

UNCLASSIFIED

AD NUMBER
AD901850
NEW LIMITATION CHANGE
TO Approved for public release, distribution unlimited
FROM Distribution authorized to U.S. Gov't. agencies only; Test and Evaluation; 17 MAR 1972. Other requests shall be referred to Army Advanced Ballistic Defense Agency, Huntsville, AL.
AUTHORITY
USASSC ltr, 23 Mar 1974

THIS PAGE IS UNCLASSIFIED

# UPSTAGE

## EXPERIMENT

AD901850

**MCDONNELL DOUGLAS ASTRONAUTICS COMPANY**

**MCDONNELL DOUGLAS**



**CORPORATION**

**MCDONNELL  
DOUGLAS**

**UpSTAGE TECHNOLOGY REPORT:  
SPECIAL MANUFACTURING AND FABRICATION PROCESSES**

JULY 1972

MDC G3230

PREPARED BY

*D. E. Schwab*

D. E. SCHWAB  
GROUP ENGINEER - UpSTAGE PROGRAM  
MATERIALS AND METHODS - RESEARCH  
AND ENGINEERING

APPROVED BY

*B. D. Pool*

B. D. POOL  
CHIEF PROGRAM ENGINEER  
UpSTAGE EXPERIMENT

APPROVED BY

*D. B. Harmon Jr.*

DR. D. B. HARMON, JR.  
MANAGER  
SYSTEM ENGINEERING/TECHNICAL DIRECTION  
UpSTAGE EXPERIMENT

APPROVED BY

*W. H. Branch*

W. H. BRANCH  
PROGRAM MANAGER  
UpSTAGE EXPERIMENT

"LIMITING STATEMENT: DISTRIBUTION LIMITED TO U.S. GOVERNMENT  
AGENCIES ONLY; TEST AND EVALUATION; 17 MARCH 1972. OTHER REQUESTS  
FOR THIS DOCUMENT MUST BE REFERRED TO ASDMA, HUNTSVILLE OFFICE,  
ATTN: RDMH-M."

*Huntsville, Ala. 35809*

**MCDONNELL DOUGLAS AERONAUTICS COMPANY-WEST**

5301 Bolsa Avenue, Huntington Beach, CA 92647

## ABSTRACT

In the conduct of the UpSTAGE Experiment, a number of special manufacturing processes were developed to meet the advanced state-of-the-art performance requirements of the interceptor design. Significant technological advances in materials processing were made to enable the successful manufacture of fuel tanks, fuel manifold frames, thick-film electronic assemblies, heat shield insulation, internal hot gas duct insulation, and solid propellant booster motors. A description of these process developments emphasizes the methods used to manufacture these components and to resolve the processing problems encountered.

## PREFACE

This report is submitted by the McDonnell Douglas Astronautics Company (MDAC) in response to Paragraph 5.7, Technical Requirements (TR) Document Number 2114, revised issue 24 May 1968. This report also reflects the title and outline revisions made to the TR by Technical Directives (TD's) from the Advanced Ballistic Missile Defense Agency (ABMDA).

This report is organized to explain the special manufacturing and fabrication processes identified with the UpSTAGE Experiment vehicle subsystems design. The design constraints imposed on the manufacture of subsystems and components were based on analysis, design tradeoffs, and ground testing, and were due primarily to the vibration, shock, and acoustical environments as well as the functional dynamics of the subsystem or components.

Other technology reports provided as a part of the UpSTAGE Experiment are as follows:

Vehicle Aerodynamics and Thermodynamics	MDC G3229
Airborne Guidance and Control	MDC G3231
EB Control System	MDC G3232
Airborne and Ground Guidance Electronics	MDC G3233
Guidance Analysis and Simulation	MDC G3234
Vibration Analysis and Testing	MDC G3235
Laser Triad Rate Gyro	MDC G3236
JI Control System	MDC G3237
Final Report	MDC G3263

This research was sponsored by and under the technical direction of AEMDA.

Requests for further information will be welcomed by the following MDAC representatives:

- Mr. W. H. Branch  
Program Manager—UpSTAGE Experiment  
Advance Systems & Technology
- Dr. D. B. Harmon, Jr.  
Manager—System Engineering & Technical Direction  
UpSTAGE Experiment  
Advance Systems & Technology
- Mr. K. M. McKenzie  
Contract Administrator  
UpSTAGE Experiment

PRECEDING PAGE BLANK - NOT FILMED

## ACKNOWLEDGMENTS

The primary contributors to this report were:

- D. E. Schwab - Principal Author
- Keith G. Morrow - Fuel Tank Processing
- Richard F. Sporny and Gerald R. Stoeckinger - Fuel Manifold Processing
- Edward G. Babiracki, Harlan R. Isaak, John W. Kanz, and Richard T. Lamoureux - Electronics Processing
- Frank P. Chiavetta and Arnold Jack Olson - External Heat Shield and Internal Hot Gas Insulation

Also participating were:

- G. V. Bennett - Overall Supervision and Technical Guidance
- John L. Cook - Nondestructive Testing
- George H. Tsuda - Technical Editor and Technical Documentation Management

## CONTENTS

Section 1	INTRODUCTION	1-1
	1.1 Design Approach	1-1
	1.2 Report Content	1-3
Section 2	SUMMARY	2-1
	2.1 Fuel Tank Processing	2-1
	2.2 Fuel Manifold Processing	2-3
	2.3 Electronics Processing	2-3
	2.4 External Heat Shield Insulation	2-5
	2.5 Internal Hot-Gas Duct Insulation	2-6
	2.6 HiBEX-U Propellant Processing	2-7
Section 3	FUEL TANK PROCESSING	3-1
	3.1 Requirements	3-1
	3.2 Approach and Constraints	3-4
	3.3 Barrel Processing	3-8
	3.4 Liner Processing	3-13
	3.5 Piston Assembly Processing	3-18
	3.6 Adhesive Bonding Liners in Tank	3-19
	3.7 Shear-Ring Development	3-20
	3.8 Nondestructive Thickness and Bond Inspection	3-20
	3.9 Problems and Solutions	3-22
	3.10 Conclusions and Recommendations	3-23
Section 4	FUEL MANIFOLD PROCESSING	4-1
	4.1 Requirements	4-1
	4.2 Approach and Constraints	4-1
	4.3 Elliptical Forging	4-3
	4.4 Plate and Round Ring Welding	4-4
	4.5 Elliptical Manifold Welding	4-10
	4.6 Nondestructive Inspection	4-13
	4.7 Machining Crack Problem	4-15
	4.8 Problems and Solutions	4-17
	4.9 Conclusions and Recommendations	4-17
Section 5	ELECTRONICS PROCESSING	5-1
	5.1 Requirements	5-1
	5.2 Approach and Constraints	5-3

	5.3	Thick-Film Multilayer Artwork Preparation	5-4
	5.4	Thick-Film Multilayer Base Fabrication	5-15
	5.5	Thick-Film Chip Resistor Fabrication	5-27
	5.6	Electronic Assembly	5-30
	5.7	Problems and Solutions	5-38
	5.8	Conclusions and Recommendations	5-40
Section 6		EXTERNAL HEAT SHIELD INSULATION	6-1
	6.1	Requirements	6-1
	6.2	Approach and Constraints	6-4
	6.3	Forward Heat Shield Development	6-6
	6.4	Aft Heat Shield	6-10
	6.5	Booster Fin Insulation	6-11
	6.6	Finlet Injector Insulation	6-11
	6.7	Problems and Solutions	6-12
	6.8	Conclusions and Recommendations	6-13
Section 7		INTERNAL HOT-GAS DUCT INSULATION	7-1
	7.1	Requirements	7-1
	7.2	Approach and Constraints	7-3
	7.3	Molded Silicone Rubber Liners	7-8
	7.4	Cast-in-Place Silicone Rubber Liners	7-15
	7.5	Quartz/Phenolic Liners	7-26
	7.6	Quartz/Phenolic Nozzle Fabrication	7-37
	7.7	Problems and Solutions	7-39
	7.8	Conclusions and Recommendations	7-41
Section 8		HERCULES HiBEX-U PROPELLANT PROCESSING	8-1
	8.1	Requirements	8-1
	8.2	HiBEX-U Configuration	8-2
	8.3	Propellant Grain	8-2
	8.4	Recommendations	8-12
Section 9		SUMMARY OF RECOMMENDATIONS	9-1
		REFERENCES	10-1
Appendix A		UpSTAGE SHEAR RING DEVELOPMENT TESTS	A-1
Appendix B		NUMERICAL CONTROL WELDING DEVELOPMENT FOR THE ELLIPTICAL UpSTAGE EB FUEL MANIFOLD FRAME	B-1

Appendix C	THEρμοCONDUCTIVE MATERIALS AND INKS FOR THICK FILM SUBSTRATES	C- 1
Appendix D	ADHESIVE BONDING, CURING AND INSULATION OF THE UpSTAGE AIRFRAME	D- 1
Appendix E	EVALUATION OF WARM GAS MANIFOLD LINER MATERIALS	E- 1
Appendix F	HiBEX- U MOTOR DESCRIPTION	F- 1
Appendix G	HAZARDS EVALUATION OF HiBEX LIQUID CARRIER PROCESS	G- 1

## GLOSSARY

Aeroder attack angle	Angle of impingement of hot Aeroder gas stream on specimen. Angle is complement of the angle away from normal to the specimen surface.
AP	ammonium perchlorate
APT	automatic programmed tool
AWG	American Wiregauge
BCA	butyl cellusolve acetate
BMD	ballistic missile defense
C	conduct, or print-and-dray conductor
CEU	control electronics unit
cfh	cubic feet per hour
D	dielectric, or print-and-dry dielectric
DSCP	direct current straight polarity
EB	external burning
EMCA	Electro Materials Corporation of America
EPSU	electrical power distribution and sequencing unit
ESL	Electro Science Laboratories, Inc.
F	fire; Fahrenheit
faying	mating; touching
FEP	fluorinated ethylene propylene (a type of Teflon)
FPC	forty-pound charge
FPP	flatpack pad
GCU	guidance command unit
GN <sub>2</sub>	gaseous nitrogen
GTA	gas tungsten arc
Hg	mercury
Hz	Hertz
IC	integrated circuit
ID	inner diameter
ipm	inches per minute
JI	jet interaction

LRAD	MDAC Independent Research and Development Program
kHz	kiloherzt
LID	leadless inverted device
MCU	machine control unit
MEK	methyl ethyl ketone (a solvent)
MFE	mold-filling efficiency
MOS	metal oxide semiconductor
N/C	numerical control
NC	nitrocellulose
NDPA	nitrodiphenylamine
NG	nitroglycerin
OD	outer diameter
PC	printed circuit
pcf	pound per cubic foot
P/N	part number
P/S ratio	powder-to-solvent ratio
RT	room temperature
RTV	room temperature vulcanizing
SCR	silicon controlled rectifier
scc/sec	standard cubic centimeter per second
TA	triacetin
Thk	thick
Thor	thorium
TPC	ten-pound charge
UDM	Universal drafting machine
V	fill and dry via
v	volt
vdc	volts direct current
via	vertical thick-film circuit conductor connecting circuit elements on different layers of a multilayer circuit board (base)
$\Omega$	ohms

# NL

## Section 1 INTRODUCTION

The purpose of the UpSTAGE Experiment program was to determine feasible guidance policies consistent with terminal defense concepts (simulated engagements) and to develop within this context the required interceptor technology.

The baseline UpSTAGE Experiment consists of a two-stage interceptor vehicle (Figure 1-1) and a ground guidance system including a modified Hercules missile-tracking radar and a SEL System 86 computer. The interceptor is a high-performance vehicle whose second stage has an advanced, nonpropelled lifting-body shape. The fast reactions required of the vehicle are provided by two types of control mechanisms: external burning (EB) and jet interaction (JI). The EB control concept uses a highly pyrophoric pentaborane fuel metered to burn near the outside of the vehicle. The JI concept, similar to an attitude control device, uses exhaust from a gas generator metered to the outside of the vehicle. The attitude of the vehicle is monitored by a laser triad rate gyro (LTRG), a strapdown component. The booster stage includes a high-performance HiBEX-U motor.

The program included five flight test vehicles flown at White Sands Missile Range (WSMR), New Mexico. Three of the vehicles were designed with EB control subsystems and two with JI.

### 1.1 DESIGN APPROACH

Due to the advanced nature of the experiment, many design concepts and manufacturing and fabricating approaches were promoted to minimize vehicle weight; develop new electronic/missile packaging concepts; ensure survivability in the flight environment; develop fast-response, fast-reacting control system components; etc. State-of-the-art design concepts were used wherever possible, but the severity of the flight environment introduced new techniques

ABMDA  
UpSTAGE

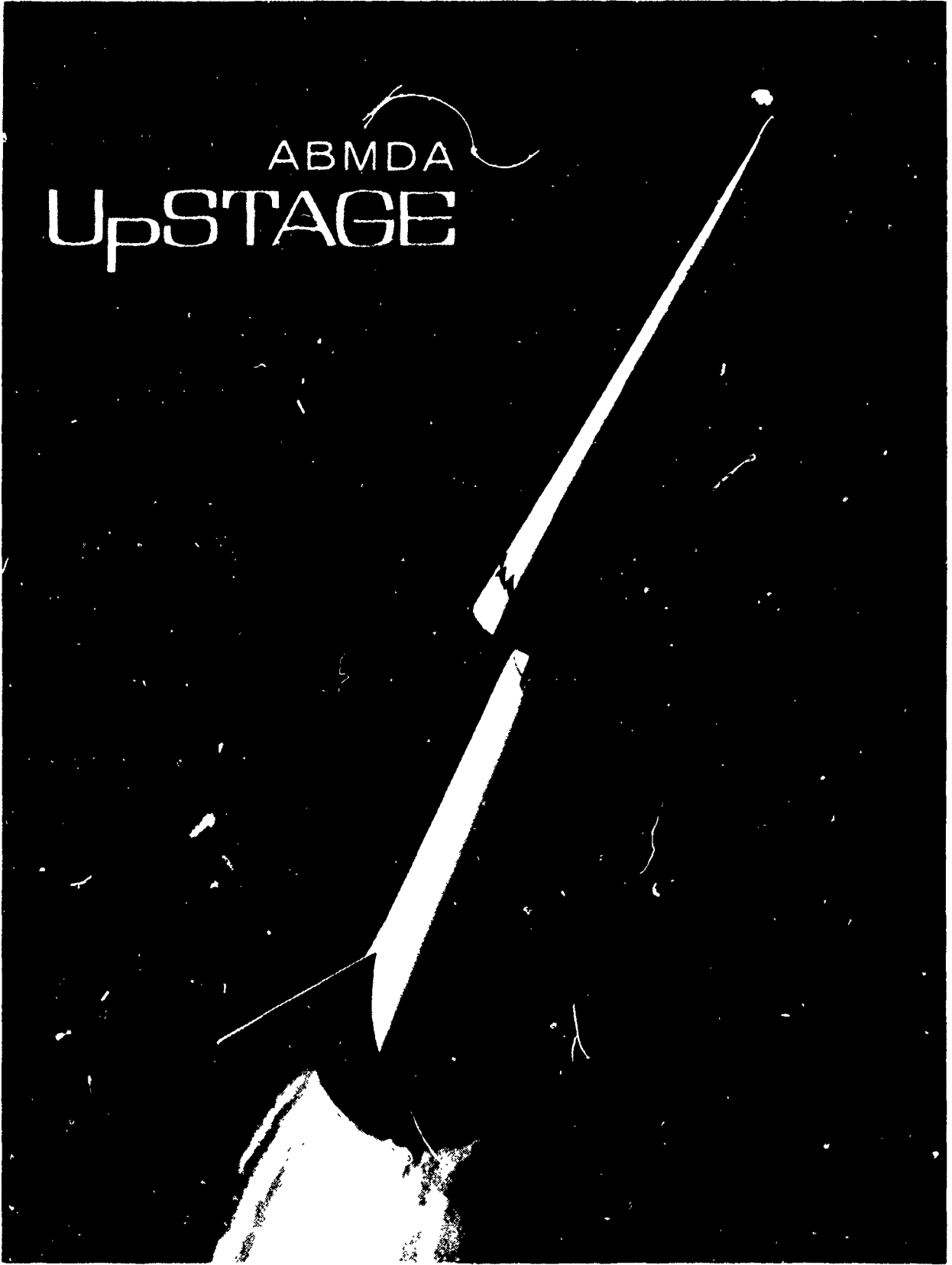


Figure 1-1. UpSTAGE Vehicle

in design and manufacturing for survivability. Severe vibration, shock, and acoustic environments established new requirements for electronics packaging and wire-bundling techniques. The electronic packaging concepts were enhanced by a thick-film approach. The EB fuel manifold machining and welding, bond and insulation development for warm gas and external application, and fuel tank processing were other areas of design implementation affected by the flight environment.

## 1.2 REPORT CONTENT

This report describes the development of several special manufacturing and processing techniques which were used to produce components of the UpSTAGE vehicles. The design and performance aspects of the components and subsystems involved are described briefly where such information is need to understand the process requirements, constraints, configuration, etc.

## Section 2 SUMMARY

This section provides an overview of the contents of this report. Table 2-1 summarizes significant advances in manufacturing process technologies and lists the sections of this report containing detailed descriptions of each development.

### 2.1 FUEL TANK PROCESSING

Manufacture of the pentaborane fuel tank assembly presented some difficult problems. The manufacturing procedures involved in shear-forming (floturning); heat treating; machining; welding; nondestructive testing; and bonding of the maraging-steel barrel, aluminum liner assembly, and the maraging-steel/aluminum piston assembly are outlined in Section 3. Significant development problems are also discussed. Material selection, fuel compatibility, and other design considerations appear in Reference 7-1.

Maraging steel in the annealed condition has excellent cold-forming characteristics; cold working does, however, induce residual stresses that are relieved in subsequent machining operations. The limitations of the equipment available for shear-forming the maraging-steel barrels made necessary additional heat-treating, straightening, and grinding to meet the dimensional and configuration requirements of the parts.

The fuel tank barrel and piston were lined on the inside surface with aluminum to prevent contact between the pentaborane fuel and the maraging-steel tank. The aluminum liners were bonded with a flexible epoxy that could withstand the loads during tank operation. The thin wall of the aluminum liner, together with the close dimensional tolerances ( $\pm 0.001$  inch) and the microfinish, made the liner a difficult part to manufacture. Shear-forming, welding, machining, bonding, and inspection created problems that required development time.

Table 2-1  
SUMMARY OF UpSTAGE MANUFACTURING PROCESS ADVANCES

UpSTAGE Application	Significant Advances in State of the Art	Applicable Sections
<b>Fuel Tank</b>	Fabrication of thin aluminum tank liners	3.1, 2, 3, 4
	Bonding thin rubber insulation liners to concave surfaces	3.5
	Bonding thin aluminum liners into slender cylindrical tanks	3.6
	In-process thickness inspection of thin cylindrical shells	3.8.1
	Nondestructive inspection of adhesive bonds between two thin cylindrical metal shells	3.8.2
<b>Fuel Manifold</b>	Fabrication of elliptical forgings with low residual stresses	4.3
	Welding longitudinal seams in small-diameter, closed aluminum ducts	4.1, 4.2, 4.4, 4.5
	Nondestructive inspection of weld drop-through in small-diameter closed ducts	4.6.1
<b>Electronics Assemblies</b>	Computerized production of multilayer thick-film circuit artwork	5.3
	Fabrication of 4- by 6- by 0.025-inch two-sided multilayer thick-film circuit bases	5.1, 5.2, 5.4
	Fabrication of solderable thick-film chip resistors	5.1, 5.2, 5.5
	Thermoconductive bonding of assemblies to withstand reflow-soldering	5.1, 5.2, 5.6.1, 5.6.2
	Fabrication of multilayer printed-circuit boards with a flexible section and plated through-holes	5.6.2
<b>Heat Shield</b>	Fabrication of thin heat shields from preimpregnated high-silica/phenolic cloth by simultaneous curing of adhesive and phenolic resin ablator	6.1, 6.2.1 through 6.2.3, 6.3 through 6.5
<b>Internal Hot-Gas Duct Insulation</b>	Bonding molded silicone rubber insulation into curved, small-diameter metal ducts	7.1.1, 7.2.1, 7.3
	Casting void-free silicone rubber insulation into aluminum and titanium ducts	7.1.2, 7.2.2, 7.4
	Fabrication, bonding, and nondestructive inspection of small-diameter, 45-deg shingle angle, quartz/phenolic hot-gas duct liners	7.1.2, 7.2.2, 7.5.1 through 7.5.3
	Fabrication of knitted quartz/phenolic continuous liners for intersecting ducts	7.2.2, 7.5.4
	Fabrication of flat-wrapped and chevron-layup quartz/phenolic nozzle exit cones	7.1.2, 7.2.2, 7.6
<b>Hercules HIBEX-U Motor</b>	Full-scale FDN propellant processing with liquid-carrier heptane	8

The piston assembly was manufactured with only minor difficulties, such as fitting the mating parts and bonding the silicone rubber boot inside the piston.

## 2.2 FUEL MANIFOLD PROCESSING

The EB fuel-manifold frames were required to conform to the elliptical cross-sectional shape of the aft control section of the vehicle and were made from two 2014-T452 aluminum ring forgings. A discussion of this process is presented in Section 4. A numerically controlled (N/C) gas tungsten arc (GTA) welding procedure was developed using three axes of an eight-axis N/C welding machine. The resultant welds were free of porosity and oxide inclusions and, when aged, resulted in guaranteed tensile yield strengths greater than 28,000 psi, even after being repaired twice. The success of the welding technique was due to the combined use of a 10-Hz pulsating welding current, in-process rotation of the weld wire feed about the tungsten electrode, and an interference fit of the two forgings. A high incidence of lack-of-penetration defects occurred during this procedure, but a satisfactory weld repair technique was employed to correct the discrepancy. Cracking that occurred during final machining (in a region not near the welds) was eliminated by reducing the stresses imposed during machining.

## 2.3 ELECTRONICS PROCESSING

The state of the art in thick-film technology, artwork generation for electronic circuits, and hybrid electronic assembly was advanced in the course of completing the UpSTAGE Experiment; these subjects are discussed in Section 5. The packaging design had to meet stringent space, weight, and environmental requirements imposed on the electronics system. Thick-film assemblies using screen-printed multilayer interconnections (vias) were chosen to meet this need. Processing problems encountered were primarily due to the large size and complexity of the thick-film circuits. Previous MDAC efforts produced 2- by 2-inch one-sided multilayer bases containing three conductor layers. For UpSTAGE, 4- by 6-inch, two-sided bases were required with six conductor layers to meet electronic packaging requirements (see Reference 5-1).

The size of the thick-film substrate (4 by 6 inches) and complexity of the circuit precluded the conventional method (20-times-scale photoreduction) of making artwork. A system was developed for making artwork which utilized

the speed and accuracy of computers and N/C drafting equipment. The approach was to treat each layer as a single entity, breaking it down into manageable parts and assembling these parts into their respective layers. Each part was stored on punched tape. Many tapes were used on one piece of artwork. As a result, the accuracy and correctness of artwork on first release exceeded 98 percent.

The multilayer fabrication process generally followed standard thick-film procedures, but several problems were encountered in scaling the process to the 4- by 6-inch substrate. One example was printing circuitry on both sides of the substrate to minimize interlayer capacitance. Initially, the thick-film multilayer fabrication yield was less than 30 percent, but improvements increased yield to 95 percent with a corresponding decrease in fabrication time.

Before bonding the thick-film substrate to the heat sink, the substrate circuitry was solder-coated by a solder-dip operation. It was necessary to redip the substrate in the solder pot in order to get a uniform solder coat. However, with repeated dip operations or repeated hand-soldering operations, solder leaching (conductive ink dissolving in solder) occurred. Process changes were developed which resulted in an adequate solder coat with two solder-dip operations. Components could be hand-soldered onto the substrate circuitry, but unsoldering of a lead often resulted in thick-film conductor pad leaching. Several approaches were taken to solve this problem including various coatings, pad/via geometry changes, multiple solder-dipping, and top-layer printing changes. The approach selected, a combination of controlled dipping, smaller vias and limited manual touchup, was the most effective practical solution to the problem.

Methods were developed for bonding the tinned thick-film multilayer base to a molybdenum heat sink, and then attaching discrete components by bonding and by reflow- and hand-soldering. Molybdenum was used to minimize forces generated by differences in thermal expansion while maximizing thermal conductivity and rigidity. An acceptable thermal transfer was obtained between the heat sink and thick-film substrate through use of a thermoconductive silicone adhesive.

Electrical assembly techniques of several types were developed. Soldering attachment of microcircuits, flexible-rigid multilayer board fabrication, conformal coating, foaming, static charge control, and repair and replacement of modules and components presented a number of processing problems that were solved.

#### 2.4 EXTERNAL HEAT SHIELD INSULATION

A process (described in Section 6) was developed to cure and bond a 0.050-inch-thick high-silica/phenolic forward heat shield to the structural sections with epoxy-phenolic film adhesive by a one-step autoclave pressure cure. Joint techniques were also examined and tested. Because of differences in thermal expansion characteristics of the composite and metallic substructure, the process required a slow, controlled-rate cooldown under pressure. Difficulties in sealing the substructure were encountered due to interference of supporting internal ribs and sealant contamination of bonding surfaces. These difficulties were overcome by capping the open ends of the structure and overbagging so that internal sealant was not required. Problems of wrinkling and unbonds were solved.

Special weaving techniques were developed to provide a 0.100-inch-thick, high-silica cloth for the aft control section heat shield. No difficulties were encountered in using this cloth as the base reinforcement for the pre-impregnated, high-silica/phenolic composite.

Booster fin insulation, 0.050-inch-thick high-silica/phenolic, was cured and bonded by the basic process developed for the forward and aft second-stage heat shields.

A transfer-molding process was developed for the fabrication of ER injector finlets from high-silica/phenolic and quartz/phenolic molding chips. A mold sticking problem was resolved by introducing zinc stearate powder with the molding compound as a premix. Finlets for evaluation tests were also fabricated using carbon/phenolic material. The developed process demonstrated repeatability and tight tolerance control.

External protection of other surfaces of the UpSTAGE vehicle was provided by conventional materials such as adhesive-bonded cork and sprayed-epoxy ablative insulation.

## 2.5 INTERNAL HOT-GAS DUCT INSULATION

Internal insulations for EB and JI ducting are summarized from Section 7.

### 2.5.1 EB Control Subsystem

Several types of moldable silicone rubber were evaluated for thermal and physical characteristics. Tubular liners were molded to close OD and wall thickness tolerances, precluding the use of extruded tubing which could not be held to close tolerances. Even by molding the insulation, it was difficult to maintain dimensions within specified tolerances. It was necessary to broaden the tolerance allowed on the wall thickness. Acceptable liners were produced to revised dimensional tolerances and successfully bonded to the interior of the manifold.

The metal surfaces of the EB crossover tube and the EB vent tubes were prepared for bonding by wet-abrasive cleaning of the Inconel 718 surface, descaling, degreasing, and priming, in this sequence. The rubber liner was degreased and primed. The liner was inserted in the tube and bonded in place with a two-part silicone adhesive. Assembly was accomplished in a vacuum chamber to minimize bonding voids. Nondestructive inspection techniques were unsuccessful with respect to the bond between the molded rubber liner and the manifold system. No method was successful in detecting small areas of unbond or adhesive voids. A resonance-loading instrument was able to distinguish gross areas of unbond, but the size of the detectable unbond areas was so great that the inspection capability was inadequate.

### 2.5.2 JI Control Subsystem

A method was developed for casting on the interior walls of the JI manifold a dense and void-free room-temperature-vulcanizing (RTV) silicone-rubber liner coating. However, poor performance of the rubber in hot-firing functional tests led to its replacement by quartz/phenolic.

A process was selected to provide a shallow-angle (10 deg), quartz/phenolic, tape-wrapped cylinder using a flat overwrap to achieve final diameter. Because of the diameter limitations for the 10-deg shingle-angle wrap (inherent in the layup technique) and poor test performance at 90-deg intersection points, a second process was developed using a 45-deg-oriented "dinked" (precut) preform made from flat washers formed to a conical shape and subsequently cured in a press. Methods were developed to post-bond these liners to the required metal components by vacuum and pressure injection techniques. Neutron radiography was found to be an effective nondestructive bond inspection technique. Exploratory work proved the feasibility of fabricating continuous liners for intersecting ducts to overcome intersection joint problems. Quartz-phenolic "socks" were knitted from yarn, impregnated with phenolic resin, and bonded and cured in metal ducts.

A successful flat-wrap technique was developed to provide insulation and erosion protection for the nozzle assembly as well as to meet structural requirements. A second technique was also developed to fabricate a 30-degree-oriented exit portion composite, subsequently overwrapped with flat wrap to achieve the required diameter in both the titanium portion and exit portion of the assembly.

## 2.6 HiBEX-U PROPELLANT PROCESSING

As subcontractor to MDAC on the UpSTAGE program, Hercules, Inc., provided an ARPA-developed HiBEX-U booster motor. The motor was a single, perforated, 11-point star grain design made from FDN-80 composite modified double-base propellant. For the UpSTAGE Experiment, several design modifications were incorporated. The nozzle was redesigned to reduce weight by eliminating the TVC and its mounting pads. FDN-80 propellant was processed with an inert carrier to reduce electrostatic hazards (refer to Section 8).

The FDN propellant was processed with heptane for full-scale HiBEX-U application in the following sequence:

- A. The propellant ingredients (ammonium perchlorate, aluminum powder, zirconium staples, nitrocellulose, nitroglycerin, resorcinol, and 2-nitrodiphenylamine) were prepared, mixed, extruded, and cut into "green" powder.

- B. The green powder in heptane was tumbled, dried, shaped, screened, and blended into finished casting powder ready for motor loading.
- C. The casting powder in heptane was loaded into a prepared motor case while being vibrated, cast, and cured.

In order to reduce the hazards inherent in propellant powder-handling, an inert liquid carrier (n-heptane) was used in the propellant manufacturing process. While the heptane did not affect the propellant burning rate, the mechanical properties of the propellant were slightly altered: that is, higher strength and modulus at nominal powder-to-solvent (P/S) ratio (70/30) were obtained, but elongation was lower. In general, as the nitrocellulose/total-plasticizer (nitroglycerin and triacetin) ratio was increased, the propellant modulus and tensile strength increased and the elongation decreased.

The heptane process also had no effect on ammonium perchlorate particle size or zirconium staple dimensions.

Mold-filling efficiency (MFE) is the ratio of density of casting powder loaded into a full-scale motor case compared to the density of powder from a standardized small-scale test mold filled by gravity-screen loading. The MFE of the original HiBEX was increased by 4 percent because low-frequency vibrations introduced into the HiBEX-U motor-loading sequence helped pack the motor more efficiently.

The mold-loading set of conditions within the demonstrated extremes produced a motor with structural capabilities better than those of the original HiBEX motor. The data at the P/S ratio extremes indicated that the HiBEX motor margin of safety was in excess of 0.2 at the critical propellant grain design area (forward groove).

The case-bond system for FDN-80 propellant grain consisted of bimodal casting-powder granules in a motor case. Embedment was accomplished by applying resin to the inside surface of the case and applying large and small powder granules which were later cured. Case-bond embedment layers were successfully applied to all HiBEX-U motors.

## Section 3 FUEL TANK PROCESSING

### 3.1 REQUIREMENTS

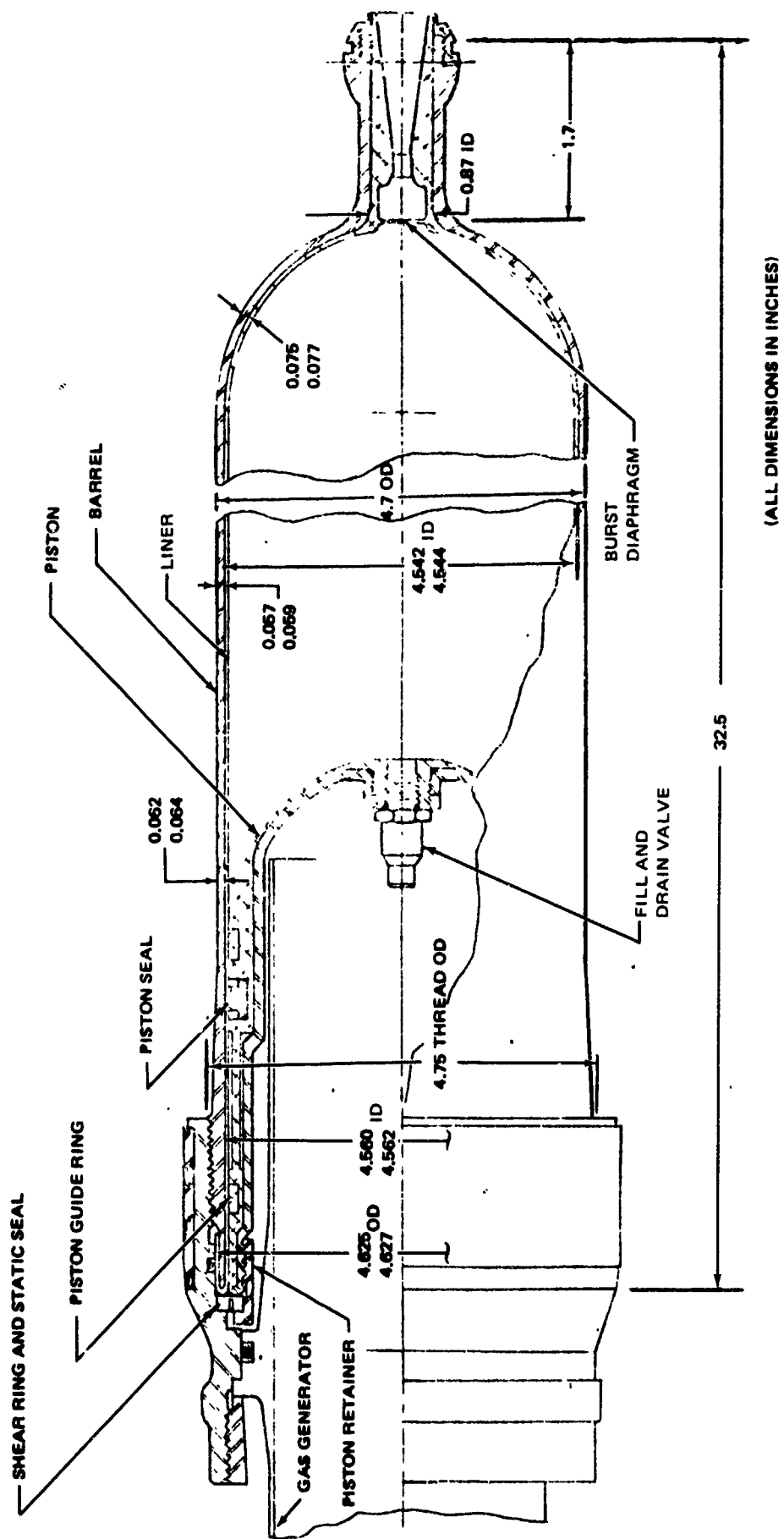
The fuel tank (Figure 3-1) consists of a flo-turned maraging steel barrel with an aluminum liner on the fuel side (to prevent contact of the pentaborane fuel with the maraging steel) and a maraging steel piston with an aluminum cover on the pentaborane fuel side and a silicone rubber insulation liner on the hot-gas side. A room-temperature adhesive-bonding process was needed to prevent thermal stresses. Dimensional requirements on detail parts and assemblies were stringent for functional reliability.

#### 3.1.1 Barrel Requirements

After forming, machining, and heat treatment, the 250-grade maraging steel barrel (Figure 3-1) was 4.7 inches in outer diameter by 32.5 inches long with a varying wall thickness of 0.057, 0.062, and 0.075 inch. The barrel had one open end. The other end was ported and hemispherical. The hemispherical end had a neck 1.7 inches long with a 2-degree tapered opening. The neck exterior had a machined hemispherical surface and threaded area. The open end of the barrel was 4.625/4.627 inches in diameter for 0.5 inch with a 4.7-inch-diameter thread, 1-inch long. The internal bore was 4.560/4.562 inches in diameter to 4.3 inches from the open end and tapered to 4.542/4.544 inch diameter for 5.5 inches. Barrels were flo-turned with a 45- to 65-percent cumulative reduction in thickness, prior to annealing. Annealing was performed after the third and fourth flo-turn passes.

#### 3.1.2 Liner Requirements

The 6061-T6 aluminum liner fitted inside the maraging steel barrel and lipped over the open end of the barrel (Figure 3-2). The liner surface had a 16-microinch finish inside and a 32-microinch finish on the outside. A burst diaphragm/diffuser assembly was electron-beam-welded to a 1.2-inch-diameter



(ALL DIMENSIONS IN INCHES)

Figure 3-1. EB Fuel Tank Flight Configuration Showing Barrel Dimensions

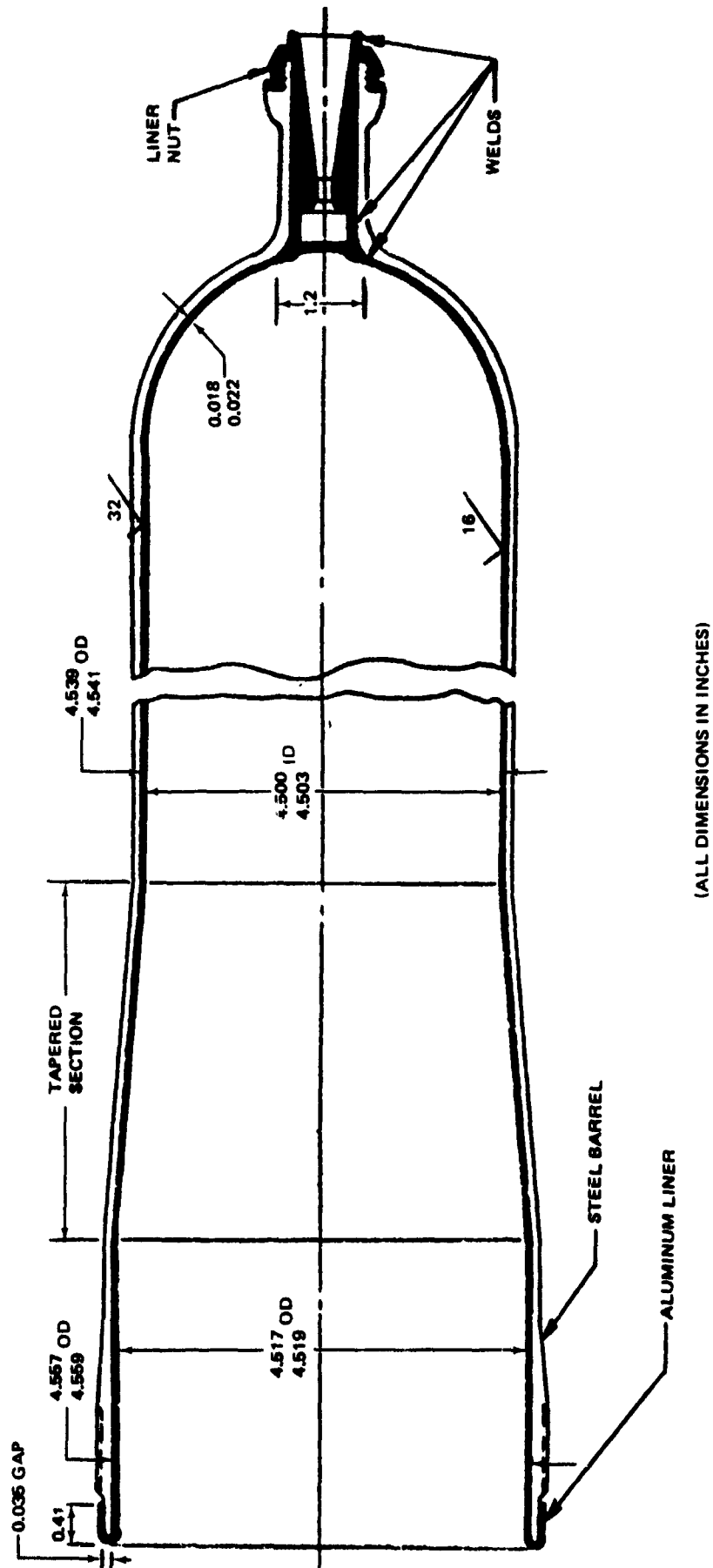


Figure 3-2. EB Fuel Tank Barrel/Liner Assembly Showing Liner Dimensions

opening in the hemispherical end of the liner. A lip formed on the open end had a 0.035-inch gap to accommodate the end of the barrel. The liner was shear-formed from 6061 aluminum and heat-treated to the T6 condition. After bonding of the liner/diffuser assembly into the barrel, an aluminum nut was threaded over the barrel and gas-tungsten-arc (GTA)-welded to the diffuser end.

### 3.1.3 Piston Requirements

The piston (Figure 3-3) was made from 250-grade maraging steel and required a hemispherical end. An aluminum cover to fit on the outside of the piston and bonded silicone rubber insulation (boot) on the inside protected the piston. The piston assembly was installed inside the barrel and liner assembly.

## 3.2 APPROACH AND CONSTRAINTS

A Lodge and Shipley Flo-Turn spin lathe was used to flo-turn the maraging steel barrel and aluminum liner. A special machine attachment was designed and fabricated to fit the lathe, as shown in Figure 3-4.

A special tail-stock adapter and guide pins were designed and fabricated to support and align the mandrel and part. Special rollers made of air-hardening tool steel were designed and fabricated. Figure 3-5 shows the adapter, rollers, and mandrel.

The equipment for shear-forming maraging steel had limitations due to the size and configuration of the barrel. Because of these limitations, it was not possible to shear-form the part to net inside dimensions. The part would not form closely enough to the mandrel during the shear-forming operation to hold the required inside dimensions. The deflection of the rollers made it difficult to control the percentage of reduction; this caused eccentricity, "banana" and "bell-mouthing" effects, and a variation in wall thickness. It was therefore necessary to reduce the diameter of the steel preform and the flo-turn mandrel and increase the outside diameter of the preform to permit subsequent grinding to achieve final dimensions.

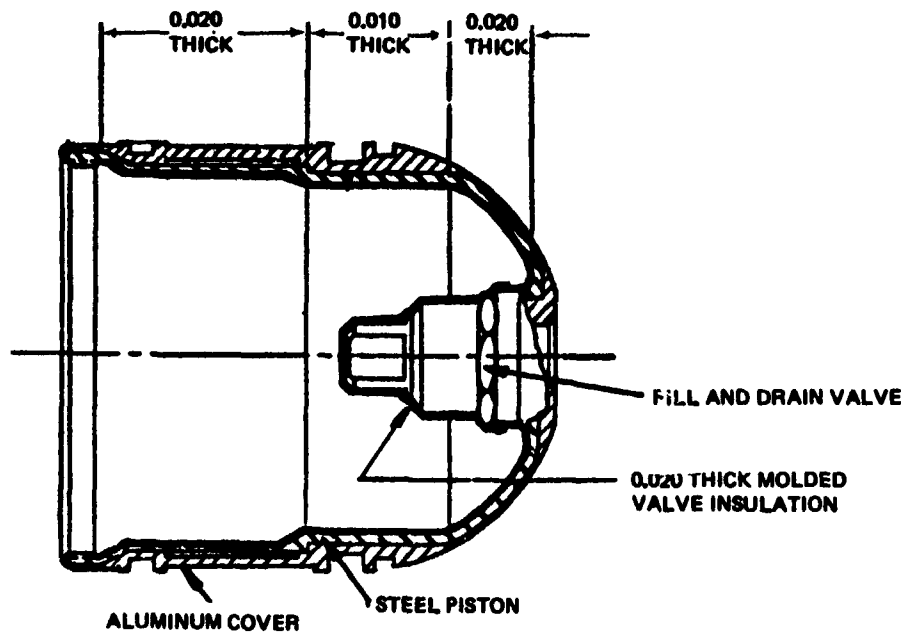


Figure 3-3. EB Fuel-Tank Piston Assembly, Showing Insulation Thickness (in Inches)

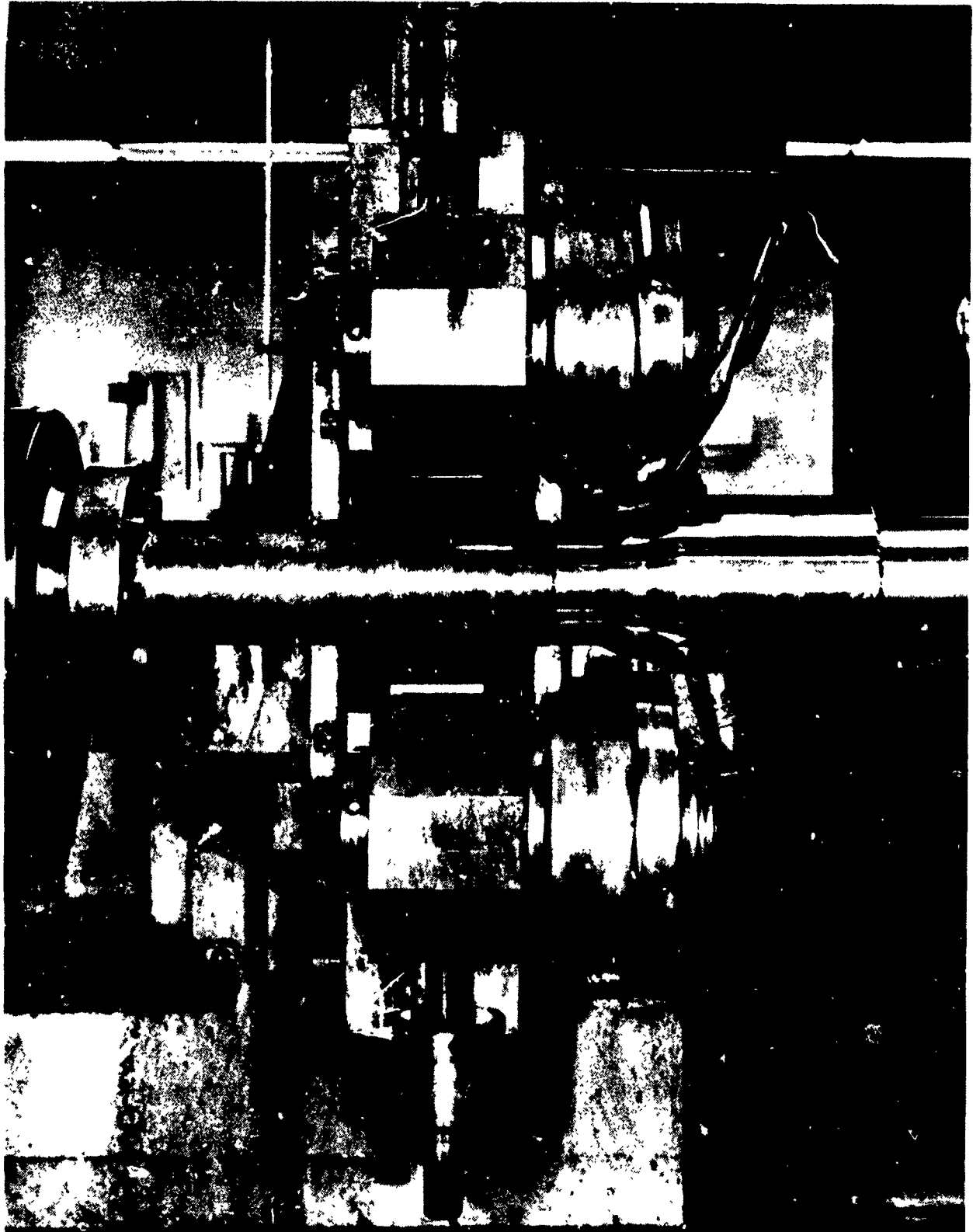


Figure 3-4. Flo-Turn Lathe and Special Roller Attachment

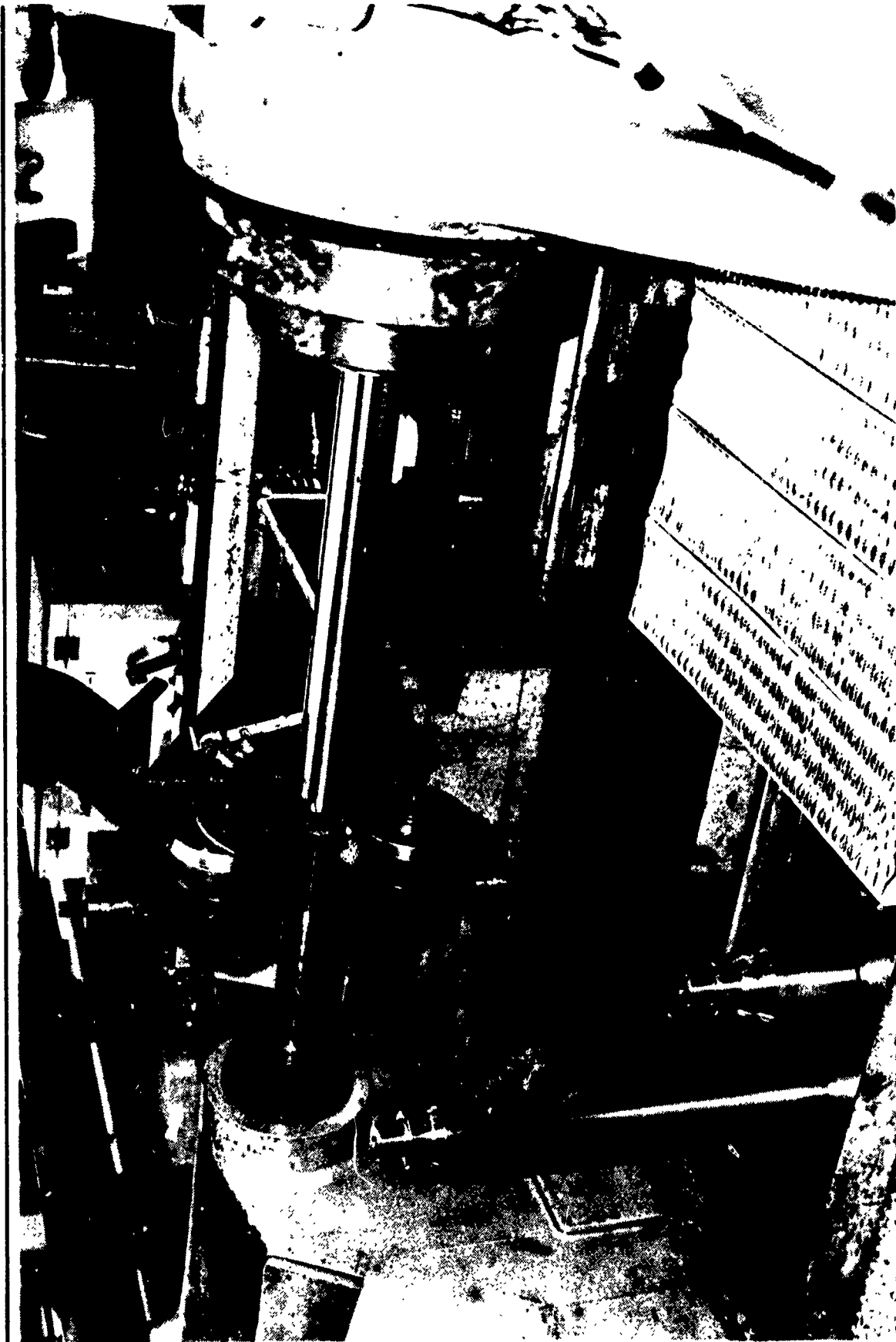


Figure 3-5. Flo-Turn Adapter, Rollers, and Mandrel

### 3.3 BARREL PROCESSING

A study was made to determine the configuration needed for the maraging steel preform blanks. Sufficient wall thickness was necessary to obtain the reductions required and to obtain the final length. Since the inside of the hemispherical end could not be machined later, it was necessary to machine the inside of the closed end of the preform to net part dimensions. A diameter was machined to fit the tail-stock adapter of the Flo-Turn machine. Also, a close-tolerance hole was machined in the closed end of the blank to fit the tail-stock alignment pin. A starting surface was machined at the tangent point of the spherical radius to allow the forming roller to start forming slightly ahead of the tangent point. Figure 3-6 shows the preform dimensions and Figure 3-7 shows the evolution of preform to postform and then to machined-barrel configurations.

#### 3.3.1 Barrel Manufacturing Sequence

The sequence for barrel processing is summarized below:

- A. Lubricate and place preform blank on mandrel.
- B. Set Flo-Turn machine to 300 rpm, 6-inch feed per minute.
- C. Set rollers to approximately 50 percent reduction. Use 0.37-inch radius, 20-deg top roller and 1.0-inch radius, 30-deg bottom roller.
- D. Shear form pass 1 and pass 2. Use feed rate of 6.0 inches per minute for pass 1 and 9.0 inches per minute for pass 2.



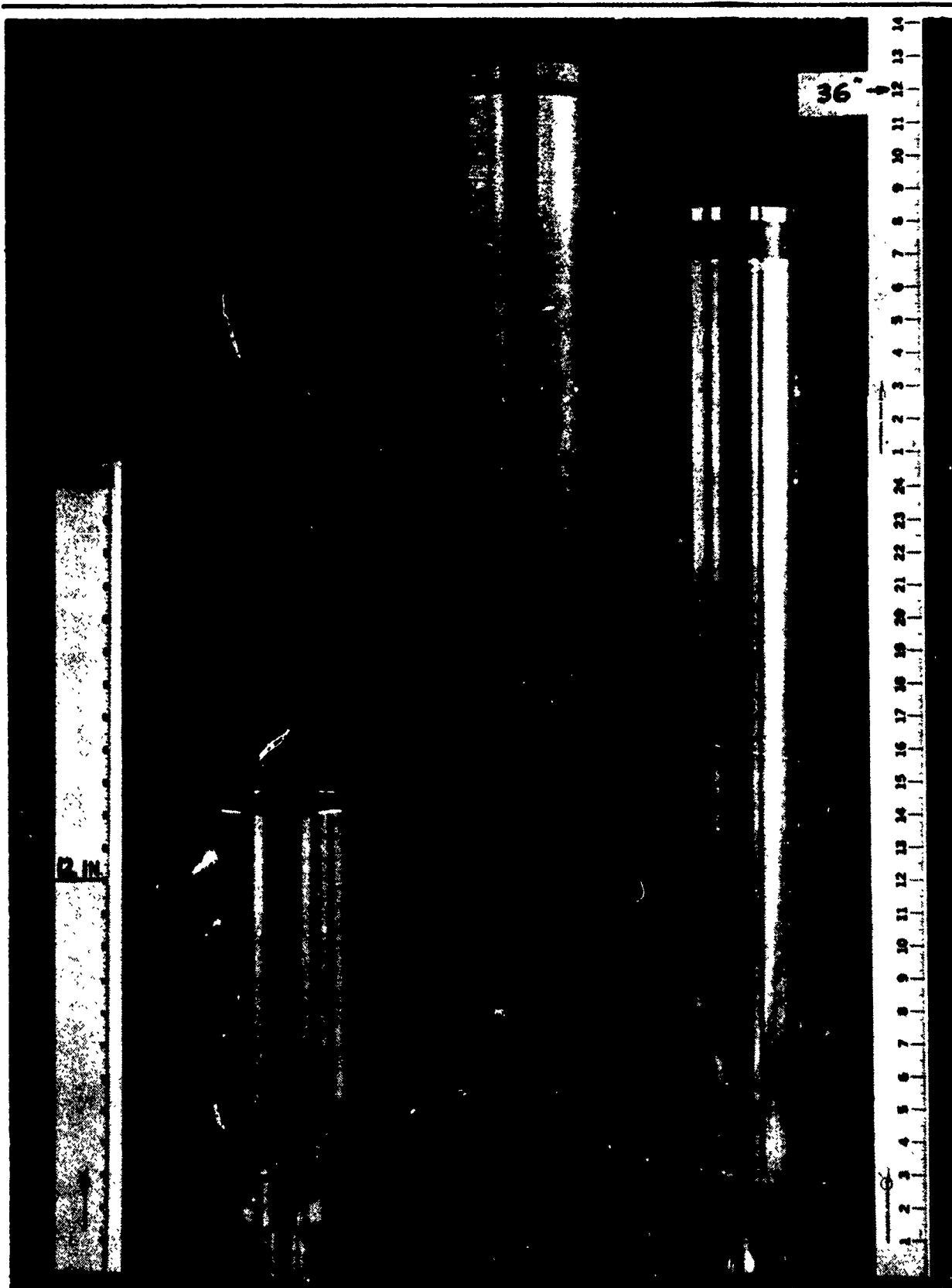


Figure 3-7. Barrel Evolution

- E. Change bottom roller to 0.37-inch radius, 30 deg, and shear-form pass 3. Use feed rate of 12 inches per minute.
- F. Solution anneal for one hour at 1,550° F.
- G. Use 0.37-inch radius, 30-deg rollers top and bottom. Shear-form pass 4. Use feed rate of 12.0 inches per minute.
- H. Solution-anneal for 1 hour at 1,550° F.
- I. Port one end.
- J. Weld cap to cover open end.
- K. Hydro-size.
- L. Remove cap.
- M. Grind inside diameter to net part dimensions. Blend spherical radius.
- N. Grind outside diameter to clean up.
- O. Set up on lathe fixture and finish machine barrel to final dimensions.
- P. Age-harden 4 hours at 900° F.
- Q. Apply corrosion-protective finish.

### 3.3.2 Shear Forming

From trial experiments, shearing-forming parameters were developed. Final parameters are listed in Table 3-1.

### 3.3.3 Straightening

A straightening operation was added which consisted of welding a maraging steel cap to the open end of the barrel and placing the welded barrel in a specially designed cylinder. The barrel was then subjected to 12,000-psig hydraulic pressure to improve the out-of-round-and-straightness condition for the grinding operation. The welded cap and barrel material adjacent to the weld were subsequently machined off.

### 3.3.4 Grinding

The inside diameter of the barrel was ground to final dimensions, blending the spherical radius of the closed end. Flat surfaces were ground on the outside diameter to support the barrel during finish machining.

Table 3-1  
 SHEAR-FORM PARAMETERS FOR MARAGING STEEL BARREL

Pass No.	t	t <sub>f</sub> (Attempt)	t <sub>f</sub> (Actual)	L <sub>o</sub> (Start)	L <sub>f</sub> (Actual)	%R (Attempt)	%R (Actual)	Feed (ipm)	Spacer-Top or Bottom	Top Roller	Bottom Roller	Bottom Roller Setting	rpm
1	0.600	0.300	0.475	15.0	17.7	50	21	6	1/2-in. bottom	3/8 R 20 deg	1.0 R 30 deg	0.600	300
2	0.475	0.240	0.395	17.7	20.0	50	17	9	1/2-in. bottom	3/8 R 20 deg	1.0 R 50 deg	0.470	300
3	0.395	0.235	0.280	20.0	26.0	41	29	12	1/4-in. top	3/8 R 20 deg	3/8 R 30 deg	0.235	300
4	0.280	0.130	0.160	24.5*	38.5	53	43	12	1/4-in. top	3/8 R 70 deg	3/8 R 30 deg	0.130	300

Legend

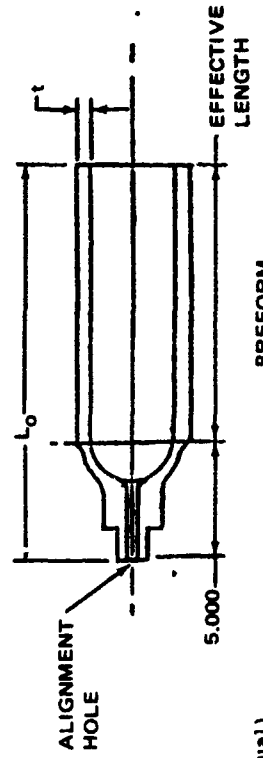
- t = Wall thickness (initial)
- t<sub>f</sub> = Thickness final (attempt) - top roller setting (actual) - result of roller deflection
- L<sub>o</sub> = Length at start
- L<sub>f</sub> = Length at final
- R = Reduction

Roller dimensions specify geometry

Effective shear-form length = 5,000 - L<sub>o</sub>

Percent of cumulative reduction through No. 3 pass = 63 percent (actual)

\* Trim length



### 3.3.5 Final Machining

The barrel was placed on a lathe mandrel. It was then finish-machined. A Freon spray coolant was used. Since the diameter of the mandrel was smaller than the diameter of the part to allow removal, perfect contact between mandrel and barrel was impossible and some variation in wall thickness resulted. Heat-resistant grease and light tool cuts were used to alleviate this problem and eliminate the necessity of making an expandable-type mandrel.

### 3.4 LINER PROCESSING

A steel mandrel was designed and fabricated to fit on the head stock of the Lodge and Shipley Flo-Turn machine. The mandrel was made to the minimum inside diameter of the aluminum liner. The end of the mandrel was made to fit the inside spherical radius of the liner. The hemispherical end cap of the mandrel was removable and was used to pull the part off the mandrel.

A special pin with a key slot was made to fit the tail stock adapter of the Flo-Turn machine. The pin and a key were inserted into the aluminum preform to prevent the preform from turning during the first three flo-turn operations.

Aluminum preforms (6061-0) were designed and made. Figure 3-8 shows the preform dimensions. A starting groove was machined on the closed end, coinciding with the tangent point of the inside spherical radius. New starting grooves were machined before each subsequent shear-form pass, as shown in Figure 3-9.

#### 3.4.1 Liner Manufacturing Sequence

The sequence for liner processing is summarized as follows:

- A. Lubricate preform and place on flo-turn mandrel.
- B. Align tail-stock guide pin.

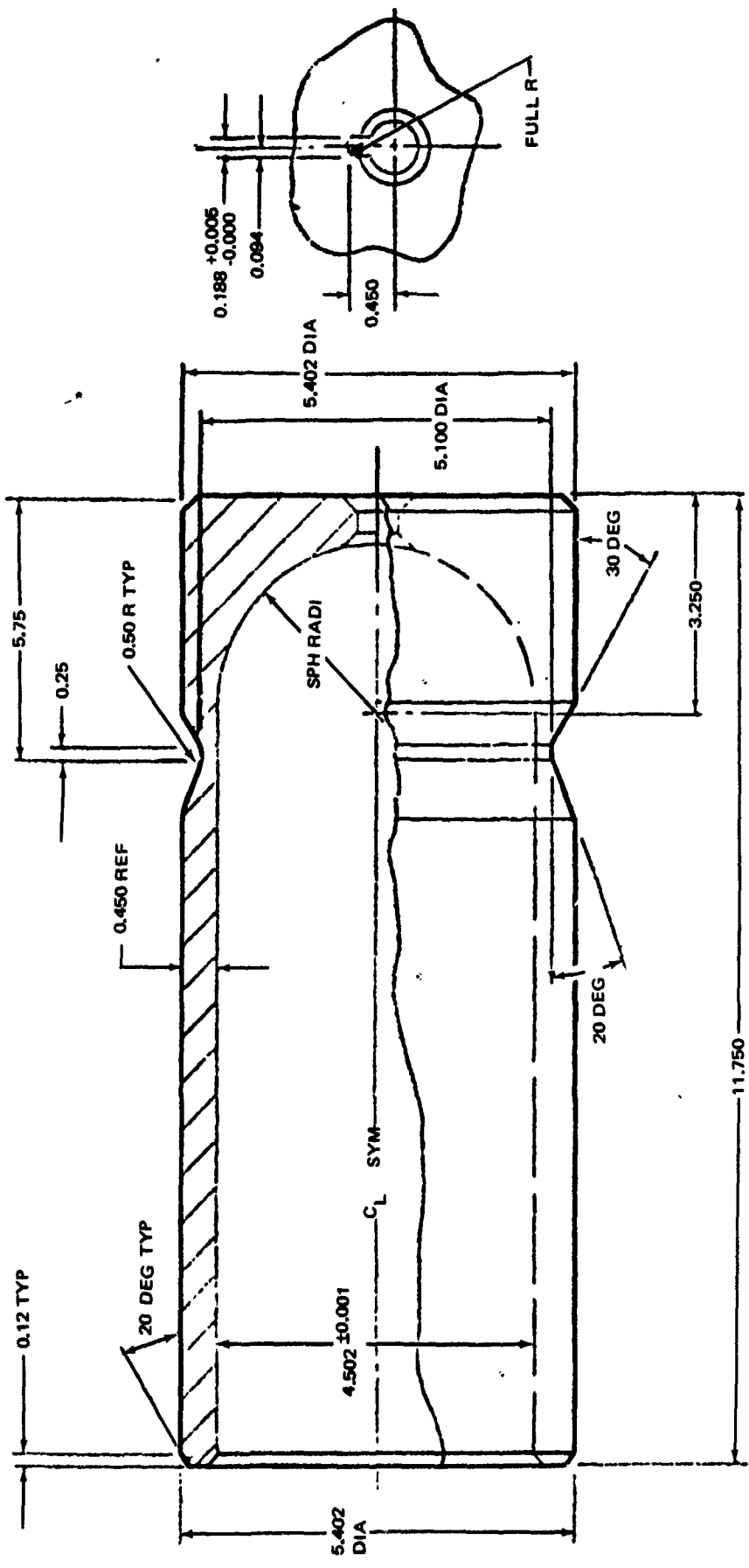


Figure 3-8. Liner Preform

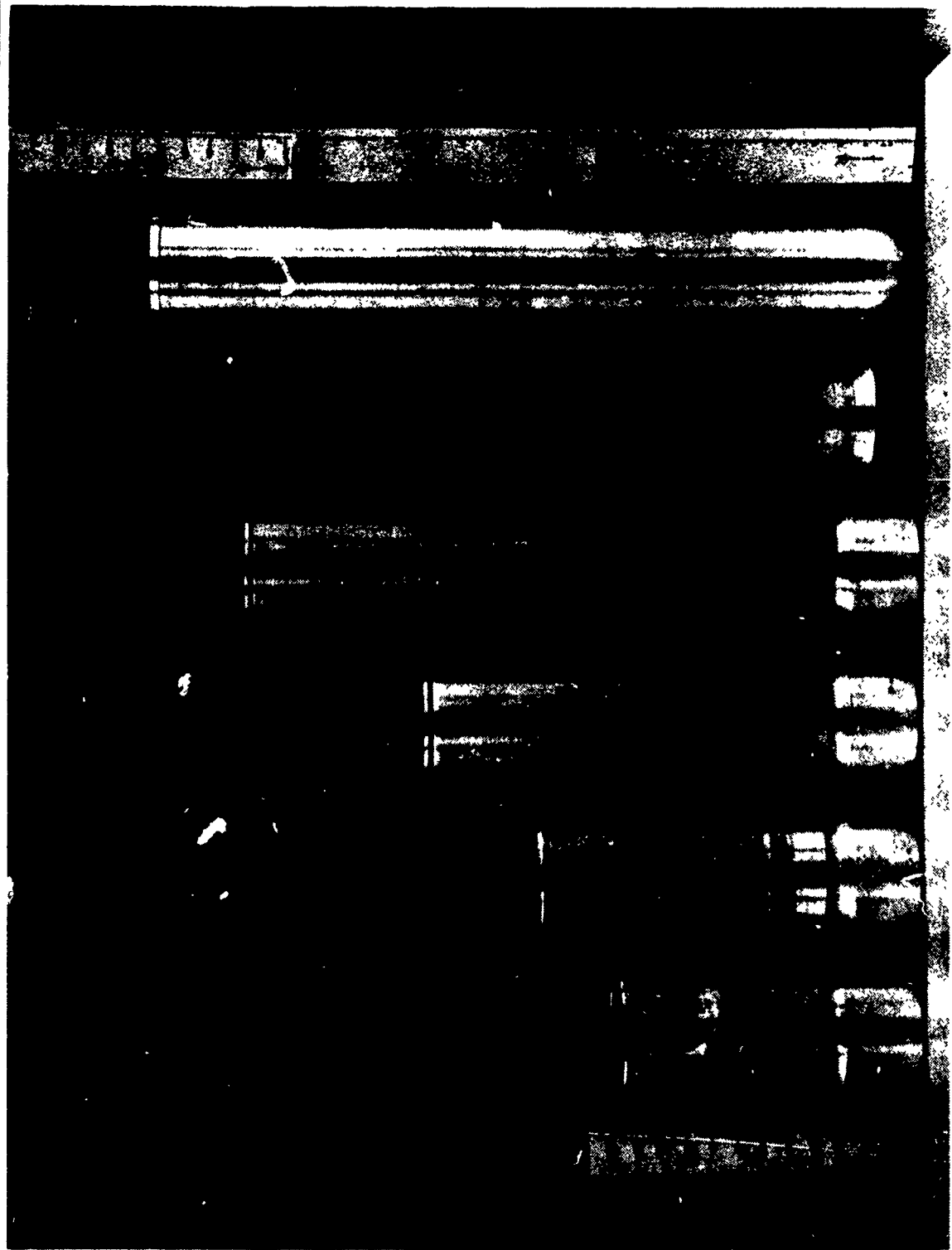


Figure 3-9. Liner Evolution

- C. Shear-form pass 1, cut off excess, clean up, and regroove.
- D. Shear-form pass 2, cut off excess, clean up, and regroove.
- E. Shear-form pass 3, cut off excess, clean up, and regroove.
- F. Solution-heat-treat to as-quenched condition.
- G. Shear form pass 4, in as-quenched condition.
- H. Leave part on mandrel and finish machine to net part dimensions except lip configuration.
- I. Heat liner to 250°F maximum to remove from mandrel.
- J. Age-harden to T6 condition.
- K. Electron-beam-weld diffuser assembly to liner.
- L. Electrically discharge machine lip configuration.

#### 3.4.2 Selection of Rollers

A number of flo-turn passes were made to obtain the correct combination of forming rollers and spacers. Scaling and distortion resulted if correct, geometrically formed rollers and dimensionally correct spacers were not used in the correct combinations. The shear-forming parameters are listed in Table 3-2.

#### 3.4.3 Machining

It was planned initially to remove the liner from the mandrel after the fourth flo-turn pass, age-harden to the T6 condition, and finish-machine on another mandrel. Heat treatment to the T6 condition caused distortion and expansion of the part, so that when the part was placed on the machining mandrel it was loose and had a tendency to stretch and move when machined to a 0.020-inch wall thickness. To solve these problems, the liners were left on the flo-turn mandrel after the fourth pass (in the as-quenched condition) and were finish-machined on the same mandrel. The liners were then removed and aged to the T6 condition. Because less than 100°F was required to remove the liner from the machining mandrel, the aging process was not affected.

Table 3-2  
SHEAR FORM PARAMETERS FOR ALUMINUM LINER

Pass No.	t Wall	t <sub>f</sub> (Attempt)	t <sub>f</sub> (Actual)	L <sub>o</sub> (Start)	L <sub>f</sub> (Actual)	%R (Attempt)	%R (Actual)	Feed (ipm)	Spacer-Top or Bottom	Top Roller	Bottom Roller	Bottom Roller Setting	rpm
1	0.450	0.300	0.320	11.7	15.0	33.0	29.0	6	1/2-in. Bottom	3/8 R 20 deg	1.0 R 30 deg	Flush	300
2	0.320	0.210	0.230	15.0	19.6	34.5	28.0	9	1/4-in. Bottom	3/8 R 20 deg	1.0 R 30 deg	0.315	300
3	0.230	0.160	0.175	19.6	25.4	30.0	26.0	9	1/4-in. Bottom	1/8 R 20 deg	1.0 R 30 deg	0.225	300
4	0.175	0.105	0.115	24.0*	34.7	40.0	34.0	12	1/4-in. Bottom	1/8 R 20 deg	1.0 R 30 deg	0.165	300

Legend

t = Wall thickness (initial)

t<sub>f</sub> = Thickness final (attempt) - top roller setting (actual) - result of roller deflection

L<sub>o</sub> = Length at start

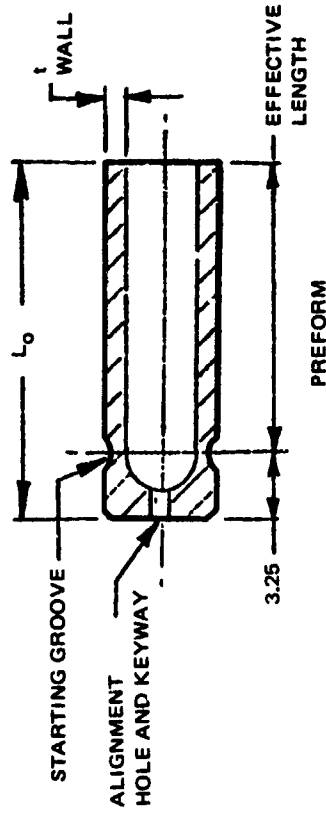
L<sub>f</sub> = Length at final

R = Reduction

Roller dimensions specify geometry

Effective shear-form length = 3.25 - L<sub>c</sub>

\* Trim length



#### 3.4.4 Electrical-Discharge Machining of Lip Configuration

A holding fixture and special electrodes of yellow brass were designed and fabricated for an electrical-discharge machine to form the lip configuration of the open end of the aluminum liner. When small particles of aluminum were flushed into the machining area, shorting occurred. Etching and cleaning of the flushing cavities of the tool eliminated this problem.

#### 3.4.5 Welding of Aluminum Liner Assembly

The electron-beam-welding process was selected to weld the diffuser to the burst diaphragm and the diffuser assembly to the liner because of the low heat input characteristics of the process. The thin-walled parts to be welded made it necessary to minimize weld distortion. In developing the weld parameters, cracking was an intermittent problem. It was found necessary to feed the 4043 aluminum filler wire into the center of the small molten puddle. This was achieved by positioning the wire guide tip precisely prior to welding each part. A stepped butt joint was used to eliminate mismatch and to reduce tooling requirements. Dimensions of the step were modified to obtain acceptable welds.

After the liner assembly was adhesive-bonded into the barrel, the diffuser end was machined to mate with the aluminum nut on the threaded neck of the barrel. The nut and liner were then GTA-welded to seal the fuel side from the steel barrel. Semiautomatic weld parameters were developed to obtain crack-free welds without overheating the barrel end.

### 3.5 PISTON ASSEMBLY PROCESSING

The tank piston was made of 250-grade maraging steel with an outer aluminum cover to prevent fuel/steel contact. Difficulty in fitting the aluminum cover over the steel piston was eliminated by hand-lapping to match-fit each assembly prior to adhesive bonding with epoxy.

A special rubber mold die was used to form a 0.010- to 0.015-inch-thick silicone rubber insulation (boot) which was subsequently bonded to the inside of the maraging steel piston. Initial attempts to bond the boot into the piston

revealed that excessive air bubbles were trapped between boot and piston. The boot material (Silastic 55) inhibited complete curing of the platinum-cured silicone adhesive (93-072). Bubbles were successfully eliminated by perforating the boot and replacing the solid bonding mandrel with a vacuum bag and appropriate bleeder-cloth layers. Curing of the adhesive was ensured by extending the cure time and raising the cure temperature. (Concurrently, a backup process was investigated to form the insulating liner by coating with liquid RTV-630 silicone rubber. This process was proven feasible.)

### 3.6 ADHESIVE BONDING LINERS IN TANK

EC-2216, a two-part, flexible, epoxy adhesive was chosen for bonding the tank liner in place. The processing characteristics are:

- A. It is a paste adhesive with adequate work life and suitable viscosity.
- B. It cures at room temperature, minimizing thermally induced stresses that could result from elevated-temperature curing of dissimilar metals.

#### 3.6.1 Processing Aids

To keep the thin-gage aluminum from buckling when the liner and tank were assembled, a precision mandrel was used. To apply a uniform thickness of adhesive to the inside wall of the tank barrel, a circular squeegee was used.

#### 3.6.2 Process Development

The mating surfaces of the aluminum liner and mating steel tank were prepared for bonding by solvent cleaning, hand sanding, and removing residual grit from the sanding operation by a final solvent wipe.

A uniform coating of adhesive was applied to the inside surface of the tank. The tank and liner were assembled with additional adhesive being applied to the liner in a rolling band at the tank and liner interface.

The adhesive was cured at ambient temperature to prevent thermal stresses developing in the dissimilar metal structure. An axial force of 100 lb was applied to maintain proper position and contact of the assembly and the assembly was allowed to cure undisturbed for 16 hr.

### 3.7 SHEAR-RING DEVELOPMENT

Tests were conducted to establish the optimum breaking groove configuration of shear rings (Figure 3-1) and to determine the spread in shear loads of rings having such breaking grooves.

Successful operation of the EB control system UpSTAGE vehicle was critically dependent upon the performance of a ring appropriately sized to shear within a prescribed load range corresponding to a tank pressure of 525 to 600 psi. The prescribed load range was 8,225 to 9,400 lb. The design specified a 2024-T4 aluminum ring with a breaking groove incorporated to produce a shear failure at the design point. Variations in the mechanical properties of the ring material were expected to affect the breaking load of the ring. Hence, the magnitude of the variation was determined. In addition, the effect on breaking load of proof loading prior to the shear test was determined.

During assembly of the UpSTAGE fuel tank, the piston retainer and piston were joined by a threaded connection (see Figure 3-1). The ability of the retainer to rotate freely without either the shear ring or Viton seal also rotating was vital to the success of the assembly operation. If either the shear ring or the seal rotated, a leak path could occur as a result of the seal being deformed. Therefore, the feasibility of using a nonmetallic torque washer to aid in assembly was determined. Details of shear-ring development tests are contained in Appendix A.

### 3.8 NONDESTRUCTIVE THICKNESS AND BOND INSPECTION

During fabrication of the tank, two problem areas in nondestructive inspection were encountered. The first of these involved measurement of the thickness of the tank and liner during machining. The second was concerned with inspection of the bond between the tank and liner.

### 3.8.1 Tank and Liner Thickness Inspection

During machining of the tank and liner it was necessary to periodically determine the thickness of the wall in the cylinder and at the hemispherical end. Inspection practice originally called for the complete removal of the work piece from the support mandrel and measurements were taken by an ultrasonic-resonance device.

In order to perform the thickness inspection without removal from the mandrel, a digital thickness gage was procured and integrated into the inspection sequence. The gage operated at 5 MHz on the pulse-echo, multiple-back-reflection concept. The transducer was only 1/4-inch in diameter and was usable in confined areas or on curved surfaces. The separation between the tank or liner and the holding mandrel was sufficient that clear reflections were seen at the back surface of the tank or liner. The small transducer worked very well on the compound curvature of the hemispherical end of the tank and liner, an area that had been very difficult to handle previously.

### 3.8.2 Tank-to-Liner Bond Inspection

To ensure the integrity of the tank-to-liner adhesive bond, it was necessary to develop a nondestructive inspection technique and procedure. The first approach was to apply a resonance-loading instrument frequently employed for metal-to-metal adhesive-bonded structure. The approach was unsuccessful because the aluminum liner was thin (about 0.020 inch) compared to the steel. The response to the transducer (located on the steel surface) was nearly the same as that of steel alone. Since the inspection had to be performed from the convex (exterior) surface of the tank (the steel surface), the resonance-loading method was not suitable.

The second approach was to use an eddy-sonic instrument. The eddy-current excitation coil operated with a frequency of approximately 15 kHz, while the pickup microphone was sensitive to a frequency of about 30 kHz. The eddy-current excitation generated a mechanical vibration which was more intense (less damped) over an unbond area. There was less material available for

damping the energy. In order to verify the effectiveness of the eddy-sonic instrument, a scrap tank (out of dimensional tolerance) was evaluated. The 1-inch test probe was fitted with a special plastic positioning shoe to maintain the probe in a fixed position with respect to the curvature of the tank. The tank was completely inspected, and all suspect areas marked. To verify the unbond indications, the tank was sectioned through the marked areas. The areas marked as unbonded came apart easily, whereas the well-bonded (unmarked) areas were extremely difficult to separate.

Based upon this test, a procedure for eddy-sonic inspection of bonded metal structures was generated and successfully employed to inspect all tank-to-liner bonds.

### 3.9 PROBLEMS AND SOLUTIONS

Problems and solutions encountered in developing the manufacturing processes for the fuel tank assembly are summarized below:

Problem	Solution
Tank barrel internal dimensions could not be maintained during flo-turning.	Reduced preform inner diameter and mandrel outer diameter; ground to final dimensions after forming.
The maraging steel barrel warped after flo-turning.	Bulge-formed the barrel to stress-relieve it.
Air gaps between the barrel and the machining mandrel caused excessive wall thickness variations during machining.	Applied heat-resistant grease to fill air gaps and made lighter tool cuts.
Aluminum liner turned on mandrel during flo-turning, causing galling.	Added a key in the guide pin of the Flo-Turn machine and a key slot in the liner preform.
Movement of material after the liner was removed from the flo-turn mandrel made it impossible to machine the wall thickness to 0.020 ±0.002 inch.	Flo-turned the part on the fourth pass in the as-quenched condition and finish-machined while the part was still on the flo-turn mandrel.

Problem	Solution
The electrical discharge machine shorted when small aluminum particles were flushed into the lip area of the liner.	Etched and cleaned the flushing cavities of the tool.
Adhesive bond between the piston and its rubber boot contained air bubbles and uncured adhesive.	Perforated the boot, vacuum-bagged the assembly, and cured at a higher temperature for longer times.
Existing thickness measurement techniques (ultrasonic-resonance) were exceedingly difficult and time consuming, especially for the aluminum liner.	Procured and applied new pulse-echo equipment (digital thickness gage).
Existing nondestructive bond testing device (resonance-loading) could not detect unbonds between tank barrel and liner.	Procured and applied new eddy-sonic device with plastic positioning shoe.
Poor weld quality was obtained in initial electron-beam welds at stepped joints.	Modified step dimensions and tolerances allowed on mating parts.

### 3.10 CONCLUSIONS AND RECOMMENDATIONS

A number of practical equipment and dimensional problems were solved to develop a satisfactory process for manufacturing a limited quantity of fuel tanks. Improved flo-turning equipment capable of producing close dimensional control would improve the economy of barrel and liner manufacture considerably. Nondestructive in-process measurement of liner wall thickness aided machining of the thin liner significantly.

## Section 4 FUEL MANIFOLD PROCESSING\*

### 4.1 REQUIREMENTS

Fabrication of the elliptical fuel manifold frame required GTA welding. The manifold frame was fabricated from two 2014-T452 aluminum rolled-ring forgings which were blocker-die-formed to an elliptical configuration. The assembly of these two partially machined forgings (Figure 4-1) created two elliptical butt joints having a major diameter of 33.75 inches and a minor diameter of 16.125 inches which produced the manifold portion of the part with a 0.875-inch inside diameter. The weld requirement was to fully penetrate in one pass the 0.165-inch-thick square edge of the weld joint without using internal tooling for puddle support. In addition, the weld-bead droptrough was not to exceed 0.050 inch and was to be reasonably smooth and consistent so as to not disturb the fluid flow in the manifold. Subsequent to welding, the manifold frame was artificially aged to the T652 condition. The aged welds (with up to two repairs) were to exceed a minimum tensile yield strength of 28,000 psi.

### 4.2 APPROACH AND CONSTRAINTS

Two welding approaches were considered. The first was manual welding and the second was N/C welding. The former method under the best conditions necessitated numerous weld starts and stops, increasing the probability of weld defects. Also, great operator skill was needed to maintain consistent weld penetration without exceeding the 0.050-inch droptrough requirement. N/C welding was selected for its ability to follow complex weld joints and provide weld puddle control on a reproducible basis.

---

\*Refer to Appendix B for details of manifold weld development.

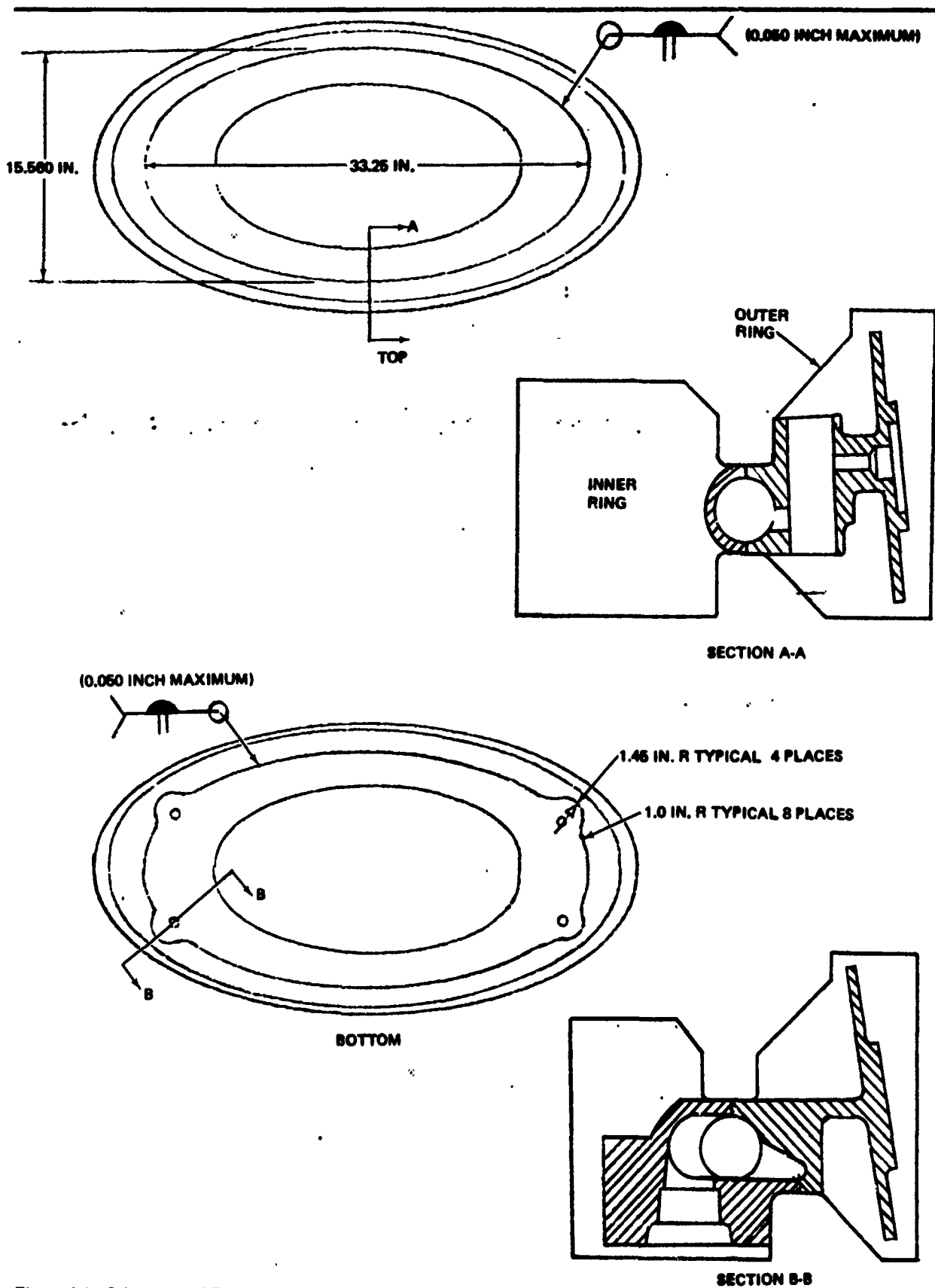


Figure 4-1. Schematic of Elliptical Manifold Frame

Preliminary welding parameters were developed on flat 2014-T4 aluminum sheet. Mechanical properties were then measured from these welded panels, which included original welds and double-repair welds, to determine if the minimum yield strength could be consistently maintained following artificial aging.

Three circular-shaped manifolds simulating the cross-sectional mass and weld length were made from 2014-T4 aluminum alloy plate and were assembled and welded to examine the performance of the N/C welding machine, weld torch accessibility, wire-guide rotational features, weld joint fit-up, weld fixturing, tape programming, and current pulsation.

The techniques thus developed were applied and optimized by welding to the flight configuration (and repairing where necessary) four elliptical manifolds machined from forgings. Dimensional and mechanical properties of the welds in these forged parts were measured and evaluated prior to committing the procedures to production.

#### 4.3 ELLIPTICAL FORGING

Aluminum alloy 2014, the alloy of highest strength and reasonable weldability, was selected as the material for making the EB elliptical manifold frames. Forgings were chosen over plate as the optimum product form for obtaining highest strength and ductility in all directions. The mandrel-forged, ring-type forging was assessed to be the most suitable and economical method for obtaining desired properties for the number of forgings required.

In the forging fabrication sequence, the ingots were heated to approximately 700°F and repeatedly hot-worked in all three directions by an upset process until the as-cast grain structure was broken down into one of uniform non-directional grains. The final upsetting terminated with the metal worked into the shape of a flattened biscuit. A hole was bored through the center of the biscuit (creating a ring-shaped forging) to permit insertion of a mandrel for the final hot-working into a ring configuration. Repeated hits were made against the mandrel-supported ring, causing an increase in ring diameter, a decrease in thickness, and a grain orientation parallel to the circumferential

direction. The forging at this point was wide enough to permit slicing to obtain a few individual frame forgings from each ring. These sliced rings were pulled diametrically to form the desired elliptical shape.

Of greatest importance was the need to minimize the amount of frame distortion during machining, as a very close tolerance fit of the opposing weld lands on the mating inner and outer frames was required. To achieve this condition, precautionary process controls were implemented to minimize residual stresses in the frame forgings prior to machining. The controls entailed holding the as-quenched forgings below 35° F (to prevent an increase in yield strength due to room-temperature age-hardening) until a compression stress relief could be applied to eliminate residual stresses induced by quenching. Then, an optimum mechanical stress relief was performed by simultaneously compressing the entire frame in its axial direction. These stress relief measures were effective, as no measurable distortion occurred during machining.

#### 4.4 PLATE AND ROUND RING WELDING

Straight-line GTA welds were made in flat panels, using the weld fixture shown in Figure 4-2. The fixture contained a cutout beneath the weld to simulate the manifold duct. The fixture was made of aluminum and was firmly clamped to the flat panel to simulate the heat-sink effect of the forgings upon the weld.

The GTA welding process was used for both the mechanized welding (direct current) and manual welding (alternating current) operations. Manual welding was being considered as a possible weld repair technique only. Mechanized weld parameters were developed to produce a single-pass, full-penetration weld with a smooth, shallow-weld droptrough shape. Several parameter combinations were evaluated, including varying mixtures of helium and argon. None of the gas mixtures effected a droptrough shape improvement. The weld parameters which produced the most consistent weld with the least practical amount of droptrough (0.034 to 0.040 inch) were used to weld three 24-inch-long panels. Additional 24-inch-long panels were welded to evaluate possible weld repair procedures by shaving the original weld flush and rewelding by mechanized or manual methods. Six to ten tensile coupons were excised from

THE SUPERIMPOSED CROSS-HATCHED AREA IS THE CROSS SECTION OF EB MANIFOLD FORGINGS AS MACHINED FOR THE WELD OPERATION. THE TEST PANEL IS SHOWN SHADED.

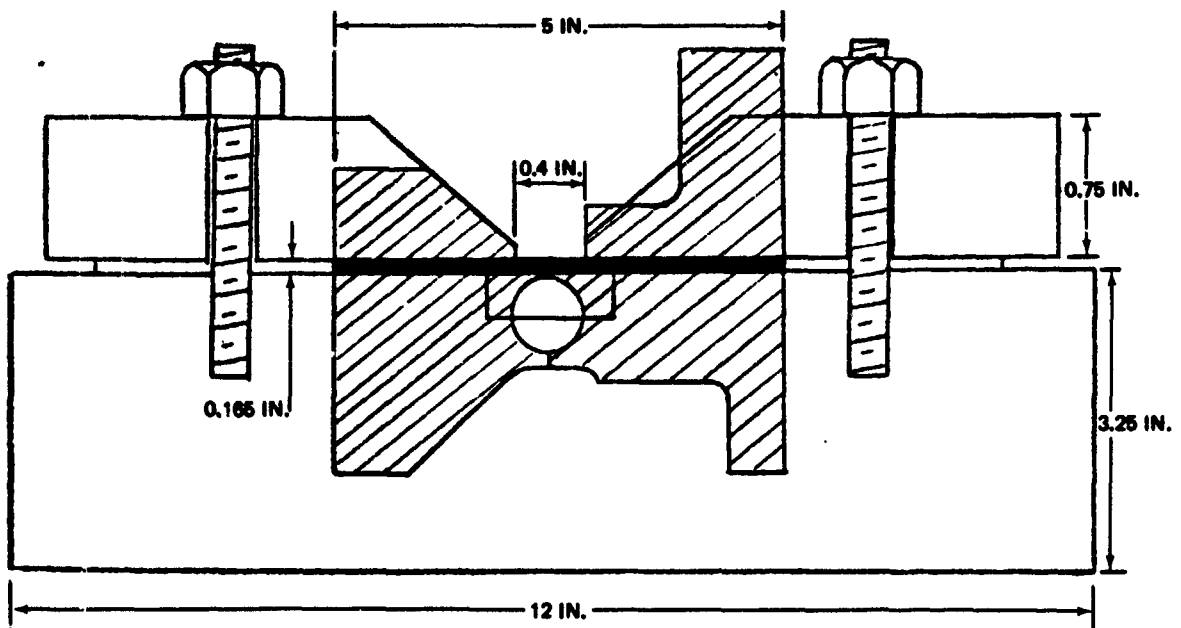


Figure 4-2. Weld Fixture—Test Panel Cross Section

each panel, aged to the T6 condition, and tensile tested. The results, shown in Table 4-1, demonstrated that the required yield strength (28 ksi) could be obtained consistently in mechanized welds with up to two mechanized repairs.

The use of pulsed-weld current was also investigated and was found to improve the consistency of weld bead shape.

To prove the capability of the newly modified N/C welder, the ability to rotate the wire guide and tungsten electrode while welding, develop weld overlap procedures, and optimize the preliminary weld parameters, three simulated circular manifold assemblies were machined from 2014-T451 plate stock. These test parts were designed with two 26.5-inch-diameter annular butt welds on opposite sides as shown in cross section in Figure 4-3. The length of the weld and mass of material were selected to simulate the conditions of the elliptical manifold.

Table 4-1  
TENSILE YIELD STRENGTH OF FLAT-PANEL WELDS\*

Welding Method	Weld Bead Shape	Tensile Yield Strength Range (ksi)
Mechanized	As-welded	40 - 44
Mechanized plus 1 mechanized repair	Shaved both sides	31 - 41
Mechanized plus 2 mechanized repairs	Shaved both sides	29 - 39
Mechanized plus 1 manual repair	Shaved both sides	27 - 36
Mechanized plus 2 manual repairs	Shaved both sides	28 - 33

\* Refer to Appendix B for detailed welding procedures.

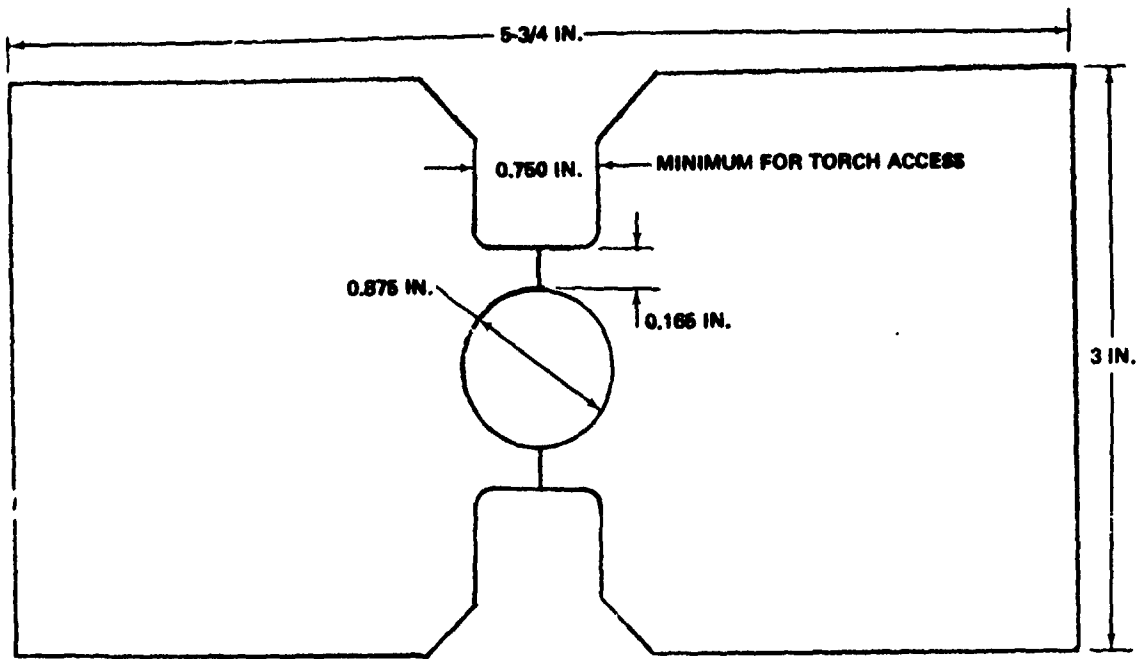


Figure 4-3. Circular Manifold Cross Section

Using the pulsation weld parameters developed on flat plate, the split circular manifold was welded in six segmented 40-deg increments. It was necessary to progressively increase the peak welding current to achieve 100-percent penetration due to the increased heat sink of the part (compared to clamped flat plates). Welding current was increased from 150 to 216 amp, arc voltage from 12.0 to 13.5 v, and wire-feed speed from 26.0 to 28.0 ipm, while the tangential travel speed remained constant at 10 ipm (50 percent of feed-rate override).

Weld overlap and tie-off parameters were developed on the same part by back-stepping in six segmented 40-deg increments. The first 20 deg of each increment was over the remaining unwelded joint followed by 20 deg of overlap. It was found that the best results were obtained by decreasing the travel speed by 10 percent in the 1.5-deg block just ahead of the weld start, increasing the arc voltage to 15.0 v in the first 3.0-deg block after overlap, and then reducing the peak welding current in four successive 3.0-deg blocks to a final value of 96 amp.

These procedures were then used to weld the other split circular manifold. During the weld the joint gap opened ahead of the arc, and in the last quadrant it spread to 0.025 inch. As a result, root-side fusion was lost. Otherwise, the weld was dimensionally satisfactory.

As a result of this condition, it was necessary to develop a technique for minimizing or eliminating the gap buildup during welding. Thus, a shrink-fitting method was devised. The remaining two circular test part details were machined with 0.003 to 0.005 inch of extra material left on the weld joint faces so that just prior to welding a dry-finish machine cut could be made, leaving the joint faces clean and ready to weld. In order to evaluate a shrink fit, these parts were left in their existing rough-machined and oversized condition and prepared for welding by lightly scraping the weld joint surfaces which removed 0.0005 inch per surface. This produced a 0.012- to 0.015-inch diametrical interference fit between the inner and outer rings, which was not considered sufficient to offset the gap observed on the previous part, but was expected to give some indication as to the value of this technique.

The outer ring was heated to 200°F, which caused a 0.060-inch increase in the inside diameter. The inner ring, which was at room temperature, was inserted into the outer ring and shimmed vertically to eliminate weld joint mismatch. When the assembly cooled to room temperature, there was metal-to-metal contact along the full length of the weld joints.

The full circular test manifold was then secured in the weld fixture. Both sides were N/C welded and no joint gap was observed. The weld bead crown was slightly convex and most satisfactory in appearance. Subsequent radiographic inspection revealed intermittent lack of penetration throughout the weld, which was attributed to the improved heat transfer due to the shrink fit. Thus, after shrink fit assembly of the last circular manifold, both joints were welded with the peak welding current increased to 234.6 amp. The crown of the weld bead was flush with the top surface of the joint. The welds were then x-rayed and found to be free of defects.

To correct the lack-of-penetration defects present in the first circular manifold, a repair technique was devised. A second hole was drilled in the manifold 180 deg from the first pressurization hole. 200 ml of methyl alcohol was poured in a beaker and aluminum welding flux was added until 400 ml of solution was obtained. The solution was poured into one of the holes and the part was rotated to coat the interior surface of the manifold. The remaining solution was poured out and then the part was dried by heating to 125°F. After shaving the defective weld beads flush, both sides were rewelded with the N/C tape having 234.6 amp of peak current. The weld ran smoothly except for some gaseous expulsion near the end of the weld on the top side. This situation was believed attributable to a heavy concentration of flux in the unfused mating surfaces of the joint. Otherwise the weld was found acceptable in subsequent radiographic inspection.

Following the radiographic inspection of each weld, the welds were inspected for surface defects using dye-penetrant. No surface defects were found in any of the welds. The two completed circular manifolds were finally inspected by a helium leak-detection method using a sensitivity of  $3 \times 10^{-9}$  scc/sec and no leaks were detected. The first full circular manifold was then cut into

sections to view the weld cross section and penetration. The weld cross section showed a consistent weld droptrough of 0.035 to 0.040 inch.

#### 4.5 ELLIPTICAL MANIFOLD WELDING

The developmental elliptical manifold was composed of inner and outer elliptical-shaped 2014-T452 aluminum roll ring forgings. When these two rings were assembled, an elliptical weld joint was created having a major diameter of 33.25 inches and a minor diameter of 15.57 inches as shown in Figure 4-1. On the opposite side, the elliptical weld path was interrupted (in the original design) to allow for the subsequent machining of four integral inlet ports. Views A-A and B-B show the cross sections of interest and the resultant cross section (shown cross-hatched) of the manifold after machining.

The weld fixture was a trunnion-type tool which was placed between the head- and tail-stock of the N/C welder. This fixturing approach permitted rotation of the entire assembly between welds by programming the A-axis 180 deg without removal of the manifold.

One of the major problems in setup and weld-joint tracking was that the welding torch was not manufactured with enough precision to allow it to be rotated through 400 deg without causing a tracking error. The error arose because the torch body was not exactly straight and the collet did not center the electrode in the torch; this caused the electrode to be located differently each time the electrode was replaced. The problem was solved by machining the torch and by shimming the torch-mounting bracket to center the electrode to the weld joint seam. The electrode eccentricity was reduced from 0.100 inch to 0.010 inch.

The preliminary N/C tape for the elliptical manifold configuration contained the same provisions for weld position, torch rotation, axis movement, and chord length deviations as for the circular manifold tape. In addition, the tungsten electrode index point was set on the centerline of the weld fixture, the weld start point was set 2 inches before the minor diameter, and the tangential travel speed was set at 10 ipm maximum.

The tape was proofed by tracking the joints as-photographed on a master Mylar-coated sheet-metal template, and several modifications were made to obtain satisfactory control of torch and wire motion.

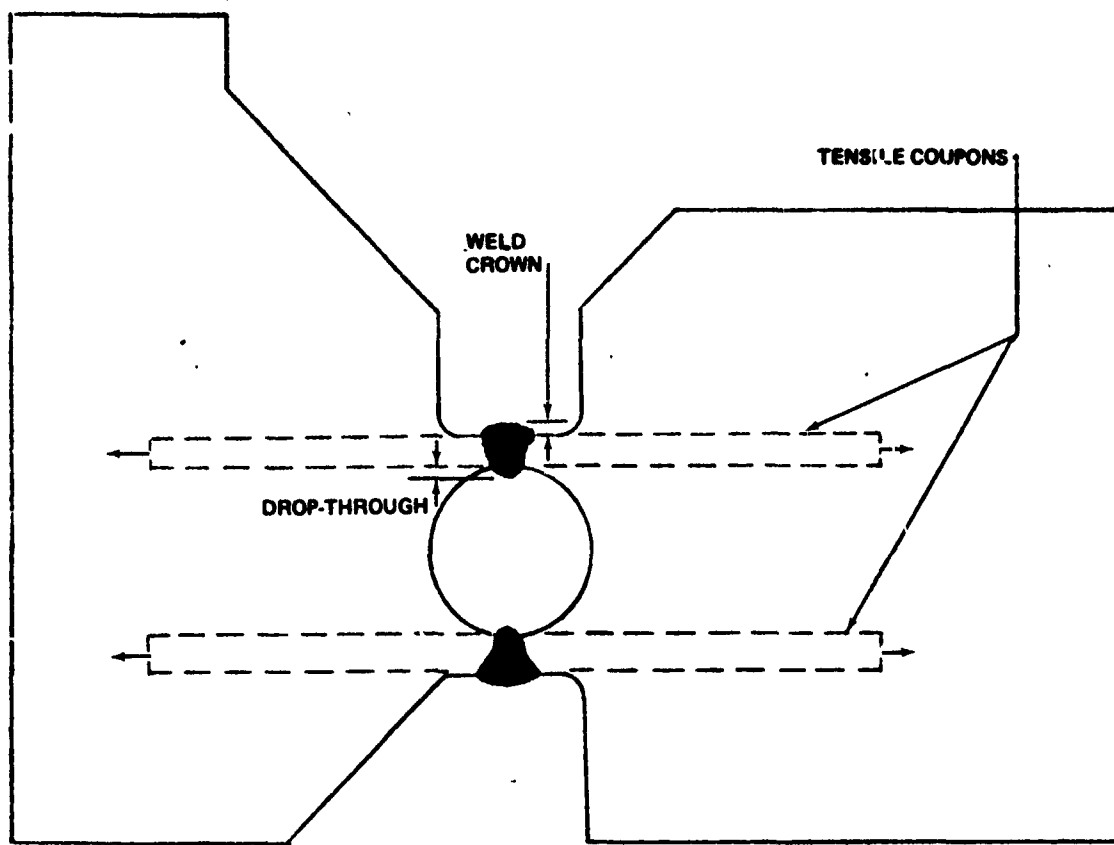
The manifold parts were N/C machined with an extra 0.005 inch of material left on the weld joint face in addition to the 0.005 inch per face required for the interference fit. The parts were brought to the final dimension by hand-filing them to a sheet-aluminum photo-template.

The weld joint preparation for welding began with degreasing and acid-etching the parts. The weld joint faces were then draw-filed and the upper and lower surfaces hand-scraped for a width of 1/4 inch. Having completed the preparation, each part was placed in a fabric-reinforced plastic bag which was evacuated and back-filled with dry nitrogen to minimize oxidation of the scraped surfaces.

Before beginning the assembly process, the outer ring was removed from its bag, four thermocouples were installed, and the outer ring was placed on hot plates for heating. The cleaned surfaces were visually inspected with white and black light and spot-scraped where necessary. The ring was then heated to 200° to 250°F, the inner ring inserted, and the joints matched. The assembly was air-cooled to room temperature.

Four manifold frames were used to determine the schedule of weld current, arc voltage, x- and y-axis travel speed, filler-wire feed rate and position, and interference-fit that produced full-penetration welds without defects or excessive droptrough. The final N/C tape required 29 wire-feed, two arc-voltage, eight welding-current, and over 400 travel-speed changes to successfully weld the two elliptical manifold weld joints.

Sections were cut from an elliptical test manifold where the weld was considered to be representative of an acceptable weld. Tensile coupons were excised from these sections, as shown in Figure 4-4, obtaining six coupons from the top weld and six from the bottom. The coupons were aged to the T6 condition and tensile tested. Tensile yield strength varied from 35 to 39 ksi, well above the required value of 28 ksi.



CROSS-SECTION OF UpSTAGE TEST MANIFOLD—FRAME P/N 1T38130  
 WELD CROWN AND DROP-THROUGH WERE LEFT AS-WELDED  
 (SMALL ARROWS SHOW LOADING DIRECTION)

Figure 4-4. Location of Tensile Coupons Excised from Forged Elliptical Manifold

Lack-of-penetration defects occurred in the bottom side weld of elliptical test parts 2 and 3 in the transition areas entering and exiting the ports. As the aluminum-welding-flux repair method produced good results on the circular test part, it was decided to repair these two elliptical parts, with some refinements in the procedure. The inside of the manifold was coated with the flux-and-alcohol mixture and the excess was drained. The manifold was then placed in a vacuum chamber which was evacuated to  $5 \times 10^{-4}$  torr. This ensured the complete evaporation of the alcohol that was suspected of causing weld expulsion on the circular part. The surface of the original weld was machined flush and hand-scraped in preparation for the repair weld. After welding, the flux was removed by flowing 180°F deionized water through the manifold to remove all traces of the flux. Dry nitrogen was then blown through the manifold to remove the remaining water and the part was again placed in the vacuum chamber and evacuated to complete the drying process.

After several production manifolds of the original design were welded, the manifold was redesigned to eliminate the discontinuities in the aft side weld path. This changed the aft side weld path to an uninterrupted ellipse like the forward side and significantly reduced the incidence of weld concavity and lack-of-penetration defects in the aft side weld.

As welding progressed on the redesigned manifolds, a lack-of-penetration problem developed in the weld-start/overlap area on both the forward and aft sides. To ensure complete penetration, the weld-start and overlap-weld parameters were modified and verified on short, straight sections that exactly duplicated the mass and cross section of the elliptical manifold. The weld-start travel speed was slowed for the first 1-1/2 inch of the weld, the current downslope was delayed for another inch after weld overlap, the overlap weld-travel speed was reduced, and the peak welding current was increased from 210.0 to 215.4 amp. It was found that the welding flux could be eliminated during these repairs, and a fully satisfactory weld was still obtained.

#### 4.6 NONDESTRUCTIVE INSPECTION

Evaluation of the welded-aluminum manifold showed that fit variations between the two mating sections were causing lack-of-penetration defects or

areas of excessive bead droptthrough. It was necessary to apply effective nondestructive inspection techniques to assess the weldment condition prior to further processing. Two techniques were employed.

#### 4.6.1 Film Radiography

The first technique employed was x-ray film radiography, an accepted inspection tool, particularly for weldments. However, if the geometry of the part becomes complex, the interpretation of the film becomes increasingly difficult. Meaningful radiographs of the manifold weldments were very difficult to obtain.

The geometry of the manifold made it difficult to produce radiographs without superimposing the images of the weldments on each other (see Figures 4-1 and 4-4).

X-ray exposure of the part at an angle sufficient to separate the weldment images clarified the individual weldment images in local areas. However, in most areas, other portions of the manifold forging blocked the view.

Weldment porosity was readily detected, as were gross lack-of-penetration defects and large cracks. However, there was no way of determining the extent of weld penetration or excessive droptthrough. It was necessary to use another inspection technique to assess the weld penetration.

#### 4.6.2 Weld Thickness and Droptthrough

The primary goal of the second inspection technique was to determine whether a full-penetration weldment existed completely about the circumference of the manifold assembly. It was impossible to examine the root (droptthrough) of the weldment because it was inside a closed passageway. Therefore, a method was needed to assess the total weld thickness from one surface only.

The technique selected for development utilized a digital thickness gage. The instrument was designed to measure metallic material thicknesses from one surface only. The results were displayed digitally on the face of the instrument. The unit operated at 5 MHz with a 1/4-inch-diameter transducer.

This method was very successful in measuring the total thickness of the weldment when the thickness of the mating parts was known initially. The height of the weld bead could be determined by mechanical measurement. The thickness measured by the instrument minus the sum of the previous two figures resulted in a figure representing the extent of the droptrough.

Areas where no signal was received indicated the presence of insufficient penetration or a defect which prevented transmission or reflection of the ultrasonic wave front. The transducer was small in diameter and operated effectively on the weld crown without degradation of the ultrasonic signal. This approach to weldment inspection was quite successful, and together with film radiography, provided adequate means of ensuring the integrity and reliability of the manifold welds.

#### 4.7 MACHINING CRACK PROBLEM

Metallurgical investigation concluded that failure of the EB manifold during proof-pressure test was caused by cracks in the manifold wall (not near the welds) that existed prior to the proof-pressure-testing operation. The cracking was caused by a tensile overload applied during removal of excess material required for a heat sink during welding. The overload resulted from excess inner ring material not being supported during the second pass of the removal cut (see Figure 4-5).

The cracking problem was eliminated by adding jacks to the mill fixture used for holding the manifold during the N/C machining operation. The jacks supported the excess heat-sink material while it was being parted from the manifold inner ring. Extensive nondestructive inspection of subsequent manifolds verified the success of this method in preventing cracking.

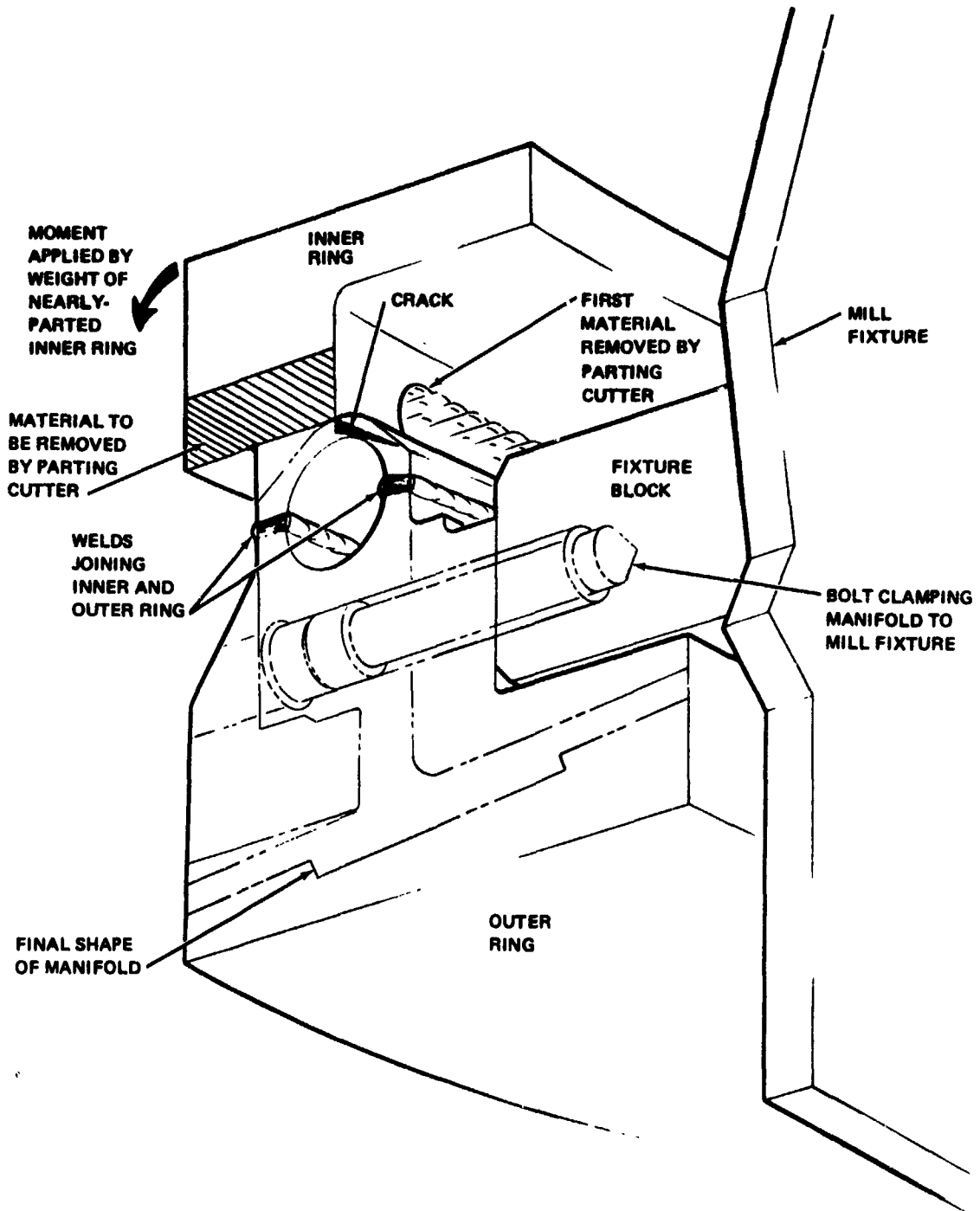


Figure 4-5. Crack Formation During Manifold Machining (U)

#### 4.8 PROBLEMS AND SOLUTIONS

Major problems and solutions encountered in processing the fuel manifold are summarized below:

Problem	Solution
A large weld-joint gap occurred during the welding of slip fit manifold test parts causing loss of weld control.	Manifold parts were machined with a 0.020-inch diametrical interference and assembled using a shrink fit.
Weld-joint tracking error occurred due to lack of concentricity of the welding torch as the weld head rotated.	Weld torch parts were modified to accurately center the tungsten electrode to the torch barrel.
Lack of weld penetration occurred in the weld overlap and tie-off area on both sides of the manifold.	The welding parameters on the N/C tape were revised in the weld overlap area. A straight-section duplication of the manifold was welded before each full elliptical manifold weld to verify the parameters and machine performance.
A nondestructive technique was required to determine depth of penetration of aluminum manifold weldments.	The digital thickness gage was effective in determining weldment thickness, thereby providing information as to complete or less-than-complete penetration.
Cracking occurred during final machining.	Machining fixtures and tools were modified to avoid forces which could cause cracking.

#### 4.9 CONCLUSIONS AND RECOMMENDATIONS

1. An uninterrupted, single-pass, free-fall butt-weld procedure was satisfactorily developed for welding the fuel manifold frame using the eight-axis N/C welding machine.
2. Through the use of low-frequency (10 Hz) weld current pulsation, excellent weld puddle control of free-fall weldments in 2014-T4 aluminum was demonstrated with the GTA welding process. In addition, this technique is believed to have contributed to the absence of oxide stringers prevalent in steady-state GTA welds in 2014 aluminum.

3. The ability to rotate the filler wire about the tungsten electrode during welding was adequately displayed in this program. It was further shown that the entry angle for the wire may vary up to 30 deg on each side of the centerline of the joint without any difficulty.
4. Numerous changes in weld heat input were required during the weld to adjust for changing heat sinks created by design of the manifold. These changes were effectively made by adjustments in the tangential travel speed and filler wire volumetric rate of addition. This condition was necessary because absolute changes in the welding current during pulsation must exceed 40 amp for the machine command unit of the N/C welding machine to be responsive.
5. To achieve weld uniformity, adjust for varying heat sinks, and provide consistency and quality in the weld overlap area, over 400 in-process changes were required in weld travel speed, filler wire feed speed, arc voltage, and welding current to weld the two sides of the manifold.
6. The interference fit of the assembly eliminated the weld-joint gap buildup during welding and is believed to have contributed to the absence of oxide stringer defects in the weld.
7. The design requirement of a minimum tensile yield strength of 28,000 psi was obtained with an average yield strength of the forging welds exceeding the minimum by more than 30 percent.
8. A combination of film radiography and ultrasonic thickness measurements was required to verify proper weld soundness and droptrough.

## Section 5 ELECTRONICS PROCESSING

### 5.1 REQUIREMENTS

Special electronic manufacturing processes were developed to meet the design requirements for four assemblies using thick-film circuit bases: the electrical power and sequencing unit (EPSU), the guidance control unit (GCU), the control electronics unit (CEU), and the signal conditioner. The performance, volume, and weight requirements which led to the design configurations selected for the units are documented in Reference 5-1 and are therefore not discussed in this report. However, technical requirements imposed by the design upon the processes and resultant materials are summarized herein.

Automated drafting processes were required to produce artwork equivalent in quality to artwork obtained by conventional 20-times photoreduction. In addition, the time and cost required to produce the artwork had to be competitive with conventional methods.

Thick-film multilayer circuit requirements included maximum conductor resistance of 0.004 ohm per square\* for gold, 0.1 ohm per square for platinum-gold (top layer conductors), and 0.01 ohm per square for solder-coated platinum gold; and a  $\pm 5$  percent tolerance on the width of conductors. Up to five conductor layers were required for the design configuration. Circuit bases were required to be as large as possible, up to a limit of 4 by 6 inches (imposed by space limitations in the GCU), in order to achieve maximum packaging density and to minimize interconnections between circuit bases

---

\*Resistance of conductor films is expressed as ohms per square, where a square is a film of the fired conductor ink of equal length and width. (A conductor film 1 inch wide and 1 inch long has the same resistance as a conductor film 1 foot wide and 1 foot long made of the same material and thickness.)

and boards. In addition, the thickness of the alumina substrate was limited to 0.025 inch to meet stack height requirements in the GCU and CEU.

When the initial series of thick-film multilayer circuit bases was made, it became apparent that interlayer capacitance between some of the signal leads and ground would exceed the rated load capacity of some integrated circuits (IC's). Therefore, the interlayer capacitance had to be reduced to permit proper functioning of the critical IC's in the assembly.

Thick-film chip resistors were required with ink resistivities of 0.1, 0.3, 3, 10, 30, 100, and 300 kilohms per square. Tolerances on the trimmed resistance value were 1 percent and 0.1 percent, depending upon function. To provide face-up mounting with reliable and inspectable solder joints, solderable conductor ink was required around the edges of the chip.

A process for adhesive-bonding flatpack IC's and heat sinks to thick-film bases was required to produce bondlines having 0.003-inch maximum thickness to enhance thermal conductance. High adhesion was required between heat sinks and thick-film bases; only moderate adhesion was required between flatpacks and thick-film bases to facilitate flatpack removal and replacement. In addition, the adhesive bond was required to retain its strength and conductivity after exposure to reflow soldering and normal test and flight thermal cycling. The number of voids in the adhesive had to be minimized to ensure adequate thermal and mechanical bonding.

Requirements for assembly of electronic packages were primarily mechanical and dimensional in nature and were set by the design drawings. The extreme static charge and thermal sensitivity of many of the IC's used in the designs was anticipated. Soldering attachment of metal-oxide semiconductor (MOS) devices required reduced heat inputs to prevent damage. Handling of IC's had to be minimized and closely controlled to prevent static discharge damage. Quantitative requirements for grounding were not established; however, it was expected that adequate grounding would be easily obtained with existing MDAC procedures.

## 5.2 APPROACH AND CONSTRAINTS

Multilayer circuit requirements allowed the use of processes, equipment, and materials which had been used previously at MDAC to make small, single-layer production circuits and 2- by 2-inch multilayer experimental circuits. The development approach taken was to obtain samples of 4- by 6-inch alumina substrates, prepare circuit artwork, and determine what screening pressure, tension, and emulsion would produce visually acceptable circuitry. Electrical and dimensional evaluations were then conducted to determine the functional acceptability of the circuit bases. As a result of these evaluations, the design and processes were modified to achieve acceptable capacitance, flatness, and electrical/structural integrity and producibility. Notably, the design of some circuits was changed to place the ground plane on the back side of the alumina substrate. This approach avoided the warpage due to thick dielectric layers on one side of the circuit base; however, it required the development of a method for producing reliable through-hole conductors.

To meet the solderability and resistivity requirements for chip resistors, conductor and resistor ink choices were limited. The resistor ink had to withstand subsequent conductor ink firing cycles, and the conductor ink had to possess good solderability. Fortunately, prior to the UpSTAGE program, one ink of each type (ESL 3800 resistor ink and ESL 5800E conductor ink) had been characterized and successfully used at MDAC. These inks were selected for chip resistor fabrication. Substrate material, ink screening, dipping and firing, and trimming techniques were adaptations of conventional thick-film technology.

The only feasible approach for applying adhesive to thick-film bases in a controlled thickness of 0.003-inch maximum was determined to be screen printing. This method was herefore selected for development. High adhesion was obtained by priming surfaces prior to bonding; low adhesion was obtained by eliminating the primer. Heat resistance was verified by testing adhesion strength samples previously exposed to temperatures of 212° and 500°F and by functional testing of prototype and flight assemblies. (See Reference 5-1 for details.) Void content was reduced by examining full-scale primed and

unprimed bonds and then making minor modifications to the bonding process. Acceptable thermal contact area was then verified by functional testing of assemblies.

The approach taken to prevent static charge damage to IC's was to minimize formation of charge wherever possible. Where this was not possible, as in the case of foam encapsulation, the charge was removed by an ionized airstream.

### 5.3 THICK-FILM MULTILAYER ARTWORK PREPARATION

The size and complexity of the circuits precluded the conventional methods of making artwork. Usually thick-film layouts are prepared 20 times actual size and photoreduced for use. The 20-times-scale layout drawings for the 4- by 6-inch substrates would be unwieldy to handle and too large for the equipment available for photoreduction. The solution was to use 2-1/2-times-scale computer-generated artwork prepared from engineering layouts of the design configuration.

#### 5.3.1 Equipment and Facilities

Digitizing was done on a Tridea Digitizer which used a closed-circuit TV system and joy-stick control to establish the coordinates of each point on the engineering sketches. The grid table was 5 by 20 ft, and the image of any point on the table was magnified to 50 diameters for accuracy in location. The positions of points on the table were punched on a tape to specify position within 0.0001 inch. Machine commands were entered onto the tape by a typewriter keyboard. The digitizer-generated tape was then processed in an IBM 360-85 computer to include such things as line straightening, component pad patterns, and interconnection (via) positions.

The complete edited tape was then drawn out at 2-1/2 times scale on a Universal drafting machine (UDM)\*. This machine drew the line to within

---

\* The UDM is manufactured by Universal Drafting Machines, Inc., a subsidiary of Eugene Dietzgen Co.; it has a 5- by 20-ft bed, a PDP-8 computer controller, and a Potter computer-grade magnetic-tape reader.

0.001 inch of the position specified on the tape. Line widths produced with an MDAC-developed pen system were uniform to within 0.005 inch.

### 5.3.2 Sequence of Operations

The method developed for making drawings is shown in Figure 5-1. The steps included were:

- A. Sketches were laid out at 5 times scale to specify component positions and types (see Figure 5-2a).
- B. The corner points of the components and types were digitized.
- C. The digitizer-made tape was put into the computer, which generated a drawing tape to outline all mounting pads needed and their positions.
- D. The drawing tape was put in the UDM, which drew the mounting pads over the engineering sketch (see Figure 5-2b).
- E. Lines were drawn manually on this artwork to interconnect the devices.
- F. The circuit runs were then digitized for each layer.
- G. These tapes were put into the computer, which added drawing commands and extracted information to build the via artwork.
- H. Each tape was put in the drafting machine and drawn at 5 times scale for check and edit.
- I. Circuit changes and error markups were made on these drawings and the tapes corrected.
- J. Corrected tapes were then used to draw production artwork for each layer at 2-1/2 times scale size.
- K. The artwork was then photoreduced to final size for production use.

### 5.3.3 Digitizing

Digitizing was done in two steps: first, the component mounting pad locations were digitized from a layout sketch. The drawing made from this tape was then used to sketch the interconnections. After the interconnections were sketched, the digitizer was used to prepare a tape of the interconnection circuitry.

A component layout sketch and computer-generated pad master drawing are shown in Figure 5-2. The numbers refer to the type of component to be located at that position. Each type of component mounting pattern was drawn

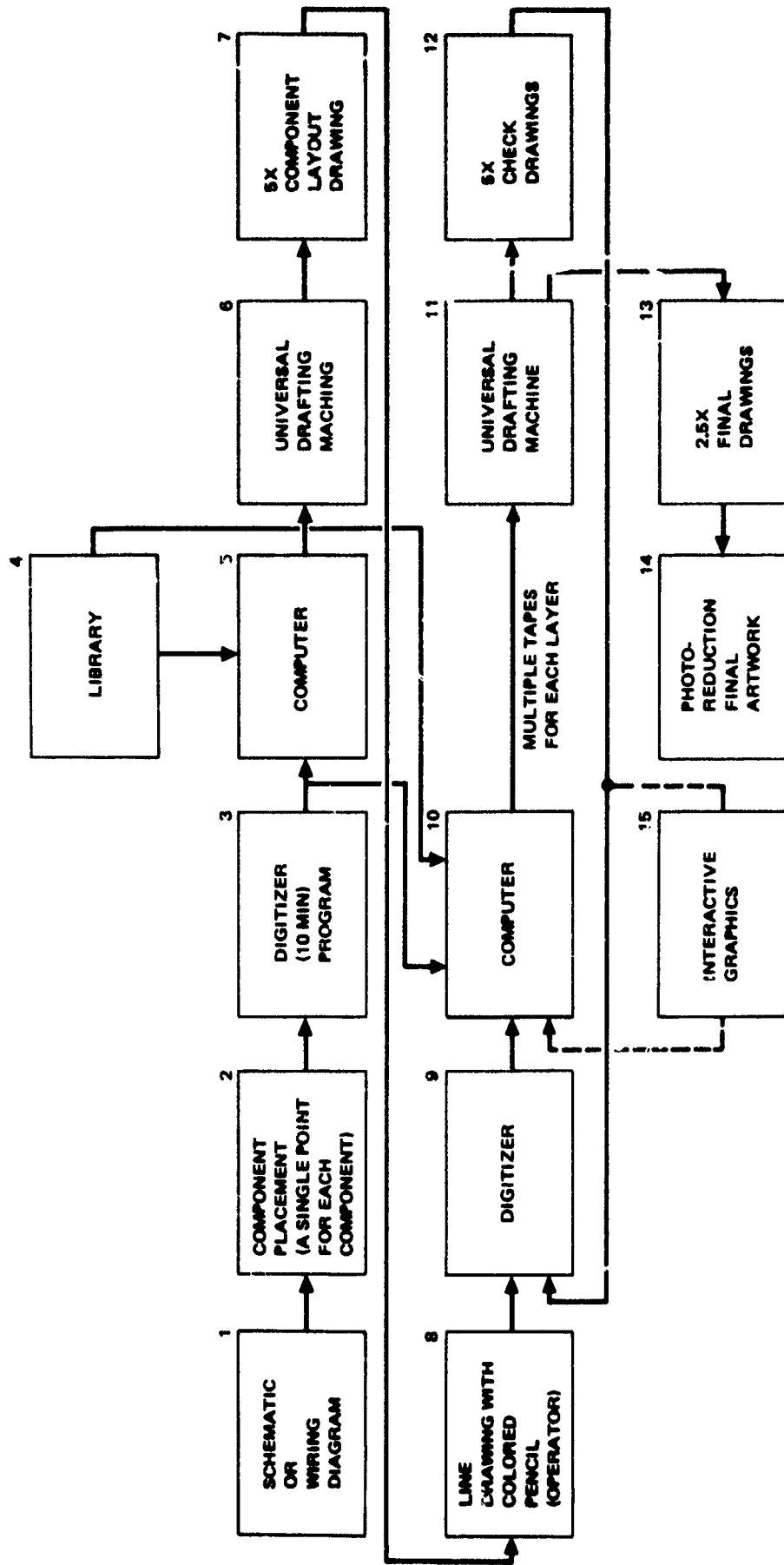


Figure 5-1. Block Diagram of Automated Artwork Generation



and checked for accuracy at 10 times scale. The pattern was then given a number and stored in a computer library for use by the digitizer. Table 5-1 lists several of the commonly used patterns.

Digitizing the interconnections was done by layers. Each layer was color-coded as shown in Table 5-2. The beginning and end points of the line were entered on the tape. The computer then added the PEN-DOWN and PEN-UP commands at the ends of each line. Information needed to draw via (vertical) connections was indicated on the layout drawing by symbols (see Table 5-2).

Table 5-1  
LIBRARY OF INTERCONNECT PAD PATTERNS

Keyboard Entry	Pad Configuration
SE F001	Two rows of 5 flatpack pads (30 x 120 mils with 20 mils spacing between pads) and 300 mils between rows.
SE F002	Two rows of 7 flatpack pads and 300 mils between rows.
SE F003	Two rows of 8 flatpack pads and 300 mils between rows.
SE F004	Two rows of 12 flatpack pads and 300 miles between rows.
SE F005	Two rows of 7 flatpack pads and 500 mils between rows.
SE F006	A single 80 x 80 mil pad.
SE F007	A single 80 x 160 mil pad with a 90 x 30 mil slot in center of pad.
SE F008	An "F" identification letter and two alignment "L's".
SE F009	A 30 x 40 mil via pad in the center of a single flatpack pad and referenced to the lower left-hand corner of this pad.
SE F010	A single 20 x 80 mil via with the 80 mil in the y-axis.

Table 5-2  
TAPE FUNCTIONS

Tape	Drawing Symbol	Function
A	---	Ground plane
B	---	Conductors in power plane
C	(green lines)	Third conductor layer conductors
D	(blue lines)	Fourth conductor layer conductors
E	(red lines)	Fifth conductor layer conductors
F	1 - 5	Flatpack pads (FPP)
G	G	All ground vias
H	9	All power vias
J	⊗	All vias under FPP originating from third conductor layer
K	⊗	All vias under FPP originating from fourth conductor layer
L	△	All 20-mil vias between conductor layers 3 and 4
M	⊗	All 20-mil vias between conductor layers 3 and 5
N	⊗	All 20-mil vias between conductor layers 4 and 5
P	8	Identification and alignment pads
R	---	Dielectric border line
S	11	Ground plane pads
T	---	Dielectric pads under flatpacks
U	6, 7	Terminal pads
W	---	Ground plane identification and alignment pads

#### 5.3.4 Tape Assembly and Editing

To allow for artwork changes, a plan was developed to make separate tapes for different functions and assemble the layer from these tapes at the UDM. Table 5-3 shows the separate tapes required for a typical multilayer circuit. The tapes are identified by letter in Table 5-2.

The assembly method included planned cases of redundancy in artwork. Figure 5-3 shows the fourth conductor artwork with the tapes used to generate it. For example, Figure 5-4 shows a via connecting a conductor on layer 2 to another conductor on layer 5. Layers 2C, 2D, 3C, 3D, 4C, 4D, and 5C contain this via tape (the suffixes C and D represent conductor and dielectric, respectively). This single tape was used seven times to ensure registration. Figures 5-4b and 5-4c show that a misplaced via was easily detected by using redundant vias.

Modifying tapes was accomplished in different ways depending on the complexity of the changes. Small changes to short tapes were usually done on the Flexowriter. Large tapes were edited with the Friden digitizer edit program. With the digitizer, the area to be corrected was redigitized on a small tape, checked, and duplicated on the tail end of the original tape. The original tape was then duplicated, omitting the changed or incorrect area. This was done on the Friden edit program by typing in a line number which duplicated the tape up to this line, then deleting by typing in keyboard character (sign) on its teletype (or typing in replacement information). This procedure was continued until all errors were corrected.

Editing with the Sigma 5 interactive graphics system was tried and found to be useful only for deleting lines. There was no reference framework to allow lines to be added.

#### 5.3.5 Automatic Drafting

The complete, corrected tape was used in the UDM to draw the artwork at 2-1/2 times scale size. At the outset, the artwork quality was poor because of poor pen control. The pen would either hit the table too hard and splash or stop too soon, not writing the line. A mechanism (Figure 5-5) was made

Table 5-3  
 TAPE COMBINATIONS REQUIRED FOR A TYPICAL MULTILAYER CIRCUIT

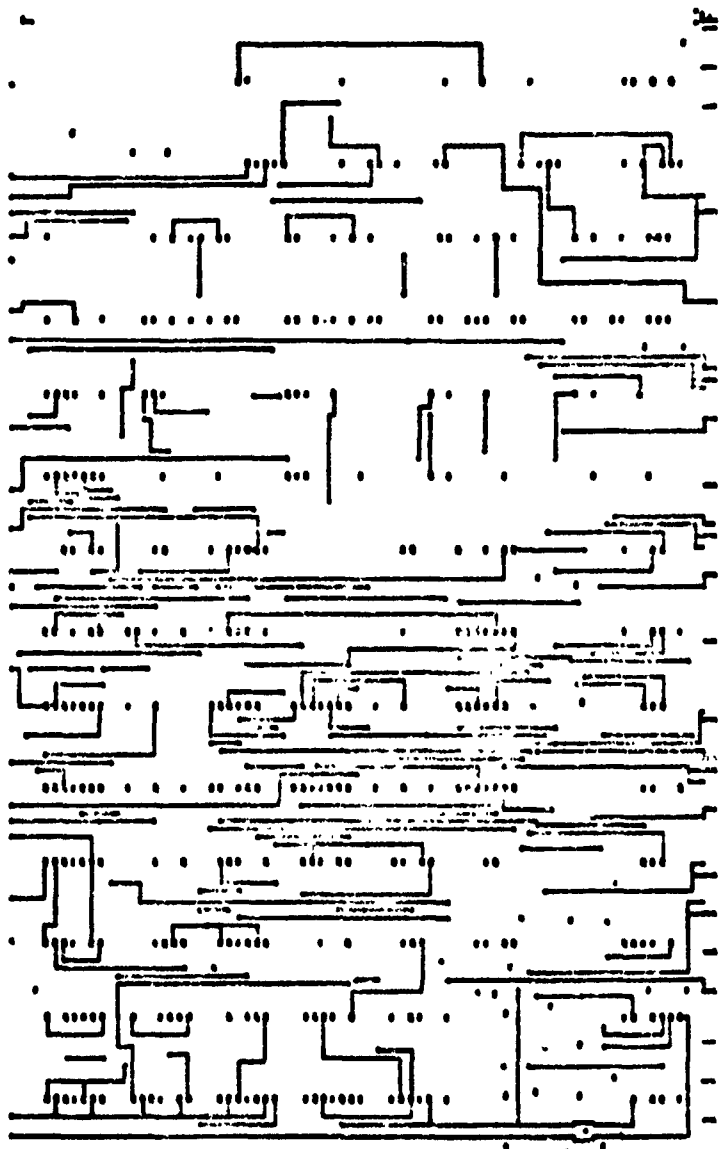
Layer	Tape	A	B	C	D	E	F	G	H	J	K	L	M	N	P	R	S	T	U	W
1	** X																			**
1D						X									X	X				** X
2		X				X	X								X	X				
2D						X	X								X	X				
3			X			X	X	X				X	X		X	X				
3D						X	X	X	X			X	X		X	X				
4				X		X	X	X	X	X	X	X	X	X	X	X				
4D					X	X	X	X	X	X	X	X	X	X	X	X				
5						X	X	X	X	X	X	X	X	X	X	X			X	
5D						X	X	X	X	X	X	X	X	X	X	X		X		
-1	*	X																		* X
-1D															X	X				X X

\* For substrates with ground plane on negative side of substrate.

\*\* For substrates with ground plane on positive side of substrate.

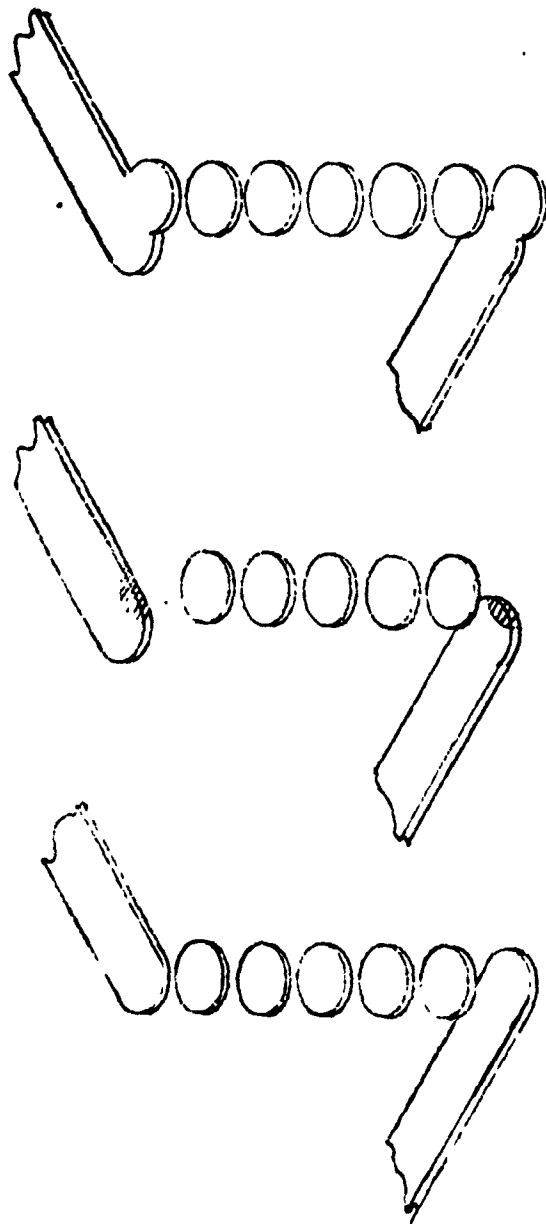
\*\*\* Each of Tapes L, M, and N must have a Q3 identification symbol at its front end.

L699101	
0ZΣJYFIU 0ZΣJYFIU	0 0



035

Figure 5-3. Completed Artwork Composed of Tapes Listed at Right



(a) CORRECT

(b) 0.015-IN. ERROR  
WITHOUT REDUNDANT VIA

(c) 0.015-IN. ERROR  
WITH REDUNDANT VIA

Figure 5-4. Expanded View of Interconnection and Misregistration of Layers 2 to 5

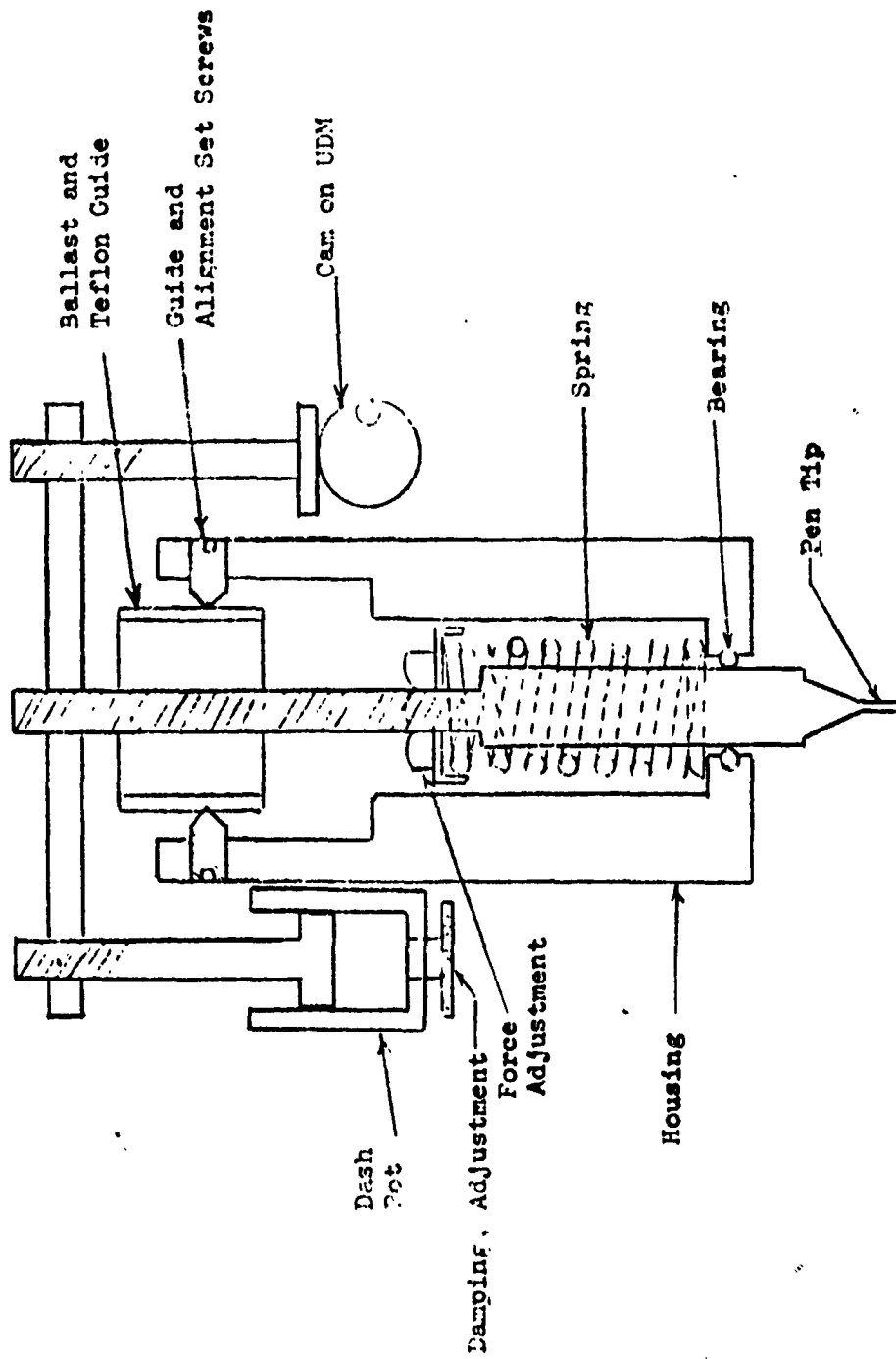


Figure 5-5. Schematic Diagram of Universal Drafting Machine Pen Mechanism

to improve the control of pen movement. To prevent ink splatter and damage to the pen tip, an air dash pot was used and set to a slightly overdamped condition.

#### 5.3.6 Artwork Evaluation

Initial attempts to manually check a 5-times-scale drawing of a five-layer circuit revealed that the check process would take at least 5 weeks. Accordingly, it was necessary to rely upon digitizing and mechanized drafting for accuracy. Of all the multilayer circuits fabricated, only one piece of artwork had to be corrected. In that case, the operator removed the tape from the UDM before the drafting of the last via point was completed.

### 5.4 THICK-FILM MULTILAYER BASE FABRICATION

The materials and most of the methods used for thick-film multilayer fabrication were previously used at MDAC; only the substrate size and complexity were unusual. The substrates were made of 96-percent alumina ceramic with holes prepunched for electrical interconnections. Commercially available gold and platinum-gold conductor inks and crystallizing dielectric inks were used.

The multilayer circuits were made by alternately screen-printing conductors and dielectric ink into substrates and firing them at 930°C. Controlled heating and cooling rates were used to obtain optimum physical properties of the finished part (Reference 5-2). Figure 5-6 shows a typical multilayer circuit base.

Limiting the capacitance between signal conductors and the ground plane necessitated double- and triple-dielectric printing, printing on both sides of the substrates, and providing interconnections through the substrates.

#### 5.4.1 Alumina Substrate Preparation

Some of the 4- by 6-inch substrates were received with so much warp that they could not be held firmly on the vacuum bed of the screen printer and could not be printed with uniform line thicknesses. A process was developed for flattening the substrates, in which twelve substrates were stacked on a

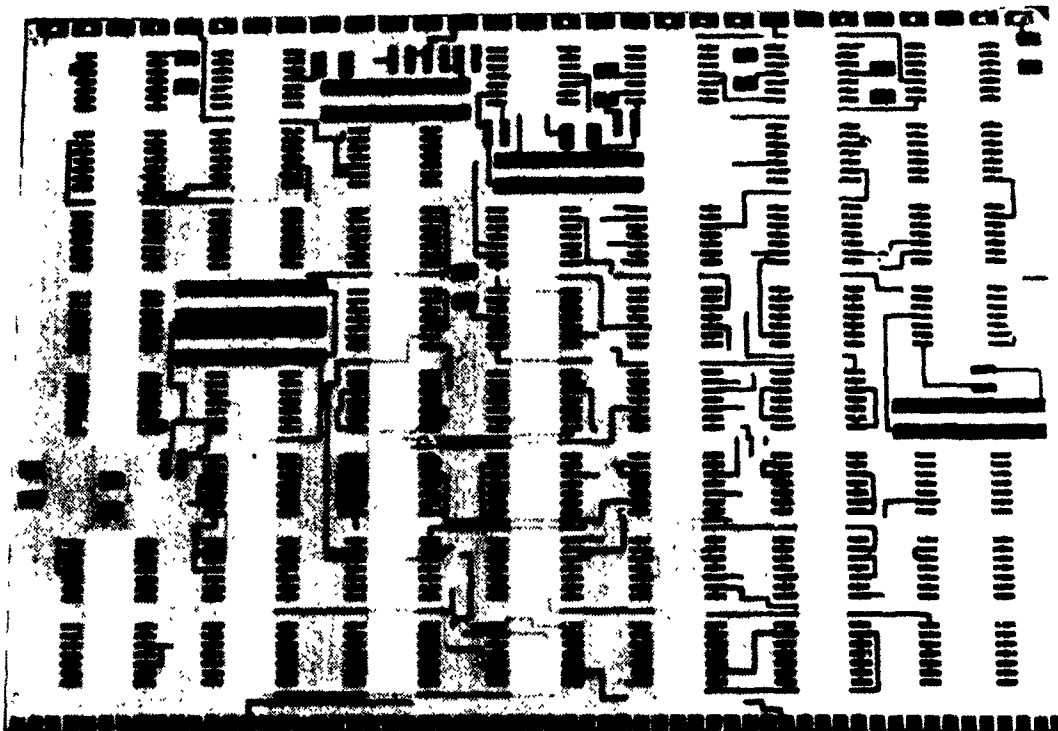


Figure 5-6. Large Thick-Film Multilayer, 4 Inches x 6 Inches x 0.025 Inch, Consisting of a Ground Plane on the Back Side, Feed-Through Holes in the Substrate, a Power Layer, and Three Signal Layers on the Front Side

1-inch-thick, flat alumina block, and a 6-lb weight was placed on top of them. The weighted stack was placed in a clean kiln, heated to 1,400°C, and cooled to room temperature. A 3-day flattening cycle was used, to allow slow cooling so that thermal stresses would be minimized. The resulting substrates were significantly flatter and less prone to distortion during subsequent firing cycles.

#### 5.4.2 Dielectric Ink Evaluation

Two dielectric inks (ESL 4608 and ESL 4610) were evaluated. The 4608 and 4610 materials have dielectric constants near 8 and 10, respectively. All other properties were reported to be the same. However, it was easier to solder conductors printed on 4610 than on 4608, whereas the thermal coefficient of expansion of 4608 was more closely matched to those of the conductor inks and substrate used on this program than 4610. On the basis of strength and appearance of the conductor/dielectric interface, the 4608 material was chosen over the 4610.

Applying dielectric as thick as 0.010 inch on a 0.025-inch-thick substrate, in order to reduce capacitance, caused the substrate to bend due to thermal expansion mismatch. Batch-to-batch variations in thermal expansion were also found. To control warpage of the final product, dielectric inks were tested and selected for use as follows. Ink lots which produced less than 0.050-inch deflection in the 6-inch substrate dimension were considered acceptable for making five-layer circuit bases. Inks causing greater bowing were used for one- and two-layer circuit bases. (Bowing of up to 0.125 inch in the 6-inch dimension was observed on occasion.) Dielectric inks were used as supplied by the manufacturer, and required no mixing or preparation at MDAC.

#### 5.4.3 Screen Printing

Two major problems were encountered in screen printing: (1) printing bases almost as large as the screen, and (2) producing pinhole-free multilayer bases. Many of the techniques of multilayer construction were developed previously on the MDAC Independent Research and Development Program. Experimental yields were roughly in the range of 60 percent for a 2- by 2-inch substrate with three layers. Initially the yield of good parts dropped

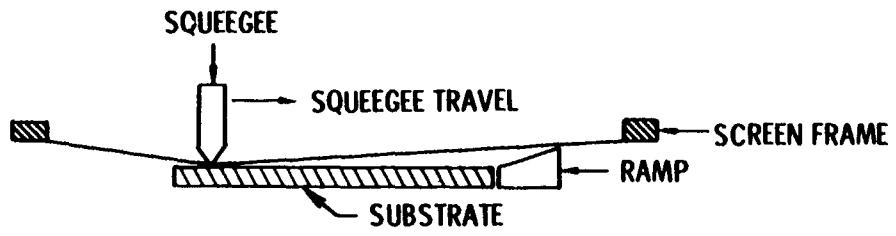
considerably when the area of the substrate was increased to 4 by 6 inches, but through refinement of procedural controls, a yield of 95 percent was achieved in production.

With 4- by 6-inch substrates and an 8- by 10-inch screen, nonuniform screen printing across the substrate was observed. When the screen was adjusted to give good prints in the center, the edges would not print properly. When the edges were optimized, the center of the pattern was spread out. When the printing parameters were optimized to yield a uniformly good print from edge to center, a rough surface texture containing sharp peaks resulted. These peaks caused the formation of pinhole shorts during subsequent firing operations.

Substrate-to-screen distance settings from 0.050 inch to zero (contact print) were unsuccessful in preventing poor printing. Analysis of the manner of operation of the screener indicated that high screen tension was necessary to provide a clean screen breakaway. This was provided by adding a silicone rubber ramp adjacent to the substrate. Figure 5-7 depicts the ramp in operation. When the ramp was used, pinhole-free dielectric layers were obtained.

Shorted conductors were caused by printing conductors on top of the dielectric with poor screening and by printing conductors on top of lint particles. Figure 5-8 shows a section of conductor removed from a substrate with a pinhole short. Much of this type of shorting was eliminated with the introduction of the ramp. Lint, the other major cause of pinholes, was eliminated by screening in a dust-controlled area and substituting polyurethane sponge wipers for cotton ones. Figure 5-9 shows a conductor with this type of short.

Random pinholes due to material inhomogeneity were eliminated by screening two layers of dielectric between each layer of conductor. The order of printing and firing was found to be important, and is discussed in Subsection 5.4.4. The total print thickness was closely controlled to minimize warpage at the thick extreme and interlayer capacitance at the thin extreme.



A. INITIAL PHASE OF PRINTING CYCLE

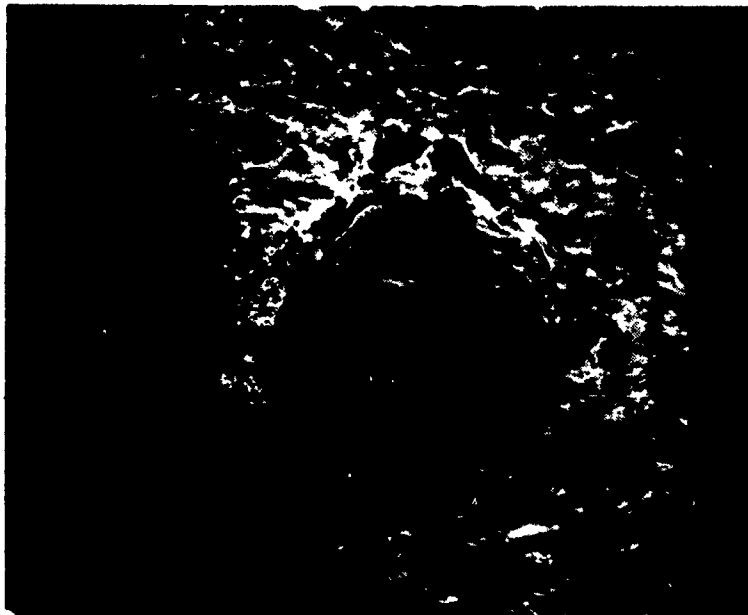


B. END OF PRINTING CYCLE SHOWING RAMP INTERACTION INCREASING SCREEN TENSION

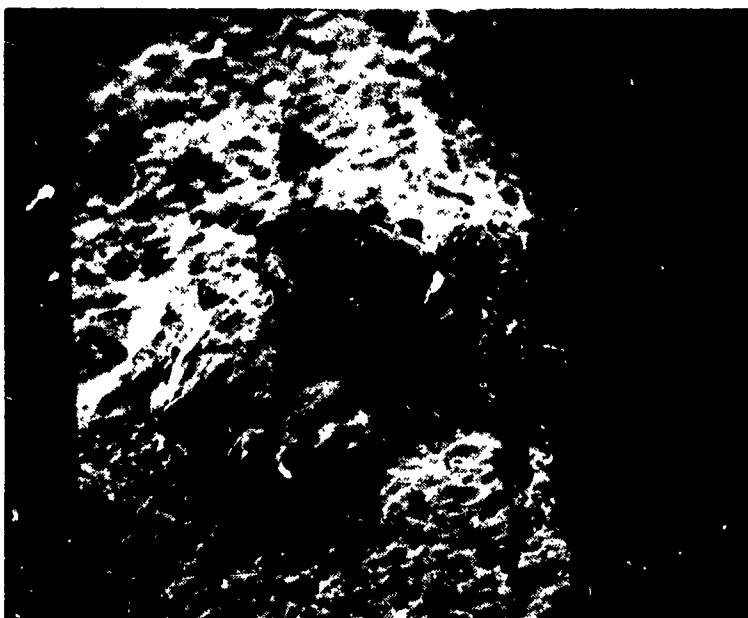


C. SQUEEGEE-RAMP INTERACTION FORCING SCREEN BREAKAWAY

Figure 5-7. Schematic Representation of Ramp Printing



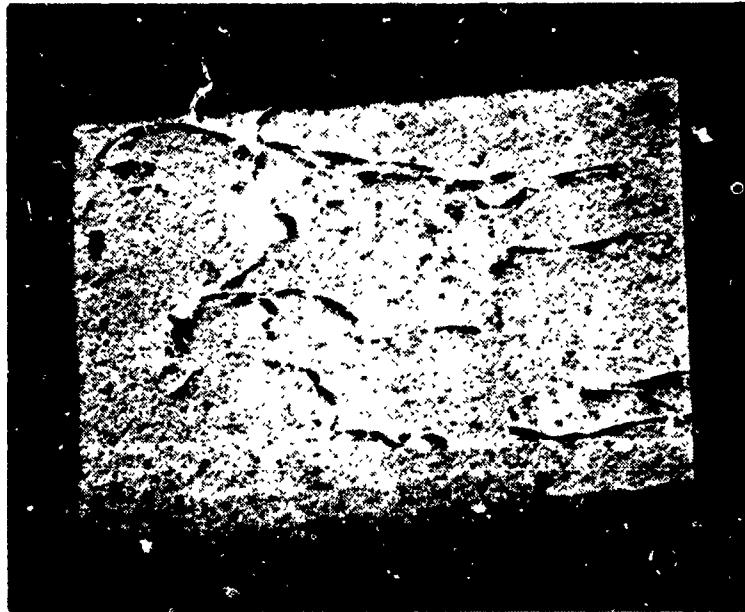
TOP VIEW (425X)



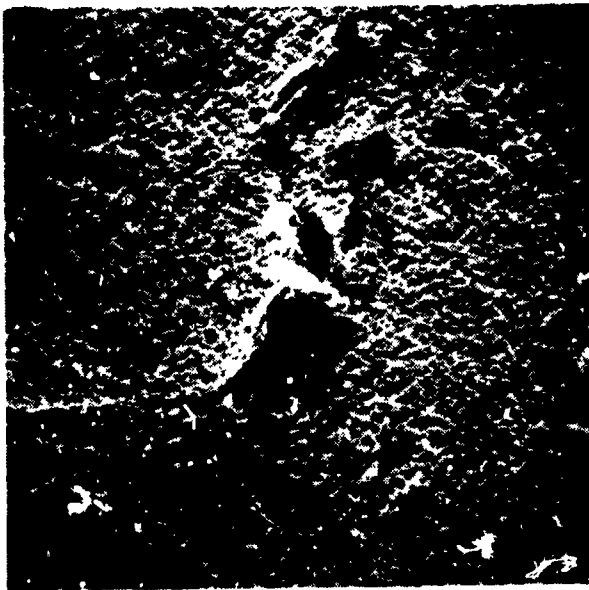
OBLIQUE VIEW (425X)

**Figure 5-8. Scanning Electron Micrograph of a Gold Conductor Short Due to a Pinhole After Removal of the Dielectric with Hydrofluoric Acid**

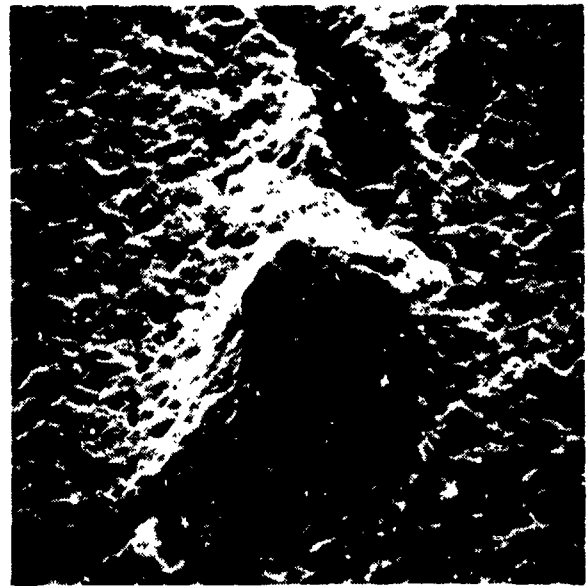
---



(42X)



(170X)



(425X)

Figure 5-9. Scanning Electron Micrograph of Voids and Bumps Left in a Fired Gold Conductor (ESL 8831)  
Due to Lint

Using conventional conductor ink, manual techniques were devised to form conductors in prepunched holes through the alumina substrate. A workable consistency was obtained by drying the ink, grinding it to powder, and adding small amounts of standard ink solvent. Figure 5-10 shows a conductor feedthrough in a substrate.

Initially, up to 4 hours were required to precisely align the screen. By interposing a clear plastic film and printing on it, alignment time was reduced to 15 minutes and less ink was wasted. In this method, the screen and plastic film were mounted solidly to the machine framework. The film was mounted just above the level of the substrate. A print was made on the film with blank substrate below it. The production board was then put in position on the table, adjusted to align the previously printed layers with that on the film.

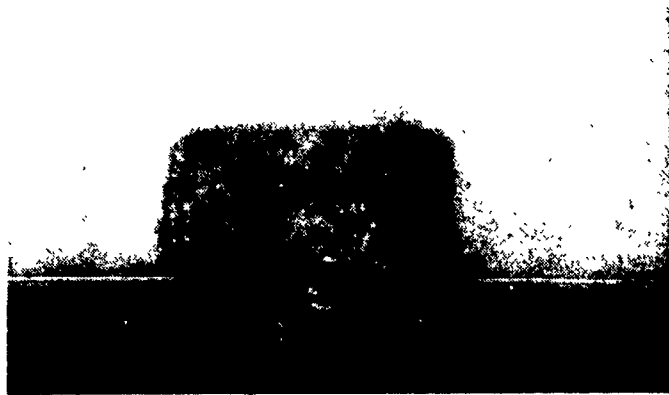
#### 5.4.4 Processing Sequence

Figure 5-11 shows the process sequence which was developed for a typical multilayer base. The letters denoting the ordering are defined as follows: C = conductor print and dry, D = dielectric print and dry, V = via fill and dry, and F = fire. (For example, C-F-D-D-C-F means the first conductor was printed, dried, and fired; a double printing of dielectric with drying between prints followed; and finally, the second conductor was printed, dried, and cofired with the dielectric.) This sequence minimized warpage, pinholes, and interlayer capacitance, while maximizing conductor adhesion to the substrate. The process sequence used produced boards of up to five layers with adhesion greater than the strength of the alumina substrate (i. e., capable of pulling a piece out of the substrate in tensile testing).

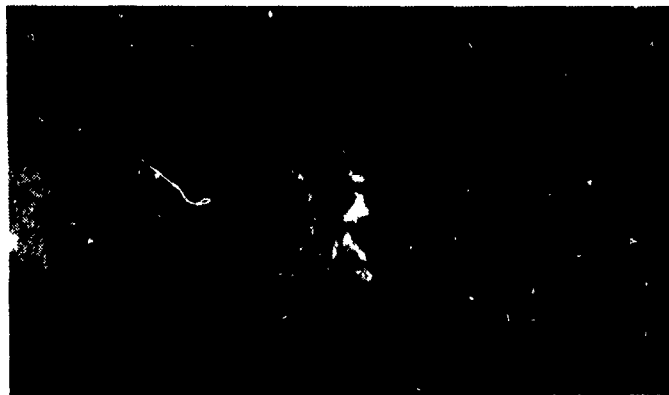
Figure 5-12 shows a cross section through a five-layer board. Only four of the conductor layers passed through the section plane, the first or bottom one being absent. Figure 5-13 shows sections through typical vias.

#### 5.4.5 Solder Coating

Once all screening and firing processes and visual inspection were completed, the circuit base was solder coated. The coat provided pretinning for subsequent component attachment and acted as a protective coating for the conductor



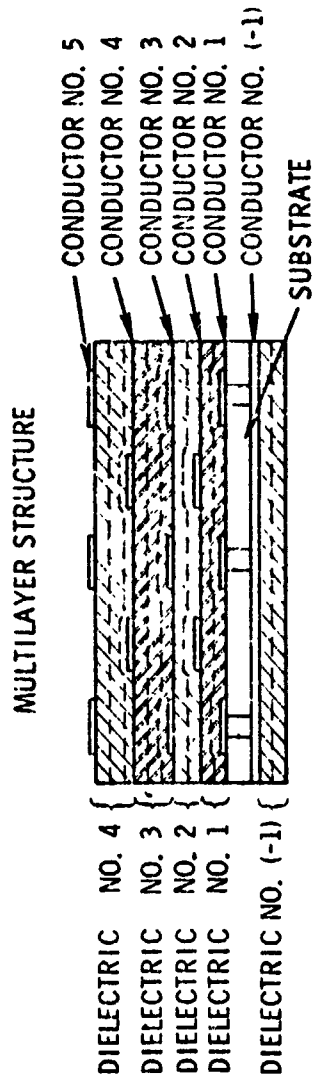
CONDUCTOR PAD SIDE (20X)  
OBLIQUE VIEW



CROSS-SECTION VIEW (36X)

Figure 5-10. Feedthrough Holes in the Substrate Showing the Gold Plug Making Connection from the Ground Plane to the Conductor Pad

---



**FABRICATION SEQUENCE**

LAYER NO.	SEQUENCE
0	FILL HOLES AND FIRE
-1	C (GROUND PLANE)-F
-2	D-D-F
1	C-F-D-D-
2	C-F-D-D-
3	C-F-D-D-V-F-D-
4	C-F-D-D-V-F-D-V-F
5	C-F-D (SOLDER MASK)-F

C = CONDUCTOR PRINT AND DRY  
D = DIELECTRIC PRINT AND DRY  
V = VIA FILL AND DRY  
F = FIRE

**Figure 5-11. Process Sequence Used for Five-Layer Multilayer Substrates with the Ground Plane on the Back Side Where Capacitance is Critical**

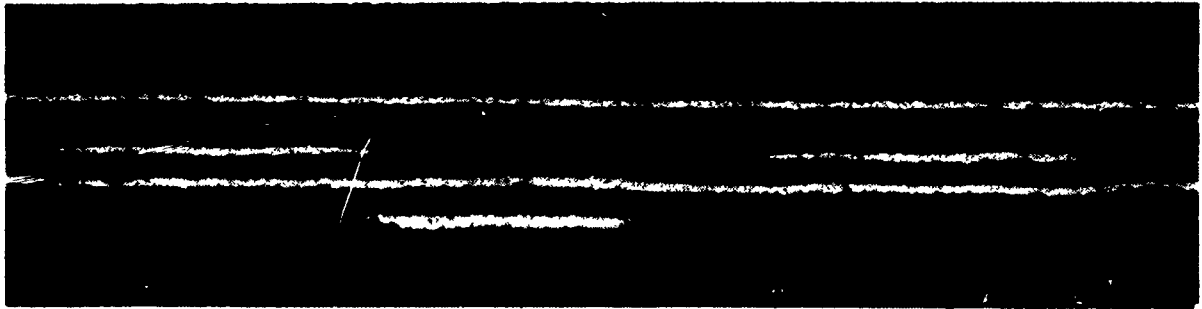


**Figure 5-12. Microsection of a Thick-Film Multilayer Showing Four of the Layers (200X)**

---

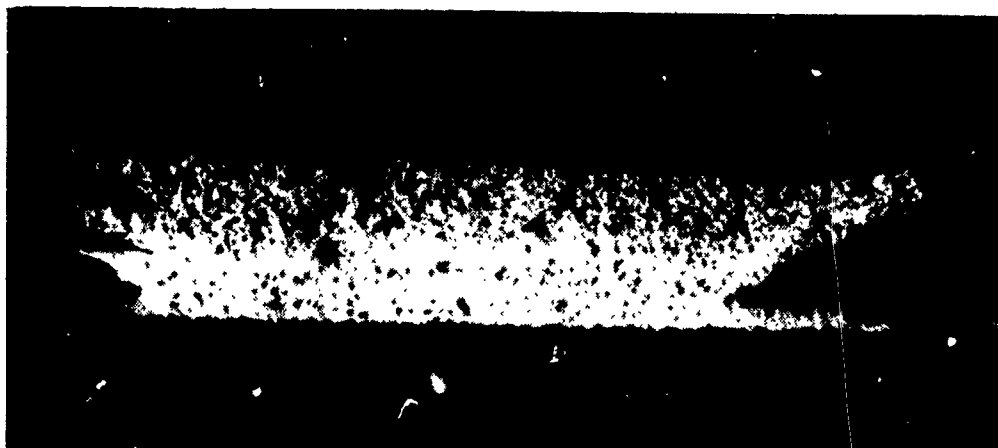


**Figure 5-13. Microsection of Typical Vias in a Five-Conductor Layer Thick-Film Multilayer (200X)**

---

pads during repeated electrical probing. Although a number of solders were studied, ordinary lead-tin eutectic solder proved the most satisfactory overall.

Complete solder-tinning could not be obtained without some solder leaching (conductors dissolving in solder). Thicker conductors were more difficult to tin. In the first tinning, the vias in the flatpack pads were centrally located under the pads and represented one-third of the pad area. With each successive solder-dip operation, additional solder would adhere to the periphery of the via until the via was bridged over with solder, leaving an untinned cavity under the solder. Also, with each successive solder-dip operation, the pads progressively leached, leaving the conductors so thin that they would leach out completely during subsequent heating for component attachment.

Several approaches were taken to tin the conductor without leaching it. Protective coatings such as plasma-sprayed copper, sputtered copper, vacuum-evaporated nickel-copper, and vacuum-evaporated nickel were unsuccessful, as they dissolved in molten solder long before the platinum-gold pad was leached. Relocating vias from under the pads increased the problem. The vias, like feedthroughs on conventional printed-wiring boards, acted like pillars or anchors and mechanically strengthened the pad. During operations where components were removed and replaced, pads without vias were significantly weaker than those with them.

A simple, two-stage solder-dipping operation, together with smaller-diameter vias, provided the best solution. The substrate was first immersed in a one-to-one mixture of peanut oil and nonactivated flux maintained at 135°C, and then immersed in molten solder. Total immersion time, and entry and exit angles and rates were closely controlled. Solder temperature was held below 232°C, and the substrates were redipped only once. Vias not tinned by dipping were later tinned carefully by hand with a soldering iron.

A more comprehensive solution to the solder-leaching problem was to strengthen the top conductor and dielectric layers and to improve the geometrical fit-up between them. The multilayer board made in this manner was dubbed a "superboard," due to its leach-free characteristics. The superboard differed from the others by having a double-thickness top conductor

layer and a triple-thickness top dielectric layer which was the negative, or complement, of the top conductor pattern. Thus, each top-layer conductor was in a dielectric trough. The top-layer processing sequence was CFCFDDC with an increase in furnace belt speed. With the standard process, fissuring was quite prevalent between vias and adjacent dielectrics and between the top conductor and the via. Manual touchup with conductor ink was required to overcome these potential defects. In the superboard process no fissuring occurred.

Six experimental superboards were fabricated, at different times, with difficult circuits and with otherwise standard production techniques. These boards all had the same leach-free characteristics. Tinning superboards was more difficult than tinning regular boards because the entire conductor surface exhibited the characteristics of vias. This was overcome by using a prefluxing step to activate the surface before solder dipping.

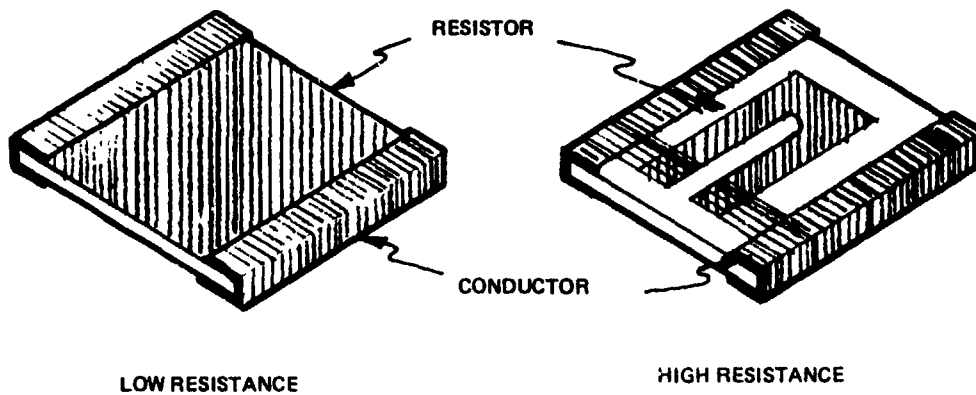
Preliminary tests on the superboard showed that leads could be soldered and unsoldered 20 times with negligible conductor leaching. Observation of pads after 20 such operations revealed (under 30-times-scale magnification) that approximately 2 percent or less of the conductor leached.

Several methods were tried to keep the holes along one side of the circuit base clear of solder to allow insertion of the ribbon cable wires (see top side of the base in Figure 5-6). The most effective and economical was to string 32 AWG Teflon-insulated wire through the holes. The Teflon was not wetted by solder and therefore the holes were not bridged during tinning.

#### 5.5 THICK-FILM CHIP RESISTOR FABRICATION

Commercially available chip resistors were made with silver terminations which dissolved extremely easily in solder. Chip resistors with solderable platinum-gold terminations were developed for UpSTAGE to allow reliable soldering.

The chip resistor structure and the fabrication sequence are shown in Figure 5-14. Conductor material was coated around the edge of the chip to allow face-up mounting on a substrate, which allowed trimming to be done



<u>STEP</u>	<u>PROCESS</u>
1	SCREEN AND FIRE RESISTOR INK
2	SCREEN AND DRY CONDUCTOR TERMINATIONS
3	BREAK SNAPSTRATE SHEET INTO STRIPS
4	DIP STRIP EDGE WITH CONDUCTOR, DRY, AND FIRE
5	BREAK STRIPS INTO INDIVIDUAL CHIPS
6	SOLDER-DIP CHIPS
7	TRIM CHIPS TO RESISTANCE VALUES

Figure 5-14. Chip Resistor Process Sequence

after installation, and precluded trapping processing residues between the resistor and circuit base. (Under electrical power, residues in contact with resistors can form electrolytic cells, causing catastrophic changes in resistance.)

#### 5.5.1 Ink Selection

To permit final conductor-dipping and firing to coat the edge of the chip without seriously affecting the resistor properties, high-firing-temperature inks (approximately 1,000°C), such as the ESL 3800 series or EMCA Firon, were evaluated. Because of availability and familiarity, ESL 3800 resistor ink was chosen.

#### 5.5.2 Fabrication Process

Resistor ink of the desired resistivity was screened onto scored substrates (snapstrates) and fired first at a peak temperature of 1,000°C. ESL conductor ink 5800E was then screened and dried but not fired. Before coating the edges of the resistor chips, the snapstrates were broken at the scored lines by holding the sheet along the bottom edge and bending it. The substrates were broken in half, then in half again, etc., until single rows remained.

The first step in dipping the strips was to prime the edges by thinning the edge conductor ink to a very thin consistency with butyl cellusolve acetate (BCA) solvent. The ratio of ink to solvent was approximately 50:50 by volume. The fluid conductor was used to soak a gauze pad. The edge of the resistor strip was then pressed on the pad to wet the edge and dried with a hot-air gun.

The second step consisted of spreading the conductor ink (no thinning or only very slight thinning) on a glass plate to a thickness of approximately 10 mils. The edge of the resistor strip was then carefully dipped into the ink to coat the edge and dried with a hot-air gun to prevent the ink from running.

After dipping and drying, the strips were fired at the standard conductor profile of 930°C. The strips were then broken apart to form individual chip resistors, solder dipped, and trimmed to the required value.

## 5.6 ELECTRONIC ASSEMBLY

Successful assembly of thick-film and epoxy-glass printed-circuit boards with flatpack and leadless inverted device (LID) integrated circuits, capacitors, resistors, and other components required development of a number of processes. Significant among these processes were thermally conductive adhesive bonding, soldering, flexible circuit boards, encapsulation, and associated static charge protection and repair.

### 5.6.1 Thermally Conductive Adhesive Bonding

Conventionally, components are reflow-soldered to relatively small thick-film circuit bases which are then mounted to carriers or heat sinks. The bow in the completed UpSTAGE 4- by 6-inch multilayer circuit bases had to be removed during bonding to the heat sinks because of tight packaging tolerances ( $\pm 0.005$  inch). The pressure and bending necessary to do this would have damaged any components previously mounted and soldered to the base. Therefore, reflow-soldering had to be done after bonding the base to the heat sink. During initial attempts to reflow-solder components, the thermal-expansion mismatch between the aluminum heat sink and alumina thick-film base bowed the assembly and destroyed the adhesive bond. The bowing was eliminated by replacing aluminum with molybdenum as the heat-sink material, obtaining near-perfect thermal-expansion matching to the alumina thick-film base. In addition, the very high elastic modulus of molybdenum ensured flatness of the bonded assembly. In cases where the molybdenum heat sinks were not received with the required flatness, they were heated to 150° to 400°F and flattened.

Candidate adhesives were chosen for thermal conductivity properties. The most promising materials were then evaluated for application properties, especially for meeting the 0.003-inch maximum bond line requirement. The following adhesives were evaluated in detail for use in bonding flatpack devices and thick-film bases: Eccosil 4852, PR 1913-2, Duroseal, DC 96-044, and Eccobond 285. It was found that all the properties desired were obtainable with Eccosil 4852. MDAC Report MP 51, 831 (contained in Appendix C of this report) includes details of the tests which led to the selection of Eccosil 4852.

Primed aluminum surfaces gave bond shear strengths of 150 to 300 lb/in.<sup>2</sup>. These were considered adequate. When the heat sink was changed to molybdenum, the strength values were redetermined. All candidate surface treatments (etching, grit-blasting, and solvent wipe) gave lap shear strengths of between 500 and 600 lb/in.<sup>2</sup>. Therefore, trichloroethane wiping was chosen as the most economical method of surface treatment for the molybdenum heat sink.

Maximum adhesion was ensured by using a silicone primer on the heat-sink and circuit-base bonding surfaces. Because of the desire to remove and replace flatpack devices, no primer was applied to their surfaces. The required thermal contact was thereby obtained without much adhesion.

A thin, uniform layer of adhesive was required for optimum heat transfer, strength, and minimum package height. A 0.003-inch maximum bond line between heat-sink and base was obtained by applying adhesive to the surface of the thick-film base, using a 325-mesh screen. The heat sink and base were held together in a vacuum bag for the 16-hour cure. Sufficient pressure was applied by this technique to ensure that the base was held flat against the rigid heat sink.

Screening was not practical for applying the adhesive between the circuit base and the components to be mounted with it. The pot life or working time of the material (approximately 2 hours) was too short to place all the components in their places on top of the screened-on material, and the circuit-base surface was too irregular for screening. Therefore, bonding of flatpack integrated circuits and small, hybrid, thick-film circuits onto the multilayer thick-film circuit bases was achieved by painting. The adhesive was thinned to make it brushable. It was painted on both surfaces to ensure complete wetting. The thickness of the adhesive was checked on the circuit base with a wet-film gage to ensure proper thickness. The component body was given only a very thin coat.

Initial adhesive bonds had voids ranging from pinholes to 1-inch-diameter holes. Ultrasonic and liquid-crystal nondestructive test techniques were tried in attempts to nondestructively detect the voids. Neither technique was

capable of detecting voids less than 1/2 inch in diameter. Liquid crystals were not sensitive enough because of the circuitry ridges caused by ink buildup and solder on the circuit-base top surface, and because of the high thermal conductivity of the materials. Ultrasonic flaw detection was complicated by responses from the molybdenum heat sink in addition to those from the adhesive layer. It was found that precoating both surfaces to be bonded together was adequate to eliminate all but the smallest voids. Thermal measurements made on production assemblies indicated that the bonding provided adequate thermal transfer despite the presence of small voids.

#### 5.6.2 Electrical Interconnections

The two major electronic packages, the GCU and CEU, each had three levels of interconnections: (1) the components connected to printed-wiring boards and thick-film circuit bases, (2) the boards and circuit bases interconnected by means of a flexible-rigid multilayer printed-wiring board, and (3) the entire assembly connected to the rest of the vehicle wiring.

Chip resistors and chip capacitors were reflow-soldered to the circuit base/heat-sink assembly. The presence of the heat sink increased the time required to heat and cool the assembly. Capacitors whose contact lands were longer than 0.1 inch required a small wire preform on each end to provide an adequate fillet; all smaller components had enough solder available from pretinning operations.

Heat sensitivity of the MOS integrated circuits (IC's) would not allow them to be reflow-soldered. Normally the leads of an IC would be preformed, placed on the substrate, and reflow-soldered with the other components; but the thermal mass of the circuit base/heat-sink assembly was too large and the flat-packs were in excellent thermal contact with the board.

The process sequence used for these components was to preform and trim the leads, then bond the component to the circuit base. After the 16-hr cure for the adhesive, the assembly was put on a heated stage controlled at 140°F and the leads soldered individually with a controlled-temperature soldering iron. The iron used was a 17w iron with tip temperature controlled at 600° to 650°F. The small tip used further limited the heat flow to allow the

operator to make a good joint and remove the iron before excessive heat was applied. A completed 4- by 6-inch multilayer circuit, with flatpacks bonded and soldered in place, is shown in Figure 5-15.

Figure 5-16 shows a completed GCU assembly with the flexible-rigid board shown. The flexible-rigid board was so named because it contained two rigid sections connected with a flexible section. The top rigid section contained components and circuit sockets for wire connections. The individual circuit assemblies were connected to the circuit sockets on the other rigid portion of the board by flexible cables. The flexible section contained four conductor layers and permitted the board to wrap around the top and side of the stack.

The initial design was to make two-sided flexible circuits and bond them together. However, adequate registration was so difficult to obtain with this approach that it had to be abandoned in favor of conventional multilayer techniques.

The thin laminate material was 0.002-inch-thick Kapton\* film with 1-oz copper on both sides of it. After the inner-layer circuitry was etched the flexible area was covered with a 0.001-inch-thick Kapton film for insulation. A rigid Cimboard-11 sheet with an oblong hole cutout (to provide the flexible joint) was bonded between the two Kapton sheets with a no-flow, epoxy, B-stage prepreg. The no-flow characteristic was used to keep the flexible area free of resin. The holes in the rigid areas were drilled and through-hole plated. A mask was used over the flexible area to prevent copper thickness buildup. Solder-plating and copper-stripping were done routinely. The solder plate was then stripped from the flexible area, and a Kapton film bonded on the area.

The Cimboard filler was sealed around the flexible area during all processing to prevent solutions from damaging the inner exposed conductors. The cutout presented some difficulties in photoresist exposure. The laminate material

---

\* E. I. Du Pont De Nemours & Co. trademark for polyimide plastic.

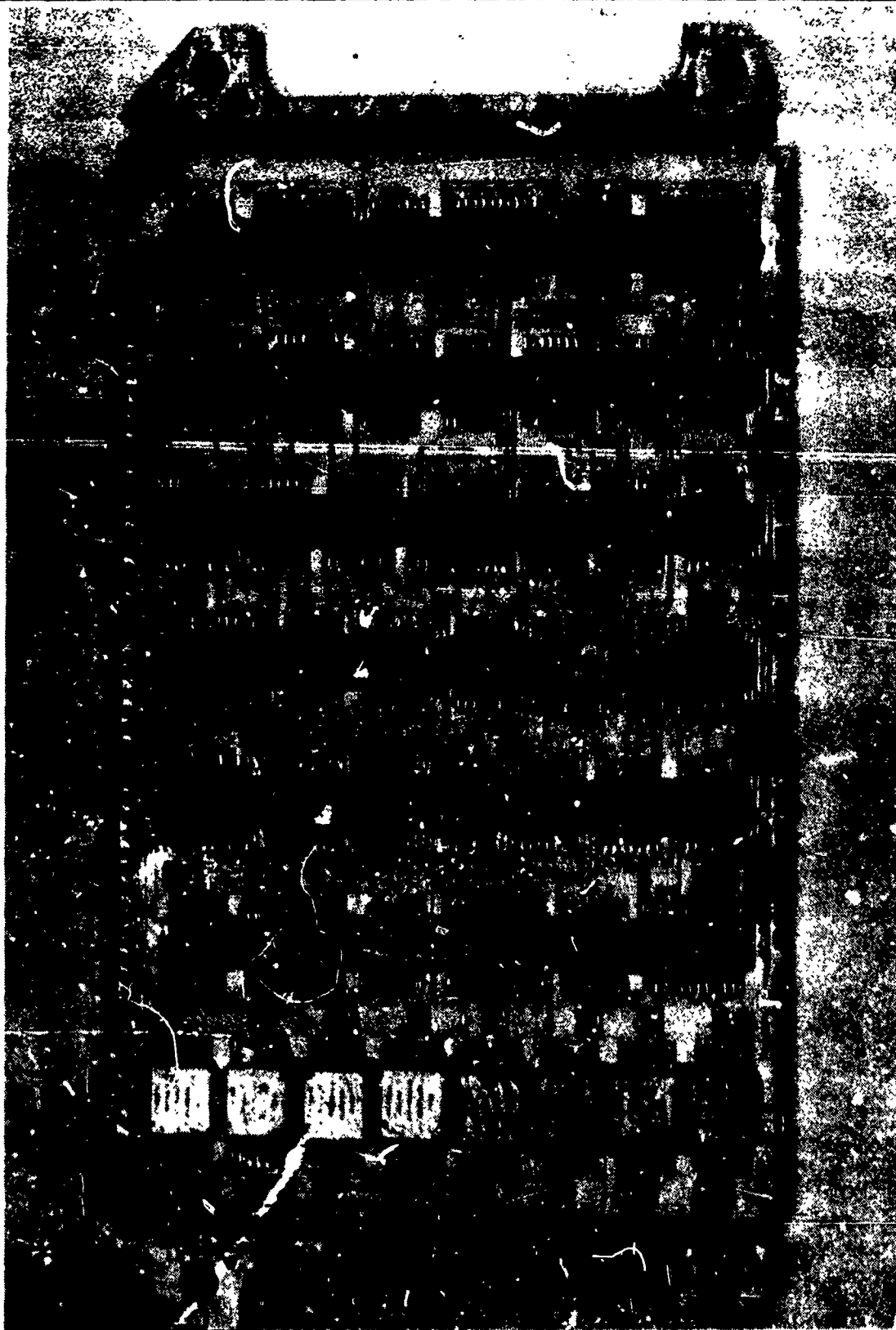


**Figure 5-15. Completed Multilayer Circuit Assembly Mounted on Heat Sink**



Figure 5-16. Assembled Guidance Control Unit

sagged into the hole, presenting a nonuniform surface which the film positive did not contact well. This problem was solved by touching up the part after photoresist developing.

Poor centering of the artwork on the panel caused the copper-plating thickness to vary across the board. Portions of the board were over-etched in order to completely etch other portions. The over-etched portions had solder hanging over the edges which broke off later in assembly. These solder slivers were potential shorts. The artwork was remade to minimize the nonuniform plating.

Adhesion of the copper to the Kapton was a constant source of trouble. A number of boards manufactured from inferior material (low peel strength between copper and Kapton) delaminated at the Kapton-copper interface during manufacture, especially during drilling. A manageable solution was to ensure good raw material by selection on a lot basis. Peel strength tests and hot peanout oil immersion (475° F for 20 sec) were used to determine the acceptability of each lot of material.

### 5.6.3 Encapsulation

The approach to ruggedness with minimum weight was implemented by using conformal coating and foam encapsulant to fill the space between circuit assemblies in each electronic package. The only exception to this was the signal-conditioning module which was mounted on the back of a connector and encapsulated in a thermally conductive epoxy.

Organic chemicals were known to cause drift in the resistivity of thick-film resistors. An extensive study indicated that silicone resins were less damaging to resistors than epoxy or polyurethane resins.\* Each printed-circuit board and thick-film circuit base was coated with silicone resin to a minimum thickness of 0.010 inch. This gave adequate protection to the thick-film resistors; however, it was found that traces of residual solder flux or

---

\* Refer to Report MP 51, 978, contained in Appendix C of this report.

certain other process solvents inhibited cure of the resin, leaving it as a low-viscosity, oily material. Thorough cleaning to remove solder flux and increasing cure temperature to 180°F alleviated this inhibition problem. The accelerated cure cycle decreased the time that the sensitive polymer component was exposed to contaminating materials.

Foaming the narrow spaces between circuit assemblies required each mold to be calibrated for determining the amount of foam required to properly fill the cavity. Thick-film modules were foamed only on the side containing components. Printed-wiring boards were foamed on both sides. Both sides of the boards were foamed at the same time, but the unequal thicknesses of foam on the two sides caused the boards to warp. Polyurethane foam shims were positioned on the thin side before foaming to maintain flatness. The foam shims were the same density as the rest of the foam and bonded readily to it. The silicone conformal coating covering the components was primed with a silicone adhesive to promote adhesion to the foam. Without the adhesive, the foam would not stick to the conformal coating.

#### 5.6.4 Static Charge Control

The electronic assemblies utilized a large number of MOS integrated-circuit devices. These devices can be electrically destroyed by application of uncontrolled static charge buildup. Static charge was measured on personnel handling devices in all phases of manufacturing. It was also shown that considerable static charge was built up during the foaming operation. This hazard was recognized early in the program, and standard procedures in use at MDAC were employed to protect electronic parts and assemblies from static charge damage.

The major static charge problem encountered on UpSTAGE was the protection of thick-film assemblies. Previously, shorted connectors, conductive tape, or 26 AWG tinned copper wire had been employed at MDAC for the shorting of internal circuitry and external grounding of printed epoxy-glass wiring boards. The same techniques were not suitable for UpSTAGE thick-film assemblies. The wire was too stiff and only provided a point contact when attached to thick-film circuit-base contact pads. The conductive tape did not have enough adhesive strength to cover the narrow width of the circuit base

pads and during processing steps, it would lose contact with the circuitry. The conductive tape also had the disadvantage of losing its conductivity when removed and reapplied. The solution was to hold a narrow, 0.002-inch-thick ribbon of aluminum foil in place over the thick-film pads with conductive tape and extend it beyond the circuitry for external grounding purposes.

#### 5.6.5 Repair Techniques

Replacement of LID components at any time prior to encapsulation was done by heating the circuit base/heat sink assembly locally. Heat was supplied by either a hot-air jet impinging on the bottom of the assembly or a pair of small soldering irons from the top. Similar heating methods were used to reattach the replacement part.

When a flatpack was known to be defective, its leads were cut with an Exacto blade at the edge of the component body. The leads were held onto the circuit pads with a stiff rubber block during this operation to minimize forces applied to the pads.

Many circuit changes were made on circuit bases by insulating flatpack pads from their circuit pads and connecting them elsewhere on the substrate by a 30 AWG jumper wire. All jumper wires were bonded to the circuit base with adhesive for mechanical strength.

#### 5.7 PROBLEMS AND SOLUTIONS

A number of technical problems encountered and solutions found in developing electronic manufacturing processes are summarized below:

Problem	Solution
Poor control of automatic drafting pen produced poor-quality drawings for photomasters.	Developed improved pen mechanism.
As-received 4- by 6-inch-thick film substrates were too warped for use.	Annealed substrates with load applied to flatten them.
Five-layer thick-film bases were bowed after circuit printing and firing were completed.	Used annealed substrates and batches of dielectric ink selected for best thermal expansion match.

Problem	Solution
Pinholes caused shorting between conductor layers in thick-film multilayer substrates.	Modified screen printer by adding a ramp to provide better screen break-away, and printed two dielectric layers between conductor layers.
Lint caused interlayer shorts on thick-film multilayer substrates.	Replaced paper wipers with polyurethane foam wipers and moved the screen printers to a dust-controlled environment.
Thick-film circuit interlayer capacitance was too high for digital circuit components.	Moved ground plane to back side of thick-film substrate and increased thickness of interlayer dielectric.
Thick-film circuit printing setup time required up to 4 hr per layer and used too much precious ink.	Added plastic "screen-on" template to screener. This reduced alignment time to 15 minutes and reduced ink amount to that needed for one printing.
Thick-film conductors were dissolved by the solder during attempts to obtain uniform tinning.	Developed two-step preheat-flux process and limited solder dip to two times.
Aluminum heat sink bowed when bonded to bowed alumina thick-film base and debonded from base during reflow-solder operation.	Replaced aluminum with a stiffer material (molybdenum) having coefficient of thermal expansion closer to alumina.
Molybdenum heat-sink material was not flat enough.	Flattened by plastic deformation at 150° to 400°F.
Voids were present in thermoconductive adhesive between circuit base and heat sink, and between flatpacks and circuit base.	Reduced size and number of voids to an acceptable level by applying adhesive to both surfaces.
Thermoconductive adhesive set up too fast for applying large number of flatpacks to thick-film circuit base.	Diluted adhesive with small amount of solvent to extend work life.
Flexible-rigid PC board delaminated during drilling.	Selected lots of material after acceptance (peel strength and hot peanut oil immersion) tests to ensure adequate bonding of copper laminate to Kapton.
Sylgard 182 conformal coating cure was inhibited by contaminants.	Removed solder flux residue more thoroughly and accelerated resin cure by curing at 180°F.

Problem	Solution
Printed-wiring-board assemblies warped during two-sided foaming operations.	Shimmed the thin side to keep them flat.
Conductive shorting tape left residue in holes of solder pads after temperature cycling and had poor adhesion to small pads.	Used narrow strip of 0.002-inch-thick aluminum foil held in place with conductive tape.
Removal of defective flatpacks caused damage to circuit base.	Cut flatpack leads at component body while supporting solder joint and removed leads one at a time; used 30 AWG wire jumpers (with suitable anchoring) to bypass damaged thick-film pads.

## 5.8 CONCLUSIONS AND RECOMMENDATIONS

Major advancements were made in the areas of computer-aided artwork preparation and in fabrication of large, ceramic, thick-film, multilayer circuit bases. Automated artwork preparation was begun and developed to a state of practicability at MDAC during this program. The system was not complex and it reduced the human layout effort to positioning the electronic packages on the circuit and drawing the interconnections. The system was developed for multilayer thick-film circuits but should be applicable to two-sided or multilayer printed wiring boards (made of reinforced plastic) with greatly increased speed and accuracy. The methods used for thick-film bases should be adapted to printed-wiring boards. Subsequently, quality, cost, and time of automated drafting should be compared with conventional (manual) methods.

Successful manufacture of 4- by 6-inch, two-sided, thick-film multilayer ceramic circuits was demonstrated.

The number of layers possible in multilayer structure is limited by the amount of bow introduced in the substrate by thermal expansion mismatch. The dielectric inks used in thick-film multilayer fabrication should be studied to determine methods for improving and/or controlling thermal expansion coefficient from batch to batch. Using inks with controlled thermal expansion,

prototype circuitry should be made to explore the limits of fabrication in terms of number of layers. Barring a significant improvement in thermal expansion match, future thick-film bases should be made from thicker alumina substrates. In addition, large, thin substrates should be annealed to relieve stresses and obtain a high degree of flatness prior to initial ink printing.

The solder leach resistance of the superboard indicates that component changes and repairs are possible more times on thick-film bases than on epoxy-based multilayer boards. This feature may be increasingly important in future programs, e. g., where alterable read-only-memories (ROM's) will have to be removed and replaced due to changing mission requirements. Further tests should be conducted to determine the number of solder repairs that can be performed on multilayer superboards.

Susceptibility of conductor pads to peeling damage during assembly operations was eliminated by proper cushioning, improved harness flexibility, and reasonable care in handling.

Experience gained in the area of flexible-rigid PC board technology points to the need for copper/Kapton laminated material having reliably higher peel strength. Improved lamination methods should be developed and tested for repeatability.

## Section 6 EXTERNAL HEAT SHIELD INSULATION

Special processes were developed to produce thin, close-tolerance insulation to protect critical external regions of the UpSTAGE vehicle from aerodynamic heating.

On the first stage (booster), high-silica/phenolic (high-silica fabric impregnated with phenolic resin) insulation was cured and bonded simultaneously on the fins. Other external booster and interstage surfaces requiring insulation were covered with adhesive-bonded cork, fiber glass, and Teflon; or with sprayed-epoxy ablative insulation, using well-known, conventional manufacturing techniques.

The second-stage surface, except for the tungsten/2-percent-thoria nose tip, was covered with a high-silica/phenolic heat shield. The heat shield thickness was 0.050 inch except in the aft controls region (Stations 88 to 107) on and around the EB fuel injectors (finlets). Finlet insulation was precision-molded, chiefly from chopped high-silica/phenolic material, and subsequently bonded to the individual finlet cores, using conventional bonding techniques. Specially woven 0.100-inch-thick high-silica/phenolic was applied to the missile surface in the region of the finlets (EB vehicle only) by the method developed for the forward heat shield. The aft face of the second stage was covered with conventional sprayed-epoxy ablative insulation. The aft control section of the JI vehicle was protected with a single layer of 0.050-inch-thick high-silica/phenolic, and additional epoxy-ablative insulation was troweled onto the region of the JI nozzle ports.

### 6.1 REQUIREMENTS

The foremost requirement for all external heat shield insulation processes was that they produce bonded insulation capable of withstanding the UpSTAGE flight environment. Aerothermodynamic requirements, as well as tests and analyses which were conducted to verify the flightworthiness of the insulation, are reported in Reference 6-1. Other requirements are discussed herein.

To minimize heat shield weight, the high-silica/phenolic insulation on the second stage was required to be relatively thin (0.050 inch thick forward of Station 88 and 0.100 inch from EB Stations 91 to 107, with a straight taper in thickness from Stations 88 to 91), and the tolerance on thickness was set at  $\pm 0.010$  inch. The high-silica/phenolic insulation on the first-stage fins was required to be  $0.100 \pm 0.020$  inch thick in the vicinity of the yaw fin leading edge and  $0.050 \pm 0.010$  inch thick on all other fin surfaces.

During curing and bonding processes, the heat-treated aluminum missile structure was not allowed to be exposed to temperatures above  $300^{\circ}\text{F}$ , and total time at temperature was set at 10 hours maximum. Forces due to autoclave pressure plus vacuum bagging were capable, in some cases, of damaging the substructure at  $300^{\circ}\text{F}$ . Accordingly, limits were set on autoclave pressure (typically 15 psig or 30 psig) for each missile section depending upon its individual load-bearing capacity.

After curing, the heat shield density was required to be 95 pcf or more, and the largest allowable unbond area was set at 0.5 inch. Aerodynamic shear stresses on the adhesive bond were approximately 1 psi at  $300^{\circ}\text{F}$ .

Finlet insulation on the EB vehicles was required to cover the core with three pieces (Figure 6-1). A cap covered the leading edge, sides, and back face; a small sliver filled the cavity under the forward nose of the cap; and a slotted disk covered the base of the finlet, blending in with the skin contour. The cured high-silica/phenolic was required to have a density of 100 pcf or more and to be radiographically sound with respect to voids, cracks, and resin-rich areas. Insulation for approximately 120 finlets was required for EB flight vehicles, tests, and spares. Dimensional requirements for the cap were typical: 2.7-inch length, 0.100-inch wall thickness, and a  $\pm 0.0025$ -inch tolerance on most dimensions.

External insulation in the nozzle region on the JI vehicles was conventional epoxy-ablative insulation, applied by troweling.

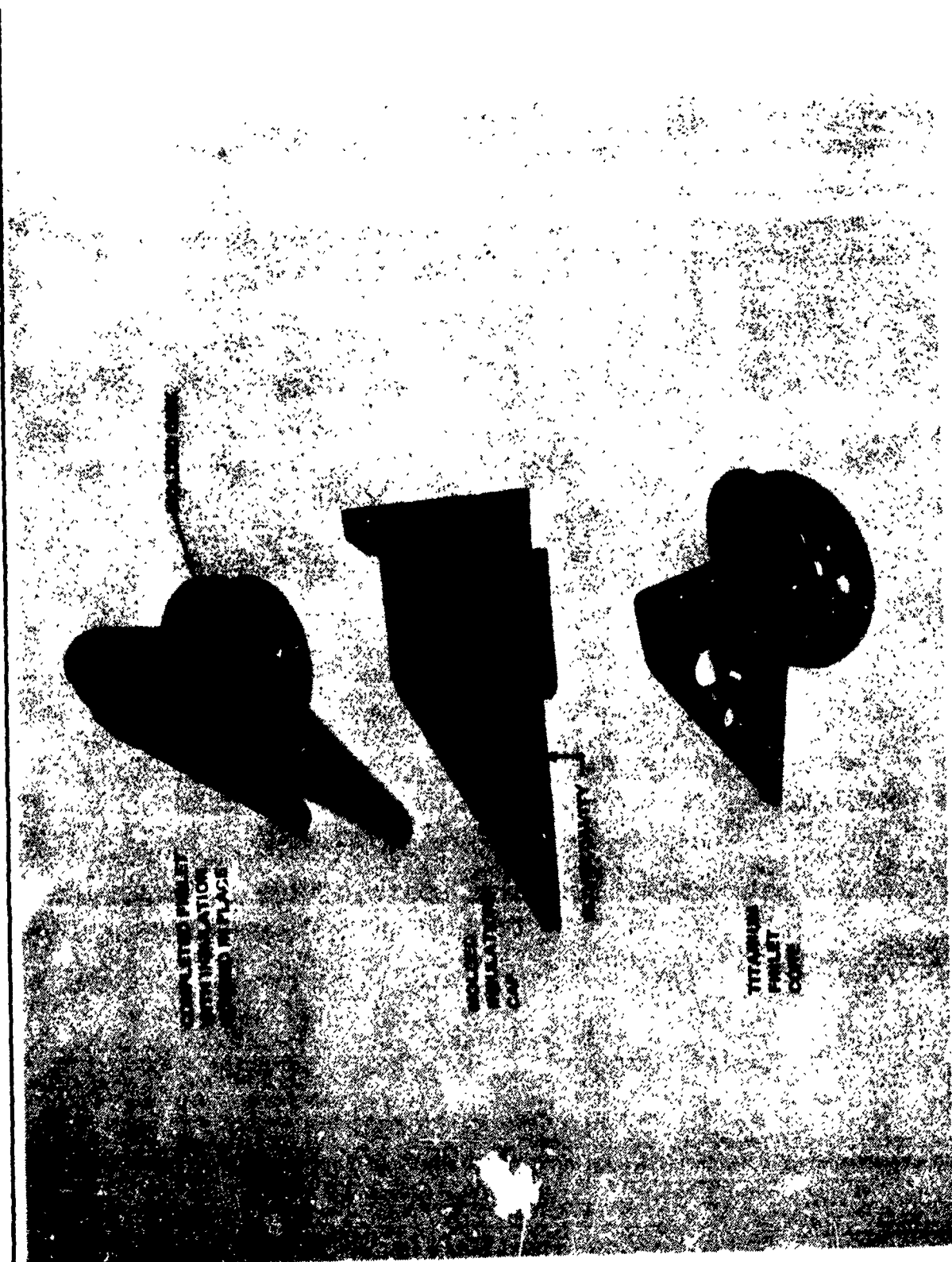


Figure 6-1. EB Finlet Insulation

## 6.2 APPROACH AND CONSTRAINTS

### 6.2.1 Forward Heat Shield

Two fabrication methods were considered as candidates for development. The first, tapé-wrapping, would require complex controls during wrapping and subsequent machining, and would present additional problems in thickness inspection for such a thin heat shield. The second method considered was to drape a single layer of prepreg (high-silica fabric preimpregnated with uncured phenolic resin) over the vehicle skin or a mandrel and then cure the heat shield. This approach took advantage of the thinness of the heat shield and was easily applied to an elliptical shape. However, it posed two possible problems: (1) a complete cure of the prepreg might require temperatures above 300°F to achieve the required density, and (2) a flight-worthy longitudinal joint was required to terminate the draped cloth edges.

Two sequences of adhesive bonding the heat shield were considered—bonding after heat shield cure, and bonding during heat shield cure. The latter sequence was chosen because it ensured geometrical fit between the vehicle skin and the flexible uncured heat shield during layup; eliminated handling problems associated with a thin, fragile, cured heat shield; and greatly reduced the tooling and time required for manufacturing. However, in order to implement the simultaneous cure method (curing heat shield and adhesive simultaneously), it was necessary to determine the compatibility of candidate adhesives with the high-silica/phenolic during the 300°F cure cycle. These compatibility tests were conducted as the first task of the process development program.

Process development for the forward heat shield was divided into three steps: (1) preliminary testing, (2) process verification, and (3) process modification. The objectives of the first step were to select process parameters and compatible processing materials and to demonstrate the feasibility of the selected process. The second step was intended to verify the producibility of the selected process by insulating full-scale UpSTAGE test structures. The third step, process modification, was later required to reduce the amount of heat shield rework by simplifying the vacuum-bagging procedure.

### 6.2.2 Aft Heat Shield

As with the forward heat shield, the process selected for the aft heat shield involved simultaneous cure of a single ply of high-silica/phenolic fabric draped over adhesive-covered structural skins. Because the EB aft heat shield was required to be 0.050 to 0.100 inch thick, and the thickest available prepreg was 0.050 inch thick, it was necessary to procure a quantity of custom-woven high-silica cloth and have it preimpregnated with phenolic resin to obtain 0.100-inch-thick prepreg.

After acceptable material was procured, a full-scale test structure simulating the second-stage aft control section (Stations 88 to 107) was insulated to verify producibility of the simultaneous cure process. The thickness taper from 0.050 to 0.100 inch was produced by conventional machining techniques.

Process modifications to improve the vacuum-bagging procedure were employed for insulation of the last two (JI) vehicles, with 0.050-inch-thick material. These modifications included elimination of foreign sealants. (Refer to Sections 6.3.2 and 6.4 for a discussion of the modified process.)

### 6.2.3 Booster Fin Heat Shield

To obtain 0.100-inch-thick leading-edge insulation adjacent to 0.050-inch-thick side-panel insulation, both composed of high-silica/phenolic, two approaches were considered: (1) a separate leading-edge insulation piece made from precured high-silica/phenolic or made from 0.100-inch-thick prepreg (simultaneously cured and bonded), or (2) a preplaced strip of 0.050-inch thick prepreg covered by a continuous layer of 0.050-inch-thick prepreg covering the side panels also. The second approach was selected because it eliminated the need for a joint between the leading edge and side panels and was more easily produced, and because the relatively weak bond between the two layers was not exposed to erosion or high stress during flight. As with the second-stage heat shield, full-scale test parts were insulated to develop detailed processing techniques for the simultaneous cure process.

#### 6.2.4 Finlet Insulation

Preliminary tests on the MDAC Aeroder (Reference 6-2) had demonstrated that with proper ply orientation, quartz/phenolic, pre-cured in block form, offered the best resistance to erosion. However, high-silica/phenolic, molded from chopped prepreg, was found to be acceptable also, based upon an aerothermodynamic analysis of available data. Molding was chosen for development because it appeared the most economical and reproducible way to make the finlet insulation pieces, given the geometry, tolerance, and quantity requirements. Initially, a simple mold was made, approximating the size and shape of the cap (the most difficult part to mold). This test mold was used to establish the molding pressures, temperatures, material preparation, etc., which would produce molded parts of the required density and soundness. Experience gained in these molding tests was applied in designing the final production molds.

### 6.3 FORWARD HEAT SHIELD DEVELOPMENT

#### 6.3.1 Subscale Tests\*

Five candidate adhesives were used to bond high-silica/phenolic prepreg to 6- by 6- by 0.250-inch aluminum plates. Prior to bonding, each plate was cleaned and primed in a similar manner. Each assembly was bagged and a vacuum of 28 inches Hg was applied. The assemblies were then cured for 3 hours at 300°F in the autoclave at 50 psig, cooled to 150°F, and the pressure removed. The purpose was to determine which adhesive was best suited for simultaneous curing with high-silica/phenolic at 300°F.

Subscale circular aluminum cylinders, approximately 6 inches in diameter, were covered with insulation and cured using the four most promising adhesive materials from the initial plate screening tests. Cylinders were insulated using a butt-splice and a single overlap joint for each adhesive used. The metal cylinders were cleaned, primed, and cured in the same

---

\*Details of subscale tests appear in Report MP 51,564, in Appendix D.

manner as were the plates. It was determined that a layer of rubber foam inserted between the vacuum bag and bleeder was required to eliminate wrinkling on the test cylinders. Each test cylinder was nondestructively tested for voids in the adhesive bondline using the immersion ultrasonic through-transmission technique. Based on the test results, a nitrile phenolic film adhesive (AF31) was selected for further evaluation.

Because both the high-silica/phenolic and the AF31 film adhesive are normally cured above 300°F, tests were conducted to verify that a cure cycle of 3 hours at 300°F would completely cure the materials to a stable state. The test methods included thermogravimetric and thermomechanical analysis, and vibrating reed (dynamic modulus) analysis. The results of these tests (which appear in Reports MP 51,736 and MP 51,731, respectively, in Appendix D of this report) were compared with existing data for higher-temperature cure cycles and verified the adequacy of the 300°F cure for 3 hours.

Using the techniques developed during the plate and 6-inch-cylinder tests, a riveted elliptical cylinder 71 inches in circumference was insulated using the high-silica/phenolic and AF31 film adhesive. In order to maintain a vacuum during cure, it was necessary to seal the internal portion of the metal substructure with silicone sealant. Nondestructive testing indicated that there were no voids in the bondline and that the procedure was acceptable for the application of insulation to the actual UpSTAGE structure.

To verify the performance of the heat shield and joints in a simulated flight environment, test specimens were prepared by bonding the high-silica/phenolic to aluminum plates using AF31 adhesive for plasma jet tests. The AF31 exhibited a general failure in the bondline with catastrophic release of the insulation material during plasma jet exposure. The failure was attributed to unexpected thermal and shock loads, the nature and magnitude of which could not be readily determined. As an expedient solution, it was decided to try replacing the AF31 adhesive with an adhesive having better high-temperature strength and thermal conductivity. The adhesive chosen was an epoxy phenolic aluminum-filled adhesive (HT-424) which was not originally considered because it is highly outgassing during curing.

Plasma jet tests of heat shield and joint specimens bonded with HT-424 were successful. Also, bonding tests on 12- by 12-inch flatplates showed that unbonds due to outgassing could be reduced, without introducing wrinkles, by increasing the number of bleeder plies and then wrapping the assembly with shrink tape prior to vacuum bagging. As a result, HT-424 was chosen to replace AF31 for all UpSTAGE heat shield bonding. (Details of the above tests appear in Reports MP 51, 732 and MP 51, 741 in Appendix D of this report, and in Reference 6-1.)

### 6.3.2 Full-Scale Tests

A full-scale aluminum mockup of the UpSTAGE forward control section was made to evaluate the proposed bonding techniques and joint design. The forward control section was chosen because it was by far the largest section of the forward heat shield, and therefore the most difficult to handle. Difficulties were encountered in finding leaks in the substructure during vacuum-bagging checkout. After all leaks had been found and sealed, the first half of the heat shield was laid up and cured. No wrinkles were found, although some unbonded areas were evident. The layup procedure and the specimen were reexamined to determine the best procedure to use for the second half of the heat shield layup. To aid in solving the unbonding problem, a large truncated cone substructure was insulated, one half at a time. Improved evacuation, simplified layup, and slower cooling techniques were devised to solve the unbonding problem. Using the improved method, the second half of the forward control section was insulated. Inspection with a resonance-loading ultrasonic instrument revealed no unbonds.

Heat shield fabrication for the first two of the three EB vehicles was quite successful; only a few isolated voids or unbonds were found, and these were readily repaired by straightforward patching and injection techniques. However, numerous large and small unbonds were found on the EB-3 heat shield sections, and numerous repetitive repairs were required.

From knowledge of the fabrication techniques and from tests of flatplate samples fabricated in different controlled ways, it was suspected that the aluminum bonding surfaces were being contaminated during layup, cure,

and repair by residues from the silicone sealant on the inside of the aluminum structure. In order to expedite completion of the EB-3 heat shield, careful tests and inspections of the aluminum surfaces were conducted prior to layup, and stringent handling procedures were strictly enforced.

Concurrently, tests were conducted to develop a modified silicone-free bonding process for the two JI vehicles. Among the alternatives considered were nonsilicone sealants, internal rubber bags, sand-fill, and end caps. All available nonsilicone sealants were either poor sealants, contaminating in other ways, or very difficult to remove. Internal bags were not feasible because of the complex internal deep-ribbed configuration of the UpSTAGE structure. Sand-filling was feasible, but added handling problems because of excessive weight and posed additional internal surface protection and cleaning problems. Accordingly, end caps and internal stiffening braces were fabricated to allow each section (nose, payload, guidance, and forward control) to be closed off and evacuated internally as well as externally, without need for silicone sealants in contact with the structure.

To demonstrate the feasibility of the end-cap approach, a spare EB nose section and guidance section were insulated. No unbonds were detected and all design requirements for density and bond strength were exceeded.

However, two problems were encountered during insulation of the first JI structure:

- A. Forward control section honeycomb panels debonded because the honeycomb adhesive (AF-126) could not withstand the stresses imposed by the new sealant-free process. HT-424 adhesive was selected to replace the AF-126 and withstood the subsequent cure cycles.
- B. Internal structural frames buckled by creep during curing of forward control and guidance sections due to (1) differential thermal expansion between the JI steel skin and the internal aluminum frames and (2) the external pressure imposed

by the new process. Buckling during subsequent cures was prevented by improving support braces and by reducing autoclave pressure from 35 to 15 psig.

#### 6.4 AFT HEAT SHIELD

The process developed for the EB aft heat shield was nearly identical to that for the forward heat shield, except that the aft heat shield thickness was 0.100 inch and the aft control section was larger in circumference than the forward control section. The only development tests necessary, therefore, were associated with production of thick prepreg and subsequent verification of its curing and bonding characteristics.

JI vehicles were insulated with 0.050-inch-thick prepreg by the sealant-free bonding process (refer to Subsection 6.3.2 for a discussion of sealant-free bonding), except that the autoclave pressure was 30 psig to improve the densification of the heat shield in the areas of the JI hot-gas nozzles. This higher pressure was permitted because of the high load-carrying capability of the JI aft control section structure.

##### 6.4.1 Weaving Development

Since no 0.100-inch-thick high-silica fabric was commercially available, a description of the properties and processing requirements was sent to various weavers for competitive bid. Several modifications in weaving techniques were made before an acceptable Refrasil fabric (0.100-inch-thick) was obtained.

The first sample of custom-woven 0.100-inch-thick prepreg was received for evaluation. The results of the inspections and tests showed that the sample did not meet most of the requirements specified in the purchase order, including density, thickness, volatile content, and resin flow. The vendor was contacted, and a second sample was prepared. Tests of the second sample showed that, although considerable improvement in thickness and density was achieved, not all of the specified properties were met. Accordingly, additional discussions were held with the weaving and impregnating vendors, and a third sample was made, received, and found to meet all UpSTAGE requirements. Authority was then given to proceed with the

manufacture of several yards of prepreg to be made in the same way as the third sample. This initial lot of material was used to lay up a prototype aft control section heat shield to verify that the 0.100-inch-thick material could be processed as the 0.050-inch-thick material was for the forward control section.

#### 6.4.2 Layup Tests

As with the forward control section, a full-scale aluminum mockup of the aft control section was made for the layup tests. Using the HT-424 adhesive system, a single layer of 0.100-inch-thick prepreg was bonded to a prototype aft control section using the curing procedures developed earlier for the forward heat shield. The first half of the prototype aft control section was successfully installed and inspected. No unbonds or wrinkles were found and it was determined that existing resonance-loading ultrasonic equipment and procedures were suitable for nondestructive inspection. The second half of the prototype aft control section was then insulated. In sealing vacuum-bag leaks prior to curing, excessive handling of the laid-up assembly occurred. As a result, the cured heat shield had a few large wrinkles on the second half. No unbonds were detected by ultrasonic inspection, however. It was concluded that a satisfactory processing technique for bonding and curing the adhesive and 0.100-inch-thick insulation simultaneously had been verified, and that careful bagging and handling were necessary.

#### 6.5 BOOSTER FIN INSULATION

A simulated fin leading edge was made from aluminum sheet and used to develop layup and simultaneous-cure techniques. It was found that the same techniques used for the forward heat shield could be successfully applied to the booster fins. No unbonds or wrinkles were found in the test specimen. The double layer of 0.050-inch-thick insulation required on the pitch stability fin leading edge was successfully cured and bonded in a single bonding cycle of 3 hours at 300°F.

#### 6.6 FINLET INJECTOR INSULATION

Initial molding process development was performed with a prototype mold which produced parts of the same approximate size and shape as would be

required for EB flight caps (See Figure 6-1). A quantity of high-silica/phenolic cloth was chopped into squares to obtain the molding compound. It was found that the size of the chopped pieces could not exceed 1/4 by 1/4 inch to obtain complete mold filling. At first, sticking problems were encountered, but these were solved by adding 1-percent zinc stearate powder (a common additive) to the chips prior to molding. Several test laminates were bonded to test structures to ensure that the zinc stearate additions would not interfere with standard adhesive-bonding techniques. All tests indicated that there were no observable effects. Numerous systematic tests were conducted to establish optimum molding parameters such as preform compaction, pre-heat, pressure and temperature cycles, postcure cycle, mold lubricants, and insertion/removal methods.

Using the prototype finlet mold, test parts were transfer-molded and prepared for the RENT performance test (Reference 6-1) using high-silica/phenolic molding chips. In addition, test parts were made by the same molding process, using carbon/phenolic chips, with excellent success.

## 6.7 PROBLEMS AND SOLUTIONS

A summary of technical problems and solutions associated with developing the heat shield insulation processes appears below.

Problem	Solution
Wrinkles formed on the heat shield surface during subscale cylinder tests.	Inserted layer of rubber foam between bleeder plies and vacuum bag during layup (see Figure 6-2a).
Difficulty was experienced in maintaining acceptable levels of vacuum during cure of the forward heat shield.	Sealed interior surface seams and fasteners with silicone rubber sealant (see Figure 6-2b).
Unbonds formed during (a) 12- by 12-inch flatplate tests and (b) forward control section full-scale prototype bonding.	(a) Increased number of bleeder plies and wrapped with shrink tape prior to bagging (see Figure 6-2c).  (b) Simplified layup, improved evacuation method, and cooled slowly to minimize gas bubble formation and thermal stresses.

Problem	Solution
Numerous and repetitive unbonds formed during heat shield bonding.	Developed a sealant-free bonding process to eliminate silicone contamination (see Figure 6-2d).
JI forward control section honeycomb panels debonded during heat shield cure.	Replaced the honeycomb adhesive with a high-temperature adhesive.
JI internal structural frames buckled during heat shield cure.	Improved internal support braces and reduced autoclave pressure during bonding (see Figure 6-2d).
No high-silica/phenolic prepreg 0.100 inch thick was available commercially.	Coordinated efforts of cloth weavers and resin impregnators to develop a satisfactory custom-made prepreg.
Molded finlet insulation pieces stuck to mold.	Added 1 percent by weight of zinc stearate to the molding chips prior to molding.

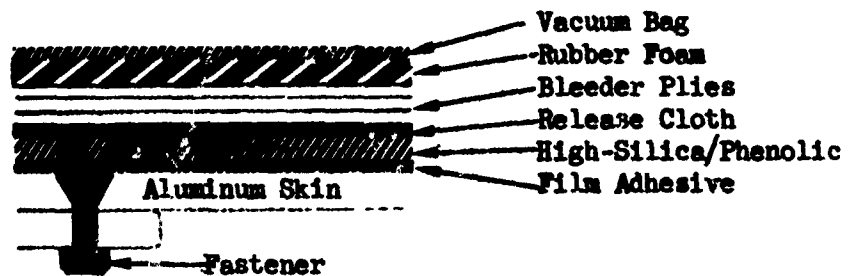
## 6.8 CONCLUSIONS AND RECOMMENDATIONS

A satisfactory process was developed to apply, bond, and cure film adhesive and high-silica/phenolic insulation to the UpSTAGE substructure simultaneously. The process was found to be an effective and economical method for applying thin heat shields (0.050 and 0.100 inch thick) to aluminum and steel surfaces.

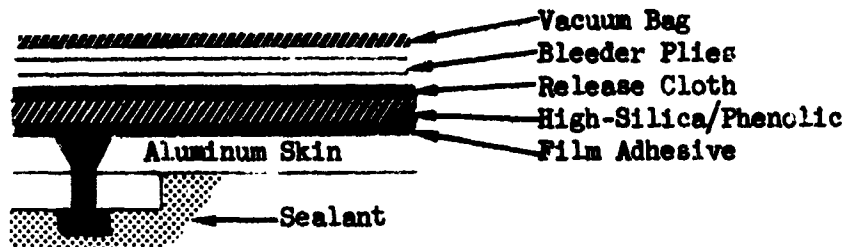
Special 0.100-inch-thick fabric was successfully developed and processed. Other custom-thickness prepregs could be produced in a similar manner to meet future requirements. Experimental heat shields of increased thickness should be fabricated in a similar manner to define the thickness limits for simultaneously cured and bonded heat shields.

Sealing the internal portion of the substructure was found to be a time-consuming operation with inherent contamination hazards. The use of end-cap plates was found to be a better method of sealing. However, the additional stresses imposed on the capped structure by the autoclave pressure required design and process changes to avoid structural damage. Noncontaminating sealants which can be easily applied and removed should be developed for use where end caps cannot be used.

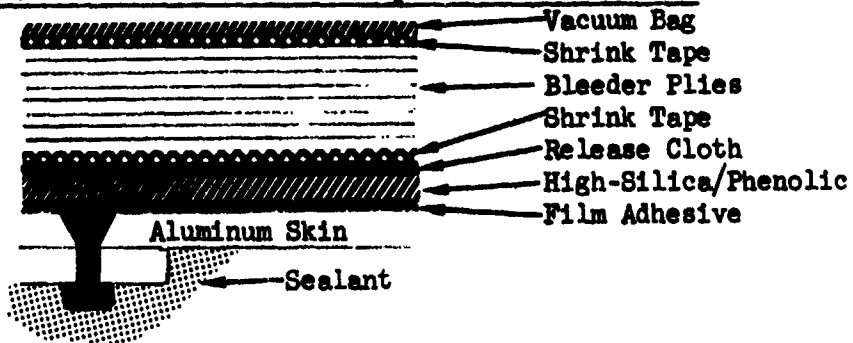
(a) Rubber Foam to Reduce Wrinkles



(b) Sealant to Reduce Leaks



(c) Increased Bleeder Plies and Shrink Tape to Reduce Unbonds



(d) Sealant-Free Layup to Reduce Unbonds

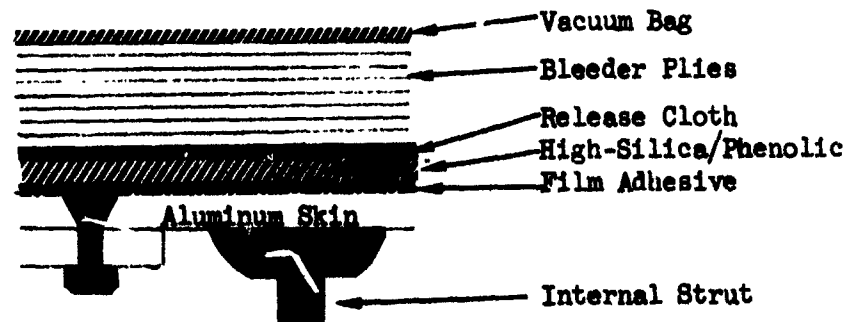


Figure 6-2. Schematic of Insulation Layups

Transfer-molding parameters established for the finlet insulation provided a method for reproducible fabrication of small parts of high-silica/phenolic and carbon/phenolic to close tolerances. For new molds, it is recommended that tooling be made that allows the mold to be mounted in a press and heated. In addition, provisions should be made to allow removal of the part from the mold without completely disassembling the die.

Section 7  
INTERNAL HOT-GAS DUCT INSULATION

7.1 REQUIREMENTS

7.1.1 EB Liners\*

The EB warm-gas ducts (Figure 7-1) required internal silicone rubber insulation to protect the tube assembly from the flowing 2, 250° F gas-generator products (at up to 4, 500 psi) for 1 to 3 sec. To meet original weight and performance goals, the wall thickness of the liner was to be 0.060 ±0.005 inch with an OD of 0.900 ±0.005 inch in the manifold (from the gas generator to the relief valve). In the vent line leading from the relief valve to the overboard dump nozzle, the liner was to 0.100 ±0.005 inch thick with an OD of 0.968 ±0.005 inch.

The liner was to be installed in straight and bent tubes made from nickel-base alloy bar and sheet having longitudinal and circumferential welds flushed to within 0.005 inch of the ID surface. The liner was required to adhere to the metal surface well enough to withstand variable flow of the warm gas during flight operation. In addition, the decomposition products of the liner and adhesive were required to be compatible with the relief valve and the unlined nickel-base tee in the system.

7.1.2 JI Liners\*\*

The JI warm-gas manifold ducts and nozzles required internal insulation to protect the metal ducts and missile structure, respectively, from flowing 2, 800° F gas-generator products (at up to 4, 000 psi) for 1.5 sec.

---

\*See Reference 7-1 for a description of EB control subsystem analysis, design, and testing. Refer to Subsection 3.5 of this report for information on fuel tank piston insulation.

\*\*See Reference 7-2 for a description of JI control subsystem analysis, design, and testing.

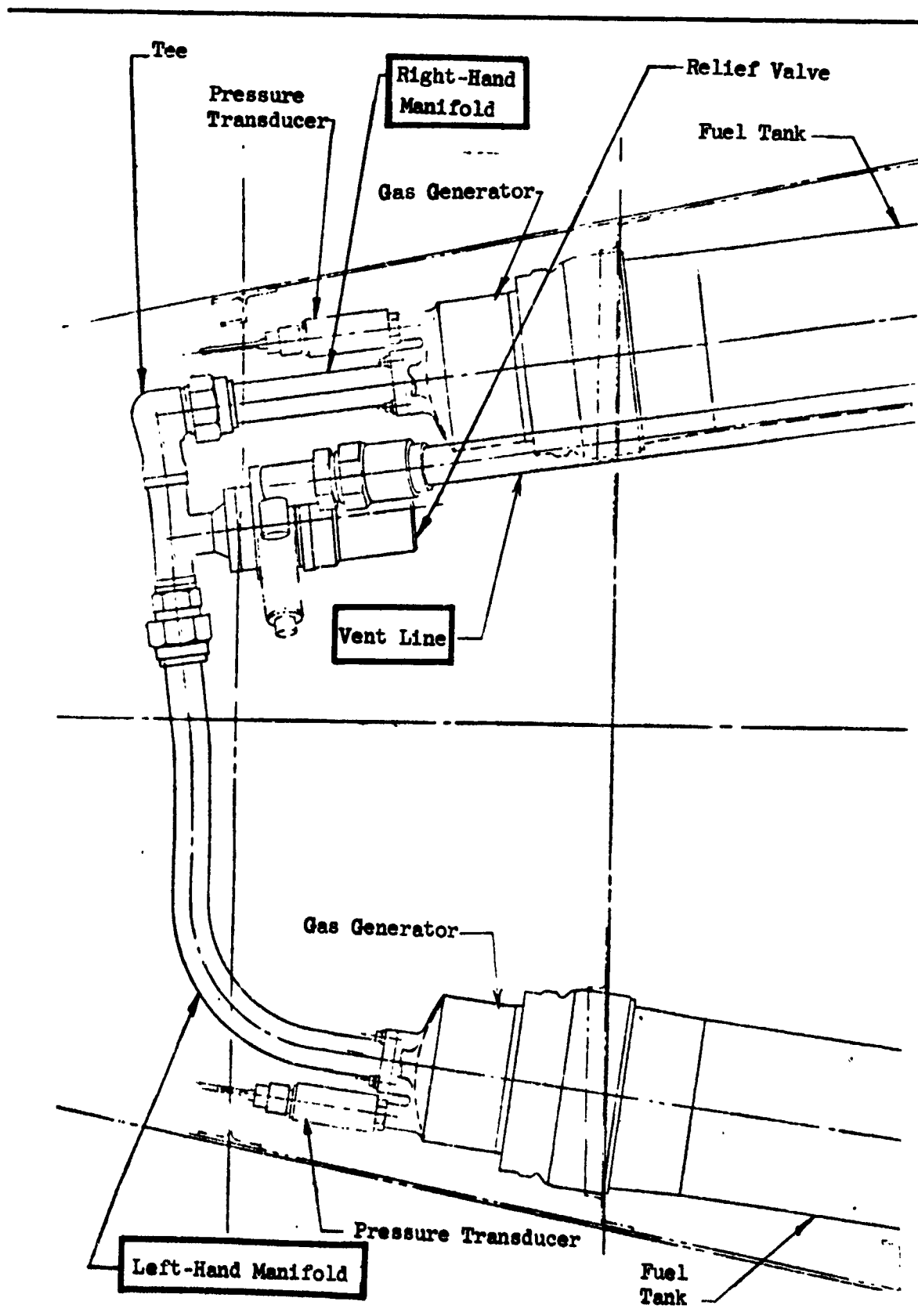


Figure 7-1. EB Hot Gas Manifold System

The original manifold design required a void-free, cast-in-place insulation coating of silicone rubber up to 0.250 inch thick, that would adhere well enough to the aluminum and titanium duct segments to withstand the gas flow. Liner ID and wall thickness tolerances were typically  $\pm 0.005$  inch. Later, the manifold design was changed to replace the silicone rubber lining with a combination of quartz/phenolic and zirconia-coated titanium liners, as shown in Figures 7-2 and 7-3. The latter liners were zirconia-coated by a proprietary spray process and then flat-wrapped with external quartz/phenolic insulation. The all-quartz/phenolic liner ID's were primarily 1.0 and 1.3 inches, and the quartz/phenolic liner thickness varied from approximately 0.100 to 0.150 inch. All dimensional requirements were met by machining the cured quartz/phenolic material. A minimum density of 100 pcf was required for all cured quartz/phenolic parts to ensure a complete cure so that proper ablation and strength properties would be obtained. In addition, the orientation of quartz cloth layers in the initial design was specified to be  $10 \pm 5$  deg to the gas flow direction. The orientation was changed later, as a result of fabrication and test experience. The adhesive bond between certain quartz/phenolic liners and the metal duct was required to be nondestructively inspected to ensure that no adhesive voids  $1/4$  inch or larger in diameter were present. In addition, the adhesive was required to be capable of curing below  $200^{\circ}\text{F}$  (to avoid overaging the 7075 aluminum ducts), and be resistant to exposure to  $200^{\circ}\text{F}$  in flight operation.

The JI nozzle density and dimensional requirements were the same as for the manifold liners. In addition, to ensure adequate strength to withstand pressure and combined loads, the cured flat-wrapped configuration was required to have a minimum of 10 continuous plies of quartz cloth within the 0.15-inch overwrap thickness; and no wrinkles greater than 0.060 inch in height were permitted.

## 7.2 APPROACH AND CONSTRAINTS

### 7.2.1 EB Liners

Only one fabrication method offered a reasonable potential for meeting the geometrical and dimensional requirements for the EB insulation. That method was to mold a silicone rubber liner to the required dimensions and to install it by insertion and adhesive bonding in the metal tube assembly.

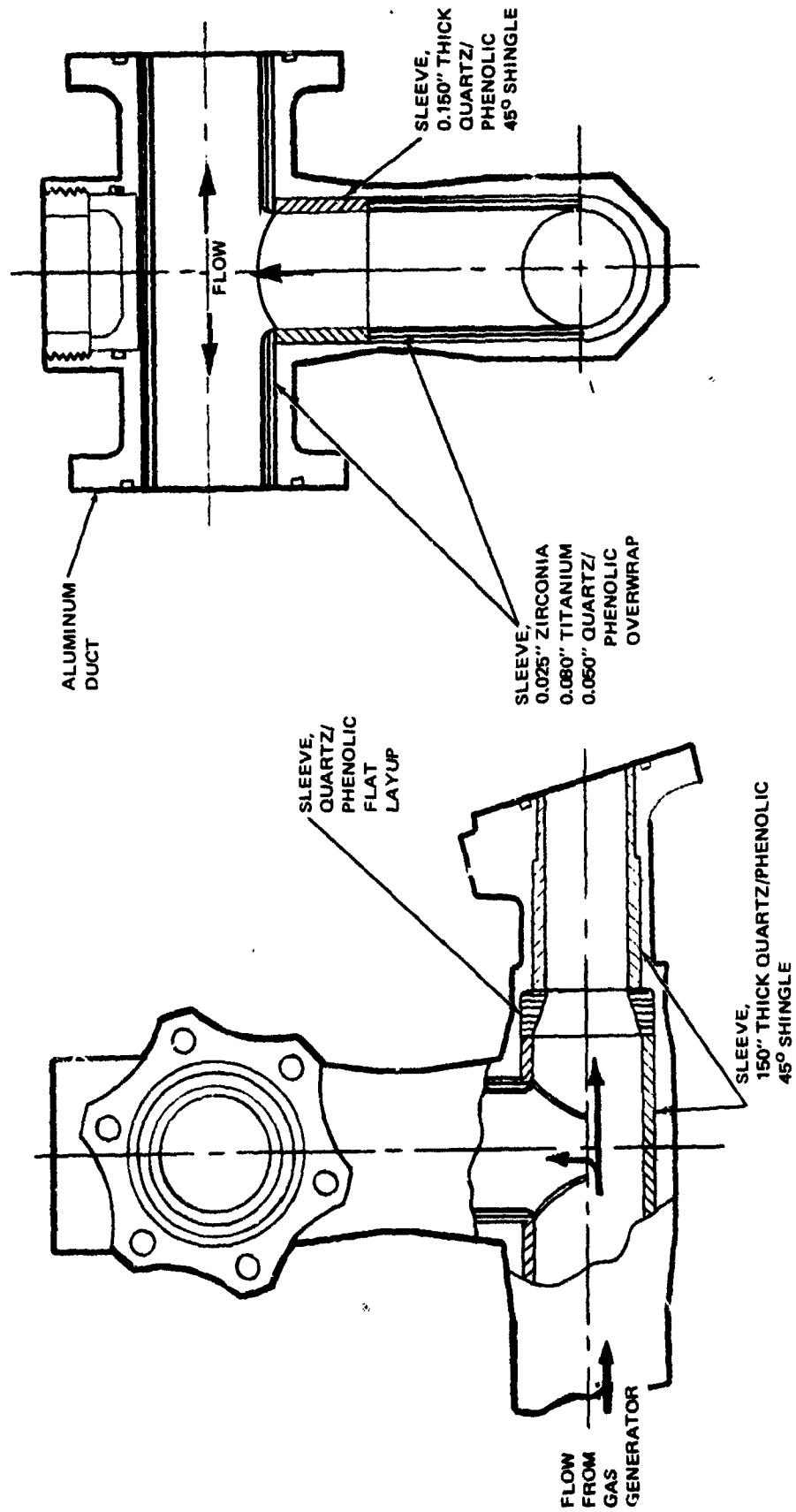
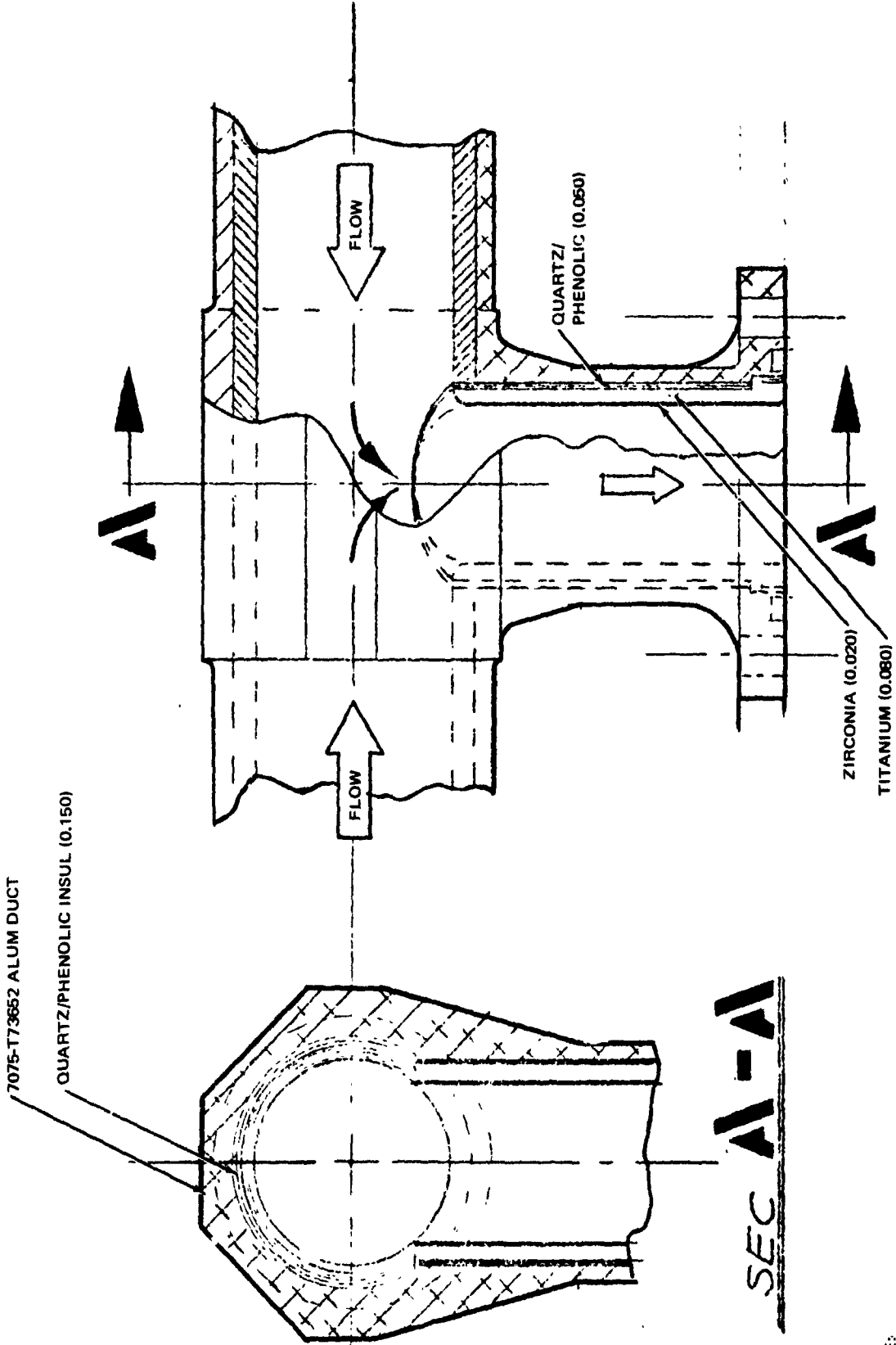


Figure 7-2. Redesigned J1 Manifold Inlet Tee Segment



NOTE:  
ALL DIMENSIONS IN INCHES.

Figure 7-3. Typical Segment of Redesigned J1 Manifold at Exit to Valve

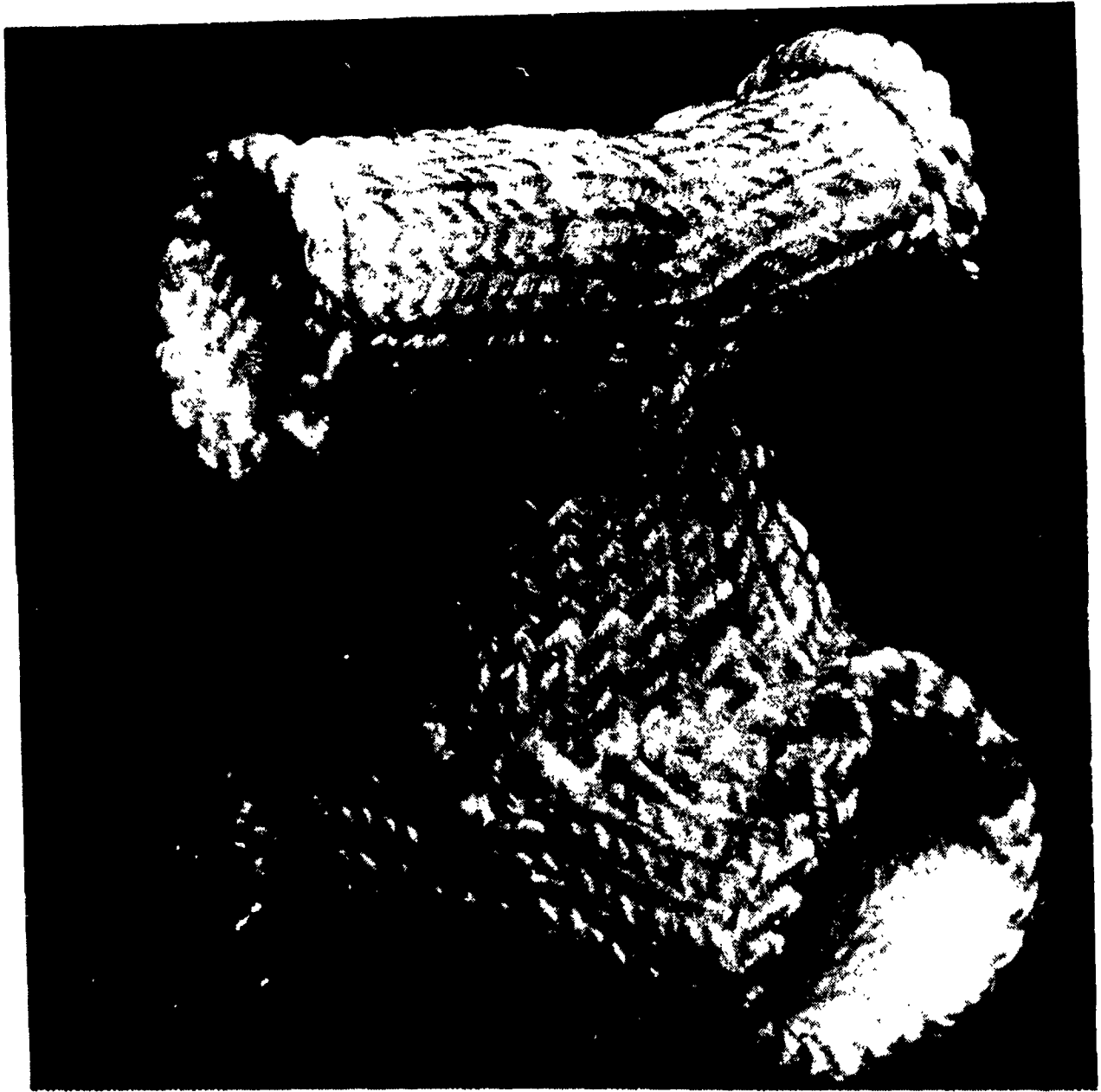
Preliminary tests were conducted to select the moldable silicone rubber with the best combination of moldability, tensile strength, bondability, and erosion properties. Subsequently, techniques for molding, insertion, adhesive bonding, and nondestructive bond inspection were developed for use on test hardware. As experience was gained in fabrication and functional testing, a number of design and process changes were made to obtain a satisfactory flight product.

### 7.2.2 JI Liners

The approach taken to develop cast-in-place silicone rubber liners was as follows:

- A. Determine the most suitable material by testing erosion and adhesion of the candidate materials.
- B. Design and fabricate practice parts and tooling to aid in cast-in-place technique development.
- C. Develop cast-in-place techniques.
- D. Using developed techniques, insulate test parts for experimental firings.

In developing the quartz/phenolic liners, prototype liners of the initial design (10-deg shingle angle) were wrapped manually on a mandrel using quartz/phenolic prepreg cut to the required tape width. Because the specified cloth orientation and liner wall thickness combination could not be successfully fabricated, alternate layup designs were developed and functionally tested to arrive at a satisfactory configuration. The final configuration for flight use included a "dinked" layup of conical washers, rather than a wrapped layup. Conventional layup, curing, and machining procedures were used throughout, with geometrical modifications. In addition, exploratory tests were conducted to develop a prefabricated quartz cloth "sock" (Figure 7-4). This approach was taken to relieve the erosion of internal tubular insulation at 90-deg intersecting joints by providing a rounded path to minimize turbulent flow conditions at these locations. The reinforcement in woven, braided, or knitted form was required to be capable of accepting phenolic resin and a "B" stage operation to provide a preimpregnated sock for insertion and curing within the metal ducts.



© DONNELLY GOLF COMPANY

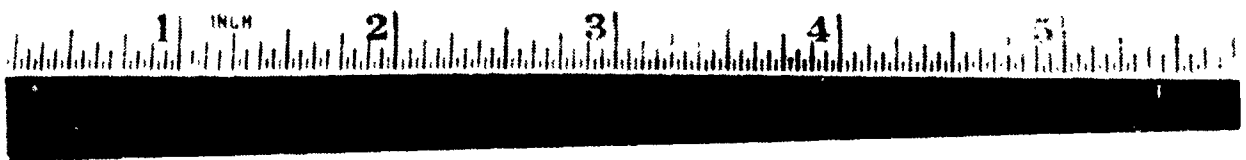


Figure 7-4. Knitted Liner (Double-Tee Configuration)

The approach taken to develop the nozzle insulation (see Figure 7-5) was to (1) flat-wrap the core of the nozzle exit cone; (2) densify (partially cure) and machine it; (3) assemble the titanium entrance nozzle, adhesive, and densified core (preform); (4) join the entrance nozzle and core with the flat-wrapped outer exit cone; (5) cure the assembly; and (6) machine final internal and external surfaces to the specified dimensions. As a result of functional tests, modifications were made to the design and process to obtain a satisfactory nozzle. Manual wrapping on a rotating mandrel was selected as the most economical method of wrapping the required quantity of parts to meet the schedule for ground test and flight parts.

Because of its success in producing void-free JI rubber liners, a cast-in-place technique was selected for void-free adhesive-bonding evaluation. Plexiglas practice parts and tools were designed, fabricated, and used to establish filling procedures and to select the most suitable adhesive. Tooling and processing concepts developed for the cast-in-place liners were applied directly to this adhesive-bonding problem. In addition, a pressure-injection method was selected and developed to bond quartz/phenolic liners inside existing quartz/phenolic liners. The approach to the nondestructive inspection of the bond integrity for the quartz/phenolic liner to metal tube bond was based on investigation of five potential techniques. These were ultrasonic pulse-echo, resonance-loading, eddy-sonic, x-radiography, and neutron-radiography. To evaluate these potential techniques, prototype standards and full-scale parts were made and subjected to nondestructive tests. From these tests, the most effective nondestructive test method was selected.

### 7.3 MOLDED SILICONE RUBBER LINERS

#### 7.3.1 Preliminary Tests

Five candidate solid moldable silicone rubber formulations and two liquid silicone adhesive systems were selected for preliminary processing and property tests on the basis of published properties, processing experience, and availability.

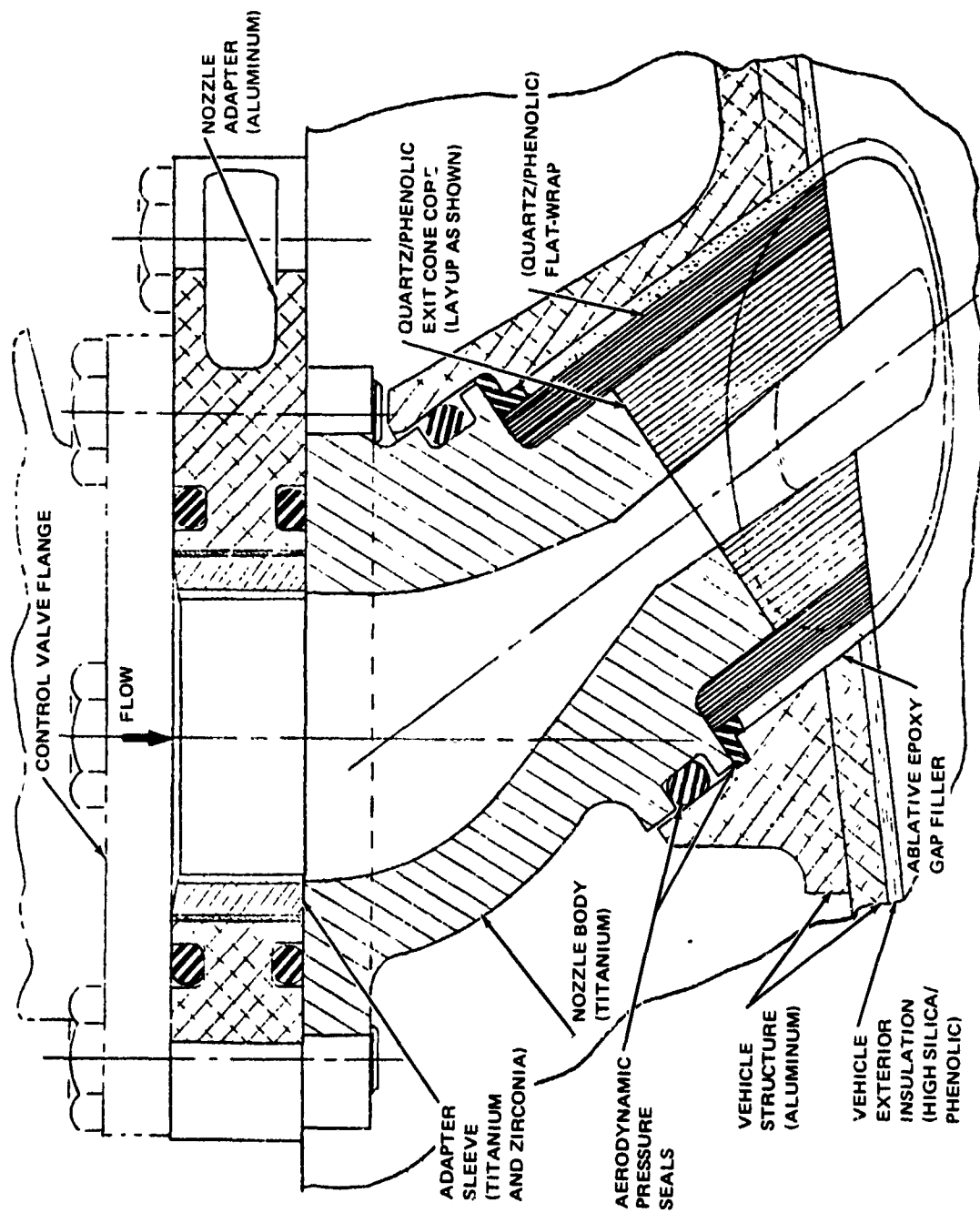


Figure 7-5. J1 Nozzle and Insulation Cross Section (U)

(U)

To assess the moldability and bondability of candidate liner materials, straight cylindrical tubes were molded and installed with the candidate adhesives in straight steel tubes. After curing, the lined tubes were sawed open and the strength and uniformity of the liner and bond were evaluated. Similarly, each of the candidate materials was molded into flat sheets from which samples were cut and prepared for tensile and erosion tests (refer to Report MP 51,603 in Appendix E).

Of the candidate materials, Silastic 55 bonded with RTV-731 exhibited (1) the best combination of bond strength and uniformity, (2) the highest tensile strength and elongation, and (3) good erosion performance based on material loss, backside temperature rise, and lack of charring ablation products.

### 7.3.2 Molding and Curing

Tests were performed to determine the linear shrinkage of Silastic 55 during curing so that correct compensations could be made in the mold cavity dimensions to produce a cured liner within the dimensional tolerances specified. A two-plate, single-cavity mold was machined from aluminum and provided with a steel rod core. Silicone rubber was sheeted to the correct thickness, wrapped longitudinally over the steel core, and "stitched" at the seam with a knurled roller to form an uncured tube of rubber around the core. This preform and core assembly was then placed in a two-plate mold, and the mold closed in a platen press under 10 tons of pressure at 320°F. The part was then cured for 30 minutes at this temperature and pressure. A mold release lubricant was applied to the core and the mold before pressing the rubber to facilitate removal of the part from the mold and core. At the conclusion of the press molding and subsequent to the removal of the part from the mold and core, the molded liner tube was postcured in a circulating air oven for 16 hours at 400°F. In order to inspect the liner wall thickness over the entire length, a rigid metal mandrel with an OD equal to the liner ID was made, supported horizontally, and numerous dial gage measurements were taken before and after the liner was placed on the mandrel.

Inspection of initial liners revealed three problem areas: (1) voids, (2) wall thickness variations, and (3) longitudinal stepped seams. The voids were caused by air bubbles entrapped during loading of the mold. It was found that if the core mandrel was wrapped with one ply of rubber having a carefully controlled thickness, and if the single seam was positioned at the mold parting line, that voids were eliminated.

Wall thickness variations were primarily caused by a center core mandrel that was not sufficiently straight. However, even when a new, straight core mandrel was used, wall thickness variations exceeded the specified  $\pm 0.005$  inch. Accordingly, the design was changed to allow wall thickness to vary up to  $\pm 0.010$  inch, which could be satisfactorily achieved in production. Stepped longitudinal seams were caused by lateral shifting of the mold halves relative to each other during heated-press curing of the liners. This problem was solved by adding dowel pins and holes to the mold halves to prevent sidewise movement.

### 7.3.3 Adhesive Bonding

Although preliminary tests with 6-inch-long straight tubes had produced satisfactory bonds, the first attempts to install a liner in a bent tube were unsuccessful. Apparently, the change in the internal dimensions of the metal tube in the bent region was too great to allow the liner to be drawn through. Accordingly, new liners were molded with slightly smaller OD's. These liners were successfully inserted.

During the manufacture and functional testing of the lined tubes, four problems occurred intermittently: (1) poor adhesion between the liner and the metal, (2) voids in the adhesive, (3) blistering following pressure testing, and (4) incomplete curing of the adhesive. As a result of these problems, the vent tube was redesigned to replace the lined configuration with an uninsulated heavy-wall design, and the process and test procedure for bonding the liners into the manifold tubes were changed in several ways.

Adhesion between the liner and the metal was affected by the methods used to clean and prime the metal and rubber surfaces, and apply and cure the adhesive. Numerous tests were conducted to determine a satisfactory combination of these methods.

Cleaning tests of the metal (Inconel 718) surface revealed that the conventionally descaled, cleaned, degreased surface could not be wetted by water. A light abrasive scrub activated the metal surface so that it could be water-wetted and thus be capable of being wetted by the adhesive primer. It was further observed that the descaling process was more effective when the metal surface was wetted by water. When the nonwetable metal covered with heat-treat scale was scrubbed with a paste of 400-grit aluminum oxide and water, the subsequent descaling treatment produced a bright, clear surface. This surface could be wetted for 1 hour after treatment at which time a water film on the surface would begin to bead. As a result, it was determined that proper surface preparation of the metal required priming within 1 hour of descaling and solvent degreasing. It was also determined that the metal primer had to dry and cure at ambient temperature for 1 hour minimum for best adhesion. To verify proper surface preparation, a strip of liner material was bonded to the metal OD surface of each manifold and tested for bond peel strength.

The rubber-cleaning method found to be most effective was methyl ethyl ketone (MEK) solvent wiping. (In addition, a water-soluble mold release was specified for the rubber molding operation. The mold release was easily removed from the cured liner surfaces by water washing.) Two primers were examined: a resin type, and an elastomeric type. The elastomeric primer produced liner-to-adhesive bonds that were more reproducible, and was therefore selected for use.

Voids in the adhesive were primarily a result of air entrapment during insertion of the liner. Changes in the insertion method were required to eliminate any possibility of air entrapment. Therefore, the vent tube liners were installed inside a vacuum chamber. Outside the chamber the liner and the tube ID were covered with adhesive. The liner was

collapsed around a mandrel (consisting of a 1/2-inch OD, 0.050-inch-wall plastic tube slit lengthwise) and positioned within the metal tube. These parts were placed in a vacuum chamber which was later evacuated. Next, the collapsed tube was expanded, in vacuum, against the ID of the tube wall with internal atmospheric pressure. The parts were removed from the vacuum, the mandrel was removed, the liner was pressurized to 14 psig, and the pressurized assembly was cured at 300°F for 1 hour.

Blisters which were found on the inside of lined tubes were observed to decrease in size and disappear after several hours. The blisters apparently formed when high-pressure gas diffused to the bondline during pressure testing and were unable to return to the inside of the liner during depressurization. The blisters were of concern because, in forming, they created unbonded areas. Blister formation was prevented on subsequent parts by (1) using a liquid pressurizing medium where possible, (2) requiring gas pressurization to be brief, and (3) allowing sufficient time during depressurization for entrapped gases to return to the liner ID.

Incomplete curing of the adhesive occurred first when RTV-731 was used. RTV-731 requires the presence of moisture to cure. Complete reaction was difficult to ensure with the tube liner configuration. Accordingly, 93-072, an elastomeric adhesive capable of curing without foreign reactants, was chosen to replace RTV-731. Unfortunately, 93-072 also exhibited incomplete curing from time to time, probably as a result of a weak inhibition reaction with the liner material. To overcome this problem, the liner was primed with diluted RTV-731, the curing temperature was raised to 300°F, and complete curing was verified by the bond test of a strip of liner material on the external surface of the metal.

#### 7.3.4 Nondestructive Bond Inspection

To determine the integrity of the bond, inspection had to be performed from the exterior of the tubing, working on the convex surface. Four techniques were considered potentially applicable. These were eddy-sonic, resonance-loading, interferometric holography, and ultrasonic pulse-echo.

The small diameter of the metal tube (approximately 1 inch) and the wall thickness (0.100 inch) were such that the eddy-sonic method was not effective. The means of excitation of the transducer was insufficient to discriminate between bonded liner and no liner at all. Therefore, it was not possible to detect the unbond conditions present in the test standard.

The resonance-loading method was successful to a limited extent in areas of large unbond. It was necessary to fabricate a special "V" block to keep the transducer properly aligned on the cylindrical surface of the tube. When small discrete areas of unbond were incorporated into the standard, the instrument could not clearly discriminate these unbonds.

Interferometric holography techniques were explored as a possible means of inspecting the rubber-lined manifold system. This approach had the advantage of being a noncontacting system, and no couplants such as oil or water were needed. To accomplish the test, two holograms were made of the test part, one with the part at rest and the second with the part under some minor stress. When these two holograms were superimposed, any defects, such as an unbond or an adhesive void, were expected to be displayed as an interference pattern. Holographic inspection of the test standard did not reveal any of the unbond conditions present. This is attributed to the fact that the elastic modulus of the metal tube was very much greater than that of the rubber liner, and the strains imposed on the metal were so small that no movement was detected at the exterior surface.

The pulse-echo approach required the use of a couplant material between the hand-held transducer and the surface of the test part. The wave front generated by the transducer was expected to traverse the metal and pass into the adhesive if there was a good bond. Ultrasonic energy absorbed in this way was expected to produce a highly damped signal on the oscilloscope screen. If, however, an unbond condition existed between the adherend and the adhesive,

the ultrasonic wave front was expected to be reflected and bounce back and forth several times. This would provide an oscilloscope screen presentation showing many back reflections, clearly different from the damped signal resulting from a good bond.

In the case of the metal tube and rubber liner, the pulse-echo approach proved unsatisfactory. It was not possible to distinguish between areas of unbond and those areas properly bonded. All areas provided multiple back-reflections on the oscilloscope screen. This behavior probably resulted from the large difference in acoustic impedance between the metal and the rubber.

#### 7.4 CAST-IN-PLACE SILICONE RUBBER LINERS

##### 7.4.1 Ablation and Adhesion Tests

Four candidate RTV silicones were tested on the MDAC Aeroder with the EB liner material (Silastic 55) and Teflon as controls. An attack angle of 10 deg was used. Results are given in Report No. MP51, 603 in Appendix E and in Table 7-1. On the basis of these data, RTV-630 was selected for further tests, because it exhibited a low erosion rate and no charring of the surface during ablation. A second series of Aeroder tests was conducted on RTV-630 at attack angles of 10 and 60 deg with  $\text{GN}_2$  stream temperatures of 3, 500 and 4, 000°F. Results are given in Table 7-1. As the results obtained for RTV-630 in the second series were substantially better than those obtained in the first series, a third series of Aeroder tests was initiated on RTV-630 at attack angles of 10, 30 and 60 deg with  $\text{CN}_2$  stream temperatures of 2, 400, 2, 900, and 3, 400°F. Teflon and Silastic 55 specimens were used as controls. In addition, specimens of 28-mil quartz cloth impregnated with RTV-630 were tested. The quartz cloth was impregnated with an excess of 8 mils of RTV-630 above and below the cloth. Data on these tests are also given in Table 7-1.

Table 7-1

RESULTS OF AERODER TESTS

Test Series	Date Tested	Material	GN <sub>2</sub>		Specimen Thickness (Mils)	Attack Angle (Deg)	Time of Test Exposure (Sec)	Erosion Depth (Mils)	Erosion Rate (Mils/Sec)	Surface Temperature (°F)
			Stream Temp (°F)	Temp (°F)						
1	8-20-69	Teflon	3,500	3,500	125	10	9.76	47	4.8	985
		RTV-630								
		RTV-630								
		Silastic 55								
2	5-10-71	Teflon	3,500	3,500	125	10	9.96	56	5.8	1050
		RTV-630								
		RTV-630								
		Teflon								
3	7-10-71	Teflon	2,400	2,400	125	30	5.96	17	2.9	1112
		RTV-630								
		RTV-630/Quartz								
		Teflon								
		Teflon	2,400	2,400	100	10	9.30	18	1.9	1436
		RTV-630								
		RTV-630/Quartz								
		Teflon								
		Teflon	2,400	2,400	45	60	5.90	19	3.2	1040
		RTV-630								
		RTV-630/Quartz								
		Teflon								
		Teflon	2,400	2,400	100	60	5.98	72	12.1	1202
		RTV-630								
		RTV-630/Quartz								
		Teflon								
		Teflon	2,400	2,400	45	60	4.04	52	12.9	1130
		RTV-630								
		RTV-630/Quartz								
		Teflon								

Table 7-1  
RESULTS OF AERODER TESTS (Continued)

Test Series	Date Tested	Material	GN <sub>2</sub>		Stream Temp (°F)	Specimen Thickness (Mils)	Attack Angle (Deg)	Time of Test Exposure (Sec)	Erosion Depth (Mils)	Erosion Rate (Mils/Sec)	Surface Temperature (°F)						
			Temp	Thickness													
3 (Contd)	7-10-71	Teflon	2,900	125	10	9.82	25	2.6	-	1427							
		RTV-630									100	9.71	22	2.3	1382		
		RTV-630/ Quartz									45	9.84	16	1.6			
		Teflon	2,900	125	30	2.22	10	4.5	-	1166							
		RTV-630									100	2.25	11	4.9	1058		
		RTV-630/ Quartz									45	2.18	11	5.1			
		Teflon	2,900	125	60	2.10	28	13.3	-	1040							
		RTV-630									100	2.19	43	19.6	1094		
		RTV-630/ Quartz									45	2.10	43	20.5			
			Silastic 55	3,400	125	10	9.88	54	5.5	-	1604						
												RTV-630	100	9.95	41	4.1	1562
												RTV-630/ Quartz	45	6.88	10	1.5	
			Silastic 55	3,400	100	10	9.85	71	7.2	-	932						
												Teflon	125	3.77	27	7.2	1292
												RTV-630	100	5.79	60	10.4	
		Silastic 55	3,400	100	30	3.87	34	8.8	-	-							
											RTV-630/ Quartz	45	5.83	91	16.0		

Table 7-1  
RESULTS OF AERODER TESTS (Continued)

Test Series	Date Tested	Material	GN <sub>2</sub>		Stream Temp (°F)	Specimen Thickness (Mils)	Attack Angle (Deg)	Time of Test Exposure (Sec)	Erosion Depth (Mils)	Erosion Rate (Mils/Sec)	Surface Temperature (°F)
			Temp (°F)	Thickness (Mils)							
3 (Contd)	7-10-71	Teflon				125	60	2.99	43	14.4	-
		RTV 630				45	60	2.00	BT	-	1094
		RTV 630				45	60	1.37	BT	27.0	1022
		RTV 630		3,400		100	60	2.93	77	26.0	1220
		RTV 630				200	60	3.93	134	34.0	1202
		RTV 630/ Quartz Silastic 55				45	60	1.67	34	20.4	1238
					100	60	2.05	53	25.9	-	

BT = Burn-through

The peel adhesion of RTV-630 was tested on flat 4- by 6-inch panels of titanium of the type used for the manifold functional test parts. As the conventional methods of surface preparation and priming did not yield reproducible results, a study of primers and surface preparation methods was initiated. The results of this study are presented in Table 7-2. The most consistent method of surface preparation was found to be as described for Specimen No. 33 in the table using SS-4155 primer.

#### 7.4.2 Casting and Curing

An aluminum practice part similar to the flight configuration manifold was fabricated. Cores, mandrels, and end rings were fabricated to provide the assembly shown in Figures 7-6 through 7-9. When assembled, the cores provided a 0.200-inch-thick coating on the walls of the central tube of the assembly. Figures 7-8 and 7-9 show cutaway views of the central tube and of one side tube.

##### 7.4.2.1 Gravity Flow into an Evacuated Cavity - Test A-1

A vacuum bag with bleeder cloth was sealed over the bottom of the assembly, the side openings were vacuum sealed, and a reservoir assembly was affixed to the top of the assembly as shown in Figure 7-8. A 29-inch-Hg vacuum was applied to the part and the reservoir was filled with catalyzed and degassed RTV-630. The assembly was left with vacuum on for 1 hour and then the entire assembly was put in an oven at 210°F for 1 hour. After cooling and disassembly, it was found that very little RTV-630 had gone into the cavity. The RTV-630 had run rapidly to the bottom, blocking off the vacuum source. The cores were removed and, as the interior walls of the practice part had not been primed, the cured RTV-630 was cut and pulled out of the cavity.

##### 7.4.2.2 Gravity Flow into an Evacuated Cavity - Test A-2

Test A-2 was conducted in the same manner as Test A-1 except that the vacuum bag seal and bleeder cloth were extended around the entire part except for the reservoir on top. After cure and cooling, it was found that 60 percent of the cavity was filled, with material still remaining in the reservoir. The coating was removed from the practice part.

Table 7-2

## PEEL ADHESION TEST RESULTS

Specimen Number	Cleaning Method	Primer/ Lot No.	Primer Drying Time	Load (psi)	Type of Failure	
					% Cohesion	% Adhesion
1	Methyl ethyl ketone cleaned	SS-4155 Lab Lot 1	1 hr RT*	16	25	75
7	Vapor-honed	SS-4155 Lab Lot 1	1 hr RT	0	0	100
8	Grit-blasted	SS-4155 Lab Lot 1	1 hr RT	21	90	10
9	Etched per PS 12050.8	SS-4155 Lab Lot 1	1 hr RT	0	0	100
11	MEK cleaned	SS-4155 Lab Lot 2	1 hr RT	22	100	0
13	MEK cleaned	SS-4155 Lab Lot 2	1 hr RT	31	80	20
14	Vapor-honed	SS-4155 Lab Lot 2	1 hr RT	0	0	100
15	MEK cleaned	SS-4155 Lab Lot 2	1 hr RT	9	10	90
		Plus Thin Coat RTV154				
19	MEK cleaned, 60 grit-sanded, MEK cleaned	SS-4155 Lab Lot 2	1 hr RT	32	100	0
22	MEK cleaned	PR-1903	1 hr RT	0	0	100
23	MEK cleaned	DC 92-056	1 hr RT	25	80	20
24	MEK cleaned	DC 1200	1 hr RT	0	0	100
29	MEK cleaned	DC 92-019	1 hr RT	0	0	100
30	MEK cleaned	DC 92-019	10 hrs RT plus 1/2 hr 180° F	0	0	100
31	MEK cleaned	SS-4120	1 hr RT	0	0	100
32	MEK cleaned	SS-4155 Lab Lot 2	1 hr RT	0	0	100
33	MEK cleaned plus power-drum sanded (30 grit) plus MEK clean	SS-4153 Lot 94218	1 hr RT	25	100	0

\*RT = Room temperature



**Figure 7-6. Practice Test Part Assembled with Cast-in-Place Silicone Liners**

---

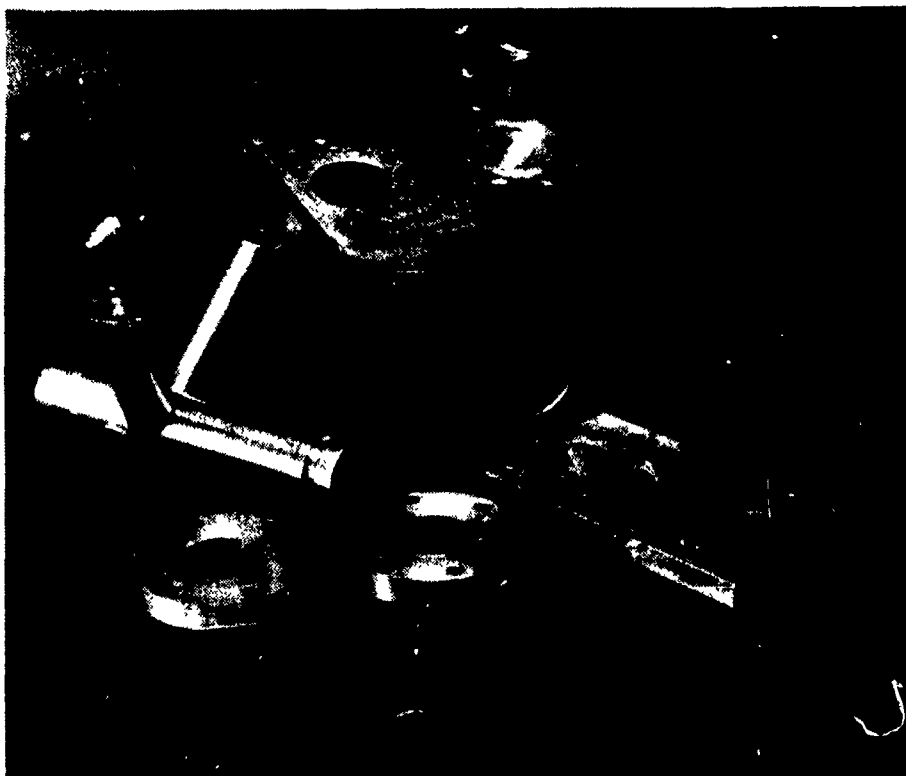


**Figure 7-7. Practice Test Part Disassembled with Cast-in-Place Silicone Liners**

---

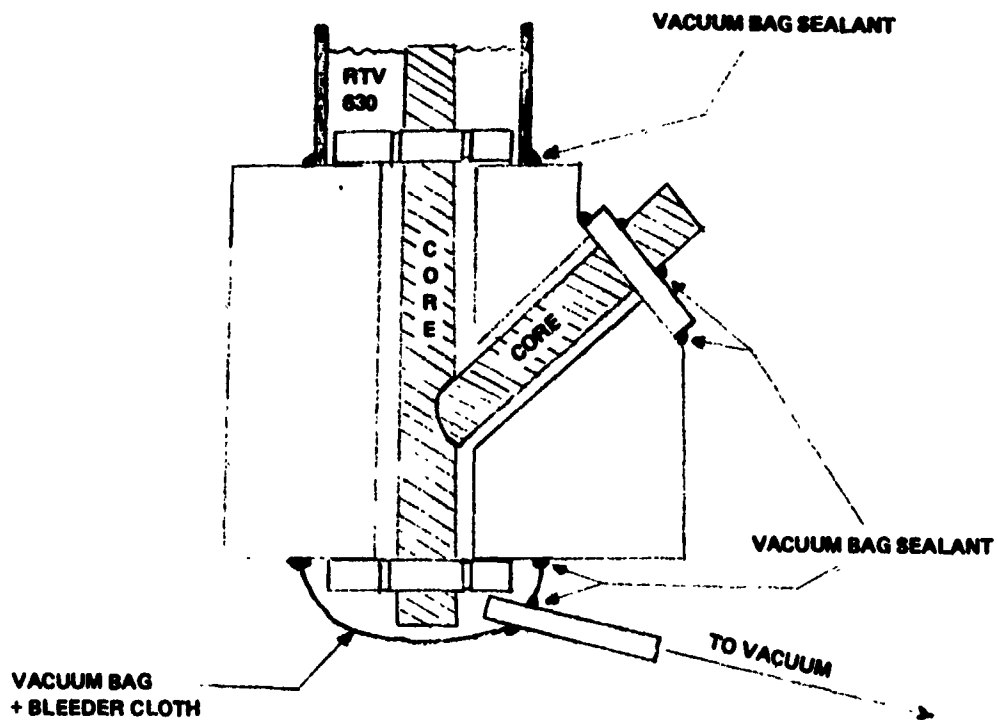


Figure 7-8. Gravity Flow into Evacuated Cavity

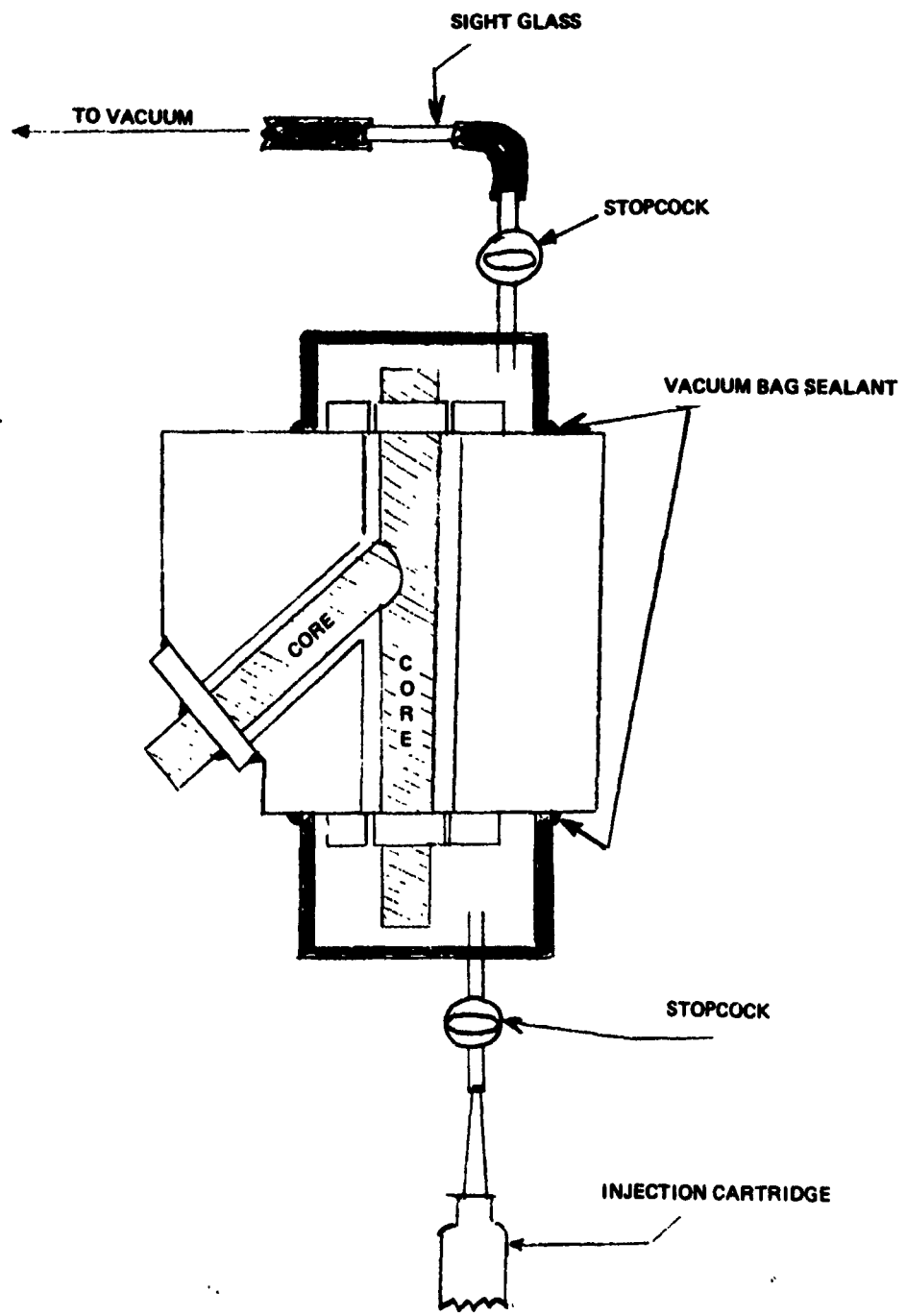


Figure 7-9. Pressure Injection into Evacuated Cavity

#### 7.4.2.3 Pressure Injection into an Evacuated Cavity - Test B-1

Closed reservoir caps with stopcocks were fabricated for the top and bottom of the practice part as shown in Figure 7-9. These caps were adhered and sealed to the part, as shown, with vacuum bag sealant. An injection cartridge was filled with catalyzed and degassed RTV-630. After the assembly was checked for leakage at 29 inches of vacuum, the RTV-630 was injected at 5 psig into the assembly, at full vacuum, by inserting the injection nozzle into the opening below the stopcock and opening the stopcock. The RTV-630 was injected into the assembly until it appeared in the sight glass above the assembly. The vacuum was released and the assembly was transferred to an oven at 210°F for 2 hours. After cooling, the side cores were pulled out and the central core was forced out on an arbor press. Although the upper reservoir cap was filled with RTV-630, there was a void about 1 inch in depth below the upper retaining ring. The RTV-630 expanded under vacuum and the void, formed by contraction after release of vacuum, did not fill from the upper reservoir. The coating was removed.

#### 7.4.2.4 Pressure Filling of Evacuated Cavity - Test B-2

Test B-2 was conducted in the same manner as Test B-1 except that after the RTV-630 appeared in the upper sight glass, the vacuum was released and the vacuum hose removed from the upper stopcock. The injection of RTV-630 was resumed at 5 psig without vacuum until there was an uninterrupted flow of the material out of the upper stopcock. The assembly was transferred to an oven at 210°F for 2 hours. On being disassembled as in Test B-1, the part was found to be completely filled with RTV-630 and was void-free.

#### 7.4.2.5 Pressure-Vacuum Filling of Manifold Functional Test Parts

The interior surfaces to be coated with RTV-630 were prepared as described for Specimen No. 33 in Table 7-2. A rotary power-sanding drum was used for abrading the interior surfaces. The parts were filled as in Test B-2 except that improved tooling was used as shown in Figure 7-10. The parts were cured a minimum of 4 hours at 210°F. After cooling, the cores were removed. The insulation coatings were found to be dense and void-free.

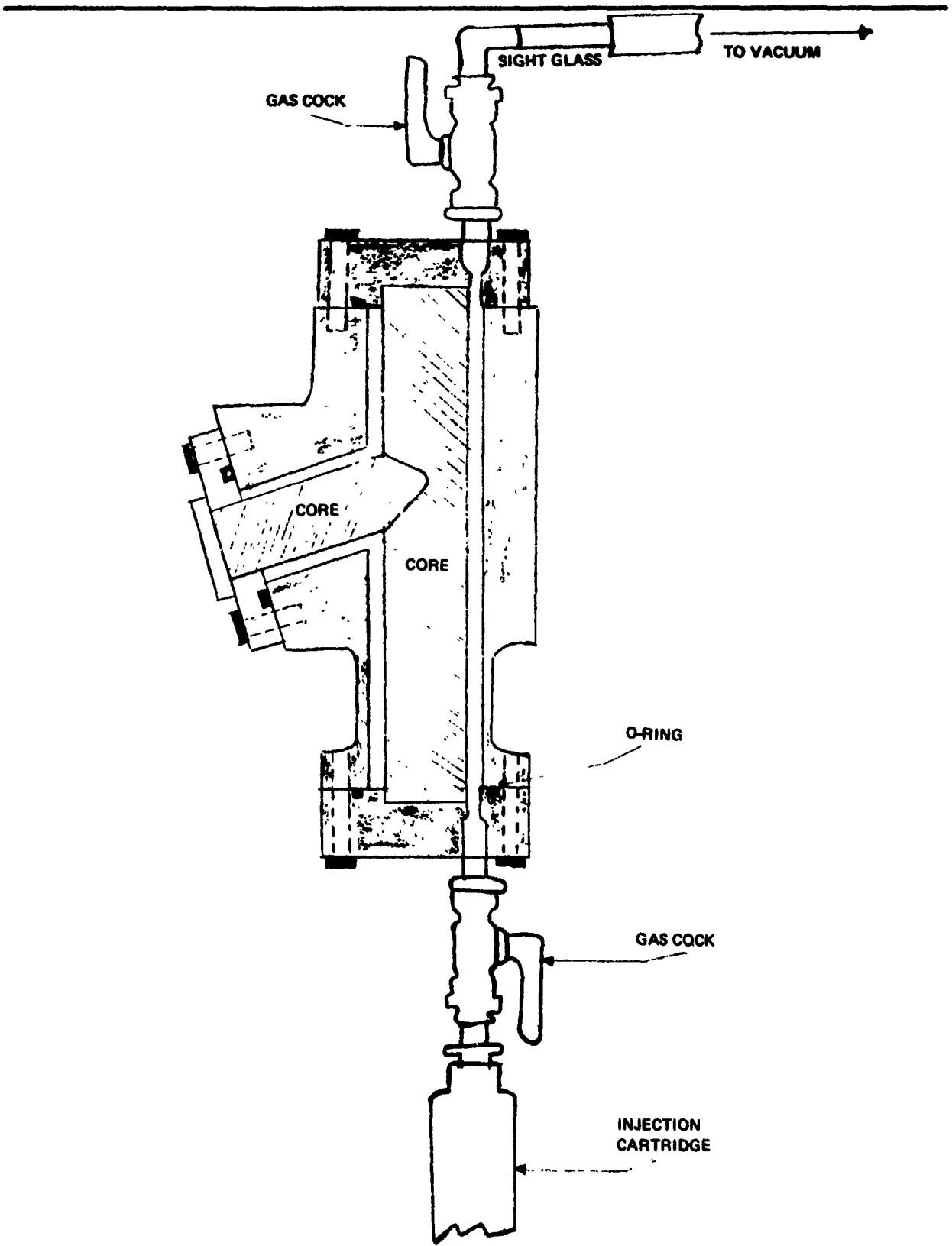


Figure 7-10. Pressure Injection into Evacuated Cavity of Manifold Functional Test Part

As described in Reference 7-2, the erosion resistance of the cast-in-place RTV-630 liners was unsatisfactory. The design of the manifold was subsequently changed to eliminate RTV-630 and no further process development was pursued.

## 7.5 QUARTZ/PHENOLIC LINERS

### 7.5.1 Layup and Curing

#### 7.5.1.1 Flat Shingle Angle Configuration

A tape-wrapping procedure was employed to provide a shallow (10 deg) angle configuration tubular composite. It became evident early in initial fabrication efforts that the method was limited in providing the required thickness when quartz/phenolic tape was wrapped around a relatively small (1 inch) diameter mandrel. The reason for this was that the OD edge of the tape would not stretch sufficiently to conform to the required conical shape for the entire liner thickness. A two-step process was therefore followed in which the 10-deg shingle angle configuration was wrapped using narrow tape, densified and machined to a smaller OD, and then over-wrapped with a flat-wrap of the same material to obtain the required liner wall thickness. The two-step-fabricated "green" part was then vacuum-bagged and autoclave-cured. Sufficient over-wrap material was provided so the cured part could be machined to the required OD.

The cure procedure employed a preliminary densification step at 160°F and 50 psig autoclave pressure under vacuum, followed by stepwise increases in pressure and temperature to a final cure dwell at 350°F and 180 psig for a period of 3 hours while still employing vacuum. Part density achieved varied from a low of 102 pcf to a maximum of 140 pcf.

Test firings were completed on components employing the flat shingle angle configuration. It was observed that in the insulated straight sections, erosion did not reach the flat-wrap portion of the insulation. However, in the high-erosion locations (one or two diameters from 90-deg turns), erosion was

observed in the flat-wrap layer. Consequently, the design was changed to require a  $45 \pm 5$  deg shingle angle, which required development of a new process.

#### 7.5.1.2 45-Deg Shingle Angle Laminate

To obtain a 45-deg shingle angle, the use of pre-cut (dinked) disks in flat washer form was investigated. Tooling was provided to assemble these disks at a 45-deg angle over a central shaft mandrel as a preform assembly within a restraining cylinder. This preform assembly became the curing tool when the required end-cap tooling was added. Moderate preforming pressure was applied to locate the disks initially until the required number of disks were loaded to achieve the desired part length. The preform was then cured in a platen press in a stepwise fashion.

Initially, the assembly was subjected to a dwell at  $160^{\circ}\text{F}$  for a period of 1 hour at contact pressure to provide initial resin flow. Subsequently, the part temperature was raised to  $220^{\circ}\text{F}$  and the load increased to 6 tons. While maintaining this load, the part was raised to  $350^{\circ}\text{F}$  for the final dwell cure of 3 hours at load.

The above process provided a molded-quartz/phenolic 45-deg-angle composite with densities of 109.4 pcf minimum to 111.3 pcf maximum. The procedure overcame the limitation of maintained angle versus thickness experienced with the wrapped technique as well as the OD/ID limitations previously experienced.

#### 7.5.1.3 Nondestructive Inspection

Tests were conducted to develop a nondestructive method for determining the shingle-angle orientation of fully machined liners. X- and neutron-radiography, as well as microscopic and visual examination, were investigated. It was found that the laminate orientation of installed liners could best be determined by careful examination of tangential x-rays with the aid of a low-power magnifying glass, using a high-intensity x-ray film viewer.

### 7.5.2 Adhesive Bonding

A double-tee manifold practice part was designed and fabricated from a Plexiglas block. Simulated quartz/phenolic insulation liners and end caps were fabricated from aluminum. The Plexiglas part with the simulated insulation bonded in place is shown in Figures 7-11 and 7-12. Three mutually perpendicular liners were required: a lower (inlet) liner, a vertical liner, and an upper liner.

#### 7.5.2.1 Bonding the Lower Insulation Liner

All tooling aids and the interior of the Plexiglas block were coated with mold release to aid in removal, if required, of the cured or uncured resin. The lower insulation liner was inserted. Small shims to hold the liner to allow a concentric gap of 7 to 10 mils around the liner were positioned in three places at each end. Several tests employing various combinations of vacuum and resin introduction were made. The best technique was as illustrated in Figure 7-13. The resin used was catalyzed and degassed and placed in the injection cartridge with the adjacent valve closed. A vacuum of 29 inches of mercury was applied to the part and the part was checked for leakage. After all leakage was eliminated, the valve adjacent to the resin reservoir was opened. The resin flowed easily around the lower insulation liner, which was plugged on each end as shown.

Epon 919 epoxy resin was the first resin tested. While curing 24 hours at room temperature, this resin exhibited a large amount of shrinkage which was manifested in large areas of debonding. Stycast 2850-FT epoxy resin was tested next. This resin required a 160°F oven cure and also exhibited debonding due to unequal expansion and contraction between the plastic block and the metal liner. EC-2216 epoxy resin was tested next. This resin proved, on curing 16 hours at room temperature, to have low shrinkage, and a continuous bond line was achieved. EC-2216 was used in the balance of the tests described herein, and for all vacuum bonding of JI liners.

A laboratory comparison of the volume shrinkage during cure of Epon 919 and EC-2216 was also made. These data are presented in Table 7-3, and show the relatively low volumetric shrinkage of EC-2216. After curing, the top

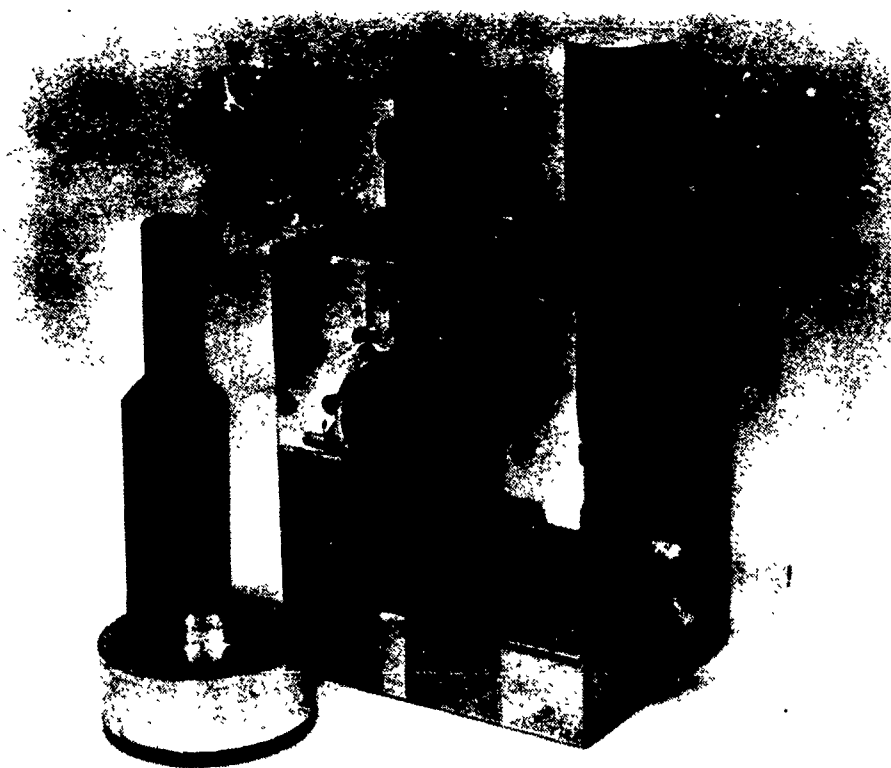


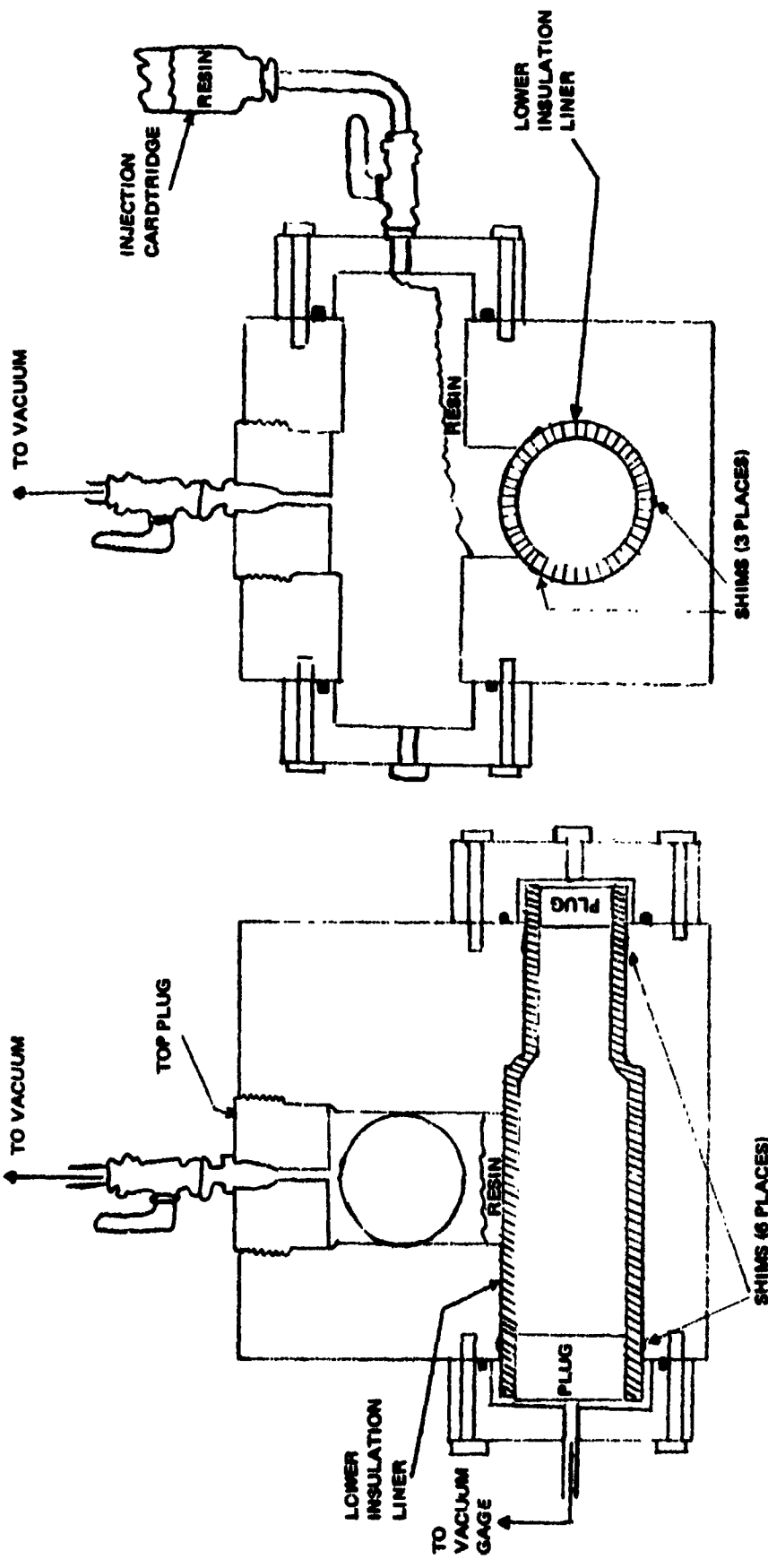
**Figure 7-11. Plexiglas Simulation of JI Double-Tee Manifold Part - Side View with Tooling Aids**

---



**Figure 7-12. Plexiglas Simulation of JI Double-Tee Manifold Part - Front View**

---



FRONT VIEW  
 LOWER END CAP OMITTED  
 FOR CLARITY

SIDE VIEW  
 UPPER END CAP OMITTED  
 FOR CLARITY

Figure 7-13. Bonding the Lower Insulation Liner into Plexiglas Simulation of J1 Double-Tee Manifold Part

Table 7-3

## COMPARISON OF VOLUME SHRINKAGE OF EPON 919 AND EC-2216

	Epon 919	EC 2216
Volume of Mold (cc)	160.7	161.1
Weight of Cured Block (g)	167.7	205.9
Specific Gravity	1.12	1.30
Volume of Cured Block (cc)	149.7	158.4
Volume Loss (cc)	11.0	2.7
Volume Shrinkage (%)	6.6	1.7

plug was removed and a hole of the same diameter as the vertical shaft was drilled through the excess cured resin and through the upper wall of the lower insulation liner, in the same manner as would be done in production.

#### 7.5.2.2 Bonding the Vertical Insulation Liner

The vertical insulation liner, a duplicate piece of which is seen on the right top of the Plexiglas block in Figure 7-11, was placed in the vertical shaft and three shims were placed around it at the upper edge of the vertical shaft. A precast epoxy mandrel, seen standing to the left of the Plexiglas block in Figure 7-11, was inserted into the bonded lower insulation liner. With the assembly as shown in Figure 7-14, the resin was catalyzed, degassed, and placed in the reservoir above the block with the valve below the reservoir closed. Vacuum at 29 inches of mercury was applied to the parts. After leaks were sealed, the valve was opened and the resin allowed to flow around the vertical liner. After curing 16 hours at room temperature, the end caps were removed and the excess upper vertical liner section and the excess cured resin were drilled out horizontally through the upper tube.

#### 7.5.2.3 Bonding the Upper Insulation Liner

The upper insulation liner, which had a hole predrilled in the side, was placed in the block with shims at each end and the side holes lined up with

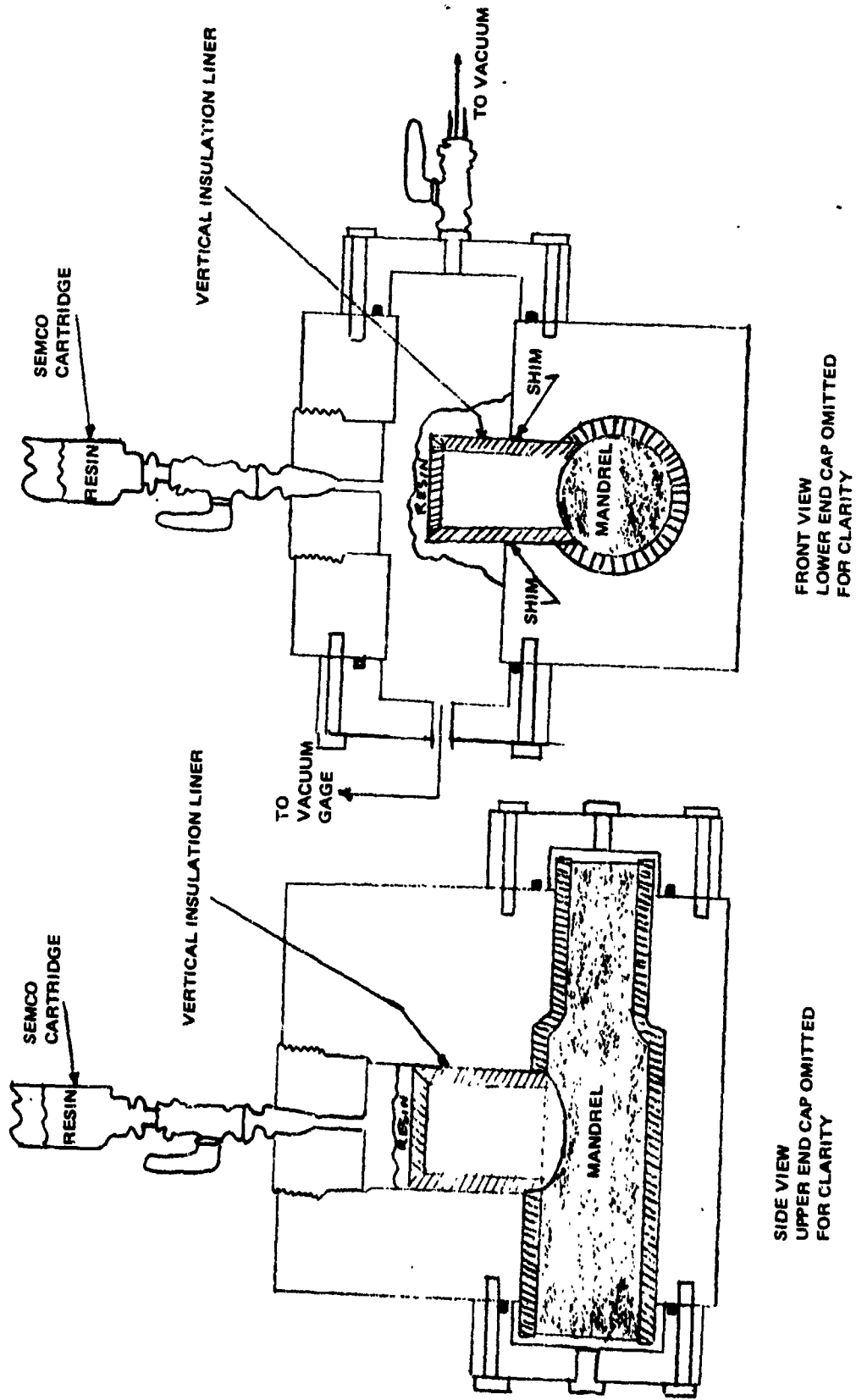


Figure 7-14. Bonding the Vertical Insulation Liner into Plexiglas Simulation of JI Double-Tee Manifold Part

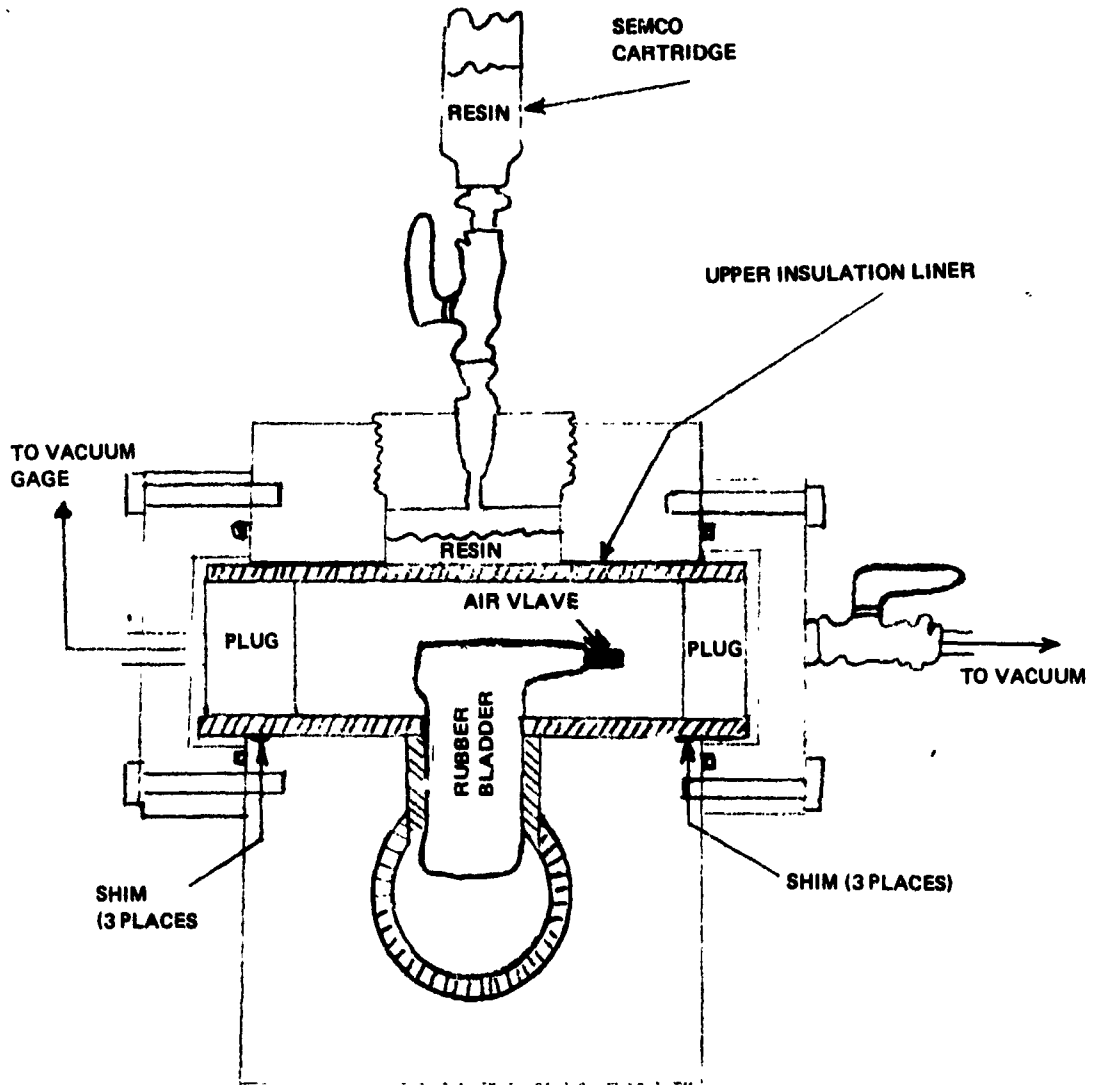
the vertical shaft as shown in Figure 7-15. A rubber bladder was fabricated to fill the vertical shaft area. The function of this bladder was to keep the resin out of the vertical shaft area, which is inaccessible for post-cure cleaning. The bladder was inflated to 5 psig. With the upper insulation liner plugged at each end, vacuum at 29 inches of mercury was applied to the part. After leakage was sealed, the catalyzed and degassed resin was allowed to flow around the upper insulation liner. Before cure, the excess resin was removed below the top plug.

#### 7.5.2.4 Bonding Liners to JI Manifold Functional Test Parts

Various liners of quartz/phenolic, quartz/phenolic-wrapped ceramic, and quartz/phenolic-wrapped titanium-zirconia were bonded to JI manifold test parts using techniques described above with minor variations. As the parts were metal, the end caps were fabricated from Plexiglas to facilitate observation of the resin flow. Results of the tests appear in Reference 7-2.

#### 7.5.2.5 Pressure Injection Bonding

A design change to add additional internal insulation to the JI manifold required the bonding of a 0.150-inch-thick quartz/phenolic "patch" liner in an existing 1.3-inch-ID quartz/phenolic-lined segment. Because of the configuration, vacuum bonding was difficult, and a new method was developed. The new method involved machining longitudinal grooves 0.080 inch wide and 0.025 inch deep on the patch liner OD. A special injection tool was designed and fabricated to allow adhesive to be injected from a standard 90-psig injection cartridge into an annular space at one end of the patch liner, forcing the adhesive to fill the grooves. Using a Plexiglas model, a low-viscosity epoxy adhesive was injected in this manner, filling the 2-inch-long grooves completely. Two test specimens were fabricated with this method, using grooved patch liners which fit snugly into cylindrical outer liners, both made of quartz/phenolic. Shear tests of these test parts were conducted and showed that the shear strength of the bond exceeded the design requirement by a factor of six.



FRONT VIEW  
 LOWER END CAP OMITTED  
 FOR CLARITY

Figure 7-15. Bonding Upper Insulation Liner into Plexiglas Simulation of JI Double-Tee Manifold Part

### 7.5.3 Nondestructive Bond Inspection

Two test standards were constructed, each containing four sizes of simulated discrete defects. Aluminum tubing of 1-3/4-inch OD with a 1/8-inch wall was used. A quartz/phenolic liner with a 3/16-inch-thick wall was made to fit inside the tube. Both were cut 12 inches long and were split lengthwise before bonding. Four sizes of holes were drilled in each half of the liner: 1/8-, 1/4-, 3/8-, and 1/2-inch diameter. Quartz/phenolic plugs were made to fit the holes. The liners were then bonded to the inside surface of the tube halves. After curing, the holes in the liner of each assembly were cleaned of all excess adhesive. In one of the standards, the plugs were inserted and bonded in the holes, leaving an air gap between the plug and the aluminum wall equivalent to the original bond line thickness, to simulate voids in the adhesive. For the second standard, the plugs were coated on one surface with adhesive and cured, then inserted with the cured adhesive against the aluminum surface to simulate unbonds between the aluminum and the adhesive.

Using these prototype standards, four potentially applicable and available nondestructive test techniques were evaluated. Limited effort with resonance-loading, eddy-sonics, and x-radiography indicated that none of these methods effectively detected the simulated defects. Based on the initial work, it appeared that manual contact pulse-echo ultrasonic inspection would be the only usable method. The minimum size of detectable unbond or adhesive void by this method was 1/4 inch, except that defects beneath nonuniform metal cross sections could not be detected at all.

Additional investigations later showed that very careful inspection of enhanced x-radiographs was capable of detecting some adhesive voids. Also, neutron radiography was found capable of revealing voids as small as 1/8 inch in diameter with ease and clarity. Accordingly, neutron radiography was employed to inspect all manifold segments for voids.

#### 7.5.4 Knitted Quartz/Phenolic Liners

A number of right-angle and Y-sections were braided. Upon examination of these articles, it was observed that in the most critical area (the rounded corners at the intersections), the fiber density was low and variable. This was an inherent characteristic of the braiding process and unsatisfactory. Vendors were also contacted relative to the feasibility of obtaining woven or knitted articles. Although this approach appeared promising, time and budget constraints did not permit its further pursuit. Accordingly, two quartz-fiber sock liners were knitted manually at MDAC to examine straight sections with and without a flared end. The flared-end approach provided the desired rounded edge at an intersection (to promote a more streamlined flow). The hand-knitted quartz liners were impregnated with phenolic resin and partially cured (B-staged) by heating at 180° F for a dwell period of 30 to 40 minutes.

The straight liner prepreg was slipped over a metal mandrel and given an over-wrap with quartz/phenolic tape. The liner was then vacuum-bagged and cured using procedures similar to those employed for dinked liners.

The flared-end liner prepreg was inserted into a matching primed metal sleeve and cured by inserting a rubber bladder (for internal pressurization), vacuum-bagging, and curing.

The knitted liners were subsequently bonded into a JI functional test manifold, using epoxy adhesive. The bonding process used was a standard one. No processing problems were observed. Results of the functional test of the knitted material are reported in Reference 7-2.

In addition to the functional test knitted parts, additional knitted liners were made, but not impregnated, to establish the feasibility of knitting complex tee and cross configurations. Figure 7-4 shows the most complex configuration that was made. It was found that glass, high-silica, and quartz fibers had very similar knitting characteristics, and that ordinary knitting needles

could be used, although frequent replacement was required because of abrasive wear by the yarn. No additional sock development was pursued because the design baseline approach (dinked quartz liners) performed satisfactorily.

#### 7.6 QUARTZ/PHENOLIC NOZZLE FABRICATION

Figure 7-5 shows a cross section of the JI nozzle assembly, as originally designed. The initial manufacturing sequence for the insulation began with the fabrication of a machinable quartz/phenolic flat-wrapped core preform. The preform was given a preliminary densification step in an autoclave at 160°F, 50-psig pressure, with vacuum, for a dwell period of 50 minutes. After densification, the preform was machined to match the titanium nozzle body end. The titanium was then grit-blasted and primed, and adhesive was applied to the OD and end surfaces. The assembly, consisting of the titanium body and mated quartz/phenolic preform, was then over-wrapped (flat) with quartz/phenolic tape and cured.

The first approach was to flat-wrap the core preform to obtain the configuration shown in Figure 7-16a. The densification, machining, assembly, bonding, over-wrap, and curing steps were as described for the liners in Subsection 7.5.1.1. Initial functional testing with this configuration was successful, except that an undesirable amount of erosion was measured in the insulation. As an added factor of safety, it was desired to try to reduce the observed erosion by changing the ply orientation in the core insulation, as shown in Figure 7-16b.

Preform tooling was provided to permit fabrication of a vee- or chevron-shaped preform having a 30-deg angle. Rectangular pieces were precut from a quartz/phenolic prepreg and preformed at 1,000-psi pressure to provide a preform of the required geometry in terms of angle, width, depth, and height. This preform was densified, machined, assembled to the titanium nozzle body, and cured as the flat-wrap configuration was. The orientation of the angled preform assembly to the nozzle body was such that the desired laminate angle was presented to the internal gas flow to minimize peeling effects (30 deg to the flow direction). In functional tests, this configuration failed structurally (see Reference 7-2), so no additional development was pursued.

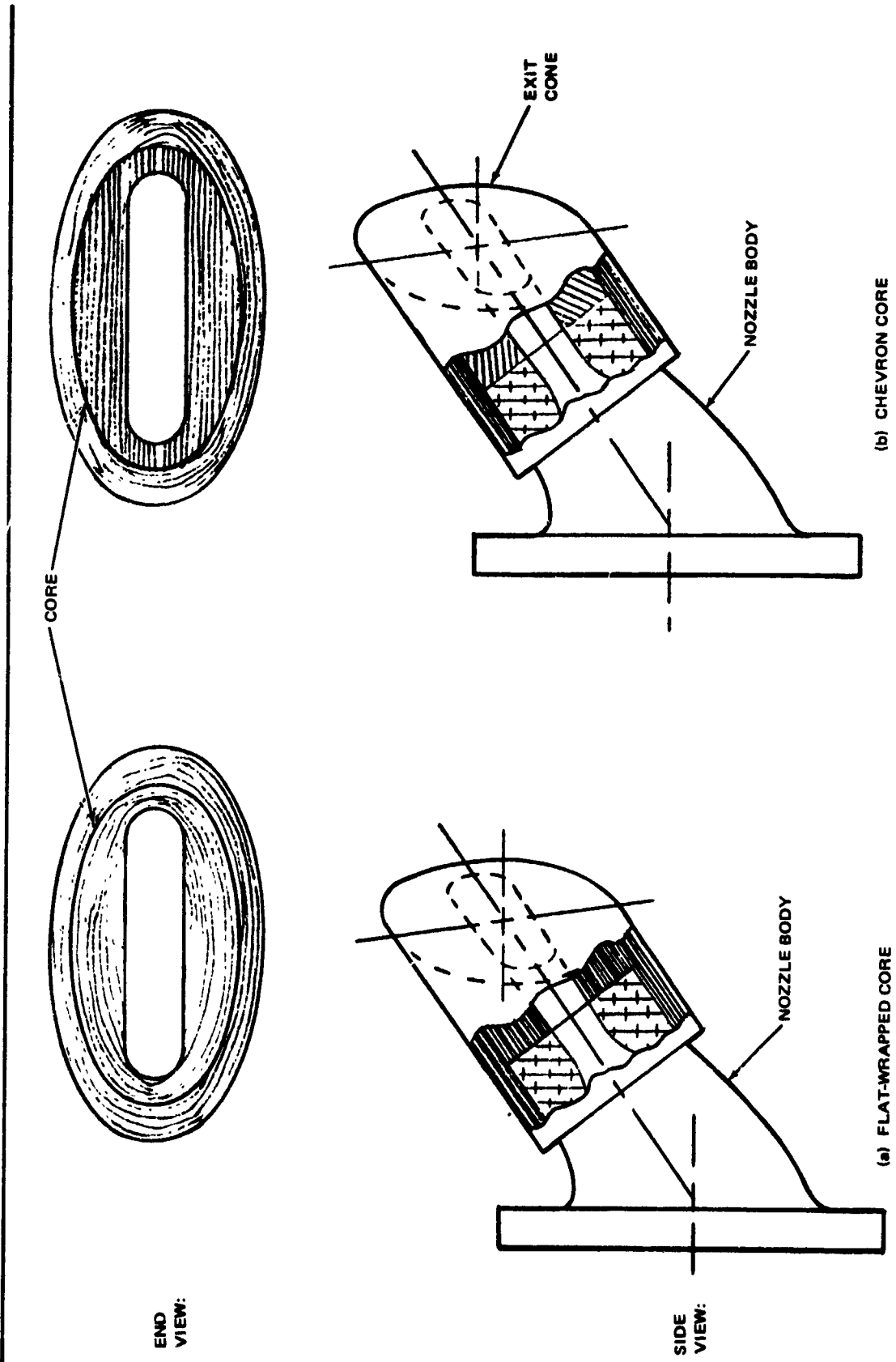


Figure 7-16. Exit Cone Insulation Layouts

Later, it was found necessary to cure the flat-wrapped core completely prior to assembly to reduce wrinkling and distortion of the over-wrapped insulation during the over-wrap cure cycle and to assure that an adequate number of continuous circumferential plies would remain in the over-wrapped insulation after final machining.

#### 7.7 PROBLEMS AND SOLUTIONS

The following is a summary of the problems encountered and solutions found during the internal insulation process development tests.

---

Problem	Solution
Molded rubber liners had voids.	Improved method of loading uncured rubber into the mold cavity.
Wall thickness variations in molded rubber liners exceeded the specified tolerance.	(a) Fabricated a straighter core mandrel. (b) Changed the duct design to allow greater wall thickness variations.
Molded rubber liners had stepped seam longitudinally.	Added dowel pins and holes to mold halves.
Straight molded tubes could not be installed into bent segments of metal ducts.	Reduced liner OD to allow for changes in duct geometry at bends.
Adhesion of the rubber to the metal ducts was not reproducible using the standard degreasing and priming methods.	(a) Developed a new metal surface preparation: abrasive scrub, descale, dry, solvent wipe, and prime within 1 hour after descaling. (b) A mold-release solution of mixed alkyl sulfonates in water was used, which could be washed off the molded liners, thereby providing consistently acceptable adhesion to metal.

---

Problem	Solution
Voids were found in the adhesive between the rubber and the metal.	<p>(c) Wiped the liner with MEK and primed it with RTV-731.</p> <p>(d) Added a peel test using a strip of liner material bonded to the duct OD to verify proper surface preparation and curing.</p>
Blisters formed in the lined duct during rapid depressurization after pneumatic testing.	<p>Assembled the liner into the metal tube in a vacuum chamber, and pressurized the liner during curing to exclude entrapped air.</p>
Incomplete curing was found in RTV-731 and 93-072 adhesives.	<p>Changed test procedures to eliminate gas entrapment behind the liner.</p>
A nondestructive test was desired to detect voids and unbonded regions in the liner.	<p>(a) Eliminated use of RTV-731 adhesive where presence of moisture was not assured.</p> <p>(b) Raised cure temperature of 93-072 to 300° F and verified cure by peel test of liner material bonded on the duct OD.</p>
A method of applying void-free insulation coatings up to 0.25 inch thick to the interior walls of the JI manifold was required.	<p>As no effective method of nondestructive inspection was found, imposed close controls and supervision of bonding process and functionally tested lined ducts from each batch to verify acceptable bonding.</p>
Adhesion of the RTV insulation coating to titanium using conventional cleaning and priming techniques was unsatisfactory.	<p>Special tooling was fabricated and a technique of pressure injecting the RTV insulation material into an evacuated cavity was developed.</p> <p>An improved method of surface preparation was developed in which the part was thoroughly degreased, power drum-sanded with 30-grit paper, and primed with SS-4155 primer.</p>

Problem	Solution
Tape wrapping at 10-deg shingle angle provided inadequate insulation thickness.	Developed a dinked laminate process to obtain a 45-deg shingle angle.
The adhesive migrated into a JI manifold area inaccessible for cleaning during processing.	A special rubber bladder was fabricated and inflated in the inaccessible area to hold resin out.
The progress of the resin was not observable within metal parts.	Plexiglas end caps were fabricated.
Wrinkling and distortion of the nozzle preform core assembly occurred during curing.	Cured the core completely prior to assembly to allow tighter over-wrapping and reduce distortion.
Braiding process produced low and variable fiber density.	Used hand-knitting process.

#### 7.8 CONCLUSIONS AND RECOMMENDATIONS

A liner molded from Silastic 55 silicone rubber was produced and successfully bonded into the interior of the EB warm-gas manifold liner. The liner had to be bonded with an elastomeric adhesive using an assembly process that eliminated observable voids. However, a liner made by the same process failed to withstand the flow environment in the vent tube. Improved processes should be developed to fabricate liners which can withstand severe flow conditions.

The attempts to develop and refine a nondestructive inspection technique for the molded rubber liners bonded inside metal tubing were largely unsuccessful. Further work in this area is recommended. There may be some potential in shear-wave pulse-echo evaluation, neutron radiography, and Lamb wave propagation and damping. In addition, some material or design changes may enhance inspectability.

A technique that applied a dense, void-free insulation coating to the interior of the JI manifold was developed. It is recommended that other castable materials be tested to develop acceptable fabrication and improved performance in hot-gas ducts.

The 45-deg-angle composite produced a tube lining with satisfactory density for good ablation characteristics without thickness limitations.

Both JI nozzle preform processes produced satisfactory laminates. However, the vee-shaped preform was produced at considerable increase in labor cost.

Neutron radiography was an effective method for detecting voids in adhesive between metal ducts and quartz/phenolic liners, and is highly recommended for future inspection of similar bonded assemblies.

A method of applying a dense, relatively void-free adhesive layer between the liner and the JI manifold wall was developed, using vacuum injection and pressure injection into grooves.

Knitting and impregnating of quartz socks to provide continuous insulation in intersecting ducts was demonstrated to be feasible. Mechanized knitting methods should be developed, and prototype liners for intersecting ducts should be made and tested in hot-gas environments to assess the performance of this type of liner in flow around corners.

## Section 8

### HERCULES HiBEX-U PROPELLANT PROCESSING

The HiBEX motor which was developed under the ARPA HiBEX Project (Reference 8-1) was used in the UpSTAGE Experiment program (Reference 8-2) with some design modifications. The modifications complying with experiment requirements included design changes to the nozzle by removing the TVC hardware, thus reducing weight; incorporation of safety improvements to the igniter; and use of an inert liquid carrier, n-heptane, as a casting-powder processing aid. The design modifications to the nozzle increased boost burnout velocity. The use of heptane was verified in full-scale motor manufacture and subsequent static and flight tests.

A process study using heptane was conducted in conjunction with and supplementary to ABMDA/Hercules inert-carrier studies (Phase I is described in Reference 8-3 and Phase II in Reference 8-4).

The objective of Phase I was to demonstrate a safer FDN propellant-manufacturing process and to define the growth potential of high-burn-rate, FDN-type propellants via formulation changes.

The objective of Phase II was to evaluate the feasibility of using heptane in the key FDN propellant processing operations and to establish requirements for the planned process of manufacturing HiBEX motors for the UpSTAGE program.

#### 8.1 REQUIREMENTS

The program requirements for the UpSTAGE Experiment specified use of the HiBEX Phase D rocket motor and its components for the boost phase of the flights. Minimum redesign and engineering analyses of the HiBEX nozzle were also specified for eliminating the HiBEX TVC and TVC system mounting provisions.

The modified composite double-base propellant processed with inert liquid carrier (n-heptane), designated FDN-80, was specified for the grains of all UpSTAGE motors.

## 8.2 HiBEX-U CONFIGURATION

The rocket motor assembly (Figure 8-1) consists of three major components: the loaded case assembly, the nozzle and closure assembly, and the loaded igniter assembly. Only the loaded case assembly is discussed in this section. The nozzle and closure assembly and the loaded igniter assembly are discussed in Appendix F.

The loaded case assembly consists of the case subassembly, the propellant grain, a hot-gas seal, and miscellaneous case components. The conical fiber glass case, with metal skirt attachment (splice) rings and adapters, contains FDN-80 propellant. Of particular interest is the effect of liquid-carrier heptane on FDN propellant processing and its subsequent loaded effects upon propellant structural integrity and motor performance. Therefore, propellant processing and motor loading are subsequently discussed in depth.

## 8.3 PROPELLANT GRAIN

The HiBEX-U propellant grain is an FDN-80 composite modified double-base propellant in a single-perforated 11-point star configuration. Radial stress relief grooves are contained at the port openings in both the forward and aft dome areas. The propellant is bonded to the case with a bimodal powder-embedding case-bond system. The propellant burn rate is increased by the use of zirconium staples randomly dispersed throughout the propellant mass. Inert slivers placed against the case wall at the base of each star point modify the final propellant burning surface to control excessively long motor-pressure-time tailoff.

### 8.3.1 Casting Powder Process

As described in Appendix G, the objective of using heptane with FDN was to minimize or eliminate the processing hazards (electrostatic-charge buildup) of dry-powder handling during manufacture of FDN. The inert-liquid process consisted of several manufacturing operations that had common sensitivity characteristics such as impact, impingement (granule-to-granule friction),

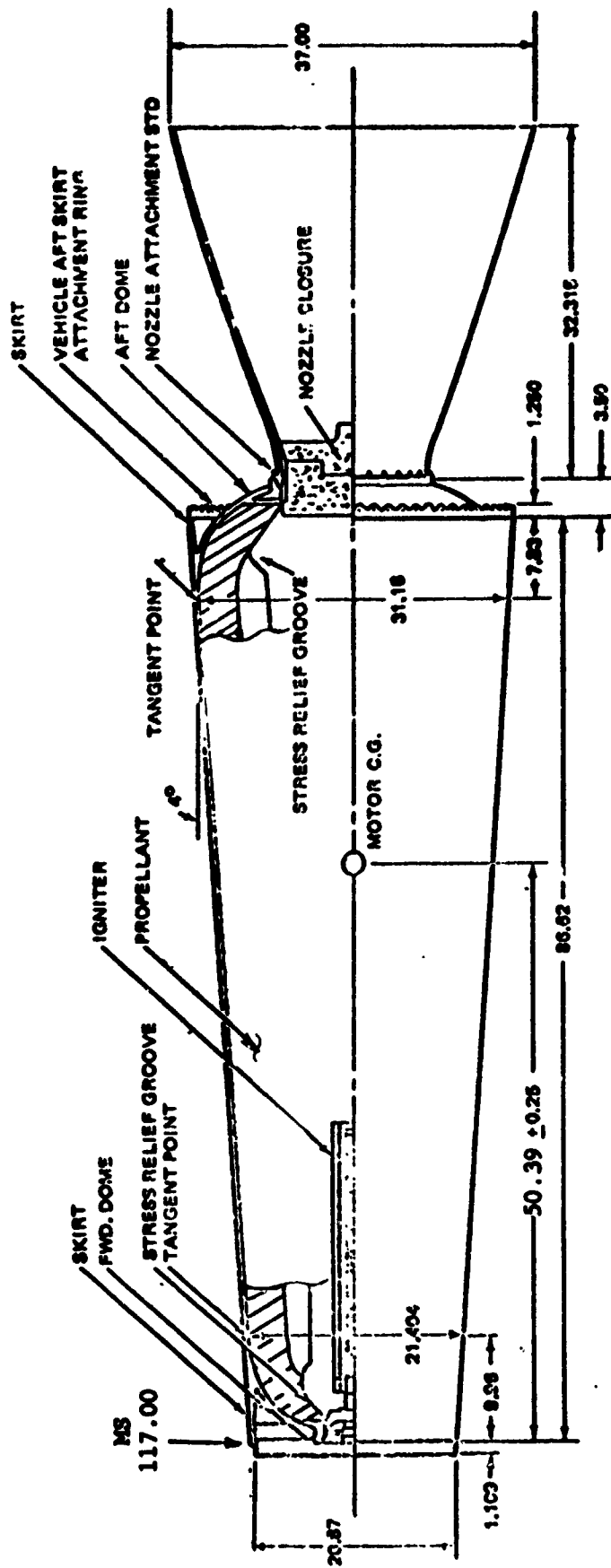


Figure 8-1. HIBEX Rocket Motor Assembly

electrostatic discharge initiation, electrostatic generation, and transition.

The results of the tests were as follows:

- A. The impact sensitivity of FDN powder was not mitigated by submergence in heptane.
- B. Granule friction was reduced by submergence in heptane.
- C. Powder-to-powder friction did not improve with submergence in heptane.
- D. The electrostatic potential of casting powder in heptane was dissipated through proper grounding.
- E. Transition height was increased 5-1/2 times (small diameter) through the use of heptane.
- F. FDN powder in heptane increased the handling margin of safety by:
  1. Elimination of dust.
  2. Improvements in control of powder granule velocity.
  3. Increase in transition height.
  4. Positive control of electrostatic dissipation.

Figures 8-2 and 8-3 are flow diagrams of FDN casting-powder manufacture and motor-loading processes with heptane. With the exception of the precutting and cutting operations, the powder was stored, handled, and loaded under heptane from the time casting-powder extrusions were cut until the propellant was loaded into the motor case.

The process from manufacture of casting powder through casting-powder cutting included:

- A. Grinding ammonium perchlorate (AP).

The grinding of AP is directly related to the burning rate of the FDN propellant. Based on the original HiBEX data, the maximum statistical limits for particle size were established as:

  1. 100 weight-percent to be no greater than 20 microns
  2. 50 weight-percent to be no greater than 8 microns
- B. Preparation of premix.

This process included the formulation of nitrocellulose, nitroglycerin, acetone, and alcohol.
- C. Preparation of oxidizer/stabilizer slurry.

The slurry was a mixture of resorcinol, AP, and acetone.

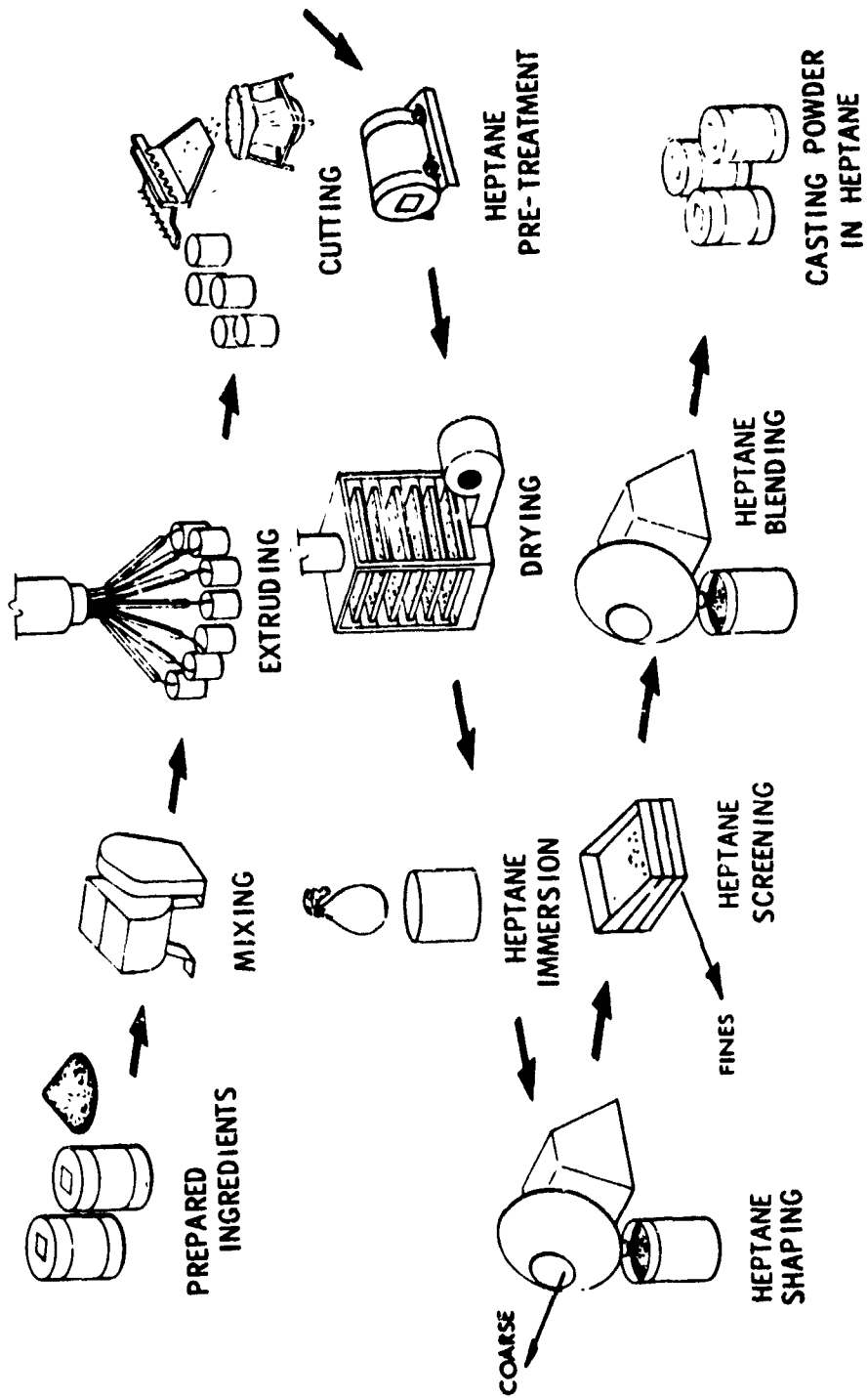


Figure 8-2. FDN Casting Powder Manufacture

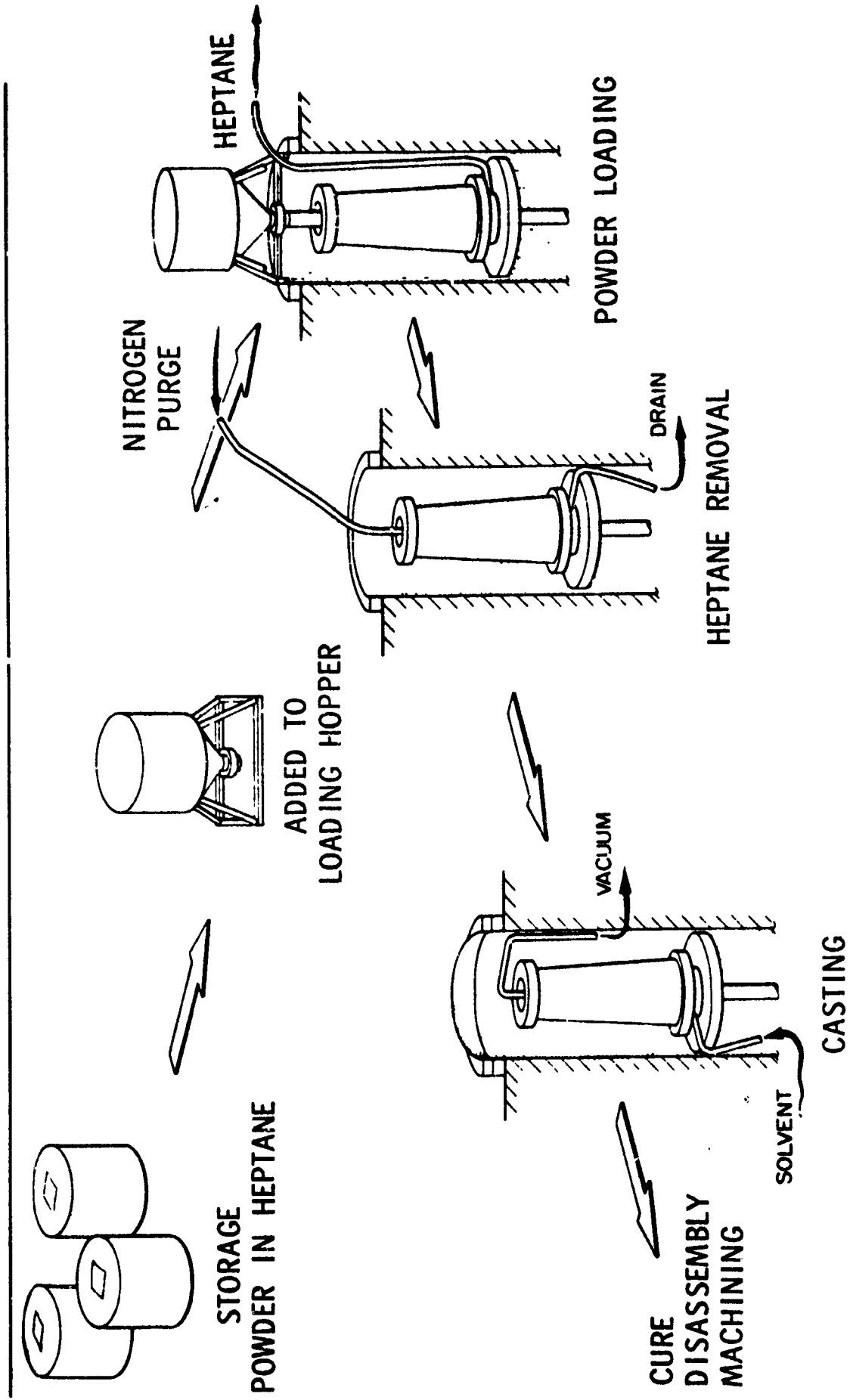


Figure 8-3. Propellant Grain Manufacturing Using Heptane

D. Mixing.

The final mixing operation combined 2-nitrodiphenylamine (2-NDPA), acetone, premix, oxidizer/stabilizer, aluminum powder, and zirconium staples, forming a casting-powder dough.

E. Pressing and cutting.

The zirconium staples were added to the dough in a mixer, then pressed and cut into cylindrical-shaped casting-powder granules (green powder). The granule specification indicated an acceptable diameter range of 0.125 to 0.145 inch and an L/D ratio of  $1.15 \pm 0.05$ . The granules were placed in heptane and 2-NDPA solution for storing and handling. The zirconium staple dimensions (in inches) were:

1. length:  $0.125 \pm 0.00$
2. width:  $0.0045 +0.001, -0.0005$
3. thickness:  $0.0005 \pm 0.00005$

F. Green powder.

The pressed and cut granule composition, at this stage called green powder, was immersed in heptane for the first time and agitated by rotation to prevent granule clustering or agglomeration. Then the heptane was drained and the powder dried and reimmersed in heptane. The shaping, screening, and blending operations were conducted while the powder was wet or immersed in heptane.

G. Mold loading.

One of the major advantages of the heptane process was in the mold-loading operation. The presence of heptane limited and reduced the velocity of powder-granule flow into the mold, thus reducing electrostatic charge, etc. However, reduced velocity caused low-density loading.

Of greatest concern in the manufacture of the HiBEX-U motor was that the propellant in the motor maintain the same ballistic properties as the previously manufactured FDN propellant. Therefore, three areas were monitored during the manufacture of the HiBEX-U motor: powder/solvent ratio, mechanical effects, and ballistic characteristics.

### 8.3.2 Powder/Solvent Ratio and Ballistics

The ratio of the weight of casting powder loaded into a full-scale motor case

to the weight of casting solvent is called the powder-to-solvent (P/S) ratio. The ballistic characteristics of the propellant are sensitive to P/S ratio. A direct comparison of propellant rates from different propellant lots was not a valid method of evaluating propellant powder unless the P/S ratios from the lots were normalized or adjusted to the same P/S values. A comparison of burning rates between the original HiBEX and UpSTAGE HiBEX-U is shown in Table 8-1. The HiBEX-U burning rate was outside the accept/reject criteria established for the UpSTAGE program. When the HiBEX-U P/S ratio was adjusted to that of the original HiBEX ( $\frac{70.29}{29.71}$  to  $\frac{73.64}{26.36}$ ), the burning rate fell within the acceptable range. In fact, the ballistics for the propellant processed with heptane showed a higher propellant burn rate at the same P/S ratio. Based on the development of the HiBEX FDN propellant with heptane, it was concluded that a 1-percent increase in P/S ratio increased the burning rate by 0.13 in. /sec.

A comparison of the normalized specific impulse of the HiBEX-U propellant with the original HiBEX propellant showed an increase of 0.7 percent in specific impulse (Table 8-1). The difference was attributable to the method of determining propellant weight. That is, the original HiBEX specific impulse included all consumable weights; i. e., propellant and inhibitor (propellant weight less grain weight). The specific impulse for HiBEX-U was determined with consumable propellant weight only.

Table 8-1  
BALLISTIC COMPARISONS

Propellant	P/S	Burning Rate <sup>(1)</sup> Comparisons (Percent from Nominal)	Normalized Specific Impulse (Percent)
(Accept/reject criteria)	$\frac{73.64}{26.36}$	±3.00	
Original HiBEX	$\frac{73.64}{26.36}$	-2.56	1.0000 <sup>(3)</sup>
HiBEX-U	$\frac{70.29}{29.71}$	-4.09	1.0068 <sup>(4)</sup>
Adjusted HiBEX-U	$\frac{73.64}{26.36}$ <sup>(2)</sup>	-0.77	1.0056 <sup>(4)</sup>

(1) 2,000 psi at 70° F

(2) Adjusted to original HiBEX P/S

(3) Included inhibitor weight

(4) Consumable propellant weight only

Mold filling efficiency (MFE) is the ratio of the density of powder loaded into a full-scale case compared to the density of powder from a standardized small-scale test mold filled by gravity-screen loading. In other words,

$$\text{MFE} = \frac{\text{Unit packing density}}{\text{Screen loading density}}$$

$$\text{where packing density} = \frac{\text{powder weight}}{\text{mold volume}}$$

The predicted P/S ratio (percent of casting powder) was determined by the following equation:

$$\text{Percent of casting powder} = \frac{(\text{SLD})(\text{MFE})(100)}{P_s + (\text{SLD})(\text{MFE}) \left(1 - \frac{P_s}{P_{cp}}\right)}$$

and

$$\text{Percent of casting solvent} = 100 - \text{Percent of casting powder}$$

where

SLD = screen loading density

MFE = mold loading efficiency

$P_s$  = density of casting solvent

$P_{cp}$  = density of casting powder

After the successful static firing of the first FDN HiBEX-U motor manufactured by the liquid-carrier process, an acceptable range of MFE values was established between 101.1 and 104.5 percent based on a static motor MFE of 103.4 percent. The limits of the mold-filling efficiency were based on frequency/force values (sufficient vibration necessary to impart movement to the powder bed) obtained from the study and motor loading of the static motor to facilitate adequate packing of casting powder immersed in heptane.

The subscale test results were within the MFE and P/S ratio range of three HiBEX motors from the original HiBEX program, thus verifying the use of the original P/S ratio range. The use of heptane in the propellant process improved control over MFE and P/S ratio, which were functions of vibration characteristics established for the loading operation. For example, high frequency and low amplitude vibration during motor loading produced loaded motors with lower than expected burn rates; low frequency and high amplitude produced motors of higher than expected burn rates. Thus, the vibration levels used during motor loading controlled the MFE and P/S. The ability to adjust the vibration levels during motor loading provided the means to obtain a uniform density from the forward to the aft end of the motor. Table 8-2 shows the HiBEX-U MFE range to be higher than that of the original HiBEX MFE.

### 8.3.3 Mechanical Effects

The mechanical property data are shown in Figure 8-4. The curves show that at the nominal 70/30 P/S ratio, the HiBEX-U propellant has higher strength and modulus, but lower elongation. Previous data have shown that the nitrocellulose (NC) to plasticizer (NG + TA) ratio is a good determinant of the variability of propellant physical properties. The ratio accounted for the binder (NC), which imparted the strength to the propellant, and also for the plasticizer, which imparted elongation qualities. In general, as the NC-to-total-plasticizer ratio increased, the propellant modulus and tensile strength increased and the elongation decreased, as shown in Figure 8-4.

Table 8-2  
MOLD FILLING EFFICIENCY

	Original HiBEX (D series)	HiBEX-U
P/S Range	$\frac{69.74}{30.26}$ to $\frac{71.44}{28.56}$	$\frac{71.74}{28.26}$ to $\frac{72.60}{27.40}$
MFE Range	99.1 to 102.05	103.4 to 104.8

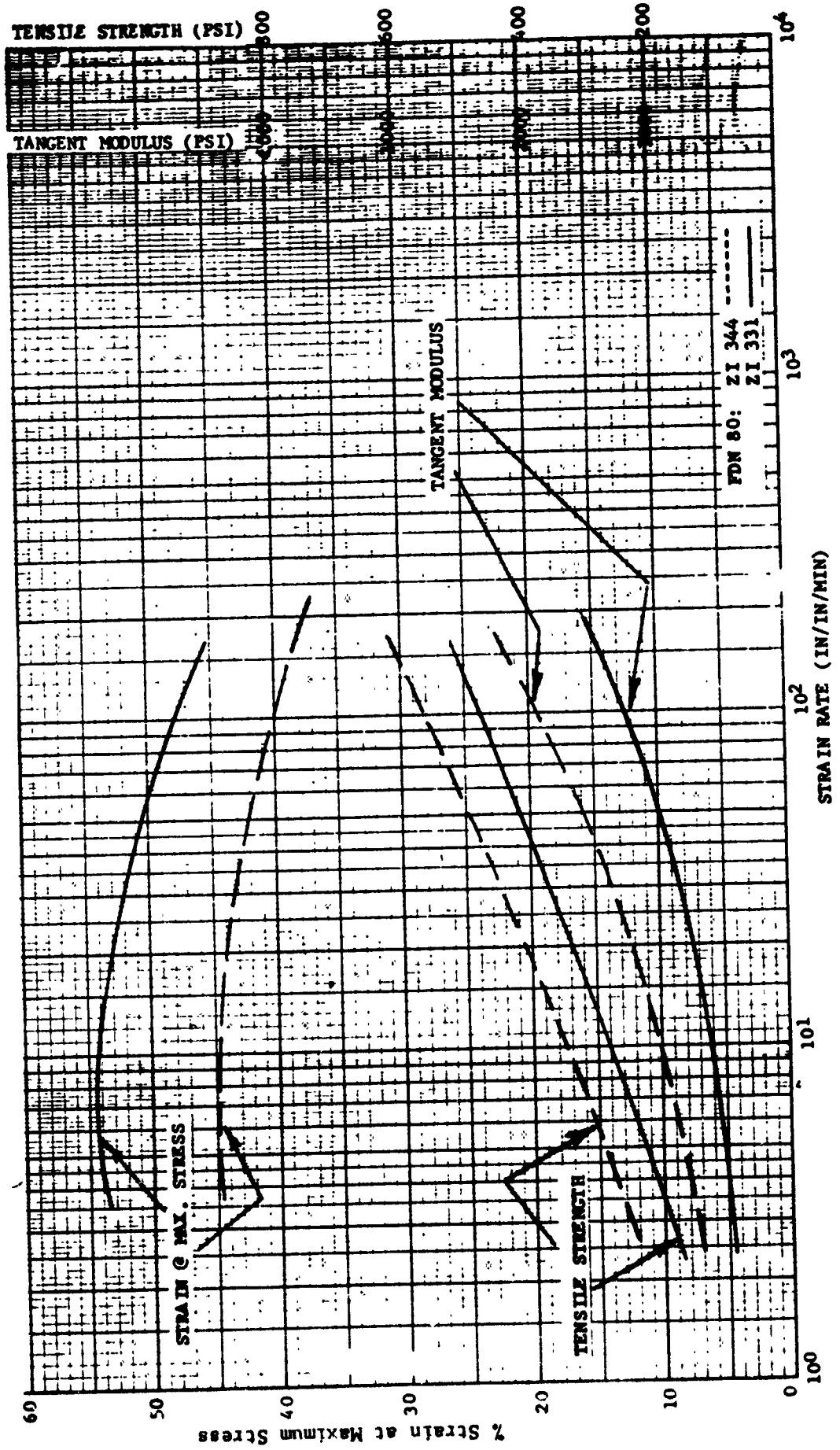


Figure 8-4. Master Curves Comparison - Ref. Temp. = 77°F, Ref. P/S Ratio = 70/30

Figures 8-5 and 8-6 show the comparison between the HiBEX-U propellant and the original HiBEX propellant. In general, the HiBEX-U propellant (Z1-344) exhibited better shear properties (strength and modulus) than those of the original propellant, considering the difference in NC (NG + TA) ratio and grain P/S ratio between the sample propellants.

For case bond strength, Figures 8-7 and 8-8 show that HiBEX-U propellant has higher tensile and shear strength than the original propellant. It can be concluded that the HiBEX-U showed adequate case bond physical properties.

#### 8.3.4 Casting Solvent

Solvent for casting HiBEX-U propellant grains was made up of a nominal composition of nitroglycerin (NG), triacetin (TA), and 2-NDPA. NC was tested for moisture, acidity, and stability; TA was tested for acidity and ester content; and 2-NDPA was tested for complete specification requirements.

#### 8.3.5 Case Bond System

The case bond system for the FDN-80 propellant grain consisted of the embedment of bimodal casting-powder granules in a case. Embedment was accomplished by applying a resin system (EA 946) to the inside surface of the case and introducing large (0.070-inch-diameter) and then small (0.045-inch-diameter) powder granules, followed by a cure.

The embedment layer in each case was visually inspected and accepted on the basis of criteria set forth in Specification S67-1-014, which stated that no area greater than 10 percent was to contain multilayers, encapsulated granules, or lack of granules and that no cracks were to exist in the embedment resin. In addition to the visual acceptance inspection, stereo photomicrographs were taken of each case bond system.

### 8.4 RECOMMENDATIONS

High-burn-rate propellant technology has been demonstrated by the HiBEX motor development program and the UpSTAGE Experiment application. However, several propellant development areas should be investigated which would allow expanded use of the HiBEX propellant/motor technology:

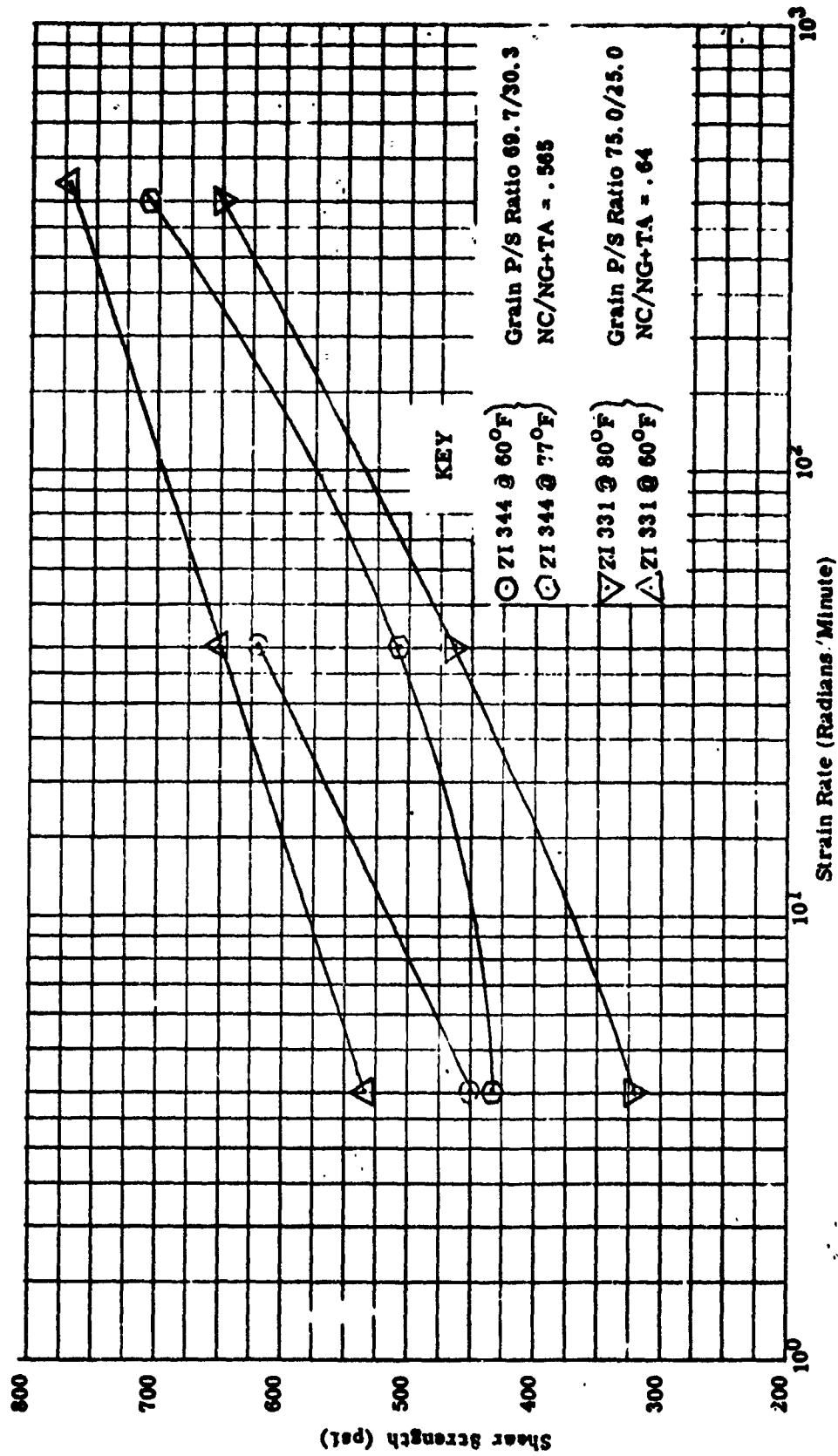


Figure 8-5. FDN 80 Propellant Shear Strength, Comparison of ZI 344 With ZI 331 Data  
(1 x 2 x 1/2 Double Lap Shear Sandwich)

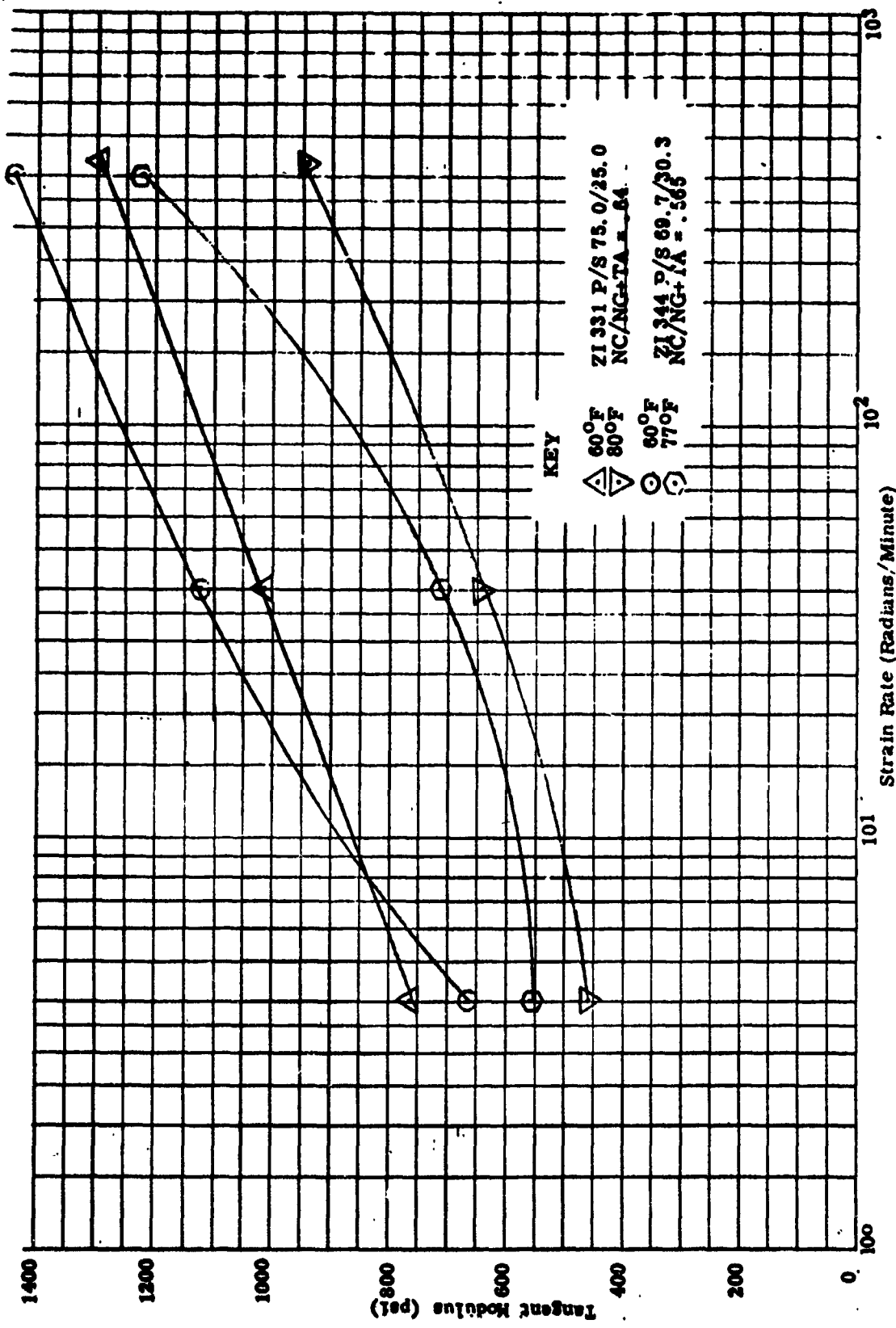


Figure 8-6. FDN 80 Propellant Shear Tangent Modulus, Comparison of ZI 344 Data With ZI 331 Data (1 x 2 x 1/2 Double Lap Shear Sandwich)

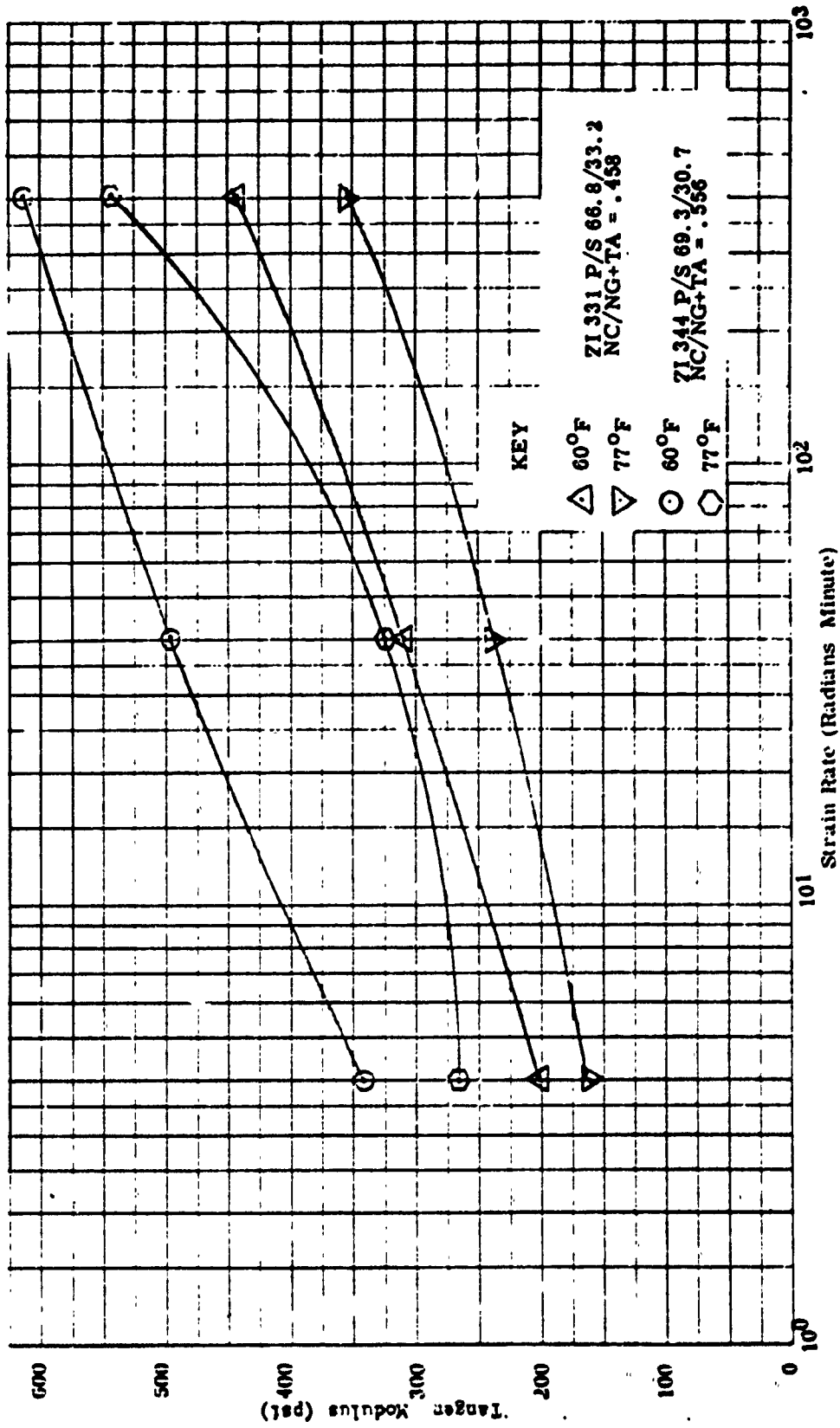


Figure 8-7. FDN 80 Case-Bond Shear Tangent Modulus, Comparison of ZI 344 Data (1 x 2 x 1/2 Double Lap Shear Sandwich)

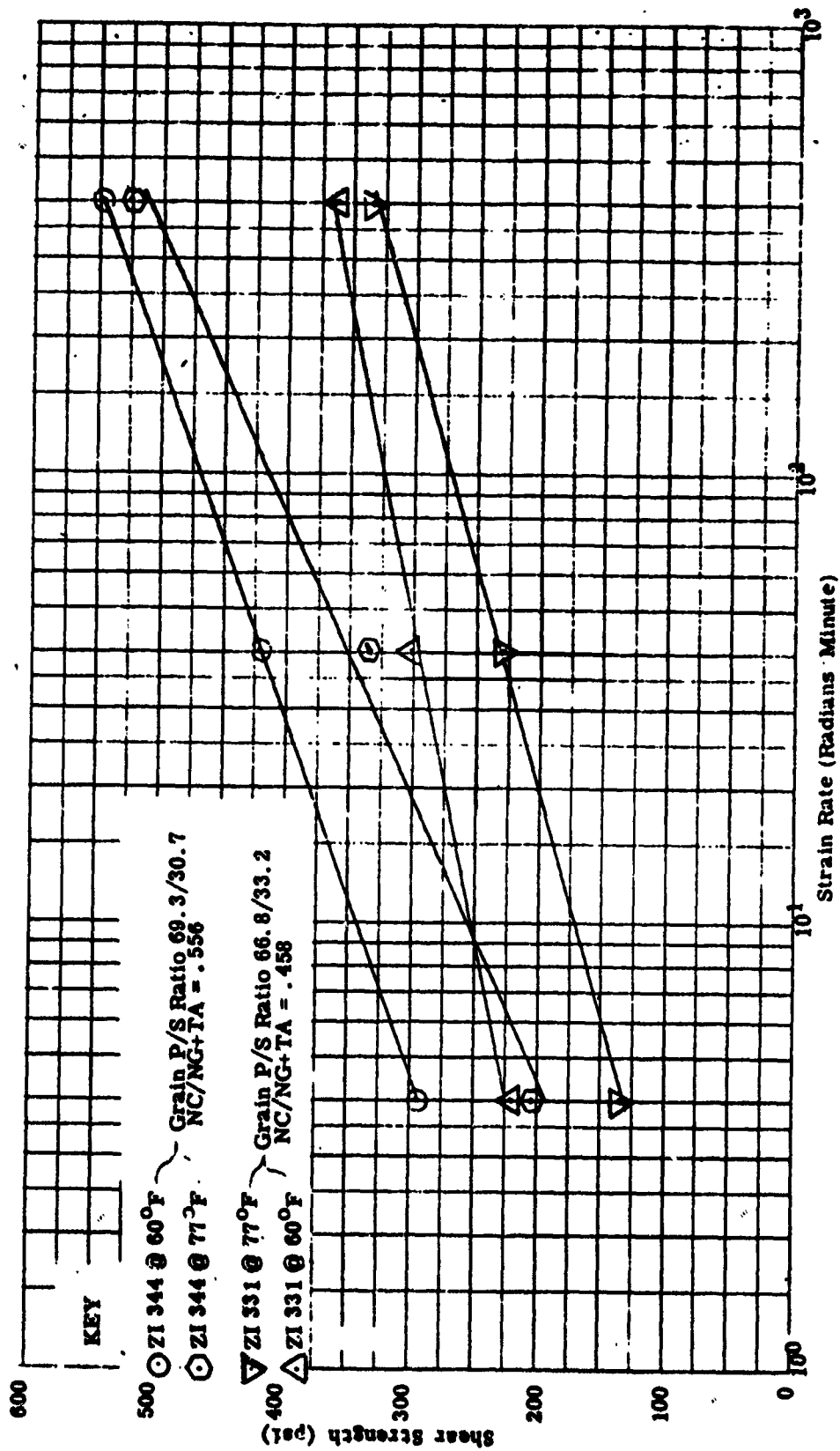


Figure 8-8. FDN 80 Case-Bond Shear Strength, Comparison of ZI 344 P/S Ratio 69.3/30.7 With ZI 331 Data (1 x 2 x 1/2 Double Lap Shear Sandwich)

- A. A definition of the upper limit of FDN-80 propellant burn rate is desirable to provide performance flexibility in vehicle-sizing tradeoff studies for system application. Of particular interest would be reproducibility at these high burn rates.
- B. Along with the higher propellant burn rate, an investigation of the effects on propellant physical properties of environments higher than that of UpSTAGE is desirable. Strenuous vibration and/or high lateral maneuver levels may cause propellant stresses to go beyond adequate margins of safety. Consideration should also be given to nonpressurized propellant applications.

Section 9  
SUMMARY OF RECOMMENDATIONS

Additional research and development should be pursued in the following areas:

1. Automated drafting should be adapted to plastic PC board fabrication and compared to manual drafting quality, cost, and time.
2. Thick-film dielectric inks should be characterized and studied to determine methods of controlling thermal expansion properties. Improved inks should be used to determine how many layers can be successfully fabricated in large, thin, thick-film multilayer circuit bases.
3. Tests should be conducted to determine how many soldering repairs are feasible on thick-film multilayer circuits of superboard construction.
4. Studies are needed to develop higher reproducible peel strength of copper-cladding on Kapton PC board material.
5. Simultaneous curing of preimpregnated high-silica/phenolic cloth and fiber adhesive is a recommended method of fabricating thin heat shields, and should be further explored to determine its limits of applicability in terms of thickness, materials, and performance.
6. Noncontaminating sealants should be developed for use where assemblies cannot be pressure-capped during bonding. The sealants should also be easily applied and easily removable.
7. Improved processes should be developed for molded and bonded rubber liners in hot-gas ducts. A nondestructive technique should be developed to detect voids and unbonded areas between metal ducts and internal rubber liners.
8. Castable insulation materials should be developed which can withstand hot-gas flow in ducts.
9. Further development and functional testing should be pursued to develop techniques for mechanized knitting, impregnating, and low-temperature bonding and curing of quartz/phenolic sock liners for intersecting hot-gas ducts. Subsequently, such liners should be installed in intersecting ducts and tested with hot gas to determine performance in flow around corners.

10. Studies and tests for high burn rate and adequate propellant physical properties are recommended for advanced interceptor technology. Subscale and full-scale motor tests are needed to verify feasibility and performance repeatability.

## REFERENCES

- 5-1 UpSTAGE Technology Report: Airborne and Ground Guidance Electronics, MDC G3233, August 1972.
- 5-2 Isaak, H. R., Kanz, J. W., and Babiracki, E. G., Development of Large Thick-Film Multilayer Assemblies, MDAC Paper WD1704, September 1971.
- 6-1 UpSTAGE Technology Report: Vehicle Aerodynamics and Thermodynamics, MDC G3229, May 1972.
- 6-2 UpSTAGE Task I Report, MDAC-62424, October 1968.
- 7-1 UpSTAGE Technology Report: EB Control System, MDC G3232, July 1972.
- 7-2 UpSTAGE Technology Report: JI Control System, MDC G3237, August 1972.
- 8-1 HiBEX Final Technical Report, Report No. D2-99600-1, Contract No. DA-01-021-AMC-10696(Z), 5 March 1966.
- 8-2 UpSTAGE Program-HiBEX-U Rocket Motor, Final Technical Report, Volumes I and II-Technical, Volume III-Appendixes, Hercules, Inc. Report No. UPC/72-7, Contract No. DACA68-8012, February 1972.
- 8-3 FDN Propellant Studies-Final Report, Hercules Report No. ABL-TR-67-14, Contract No. DA-01-021-AMC-1555(Z), April 1967.
- 8-4 FDN Propellant Studies-Final Report, Hercules, Inc. Report No. ABL-TR-68-12, Contract No. DAAH-01-68-C-0249, November 1968.

Appendix A  
UpSTAGE SHEAR RING DEVELOPMENT TESTS  
(This Appendix is Unclassified)

Prepared by  
M. L. Tarkanian  
Metallics Branch  
Materials & Methods—Research & Engineering

Appendix A  
UpSTAGE SHEAR RING DEVELOPMENT TESTS

OBJECT

To establish the optimum breaking groove configuration of shear rings and to determine the spread in shear loads of rings having such breaking grooves.

INTRODUCTION

Successful operation of the UpSTAGE vehicle is critically dependent upon the performance of a ring appropriately sized to shear within a prescribed load range corresponding to a tank pressure of 525 to 600 psi. The prescribed load range is 8,225 to 9,400 lb. The design specifies a 2024-T4 aluminum ring with a breaking groove incorporated to produce a shear failure at that location. Variation in the mechanical properties of the ring material will affect the breaking load of the ring. Hence, the magnitude of the variation must be determined. In addition, the effect on breaking load of proof loading prior to the shear test must be determined.

During assembly of the UpSTAGE fuel tank, a piston retainer and piston are joined by a threaded connection (see 1T34606D). The ability of the retainer to rotate freely without either the shear ring or viton seal also rotating is vital to the success of the assembly operation. If either the shear ring or the seal rotates, a leak path may occur as a result of the seal being deformed. Therefore, the feasibility of using a nonmetallic torque washer to aid in assembly must be determined.

PROCEDURE AND RESULTS

The initial efforts were directed at determining the feasibility of using a non-metallic torque washer to aid in assembly of the piston and piston retainer. Once this objective was accomplished, it was then necessary to determine the torque values of the piston bolts and the cylinder bolts required to achieve

the design clamping force of 10,000 lb between the piston and piston retainer as well as between the cylinder cap and cylinder (in these tests, the EB fuel tank's forward closure retainer and barrel were simulated by the cylinder cap and cylinder, respectively (see 1T34606D).

Initial shear ring tests established the optimum net section thickness. Subsequent shear ring tests provided data that was statistically analyzed to qualify remaining shear rings for use on future UpSTAGE fuel tank tests. To more closely duplicate the actual fuel tank production schedule, the rings were subjected to a simulated viton bonding operation which consisted of heating the rings to 180°F for 16 hours.

The following materials were used:

- 1T35832 Viton Seal
- 1T34697 Torque Washer
- 1T35968 Aluminum Shear Ring
- DPM 312 Graphite Lubricant

The aluminum shear rings were heat treated to the 2024-T4 temper in a salt bath to minimize distortion. All shear rings used in this study came from the same sheet (procured as a sheet of 0.100- by 48- by 120-inch Alclad 2024-0).

The design drawing for the 1T34697 torque washer initially specified Teflon. However, considerable difficulty was encountered during installation of the washer into the test fixture due to Teflon's inherent lack of rigidity. It was therefore decided to substitute a more rigid Armalon washer (produced by DuPont and designated as Armalon 410-128) for this test. The material consisted of woven fiber glass impregnated with Teflon.

To simulate the piston-to-piston retainer assembly operation, the piston and piston caps (see Figure A-1) were assembled using a viton seal, an Armalon torque washer and an aluminum shear ring. The assembly was not bolted together, however. The assembly was axially loaded to 10,000 lb and the cap torque was measured with the aid of a calibrated spring scale. The three

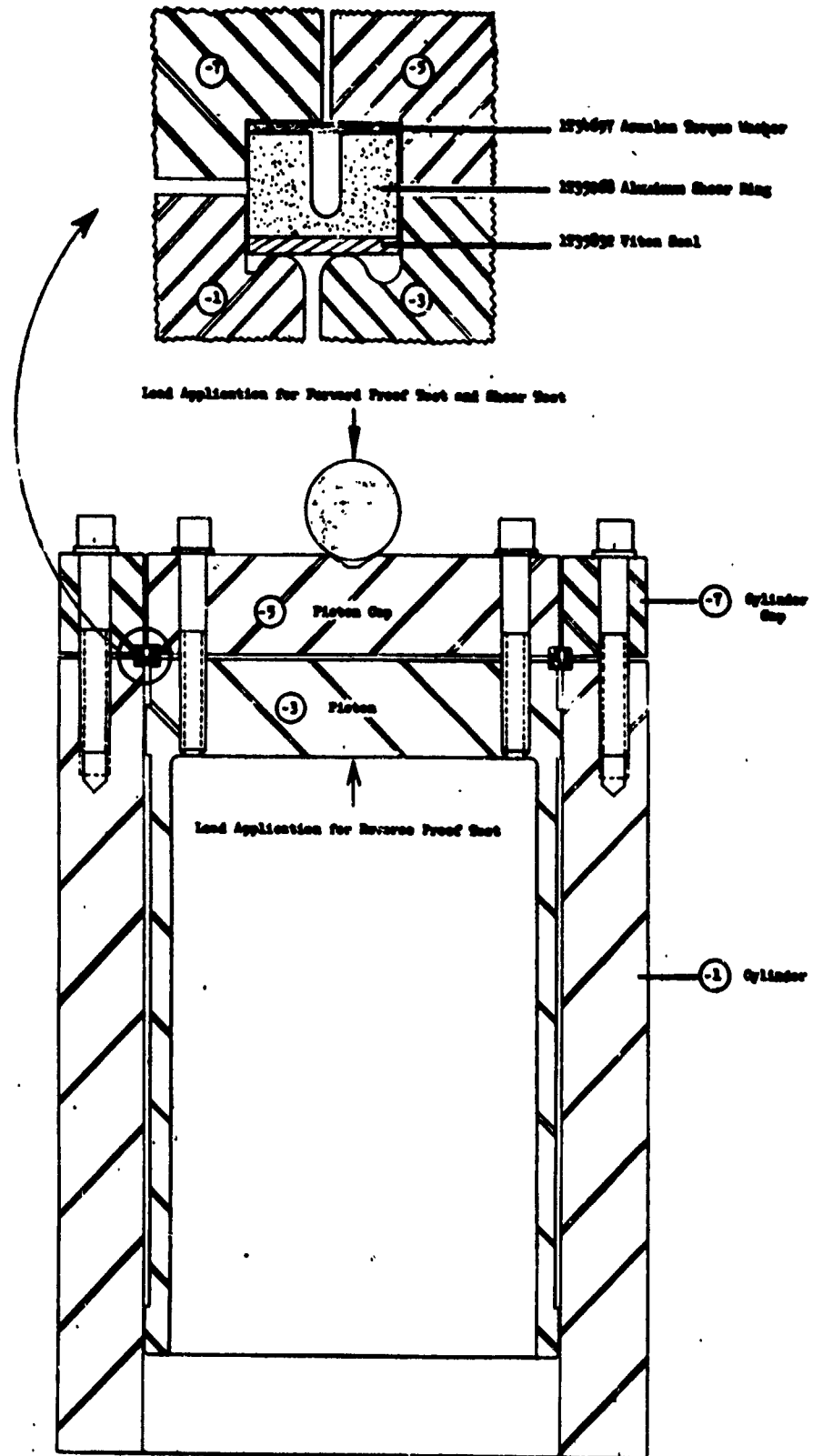


Figure A-1. Shear Test Fixture

conditions investigated and the resultant torques required to rotate the cap were as follows:

	<u>Condition</u>	<u>Torque</u>
A.	No Armalon washer; shear ring and piston cap lubricated with DPM 312 graphite.	400 in-lb
B.	With Armalon washer, shear ring and piston cap unlubricated.	250 in-lb
C.	With Armalon washer, shear ring and piston cap lubricated with DPM 312 graphite.	200 in-lb

An existing load cell, especially constructed for this type of test, was calibrated and used to establish a relationship between bolt torque and resultant axial load. This was accomplished by first plotting the instrument readout versus imposed axial load and secondly by plotting instrument readout versus bolt torque. The correlation between axial load and bolt torque could then be made (see Figure A-2). Using this technique, it was determined that each of eight cylinder bolts should be torqued to 115 in-lb while each of the six piston bolts should be torqued to 150 in-lb to achieve the desired clamping force of 10,000 lb required by design engineering.

Three rectangular specimens, each being 0.016 by 0.75 by 2.00 inch, were tested in double shear to determine the ultimate shear strength of the sheet of material used in this study. The shear strengths of the three specimens were 35,800, 36,000, and 36,900 psi. Based on these results, the net section thickness of the initial shear ring was determined. The section thickness was sized to fail at the nominal breaking load of 8,812 lb. Subsequent section thicknesses were selected based on the previous test results. The results of these initial tests are shown in Table A-1 and Figure A-3. When it was decided that the optimum section thickness (0.020 inch) had been discovered, a series of five shear rings having this particular net section thickness were machined and tested. The standard shear test procedure used is described in the following paragraph. The results of this series of tests confirmed the selection of 0.020 inch as the optimum net section thickness. The average breaking load of the five tests was 8,700 lb (see Table A-2).

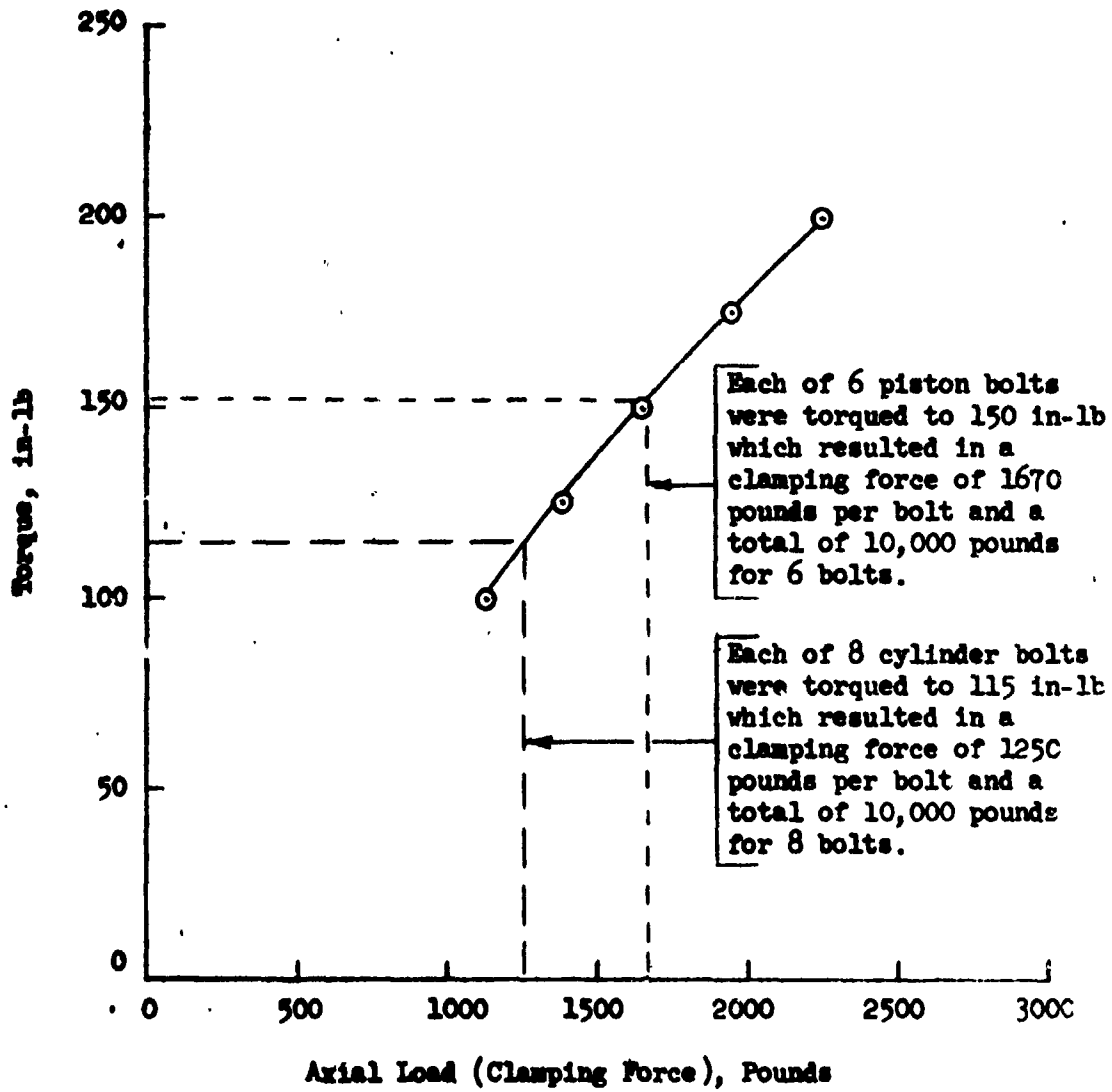


Figure A-2. Correlation Between Bolt Torque and Clamping Force

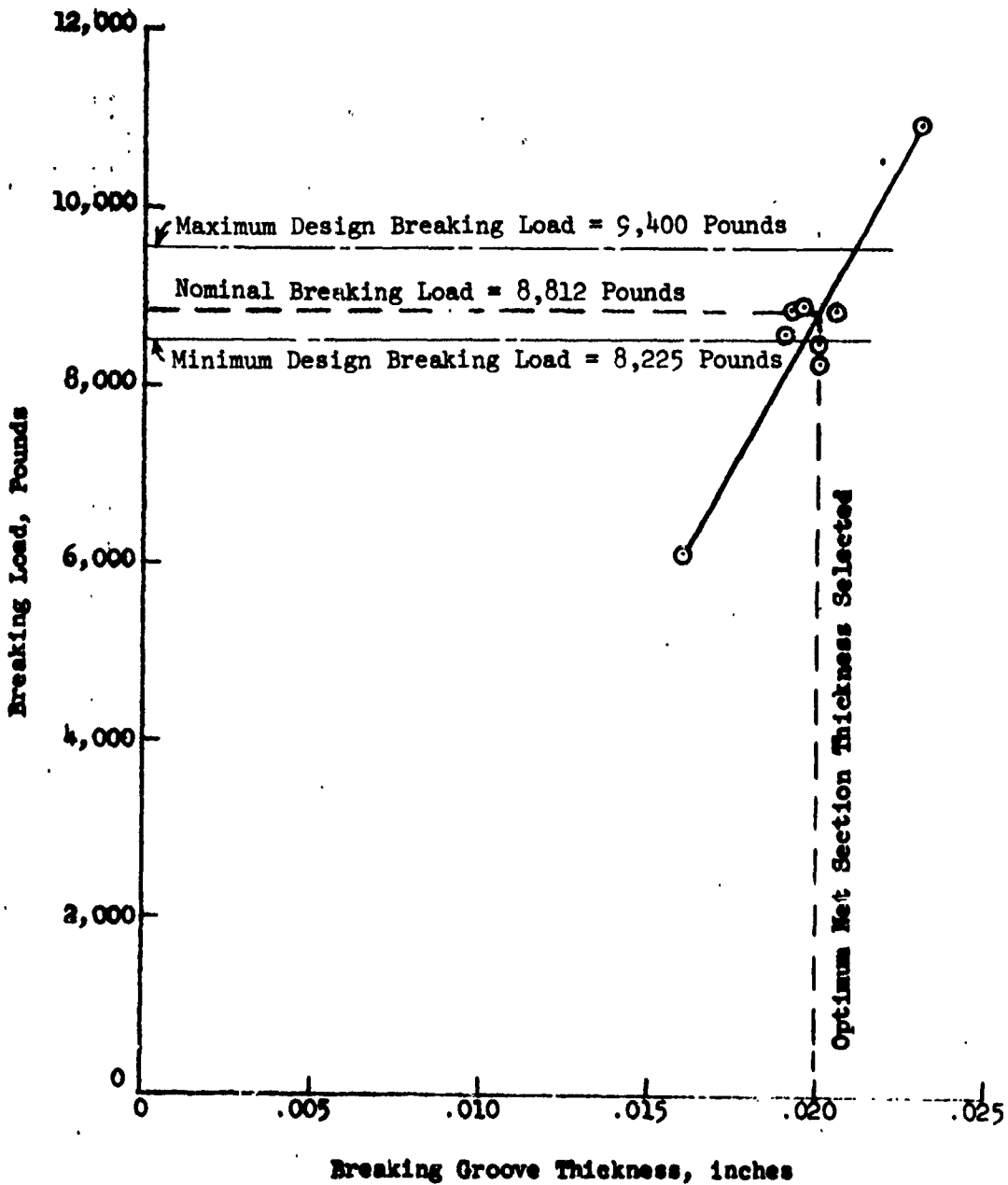


Figure A-3. Selection of Optimum Breaking Net Section

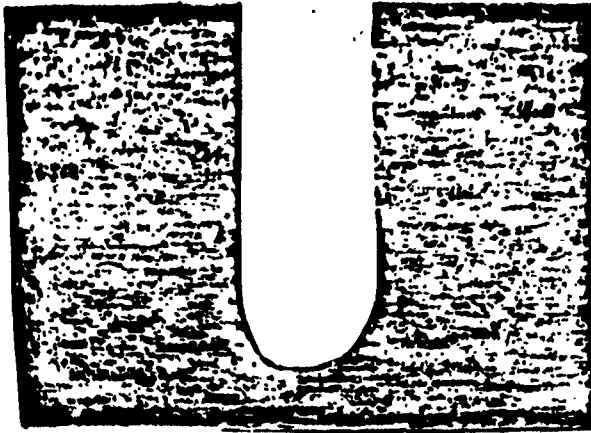
Table A-1  
BREAKING LOADS OF INITIAL TESTS

Ring Number	Net Section Thickness (inch)	Breaking Load (lb)
1	0.0192	8,820
5	0.0190	8,880
8	0.0200	8,250
16	0.0200	8,520
20	0.0190	8,600
22	0.0205	8,840
28	0.0160	6,110
34	0.0230	10,950

Table A-2  
BREAKING LOADS OF CONFIRMING SHEAR RINGS

Ring Number	Net Section Thickness (inch)	Breaking Load (lb)
9	0.0200	8,500
10	0.0200	8,700
12	0.0200	8,700
14	0.0195	8,590
32	0.0202	9,010

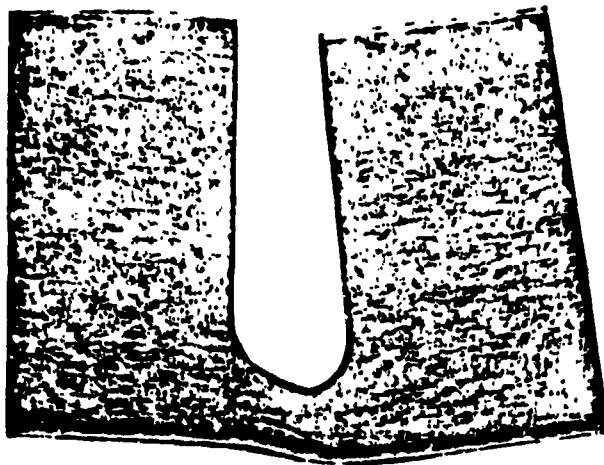
Another series of shear rings was machined having the optimum net section thickness. The results of these tests were used to qualify remaining shear rings for use on future UpSTAGE fuel tank tests. The rings were put through a simulated viton-bonding operation which consisted of heating the rings to



Ring #21  
Photo M5493  
Mag. 25X  
Keller's Etch

Figure A-4. As Machined

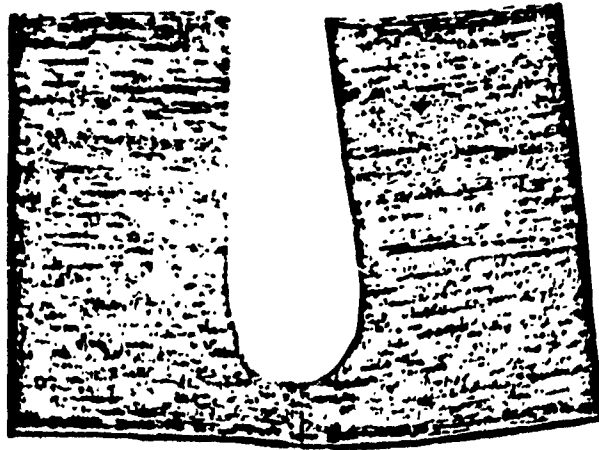
---



Ring #1  
Photo M5494  
Mag. 25X  
Keller's Etch

Figure A-5. After Forward Proof Test

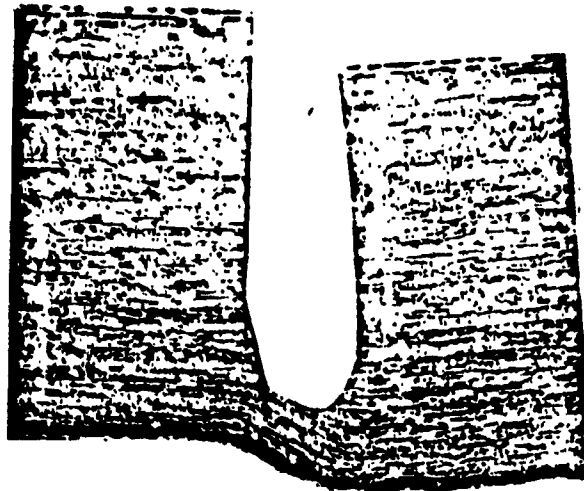
---



Ring #59  
Photo M5495  
Mag. 25X  
Keller's Etch

Figure A-6. After Forward and Reverse Proof Tests

---



Ring #61  
Photo M5496  
Mag. 25X  
Keller's Etch

Figure A-7. After Loading to 8,000 Pounds (Just Prior to Failure)

---

Table A-3  
BREAKING LOADS OF QUALIFYING SHEAR RINGS

Ring Number	Net Section Thickness (inch)	Breaking Load (lb)
13	0.0210	8,460
23	0.0200	9,200
33	0.0200	9,100
39	0.0200	8,960
44	0.0202	8,090
45	0.0203	8,760
51	0.0202	8,810
52	0.0200	8,675
54	0.0210	8,475
57	0.0205	8,325
58	0.0200	8,780
67	0.0200	8,180

Table A-4  
BREAKING LOADS OF SHEAR RINGS SUBJECTED TO  
250°F FOR 4 HOURS

Ring Number	Net Section Thickness (inch)	Breaking Load (lb)
49	0.0205	8,760
50	0.0205	8,620
55	0.0205	8,600

Table A-5  
EFFECT OF PROOF LOADING ON ULTIMATE STRENGTH OF 2024-T4

Specimen	Tensile Test Procedure	Ultimate Strength (psi)
T1T3	Tested to failure without interruption of loading.	64,600
T1T4	Tested to failure without interruption of loading.	63,100
T1T5	Loaded to 2,500 lb, unloaded, held for one minute and then tested to failure.	64,700
T1T6	Loaded to 2,500 lb, unloaded, held for one minute and then tested to failure.	64,200
T1T7	Loaded to 2,500 lb, unloaded, held for 220 hours and then tested to failure.	64,000
T1T8	Loaded to 2,500 lb, unloaded, held for 220 hours and then tested to failure.	64,800
T1T9	Tested to failure without interruption of loading.	64,700
T1T10	Tested to failure without interruption of loading.	64,000

**SIGNIFICANCE OF DATA**

Lubrication of the Armalon torque washer, aluminum shear ring and piston cap with graphite resulted in the minimum torque required to rotate the piston cap. Based on the results of this series of tests, the assembly drawing has been changed to specify an Armalon torque washer lubricated with graphite.

The range of breaking loads was 8,090 to 9,200 lb. This spread may be attributed to differences in mechanical properties and cladding thickness throughout a sheet. A difference of only 0.0005 inch in cladding thickness

would result in a difference of nearly 200 lb in the breaking load. It has been shown metallographically that cladding thickness differences of 0.0005 inch do exist in the sheet.

A statistical analysis of these data has been performed by UpSTAGE Effectiveness Engineering. The result of the analysis was that the shear rings would perform as required in the UpSTAGE vehicle (Reference A-1).

A set of 10 shear rings has been set aside for use by the UpSTAGE program for the EB Fuel Tank Tests. These rings were produced coincidentally with those used for the shear tests.

If a viton-bonding cycle of 250°F for 4 hours is selected, the breaking load of the shear rings will not be affected.

Through tensile testing, it was shown that proof loading does not affect the ultimate strength. It was also shown that a time delay between the proof test and the shear test does not affect the ultimate strength.

#### REFERENCES

A-1 "Statistical Evaluation of P/N 1T35968 Shear Ring Development Tests," UpSTAGE Record of Discussion, 11-5-69, E. M. Skinner.

A-2 Case Sheets

79029  
82667  
89691  
89692  
89704  
89706  
89721

A-3 UpSTAGE Drawings

1T34606D - Test Fixture - EB Fuel Tank Piston Seal  
1T34697A - Washer, EB Fuel Tank Piston, Torque  
1T35832A - Seal, Shear Ring  
1T35968B - Ring, Shear

Appendix B

NUMERICAL CONTROL WELDING DEVELOPMENT FOR THE  
ELLIPTICAL UpSTAGE EB FUEL MANIFOLD FRAME

REPORT NO. MDC G2066

DATE: 1-21-72

Prepared by: R. F. Sporny and  
G. R. Stoeckinger

  
Approved by: R. A. Rawe, Branch Chief  
Metallics  
Materials & Methods -  
Research & Engineering

Prepared for: The U.S. Army Missile  
Command  
Huntsville, Alabama

Contract: DAAH01-68-C-1237

## ABSTRACT

A requirement arose to weld an elliptical shaped external burning fuel manifold frame P/N 1D15693 for the UpSTAGE program. The manifold was made from two 2014-T452 aluminum roll ring forgings that were blocker die formed into the elliptical configuration. A numerically controlled GTA welding procedure was developed using three axes of the 8-axis N/C welding machine. Resultant welds were free from porosity and oxide inclusions, and when aged resulted in minimum tensile yield strengths greater than 28,000 psi even if repaired twice. The success of the technique is believed due to the combined use of a 10 Hz pulsating welding current, in-process rotation of the weld wire feed about the tungsten electrode and an interference fit of the two forgings. A high incidence of lack of penetration defects plagued the total success of this procedure but nonetheless, a satisfactory N/C weld technique was employed to correct the discrepancy.

## 1.0 INTRODUCTION

A requirement arose to weld an elliptical shaped part (P/N 1D15693) which was a combination fuel manifold and structural frame for the UpSTAGE experimental missile program. This manifold-frame was to be fabricated from two 2014-T452 aluminum roll ring forgings which were blocker die formed to an elliptical configuration. The assembly of these two partially machined forgings create two elliptical butt joints having a major diameter of 33.75 inches and a minor diameter of 16.125 inches which produces the manifold portion of the part with a 0.875 inch inside diameter. The weld requirement was to fully penetrate in one pass the 0.165 inch thick square edge of the weld joint without any internal tooling for puddle support. In addition, the weld bead drop through was not to exceed 0.050 inch as well as be reasonably smooth and consistent so as to not disturb the fluid flow in the manifold. Subsequent to the welding, the manifold-frame was to be checked and straightened, if necessary, before artificially aging to the T-6 condition. The welds with up to two repairs were to exceed a minimum tensile yield strength of 28,000 psi once the artificial aging had been accomplished.

To satisfy these requirements two welding approaches were considered. The first was manual GTA (Gas Tungsten Arc) welding and the second was N/C (Numerical Control) GTA welding. The former method under the best conditions would necessitate numerous weld starts and stops plus a tremendous challenge for the operator to maintain consistent weld penetration not exceeding the 0.050 inch drop through requirement. The modified USAF-owned N/C welding machine\* was selected for its ability to follow complex weld joints, rotate the filler wire guide about the electrode and provide weld puddle control by pulsating the welding current.

To achieve the ultimate objective of developing an N/C fusion welding technique for the UpSTAGE external burning fuel manifold frame while simultaneously training personnel for ultimate production implementation, the following approach was taken.

Preliminary welding parameters were developed on flat 2014-T4 aluminum sheet with and without weld current pulsation. Mechanical properties were then obtained from these welded panels which included original welds and double

---

\*Machine No. USAF-053912, manufactured by Sciaky Bros., Inc.

repair welds to determine if the minimum yield strength could be consistently maintained following the artificial aging.

Three circular shaped manifolds simulating the cross sectional mass and weld length were designed, assembled and welded using 2014-T4 aluminum alloy plate stock to examine the performance of the modified N/C welding machine, the weld torch accessibility, wire guide rotational features, weld joint fit-up requirements, weld fixturing, tape programming, and current pulsation benefits.

The technology thus developed, was applied and optimized by welding and repairing where necessary four elliptical manifolds machined from forgings with the production configuration. Dimensional and mechanical properties of the welds in these forged parts were obtained and evaluated prior to committing the procedures and necessary documentation to production.

The successful effort to attain this end objective is reported herein.

## 2.0 EXPERIMENTAL PROCEDURE

### Equipment:

The welding equipment used in the preliminary steady state parameter development consisted of the following:

1. Welding Power Supply - Linde Missile Maker S/N 015
2. Wire Feeder - Linde Type SEH-2
3. Welding Torch - Linde HW-27 with #8 Gas Cup
4. Torch Travel - Linde Type OM-48
5. Manual Welding Power Supply - P&H AC-DC 300 amp with a Linde HW-20 Torch
6. Welding Fixture - Aluminum Fixture as shown in Figure 1

Subsequent welding was conducted on the Sciaky 8-axis N/C (Numerically Controlled) welding machine which is partially shown in Figure 2. The various axes and eight welding parameters are servo controlled and inputted by a punched tape coded in the binary decimal format to the Bendix Dynapath 20 MCU (Machine Control Unit). The three linear axes (x, y, z) are programmable in 0.0002 inch increments. The angular axes (a - turntable rotation, b - turntable tilt, c - wire feed and head rotation, d and e - head attitude)

THE SUPERIMPOSED CROSS-HATCHED AREA IS THE CROSS SECTION OF EB MANIFOLD FORGINGS AS MACHINED FOR THE WELD OPERATION. THE TEST PANEL IS SHOWN SHADED.

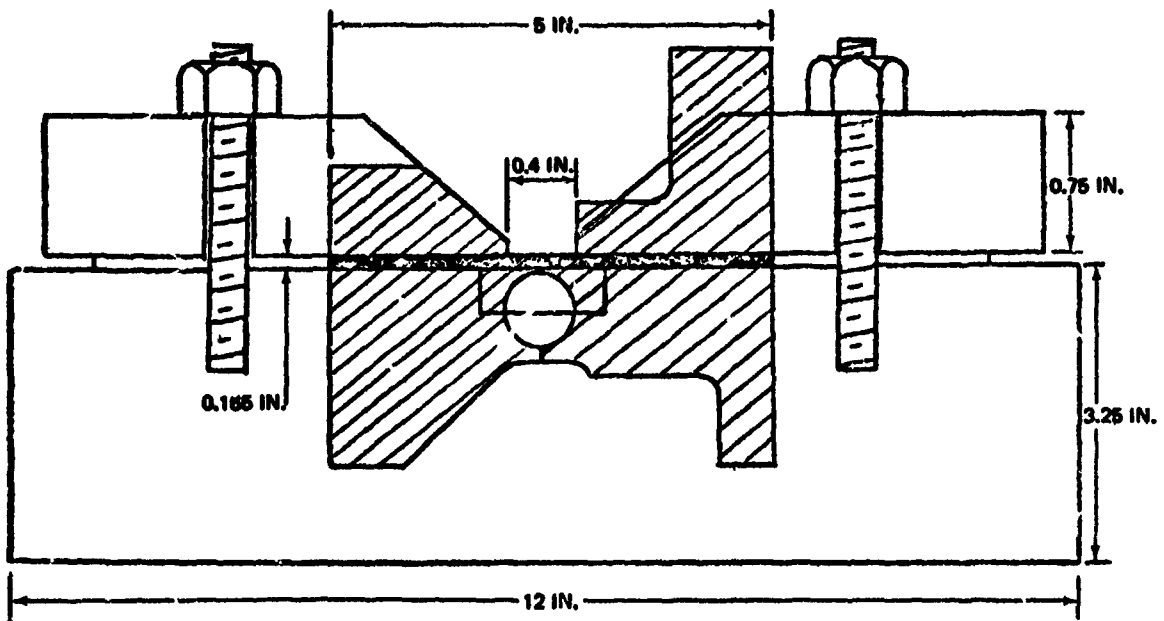


Figure 1. Weld Fixture--Test Panel Cross Section



Figure 2. 8-Axis Numerical Control Welding Head and Control Panel

are programmed in 0.002° increments. The welding current (programmed in 0.6 ampere steps), arc voltage (0.03 volts) and wire feed speed (0.1 ipm) can be individually changed as desired within a weld sequence. These in-process changes require 1.3 seconds which is the time for the electromechanical relays in the MCU to input a new parameter. The power supply is a 600 ampere SCR (Silicon Controlled Rectifier) with a choice of either constant current or constant potential static DC output characteristics. Welding currents can be pulsed at a given polarity up to 30 hertz maximum with independent adjustment of peak and base current duration. The machine is operated from the control panel as shown in Figure 2. During a weld sequence the operator may vary the filler wire feed rate  $\pm 10\%$  from the programmed tape value, override the travel speed if necessary, and adjust the filler wire entry angle either vertically or horizontally with a remote motorized wire guide control. The basic welding parameters are recorded during a weld on a Honeywell Oscillographic recorder equipped with a 1508 Visicorder and Accudata 117 Amplifiers, see Figure 3.

#### Materials:

The material used was as follows:

1. The test panels were 0.165 inch thick 2014-T4 aluminum alloy sheet per MSFC-104.
2. The filler wire was 1/16 inch diameter 4043 high quality aluminum alloy per DPM 3014-1.
3. Helium shielding gas per 1P20115 (DPM 152-2) was used in mechanized welding and argon per DPM 150-3 was used in manual welding operations.
4. Circular Test Manifolds - 3.0 inch thick 2014-T451 Aluminum Alloy plate per MSFC 105.
5. Elliptical Manifolds - 2014-T452 Aluminum Alloy Roll Ring Forgings per QQ-A-367.

#### PRELIMINARY PARAMETER DEVELOPMENT

The 0.165 inch thick 2014-T4 aluminum plates (5 inches wide by 15 inches long) were prepared for welding as follows:

- a. Degrease - Acetone

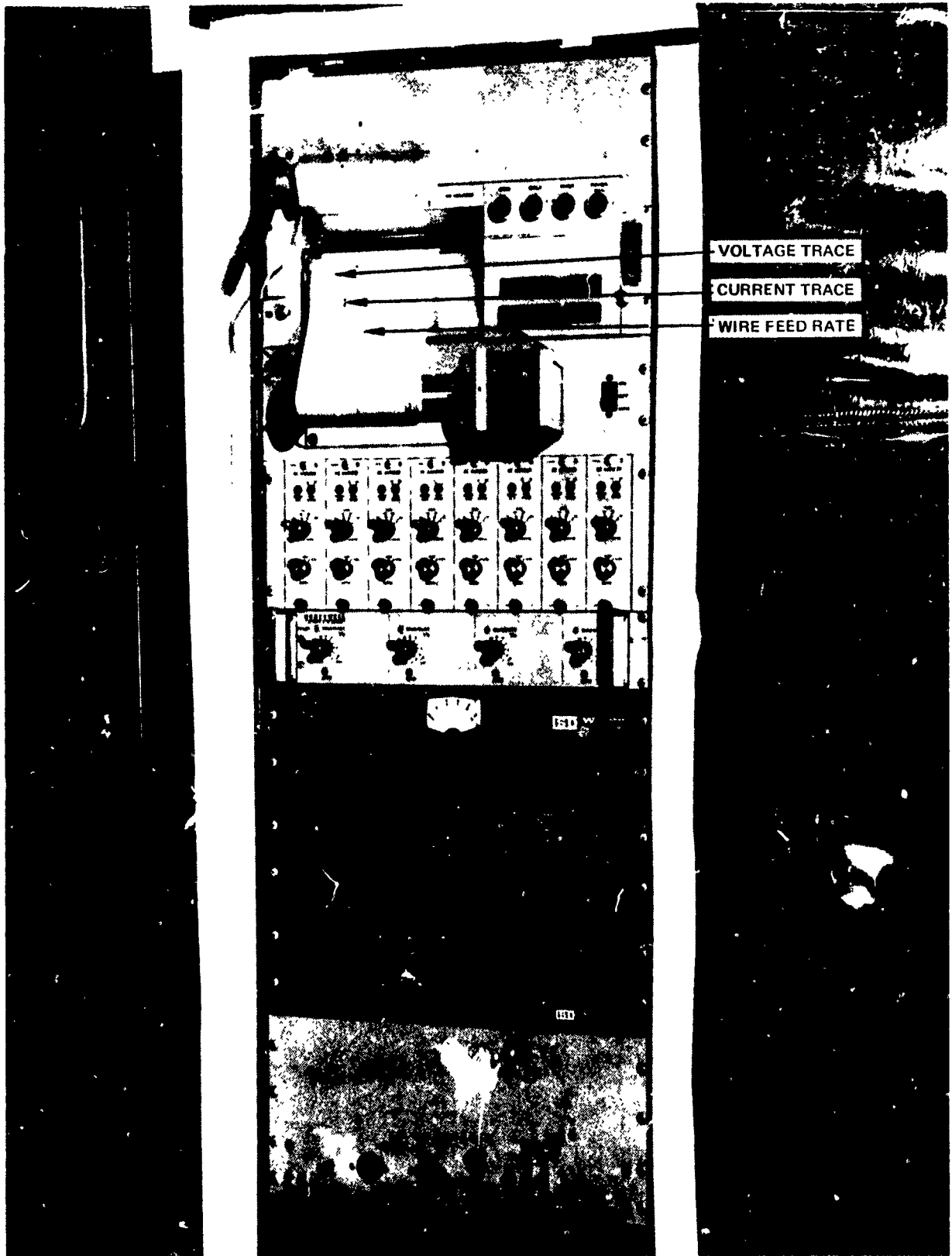


Figure 3. Honeywell Oscillographic Recorder

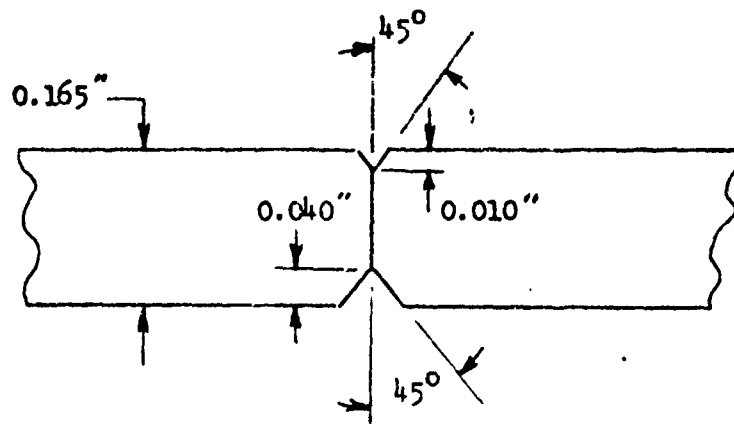
2. Etch - Paaajel & British Etch
3. Wire Brush - Fine Stainless Steel
4. Hand File - Draw File Along 15 inch length
5. Hand Scrape - 1/4 inch width ~~along edge~~ along edge to be welded - top & bottom

The joint designs are shown in Figure 4. The aluminum butt weld fixture (Figure 1) was used to approximate the mass of the actual part. No back-up bar was installed in the fixture in order to obtain free-fall penetration welds.

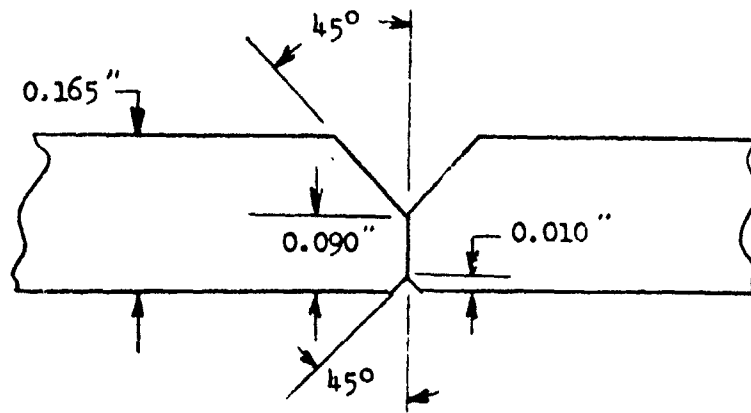
The GTA welding process was used for both the mechanized welding (direct current) and manual welding (alternating current) operations. Manual welding was being considered as a possible weld repair technique only. Mechanized weld parameters were developed to produce a single pass, full penetration weld attempting to produce a smooth, shallow weld drop-through shape. Several parameter combinations were evaluated including varying mixtures of helium and argon. None of the gas mixtures effected a drop-through shape improvement so pure helium was decided upon as the shielding gas to be used. The weld parameters which produced the most consistent weld with the least practical amount of drop-through are shown in Table I. The resultant weld geometry is shown in Figure 5.

Three 24 inch long panels were welded with these developed parameters and x-rayed. The welds were found to be free from defects. Ten tensile coupon blanks were excised from each panel (30 total), machined per 1T13007-5, and directly aged to the T6 condition per DPS 11150 (320°F for 18 hours). The coupons were tensile tested with the results being shown in Table 2.

Five additional 24 inch long panels were welded to evaluate possible weld repair procedures. One panel was manually welded using AC current, X-rayed, heat-treated, and excised into 10 tensile coupons and tested to compare manual weld properties to mechanized weld properties (Table 3). Four panels were mechanized welded, inspected, and rewelded to simulate repair welds. Each original weld was shaved flush and rewelded over its full length. The procedure was then repeated a second time over half the weld length. Mechanized welding was used on two panels and manual welding was used on the two remaining



Mechanized Weld Joint



Manual Weld Joint

Figure 4. Weld Joint Designs

Table I

Preliminary Weld Parameters

Amperage	-	120 DCSP
Voltage	-	11.5 VDC
Travel Speed	-	15 IPM
Filler Wire	-	1/16 IN. DIA. 4043 A1
Wire Speed	-	34 IPM
Tungsten	-	1/8 IN. DIA. 2% THOR
Tungsten Shape	-	75° WITH 0.030 FLAT.
Shielding Gas	-	Helium at 100 CFH using a #8 Cup

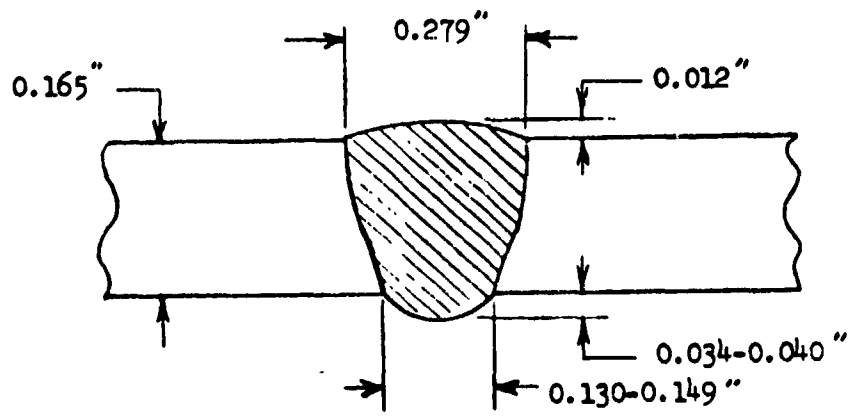


Figure 5. Weld Bead Dimensions

Table 2  
Tensile Properties of Initial Flat Plate Welds  
Welded 0.165 in. Thick 2014 Aluminum Alloy  
Using 4043 Aluminum Alloy Filler

Welding Procedure	Weld Bead Shape	Temper		Coupon Number	Yield Fty KSI	Ultimate Ftu KSI	% Elongation in 1 Inch	Location of Failure <sup>2</sup>
		Welded	Tested					
Control Coupons -No Weld-		T4	T6 <sup>1</sup>	C-1	47.3	67.5	21	
		T4	T6	C-2	50.1	67.8	19	
Mechanized Welds DC - GTA	As-welded ↓	T4 ↓	T6 <sup>1</sup> ↓	11-2	41.7	52.2	5	3
				-3	41.4	51.1	4	3
				-4	39.9	50.1	3	3
				-5	43.1	51.9	4	3
				-7	41.1	52.5	5	3
				-8	40.9	52.4	4	3
				-9	41.6	51.2	3	3
				-10	42.0	52.3	4	3
				12-1	42.4	52.7	4	3
				-2	41.0	50.0	3	3
				-3	40.5	48.3	3	3
				-6	41.4	50.4	4	3
				-7	40.9	48.9	3	3
				-8	41.3	47.5	2	3
				13-1	44.0	52.8	3.5	3
				-2	43.7	52.7	3.5	3
				-3	41.7	50.4	2	3
				-4	43.2	52.8	2	3
				-5	43.4	51.9	3	4
				-6	43.5	52.3	4	3
-7	43.0	51.6	3	3				
-8	43.7	52.4	3.5	3				
-10	42.0	51.4	4	3				

NOTES:

1. Welded coupons aged at 320°F for 18.5 hours.
2. See Figure 6.

**Table 3**

**Tensile Properties of Flat Plate Welds  
Welded 0.165 in. Thick 2014 Aluminum Alloy  
Using 4043 Aluminum Alloy Filler**

Welding Procedure	Weld Bead Shape	Temper		Coupon Number	Yield Fty KSI	Ultimate Ftu KSI	% Elongation in 1 Inch	Location <sup>2</sup> of Failure
		Welded	Tested					
Manual Weld AC Current	As-Welded	T4 ↓	T6 <sup>1</sup> ↓	HW-1	NA	53.4	6	3
				-2	33.1	54.0	6	2
				-3	33.2	49.0	4.5	3
				-4	33.2	54.7	7	3
				-5	NA	53.6	7	4
				-6	30.6	50.7	5	4
				-7	30.7	50.6	5	4
				-8	30.3	51.9	5	4
				-9	30.2	52.6	7	3
				-10	32.2	54.9	8	2
Mechanized Weld Plus 1 Mech. Repair	Shaved Both Sides	T4 ↓	T6 ↓	ARW-1	37.4	51.1	4	3
				-2	37.4	52.7	3.5	3
				-3	37.1	51.7	3.5	3
				-4	37.8	51.4	3.5	3
				-5	40.7	53.1	3.5	3
				-7	30.5	49.5	5	3
Mechanized Weld Plus 2 Mech. Repairs	Shaved Both Sides	T4 ↓	T6 ↓	ARW-8	38.9	51.1	3.5	4
				-9	36.4	51.3	3.5	3
				-10	36.0	51.7	3	3
				-11	37.6	52.2	3	3
				-12	35.9	50.7	3	3
				-13	35.8	50.7	3	3
				-14	28.9	48.3	5	3
Mechanized Weld Plus 1 Manual Repair AC Current	Shaved Both Sides	T4 ↓	T6 ↓	MRW-1	33.4	47.3	4	4
				-2	33.7	47.3	3	4
				-3	35.6	48.6	2.5	4
				-4	34.3	49.2	3.5	4
				-5	34.2	49.6	3	4
				-6	35.9	48.8	3	4
				-7	27.1	44.2	5	4
Mechanized Weld Plus 2 Manual Repairs AC Current	Shaved Both Sides	T4 ↓	T6 ↓	MRW-8	30.9	43.0	3	4
				-9	32.6	44.9	3	4
				-10	31.5	46.0	3.5	4
				-11	30.2	46.9	3.5	4
				-12	28.2	46.1	3.5	4
				-13	30.8	48.2	3.5	4
				-14	27.7	45.1	5	4

**NOTES:** 1. Welded coupons aged at 320°F for 18.5 hours.  
2. See Figure 6.

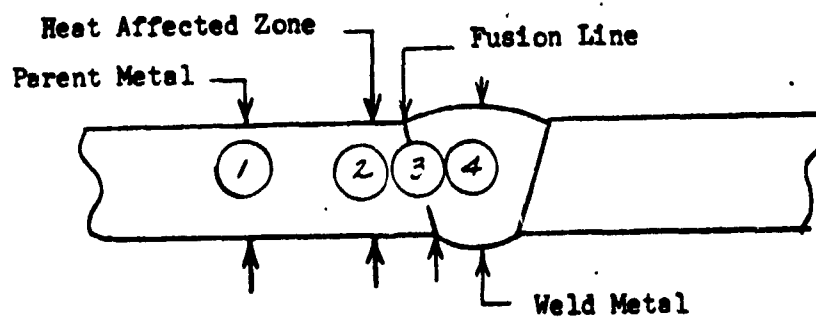


Figure 6. Location of Welded Tensile Coupon Failures

panels. The panels were then X-rayed, heat-treated, excised into tensile coupons and tensile tested (Table 3). All of the welds were free from defects.

#### PULSATION WELDS

The weld development was transferred to the 8-axis N/C welding machine in order to evaluate pulsed weld current. It was thought that a narrower weld with a flatter weld drop-through as compared with the steady state welds might be achieved by current pulsation. Various pulse rates and pulse durations were evaluated while adjusting the peak current to obtain an average current equal to the current used in the steady state welding. An equal pulse duration of 3 cycles at peak current and 3 cycles at base current (10 Hz pulse frequency) produced a weld bead having the same shape as the steady state current weld but with improved consistency. Several panels were welded and X-rayed. The welds were water clear.

#### CIRCULAR MANIFOLD WELD DEVELOPMENT

To prove the capability of the newly modified N/C welder, the ability to rotate the wire guide and tungsten electrode while welding, develop weld overlap procedures and optimize the preliminary weld parameters, three simulated circular manifold assemblies were machined from 2014-T451 plate stock. These test parts were designed with two 26.5 inch diameter annular butt welds on opposite sides as shown in cross-section in Figure 7. The length of the weld and mass of material were selected to simulate the conditions of the elliptical manifold.

#### WELD FIXTURE

An all aluminum weld fixture was fabricated to secure and align the circular manifold assembly, see Figure 8. This fixture contains an annular groove in which the inner and outer rings were placed. Eighteen holes were drilled through the bottom of this groove for viewing the weld drop-through. Four thru bolts were used to secure each ring to the baseplate. This fixture was secured concentrically on the turntable baseplate.

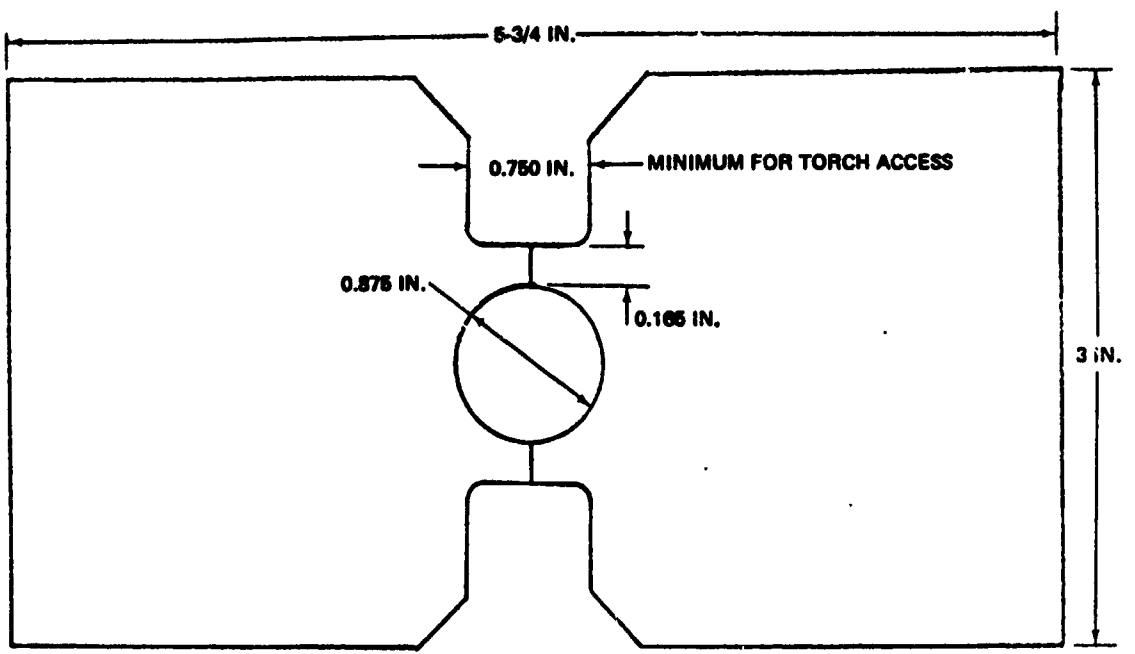


Figure 7. Circular Manifold Cross Section

---

Hold Down Bolt Holes  
8 Bolts

Viewing Holes  
15 Holes

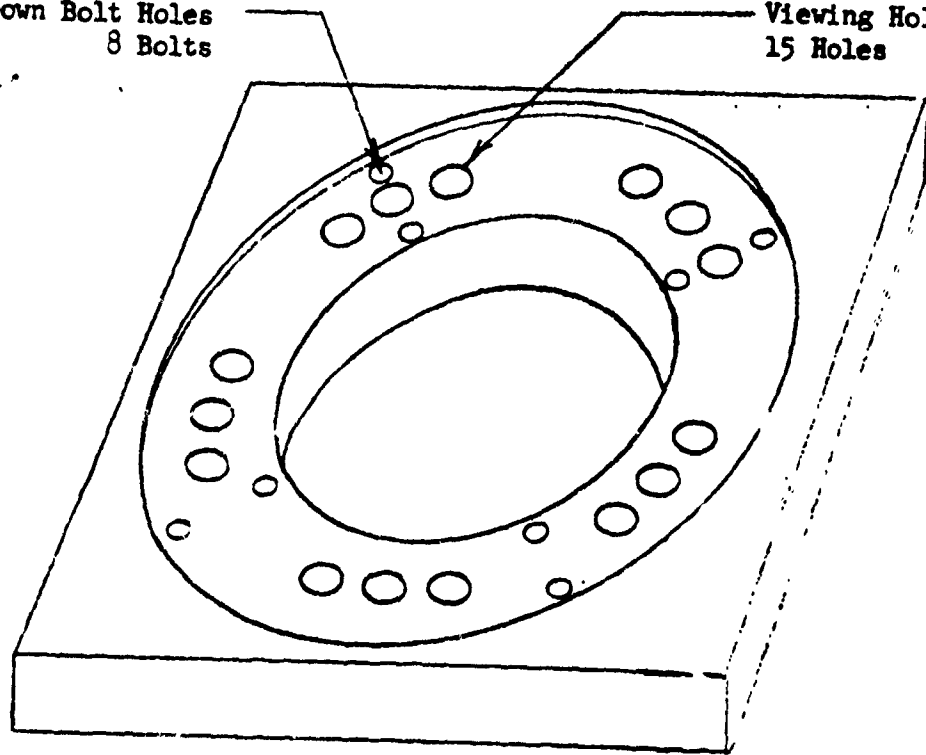


Figure 8. Circular Manifold Weld Fixture

---

## N/C TAPE PREPARATION

A preliminary N/C welding tape was prepared with the following provisions. The circular manifold remained stationary in the x-y plane of the machine while the torch traversed the circular joint in incremental movements of the x and y axes. The chord length generated by the combined motion was programmed so that deviation from the true arc of the joint did not exceed 0.005 inch at chord midpoint. The c-axis (convertible with the z-axis) was programmed to rotate the wire guide about the tungsten electrode simultaneously with the individual chord movements always keeping it ahead and in line with the joint. The total angular rotation of the wire guide was 400° (40° for weld overlap) followed by one 400° reverse movement to unwind the cables after the weld. The tangential travel speed of the torch was 20 rpm for the first 370° of the program, followed by successive increases to 40 rpm up to the 400° point. (The formula for calculating the feed rate is shown in Appendix A.) Through use of the feedrate override control, the final optimized speed can be chosen as a percentage of the programmed value - never greater.

### 2.1 CIRCULAR MANIFOLD WELD DEVELOPMENT

#### PARAMETER DEVELOPMENT

Using the pulsation weld parameters developed on flat plate, the split circular manifold was welded in six segmented 40° increments as shown in Figure 9. It was necessary to progressively increase the peak welding current to achieve 100% penetration due to the increased heat sink of the part. Welding current increased overall from 150 to 216 amps, arc voltage from 12.0 to 13.5 volts, wire feed speed from 26.0 to 28.0 ipm while the tangential travel speed remained constant at 10 ipm (50% of feedrate override).

Weld overlap and tie-off parameters were developed on the same part by backstepping in six segmented 40° increments. The first 20° of each increment was over the remaining unwelded joint followed by 20° of overlap. It was found that the best results were obtained by decreasing the travel speed by 10% in the 1.5° block just ahead of the weld start, increasing the arc voltage to 15.0 volts in the first 3.0° block after overlap and then reducing the peak welding current in four successive 3.0° blocks to a final value of 96 amps.

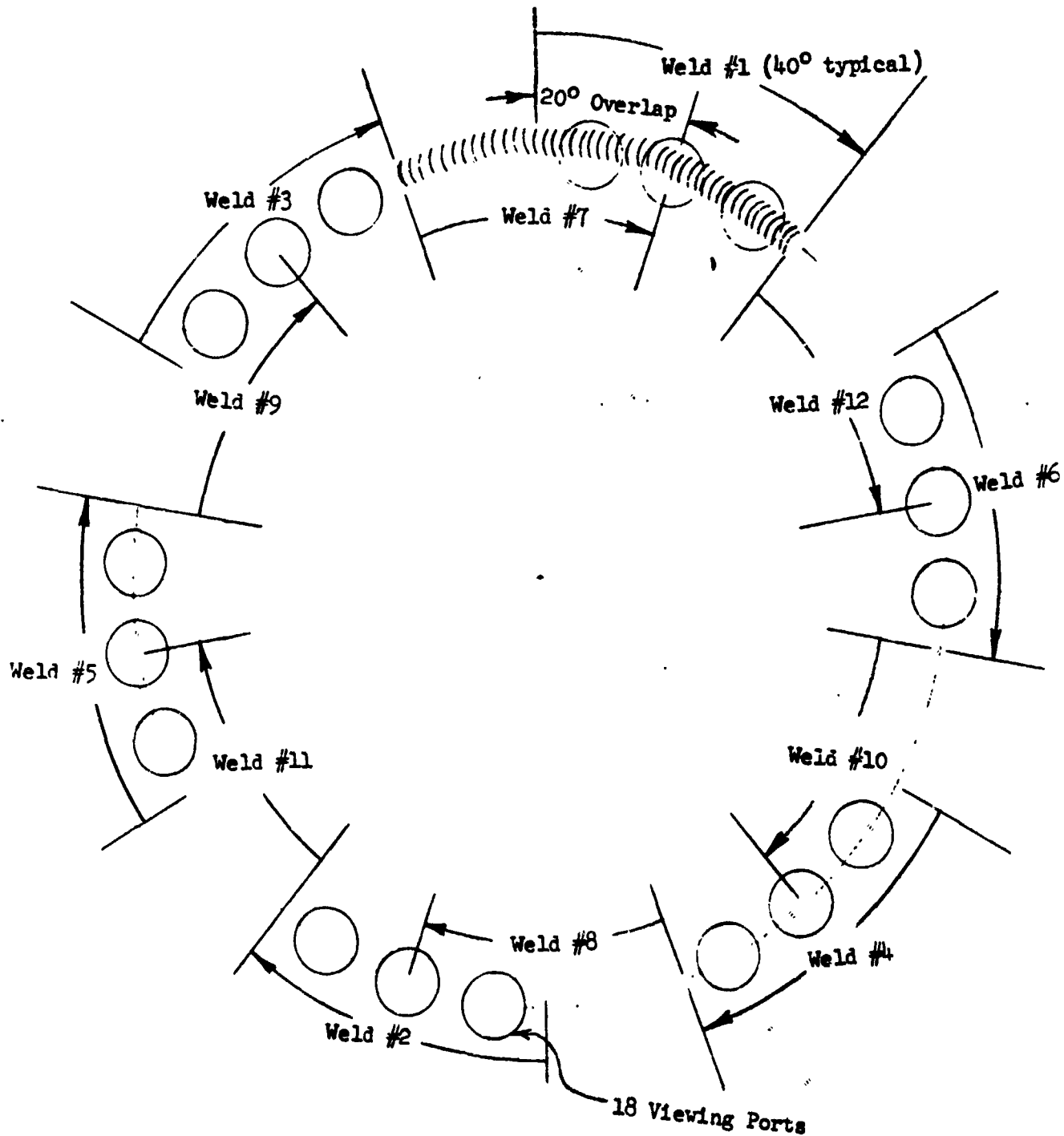


Figure 9. Circular Manifold Weld Parameter Development Test Sequence

These procedures were then used to weld the other split circular manifold. During the weld the joint opened ahead of the arc, and in the last quadrant it spread to 0.025 inch and as a result root side fusion was lost. Otherwise, the weld was dimensionally satisfactory.

As a result of this condition, it was necessary to develop a technique for minimizing or eliminating the gap buildup during welding. Thus, a shrink fit approach was devised.

The remaining two full circular test part details were machined with 0.003 to 0.005 inch of extra material left on the weld joint faces so that just prior to welding, a dry finish machine cut could be made leaving the joint faces clean and ready to weld. In order to evaluate a shrink fit, these parts were left in their oversized condition and prepared for welding by lightly scraping the weld joint surfaces which removed 0.0005 inch per surface. This produced a 0.012 to 0.015 inch diametrical interference fit between the inner and outer rings which was not considered to be sufficient to off-set the gap observed on the previous part, but it was thought that it would give some indication as to the value of this technique. The outer ring was heated to 200°F which caused a 0.060 inch increase in the inside diameter. The inner ring, which was at room temperature, was inserted into the outer ring and shimmed vertically to eliminate weld joint mismatch. When the assembly cooled to room temperature, there was metal-to-metal contact along the full length of the weld joints.

The full circular test manifold was then secured in the weld fixture. The N/C tape was modified 0.065 inch in the X-axis to correct for a difference in part diameter. Both sides were N/C welded during which no joint gap was observed (See Figure 10). The weld bead was slightly convex and most satisfactory in appearance. Subsequent radiographic inspection revealed intermittent lack of penetration throughout the weld which was attributed to the improved heat transfer due to the shrink fit. Thus, after shrink fit assembly of the last circular manifold, both joints were welded with the peak welding current increased to 234.6 amperes (other parameters are detailed in Appendix B). The face of the weld bead was flush with the top surface of the joint. The welds were then X-rayed and found to be free from defects.



**Figure 10. N/C Welded Circular Manifold**

Shrinkage measurements were taken at 60° intervals on this weld from 2 inch gage marks placed transverse with the weld. On the first side the shrinkage averaged .030 inch and on the second side it averaged .012 inch. These measurements gave an indication of the loss in volume within the manifold which was critical from a design standpoint.

#### WELD REPAIR

With the lack of penetration defects present in the first circular manifold, a repair technique was devised. A second hole was drilled in the manifold 180° from the first pressurization hole. 200 ml of methyl alcohol was poured in a beaker and Solar 202 aluminum welding flux was added until 400 ml of solution was obtained. The solution was poured in one of the holes and the part was rotated to coat the interior surface of the manifold. The remaining solution was poured out and then the part was dried by heating to 125°F. After shaving the defective weld beads flush, both sides were rewelded with the N/C tape having 234.6 amps of peak current. The weld ran smoothly except for some gaseous expulsion near the end of the weld on the top side. This situation was believed attributable to a heavy concentration of flux in the unfused faying surfaces of the joint. Otherwise the weld was found acceptable in subsequent radiographic inspection.

#### Evaluation

Following the radiographic inspection of each weld, the welds were inspected for surface defects using dye-penetrant per DPS 15101. No surface defects were found in any of the welds. The two completed circular manifolds were finally inspected by helium leak detection method using a sensitivity of  $3 \times 10^{-9}$  scc/sec and no leaks were detected.

The first full circular manifold was cut into sections to view the weld cross-section and penetration. The weld cross-section was basically the same as shown in Figure 6 with a consistent weld drop-through of 0.035 to 0.040 inch.

## 2.2 ELLIPTICAL MANIFOLD WELD DEVELOPMENT

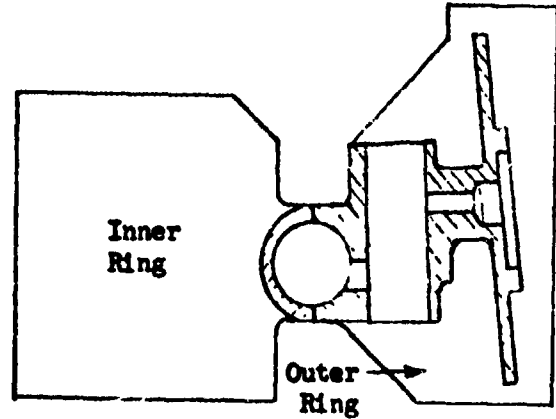
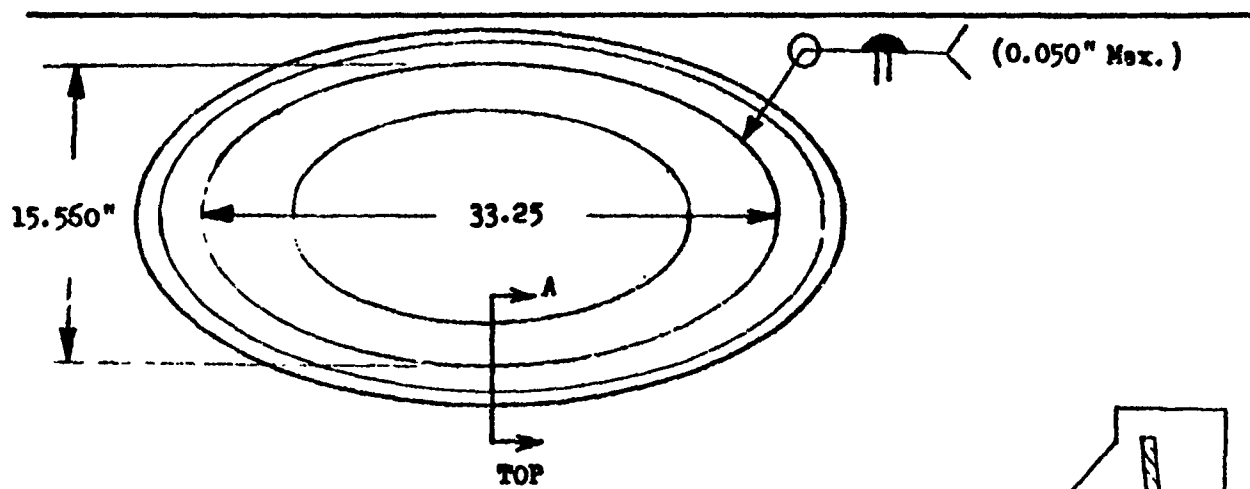
The developmental elliptical manifold was configured like the production part. It was composed of an inner and outer elliptical shaped 2014-T452 aluminum roll ring forging. When these two rings are assembled one inside the other, an elliptical weld joint is created having a major diameter of 33.25 inches and a minor diameter of 15.560-inches as shown in a schematic sketch of the manifold in Figure 11. On the opposite side the elliptical weld path is interrupted to allow for the subsequent machining of four integral actuation ports. Views A-A and B-B show the cross sections of interest and reveal in phantom the resultant cross section of the manifold after machining.

### WELD FIXTURE

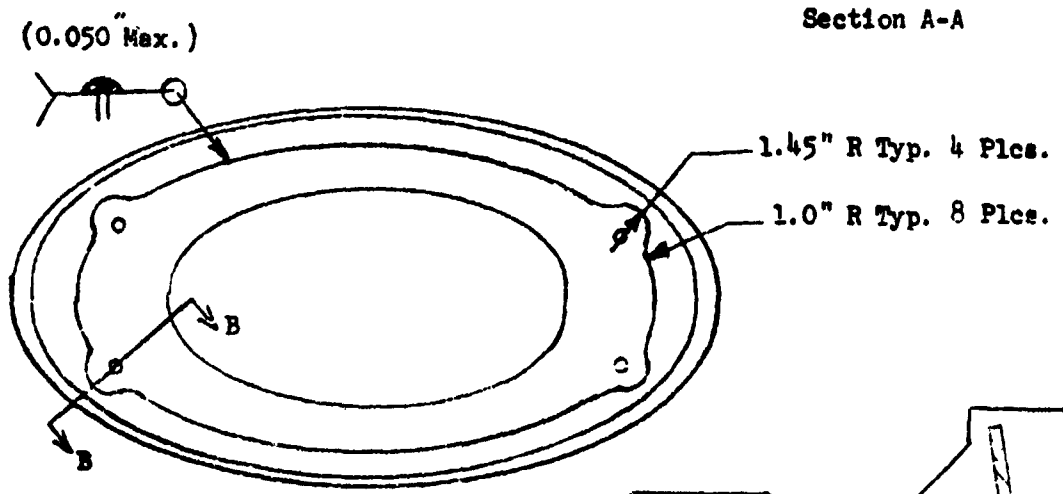
The weld fixture was designed and fabricated as a trunnion type tool so that it could be placed between the head and tail stock of the N/C welder. This fixturing approach permitted rotation of the entire assembly between welds by programming the A-axis  $180^{\circ}$  without removal of the manifold. The fixture, shown in Figure 12 was made entirely of aluminum to reduce overall weight. The assembled manifold was placed in the cavity and accurately located with two fixture index pins. Stainless steel bolts were advanced laterally to prevent any movement during welding.

### WELD TORCH MODIFICATIONS

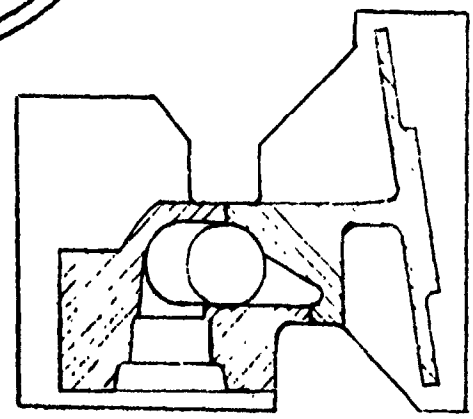
One of the major problems in set-up and weld joint tracking was that the welding torch, a Linde HW-20 machine welding torch, was not manufactured with enough precision to allow it to be rotated through  $400^{\circ}$  without causing a tracking error. The error resulted from the torch body not being exactly straight, the collet not centering the electrode in the torch as well as locating the electrode differently each time the electrode was replaced. It was initially decided to manufacture a new precision torch, similar to the HW-20, to eliminate this problem but after further consideration it was decided to modify an existing Linde HW-20 torch. The torch body was machined concentrically in a lathe, with a plug placed in the center of the collet body hole. The collet body threads were re-machined to improve the tolerance and concentricity of the electrode location. These modifications did minimize the



Section A-A



BOTTOM



Section B-B

Figure 11. Schematic of Elliptical Manifold Frame



Figure 12. Weld Fixture for Elliptical Manifold

tracking problem but did not completely eliminate it. Each time the electrode was replaced, a small correction was necessary. This was accomplished by shimming the torch mounting bracket to center the electrode to the weld joint seam. The electrode eccentricity was reduced from 0.100 inch to 0.010 inch.

#### N/C TAPE PREPARATION AND PROOFING

The preliminary N/C tape for the elliptical manifold configuration contained the same provisions for weld position, torch rotation, axes movement and chord length deviations as that for the circular manifold tape. In addition, the tungsten index point was on the centerline of the weld fixture, the weld start point two inches before the minor diameter and the tangential travel speed at 10 ipm maximum. These requirements were inputted to a computer using the APT III (Automatic Programmed Tool) program. Two tapes were generated having 229 blocks of information for the top side and 195 blocks for the bottom side. Included in these tapes were the welding parameters developed on the circular manifold, overlap and tie-off data plus torch movements at the start of the weld. The first tape includes a movement for moving the torch away from the weld fixture while the assembly is rotated, followed by a return torch movement to the workpiece.

The tape was initially proofed by tracking the joints as photographed on a master mylar coated sheet metal template. It was found that some of the c-axis (torch rotation) movements were too rapid causing the N/C machine to lose synchronization. In addition, the acceleration (g08) and deceleration (g09) codes that were programmed in the tape when the c-axis reversed direction caused the torch to temporarily stop. This condition was improved by removing the g08 and g09 codes and by reducing the angular change in those blocks where synchronization was lost. Further tape proofing was performed by placing just the inner forging in the weld fixture. During the first trial run, it was found that the top face plate of the tool protruded too far toward the joint in the area where the two index pins were located. By removing the excess material it was then possible for the torch and wire guide to pass this area without obstruction.

Continued tape proofing revealed a problem with the wire feed guide tube hitting the side walls of the manifold in the four port areas on the bottom side. This problem was manifested by the desire to have the filler wire enter the weld puddle directly in line with the joint. To satisfy this requirement it was necessary for the wire guide to rotate  $+47.308^\circ$ , then  $-110.008^\circ$ , and then  $+43.484^\circ$  in the span between the respective tangent points in the port area as shown in Figure 13. To resolve this problem, it was necessary to deviate from the requirement of having the wire enter normal and in-line to the weld puddle and accept angular deviation up to  $\pm 30^\circ$ . Consequently the tape was revised where this area was traversed with total angular movements of  $+17.954^\circ$ ,  $-81.026^\circ$  and  $+18.278^\circ$  respectively. It was also necessary to increase C-axis movements prior to the first tangency point by  $25.578^\circ$  to make the net change the same.

#### ASSEMBLY PROCEDURE - ELLIPTICAL

The manifold parts were N/C machined with an extra 0.005 inch of material left on the weld joint face in addition to the 0.005 inch per face required for the interference fit. The parts were brought to the final dimension by hand filing them to a sheet aluminum photo template as shown in Figure 14.

The weld joint preparation for welding began by degreasing and acid etching the parts per DPS 41006 Method 1. The weld joint faces were then draw filed and the upper and lower surfaces hand scraped for a width of a quarter inch as shown in Figure 15. Having completed the preparation, the parts were each placed in a fabric reinforced plastic bag which was evacuated and back filled with dry nitrogen to minimize oxidation of the scraped surfaces.

When the assembly process was ready to begin, the outer ring was removed from its bag, four thermocouples installed, and set-up on laboratory type hot plates for heating as shown in Figure 16. The cleaned surfaces were visually inspected with white and black light and spot scraped where necessary. The ring was then heated to  $200^\circ\text{F}$  to  $250^\circ\text{F}$  at which time the inner ring was inserted and the joints matched. The assembly was air cooled to room temperature.

	Span	Original <sup>o</sup>	Revised <sup>o</sup>
before	①	---	+25.578
	①	+ 47.308	+17.954
	②	-110.008	-81.026
	③	+ 43.484	+18.278
$\Delta =$		<u>- 19.216"</u>	<u>- 19.216"</u>

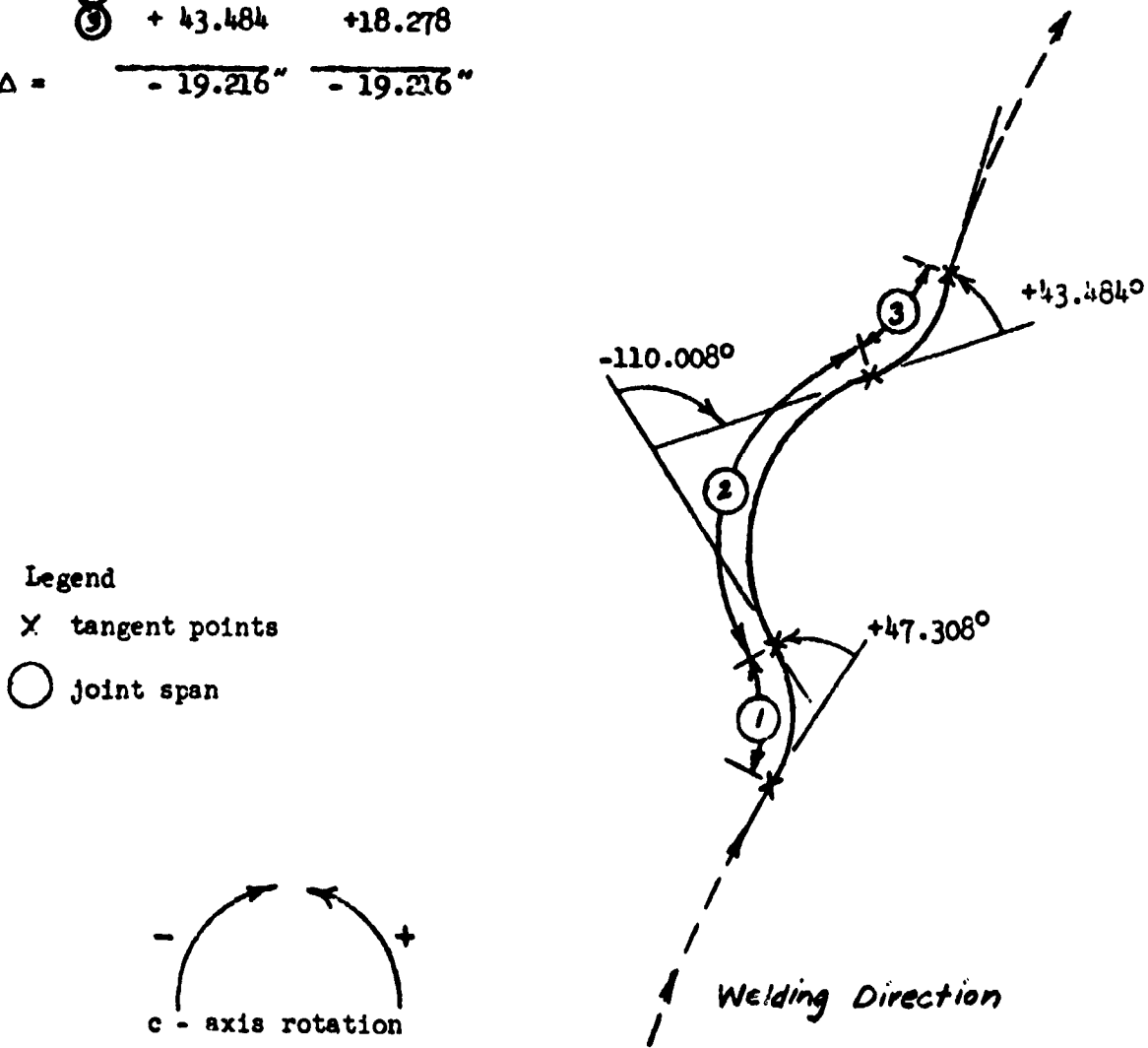


Figure 13 Wire Feed Movements in Port Area

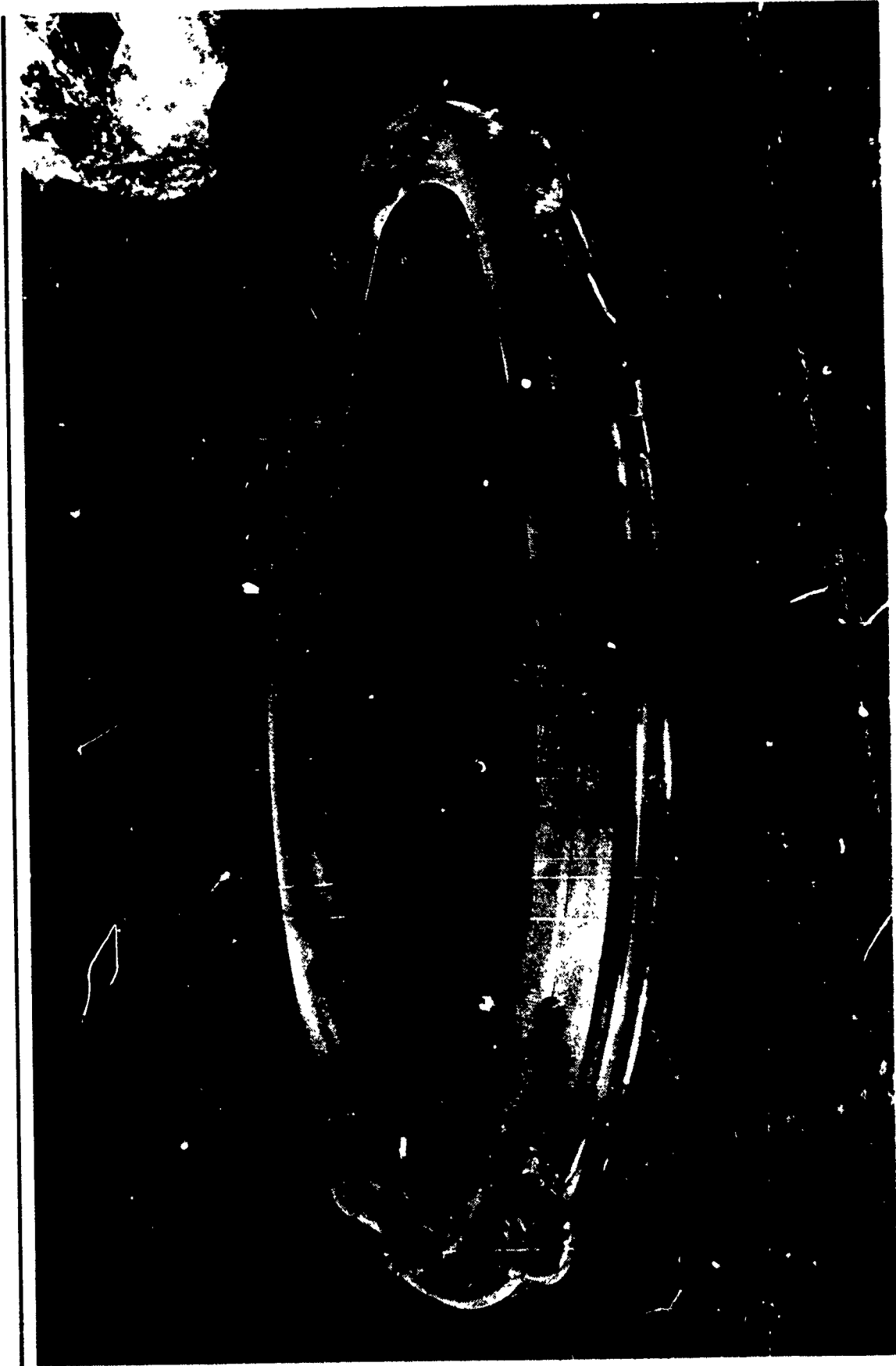


Figure 14. Inner Elliptical Forging as Machined for Welding



Figure 15. Scraping of Weld Joint Area for Welding

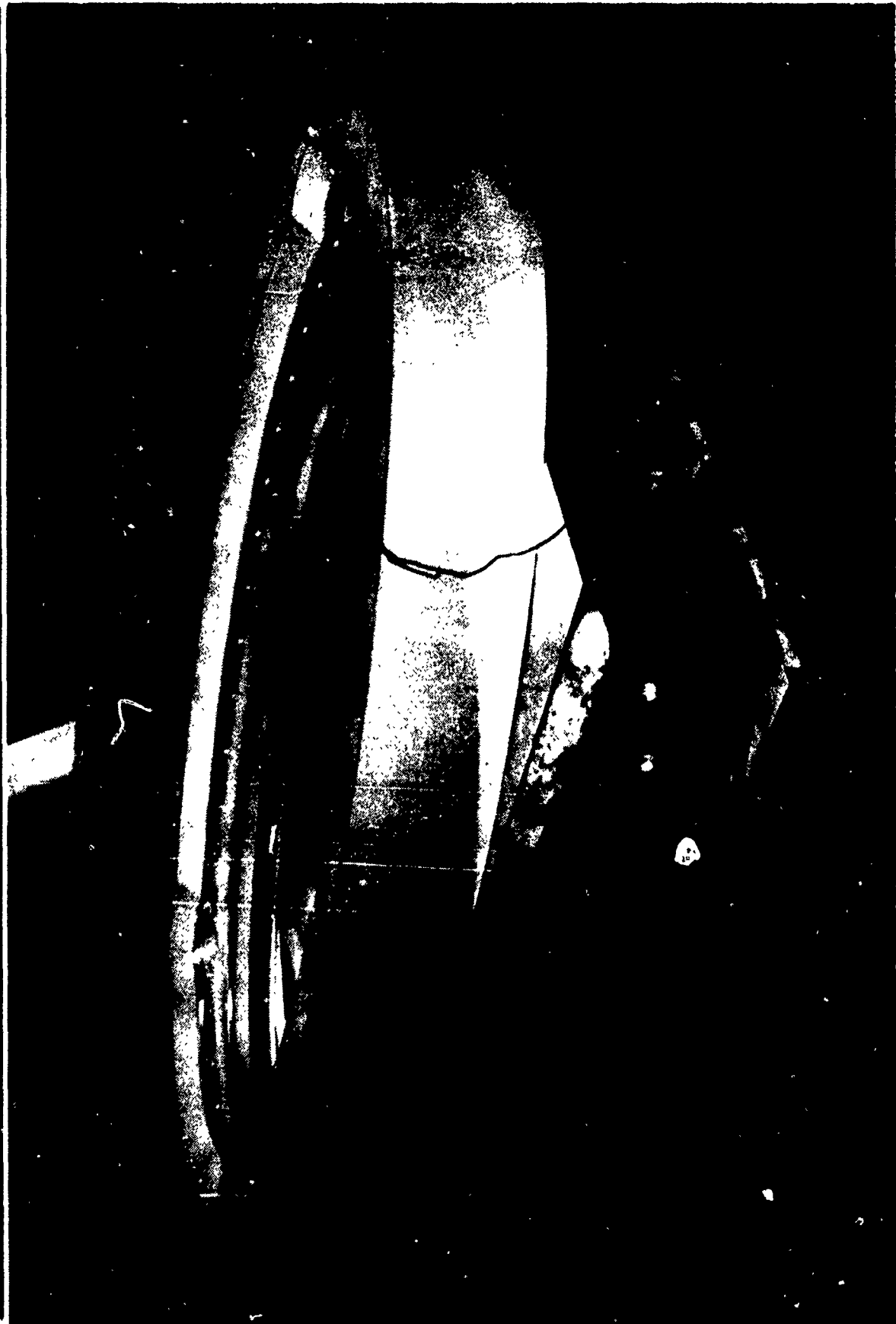


Figure 16. Heating of Outer Forging for Shrink Fitting

### WELDING PARAMETER OPTIMIZATION

The first elliptical manifold was assembled in the manner just described and secured in the weld fixture. The top side joint was tracked to within  $\pm 0.010$  inch after several adjustments of the welding torch mounting bracket. The joint was welded with a peak current of 234.6 amperes without interruption.

The weld was flat to slightly concave on the face and sunk to a maximum of 0.070 inch in those areas where the inside cavity was enlarged for the actuation ports. Figure 17 shows a section subsequently removed from this area and sectioned longitudinally to examine the underbead. Note the affect of this loss of mass on the root bead width.

After the top side weld, the part was rotated  $180^\circ$  and the second side welded with the same peak welding current approximately 30 minutes later. During the weld it became so hot and concave that the program was stopped and the machine switched from the tape value of welding parameters to manual potentiometer input. This allowed for adjustment of welding current during welding and a value of 204 amperes peak current was found to eliminate concavity and restore bead convexity without a loss of penetration. Only in the small radius portion of the port areas did concavity still exist. A section through this area is shown in Figure 18.

On both joints the weld start and overlap area was irregular due primarily to the large button that existed from the weld start causing the wire to raise, hit the tungsten electrode and disturb equilibrium conditions in the weld puddle. As a result several trial N/C tapes were prepared to resolve this problem. By running beads on plate, adjustments were made to arc voltage, travel speed and filler wire feed speed. In essence a ramp of filler wire was created by starting at 20 ipm and increasing to 28 ipm 0.400 inch after the start. Then upon overlap, the travel speed was reduced from 10 to 9 ipm 0.5 inch before the weld start and then returned to 10 ipm once the arc was on top of the weld start. The arc voltage was increased at this point to prevent the filler wire from shorting against the tungsten. Then the welding current was reduced in four increments to 66 amperes while maintaining the pulsing condition. These tests also displayed the need for accurate positioning of

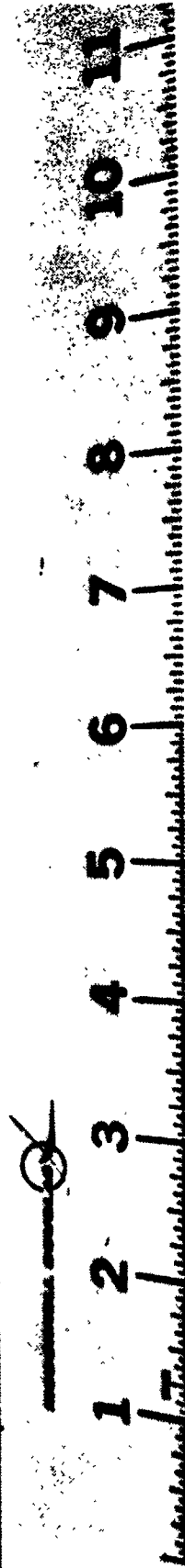
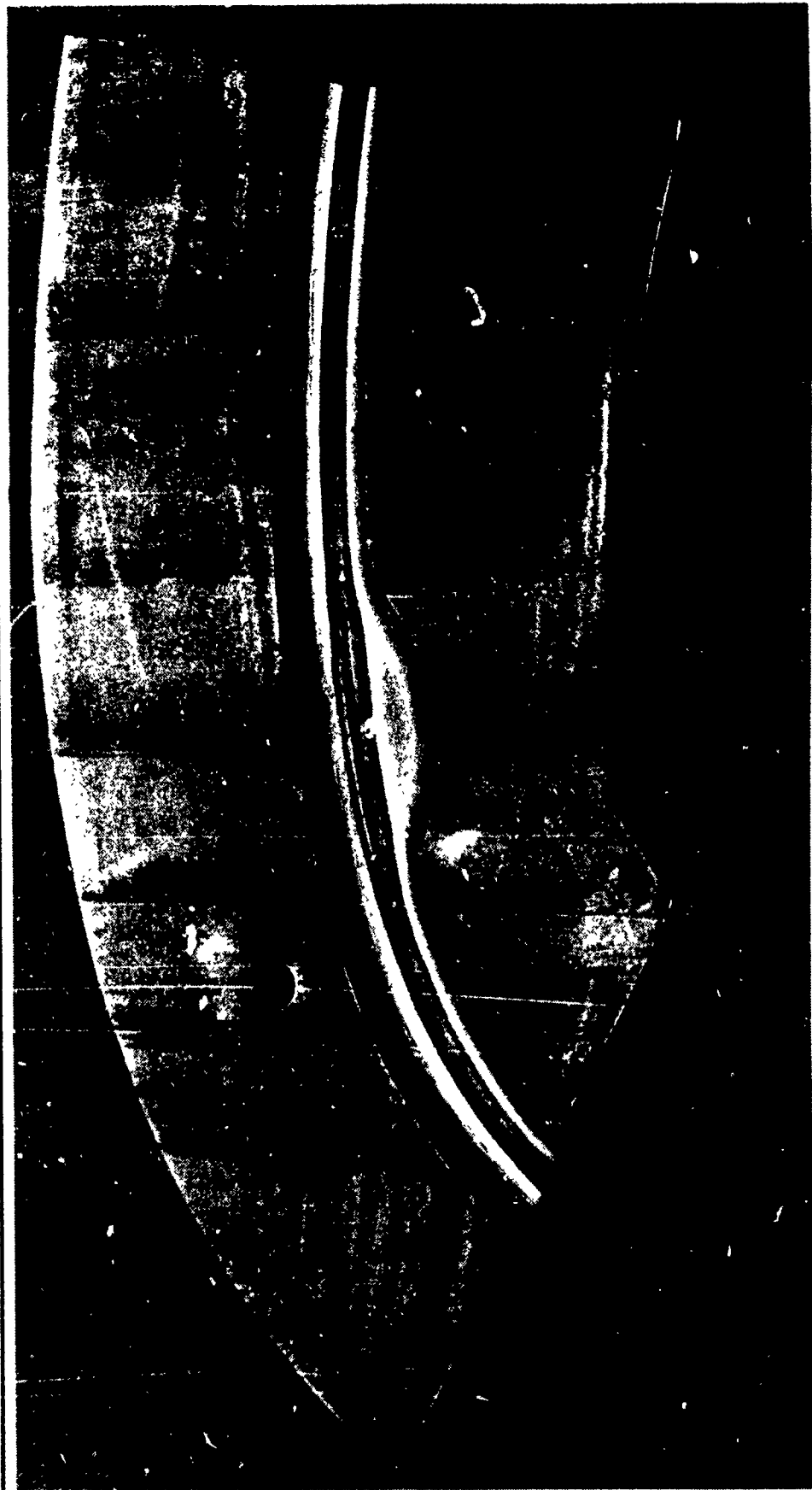


Figure 17. Longitudinal Section of Elliptical Manifold Showing Underbead in Port Area

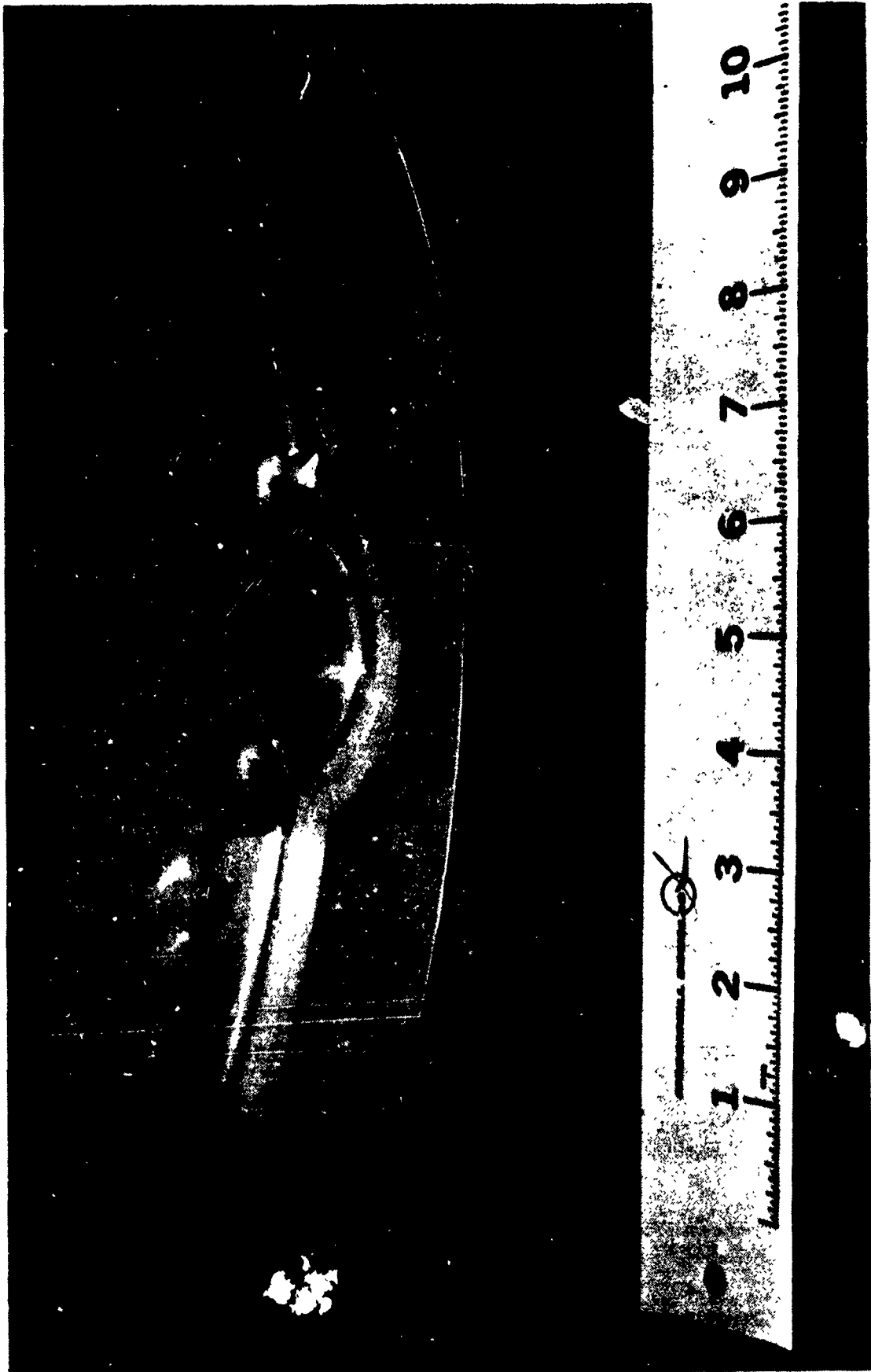
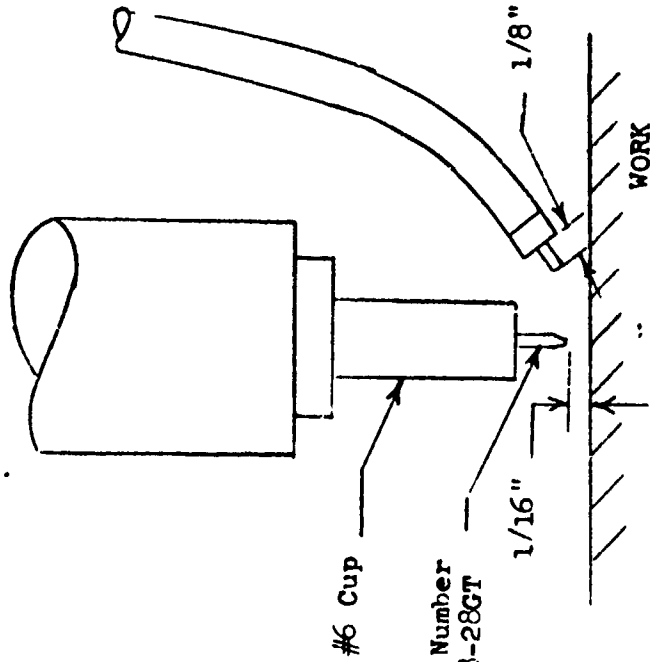


Figure 16. Section of Elliptical Manifold Indicating Areas of Weld Concavity

the filler wire and tungsten electrode with relationship to the cup as shown in Figure 19.

This first elliptical test manifold was then X-rayed, knowing that there were several unacceptable areas caused by weld parameter errors, to get some ideas as to the internal weld quality as might be affected by the pre-weld cleaning procedure. The welds were found to be free from any internal defects. Sections were cut from the manifold where the weld was considered to be representative of an acceptable weld. Tensile coupons (per 1T13007-3) were excised from these sections as shown in Figure 20 obtaining six coupons from the top weld and six coupons from the bottom weld. The coupons were aged to the T6 condition and tensile tested. The results are shown in Table 4.

A second elliptical manifold was then welded with a revised N/C tape that included the starting and weld overlap procedures developed on plate. In addition a reduction of 5 amperes in the peak welding current was programmed for the critical port areas on both sides of the joint except for an 11 ampere increase in the back side of the port on the bottom side to account for the greater mass of material. The weld was flat on the top side and slightly convex on the bottom side. However, the welding current changes were not great enough to correct the concavity present in the port areas. In addition it was noted on the oscillographic trace of the pulsing welding current, that the small 5 and 11 ampere programmed peak current changes were not compatible with the N/C Machine Control Unit. Since 1.3 seconds of raw time is required for the electromechanical relays to read and store a new value, the peak welding current drops to the base current value during this period followed by an exponential rise back to the new programmed value. With the base current set at 75% of the peak current, this results in an instantaneous drop of  $227 - (.75 \times 227) = 57$  amperes, and can cause an interruption in weld penetration for a free fall weldment.



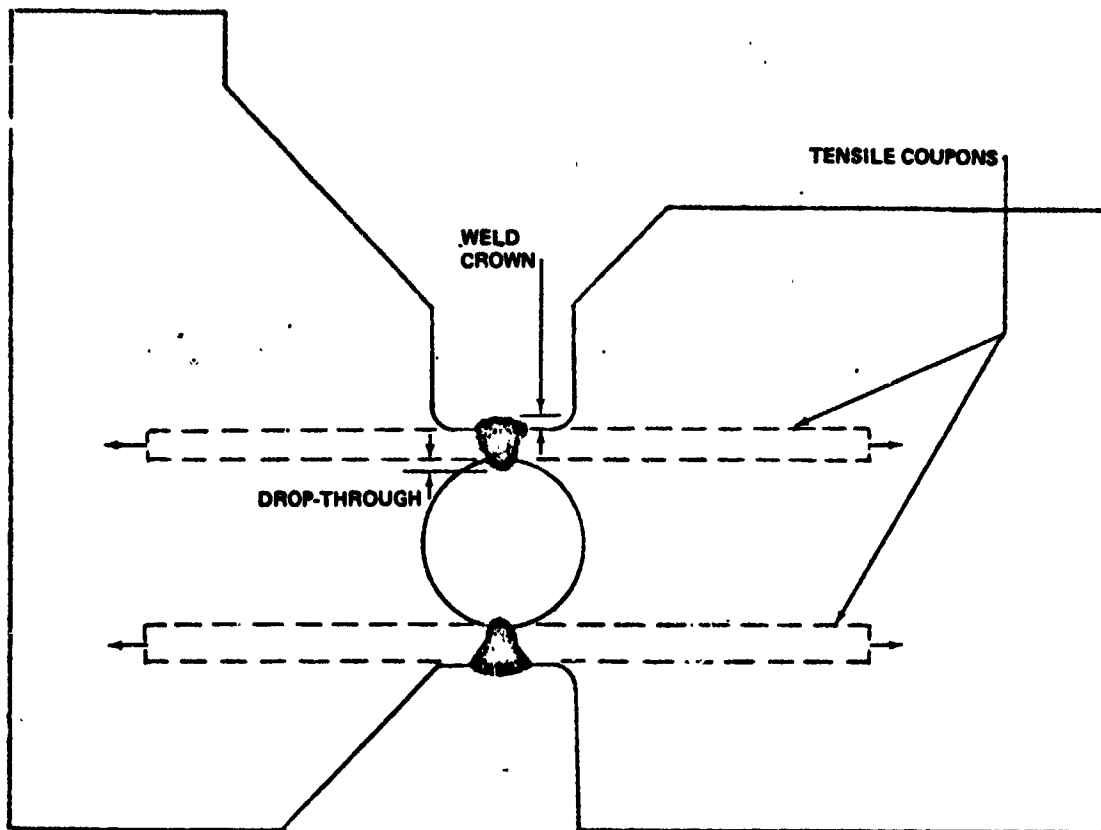
Electrode Extension from Cup  
and Wire-to-Electrode Set-up  
Dimensions

A

Electrode-to-Work Dimension  
and Wire Extension Prior to  
Arc Initiation

B

Figure 19. Torch and Filler Wire Set-Up



CROSS-SECTION OF UpSTAGE TEST MANIFOLD—FRAME P/N 1T36130  
 WELD CROWN AND DROP-THROUGH WERE LEFT AS-WELDED  
 (SMALL ARROWS SHOW LOADING DIRECTION)

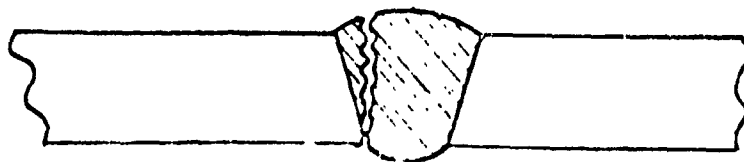
Figure 20. Location of Tensile Coupons Excised from Forged Elliptical Manifold

Table 4

EB Manifold Frame Tensile Test Results  
Forged 2014 Aluminum Welded in the T<sup>4</sup> Condition  
and  
Aged to T6

	Coupon No.	Yield, Psi	Ultimate, Psi	% Elongation	
				1/2"	1"
FWD. (Top)	1F	38,280	41,510	5	3
	2F	----	38,850	6	3
	3F	35,900	40,970	4	2
	4F	35,120	40,190	4	2
	5F	36,360	39,260	6	3
	6F	34,890	39,050	4	2
	AVG.	36,110	39,970	5	2 1/2
AFT (Bottom)	1A	37,080	38,360	4	2
	2A	35,940	36,230	2	2
	3A	35,440	37,250	4	2
	4A	37,920	38,940	4	2
	5A	38,820	40,790	4	2
	6A	36,000	38,440	4	2
	AVG.	36,870	38,500	4	2

NOTE: All Failures Occurred as Shown Below:



The weld overlap was considerably improved but contained isolated blips due to a depression in the weld start as a result of a high initial current condition. However, it was interesting to find that as the peak welding current was programmed to lower values in the overlap area, the oscillographic trace revealed a smooth transition to the new value. Thus, it is apparent that when the current is reduced in greater than 50 ampere increments, the lag in the electro-mechanical relays is not problematic.

The X-rays of this second elliptical test part indicated a loss of penetration for a length of  $3/8$  of an inch at each spot where a slight current change had been programmed as well as a lack of penetration at each port area in the bottom weld.

The limitation in making small in-process changes to the welding current necessitated using the travel speed to reduce heat input for correction of the bead concavity problem. Thus the tangential travel speed was adjusted linearly by a percentage change in the feed rate,  $f$ . The filler wire feed speed was likewise adjusted the same percentage so that the volumetric rate of fill was consistent with the remainder of the weld. These parameters were increased where concavity existed and were decreased in the back side of the parts where the chill was greater.

Having made these tape changes, it was decided to reweld this part using the new tape and procedure used earlier for the circular manifold which is described in detail in a later section - REPAIR TECHNIQUES. Both joints were rewelded and re-X-rayed. The re-welds were found to be free from defects. Dye-penetration inspection of the weld surfaces also indicated no defects.

Additional adjustments to filler wire speed and travel speed were necessary because the third manifold contained machined slots through the side wall of the manifold I.D. wall. Some of these slots which were approximately 1 inch long, 1/4 inch deep and 0.250 inches high were machined under the weld land going into ports #1 and #3, and going out of ports #2 and #4.

With these parameter adjustments the third manifold was N/C welded. The resultant welds were visually quite satisfactory except that concavity of the bead was nearly 0.040-inch deep in those areas where the machined slots existed. Concavity in the other areas was reduced to 0.010-0.020 inch. These dimensions were the maximum recorded with a symmetrical tapering up to a flush condition approximately one inch to each side. Thus, the logical correction to the travel speed and filler wire feed speed was to adjust them in an exponential manner as shown in Figure 21 and 22. It should be noted that the increase is nearly 7% in the area containing the machined slot under the weld joint; whereas, only a 4% increase is required in the absence of the machined slot. The X-rays indicated the welds to be defect free except for a 3/4 inch length of lack of penetration where the weld starts around port #1 and a 1-1/4 inch length of lack of penetration where the weld exits around port #4 in the bottom weld. Additional tape modifications were made to correct these two areas and the bottom joint rewelded. X-rays showed the weld to be free from defects.

Thus the fourth and final pre-production elliptical manifold was welded with these tape modifications plus minor adjustments to the initial welding current to smooth the weld overlap area. The resultant welds were visually most satisfactory and found to be defect free using dye penetrant and X-ray inspection methods. This manifold and the third manifold were helium leak checked using a sensitivity of  $3 \times 10^{-9}$  scc/sec and no leaks were detected.

The final N/C tape printouts for both sides of the manifold are to be found in Appendix C along with the welding data sheet containing secondary welding parameters. Close examination of the N/C tape printouts show that 29 wire feed, 2 arc voltage, 8 welding current and over 400 travel speed changes are required to successfully weld the two elliptical manifold weld joints.

The final variations necessary to achieve good weld start and overlap conditions for each joint are shown in Figure 23.

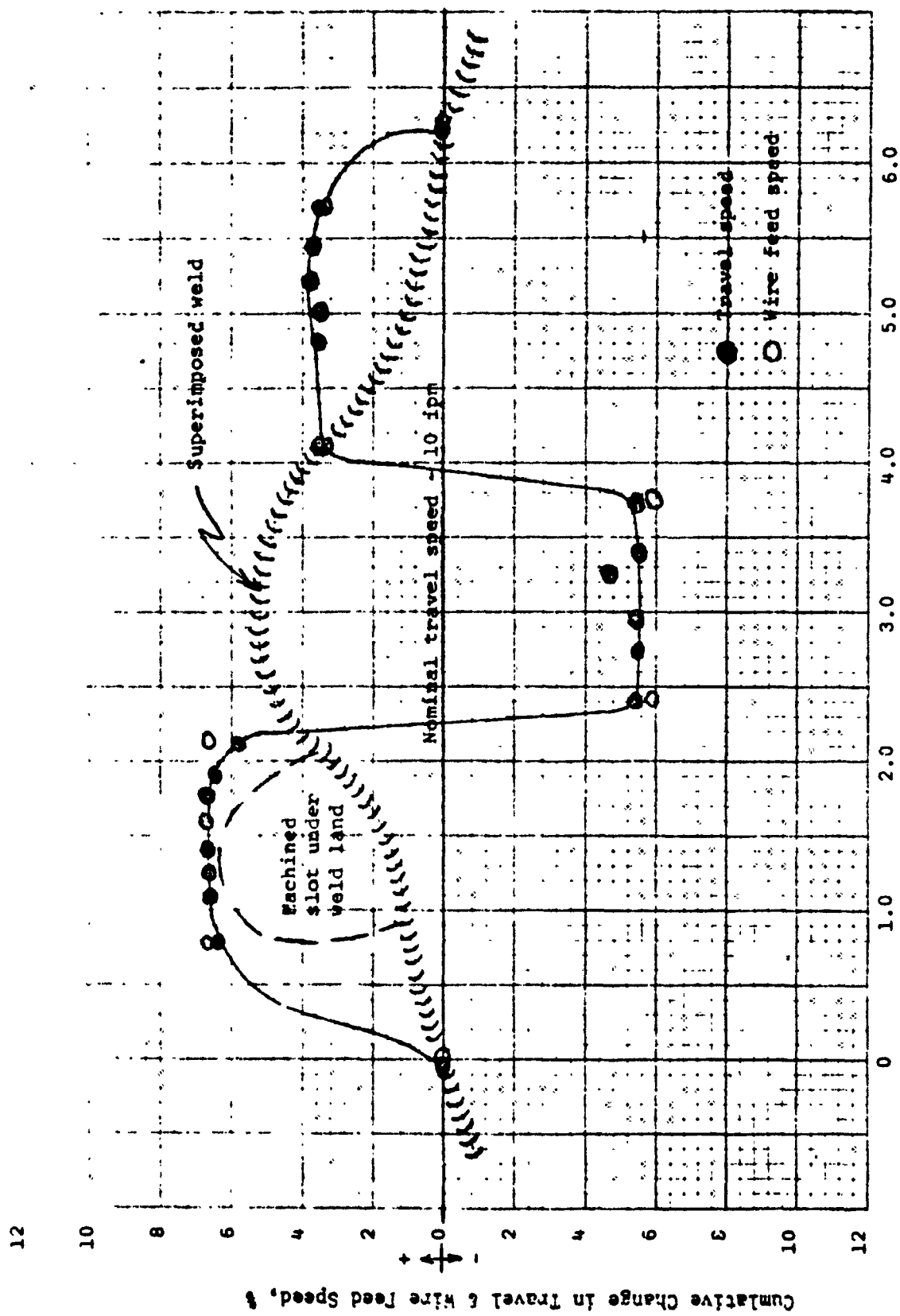


Figure 21. Typical Parameter Changes Required for the Port Area on Aft Side of Elliptical Manifold

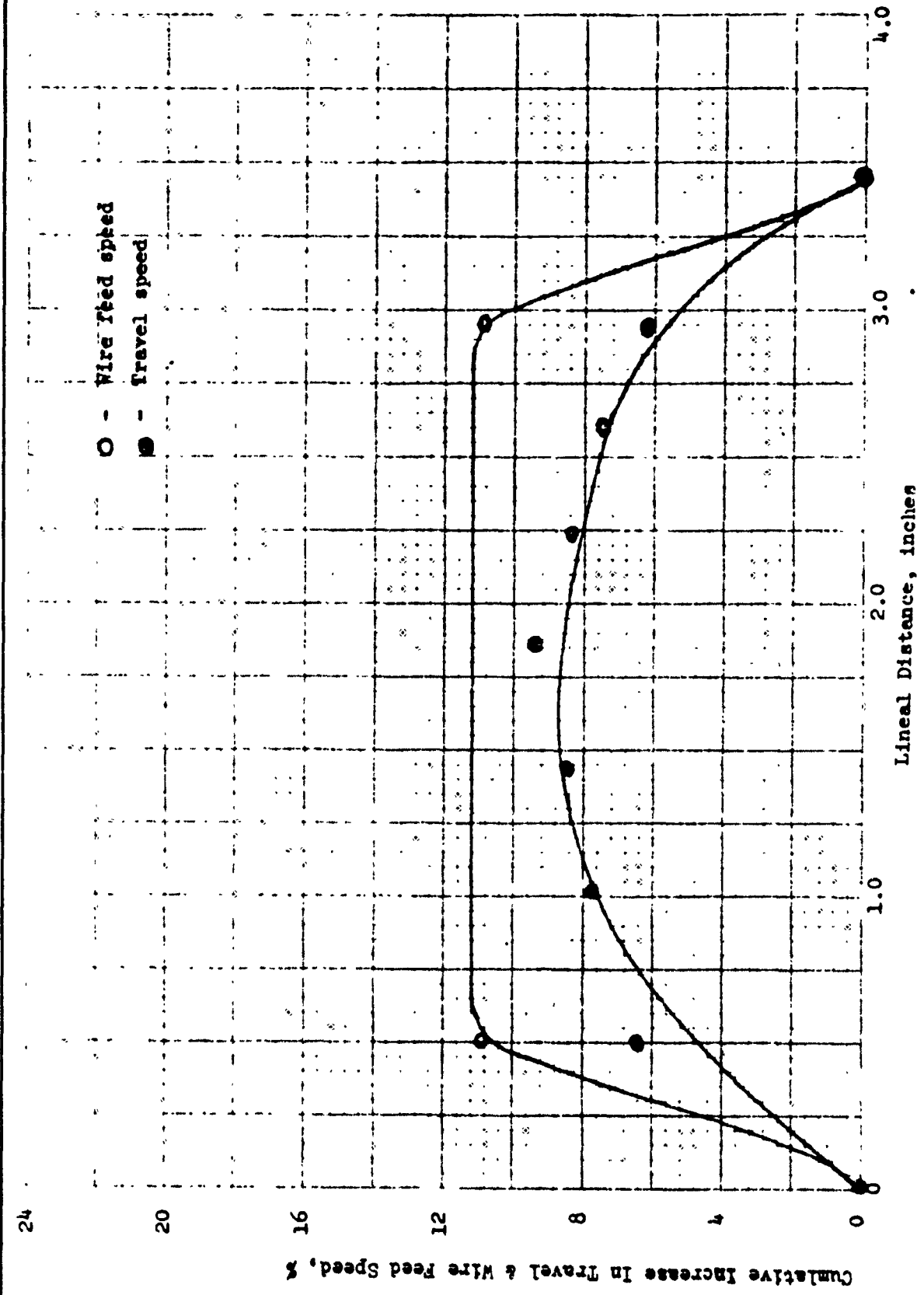
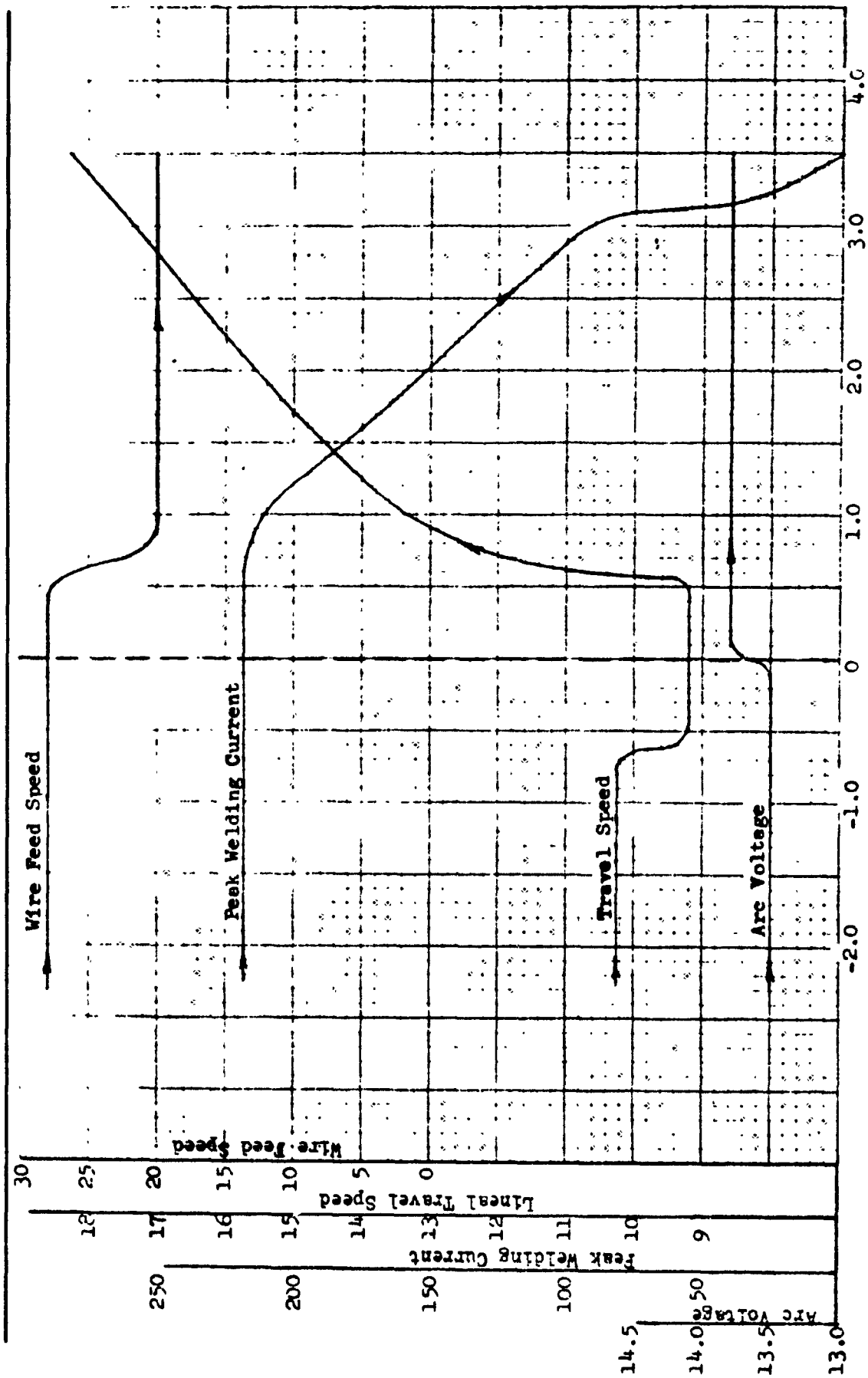


Figure 22. Typical Welding Parameter Changes Required for Joint on Forward Side Opposite Port Area



Inches Relative to Weld Initiation Point

Figure 23. Weld Parameter Variations Required for Overlap and Tie-Off

## REPAIR TECHNIQUES

When the development program was initially planned it was thought that repair procedures should be established for each of the common types of defects which occur in aluminum welds, but it later became apparent that the only type of defect that was of any concern was lack-of-penetration. This defect occurred in the bottom side weld of elliptical test part numbers 2 and 3 in the transition areas entering and exiting the ports. Since the Solar 202 aluminum welding flux produced such good results as described earlier on the circular test part, it was selected for use to repair these two parts but with some refinements in the procedure. After the inside of the manifold had been coated with the flux and alcohol mixture and the excess drained, the manifold was placed in a vacuum chamber which was evacuated to  $5 \times 10^{-4}$  TORR which insured the complete evaporation of the alcohol that was suspected of causing weld expulsion on the circular part. The surface of the original weld was machined flush and hand scraped in preparation for the repair weld. The part was rotated  $180^\circ$  and placed in the weld fixture to avoid having the weld overlap occur in the same area. The reweld was made with the same N/C tape which had been used to weld the joint originally. After welding, the flux was removed by flowing  $180^\circ\text{F}$  deionized water through the manifold and testing the exit water for chemical traces of the highly corrosive flux. When it was indicated that the flux was removed, dry nitrogen was blown through the manifold to remove the remaining water and then the part was again placed in the vacuum chamber and evacuated to complete the drying process.

## PRODUCTION OPTIMIZATION

After several production manifolds were welded, design engineering re-designed the actuation port configuration thereby changing the aft side weld path to an uninterrupted ellipse like the forward side. This change significantly reduced the incidence of weld concavity and lack-of-penetration defects experienced in the actuation port areas of the aft side weld. The N/C tape prepared to weld the aft side was identical to that used for the forward side except for peak welding current - 217.8 amps for the forward side and 210 for the aft side.

As welding progressed on the redesigned manifolds a lack-of-penetration problem developed in the weld start and overlap area on both the forward and aft sides. It was not apparent if this problem was caused by machine malfunction, joint compression, weld shrinkage or material thickness. Nonetheless, to assure complete penetration the weld start and overlap weld parameters were modified and verified on short straight sections that exactly duplicated the mass and cross sectional configuration of the elliptical manifold. In essence the weld start travel speed was slowed for the first inch and a half of the weld, the current downslope was delayed for another inch after weld overlap and the overlap weld travel speed was reduced. These changes are incorporated in the N/C tape printout shown in Appendix D. This printout is identical for both sides of the manifold except for the difference in peak welding current mentioned previously. Shown in Appendix E is the N/C tape printout for the straight line simulated sections which were subsequently used for pre-production verification of the overlap procedure.

Even with these modified welding parameters there were several manifolds that still had lack-of-penetration in the overlap area on the aft side weld. Thus the peak welding current was increased from 210.0 to 215.4 amperes for the last manifold which resolved the problem. Those manifolds containing lack-of-penetration prior to this change were repair welded in the same manner described earlier. It was found that the Solar 202 flux could be eliminated during the latter repairs and a fully satisfactory weld obtained.

### 3.0 CONCLUSIONS

1. An uninterrupted single-pass free fall butt weld procedure was satisfactorily developed for welding the 2014-T452 aluminum elliptical shaped UpSTAGE EB Fuel Manifold Frame P/N 1D15693 using the 8-axis Numerically Controlled welding machine.
2. Through the use of low frequency (10 hz) weld current pulsation, excellent weld puddle control of free fall weldments in 2014-T4 aluminum was demonstrated with the GTA (Gas Tungsten Arc) welding process. In addition, this technique is believed to have contributed to the absence of oxide stringers prevalent in steady state GTA welds in 2014 aluminum.
3. The ability to rotate the filler wire about the tungsten electrode during welding was adequately displayed in this program. It was further shown that the entry angle for the wire may vary up to 30° each side from the center line of the joint without any difficulty.
4. Numerous changes in weld heat input were required during the weld to adjust for changing heat sinks created by design of the manifold. These changes were effectively made by adjustments in the tangential travel speed and filler wire volumetric rate of addition. This condition was necessitated since absolute changes in the welding current during pulsation must exceed 40 amperes for the MCU of the N/C welding machine to be responsive.
5. To achieve weld uniformity, adjust for varying heat sinks, and provide consistency and quality in the weld overlap area over 400 in-process changes were required in weld travel speed, filler wire feed speed, arc voltage and welding current to weld the two sides of the manifold.
6. The interference fit of the assembly eliminated the weld joint gap build-up during welding and is believed to have contributed to the absence of oxide stringer defects in the weld.
7. The design requirement of a minimum tensile yield strength of 28,000 psi was obtained with an average yield strength of the forging welds exceeding the minimum by more than 30 percent.

## APPENDIX A - N/C TAPE CALCULATION FOR FEEDRATE, f

The following equation is used for calculating feedrate, f, for the z-axis N/C welder using the x and y axes to trace the weld path and the c-axis for wire feed rotation.

$$f = \frac{0.0041 (2^n) FR}{\sqrt{x^2 + y^2}}$$

where f = feedrate (dimensionless)

0.0041 = machine constant

$2^n$  = binary number that exceeds the longest movement when divided by pulse length of 0.0002

FR = lineal travel speed in inches per minute

x = lineal distance in x-axis

y = lineal distance in z-axis

Note: The longest movement should include the c-axis converted to lineal movement in the z-axis to four decimal places.

APPENDIX B - FINAL N/C TAPE PRINTOUT FOR CIRCULAR MANIFOLD - 3-18-70

x670ky-178z3000r444	x-555y-394z3000r456	x192dy6506z3000r677r10160
x6766y-53z3000r444	x-5746y-354z3000r456	m82
x6728y-88z3000r444	x-5924y-323z3000r456	m00
x6672y-121z3000r444	x-5104y-292z3000r456	x2266y6398z3000r632
x6588y-154z3000r445	x-6250y-259z3000r457	x2596y6270z3000r677
x6496y-192z3000r445	x-6373y-226z3000r457	x2722y6124z3000r723
x6378y-222z3000r445	x-6496y-192z3000r457	x3238y5954z3000r768
x6299y-257z3000r445	x-6584y-159z3000r458	x344y5592z3000r858
x6104y-272z3000r446	x-6672y-121z3000r458	x3672y4732z2636r1028
x5924y-323z3000r446	y-6723y-88z3000r458	x166y218z122z523
x5746y-354z3000r446	x-6756y-53z3000r458	x168y218z122z349
x5554y-404z3000r446	x-6784y-17z3000r459	m040
x5344y-413z3000r447	x-6784y173z3000r459	m00
x5120y-440z3000r447	x-6784y173z3000r459	m30
x4974y-467z3000r447	x-6784y173z3000r459	608x100376/-01250z-397576r1283
x4640y-492z3000r447	x-6784y173z3000r459	609x360y-292z-144r1397
x4378y-515z3000r448	x-6520y152z3000r460	n997
x4100y-538z3000r448	x-6506y192z3000r460	m00
x3914y-557z3000r448	x-6124y202z3000r460	m30
x3726y-574z3000r448	x-6124y202z3000r461	
x3526y-574z3000r448	x-5961y323z3000r461	
x33218y-594z3000r449	x-5786y354z3000r461	
x3202y-612z3000r449	x-5528y384z3000r461	
x2576y-627z3000r449	x-5384y413z3000r462	
x1904y-650z3000r450	x-5160y440z3000r462	
x1564y-659z3000r450	x-4924y467z3000r462	
x1216y-672z3000r450	x-4670y492z3000r462	
x866y-672z3000r450	x-4400y515z3000r463	
x512y-676z3000r451	x-4130y538z3000r463	
x178y-676z3000r451	x-3844y559z3000r463	
x-178y-676z3000r451	x-3546y578z3000r463	
x-512y-676z3000r451	x-3238y596z3000r464	
x-866y-672z3000r452	x-2924y612z3000r464	
x-1216y-667z3000r452	x-2576y627z3000r464	
x-1564y-659z3000r452	x-2266y640z3000r464	
x-1904y-650z3000r452	x-1928y650z3000r465	
x-2246y-639z3000r453	x-1584y657z3000r465	
x-2576y-627z3000r453	x-1236y667z3000r465	
x-2902y-612z3000r453	x-886y672z3000r465	
x-3218y-596z3000r453	x-532y676z3000r465	
x-3526y-578z3000r454	x-128y339z3000r451	
x-3814y-550z3000r454	x178y676z3000r451	
x-4100y-538z3000r454	x532y676z3000r457r30500	
x-4340y-492z3000r455	x886y676z3000r542r10310	
x-4894y-467z3000r455	x1236y667z3000r587r10260	
x-5120y-440z3000r455	x1564y659z3000r632r10210	
x-5344y-413z3000r455		

**APPENDIX B  
WELDING PARAMETERS--N. C. WELDER**

CURRENT SOURCE	TAPE	DIAL
INITIAL CURRENT IN AMPS	T 40014	84
INITIAL SLOPE IN SEC'S	T 60015	1.5
FINAL CURRENT IN AMPS	T 50011	66
FINAL SLOPE IN SEC'S	T 70010	1.0
CURRENT STOP DELAY IN SEC'S	T 90002	0.66
SURGE SUPPRESSION SETTING		
VOLT AMPERE CONTROL SETTING		
BACKGROUND CURRENT PERCENT		
GMA PULSED ARC SWITCH	ON	OFF
VOLT/AMPERE SWITCH	ON	OFF
CONSTANT CUR. (CONST. POTEN.) SWITCH	(CC)	CP
OPEN CIRCUIT VOLTAGE SWITCH	85	(150)
POLARITY SWITCH	(STR)	REV
INDUCTANCE TAP SWITCH (FRONT)	1 2	3 4
INDUCTANCE JUMPER TAP (REAR)	PULSE	(NO PULSE)

PULSED ARC DRAWER	SEC'S	DIAL
PULSE START DELAY	1.0	0.1
PULSE STOP DELAY	0.0	2.0
PEAK CYCLES LEVEL #1 SETTING		03
BASE CYCLES LEVEL #2 SETTING		03
BASE CURRENT PERCENT SETTING		7.50
PULSE SWITCH	(ON)	OFF

ARC HEAD DRAWER & HIGH FREQ.	SEC'S	DIAL
HEAD LOCK DIAL	2	0.20
HEAD UNLOCK DIAL	0	0.00
RATE OF RESPONSE DIAL SETTING		5.00
POLARITY SWITCH	(STR)	REV.
HIGH FREQUENCY INTENSITY SETTING		100%
HIGH FREQUENCY SWITCH	(ON)	OFF

AUTOMATIC SEQUENCE DRAWER	SEC'S	DIAL
WIRE FEED START DELAY	1.0	2.0
WIRE FEED STOP DELAY	1.0	2.0
TRAVEL START DELAY	1.0	2.0
TRAVEL STOP DELAY	0.0	0.0
TORCH GAS PREFLOW SWITCH - 10	10.0	10.0
TORCH GAS POSTFLOW SWITCH - 10	10.0	10.0
TORCH GAS SWITCHOVER DELAY	0.0	0.0
TORCH GAS SWITCHOVER SWITCH	ON	OFF
GAS MIXTURE SWITCH	ON	OFF
TORCH GAS SWITCH	(AUTO)	OFF
BACKUP GAS SWITCH	AUTO	OFF
GAS TYPE SWITCH	(M)	A

PART OR TAPE NO.	CIRCULAR MANIFOLD
PROJECT NAME	UPSTAGE
WELDING ENGINEER	GRS - JJJ - FD
DEPT. NO. & GROUP	A255
DATE:	3-23-70

AXIS TRANSFER		
Z AXIS TO C AXIS	2	(C)
A AXIS TO D AXIS	(A)	D
B AXIS TO E AXIS	B	(E)

WIRE FEED DRAWER		DIAL
GTA RETRACT DIAL SETTING		0.00
GMA APPROACH DIAL SETTING		--
SENSITIVITY DIAL SETTING		--
DAMPING DIAL SETTING		--
GTA/GMA SWITCH	(GTA)	GMA
CONSTANT/DEMAND SWITCH	(CONST)	DEMAND

PENDANT CONTROL	TAPE	DIAL
RUNNING CURRENT IN AMPS	T 10391	234.6
WIRE FEED SPEED IN IPM	T 20230	23.0
VOLTAGE IN VOLTS	T 30450	13.5
WELDING TRAVEL SPEED IPM	*	
WELD OR SET UP SEQUENCE	(OPER)	SETUP
TRAVEL FEEDRATE OVERRIDE PERCENT	55%	
WIRE FEED FEEDRATE OVERRIDE SETTING	**	
MANUAL OR TAPE DATA SWITCH	MAN	(TAPE)
TAPE MODE SWITCH & MCU SWITCH	(ON)	OFF
ARC HEAD SWITCH SETTING	LOCK	UNLOCK

TRAVEL SEQUENCE	DIAL	DIRECT	SEQ MAN	OFF ON
X AXIS			(SEQ/MAN)	OFF (ON)
Y AXIS			(SEQ/MAN)	OFF (ON)
Z OR C AXIS			(SEQ/MAN)	OFF (ON)
A OR D AXIS			(SEQ/MAN)	OFF (ON)
B OR E AXIS			(SEQ/MAN)	OFF (ON)
WIRE FEED SPEED SWITCH			(SEQ/MAN)	OFF (ON)

PURGE GAS	TYPE	CFH
TORCH PURGE GAS	7E	70
BACKUP PURGE GAS	--	--
MIXTURE GAS	--	--
TRAIL SHIELD GAS	--	--

MISC. DATA	
FILLER WIRE TYPE	AL 4043
FILLER WIRE DIA.	.063
ELECTRODE TYPE	FWG 290 TMR
ELECTRODE DIA.	.125 #
ELECTRODE EXTENSION	--
CONTACT TUBE SIZE	--
CONTACT TUBE SETTING (INCHES)	--
TYPE OF JOINT	SO. BUTT
TYPE OF MATERIAL	2014-T6
MATERIAL THICKNESS	1/16

NOTES \* N/C TAPE IS PROGRAMMED AT 18 IPM, 55% ON THE FEED RATE OVERRIDE IS 10 IPM TRAVEL SPEED \*\* WIRE FEEDRATE OVERRIDE STARTS AT 0, INCREASED GRADUALLY TO 50% AT 180°, THEN 75% AT 270°  
 1) ELECTRODE GROUND PER K652-54149-10 (84° X .050 FLAT)  
 FILLER WIRE IS LOCATED .190 BEHIND THE ELECTRODE AND 3/16" IN FRONT.





**APPENDIX C  
WELDING PARAMETERS—N. C. WELDER**

CURRENT SOURCE	TAPE	DIAL
INITIAL CURRENT IN AMPS	54	
INITIAL SLOPE IN SEC'S	1.5	
FINAL CURRENT IN AMPS	60	
FINAL SLOPE IN SEC'S	10	
CURRENT STOP DELAY IN SEC'S	0.66	
SURGE SUPPRESSION SETTING		
VOLT AMPERE CONTROL SETTING		
BACKGROUND CURRENT PERCENT		
GMA PULSED ARC SWITCH	ON	(OFF)
VOLT AMPERE SWITCH	ON	(OFF)
CONSTANT CUR. / CONST. POTENTIAL SWITCH	(CC)	CP
OPEN CIRCUIT VOLTAGE SWITCH	85	(150)
POLARITY SWITCH	(STR)	REV
INDUCTANCE TAP SWITCH (FRONT)	1 2	3 4
INDUCTANCE JUMPER TAP (REAR)	PULSE	(NO PULSE)

PULSED ARC DRAWER	SEC'S	DIAL
PULSE START DELAY	0	0.00
PULSE STOP DELAY	0	0.00
PEAK CYCLES LEVEL #1 SETTING		3
BASE CYCLES LEVEL #2 SETTING		3
BASE CURRENT PERCENT SETTING		75%
PULSE SWITCH	(ON)	OFF

ARC HEAD DRAWER & HIGH FREQ.	SEC'S	DIAL
HEAD LOCK DIAL	0	0.00
HEAD UNLOCK DIAL	0	0.00
RATE OF RESPONSE DIAL SETTING		4.50
POLARITY SWITCH	(STR)	REV.
HIGH FREQUENCY INTENSITY SETTING		100%
HIGH FREQUENCY SWITCH	(ON)	OFF

AUTOMATIC SEQUENCE DRAWER	SEC'S	DIAL
WIRE FEED START DELAY	1.75	3.5
WIRE FEED STOP DELAY	1.0	2.0
TRAVEL START DELAY	1.5	3.0
TRAVEL STOP DELAY	0.0	0.0
TORCH GAS PREFLOW SW-10	10.0	10.0
TORCH GAS POSTFLOW SW-10	10.0	10.0
TORCH GAS SWITCHOVER DELAY	0.0	0.0
TORCH GAS SWITCHOVER SWITCH	ON	(OFF)
GAS MIXTURE SWITCH	ON	(OFF)
TORCH GAS SWITCH CONST PURGE	AUTO	OFF
BACKUP GAS SWITCH	AUTO	(OFF)
GAS TYPE SWITCH	(He)	A

PART OR TAPE NO.	DIS693-40	MCM1-MCM2
PROJECT NAME	UPSTAGE	
WELDING ENGINEER	RES - LLK	
DEPT NO. & GROUP	A255	
DATE	6-15-70	

AXIS TRANSFER		
Z AXIS TO C AXIS	Z	(C)
A AXIS TO D AXIS	(A)	D
B AXIS TO E AXIS	B	(E)

WIRE FEED DRAWER	DIAL
GTA RETRACT DIAL SETTING	0.60
GMA APPROACH DIAL SETTING	—
SENSITIVITY DIAL SETTING	—
DAMPING DIAL SETTING	—
GTA/GMA SWITCH	(GTA) GMA
CONSTANT/DEMAND SWITCH	(CONST) DEM

PENDANT CONTROL	TAPE	DIAL
RUNNING CURRENT IN AMPS	1ST SIDE 2.18 2ND SIDE 2.10	
WIRE FEED SPEED IN IPM	*	
VOLTAGE IN VOLTS	13.5	
WELDING TRAVEL SPEED IPM	9.75-10.25	
WELD OR SET UP SEQUENCE	(OPER)	SETUP
TRAVEL FEEDRATE OVERRIDE PERCENT	100%	
WIRE FEED FEEDRATE OVERRIDE SETTING	*	
MANUAL OR DATA SWITCH	MAN	(TAPE)
TAPE MODE SWITCH & MCIU SWITCH	(ON)	OFF
ARC HEAD SWITCH SETTING	LOCK	(UNLOCK)

TRAVEL SEQUENCE	DIAL	DIRECT	SEQ. MAN	OFF ON
X AXIS			(SEQ. MAN)	OFF ON
Y AXIS			(SEQ. MAN)	OFF ON
Z OR C AXIS			(SEQ. MAN)	OFF ON
A OR D AXIS			(SEQ. MAN)	OFF ON
B OR E AXIS			(SEQ. MAN)	OFF ON
WIRE FEED SPEED SWITCH			(SEQ. MAN)	OFF ON

PURGE GAS	TYPE	CFH
TORCH PURGE GAS	He	70
BACKUP PURGE GAS	—	—
MIXTURE GAS	—	—
TRAIL SHIELD GAS	—	—

MISC. DATA	
FILLER WIRE TYPE	AL. 9043
FILLER WIRE DIA.	.063
ELECTRODE TYPE	TUNG. 2% THOR.
ELECTRODE DIA.	.125
ELECTRODE EXTENSION	SEE SPEC'N
CONTACT TUBE SIZE	—
CONTACT TUBE SETTING (INCH)	—
TYPE OF JOINT	50. BUTT
TYPE OF MATERIAL	2014-T4
MATERIAL THICKNESS	.170

NOTES \* WIRE FEED 28.0 IPM AND VARIES AT PORTS. WIRE FEED OVERRIDE STARTS AT 0 AND IS INCREASED AS REQUIRED.  
BENDIX TRAVEL SWITCH ON "Z-C" AXIS MUST BE "INVERTED"

**TURN OFF AIR-CONDITIONING BEFORE WELDING**

APPENDIX E - STRAIGHT LINE PRE-PRODUCTION OVERLAP TAPE PRINTOUT  
FOR ELLIPTICAL EB MANIFOLD FRAME P/N 1D15693-401 - 3-31-71

n010  
t10363 ← t10359 for AFT side  
t20200  
t30450  
t40009  
t50010  
t60015  
t70010  
t80001  
n020  
m00  
m81  
g08x3860f196  
x3860f201  
x6980f228  
x4320f378t20280  
x5520f296  
x3780f216  
x7170f228  
x7225f226  
x7225f226  
x6400f255  
m82  
n030  
m00  
g08x-110830f400  
n040  
m00  
m81  
g08x6230f273  
x6450f264  
x6490f262  
x6690f254  
x6700f254  
x6860f248  
x6920f246  
x5650f301  
x5010f312  
x5170f315t30461  
x5340f322  
x4550f415  
x5690f376t20200  
x4940f477t10310  
x5390f487t10260  
x3490f676t10210  
m82  
m00



Appendix C  
THERMOCONDUCTIVE MATERIALS AND  
INKS FOR THICK FILM SUBSTATES

- MDAC Report MP 51,831 (L. H. Kram), Materials for Attaching Flat Packs and Thick Film Substrates, 21 July 1970.
- MDAC Report MP 51,978 (C. T. McMurray), Stability of Thick Film Resistors in the Presence of Dynamic Materials, 13 August 1971.

MISSILE & SPACE SYSTEMS DIVISION  
DOUGLAS AIRCRAFT COMPANY, INC.

FORM 37-86 (REV. 1-62)

MATERIAL & PROCESS ENGINEERING  
LABORATORY REPORTCATALOG NO. PDL 4448  
SERIAL NO. MP 51,831

DATE 7-21-70

TITLE MATERIALS FOR ATTACHING FLAT PACKS  
AND THICK FILM SUBSTRATES

ASSIGNED TO L. H. Ryan, A-255

MATERIALS

See Materials Index.

OBJECT

1. To evaluate and select thermoconductive materials for thick film.
2. To develop a method for mechanical attachment of flat packs to alumina thick film, and alumina thick film to aluminum heat sink.
3. To develop a method for removal of defective flat packs from the thick film assemblies.

INTRODUCTION

A thermoconductive material is needed to provide temporary adhesion and heat transfer between gold plated and glass flat packs and alumina thick film substrates during solder operation. The adhesion between flat packs and thick film shall be weak, so that flat packs can be removed easily when needed.

Thermoconductive material is also needed to provide good adhesion and heat transfer between alumina thick film substrate and aluminum heat sink.

SIGNIFICANCE OF DATA

Eccosil 4852 thermoconductive silicone was selected as the best material for bonding flat packs to alumina thick film and also for bonding alumina thick film substrate to aluminum heat sink structure. This material has a comparatively good thermoconductive: 6.6 BTU/(hr) (Ft<sup>2</sup>) (F<sup>o</sup>/in) and percent elongation (100%) which permits it to transfer heat away from the flat packs during soldering operation and to absorb the difference between thermal coefficient of expansion of alumina and aluminum during thermocycling (0° to 100°C).

It can be applied in less than .002" thickness, thus providing maximum heat dissipation since heat transfer is inversely proportional to the thickness of the material.

Without primer, Eccosil 4852 provides temporary adhesion for flat packs to alumina thick film during soldering operation, and good adhesion between thick film and aluminum heat sink when primer is used.

Out of five evaluated primers, SS-4004 and S-11 primers were selected as the best primers for bonding alumina to aluminum.

In bonding 4" x 6" x 0.002" alumina to aluminum, using epoxy adhesive, the specimen developed extensive warpage. On two specimens, using Eccosil 4852 adhesive with primers, there was no warpage. There was no cracking of alumina or failure of the adhesive on any of the three specimens tested.

PROCEDURE AND RESULTSA. Lap Shear Test1. Preparation of the specimens

The following materials were used as adhesives in preparation of the lap shear specimens:

- a. Eccosil 4852 silicone with SS-4004 and S-11 primers
- b. Eccobond 285 epoxy, no primer
- c. DC96-044 silicone with DC1203 primer
- d. Duroseal epoxy, no primer
- e. PR1913-2 silicone with PR1903 primer

72 aluminum 7075 T6 panels, measuring 1 x 4 x .060 inches, were prepared. Panels were cleaned with MEK and sandblasted on one side with #80 mesh grit.

36 alumina plates measuring 1 x 2 x .028 inches were cleaned with MEK.

2. Priming

Both sides of the alumina plates and sandblasted sides of the aluminum panels were primed as recorded in Table 1. Primers were allowed to dry at ambient temperature for 30 minutes.

3. Application of the Adhesives

A thin coat of the adhesive material (see Table 1 for details) was applied on prepared surfaces of aluminum or alumina. Adhesive materials were screened using 200 mesh screen. The total thickness of the adhesive varied between .001 to .002 inch. Alumina plates were sandwiched between two aluminum plates and cured overnight under 20 Hg inches vacuum at ambient temperature.

Specimens were then postcured for 3 hours at 150°F.

Duroseal adhesive specimens were prepared and cured per manufacturer's recommendation.

4. Testing

Half of the cured specimens were tested for lap shear strength per Federal Test Method Std. No. 175, Method 1033. Another half was cycled 30 times, each cycle scheduled as follows:

- 10 minutes at 212°F
- 10 minutes at ambient
- 10 minutes at 32°F
- 10 minutes at ambient

At the end of 30 cycles, specimens were tested for lap shear strength as above. All results are recorded in Table 1.

PROCEDURE AND RESULTS - ContinuedB. Tensile Strength - Ultimate Elongation

Using Eccosil 4852 silicone material, ten specimens were prepared per ASTM D412 requirements. Specimens were initially cured for 3 days at ambient temperature plus 3 hours at 150°F. Five out of ten specimens were postcured further, up to 500°F, by increasing temperature 50°F every 4 hours, until 500°F was reached.

All specimens were tested for tensile strength and ultimate elongation per ASTM D412. Results are recorded in Table 2.

C. Adhesion Study

Five different primers were evaluated, to check the adhesion of Eccosil 4852 silicone to 7075 T6 aluminum panels.

Ten 1 x 6 x 1/8 inch aluminum panels and ten 1 x 2 x .028 alumina chips were cleaned with MEK.

Five out of ten aluminum panels were sandblasted. Primers were applied to the surfaces of the panels and alumina chips per manufacturer's recommendations.

A thin layer of Eccosil 4852 silicone (.002") was applied on prepared aluminum panels. Primed alumina chips were bonded to the aluminum panels.

Specimens were cured under light pressure for 24 hours at ambient temperature, followed by 3 hours at 150°F. Adhesion was evaluated qualitatively by pulling alumina substrate away from the aluminum. Results of this test are recorded in Table 3.

D. Removal of Flat Packs

Eccosil 4852 silicone was applied to the glass deposits on alumina thick film as described in A.3.

Three glass Signetic G flat packs and three gold plated flat packs were placed on screened Eccosil 4852 material. Slight pressure was applied to the surface of the flat packs. After material was cured overnight at ambient temperature, flat packs were removed by turning them gently with forceps until the adhesive bond was broken. Cured film of silicone adhesive was then peeled off.

E. Bonding Alumina Plates to Aluminum Heat Sinks

Using 7075 T6 clad aluminum, three heat sinks, measuring 4 x 6 x .063 inches were prepared. The surfaces of the heat sinks were cleaned with MEK and then sandblasted with #80 mesh grit. Three alumina plates, measuring 4 x 6 x .028 inches were cleaned with MEK.

PROCEDURE AND RESULTS - Continued

E. Bonding Alumina Plates to Aluminum Heat Sinks - Continued

Using three different adhesives, the above substrates were bonded together as described below:

1. The surfaces of heat sink and alumina plate were primed with S-11 primer. The primer was allowed to dry at ambient temperature for 30 minutes. Using #285 mesh screen, Eccosil 4852 silicone adhesive was screened on primed surface of a heat sink. The thickness of the bond line did not exceed .002 inch. Primed alumina plate was bonded to the heat sink. Eccosil 4852 material was cured under 20 Hg inches vacuum for 16 hours.
2. The surfaces of heat sink and alumina plate were primed with PR1903 primer. Primer was allowed to air dry at ambient temperature for 30 minutes. PR1913-2 silicone was screened on primed surface of a heat sink using #225 mesh screen. Alumina plate was bonded to the heat sink and material was cured as in E.1 above.
3. .003 inch thick Duroseal B fiber-filled epoxy film was cut to 4 x 6 inches dimension and sandwiched between heat sink and alumina plates. The material was cured for 30 minutes at 350°F and 50 grams per square inch pressure.

All specimens were thermocycled for 30 cycles as described in A.4. After cycling, specimens were subjected to 500°F for 3 minutes. All specimens were examined visually for adhesion, warpage or any other defects, after cycling and after exposing the specimen to 500°F.

RESULTS

There was a definite warpage in specimen 3 above where epoxy was used as an adhesive. Specimens 1 and 2 above where silicone was used as adhesive, showed no warpage. Upon exposure of specimens to 500°F, specimen 3 showed increase in warpage. However, this warpage decreased when specimen was cooled to room temperature. Adhesion in all specimens was good.

SUMMARY OF RESULTS

Out of five materials tested for the lap shear strength, Duroseal epoxy gave the highest value. Eccosil 4852 silicone gave highest lap shear strength value, as compared to two other silicones, DC96-044 and PR1913-2. Comparing lap shear values for cycled and non-cycled specimens, lap shear strength values for most materials increased slightly after specimens were cycled.

Percent elongation of Eccosil 4852 material was not effected by postcure however, tensile strength was reduced approximately by 10 percent.

Out of five evaluated primers, S-11 and SS-4004 primers gave the best adhesion between Eccosil 4852 and aluminum panels.

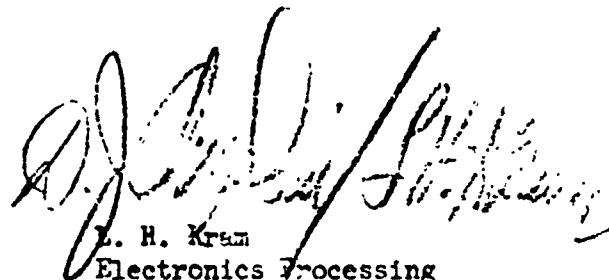
SUMMARY OF RESULTS - Continued

There were no problems in removing flat packs from the alumina thick film substrates. Flat packs were removed easily with the use of forceps.

Bonding alumina thick film to aluminum heat sink with epoxy adhesive produced warpage. Warpage increased when specimen was exposed to 500°F, and decreased when specimen was cooled to room temperature. There was no warpage in the two other specimens where silicone was used as an adhesive.

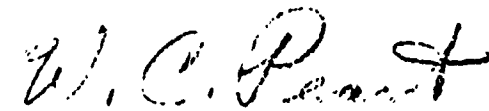
REFERENCES

Case Sheet #85086  
Technical Record Book No. 12271  
ASTM D412 - Tension Testing of Vulcanized Rubber  
Federal Test Method Standard 175, Method 1033T  
EWO 11134  
SA 7002  
SO 3859-6320



L. H. Kram  
Electronics Processing  
Materials & Methods -  
Research & Engineering

Approved by:



W. C. Peart, Section Chief  
Electronics Processing  
Materials & Methods -  
Research & Engineering

MATERIALS INDEX

- Eccosil 4852 - A red, thermoconductive silicone that is mixed with Catalyst 50 in the ratio of 100% base to 0.1 - 0.5% catalyst.
- Eccosil TP51 - A thixotropic, thermoconductive silicone rubber paste.
- Stycast 2850FT - A black, general purpose casting resin with high thermoconductivity.
- Eccobond 285 - A thixotropic, thermoconductive paste.
- S-11 - A colorless, one system primer used with Eccosil 4852 silicone.  
Emerson and Cuming, Inc.  
Gardena, California
- Duroseal - 0.003 mils thick B fiber filled thermoconductive epoxy film.  
Singer  
Physical Science Corp.  
Arcadia, California
- Vigor-Kool-It - One part, thermoconductive adhesive  
Raiko Product, Box 375  
Farmingdale, N.Y. 11735
- DC 96-044 - A thermoconductive, white silicone compound that cures at room temperature.
- DC 1200 (DPM 3202) (1P20040) One part, pink silicone primer  
Dow Corning Corporation  
Midland, Michigan
- SS 4004 (DPM 2072-1) (MRD9709139), One part, fluorescent pink, silicone primer  
General Electric  
Waterford, New York
- PR1913-2 (DPM 4331), Two part thixotropic, room temperature curing silicone compound.
- PR1903 (DPM 3510) (MRD11247174-01) One part, fluorescent pink silicone primer  
Product Research & Chem. Corp.  
Burbank, California
- Glass Signetic G Packs (1/4" x 3/8")  
Signetic Corp.  
Sunnyvale, Calif.
- Gold Plated Flat Packs (1/4" x 3/8")  
General Instrument Corp.  
Long Island, New York

TABLE 1. LAJ SHEAR STRENGTH (PSI)  
(FEDERAL TEST METHOD STANDARD 175, METHOD 1033-1T)

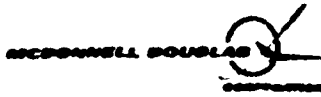
MATERIAL	PRIMER	NON-CYCLED SPECIMENS			CYCLED SPECIMENS		
		BOND THICKNESS (INCHES)	LOAD (LBS)	PSI	BOND THICKNESS (INCHES)	LOAD (LBS)	PSI
Eccobond 4852	S-11	.0005	442	216	.0015	702	351
		.0006	311	155	.0015	694	347
		.0005	593	296	.0020	669	334
		.0012	310	155	.0015	772	386
PR1913-2	FR1903	.0010	163	81	.0006	192	96
		.0008	216	108	.0008	32	16
		.0020	645	322	.0015	422	211
		.0013	541	270			
Duroseal	None	.0032	1525	762	.003	1662	831
		.0029	1525	762	.003	1300	650
					.003	1465	732
DC 96-044	DC 1200	.0015	190	95	.0025	222	111
		.0014	195	97	.0025	223	111
					.0025	182	91
Eccobond 285	None						

TABLE 2. TENSILE STRENGTH AND ULTIMATE ELONGATION OF ECCOSIL 4852 MATERIAL  
(ASTM D412)

FULLY CURED SPECIMENS			POSTCURED SPECIMENS				
THICKNESS OF THE SPECIMEN (INCHES)	LOAD (LBS)	% ELONGATION	PSI	THICKNESS OF THE SPECIMEN (INCHES)	LOAD (LBS)	% ELONGATION	PSI
.021	4.3	100	819.0	.024	4.1	100	632.3
.022	4.0	100	727.2	.024	4.1	100	683.3
.018	3.5	100	777.7	.023	4.1	100	713.0
.022	4.3	100	781.8	.026	4.8	100	738.4
.023	4.5	100	782.6	.025	3.9	100	624.0

TABLE 3. ADHESION OF ECCOSIL 4852 MATERIAL TO 7075 T6 ALUMINUM PANELS

PRIMER	PANEL SURFACE NOT TREATED		PANEL SURFACE SANDBLASTED	
	ADHESION	PRIMER	ADHESION	PRIMER
SS-4004	Fair	SS-4004	Good	
PR1903	Poor	PR1903	Poor	
SS-4155	Poor	SS-4155	Poor	
DC 1200	Fair	DC 1200	Poor	
S-11	Poor	S-11	Fair	



FORM 40-529 (8-70)

MATERIAL & METHODS - RESEARCH & ENGINEERING  
LABORATORY REPORT

TITLE STABILITY OF THICK FILM RESISTORS IN  
THE PRESENCE OF ORGANIC MATERIALS

CATALOG NO. PDL 111238  
REPORT NO. MP 51,978

DATE 8-13-71

MATERIALS AND EQUIPMENT

PREPARED BY C. T. Mc Murray, A-255

See Materials and Equipment Index.

OBJECT

To determine the effects of fluxes, organic coatings and hermetic packaging on the stability of du Pont's Birox and 8000 series resistor inks.

INTRODUCTION

Past experience has indicated that under certain not completely understood conditions, thick film resistor values are changed by the presence of certain materials or materials-sealing methods. The purpose of this study was to determine the effects of fluxes, organic coatings and hermetic sealing on the stability of du Pont's Birox and 8000 series resistors by accelerated thermal aging. In the first part of this work, the effects of various materials and hermetic sealing were studied with all specimens exposed to each other and to a possibly contaminated oven environment. Later, (Part 2) an additional material was tested but without exposing the specimens to the questionable oven contamination.

SIGNIFICANCE OF DATA

Careful examination of individual percentage changes (see Appendix) shows that the overall mean value does not always give a true indication of what has taken place. Looking closely at the tables in the Appendix and remembering that there are 5 resistors on each substrate, one can detect many cases of distinct groupings of 5 values particularly with (but not limited to) the hermetically sealed substrates. For an obvious example, see the data for the hermetically sealed DP1033 specimens on the third page of Table A5. Here the pure rosin coated substrates have substrate means ranging from 0.04% to 0.50%. This indicates an unknown factor which influences the stability of both Birox and 8000 series resistors. In the case of the hermetically sealed packages it could be argued that the differences might be due to the degree of the hermetic seal, (this has not yet been determined). But since this data grouping exists to a lesser extent for non-hermetically sealed substrates (see data for the HA 7236/Kester 1544 coated specimens in Figure 4), some additional factor such as an accidental finger print must be involved. In order to determine the cause or causes of these substrate-to-substrate variations, additional experimentation must be performed. (In the case of the hermetically sealed substrates, this will most likely involve only a precisely controlled leak test.)

SIGNIFICANCE OF DATA - (Cont'd)

The majority of the resistance drift is accounted for within the first ten days. After that the drift rate of the Birox inks was very low. The hermetically sealed resistors continued to drift throughout the period of the experiments at an appreciable rate.

Birox resistors were more stable than the 8025 resistors in the presence of the materials tested. The silicone and urethane coatings had about the same magnitude of effect on the resistors while the epoxy was considerably worse.

The resistance changes seen are the net result of at least two reactions. The resistance changes for resistors coated with silicones and urethane have indications of reactions of different rates and opposing effects. This is not seen in the epoxy coated samples because of the magnitude of the epoxy caused shift. Further work should be done to separate the two reactions.

PROCEDURE

Part 1 - 125 substrates, each containing 5 resistors, were printed with Birox DP1033 and fired per DPS 51042 on previously fired ESL 5800C conductors giving an initial mean resistance of 10.3K ohms for the 625 resistors. One hundred similar substrates printed with du Pont's 8025 resistor ink for a previous study (Reference 3) were glass coated with du Pont's 8185 and stabilized as specified in DPS 51042. All resistors were then trimmed to 20K ohms  $\pm$  1/2%.

Five DP1033 substrates and four 8025 substrates were set aside for use as controls. The remaining substrates were divided into four groups and coated with a thin coat of the following fluxes:

- Group 1    Alpha 611 (RMA)
- Group 2    Kester 1544 (RA)
- Group 3    Pure Rosin dissolved in an equal volume of isopropyl alcohol (w)
- Group 4    Not coated with flux

Each of these groups were divided into six subgroups and coated or packaged as follows:

- Subgroup 1    Coated with Sylgard 182 (silicone)
- Subgroup 2    Coated with GE's RTV 511 (silicone)
- Subgroup 3    Coated with Stycast 2850GT (epoxy)
- Subgroup 4    Coated with Hathane HA 7236 (polyurethane foam)
- Subgroup 5    Coated with Eccosil (silicone)
- Subgroup 6    Hermetically sealed

(The above grouping results in 5 substrates per condition for the DP1033 resistors and 4 substrates per condition for the 8025 ink. In each case there were 5 resistors on each substrate).

PROCEDURE - (Cont'd)

Resistors were measured immediately before coating and again 24 hours after coating using a Dymec 2010B data acquisition system. (The digital ohmmeter in this system has a rated accuracy of 0.01% of reading  $\pm$  0.005% full scale  $\pm$  1 digit. Measurement repeatability was tested several times during this study with a 20,000 ohm standard resistor and found to be within  $\pm$  2 digits giving a repeatability accuracy of 0.01%). All specimens except the controls were placed on trays and exposed to thermal aging in a forced draft oven. The resistors were measured again at the following time-temperature intervals:

After 11 days at 150°C.

After 11 days at 150°C + 9 days at 100°C.

After 11 days at 150°C + 17 days at 100°C  
+ 11 days at 125°C.

After 11 days at 150°C + 17 days at 100°C  
+ 76 days at 125°C.

The control resistors were measured at the same time intervals but were not thermally aged.

Part 2 - Five substrates with Birox resistors, a blend of equal parts by weight of DP1031 and DP1041, and five substrates with 8025 resistors made according to the established manufacturing process (DPS 51046) but rejected because of minor defects were selected for testing resistor sensitivity to the silicone coating DC3140.

Each of these substrates was broken in half and divided into two groups containing five half substrates each. Five trimmed resistors on each half substrate were connected using Sn 63 solder with an RMA flux core with 28 gauge Teflon insulated wire to a thick film conductor terminal strip (separate strip for each group). The groups, supported only by interconnecting wires, were thoroughly cleaned in 1,1,1-trichloroethane, dried and initial resistance measurements taken. One DP1031/DP1041 group and one 8025 group was coated with a 0.050 to 0.100 inch layer of DC3140 silicone coating which was cured overnight at room temperature. The resistors were measured again, then placed in large sealed glass containers (one container for the uncoated controls and one for the coated specimens) and placed in a 125°C oven. The resistors were measured after 1, 7, 14, 28, 64, 76, and 95 days exposure to the thermal environment. After the 64 day measurement, the specimens remained exposed to the laboratory environment overnight before returning to the heated glass containers.

RESULTS

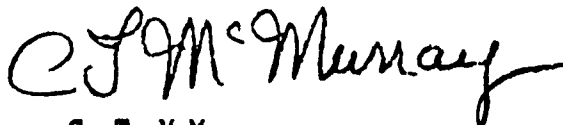
The results are discussed in terms of changes in resistance from the initial resistance (that is the resistance before coating). Standard deviations are listed with each value to show the data spread. The individual resistance changes are listed in the Appendix for use in detailed studies.

Part I - The resistance changes for the DP1033 ink are summarized in Table I. These changes are shown graphically in Figures 1-6. Resistance changes for the 8025 ink are summarized in Table II and shown graphically in Figures 7-12.

Part II - The resistance changes and standard deviations for the closed container ageing experiment are listed in Table III, and shown graphically in Figure 13.

REFERENCES

1. Technical Record Book No. 12085 pgs. 12 to 25
2. MP 51,412, Thick Film Printing and Resistor Ink Blending
3. EWO 66145  
S.O. 80611-012



C. T. McMurray  
Electronics Processing  
Materials & Methods -  
Research & Engineering

Approved by:



W. C. Peart, Section Chief  
Electronics Processing  
Materials & Methods -  
Research & Engineering

rvt

MATERIALS AND EQUIPMENT INDEX

1. Electro Science Lab 5800C Platinum-gold conductor ink.
2. du Pont Birox DP1033 resistor ink.
3. du Pont 8025 palladium silver resistor ink.
4. du Pont 8185 resistor glaze coating.
5. AlSi Mag 614 substrates, 1-inch by 1-inch by .025-inch.
6. Alpha 611 flux, mildly activated (RMA), MIL-F-14256C, Type A.
7. Kester 1544 flux, activated (RA), MIL-F-14256C, Type A.
8. Non-activated flux (equal parts by volume of isopropyl alcohol and rosin), MIL-F-14256C, Type W.
9. Dow Corning Sylgard 182 silicone encapsulating resin.
10. General Electric RTV 511 silicone encapsulating resin.
11. Emmerson and Cuming Eccosil silicone resin.
12. Emmerson and Cuming Stycast 2850GT, with Catalyst 11 epoxy encapsulating resin.
13. Hastings Plastics HA7236 polyurethane foam.
14. Cold welded packages (MP 51,547).
15. Dymec Data Acquisition System, model DY-2010B, MDAC Tag No. 622060.

Table I  
PERCENTAGE CHANGE SUMMARY FOR DUPONT'S BIROX DPI033 INK

Coating or Package	Percentage Changes:																	
	Before Thermal Aging (After Coating)				After 11 days at 150°C + 9 days at 100°C				After 11 days at 150°C + 17 days at 100°C				After 11 days at 150°C + 17 days at 100°C + 76 days at 125°C					
	Alpha 611 Flux (RMA)	Kester 1544 Flux (RA)	Pure Rosin Flux (U)	No Flux	Alpha 611 Flux (RMA)	Kester 1544 Flux (RA)	Pure Rosin Flux (U)	No Flux	Alpha 611 Flux (RMA)	Kester 1544 Flux (RA)	Pure Rosin Flux (U)	No Flux	Alpha 611 Flux (RMA)	Kester 1544 Flux (RA)	Pure Rosin Flux (U)	No Flux		
Standard 150 (Silicone)	M(1) S(2)	0.109 0.011	0.129 0.060	-0.007 0.009	0.016 0.012	-0.230 0.025	-0.110 0.060	-0.091 0.062	-0.218 0.028	-0.210 0.043	-0.266 0.055	-0.278 0.049	-0.098 0.065	-0.233 0.27	-0.271 0.151	-0.097 0.070	-0.289 0.037	-0.217 0.040
GE 511 Silicone	M S	0.110 0.102	0.047 0.005	0.009 0.005	0.022 0.006	-0.266 0.027	-0.117 0.044	-0.096 0.044	-0.232 0.023	-0.268 0.038	-0.251 0.024	-0.262 0.026	-0.101 0.044	-0.252 0.027	-0.242 0.030	-0.106 0.042	-0.264 0.023	-0.275 0.029
Styrene 2000 (Epoxy)	M S	0.083 0.020	0.119 0.073	-0.008 0.017	0.117 0.233	2.046 0.279	1.808 0.299	1.870 0.308	2.132 0.282	1.531 0.401	1.997 0.240	2.052 0.252	1.920 0.320	2.182 0.288	2.652 0.481	2.163 0.312	2.317 0.312	1.790 0.190
Hachure 7236 (Polyurethane Foam)	M S	0.097 0.012	0.111 0.049	-0.011 0.018	-0.050 0.013	-0.234 0.043	-0.119 0.046	-0.094 0.059	-0.232 0.042	-0.344 0.036	-0.248 0.050	-0.260 0.050	-0.101 0.052	-0.217 0.045	-0.266 0.044	-0.098 0.046	-0.297 0.043	-0.333 0.052
Ecocoll Silicone	M S	0.102 0.015	0.162 0.061	0.009 0.009	0.019 0.006	-0.247 0.046	-0.099 0.060	-0.071 0.064	-0.277 0.048	-0.257 0.036	-0.286 0.029	-0.268 0.030	-0.086 0.061	-0.237 0.140	-0.236 0.063	-0.090 0.063	-0.269 0.029	-0.266 0.027
Mathematically Packaged	M S	0.010 0.034	0.111 0.121	-0.134 0.026	-0.149 0.033	0.063 0.037	0.097 0.099	0.186 0.104	0.108 0.055	-0.247 0.132	0.017 0.110	0.017 0.110	0.095 0.086	0.160 0.058	0.478 0.161	0.110 0.095	0.355 0.204	-0.240 0.021
Controls (3) Not Coated or Thermally Aged	M S	0.034 0.009		0.055 0.018		0.067 0.022		0.074 0.016					0.074 0.016			0.071 0.019		

NOTE: 1) Mean Value  
2) Standard Deviation  
3) Controls were not thermally aged but were measured along with other resistors.

Table II  
 PERCENTAGE CHANGE SUMMARY FOR DuPONT'S 8025 INK

Coating or Package	Percentage Changes:															
	Before Thermal Aging (After Coating)				After 11 days at 150°C + 9 days at 100°C				After 11 days at 150°C + 17 days at 100°C + 11 days at 125°C				After 11 days at 150°C + 17 days at 100°C + 76 days at 125°C			
	Alpha Flux (MA)	Kester Flux (RA)	1544 Flux (VA)	Pure Rosin Flux (V)	Alpha Flux (MA)	Kester Flux (RA)	1544 Flux (VA)	Pure Rosin Flux (V)	Alpha Flux (MA)	Kester Flux (RA)	1544 Flux (VA)	Pure Rosin Flux (V)	Alpha Flux (MA)	Kester Flux (RA)	1544 Flux (VA)	Pure Rosin Flux (V)
M (Silicone)	0.071	0.101	0.155	0.053	0.104	0.087	0.054	0.085	0.290	0.347	0.062	0.297	0.304	0.286	0.129	0.286
S (Silicone)	0.054	0.161	0.254	0.025	0.039	0.054	0.025	0.039	0.129	0.062	0.062	0.024	0.042	0.042	0.042	0.042
M (Silicone)	0.008	0.155	0.254	0.023	0.104	0.087	0.054	0.085	0.290	0.347	0.062	0.297	0.304	0.286	0.129	0.286
S (Silicone)	0.005	0.161	0.254	0.025	0.039	0.054	0.025	0.039	0.129	0.062	0.062	0.024	0.042	0.042	0.042	0.042
S (Silicone)	0.004	0.126	0.074	0.018	0.018	0.018	0.018	0.018	0.018	0.018	0.018	0.018	0.018	0.018	0.018	0.018
S (Silicone)	0.005	0.074	0.018	0.018	0.018	0.018	0.018	0.018	0.018	0.018	0.018	0.018	0.018	0.018	0.018	0.018
M (Silicone)	0.011	0.065	0.028	0.011	0.116	0.042	0.015	0.015	0.255	0.340	0.041	0.396	0.422	0.248	0.016	0.281
S (Silicone)	0.005	0.028	0.011	0.011	0.042	0.042	0.015	0.015	0.016	0.024	0.024	0.078	0.059	0.016	0.016	0.016
M (Silicone)	0.021	0.071	0.033	0.017	0.228	0.101	0.017	0.017	0.271	0.314	0.038	0.393	0.427	0.253	0.014	0.285
S (Silicone)	0.005	0.033	0.017	0.017	0.101	0.101	0.017	0.017	0.014	0.037	0.037	0.084	0.089	0.017	0.017	0.017
M (Silicone)	0.001	0.118	0.032	0.050	0.179	0.051	0.050	0.050	0.477	0.308	0.092	0.743	0.569	0.477	0.065	0.064
S (Silicone)	0.013	0.032	0.050	0.050	0.078	0.078	0.050	0.050	0.038	0.065	0.065	0.142	0.081	0.061	0.061	0.061
M (Silicone)	0.050	0.026	0.026	0.026	0.026	0.026	0.026	0.026	0.026	0.026	0.026	0.026	0.026	0.026	0.026	0.026
S (Silicone)	0.026	0.026	0.026	0.026	0.026	0.026	0.026	0.026	0.026	0.026	0.026	0.026	0.026	0.026	0.026	0.026

NOTES: 1) Mean Value  
 2) Standard Deviation  
 3) Controls were not thermally aged but were measured along with other resistors.

Table III  
PERCENTAGE CHANGE SUMMARY FOR DC3140 COATED RESISTORS

Coating		After Coating	After 7 Days at 125°C	After 14 Days at 125°C	After 28 Days at 125°C	After 64 Days at 125°C	After 76 Days at 125°C	After 95 Days at 125°C
Birox (1) coated with DC3140	M	-0.053	0.008	0.027	0.027	0.019	-0.053	0.026
	S	0.115	0.019	0.022	0.021	0.025	0.050	0.023
Birox Control	M	0.002	0.002	0.013	0.036	-0.114	-0.118	-0.116
	S	0.019	0.010	0.021	0.025	0.071	0.071	0.079
8025 Coated with DC3140	M	0.008	0.098	0.143	0.166	0.209	0.085	0.244
	S	0.037	0.062	0.085	0.081	0.095	0.157	0.114
8025 Control	M	-0.028	0.109	0.203	0.233	0.280	0.171	0.296
	S	0.128	0.034	0.067	0.056	0.100	0.143	0.111

(1) Birox is a blend of DP1031 and DP1041 inks.

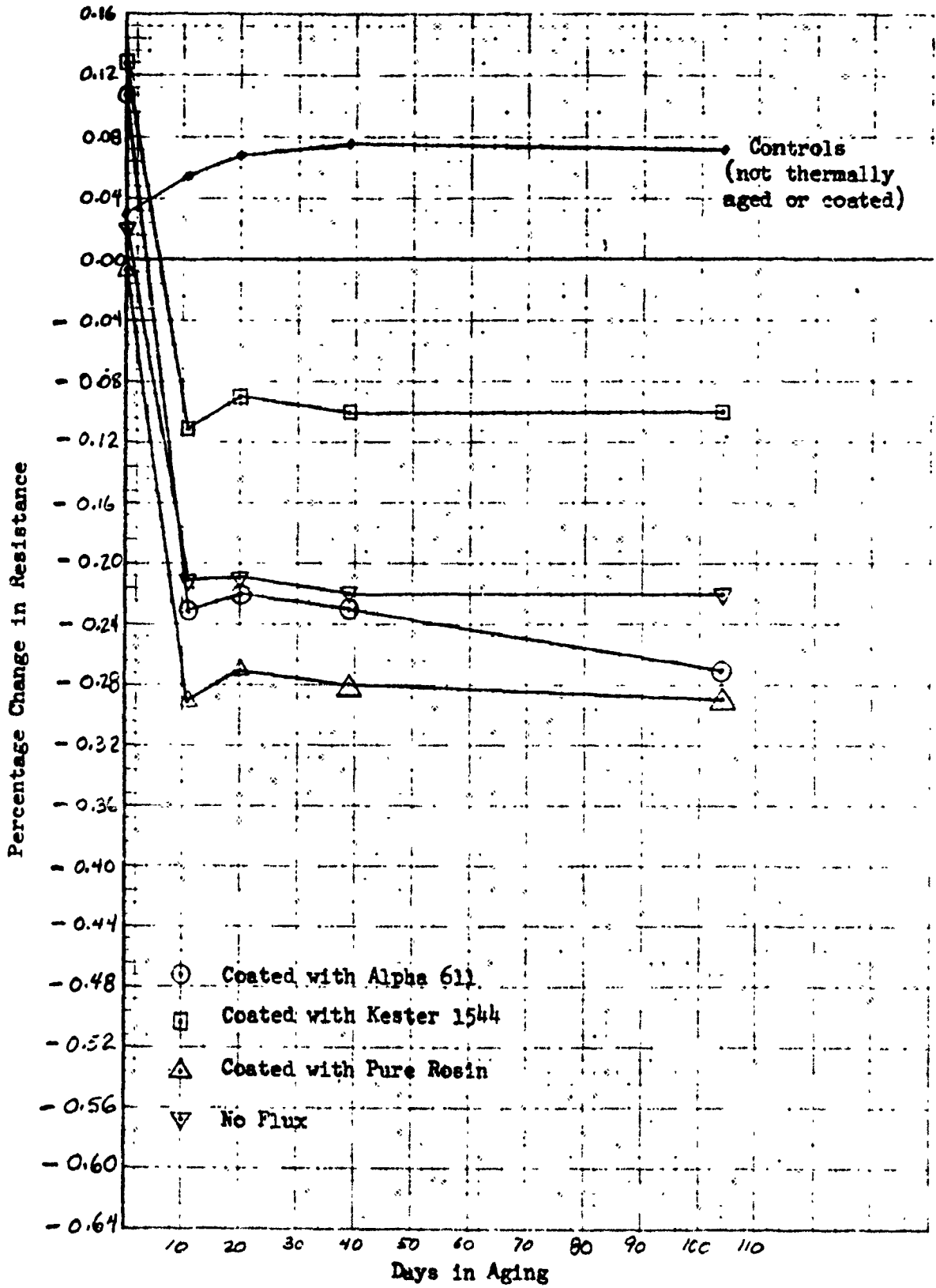


Figure 1. DP1033 Resistors Coated with Sylgard (Silicone)

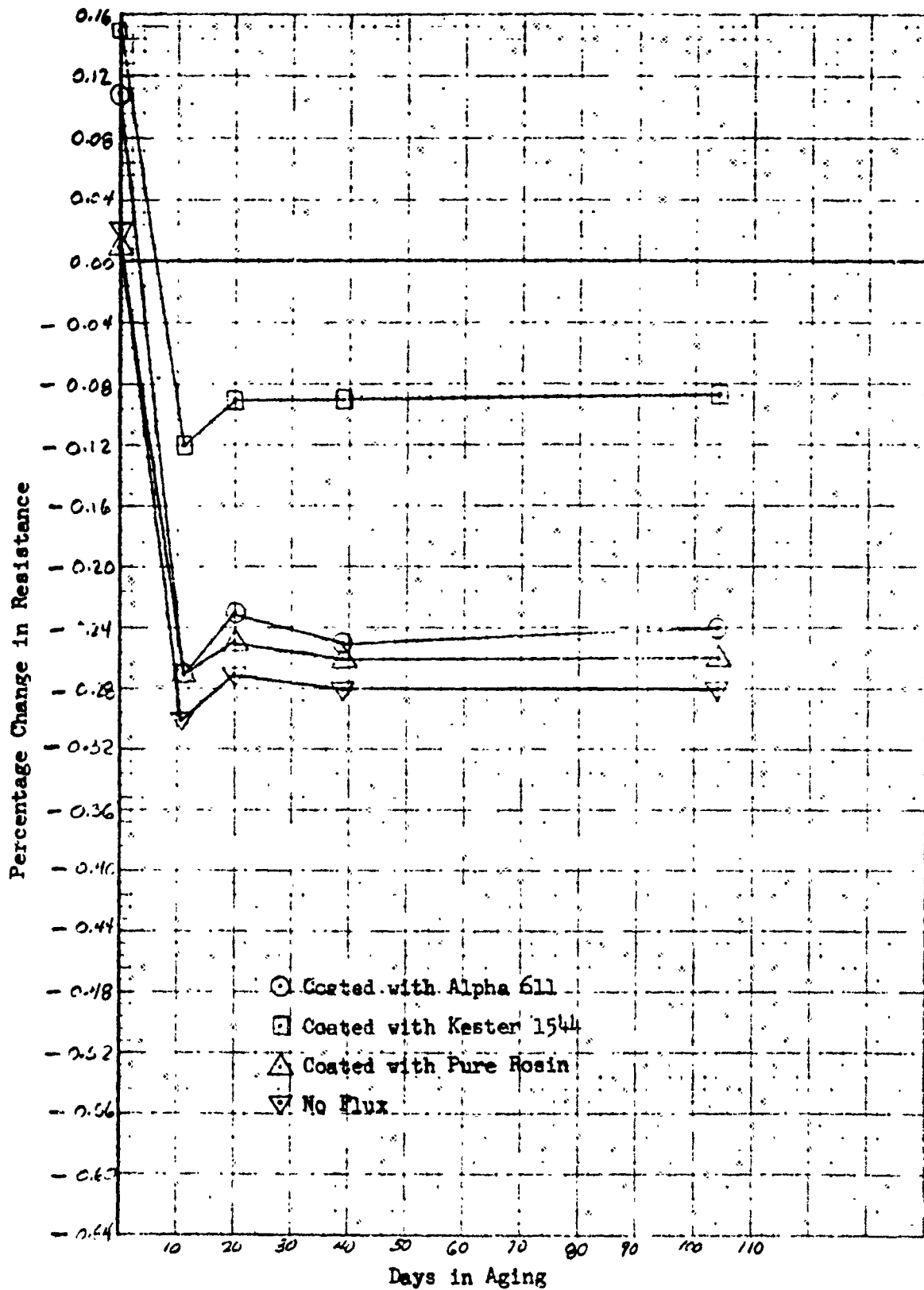


Figure 2. Biros DP1033 Resistors Coated with GE 511 (Silicone)

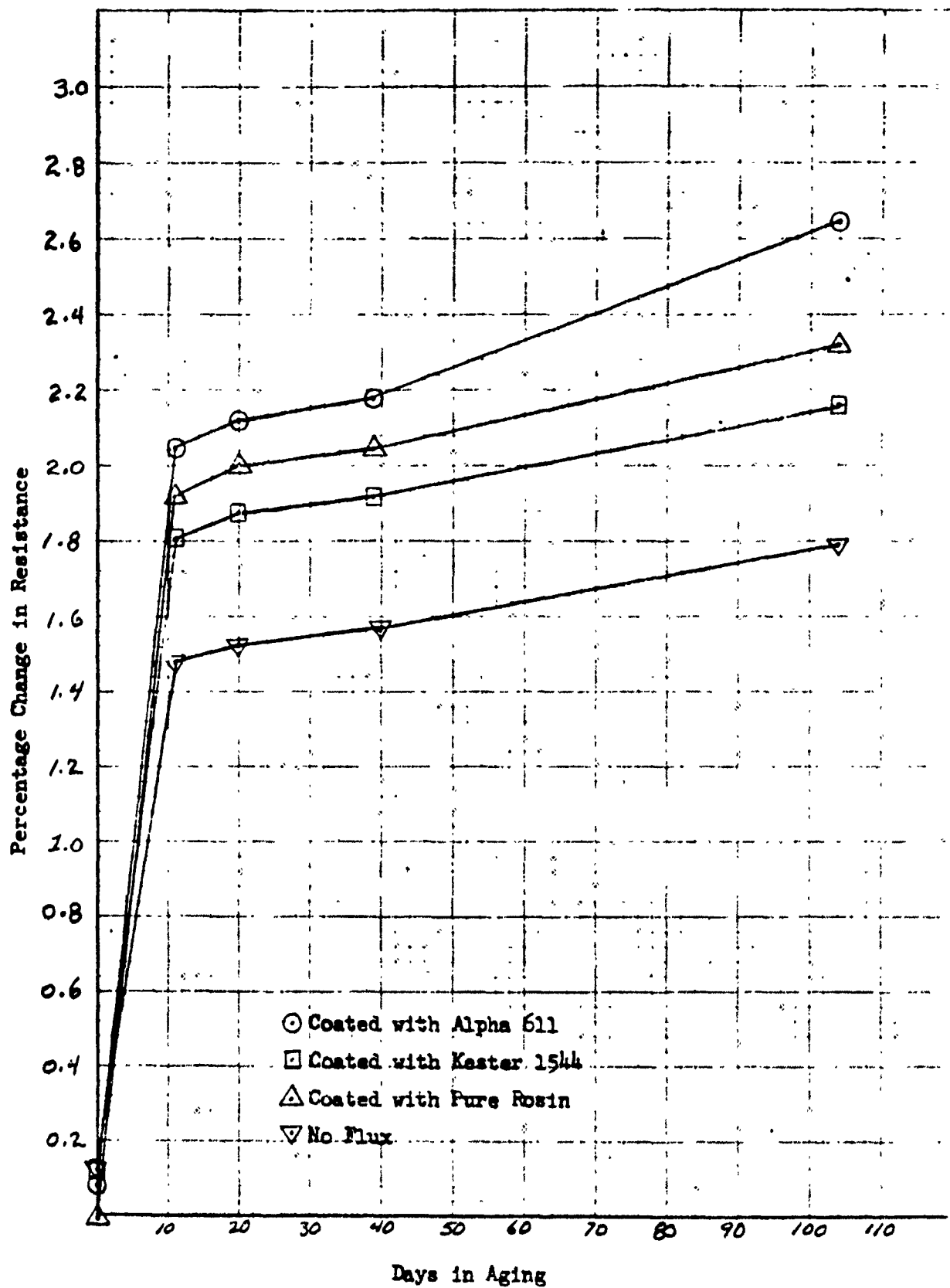


Figure 3. Biorex DP1033 Resistors Coated with Stycast 2850GT (Epoxy)

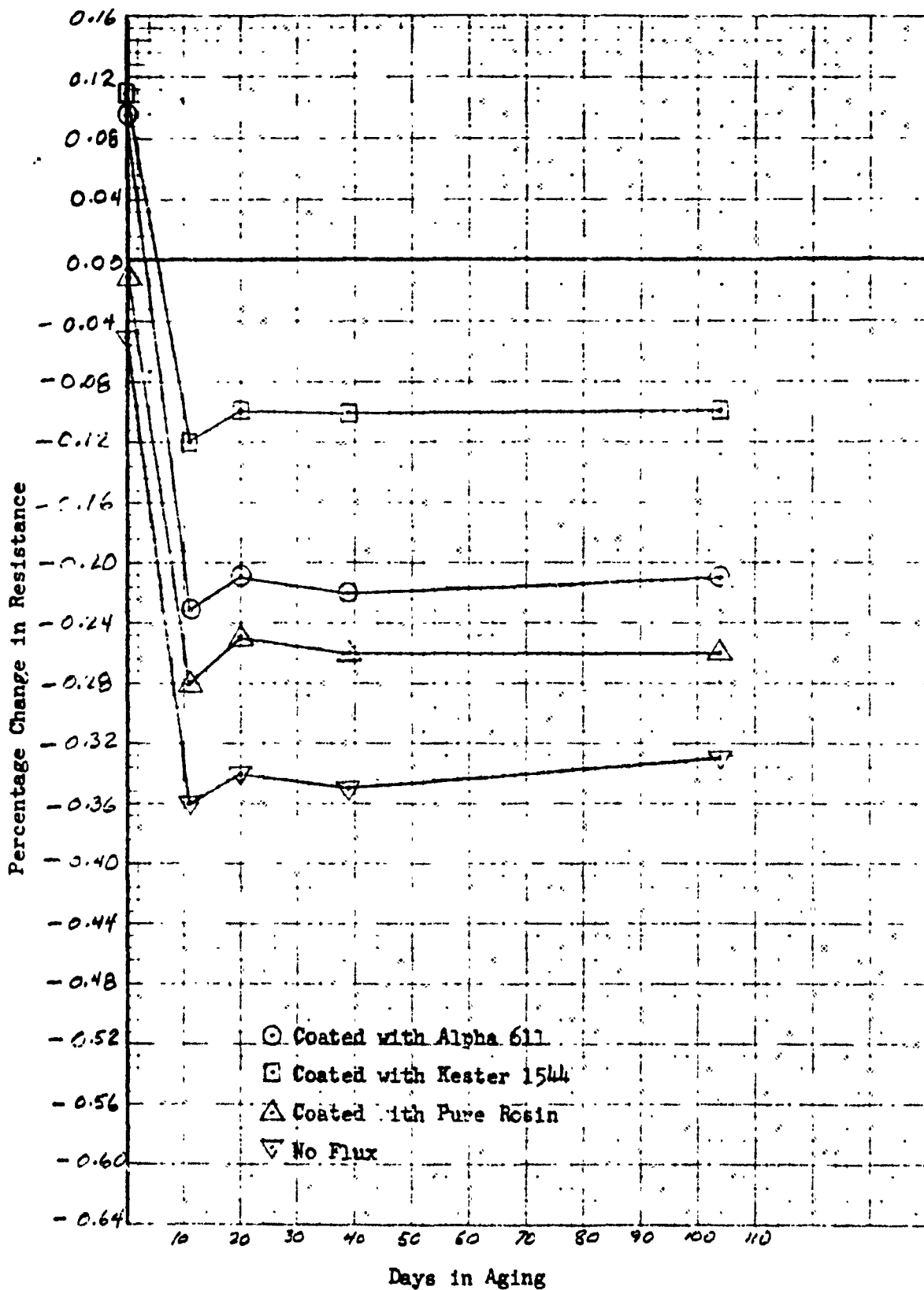


Figure 4. Biorex DP1033 Resistors Coated with HA7236 (Polyurethane Foam)

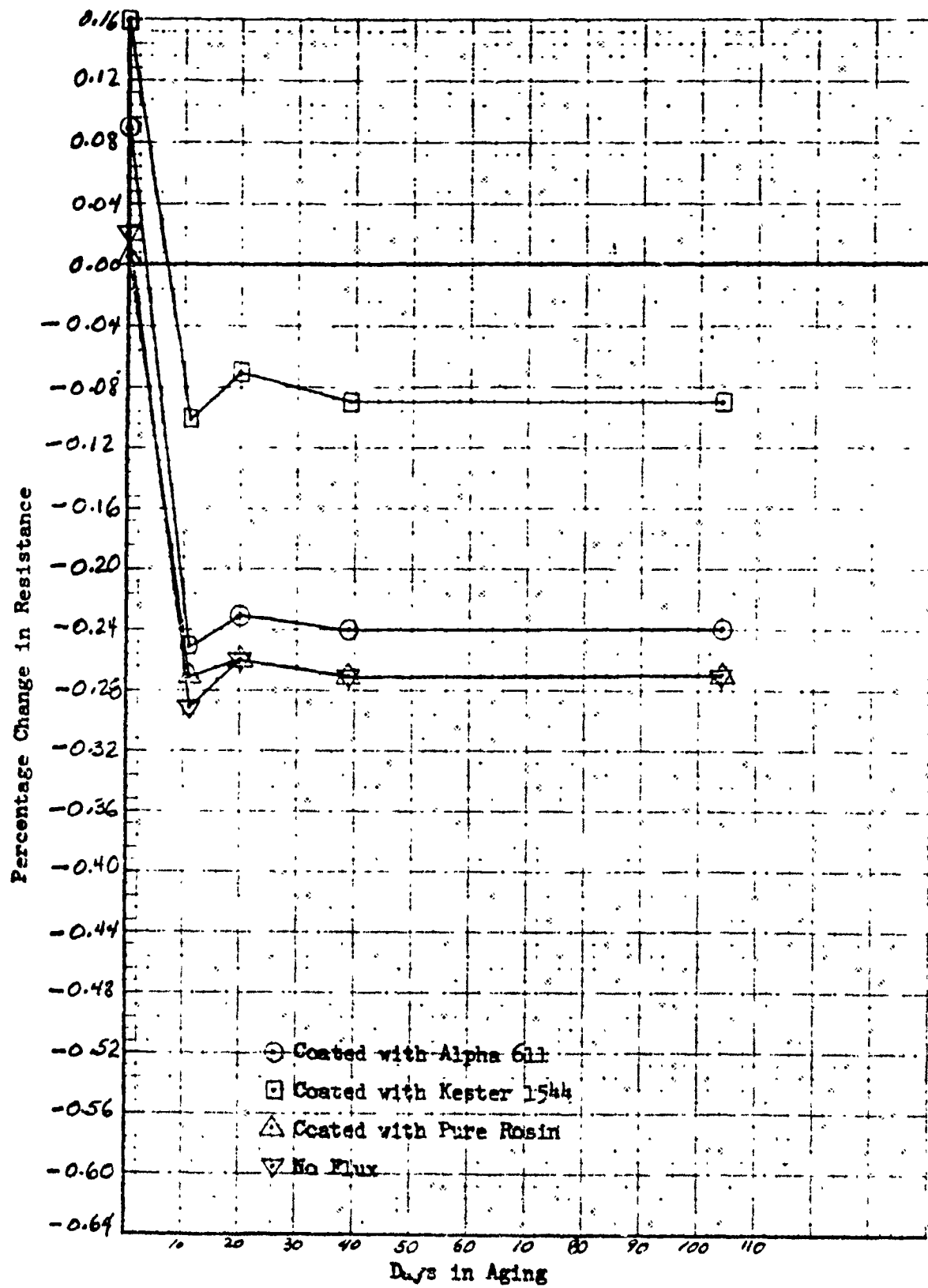


Figure 5. Birox DP1033 Resistors Coated with Eccosil (Silicone)

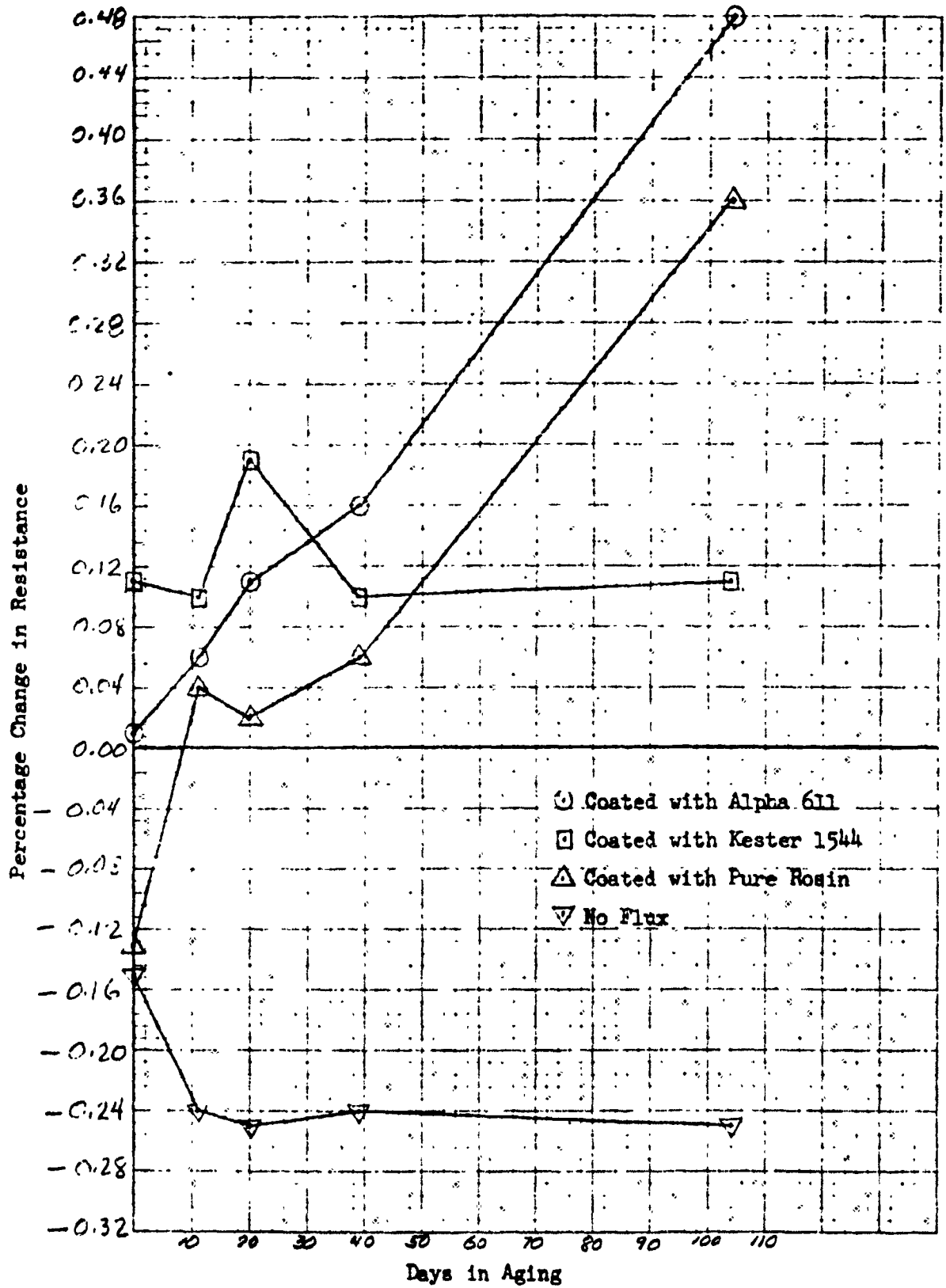


Figure 6. Birox DP1033 Resistors Horizontally Sealed

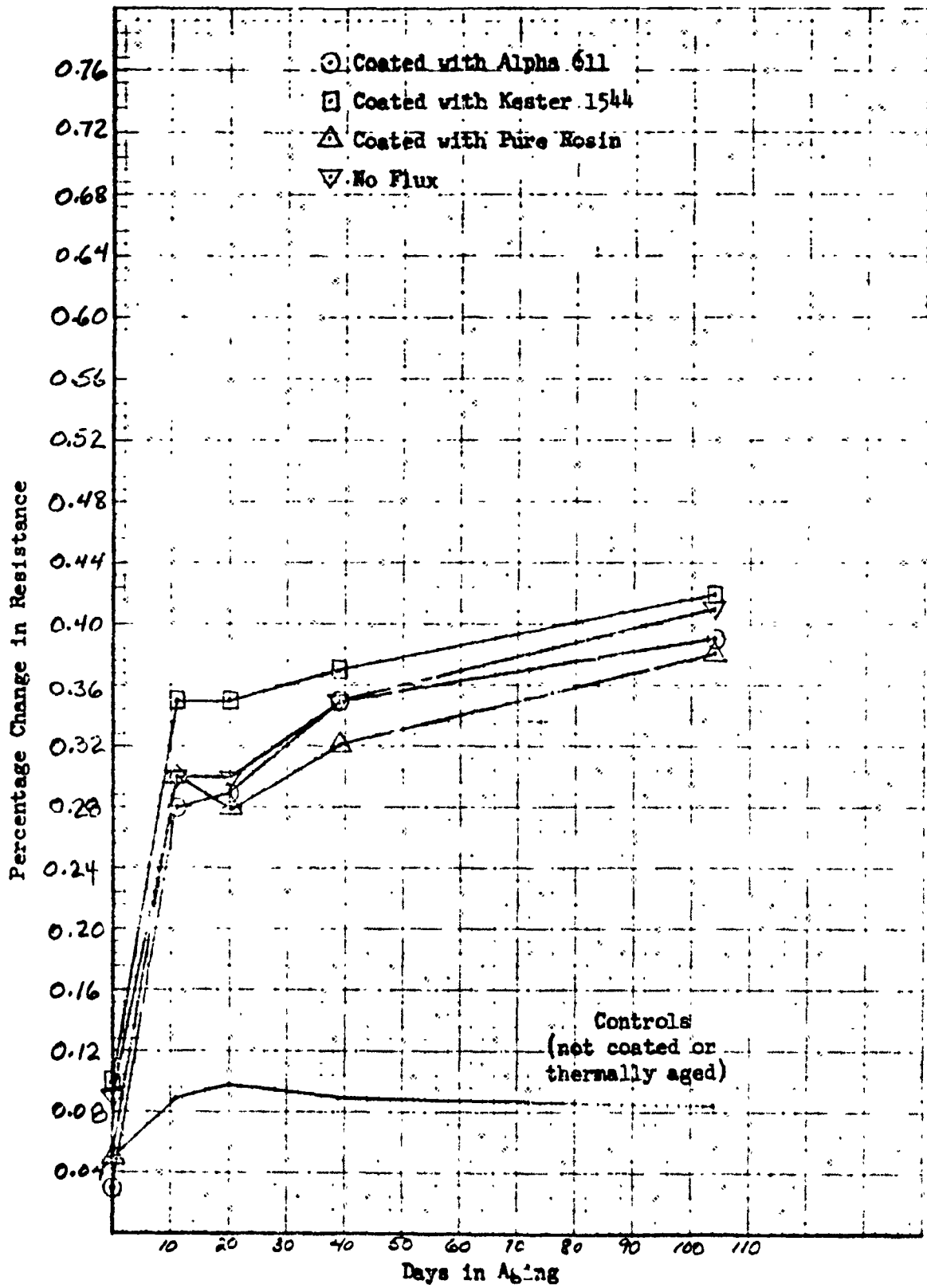


Figure 7. 8025 Resistors Coated with Sylgard 182 (Silicone)

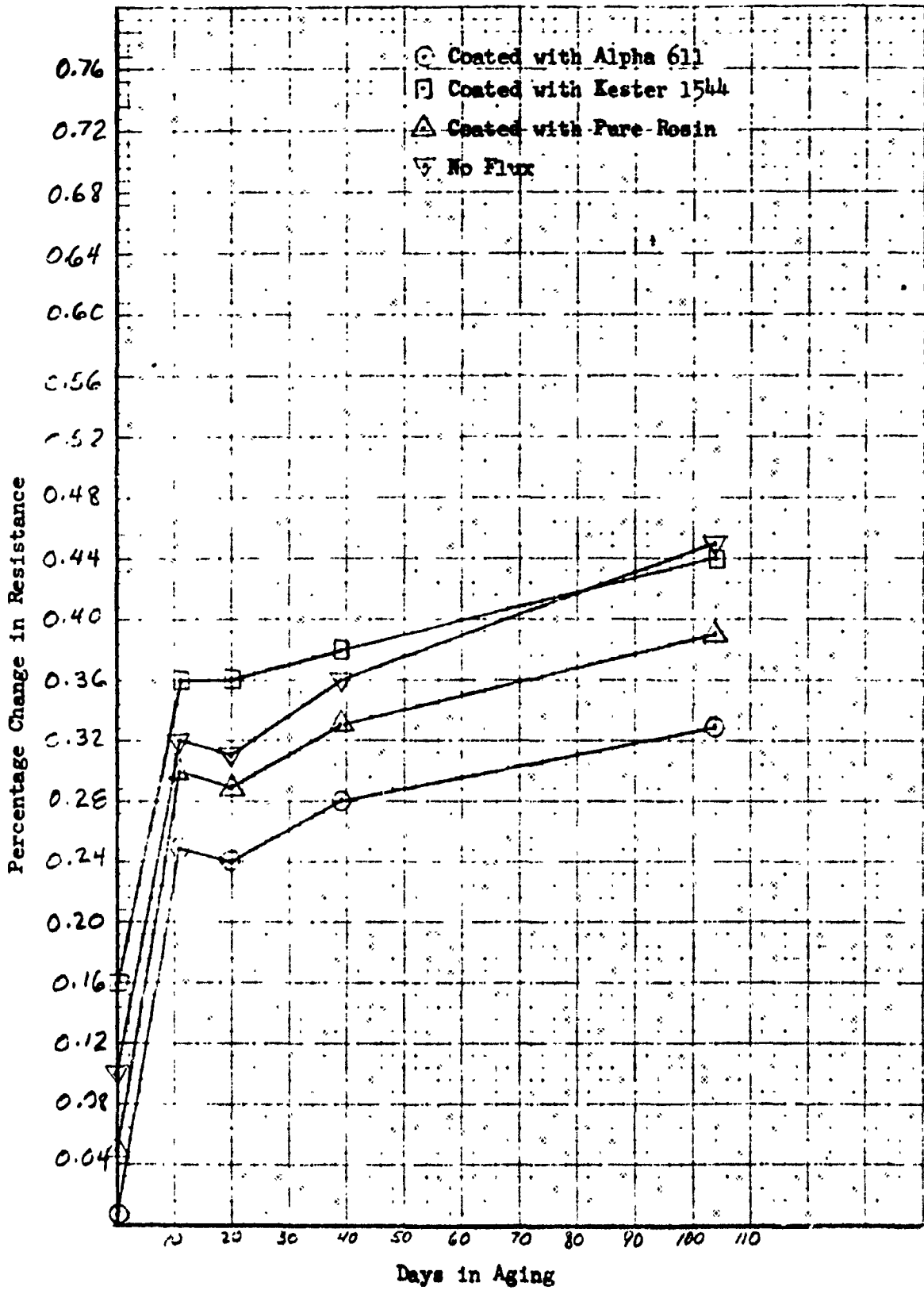


Figure 8. 8025 Resistors Coated with GE 511 (Silicone)

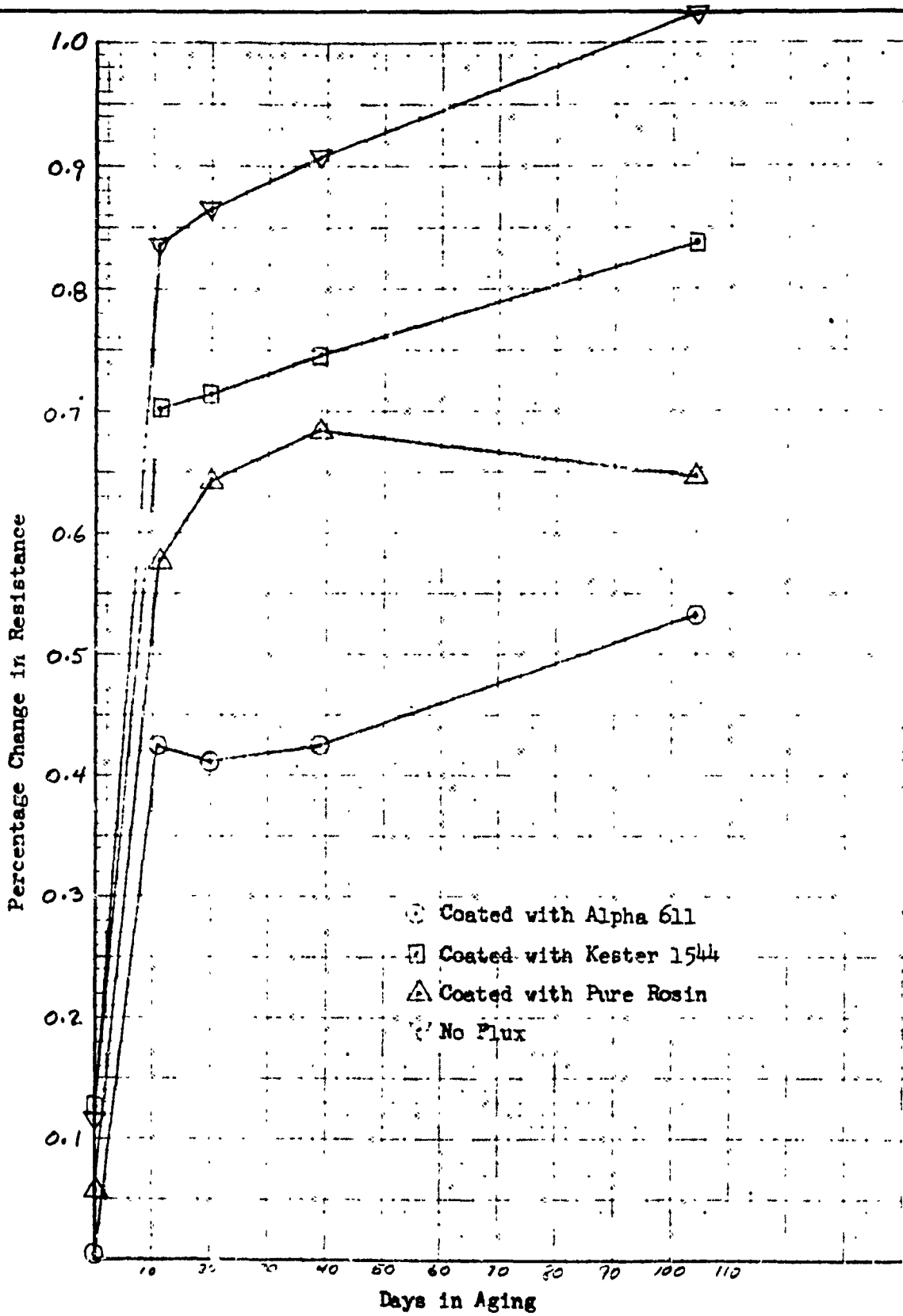


Figure 9. 802C Resistors Coated with Stycast 2850GT (Epoxy)

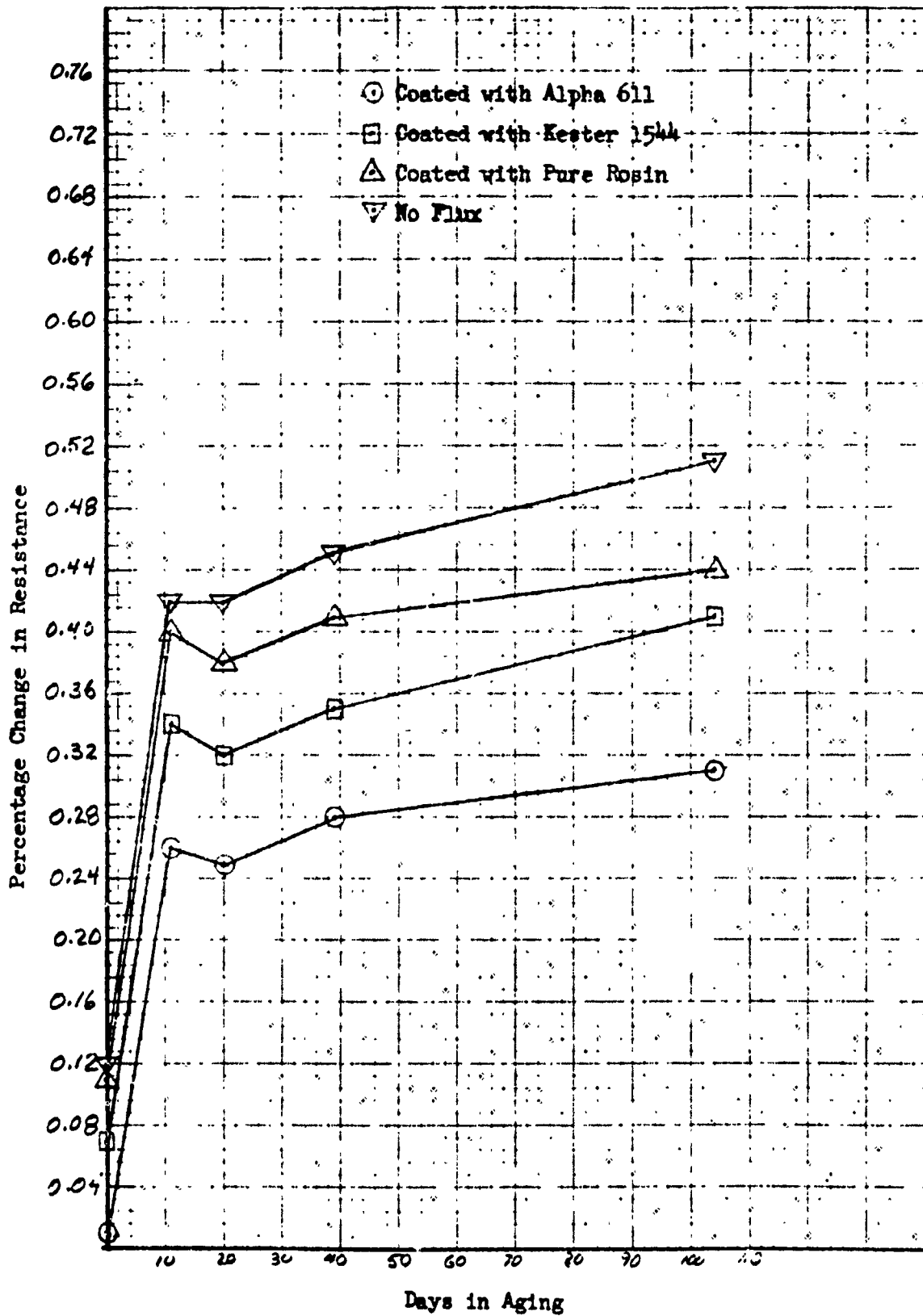


Figure 10. 8025 Resistors Coated with HA7236 (Polyurethane Foam)

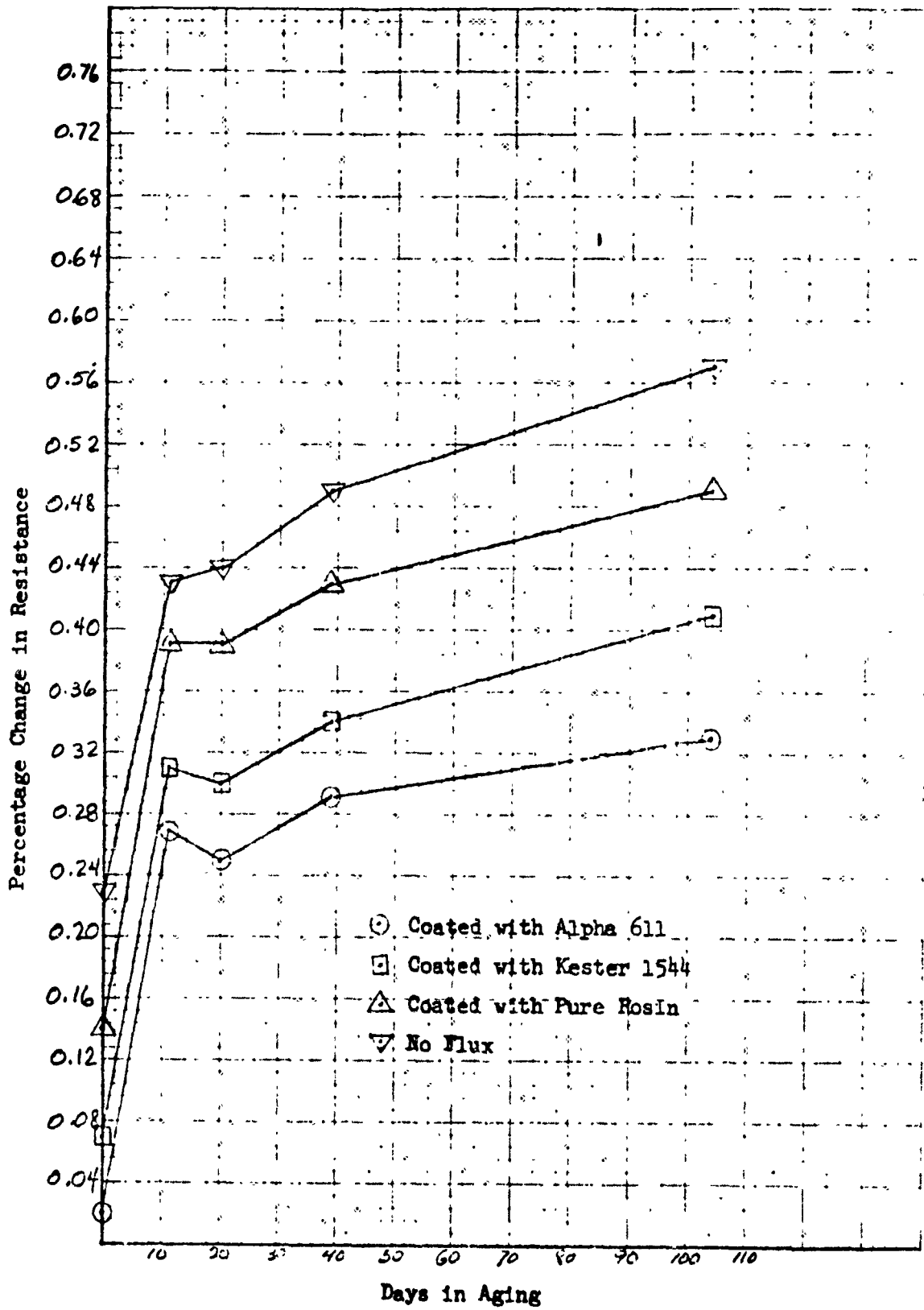


Figure 11. 8025 Resistors Coated with Eccosil (Silicone)

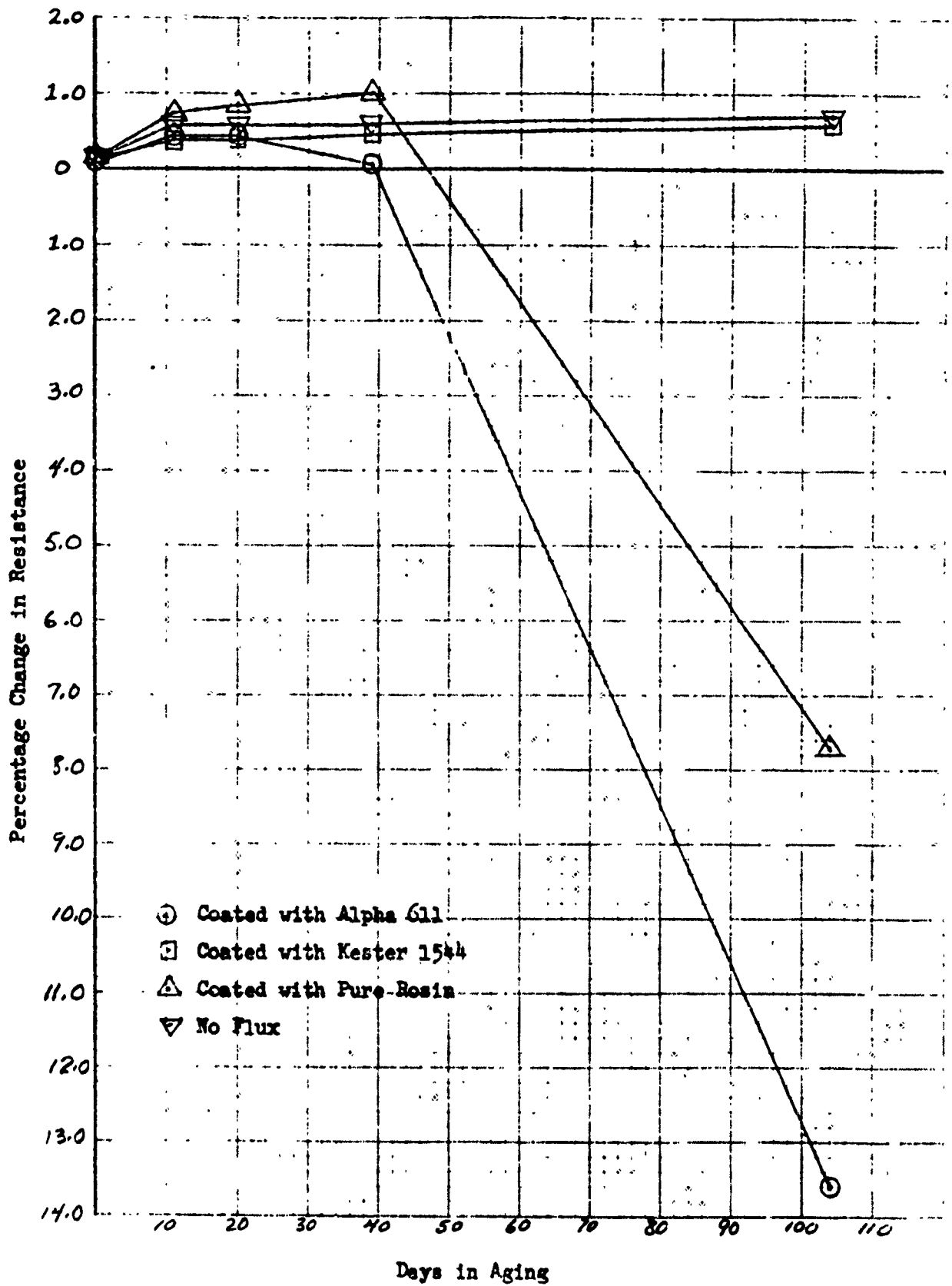


Figure 12. 8025 Resistors Hermetically Sealed

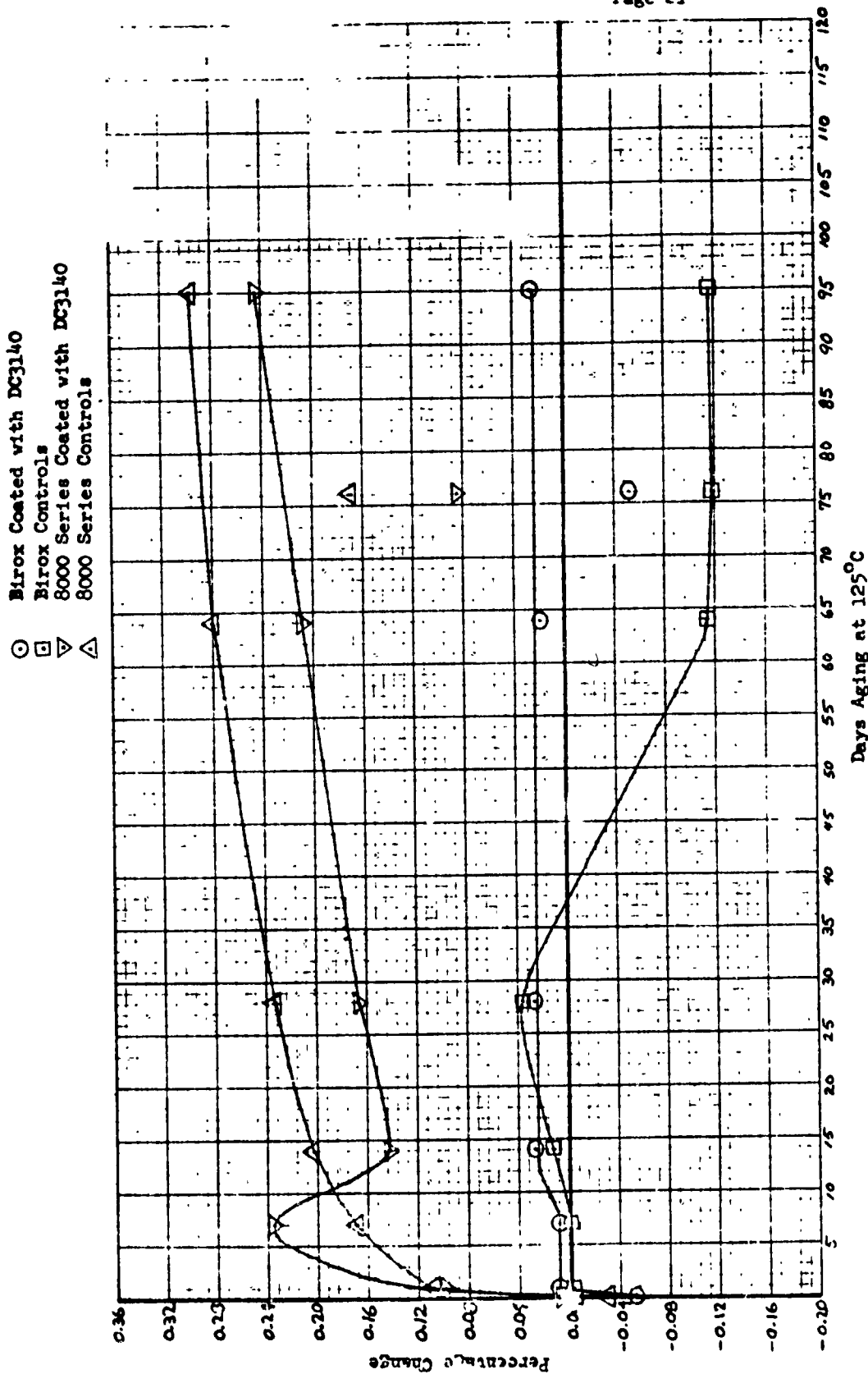


Figure 13. Effect of Thermal Aging on Birox and 8000 Series Resistors Coated with DC 3140 Silicone

### APPENDIX

In this Appendix are collected the percentage resistance changes calculated from resistance measurements made at various intervals. All percentage changes are with respect to the initial trimmed value of 20K ohms  $\pm$  .5%. Percent resistance was calculated by the equation

$$\% \Delta R = \frac{R - R_0}{R_0} \times 100$$

These data are listed for future studies wishing to further examine reasons for the definite grouping of some of the resistance changes.

Table A1  
Birox Resistors

Percentage Changes of Individual Resistors After Coating (Before Aging)

Coating or Package	Flux			
	Alpha 611	Kester 1544	Pure Rosin	No Flux
Sylgard 182	0.105	0.125	0.000	0.010
	0.105	0.149	0.010	0.005
	0.120	0.129	0.015	0.015
	0.100	0.144	0.000	0.015
	0.131	0.134	0.000	0.010
	0.120	0.065	-0.005	0.030
	0.110	0.120	0.000	0.040
	0.115	0.120	-0.010	0.035
	0.120	0.100	-0.020	0.030
	0.105	0.090	-0.010	0.020
	0.095	0.135	0.010	0.025
	0.100	0.119	0.010	0.030
	0.100	0.080	-0.005	0.015
	0.095	0.065	-0.005	0.020
	0.115	0.075	-0.005	0.020
	0.121	0.080	-0.010	0.015
	0.125	0.105	0.000	0.015
	0.120	0.050	-0.005	0.025
	0.090	0.080	-0.010	0.010
	0.090	0.100	-0.140	0.010
0.100	0.245	-0.005	-0.005	
0.105	0.269	0.000	0.005	
0.110	0.259	0.005	0.005	
0.105	0.209	0.005	0.005	
0.115	0.149	0.000	-0.010	
GE 511	0.140	0.105	0.000	0.015
	0.115	0.110	0.010	0.020
	0.115	0.105	0.010	0.025
	0.110	0.115	0.010	0.025
	0.105	0.095	0.010	0.020
	0.085	0.165	0.005	0.020
	0.105	0.204	0.015	0.025
	0.100	0.169	0.010	0.025
	0.100	0.120	0.015	0.025
	0.120	0.119	0.000	0.010
	0.140	0.130	0.020	0.015
	0.135	0.155	0.010	0.020
	0.120	0.200	0.015	0.025
	0.115	0.190	0.015	0.025
	0.100	0.155	0.005	0.025
	0.090	0.145	0.005	0.020
	0.090	0.159	0.000	0.030
	0.100	0.105	0.005	0.035
	0.090	0.085	0.010	0.020
	0.105	0.094	0.000	0.015
0.135	0.155	0.010	0.025	
0.125	0.190	0.010	0.030	
0.115	0.200	0.010	0.020	
0.110	0.215	0.015	0.015	
0.090	0.265	0.005	0.015	

Table A1  
Continued

Coating or Package	Flux			
	Alpha 611	Kester 1544	Pure Rosin	No Flux
Stycast 2850GT	0.080	0.110	-0.005	0.070
	0.090	0.119	0.005	0.045
	0.080	0.099	0.005	0.035
	0.085	0.100	0.000	0.060
	0.050	0.427	-0.015	0.030
	0.125	0.140	-0.025	0.070
	0.115	0.115	-0.015	0.258
	0.110	0.105	-0.015	0.060
	0.090	0.065	-0.020	0.091
	0.065	0.085	-0.025	0.050
	0.085	0.130	-0.035	0.160
	0.065	0.159	-0.020	-0.010
	0.055	0.174	-0.015	0.065
	0.070	0.070	-0.015	0.018
	0.090	0.075	-0.015	-0.015
	0.080	0.140	-0.015	0.160
	0.065	0.100	-0.025	0.050
	0.105	0.070	-0.010	1.200
	0.075	0.175	-0.010	0.124
	0.110	0.060	-0.015	0.030
0.050	0.110	0.030	0.085	
0.095	0.114	0.025	0.090	
0.095	0.104	0.005	0.065	
0.075	0.075	0.000	0.035	
0.070	0.045	0.025	0.109	
EA7236	0.100	0.025	0.005	-0.055
	0.110	0.065	-0.005	-0.065
	0.110	0.080	0.005	-0.060
	0.105	0.075	0.000	-0.050
	0.105	0.095	0.005	-0.030
	0.095	0.070	-0.030	-0.045
	0.105	0.105	-0.055	-0.070
	0.090	0.105	-0.050	-0.075
	0.100	0.124	-0.025	-0.075
	0.105	0.080	-0.005	-0.035
	0.075	0.090	0.000	-0.040
	0.075	0.080	0.000	-0.060
	0.085	0.105	0.010	-0.060
	0.095	0.080	0.015	-0.060
	0.095	0.125	0.010	-0.045
	0.105	0.090	-0.025	-0.035
	0.100	0.099	-0.025	-0.045
	0.095	0.104	-0.020	-0.055
	0.095	0.095	-0.010	-0.050
	0.080	0.094	0.000	-0.035
0.080	0.175	-0.025	-0.040	
0.090	0.205	-0.030	-0.045	
0.100	0.170	-0.015	-0.045	
0.115	0.230	-0.005	-0.045	
0.120	0.200	0.000	-0.040	

Table A1  
Continued

Coating or Package	Flux			
	Alpha 611	Kester 1544	Pure Rosin	No Flux
Eccosil	0.075	0.115	-0.005	0.025
	0.075	0.134	-0.010	0.020
	0.100	0.149	-0.005	0.025
	0.095	0.229	0.005	0.015
	0.115	0.060	0.000	0.020
	0.100	0.085	0.000	0.010
	0.110	0.120	-0.005	0.015
	0.114	0.120	0.000	0.025
	0.105	0.100	0.005	0.020
	0.095	0.085	-0.010	0.020
	0.080	0.140	0.005	0.020
	0.090	0.209	0.005	0.020
	0.100	0.179	0.010	0.015
	0.085	0.125	0.025	0.025
	0.095	0.164	0.025	0.010
	0.125	0.135	0.010	0.015
	0.105	0.230	0.015	0.025
	0.119	0.180	0.015	0.015
	0.110	0.210	0.005	0.030
	0.100	0.270	0.005	0.005
0.095	0.285	0.010	0.010	
0.110	0.243	0.015	0.020	
0.130	0.214	0.005	0.020	
0.100	0.144	0.000	0.020	
0.130	0.114	0.005	0.020	
Hermetically Sealed	0.040	-0.010	-0.125	-0.150
	0.030	0.005	-0.144	-0.130
	0.025	0.050	-0.149	-0.114
	0.125	0.020	-0.154	-0.179
	-0.005	-0.010	-0.164	-0.189
	0.005	0.030	-0.120	-0.140
	-0.005	0.030	-0.150	-0.170
	-0.015	0.080	-0.150	-0.010
	-0.015	0.005	-0.145	-0.170
	-0.020	-0.045	-0.150	-0.179
	-0.015	0.290	-0.120	-0.150
	-0.035	0.280	-0.144	-0.150
	-0.020	0.329	-0.149	-0.149
	-0.030	0.310	-0.149	-0.150
	-0.030	0.331	-0.164	-0.149
	0.035	0.105	-0.120	-0.150
	-0.005	0.140	-0.085	-0.150
	0.015	0.080	-0.155	-0.149
	0.020	-0.035	-0.135	-0.149
	-0.010	0.010	-0.145	-0.149
0.015	0.095	-0.095	-0.145	
0.020	0.190	-0.055	-0.150	
0.040	0.150	-0.134	-0.150	
0.040	0.170	-0.109	-0.130	
0.035	0.190	-0.134	-0.150	

Table A2  
Birox Resistors

Percentage Changes of Individual Resistors after 11 days at 150°C

Coating or Package	Flux				
	Alpha 611	Kester 1544	Pure Rosin	No Flux	
Sylgard 182	-0.20576	-0.09485	-0.23486	-0.20521	
	-0.22599	-0.06969	-0.26917	-0.26538	
	-0.24052	-0.10943	-0.27384	-0.25516	
	-0.26074	-0.11936	-0.33697	-0.29531	
	-0.21597	-0.10442	-0.31298	-0.28032	
	-0.18039	-0.15477	-0.25495	-0.16022	
	-0.22058	-0.13487	-0.3148	-0.1939	
	-0.22464	-0.12988	-0.31963	-0.19331	
	-0.22451	-0.12981	-0.30445	-0.1693	
	-0.23036	-0.15978	-0.32962	-0.17433	
	-0.2404	-0.05002	-0.28472	-0.24504	
	-0.26053	-0.07459	-0.27873	-0.27544	
	-0.25074	-0.1742	-0.3083	-0.27506	
	-0.27113	-0.20899	-0.33299	-0.24531	
	-0.24078	-0.20883	-0.33723	-0.19538	
	-0.16067	-0.10503	-0.27455	-0.19508	
	-0.21028	-0.12473	-0.30479	-0.22452	
	-0.215	-0.18486	-0.35461	0.2698	
	-0.24044	-0.14507	-0.32954	-0.22374	
	-0.24505	-0.14006	-0.28988	-0.17925	
	-0.21035	9.99E-03	-0.22518	-0.26999	
	-0.24613	9.96E-03	-0.28872	-0.24999	
	-0.25554	0	-0.23872	-0.28001	
	-0.24581	-0.06964	-0.28362	-0.28027	
	-0.22586	-0.08945	-0.26381	-0.2851	
	GE 511	-0.22067	-0.10505	-0.27485	-0.22528
		-0.26049	-0.13992	-0.25499	-0.26427
		-0.26469	-0.13988	-0.26958	-0.25858
-0.26541		-0.14995	-0.3197	-0.26838	
-0.28494		-0.15517	-0.26499	-0.24417	
-0.24106		-0.10493	-0.23018	-0.26528	
-0.27113		-0.06479	-0.25403	-0.30912	
-0.28574		-0.15294	-0.27877	-0.31403	
-0.28034		-0.17935	-0.29363	-0.34887	
-0.29044		-0.19874	-0.29852	-0.31414	
-0.21546		-0.12002	-0.21992	-0.28534	
-0.22995		-0.11987	-0.32193	-0.30906	
-0.26464		-0.08992	-0.30282	-0.33343	
-0.30949		-0.07496	-0.26372	-0.31418	
-0.28452		-0.11498	-0.2585	-0.30412	
-0.26606		-0.08493	-0.26475	-0.25513	
-0.28127		-0.0995	-0.29468	-0.26402	
-0.29963		-0.13455	-0.28958	-0.32264	
-0.29616		-0.15463	-0.29001	-0.3431	
-0.26606		-0.17879	-0.24001	-0.33801	
-0.20541		-0.08994	-0.24499	-0.28999	
-0.23499		-0.08996	-0.25904	-0.26997	
-0.27027		-0.10496	-0.23892	-0.32987	
-0.27455		-0.06498	-0.27827	-0.31502	
-0.26501		0	-0.26366	-0.3347	

Table A2  
Continued

Coating or Package	Flux			
	Alpha 611	Kester 1544	Pure Rosin	No Flux
Stycast 2850GT	1.65699	1.32447	1.7507	1.23907
	2.06665	1.65655	2.06417	1.52398
	2.09084	1.91371	2.03459	1.6121
	2.09159	1.98626	1.9902	1.5862
	1.96639	2.1358	2.06583	1.25921
	1.42907	1.44522	1.62187	1.44551
	1.73364	1.9893	1.96646	1.29735
	1.9107	2.11152	2.0001	1.24378
	2.10579	1.97125	2.16612	0.74534
	1.872	2.06993	2.23981	1.31848
	1.77838	1.63386	1.78366	1.16547
	1.95215	2.21582	2.08167	1.59521
	2.10437	2.34949	2.13521	1.42928
	2.08438	2.16558	2.14075	0.97284
	1.84357	1.81038	2.16105	0.9853
	1.90276	1.45971	1.43752	1.29513
	2.36967	1.67715	1.84306	1.54106
	2.22	1.7158	1.69997	2.74764
	2.44426	1.7719	1.90476	1.77941
	2.69813	1.62756	1.8054	1.86934
	1.74183	1.05894	1.33213	1.25494
	2.35606	1.68556	1.60388	1.47506
	2.27966	1.73468	2.02835	1.87919
	2.18196	1.89486	2.09209	1.65075
2.26362	1.78251	2.13917	1.85342	
BA7236	-0.22519	-0.15498	-0.16531	-0.31014
	-0.24688	-0.15997	-0.20954	-0.38926
	-0.29404	-0.14938	-0.21471	-0.36927
	-0.29879	-0.13499	-0.21918	-0.36919
	-0.2638	-0.11491	-0.20932	-0.30428
	-0.18504	-0.12483	-0.22054	-0.33515
	-0.2094	-0.11962	-0.2857	-0.38419
	-0.23946	-0.13442	-0.27555	-0.41866
	-0.23406	-0.12434	-0.28587	-0.41415
	-0.19434	-0.164	-0.22066	-0.35925
	-0.24511	-0.10438	-0.2448	-0.32061
	-0.2501	-0.15504	-0.28412	-0.35944
	-0.23516	-0.12001	-0.28864	-0.36886
	-0.2449	-0.14489	-0.2589	-0.37399
	-0.21016	-0.09502	-0.28851	-0.3391
	-0.19016	-0.13487	-0.31489	-0.28573
	-0.16961	-0.15395	-0.37015	-0.33963
	-0.16977	-0.14415	-0.34436	-0.36926
	-0.21951	-0.1692	-0.31222	-0.3986
	-0.19858	-0.15406	-0.28066	-0.35926
	-0.19008	-0.04495	-0.25537	-0.3305
	-0.30018	-0.03999	-0.3388	-0.37373
	-0.21497	-0.08002	-0.31375	-0.37638
	-0.30992	-0.03498	-0.35304	-0.42867
-0.30535	0	-0.33826	-0.36398	

Table A2  
Continued

Coating or Package	Flux			
	Alpha 611	Kester 1544	Pure Rosin	No Flux
Eccosil	-0.26023	-0.08013	-0.2255	-0.23032
	-0.30502	-0.08468	-0.30081	-0.26439
	-0.30535	-0.09456	-0.31073	-0.27415
	-0.28516	-0.02492	-0.28058	-0.31429
	-0.25994	-0.20881	-0.27587	-0.29912
	-0.21506	-0.14999	-0.27992	-0.22541
	-0.21945	-0.14984	-0.29399	-0.2496
	-0.25877	-0.13001	-0.31373	-0.28913
	-0.24394	-0.14996	-0.31819	-0.29936
	-0.20398	-0.16996	-0.32311	-0.309
	-0.25481	-0.10512	-0.23509	-0.24023
	-0.27994	-0.08463	-0.31017	-0.29946
	-0.26495	-0.10959	-0.29493	-0.32403
	-0.25465	-0.1744	-0.2602	-0.32916
	-0.21542	-0.13921	-0.26047	-0.31909
	-0.20997	-0.09505	-0.22011	-0.28036
	-0.27397	-0.05003	-0.23437	-0.29967
	-0.2984	-0.11487	-0.22382	-0.314
	-0.29872	-0.07503	-0.26381	-0.3341
	-0.34392	0.01	-0.2638	-0.3092
-0.15005	0.05996	-0.24012	-0.26554	
-0.21502	-0.06445	-0.28021	-0.30927	
-0.18965	-0.03481	-0.27504	-0.29924	
-0.20024	-0.1143	-0.31002	-0.31906	
-0.16512	-0.14417	-0.25013	-0.30929	
Hermetically Sealed	0.10995	-0.02496	-0.04508	-0.18023
	0.08974	0	-0.0597	-0.22451
	0.07962	0.01995	-0.06961	-0.22401
	0.05977	-0.01497	-0.06952	-0.22925
	0.0648	-0.04503	-0.06958	-0.23925
	0.07006	0.09992	0.16029	-0.20017
	0.05988	0.07968	0.11509	-0.24441
	0.0448	0.15936	0.14499	-0.25447
	4.96E-03	0.03991	0.1804	-0.25944
	0.04981	-4.98E-03	0.21029	-0.26413
	0.04502	0.01498	-0.09006	-0.2301
	0.02001	-4.99E-03	-0.03973	-0.23992
	0.04994	0.06982	-0.05433	-0.23917
	0.01001	0.02497	-0.0747	-0.25419
	0.04501	0.08012	-0.06972	-0.2789
	0.11996	0.23022	-0.04499	-0.22019
	0.07978	0.25951	-0.055	-0.24436
	9.94E-03	0.19401	-0.05503	-0.22422
	0	0.0647	-0.06999	-0.24376
	0.08958	0.12955	-0.08008	-0.24882
0.05003	0.12004	0.20536	-0.2205	
0.07003	0.26487	0.22372	-0.22958	
0.10999	0.20477	0.21893	-0.23455	
0.12497	0.22014	0.22365	-0.25962	
0.11495	0.23487	0.2088	-0.22473	

Table A3  
Birox Resistors

MP 51,978  
Page 29

Percentage Changes of Individual Resistors After 11 Days at 150°C +9 Days at 100°C

Coating or Package	Flux			
	Alpha 611	Kester 1544	Pure Rosin	No Flux
Sylgard 182	-0.19071	-0.10464	-0.21767	-0.19071
	-0.21595	-0.07965	-0.23427	-0.25036
	-0.22047	-0.05969	-0.25689	-0.24017
	-0.25071	-0.06952	-0.31715	-0.27020
	-0.18584	-0.07458	-0.30305	-0.25073
	-0.17536	-0.15976	-0.24995	-0.13519
	-0.2256	-0.11988	-0.29481	-0.16097
	-0.23484	-0.11989	-0.28967	-0.15930
	-0.20954	-0.11483	-0.28449	-0.15436
	-0.22534	-0.11484	-0.29966	-0.13946
	-0.22036	-0.03001	-0.23976	-0.20030
	-0.25552	-0.08453	-0.25682	-0.21534
	-0.25575	-0.14931	-0.29339	-0.23575
	-0.27113	-0.17416	-0.2982	-0.22020
	-0.23577	-0.179	-0.32236	-0.15506
	-0.15063	-0.10503	-0.27455	-0.17507
	-0.18525	-0.14968	-0.29479	-0.20430
	-0.215	-0.15988	-0.32464	-0.17400
	-0.23043	-0.09504	-0.32455	-0.20632
	-0.20504	-0.10504	-0.05611	-0.17487
	-0.14532	0.03497	-0.21017	-0.24990
	-0.22604	0.02986	-0.24391	-0.23993
	-0.23549	0.05468	-0.25862	-0.27001
	-0.23578	-0.04477	-0.25377	-0.26525
	-0.20578	-0.06945	-0.23892	-0.26039
	GE 511	-0.1956	-0.07504	-0.24467
-0.23545		-0.13992	-0.25999	-0.23934
-0.23474		-0.13489	-0.26958	-0.23869
-0.24037		-0.08997	-0.28972	-0.24355
-0.24995		-0.0951	-0.22999	-0.20431
-0.21595		-0.09494	-0.21017	-0.24025
-0.22092		-0.03489	-0.24905	-0.26425
-0.24564		-0.13907	-0.26384	-0.27913
-0.23528		-0.15444	-0.26875	-0.30401
-0.25038		-0.16893	-0.27365	-0.28422
-0.21045		-0.11002	-0.21492	-0.2563
-0.20496		-0.10988	-0.29716	-0.27915
-0.24467		-0.09491	-0.26807	-0.28364
-0.26956		-0.07496	-0.25377	-0.33413
-0.25956		-0.09499	-0.2237	-0.28916
-0.23092		-0.05995	-0.25476	-0.23012
-0.25113		-0.08457	-0.26469	-0.19926
-0.26512		-0.12957	-0.25962	-0.31768
-0.26604		-0.12969	-0.27001	-0.31326
-0.23594		-0.14899	-0.22001	-0.2883
-0.17535		-0.06494	-0.21999	-0.24900
-0.21499		-0.05997	-0.22915	-0.25997
-0.22022		-0.06998	-0.23892	-0.30980
-0.21465		-0.03999	-0.24846	-0.31002
-0.22001		0.02996	-0.23878	-0.28471

Table A3  
Continued

Coating or Package	Flux				
	Alpha 611	Kester 1544	Pure Rosin	No Flux	
Stycast 2850G7	1.72207	1.36945	1.79572	1.28404	
	2.13171	1.72122	2.12915	1.57378	
	2.16587	1.95347	2.10458	1.66683	
	2.16683	2.05098	2.06021	1.64587	
	2.0316	2.1954	2.13585	1.31893	
	1.50429	1.46522	1.67192	1.49052	
	1.83886	2.05928	2.02635	1.34705	
	2.02045	2.17641	2.08489	1.28358	
	2.19561	2.0511	2.23085	0.75613	
	1.97185	2.14475	2.29954	1.37841	
	1.86354	1.67882	1.83877	1.20345	
	2.02222	2.28041	2.15673	1.66002	
	2.17935	2.43394	2.21022	1.45916	
	2.17457	2.2303	2.23576	1.04437	
	1.93399	1.87522	2.24128	1.03531	
	1.9979	1.4997	1.50263	1.30513	
	2.45443	1.767	1.91799	1.63551	
	2.33974	1.77066	1.95981	2.78746	
	2.52407	1.83679	1.95961	1.85307	
	2.77776	1.70245	1.89018	1.90912	
	1.60189	1.09391	1.39223	1.29994	
	2.42109	1.79992	1.65384	1.57971	
	2.39964	1.76947	2.09345	1.92891	
	2.29707	1.94957	2.14214	1.94006	
	2.35377	1.86218	2.19428	1.68323	
	HA7236	-0.19016	-0.16997	-0.17533	-0.30514
		-0.20906	-0.13497	-0.20954	-0.36427
		-0.27909	-0.07994	-0.20472	-0.35930
-0.29381		-0.12999	-0.19925	-0.39912	
-0.22896		-0.10492	-0.1246	-0.3392	
-0.17504		-0.11484	-0.19548	-0.33015	
-0.19943		-0.1246	-0.26064	-0.34927	
-0.23946		-0.10952	-0.24048	-0.38876	
-0.1992		-0.11439	-0.24575	-0.36924	
-0.17441		-0.13418	-0.19559	-0.34428	
-0.24011		-0.10988	-0.21982	-0.30558	
-0.22009		-0.13503	-0.2592	-0.33448	
-0.22516		-0.11001	-0.26376	-0.36387	
-0.21991		-0.134	-0.23898	-0.34906	
-0.17513		-0.07002	-0.24872	-0.30419	
-0.16514		-0.11988	-0.2949	-0.29074	
-0.13968		-0.12416	-0.32013	-0.34483	
-0.1498		-0.1193	-0.31941	-0.35429	
-0.20953		-0.13935	-0.29207	-0.36871	
-0.17949		-0.12424	-0.25059	-0.33431	
-0.20008		-0.02497	-0.23033	-0.30546	
-0.27517		-0.015	-0.28399	-0.2641	
-0.16997		0.06001	-0.28386	-0.36393	
-0.27497		0.01999	-0.32321	-0.42369	
-0.25577		0.02503	-0.31339	-0.32908	

Table A3  
Continued

Coating or Package	Flux				
	Alpha 611	Kester 1544	Pure Rosin	No Flux	
Eccosil	-0.24522	-0.06511	-0.22049	-0.23555	
	-0.27001	-0.06974	-0.28076	-0.2594	
	-0.26531	-0.07465	-0.29569	-0.23427	
	-0.24513	-9.97E-03	-0.26053	-0.26441	
	-0.22494	-0.17898	-0.23574	-0.25924	
	-0.25008	-0.14999	-0.25992	-0.16533	
	-0.24936	-0.10988	-0.289	-0.20966	
	-0.24682	-0.065	-0.29331	-0.24925	
	-0.24892	-0.12496	-0.28836	-0.27441	
	-0.24936	-0.13997	-0.3082	-0.26913	
	-0.20984	-0.0901	-0.23509	-0.22021	
	-0.25495	0.02489	-0.26015	-0.26948	
	-0.24995	-0.05488	-0.26993	-0.30907	
	-0.22986	-0.15945	-0.24018	-0.28926	
	-0.17033	-0.10938	-0.23542	-0.29416	
	-0.19497	-0.07004	-0.2051	-0.25534	
	-0.2142	-0.01501	-0.22938	-0.15982	
	-0.27851	-0.09969	-0.21885	-0.26415	
	-0.28378	-0.04003	-0.24656	-0.29919	
	-0.31401	0.04001	-0.23891	-0.27426	
	-0.16503	0.06494	-0.22511	-0.23047	
	-0.20002	-0.02479	-0.24515	-0.28433	
	-0.15471	-0.01492	-0.27504	-0.2743	
	-0.18022	-0.08448	-0.26501	-0.27419	
	-0.14511	-0.11434	-0.23512	-0.2594	
	Hermetically Sealed	0.12994	0.14975	-0.06011	-0.17021
		0.10968	0.17469	-0.04975	-0.19457
0.11446		0.19952	-0.05463	-0.2041	
0.11456		0.1647	-0.07946	-0.26414	
0.07975		0.14009	-0.07455	-0.22928	
0.05504		0.2498	-0.03005	-0.20517	
0.09462		0.27887	-0.04503	-0.23444	
0.07964		0.45817	-0.045	-0.24449	
0.04467		0.33925	-0.0451	-0.24447	
0.07472		0.26385	-0.03004	-0.25416	
0.08004		0.02996	-0.03002	-0.2201	
0.04002		0.02497	0	-0.25491	
0.09488		0.08977	-4.97E-03	-0.24914	
0.04502		0.04494	-0.01992	-0.24422	
0.07502		0.06513	-0.01992	-0.8616	
0.16995		0.2102	-0.025	-0.20517	
0.09973		0.2645	-0.01	-0.12468	
0.09945		0.19401	-0.02001	-0.20429	
0.04981		0.05474	-0.03	-0.23381	
0.07465		0.12456	-0.02502	-0.24384	
0.13005		0.13005	0.25935	-0.20546	
0.20506		0.27456	0.24653	-0.18965	
0.22499		0.21476	0.22865	-0.22457	
0.20495		0.23015	0.24353	-0.25962	
0.21491		0.26485	0.22371	-0.21974	

Table Aa

Birox Resistors

Percentage Changes of Individual Resistors After 11 Days at 150°C  
+17 Days at 100°C + 11 Days at 125°C

Coating or Package	Flux			
	Alpha 611	Kester 1544	Pure Rosin	No Flux
Sylgard 182	-0.206	-0.065	-0.215	-0.195
	-0.221	-0.055	-0.249	-0.255
	-0.236	-0.075	-0.269	-0.250
	-0.261	-0.094	-0.332	-0.290
	-0.211	-0.094	-0.313	-0.270
	-0.185	-0.130	-0.260	-0.125
	-0.236	-0.125	-0.305	-0.174
	-0.245	-0.130	-0.305	-0.164
	-0.239	-0.140	-0.304	-0.169
	-0.240	-0.135	-0.315	-0.149
	-0.235	-0.035	-0.255	-0.205
	-0.266	-0.104	-0.269	-0.220
	-0.266	-0.164	-0.303	-0.240
	-0.281	-0.199	-0.313	-0.240
	-0.256	-0.194	-0.337	-0.185
	-0.161	-0.095	-0.265	-0.175
	-0.215	-0.130	-0.305	-0.220
	-0.225	-0.175	-0.325	-0.184
	-0.245	-0.135	-0.320	-0.214
	-0.250	-0.135	<del>-0.168</del>	-0.189
	-0.200	0.035	-0.215	-0.250
	-0.236	0.045	-0.259	-0.240
	-0.256	0.020	-0.269	-0.275
-0.241	-0.050	-0.269	-0.270	
-0.221	-0.080	-0.264	-0.290	
OE 511	-0.196	-0.105	-0.245	-0.205
	-0.245	-0.130	-0.265	-0.249
	-0.265	-0.135	-0.285	-0.259
	-0.255	-0.125	-0.300	-0.268
	-0.265	-0.125	-0.250	-0.234
	-0.236	-0.075	-0.210	-0.240
	-0.256	-0.050	-0.249	-0.274
	-0.266	-0.134	-0.269	-0.290
	-0.270	-0.164	-0.284	-0.334
	-0.275	-0.184	-0.299	-0.299
	-0.200	-0.110	-0.230	-0.260
	-0.215	-0.115	-0.312	-0.289
	-0.255	-0.095	-0.283	-0.314
	-0.295	-0.090	-0.269	-0.309
	-0.275	-0.105	-0.249	-0.294
	-0.236	-0.055	-0.255	-0.235
	-0.271	-0.085	-0.290	-0.249
	-0.285	-0.130	-0.275	-0.298
	-0.286	-0.150	-0.285	-0.288
	-0.246	-0.169	-0.240	-0.313
	-0.195	-0.075	-0.220	-0.255
	-0.230	-0.070	-0.234	-0.290
	-0.255	-0.075	-0.249	-0.325
-0.260	-0.055	-0.263	-0.320	
-0.255	0.015	-0.254	-0.305	

Table A4  
Continued

Coating or Package	Flux			
	Alpha 611	Kester 1544	Pure Rosin	No Flux
Stycast 2850GT	1.767	1.394	1.841	1.334
	2.207	1.761	2.179	1.624
	2.231	2.008	2.150	1.722
	2.222	2.106	2.105	1.686
	2.087	2.240	2.181	1.329
	1.524	1.545	1.737	1.556
	1.874	2.134	2.101	1.342
	2.055	2.256	2.165	1.313
	2.250	2.101	2.316	0.745
	2.017	2.210	2.384	1.383
	1.914	1.719	1.914	1.235
	2.092	2.355	2.227	1.700
	2.259	2.508	2.280	1.519
	2.240	2.295	2.306	0.992
	1.969	1.925	2.316	1.235
	2.023	1.555	1.533	1.365
	2.529	1.782	1.978	1.650
	2.345	1.806	2.010	2.832
	2.569	1.872	2.009	1.884
	2.647	1.727	1.920	1.994
1.872	1.119	1.417	1.340	
2.511	1.800	1.669	1.575	
2.425	1.849	2.118	2.008	
2.317	2.019	2.202	1.985	
2.414	1.917	2.234	1.983	
RA7236	-0.185	-0.165	-0.160	-0.300
	-0.224	-0.150	-0.205	-0.364
	-0.269	-0.140	-0.200	-0.379
	-0.274	-0.125	-0.209	-0.389
	-0.229	-0.105	-0.204	-0.319
	-0.160	-0.125	-0.190	-0.325
	-0.189	-0.125	-0.271	-0.379
	-0.234	-0.115	-0.261	-0.399
	-0.209	-0.114	-0.261	-0.404
	-0.189	-0.154	-0.221	-0.344
	-0.225	-0.105	-0.230	-0.296
	-0.220	-0.145	-0.269	-0.334
	-0.210	-0.120	-0.274	-0.354
	-0.230	-0.145	-0.254	-0.359
	-0.185	-0.070	-0.269	-0.304
	-0.175	-0.110	-0.290	-0.256
	-0.150	-0.109	-0.330	-0.320
	-0.160	-0.020	-0.334	-0.364
	-0.215	-0.154	-0.297	-0.374
	-0.194	-0.139	-0.266	-0.349
-0.180	-0.025	-0.235	-0.310	
-0.305	-0.025	-0.299	-0.364	
-0.195	-0.040	-0.309	-0.364	
-0.325	-0.010	-0.343	-0.409	
-0.280	0.010	-0.328	-0.339	

Table A4  
Continued

Coating or Package	Flux			
	Alpha 611	Kester 1544	Pure Rosin	No Flux
Eccos11	0.180	-0.065	-0.225	-0.220
	-0.290	-0.075	-0.296	-0.254
	-0.280	-0.095	-0.311	-0.259
	-0.265	-0.030	-0.276	-0.284
	-0.250	-0.204	-0.261	-0.264
	-0.205	-0.135	-0.265	-0.210
	-0.209	-0.120	-0.299	-0.215
	-0.244	-0.115	-0.294	-0.249
	-0.229	-0.145	-0.303	-0.279
	-0.190	-0.150	-0.308	-0.289
	-0.729	-0.085	-0.245	-0.220
	-0.255	-0.080	-0.295	-0.279
	-0.265	-0.100	-0.290	-0.299
	-0.265	-0.169	-0.255	-0.314
	-0.205	-0.119	-0.255	-0.289
	-0.260	-0.075	-0.210	-0.255
	-0.249	-0.020	-0.224	-0.265
	-0.283	-0.105	-0.224	-0.294
	-0.299	-0.075	-0.254	-0.314
	-0.329	0.025	-0.259	-0.309
-0.130	0.080	-0.230	-0.235	
-0.205	-0.035	-0.265	-0.274	
-0.185	-0.030	-0.290	-0.274	
-0.195	-0.099	-0.305	-0.299	
-0.155	-0.129	-0.260	-0.289	
Hermetically Scaled	0.120	0.010	-0.055	-0.180
	0.100	0.020	-0.065	-0.220
	0.100	0.040	-0.070	-0.219
	0.085	0.005	-0.079	-0.224
	0.080	-0.025	-0.084	-0.224
	0.155	0.105	-0.050	-0.190
	0.145	0.080	-0.055	-0.234
	0.144	0.147	-0.050	-0.244
	0.109	0.050	-0.060	-0.244
	0.134	0.010	-0.045	-0.249
	0.135	0.020	0.070	-0.230
	0.130	0.000	0.109	-0.250
	0.185	0.070	0.119	-0.254
	0.125	0.030	0.090	-0.269
	0.160	0.070	0.105	-0.294
	0.200	0.190	0.055	-0.230
	0.145	0.225	0.090	-0.244
	0.179	0.169	0.095	-0.244
	0.159	0.025	0.080	-0.244
	0.164	0.105	0.095	-0.259
0.165	0.120	0.220	-0.231	
0.245	0.250	0.278	-0.235	
0.265	0.200	0.279	-0.245	
0.280	0.210	0.283	-0.275	
0.295	0.245	0.249	-0.245	

Table A5

MP 51,978

Page 35

## Birox Resistors

Percentage Changes for Individual Resistors After 11 Days at  
150°C + 17 Days at 100°C + 76 Days at 125°C

Coating or Package	Flux			
	Alpha 611	Kester 1544	Pure Rosin	No Flux
Sylgard 162	-0.221	-0.075	-0.240	-0.221
	-0.984	-0.060	-0.244	-0.255
	-0.246	-0.065	-0.269	-0.250
	-0.276	-0.090	-0.337	-0.230
	-0.221	0.030	-0.318	-0.270
	-0.200	-0.150	-0.270	-0.150
	-0.236	-0.130	-0.305	-0.169
	-0.255	-0.125	-0.315	-0.174
	-0.244	-0.135	-0.304	-0.174
	-0.245	-0.130	-0.325	-0.159
	-0.245	-0.045	-0.270	-0.205
	-0.261	-0.109	-0.269	-0.225
	-0.261	-0.169	-0.313	-0.245
	-0.291	-0.199	-0.333	-0.249
	-0.261	-0.194	-0.347	-0.290
	-0.176	-0.120	-0.285	-0.185
	-0.215	-0.140	-0.305	-0.210
	-0.240	-0.180	-0.335	-0.174
	-0.255	-0.145	-0.335	-0.209
	-0.260	-0.140	<del>-0.376</del>	-0.169
-0.200	0.025	-0.220	-0.260	
-0.236	0.045	-0.234	-0.235	
-0.256	0.020	-0.254	-0.270	
-0.251	-0.060	-0.259	-0.260	
-0.231	-0.075	-0.249	-0.260	
GE 511	-0.236	-0.125	-0.260	-0.235
	-0.245	-0.135	-0.265	-0.244
	-0.255	-0.120	-0.290	-0.249
	-0.255	-0.115	-0.305	-0.260
	-0.260	-0.110	-0.245	-0.214
	-0.231	-0.090	-0.225	-0.265
	-0.231	-0.045	-0.264	-0.264
	-0.251	-0.139	-0.284	-0.299
	-0.250	-0.169	-0.284	-0.320
	-0.255	-0.179	-0.303	-0.289
	-0.195	-0.120	-0.235	-0.270
	-0.205	-0.110	-0.297	-0.274
	-0.255	-0.095	-0.278	-0.304
	-0.295	-0.080	-0.274	-0.294
	-0.280	-0.100	-0.239	-0.279
	-0.246	-0.080	-0.255	-0.230
	-0.266	-0.090	-0.275	-0.229
	-0.290	-0.130	-0.270	-0.283
	-0.276	-0.200	-0.275	-0.274
	-0.251	-0.169	-0.230	-0.293
-0.180	-0.085	-0.235	-0.265	
-0.190	-0.055	-0.229	-0.285	
-0.220	-0.075	-0.249	-0.315	
-0.225	-0.055	-0.268	-0.310	
-0.225	-0.025	-0.259	-0.300	

Table A5  
Continued

Coating or Package	Flux			
	Alpha 611	Kester 1544	Pure Rosin	No Flux
Stycast 2850CT	2.944	1.539	2.066	1.539
	3.458	1.960	2.479	1.902
	3.466	2.277	2.400	2.305
	3.471	2.389	2.375	1.944
	3.326	2.533	2.481	1.533
	1.630	1.750	1.977	1.766
	2.074	2.419	2.406	1.456
	2.320	2.571	2.469	1.473
	2.540	2.405	2.654	0.788
	2.306	2.524	2.733	1.573
	2.164	1.874	2.189	1.391
	2.403	2.663	2.572	2.014
	2.569	2.826	2.630	1.763
	2.560	2.614	2.641	1.106
	2.215	2.189	2.642	1.150
	2.308	1.730	1.688	1.535
	2.923	2.002	2.243	1.924
	2.609	2.020	2.289	3.131
	2.868	2.091	2.299	2.187
	3.021	1.920	2.105	2.332
2.127	1.199	1.532	1.510	
2.856	2.034	1.784	1.834	
2.655	2.078	2.319	2.322	
2.547	2.288	2.442	2.307	
2.749	2.171	2.490	2.266	
HATC36	-0.190	-0.170	-0.175	-0.305
	-0.214	-0.135	-0.195	-0.354
	-0.269	-0.135	-0.210	-0.354
	-0.279	-0.120	-0.209	-0.359
	-0.229	-0.095	-0.209	-0.294
	-0.175	-0.130	-0.206	-0.335
	-0.179	-0.115	-0.256	-0.364
	-0.220	-0.110	-0.251	-0.399
	-0.199	-0.099	-0.251	-0.384
	-0.184	-0.129	-0.211	-0.334
	-0.240	-0.115	-0.245	-0.291
	-0.220	-0.125	-0.269	-0.310
	-0.205	-0.095	-0.279	-0.334
	-0.225	-0.125	-0.254	-0.344
	-0.190	-0.035	-0.259	-0.314
	-0.155	-0.115	-0.290	-0.256
	-0.130	-0.124	-0.310	-0.300
	-0.140	-0.114	-0.324	-0.339
	-0.195	-0.134	-0.297	-0.354
	-0.184	-0.124	-0.261	-0.324
-0.185	-0.030	-0.240	-0.305	
-0.255	-0.010	-0.284	-0.329	
-0.135	-0.035	-0.289	-0.334	
-0.260	-0.050	-0.328	-0.379	
-0.275	0.015	-0.323	-0.329	

Table A5  
Continued

Coating or Package	Flux			
	Alpha 611	Kester 144	Pure Rosin	No Flux
Eccosil	-0.255	-0.080	-0.251	-0.225
	-0.275	-0.075	-0.321	-0.239
	-0.289	-0.090	-0.316	-0.309
	-0.265	-0.025	-0.286	-0.279
	-0.240	-0.194	-0.261	-0.264
	-0.220	-0.159	-0.280	-0.220
	-0.249	-0.125	-0.289	-0.210
	-0.239	-0.130	-0.199	-0.254
	-0.219	-0.160	-0.133	-0.274
	-0.180	-0.160	-0.323	-0.234
	-0.240	-0.110	-0.255	-0.237
	-0.255	-0.075	-0.275	-0.265
	-0.260	-0.110	-0.285	-0.234
	-0.260	-0.179	-0.260	-0.294
	-0.210	-0.114	-0.250	-0.229
	-0.215	-0.095	-0.225	-0.265
	-0.244	-0.010	-0.229	-0.255
	-0.283	-0.105	-0.229	-0.274
	-0.289	-0.075	-0.259	-0.299
	-0.324	0.025	-0.244	-0.239
	-0.150	0.065	-0.225	-0.135
	-0.200	-0.035	-0.255	-0.264
	-0.190	-0.025	-0.285	-0.264
	-0.200	-0.084	-0.300	-0.224
	-0.155	-0.124	-0.250	-0.274
	Hermetically Sealed	0.215	0.025	0.035
0.199		0.060	0.065	-0.201
0.169		0.080	0.065	-0.229
0.169		0.040	0.045	-0.239
0.179		-0.010	0.030	-0.234
0.520		0.110	0.140	-0.215
0.574		0.095	0.220	-0.244
0.577		0.159	0.230	-0.259
0.561		0.060	0.215	-0.259
0.533		0.000	0.250	-0.269
0.400		0.020	0.440	-0.250
0.455		-0.040	0.586	-0.240
0.574		0.085	0.616	-0.254
0.470		0.035	0.543	-0.269
0.545		0.055	0.558	-0.299
0.515		0.210	0.400	-0.225
0.558		0.260	0.525	-0.239
0.572		0.189	0.600	-0.234
0.553		0.055	0.530	-0.249
0.542		0.105	0.541	-0.249
0.460	0.140	0.381	-0.236	
0.620	0.300	0.487	-0.240	
0.625	0.230	0.478	-0.255	
0.655	0.235	0.482	-0.275	
0.685	0.255	0.413	-0.275	

Table A6  
8000 Series Resistors

Percentage Changes of Individual Resistors After Coating (Before Aging)

Coating or Package	Flux			
	Alpha 511	Kester 1544	Pure Rosin	No Flux
Sylgard 182	-0.015	0.198	0.052	0.055
	0.005	0.030	0.092	0.131
	0.010	0.045	0.044	0.095
	0.005	0.174	0.060	0.106
	0.000	0.069	0.044	0.100
	0.074	-0.326	0.032	0.005
	0.050	0.213	0.040	0.045
	0.243	0.228	0.024	0.065
	0.050	0.109	0.064	0.030
	0.050	0.397	0.076	0.045
	0.005	0.010	0.032	0.075
	0.010	0.079	0.080	0.175
	0.015	0.213	0.052	0.115
	0.015	0.094	0.052	0.080
	0.015	0.163	0.048	0.075
	0.005	0.104	0.025	0.050
	0.015	0.025	0.045	0.176
	0.015	0.361	0.089	0.121
0.025	-0.020	0.020	0.080	
0.025	-0.143	0.020	0.120	
GE 511	0.005	0.605	0.028	0.065
	0.020	0.035	0.044	0.120
	0.010	0.104	0.024	0.090
	0.010	0.119	0.044	0.120
	0.010	0.000	0.044	0.105
	0.000	0.000	0.040	0.060
	0.015	0.025	0.064	0.095
	0.015	0.223	0.036	0.095
	0.010	0.208	0.060	0.075
	0.010	-0.010	0.080	0.090
	0.005	0.357	0.028	0.065
	0.000	-0.059	0.088	0.136
	0.005	0.277	0.036	0.111
	0.005	0.293	0.056	0.100
	0.005	-0.050	0.064	0.125
	0.000	0.772	0.024	0.065
	0.010	-0.406	0.080	0.140
	0.010	0.079	0.052	0.125
0.010	0.352	0.056	0.105	
0.010	0.178	0.108	0.180	

Table A6  
Continued

Coating or Package	Flux			
	Alpha 611	Kester 1544	Pure Rosin	No Flux
Stycast 2850GT	-0.005	0.104	0.032	0.070
	0.005	0.010	0.044	0.245
	0.010	0.218	0.044	0.130
	0.010	0.139	0.048	0.150
	0.005	-0.010	0.064	0.170
	-0.005	0.178	0.060	0.050
	0.000	0.148	0.084	0.095
	0.000	0.178	0.028	0.130
	0.010	0.139	0.076	0.080
	0.005	0.134	0.092	0.101
	0.000	0.128	0.068	0.045
	0.010	0.247	0.056	0.121
	0.005	0.104	0.052	0.075
	0.005	0.148	0.060	0.080
	0.000	0.287	0.080	0.070
	0.005	0.045	0.032	0.060
	0.005	0.039	0.060	0.215
	0.005	0.070	0.076	0.130
0.005	0.074	0.060	0.130	
0.010	0.094	0.072	0.155	
RA7236	0.015	0.024	0.068	0.075
	0.020	0.060	0.076	0.155
	0.015	0.052	0.080	0.085
	0.010	0.060	0.076	0.145
	0.015	0.052	0.060	0.160
	0.010	0.032	0.096	0.030
	0.015	0.040	0.116	0.120
	0.010	0.068	0.116	0.120
	0.005	0.048	0.088	0.105
	0.020	0.056	0.148	0.125
	0.000	0.036	0.132	0.055
	0.010	0.072	0.124	0.115
	0.005	0.088	0.120	0.165
	0.010	0.060	0.151	0.095
	0.010	0.080	0.156	0.145
	0.005	0.044	0.135	0.045
	0.010	0.116	0.132	0.165
	0.015	0.132	0.128	0.180
0.010	0.084	0.124	0.110	
0.010	0.104	0.128	0.120	

Table A6  
Continued

Costing or Package	Flux			
	Alpha 611	Kester 1544	Pure Rosin	No Flux
Eccosil	0.010	0.036	0.092	0.055
	0.025	0.056	0.246	0.211
	0.020	0.076	0.112	0.176
	0.020	0.072	0.152	0.166
	0.030	0.080	0.302	0.236
	0.015	0.044	0.155	0.095
	0.020	0.084	0.124	0.240
	0.030	0.120	0.140	0.415
	0.025	0.084	0.112	0.382
	0.020	0.164	0.199	0.231
	0.025	0.040	0.120	0.135
	0.025	0.028	0.088	0.276
	0.015	0.056	0.112	0.366
	0.020	0.064	0.092	0.236
	0.030	0.080	0.128	0.201
	0.020	0.136	0.072	0.095
	0.015	0.044	0.080	0.201
0.025	0.032	0.072	0.231	
0.020	0.056	0.104	0.402	
0.020	0.064	0.239	0.221	
Hermetically Sealed	0.074	0.100	0.140	0.100
	0.079	0.092	0.164	0.211
	0.084	0.084	0.136	0.215
	0.094	0.096	0.184	0.191
	0.094	0.148	0.184	0.266
	0.065	0.068	0.140	0.100
	0.079	0.120	0.132	0.166
	0.074	0.108	0.156	0.166
	0.065	0.140	0.247	0.146
	0.089	0.208	0.283	0.241
	0.094	0.100	0.124	0.105
	0.069	0.104	0.208	0.186
	0.094	0.112	0.136	0.291
	0.069	0.116	0.168	0.171
	0.114	0.144	0.183	0.196
	0.074	0.100	0.120	0.145
	0.074	0.116	0.255	0.201
0.074	0.104	0.152	0.171	
0.069	0.124	0.192	0.151	
0.094	0.172	0.272	0.171	

Table A7  
8000 Series Resistors

Percentage Changes of Individual Resistors After 11 Days at 150°C

Coating or Package	Flux			
	Alpha 611	Kester 1544	Pure Rosin	No Flux
Sylgard 182	0.224	0.392	0.299	0.287
	0.233	0.297	0.332	0.341
	0.248	0.287	0.288	0.266
	0.253	0.292	0.304	0.332
	0.258	0.243	0.316	0.342
	0.333	0.370	0.292	0.242
	0.312	0.366	0.285	0.292
	0.526	0.371	0.273	0.272
	0.278	0.420	0.296	0.252
	0.327	0.372	0.320	0.302
	0.243	0.317	0.272	0.230
	0.253	0.480	0.304	0.336
	0.268	0.341	0.313	0.331
	0.243	0.371	0.297	0.291
	0.258	0.371	0.308	0.337
	0.243	0.262	0.266	0.246
	0.278	0.455	0.296	0.332
0.253	0.277	0.330	0.326	
0.273	0.321	0.261	0.312	
0.298	0.340	0.276	0.331	
GE 511	0.258	0.283	0.263	0.286
	0.243	0.248	0.292	0.336
	0.248	0.297	0.288	0.306
	0.273	0.327	0.288	0.321
	0.263	0.278	0.304	0.316
	0.278	0.302	0.296	0.256
	0.258	0.406	0.320	0.301
	0.253	0.366	0.292	0.291
	0.243	0.302	0.309	0.276
	0.263	0.471	0.344	0.297
	0.253	0.332	0.296	0.287
	0.243	0.426	0.332	0.351
	0.253	0.436	0.284	0.337
	0.243	0.322	0.292	0.301
	0.263	0.446	0.336	0.351
	0.253	0.344	0.224	0.292
	0.258	0.456	0.324	0.361
0.244	0.435	0.308	0.336	
0.238	0.411	0.296	0.306	
0.204	0.392	0.392	0.386	

Table A7  
Continued

Coating or Package	Flux			
	Alpha 611	Kester 1544	Pure Rosin	No Flux
Stycast 2850GT	0.442	0.639	0.521	0.920
	0.437	0.658	0.592	1.127
	0.452	0.639	0.536	0.918
	0.422	0.708	0.585	0.953
	0.398	0.816	0.609	0.917
	0.407	0.692	0.463	0.759
	0.417	0.795	0.543	0.733
	0.422	0.771	0.416	0.882
	0.437	0.743	0.600	0.713
	0.427	0.659	0.756	0.769
	0.288	0.702	0.408	0.743
	0.457	0.737	0.420	0.759
	0.412	0.634	0.520	0.638
	0.407	0.663	0.623	0.653
	0.378	0.703	0.696	0.613
	0.467	0.649	0.560	0.898
	0.447	0.786	0.596	1.007
0.507	0.696	0.863	0.838	
0.452	0.688	0.608	0.902	
0.422	0.672	0.641	0.973	
HA7236	0.243	0.357	0.351	0.374
	0.267	0.365	0.367	0.486
	0.258	0.377	0.384	0.331
	0.253	0.385	0.336	0.446
	0.273	0.393	0.356	0.509
	0.263	0.293	0.399	0.283
	0.263	0.301	0.411	0.401
	0.253	0.316	0.407	0.402
	0.243	0.269	0.372	0.391
	0.268	0.289	0.443	0.437
	0.248	0.297	0.148	0.391
	0.238	0.332	0.415	0.416
	0.228	0.340	0.419	0.496
	0.248	0.333	0.481	0.366
	0.258	0.357	0.451	0.426
	0.288	0.300	0.446	0.350
	0.238	0.360	0.486	0.491
0.278	0.432	0.431	0.550	
0.253	0.340	0.380	0.401	
0.239	0.361	0.443	0.441	

Table A7  
Continued

Coating or Package	Flux			
	Alpha 611	Kester 1544	Pure Rosin	No Flux
Eccosil	0.278	0.273	0.196	0.256
	0.278	0.293	0.512	0.422
	0.263	0.316	0.394	0.387
	0.273	0.312	0.359	0.377
	0.303	0.345	0.565	0.322
	0.263	0.289	0.411	0.346
	0.268	0.312	0.395	0.490
	0.268	0.352	0.407	0.641
	0.312	0.333	0.467	0.432
	0.273	0.401	0.514	0.411
	0.297	0.288	0.378	0.396
	0.273	0.261	0.356	0.506
	0.258	0.309	0.395	0.546
	0.248	0.301	0.355	0.437
	0.268	0.329	0.403	0.407
	0.273	0.401	0.332	0.381
	0.248	0.289	0.328	0.461
	0.263	0.285	0.332	0.437
	0.243	0.297	0.343	0.382
	0.278	0.289	0.423	0.447
Hermetically Sealed	0.471	0.361	0.607	0.476
	0.476	0.405	0.731	0.617
	0.457	0.377	0.608	0.626
	0.500	0.341	0.902	0.537
	0.551	0.433	0.648	0.707
	0.377	0.369	0.679	0.447
	0.422	0.473	0.779	0.627
	0.402	0.425	0.823	0.517
	0.367	0.445	1.035	0.527
	0.441	0.541	0.906	0.518
	0.416	0.369	0.623	0.482
	0.431	0.353	0.704	0.602
	0.437	0.417	0.576	0.742
	0.387	0.365	0.612	0.572
	0.511	0.457	0.608	0.553
	0.515	0.353	0.783	0.497
	0.472	0.381	0.918	0.652
	0.466	0.229	0.760	0.582
	0.422	0.132	0.759	0.547
	0.501	0.529	0.799	0.497

Table A8  
8000 Series Resistors

Percentage Changes of Individual Resistors After 11 Days at 150°C  
+ 9 Days at 100°C

Coating or Package	Flux			
	Alpha 611	Kester 1544	Pure Rosin	No Flux
Sylgard 182	0.209	0.407	0.299	0.282
	0.228	0.297	0.324	0.351
	0.243	0.292	0.268	0.291
	0.233	0.292	0.292	0.332
	0.244	0.248	0.292	0.331
	0.323	0.361	0.268	0.213
	0.308	0.366	0.269	0.257
	0.819	0.366	0.261	0.272
	0.288	0.406	0.280	0.262
	0.308	0.357	0.308	0.257
	0.238	0.322	0.256	0.295
	0.248	0.490	0.292	0.396
	0.258	0.327	0.293	0.336
	0.233	0.371	0.276	0.291
	0.253	0.371	0.288	0.312
	0.243	0.257	0.256	0.241
	0.258	0.450	0.286	0.337
0.248	0.277	0.330	0.311	
0.263	0.321	0.241	0.261	
0.278	0.331	0.246	0.396	
GE 511	0.238	0.283	0.264	0.266
	0.238	0.248	0.272	0.316
	0.243	0.288	0.280	0.286
	0.253	0.312	0.268	0.286
	0.253	0.268	0.280	0.296
	0.248	0.282	0.288	0.276
	0.248	0.401	0.304	0.316
	0.243	0.352	0.280	0.301
	0.228	0.278	0.296	0.286
	0.238	0.456	0.324	0.282
	0.229	0.332	0.260	0.297
	0.233	0.436	0.320	0.361
	0.229	0.431	0.272	0.347
	0.219	0.303	0.284	0.311
	0.244	0.436	0.312	0.351
	0.229	0.344	0.212	0.297
	0.233	0.466	0.324	0.366
0.234	0.406	0.296	0.331	
0.228	0.401	0.284	0.311	
0.204	0.401	0.356	0.401	

Table A8  
Continued

Coating or Package	Flux			
	Alpha 611	Kester 1544	Pure Rosin	No Flux
Stycast 2850GT	0.418	0.664	0.557	0.960
	0.427	0.663	0.640	1.167
	0.452	0.634	0.588	0.953
	0.407	0.718	0.637	0.983
	0.353	0.821	0.625	0.917
	0.392	0.717	0.579	0.805
	0.412	0.815	0.651	0.753
	0.412	0.786	0.512	0.907
	0.427	0.747	0.664	0.723
	0.407	0.673	0.808	0.734
	0.268	0.726	0.492	0.768
	0.437	0.752	0.532	0.774
	0.397	0.649	0.612	0.648
	0.407	0.683	0.668	0.668
	0.348	0.717	0.708	0.623
	0.467	0.659	0.612	0.968
	0.437	0.796	0.668	1.067
0.502	0.711	0.959	0.893	
0.447	0.688	0.680	0.917	
0.412	0.633	0.685	0.998	
HA7236	0.233	0.289	0.351	0.354
	0.272	0.296	0.367	0.461
	0.263	0.293	0.380	0.361
	0.253	0.297	0.332	0.441
	0.273	0.313	0.344	0.489
	0.238	0.309	0.383	0.293
	0.253	0.317	0.399	0.386
	0.233	0.328	0.383	0.407
	0.243	0.289	0.360	0.376
	0.258	0.305	0.411	0.442
	0.228	0.288	0.088	0.411
	0.233	0.324	0.391	0.401
	0.228	0.320	0.403	0.461
	0.243	0.308	0.462	0.361
	0.233	0.345	0.423	0.421
	0.278	0.284	0.450	0.345
	0.238	0.352	0.451	0.496
0.268	0.368	0.427	0.545	
0.248	0.332	0.340	0.436	
0.239	0.349	0.411	0.416	

Table A8  
Continued

Coating or Package	Flux			
	Alpha 611	Kester 1544	Pure Rosin	No Flux
Eccosil	0.253	0.261	0.180	0.256
	0.253	0.289	0.516	0.397
	0.253	0.312	0.394	0.417
	0.243	0.296	0.347	0.332
	0.273	0.321	0.569	0.297
	0.248	0.280	0.407	0.356
	0.248	0.300	0.387	0.495
	0.253	0.336	0.419	0.656
	0.283	0.313	0.451	0.517
	0.243	0.381	0.510	0.472
	0.283	0.268	0.375	0.401
	0.253	0.253	0.352	0.506
	0.243	0.296	0.387	0.566
	0.238	0.297	0.327	0.442
	0.253	0.321	0.379	0.417
	0.263	0.397	0.316	0.411
	0.238	0.277	0.328	0.481
	0.248	0.269	0.320	0.471
0.233	0.269	0.347	0.462	
0.268	0.285	0.403	0.462	
Hermetically Sealed	0.486	0.369	0.687	0.501
	0.501	0.413	0.871	0.622
	0.427	0.413	0.739	0.691
	0.505	0.349	1.025	0.602
	0.531	0.429	0.791	0.722
	0.432	0.393	0.803	0.472
	0.481	0.493	0.863	0.647
	0.461	0.437	0.895	0.522
	0.427	0.465	1.210	0.553
	0.501	0.573	1.014	0.508
	0.451	0.365	0.783	0.492
	0.476	0.365	0.780	0.617
	0.471	0.489	0.652	0.742
	0.417	0.357	0.692	0.577
	0.551	0.469	0.683	0.548
	0.520	0.353	0.891	0.507
	0.467	0.421	1.017	0.652
	0.481	0.409	0.892	0.572
0.432	0.377	0.975	0.562	
0.516	0.549	0.871	0.482	

Table A9

8000 Series Resistors

Percentage Changes of Individual Resistors After 11 Days at 150°C  
+ 17 Days at 100°C + 11 Days at 125°C

Coating or Package	Flux			
	Alpha 611	Kester 1544	Pure Rosin	No Flux
Sylgard 182	0.258	0.446	0.343	0.332
	0.273	0.317	0.364	0.387
	0.278	0.312	0.313	0.326
	0.288	0.327	0.324	0.367
	0.293	0.278	0.332	0.387
	0.367	0.390	0.320	0.277
	0.347	0.386	0.305	0.302
	1.270	0.396	0.289	0.312
	0.323	0.415	0.317	0.287
	0.337	0.382	0.352	0.332
	0.283	0.342	0.292	0.355
	0.283	0.510	0.328	0.421
	0.298	0.361	0.317	0.392
	0.268	0.381	0.321	0.332
	0.308	0.396	0.320	0.352
	0.283	0.292	0.301	0.321
	0.293	0.470	0.336	0.432
0.278	0.302	0.359	0.392	
0.298	0.351	0.256	0.337	
0.328	0.350	0.286	0.366	
GE 511	0.283	0.327	0.316	0.331
	0.273	0.277	0.308	0.381
	0.273	0.312	0.300	0.356
	0.288	0.337	0.316	0.366
	0.298	0.302	0.329	0.342
	0.303	0.322	0.328	0.316
	0.278	0.421	0.348	0.376
	0.278	0.366	0.316	0.342
	0.268	0.307	0.341	0.337
	0.288	0.485	0.372	0.347
	0.278	0.362	0.300	0.362
	0.278	0.451	0.364	0.402
	0.273	0.466	0.312	0.367
	0.273	0.322	0.316	0.352
	0.233	0.461	0.344	0.422
	0.283	0.374	0.249	0.297
	0.263	0.476	0.364	0.391
0.258	0.430	0.336	0.371	
0.273	0.436	0.328	0.346	
0.238	0.421	0.396	0.456	

Table A9  
Continued

Coating or Package	Flux			Wt %
	Alpha 611	Kester 1544	Pure Rosin	
Stycast 2850GT	0.442	0.694	0.617	1.
	0.452	0.703	0.680	1.
	0.487	0.669	0.624	3.
	0.447	0.748	0.665	1.
	0.398	0.856	0.681	3.
	0.442	0.771	0.591	3.
	0.442	0.834	0.663	3.
	0.427	0.816	0.508	3.
	0.462	0.792	0.704	3.
	0.452	0.693	0.871	3.
	0.308	0.756	0.556	0.
	0.477	0.802	0.548	3.
	0.442	0.669	0.644	3.
	0.457	0.702	0.728	3.
	0.403	0.742	0.760	3.
	0.511	0.689	0.644	3.
	0.486	0.830	0.704	1.
0.546	0.740	1.015	3.	
0.491	0.732	0.724	3.	
0.467	0.682	0.745	1.	
EA7236	0.273	0.333	0.387	0.
	0.302	0.324	0.391	0.
	0.292	0.329	0.416	0.
	0.287	0.329	0.360	0.
	0.307	0.361	0.388	0.
	0.278	0.345	0.411	0.
	0.233	0.345	0.439	0.
	0.263	0.352	0.419	0.
	0.273	0.325	0.372	0.
	0.293	0.345	0.435	0.
	0.268	0.341	0.120	0.4
	0.263	0.360	0.431	0.4
	0.258	0.356	0.431	0.4
	0.278	0.341	0.481	0.
	0.258	0.373	0.431	0.
	0.313	0.324	0.498	0.
	0.273	0.376	0.471	0.
0.293	0.396	0.463	0.	
0.283	0.352	0.364	0.	
0.263	0.377	0.451	0.	

Table A9  
Continued

Coating or Package	Flux			
	Alpha 611	Kester 1544	Pure Rosin	No Flux
Eccosil	0.278	0.325	0.208	0.296
	0.273	0.321	0.560	0.457
	0.283	0.344	0.426	0.467
	0.278	0.336	0.387	0.427
	0.308	0.353	0.613	0.362
	0.278	0.321	0.466	0.401
	0.283	0.341	0.419	0.545
	0.283	0.368	0.447	0.711
	0.317	0.357	0.483	0.542
	0.273	0.421	0.546	0.502
	0.317	0.320	0.436	0.451
	0.283	0.289	0.388	0.556
	0.273	0.333	0.431	0.616
	0.268	0.333	0.367	0.497
	0.292	0.361	0.427	0.467
	0.307	0.441	0.348	0.416
	0.258	0.325	0.352	0.516
	0.288	0.321	0.356	0.522
0.263	0.325	0.399	0.462	
0.293	0.329	0.439	0.502	
Hermetically Sealed	0.079	0.437	0.843	<del>7.177</del>
	-0.134	0.477	1.054	<del>7.264</del>
	-0.397	0.437	0.883	<del>7.177</del>
	-0.461	0.401	1.237	<del>7.241</del>
	-0.452	0.497	0.995	<del>7.177</del>
	0.526	0.461	0.967	0.492
	0.556	0.529	1.027	0.682
	0.546	0.461	1.079	0.552
	0.491	0.501	1.425	0.588
	0.590	0.657	1.162	0.553
	-0.818	0.425	0.967	0.582
	0.570	0.401	0.896	0.627
	0.546	0.585	0.764	0.767
	0.486	0.413	0.819	0.617
	-1.032	0.529	0.803	0.583
	-0.535	0.393	1.027	0.532
	0.005	0.485	1.105	0.692
	0.034	0.461	1.008	0.612
0.218	0.441	1.103	0.612	
0.382	0.633	0.947	0.528	

Table A10  
8000 Series Resistors

Percentage Changes of Individual Resistors after 11 Days at 150°C  
+ 17 Days at 100°C + 76 Days at 125°C

Coating or Package	Flux			
	Alpha 611	Kester 1544	Pure Rosin	No Flux
Sylgard 182	0.293	0.471	0.399	0.392
	-0.601	0.362	0.416	0.462
	0.338	0.357	0.385	0.397
	0.333	0.367	0.392	0.432
	0.353	0.322	0.401	0.447
	0.412	0.435	0.373	0.331
	0.387	0.440	0.369	0.357
	2.119	0.440	0.365	0.377
	0.367	0.485	0.385	0.357
	0.392	0.436	0.400	0.372
	0.315	0.381	0.361	0.415
	0.332	0.559	0.392	0.506
	0.338	0.416	0.389	0.457
	0.322	0.450	0.389	0.412
	0.347	0.440	0.384	0.418
	0.323	0.326	0.346	0.386
	0.337	0.514	0.371	0.482
	0.323	0.361	0.427	0.417
0.347	0.411	0.336	0.417	
0.367	0.404	0.337	0.447	
GE 511	0.323	0.362	0.360	0.422
	0.323	0.327	0.372	0.412
	0.328	0.372	0.377	0.427
	0.348	0.407	0.384	0.442
	0.348	0.362	0.393	0.437
	0.338	0.367	0.388	0.402
	0.323	0.485	0.404	0.462
	0.333	0.441	0.389	0.437
	0.318	0.362	0.409	0.417
	0.332	0.535	0.436	0.427
	0.323	0.407	0.356	0.418
	0.323	0.495	0.404	0.477
	0.323	0.520	0.372	0.452
	0.318	0.392	0.385	0.442
	0.343	0.505	0.416	0.487
	0.318	0.428	0.297	0.417
0.323	0.535	0.416	0.492	
0.318	0.490	0.392	0.467	
0.318	0.491	0.392	0.451	
0.308	0.481	0.456	0.556	

Table A10  
Continued

Coating or Package	Flux			
	Alpha 611	Kester 1544	Pure Rosin	No Flux
Stycast 2850GT	0.502	0.783	0.653	1.120
	0.536	0.806	0.740	1.323
	0.586	0.778	0.564	1.104
	0.531	0.847	0.685	1.198
	0.482	0.940	0.769	1.128
	0.512	0.841	0.272	0.905
	0.521	0.928	0.371	0.874
	0.516	0.924	0.304	1.063
	0.557	0.886	0.756	0.874
	0.516	0.802	0.931	0.970
	0.353	0.845	0.432	0.914
	0.561	0.866	0.284	0.929
	0.531	0.763	0.504	0.804
	0.541	0.806	0.776	0.823
	0.477	0.831	0.868	0.774
	0.591	0.808	0.700	1.088
	0.561	0.949	0.680	1.238
0.641	0.865	1.039	1.079	
0.576	0.856	0.784	1.108	
0.551	0.643	0.825	1.178	
HA7236	0.307	0.385	0.431	0.449
	0.317	0.389	0.443	0.566
	0.322	0.393	0.448	0.456
	0.317	0.393	0.420	0.536
	0.337	0.409	0.416	0.568
	0.303	0.405	0.439	0.374
	0.302	0.409	0.474	0.491
	0.293	0.420	0.463	0.497
	0.303	0.393	0.440	0.477
	0.322	0.397	0.455	0.512
	0.303	0.381	0.124	0.521
	0.303	0.416	0.455	0.501
	0.298	0.412	0.471	0.561
	0.318	0.417	0.505	0.451
	0.308	0.441	0.467	0.501
	0.352	0.381	0.530	0.456
	0.303	0.433	0.494	0.586
0.332	0.444	0.507	0.665	
0.323	0.420	0.380	0.517	
0.318	0.433	0.471	0.516	

Table A10  
Continued

Coating or Package	Flux			
	Alpha 611	Kester 1544	Pure Rosin	No Flux
Eccosil	0.327	0.361	0.224	0.367
	0.327	0.381	0.612	0.527
	0.332	0.417	0.486	0.552
	0.332	0.401	0.427	0.517
	0.352	0.417	0.692	0.433
	0.322	0.385	0.502	0.471
	0.333	0.397	0.474	0.635
	0.332	0.440	0.519	0.816
	0.367	0.417	0.543	0.623
	0.328	0.493	0.602	0.597
	0.352	0.393	0.618	0.536
	0.332	0.353	0.451	0.647
	0.317	0.393	0.483	0.726
	0.312	0.405	0.439	0.597
	0.332	0.433	0.487	0.552
	0.337	0.497	0.408	0.497
	0.317	0.385	0.420	0.602
0.328	0.385	0.416	0.612	
0.322	0.397	0.439	0.582	
0.342	0.389	0.498	0.587	
Hermetically Sealed	-24.263	0.533	-15.633	<del>90.900</del>
	-34.585	0.602	-21.331	<del>93.500</del>
	-29.573	0.553	-11.472	<del>93.900</del>
	-36.746	0.501	-20.132	<del>90.900</del>
	-33.123	0.593	-13.136	<del>93.900</del>
	-0.010	0.585	-8.062	0.572
	0.446	0.721	-9.417	0.773
	0.595	0.670	-10.340	0.648
	0.585	0.677	-15.785	0.683
	0.501	0.613	-13.132	0.654
	-4.967	0.497	-5.451	0.597
	-3.074	0.493	-4.277	0.762
	-1.836	0.718	-3.527	0.907
	-0.397	0.513	-5.113	0.728
	-6.542	0.650	-4.900	0.689
	-21.728	0.513	1.470	0.592
	-17.646	0.641	1.488	0.778
-21.056	0.686	1.432	0.722	
-19.369	0.594	1.510	0.718	
-19.064	0.814	1.318	0.623	

TABLE A10

STABILITY OF DUPONT BIROX AND 8000 SERIES RESISTORS  
COATED WITH DOW CORNING DC3140

CONDITION	PERCENTAGE CHANGES FOR:			
	BIROX COATED WITH DC3140	BIROX CONTROLS	8000 SERIES COATED WITH DC3140	8000 SERIES CONTROLS
After Coating  (No Thermal Aging)	0.010	0.011	0.113	0.000
	0.002	0.026	0.051	-0.217
	-0.080	0.000	0.074	0.048
	-0.025	0.012	-0.043	0.040
	0.179	0.018	0.044	0.051
	0.017	0.014	0.035	0.007
	0.012	0.013	0.057	-0.552
	-0.053	-0.020	0.017	0.008
	-0.033	-0.024	0.032	0.024
	0.002	0.015	-0.020	0.016
	-0.007	0.017	-0.011	0.009
	0.004	0.027	-0.035	0.008
	-0.025	0.015	-0.007	0.016
	-0.031	0.021	0.000	0.012
	-0.066	-0.006	0.004	0.012
	-0.013	-0.028	-0.012	0.017
	0.000	0.008	-0.035	0.004
	-0.122	0.012	0.007	0.008
	-0.388	0.007	-0.008	0.000
	-0.150	-0.004	-0.004	0.008
-0.021	-0.032	-0.009	0.007	
0.038	-0.042	-0.021	-0.233	
-0.110	0.015	-0.022	0.012	
-0.353	-0.021	-0.008	0.000	
-0.125	-0.004	-0.004	0.004	

TABLE A11

STABILITY OF DUPONT BIROX AND 8000 SERIES RESISTORS  
COATED WITH DOW CORNING DC3140

CONDITION	PERCENTAGE CHANGES FOR:			
	BIROX COATED WITH DC3140	BIROX CONTROLS	3000 SERIES COATED WITH DC3140	8000 SERIES CONTROLS
After 24 Hrs. At 125°C	0.017	0.001	0.305	0.089
	0.000	0.018	0.205	0.161
	0.035	0.000	0.192	0.097
	0.005	-0.006	0.107	0.193
	0.030	-0.006	0.095	0.173
	0.027	0.000	0.105	0.104
	0.031	0.021	0.155	0.159
	0.003	0.020	0.137	0.090
	0.000	-0.017	0.139	0.151
	0.011	-0.015	0.118	0.128
	0.017	0.000	0.052	0.061
	0.016	0.013	0.049	0.096
	-0.025	0.004	0.051	0.123
	-0.018	0.007	0.056	0.088
	0.000	-0.014	0.064	0.108
	0.017	0.003	0.067	0.104
	0.015	0.008	0.063	0.093
	-0.006	0.004	0.073	0.085
	-0.007	0.000	0.060	0.034
	0.002	0.000	0.060	0.093
	-0.013	-0.008	0.064	0.092
	0.057	0.000	0.076	0.084
	-0.012	0.008	0.036	0.093
	-0.015	-0.002	0.060	0.093
0.000	0.000	0.064	0.085	

TABLE A12

STABILITY OF DUPONT BIROX AND 8000 SERIES RESISTORS  
COATED WITH DOW CORNING DC3140

CONDITION	PERCENTAGE CHANGES FOR:			
	BIROX COATED WITH DC3140	BIROX CONTROLS	8000 SERIES COATED WITH DC3140	8000 SERIES CONTROLS
After 7 Days At 125°C	0.017	0.000	0.607	0.164
	0.012	0.015	0.451	0.184
	0.035	0.000	0.383	0.240
	0.000	-0.008	0.245	0.340
	0.030	-0.006	0.199	0.256
	0.027	-0.001	0.230	0.171
	0.031	0.017	0.322	0.334
	0.000	0.012	0.246	0.164
	-0.008	-0.021	0.218	0.219
	0.008	-0.021	0.397	0.215
	0.013	-0.002	0.180	0.076
	0.008	0.009	0.190	0.136
	-0.030	0.000	0.139	0.135
	-0.018	0.007	0.149	0.132
	0.003	-0.018	0.149	0.127
	0.017	0.003	0.224	0.153
	0.011	0.004	0.267	0.129
	-0.013	0.004	0.176	0.129
	-0.014	-0.004	0.125	0.133
	0.002	-0.004	0.153	0.133
0.006	-0.008	0.207	0.151	
0.069	0.005	0.250	0.133	
-0.004	0.003	0.116	0.125	
-0.004	0.002	0.132	0.137	
-0.010	0.004	0.148	0.117	

TABLE A13

STABILITY OF DUPONT B1R0X AND R000 SERIES RESISTORS  
COATED WITH DOW CORNING DC3140

CONDITION	PERCENTAGE CHANGES FOR:			
	B1R0X COATED WITH DC3140	B1R0X CONTROLS	R000 SERIES COATED WITH DC3140	R000 SERIES CONTROLS
After 14 Days at 125°C	0.040	0.014	0.396	0.201
	0.032	0.037	0.316	0.291
	0.050	0.000	0.088	0.263
	0.015	0.008	0.134	0.383
	0.030	0.006	0.147	0.260
	0.053	-0.063	0.195	0.215
	0.058	0.038	0.218	0.334
	0.023	0.033	0.164	0.198
	0.016	-0.007	0.139	0.255
	0.032	-0.012	0.287	0.259
	0.040	0.013	0.074	0.104
	0.035	0.031	0.099	0.172
	-0.015	0.018	0.139	0.095
	0.000	0.025	0.125	0.171
	0.028	-0.006	0.141	0.151
	0.044	0.015	0.045	0.190
	0.041	0.024	0.049	0.165
	0.006	0.025	0.146	0.165
	0.007	0.028	0.076	0.169
	0.025	0.014	0.121	0.169
0.019	0.000	0.132	0.187	
0.086	0.015	0.118	0.173	
0.004	0.039	0.058	0.161	
0.004	0.010	0.060	0.181	
0.010	0.016	0.116	0.157	

TABLE A14

STABILITY OF DUPONT BIROX AND 8000 SERIES RESISTORS  
COATED WITH DOW CORNING DC3140

CONDITION	PERCENTAGE CHANGES FOR:			
	BIROX COATED WITH DC3140	BIROX CONTROLS	8000 SERIES COATED WITH DC3140	8000 SERIES CONTROLS
After 28 Days at 125°C	0.0400	0.0322	0.4184	0.2453
	0.0341	0.0549	0.3125	0.2612
	0.0550	0.0000	0.2507	0.2831
	0.0200	0.0220	0.0948	0.3991
	-0.0081	0.0200	0.1748	0.2679
	0.0532	-0.0485	0.2203	0.2451
	0.0579	0.0716	0.2052	0.3239
	0.0302	0.0650	0.1868	0.2318
	0.0247	0.0195	0.1904	0.2870
	0.0296	0.0169	0.2436	0.2990
	0.0365	0.0426	0.0987	0.1502
	0.0310	0.0669	0.1198	0.2198
	-0.0100	0.0509	0.1612	0.1230
	0.0000	0.0565	0.1448	0.2153
	0.0219	0.0219	0.1691	0.1752
	0.0436	0.0413	0.0683	0.2256
	0.0298	0.0554	0.0561	0.2052
	0.0128	0.0534	0.1830	0.1972
	0.0144	0.0461	0.0965	0.2132
	0.0212	0.0434	0.1529	0.2132
0.0147	0.0162	0.1556	0.2243	
0.0837	0.0274	0.1318	0.2130	
0.0079	0.0541	0.0796	0.2012	
0.0110	0.0273	0.0919	0.2173	
0.0193	0.0358	0.1478	0.1976	

TABLE A15

STABILITY OF DUPONT BIROX AND 8000 SERIES RESISTORS  
COATED WITH DOW CORNING DC3140

CONDITION	PERCENTAGE CHANGES FOR:			
	BIROX COATED WITH DC3140	BIROX CONTROLS	8000 SERIES COATED WITH DC3140	8000 SERIES CONTROLS
After 64 Days at 125°C	0.0333	-0.0519	0.4751	0.3047
	0.0244	-0.1428	0.3788	0.4313
	0.0500	0.0000	0.3441	0.3167
	0.0150	-0.0921	0.0988	0.4860
	-0.0439	-0.0921	0.2304	0.3624
	0.0466	-0.0300	0.2681	0.3120
	0.0540	-0.1684	0.2841	0.5645
	0.0227	-0.1626	0.2341	0.2917
	0.0165	-0.0752	0.2738	0.3268
	0.0211	-0.0843	0.2790	0.3389
	0.0332	-0.0600	0.1289	0.1836
	0.0233	-0.1829	0.1480	0.2438
	-0.0250	-0.1563	0.1978	0.0953
	-0.0061	-0.1448	0.1730	0.2392
	0.0162	-0.0997	0.1973	0.1911
	0.0393	-0.0531	0.1015	0.2312
	0.0186	-0.1662	0.1053	0.2293
	0.0064	-0.1765	0.2416	0.2414
	0.0072	-0.1524	0.1246	0.2292
	0.0154	-0.1591	0.1851	0.2373
0.0126	-0.0243	0.1824	0.2131	
0.0789	-0.0713	0.1734	0.2291	
0.0079	-0.3398	0.0941	0.2253	
0.0074	-0.0799	0.1199	0.2495	
0.0096	-0.0896	0.1758	0.2177	

TABLE A16

STABILITY OF DUPONT BIRØX AND 8000 SERIES RESISTORS  
COATED WITH DOW CORNING DC3140

CONDITION	PERCENTAGE CHANGES FOR:			
	BIRØX COATED WITH DC3140	BIRØX CONTROLS	8000 SERIES COATED WITH DC3140	8000 SERIES CONTROLS
After 76 Days at 125°C	-0.1066	-0.0519	0.4342	0.2999
	-0.0707	-0.1428	0.3030	0.4713
	0.0300	0.0000	0.3269	0.2152
	-0.0050	-0.0921	-0.0553	0.3754
	0.0150	-0.0941	0.0735	0.2324
	-0.0899	-0.0599	0.1405	0.2971
	-0.1119	-0.1684	0.2173	0.5745
	-0.0151	-0.1606	0.1544	0.2252
	-0.0247	-0.0766	0.1508	0.1913
	-0.0612	-0.0843	0.1650	0.1954
	-0.1096	-0.0616	0.1216	0.1242
	-0.1397	-0.1873	0.1480	0.0912
	-0.0400	-0.1600	-0.1538	-0.0635
	-0.0307	-0.1448	0.0000	0.0837
	-0.0231	-0.1017	0.0121	0.0398
	-0.1484	-0.0545	0.1056	0.1603
	-0.1378	-0.1701	0.1263	0.0764
	-0.0192	-0.1806	-0.1318	0.0724
	-0.0215	-0.1595	-0.0523	0.0764
	-0.0635	-0.1591	0.0121	0.0825
-0.0735	-0.0324	0.1670	0.1514	
-0.0191	-0.0713	0.1803	0.0804	
-0.0118	-0.3476	-0.2534	0.0684	
-0.0074	-0.0818	-0.0559	0.0966	
-0.0289	-0.0941	-0.0040	0.0645	

TABLE A17

STABILITY OF DUPONT BIRØX AND 8000 SERIES RESISTORS  
COATED WITH DOW CORNING DC3140

CONDITION	PERCENTAGE CHANGES FOR:			
	BIRØX COATED WITH DC3140	BIRØX CONTROLS	8000 SERIES COATED WITH DC3140	8000 SERIES CONTROLS
After 95 Days At 125°C	0.0367	-0.0460	0.5736	0.3386
	0.0397	-0.1431	0.4590	0.3750
	0.0547	-0.0203	0.4041	0.2853
	0.0148	-0.0873	0.1126	0.5275
	0.0718	-0.0873	0.2646	0.4116
	0.0499	-0.0163	0.3017	0.3309
	0.0479	-0.1680	0.3453	0.6483
	0.0201	-0.1634	0.2829	0.3183
	0.0174	-0.0625	0.3396	0.3451
	0.0342	-0.0717	0.3281	0.3572
	0.0332	-0.0475	0.1818	0.2207
	0.0248	-0.1896	0.1781	0.2582
	-0.0153	-0.1571	0.1934	0.0857
	-0.0036	-0.1462	0.1959	0.2616
	0.0313	-0.0912	0.2122	0.2095
	0.0323	-0.0436	0.1643	0.2426
	0.0186	-0.1717	0.1561	0.2482
	0.0108	-0.1769	0.2152	0.2402
	0.0027	-0.1574	0.1476	0.2441
	0.0244	-0.1598	0.2000	0.2602
0.0128	-0.0403	0.2294	0.2451	
0.0861	-0.0772	0.1954	0.2440	
0.0068	-0.3885	0.0825	0.2362	
0.0111	-0.0859	0.1383	0.2483	
-0.0018	-0.0916	0.2021	0.2286	

Appendix D

ADHESIVE BONDING, CURING AND INSULATION  
OF THE UpSTAGE AIRFRAME

- MDAC Report MP 51, 564 (M. C. St. Cyr), Adhesive Bonding of Heat Shield Insulation of Aluminum Substructure, 13 May 1970.
- MDAC Report MP 51, 736 (S. E. Gordon, et al.), Thermal Analysis of Refrasil Phenolic Prepreg and AF31 Nitrile Adhesive for UpSTAGE, 11 March 1970.
- MDAC Report MP 51, 731 (R. W. Hunter), 300°F Cure Studies of C-100-96/DP 24-2 Prepreg and AF31 Film Adhesive for UpSTAGE, 22 April 1970.
- MDAC Report MP 51, 732 (F. B. Jones), Plasma Jet Specimen Preparation, 23 April 1970.
- MDAC Report MP 51, 741 (G. D. Shepherd), Bonding Refrasil Phenolic to Aluminum Using HT-424 Adhesive for UpSTAGE, 21 April 1970.

**MISSILE & SPACE SYSTEMS DIVISION  
DOUGLAS AIRCRAFT COMPANY, INC.**

FORM 37-88 (REV. 1-63)

**MATERIAL & PROCESS ENGINEERING  
LABORATORY REPORT**

CATALOG NO. PDL 104376

SERIAL NO. MP 51,564

DATE 13 May 1970

ASSIGNED TO M. C. St. Cyr, A-265

TITLE **ADHESIVE BONDING OF HEAT SHIELD  
INSULATION TO ALUMINUM SUBSTRUCTURE**

1. MATERIALS

1.1 Vendor - 3M Company  
St. Paul, Minnesota

1.1.1 EC-3515, B/A Polyurethane Adhesive  
Batch 23M8C, DPM 3396

1.1.2 EC-3901, Silane Primer  
Batch 32K8P, DPM 3688

1.1.3 EC-2216, B/A Flexible Epoxy Adhesive Paste  
Batch 22K8C, DPM 3279

1.1.4 AF-31 Nitrile Phenolic Film Adhesive  
Batch 22H, DPM 3915

1.1.5 EC-1459, Nitrile Phenolic Primer  
Batch 5B8P, DPM 2131

1.1.6 AF-126-2, Epoxy Nitrile Adhesive Film  
Batch 905, DPM 3844

1.1.7 EC-2320, Epoxy Nitrile Primer  
Batch 15M7C, DPM 3842

1.2 Vendor - Bloomingdale Department, American Cyanamid Co.  
Havre de Grace, Maryland

1.2.1 FM-123-5, Epoxy Nitrile Adhesive Film  
Batch B-204

1.2.2 BR-123, Epoxy Nitrile Primer  
Batch L-15

1.3 C-100-96 ~~Refrasil~~/DP 24-2 Phenolic Resin Prepreg, Batch 09806  
Ferro Corp/Cordo Div., Culver City, California

Note: Candidate adhesives were selected on the basis of (1) a short duration glueline temperature exposure of 93° to 140°C (200° to 300°F) and (2) a non-outgassing material during the required elevated temperature curing cycle.

## 2. OBJECT

- 2.1 To develop and evaluate a method for simultaneously bonding and curing a Refrasil/phenolic prepreg to an aluminum substructure.
- 2.2 To determine the compatibility of selected adhesive systems with the Refrasil/phenolic prepreg.
- 2.3 To evaluate joining techniques for ease of fabrication, bond integrity and aerodynamic smoothness.
- 2.4 To determine the integrity of the bond by nondestructive inspection.

## 3. PROCEDURE

### 3.1 Bonding of Refrasil/Phenolic Prepreg to Aluminum Plates

The candidate adhesives were used to bond C-100-96 Refrasil/DP 24-2 Phenolic prepreg to 6"x6"x0.250", 2024 T-3 clad aluminum plates. The aluminum plates were prepared for bonding by etching in a solution of sulfuric acid-sodium dichromate for 20 minutes at 66°C (150°F) per the procedure outlined in DPS 30,000, Type I, Rev. K. The faying surfaces of the cleaned aluminum plates were brush coated with primer, where applicable, and the primer cured per the recommendations of the manufacturer. Subsequently, the adhesive was placed (film) or trowelled (paste) onto the aluminum faying surface, the prepreg positioned on the adhesive and the assembly taped into position.

The assembly was bagged and a vacuum of 28 inches Hg, minimum, applied. Vacuum bagged specimens were then cured for 3 hours at 149°C (300°F) in the autoclave under 50 psig pressure and cooled to 66°C (150°F) before the pressure was removed. The above cure cycle was used for all subsequent bonding operations regardless of the type of adhesive system utilized. The adhesive systems used were as follows:

<u>Film Adhesive/Primer</u>	<u>Paste Adhesive/Primer</u>
AF-31/EC-1459	EC-3515/EC-3901
AF-126-2/EC-2320	EC-2216/None
FM-123-5/BR-123	
FM-123-7/BR-123	

Table I shows the thickness of cured Refrasil when bonded to aluminum.

### 3.2 Bonding of Prepreg to Aluminum Cylinders

Subscale circular aluminum cylinders, approximately 6 inches in diameter, were covered with insulation and cured using the four most promising of the

above adhesive systems. Cylinders were fabricated using a butt-splice and a single overlap joint for each adhesive used. A layer of 5/8 inch thick silicone rubber foam was inserted between the vacuum bag and bleeder cloth to alleviate ridges on the surface of the heat shield due to excess resin bleed out and bagging creases. Figure 1 depicts the bagging method used to minimize surface imperfections on the insulation. Figure 2 shows cylinders that were cured with and without the silicone rubber foam pad in the fabrication lay-up.

### 3.3 Bonding of Prepreg to an Aluminum Elliptical Cylinder

An aluminum elliptical cylinder, 71 inches in circumference, was insulated with the prepreg using AF-31 adhesive film as described in 3.2 above.

Note: The Refrasil/phenolic prepreg had a flow of 10.7%, a resin solids content of 28.8% and 5.9% volatiles and was used in the as-received condition.

### 3.4 Non-destructive Testing

All of the adhesively bonded UpSTAGE test cylinders were nondestructively tested for voids in the adhesive bond line using the immersion ultrasonic through-transmission technique. The basic operational set-up is shown in Figure 3.

#### 3.4.1 Ultrasonic Through-transmission Procedure -

The entire specimen was immersed in water which acted as a coupling medium. The ultrasonic waves generated by the transmitting transducer passed through the adhesively bonded cylinder and were detected by the receiving transducer. Changes in the strength of the received signal were attributed to changes in the attenuation because of the presence of defects in the adhesively bonded cylinder.

A void in the adhesive is highly attenuating. To obtain a map of the scan, the transducers were moved back and forth parallel to the axis of the cylinder. After each pass, the cylinder was rotated a small increment. In this manner the whole surface was covered. The record consists of a series of lines, one for each pass of the transducers. The record was arranged so that a line was written only for signals above a certain pre-set level. Thus, those regions which show the greatest attenuation because of voids appeared as light areas in the record. This type of record is called a C-scan map.

A typical C-scan map revealing voids is shown in Figure 4. The light areas represent the more highly attenuating voids. The long void shown across the top of the map is due to the air trapped between the aluminum and tape which was applied to keep the cylinder from slipping on the rollers. A typical C-scan map of an adhesively bonded cylinder without voids is shown in Figure 5.

4. RESULTS

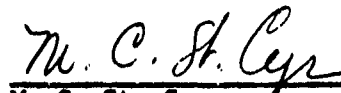
- 4.1 A large scale elliptical cylinder was insulated and bonded with Refrasil/phenolic using a nitrile phenolic adhesive (AF-31). See Figure 6.
- 4.2 The epoxy and phenolic adhesives used in this work were compatible with the Refrasil prepreg. The urethane adhesive was incompatible with the Refrasil insulation.
- 4.3 The AF-31 cylinders were bonded void free as determined by ultrasonic through-transmission technique. See Figure 5.
- 4.4 The thickness of the cured Refrasil when bonded to aluminum is shown in Table I. In all combinations checked, the total insulation thickness (cured Refrasil and adhesive) is less than the total thickness of the uncured Refrasil plus the uncured adhesive.

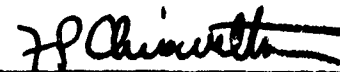
5. SIGNIFICANCE OF DATA

- 5.1 A process was developed for fabricating heat shield prepreg materials to elliptical cylindrical sections that produced an aerodynamically smooth insulation surface.

6. REFERENCES

SO 3859-6320  
EWO 11069  
SA 7014

  
\_\_\_\_\_  
M. C. St. Cyr  
Non-Metallics Materials Properties  
Materials & Methods -  
Research & Engineering

  
\_\_\_\_\_  
F. P. Chiavetta, Section Chief  
Non-Metallics Materials Properties  
Materials & Methods -  
Research & Engineering

MCStC:rtt

Table I  
Thickness Cured Refrasil  
(inches)  
Bonded to Aluminum

Adhesive Used	Adhesive Thickness (Uncured)	Refrasil Thickness (Uncured)	Total Thickness of Bonded and Cured Refrasil Heat Shield (excluding the metal)
EC-3515	*	.057	.0563
AF-31	.009	.055	.0510
EC-2216	*	.055	.0517
AF-126-2	.015	.053	.0563
FM-123-5	.011	.055	.0569
FM-123-7	.011	.053	.0563

\* Paste adhesives applied manually.



Figure D-1. Fabrication technique for Bonding Insulation

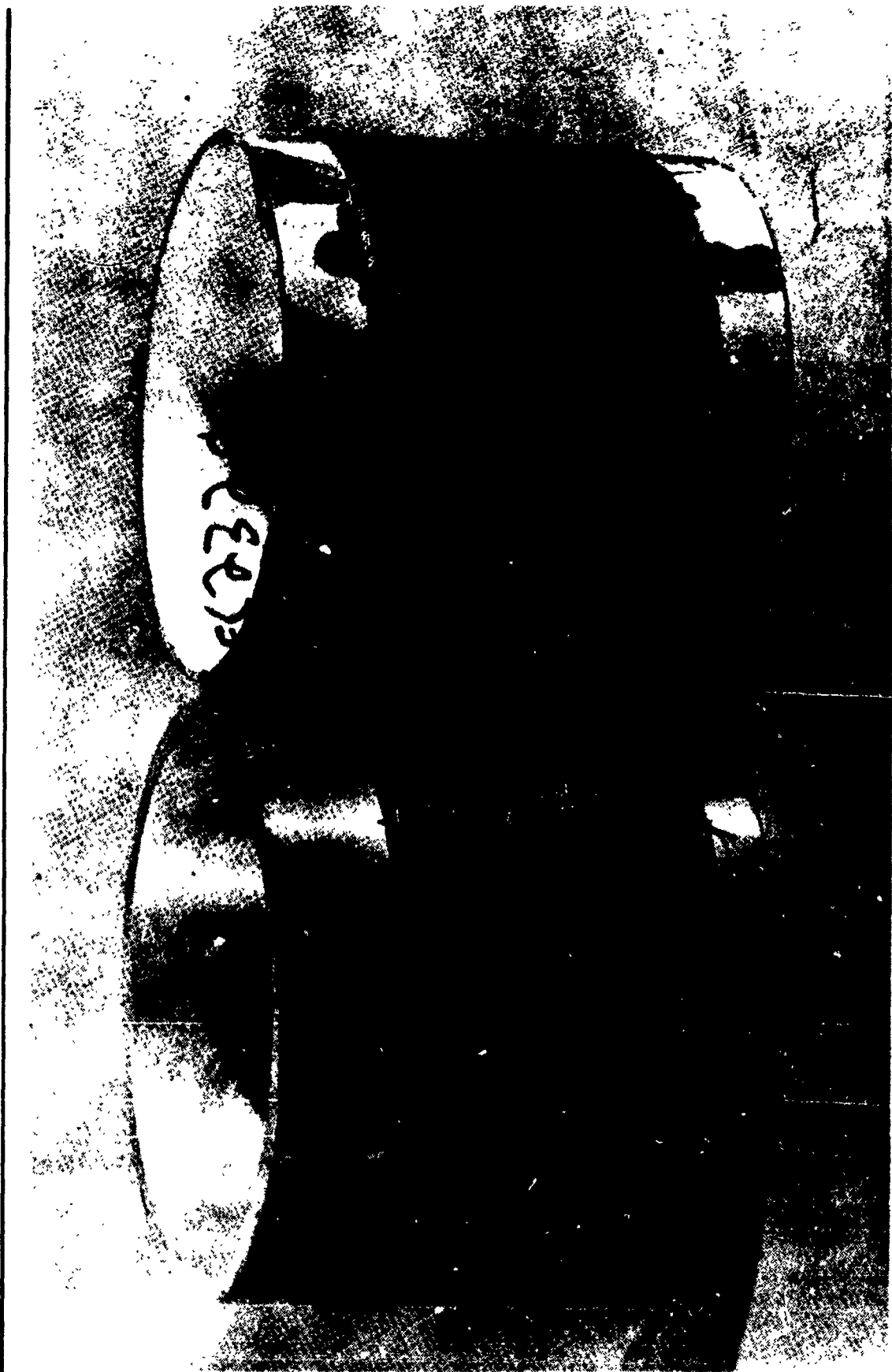


Figure D-2. Bonded Insulation Fabricated With and Without Silicone Foam Rubber

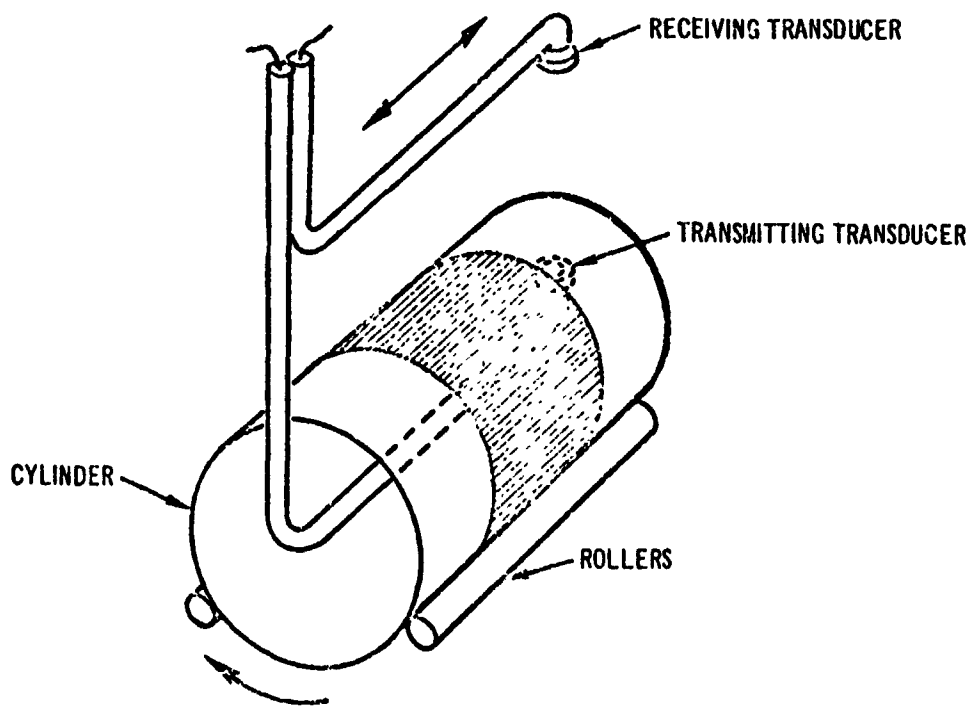
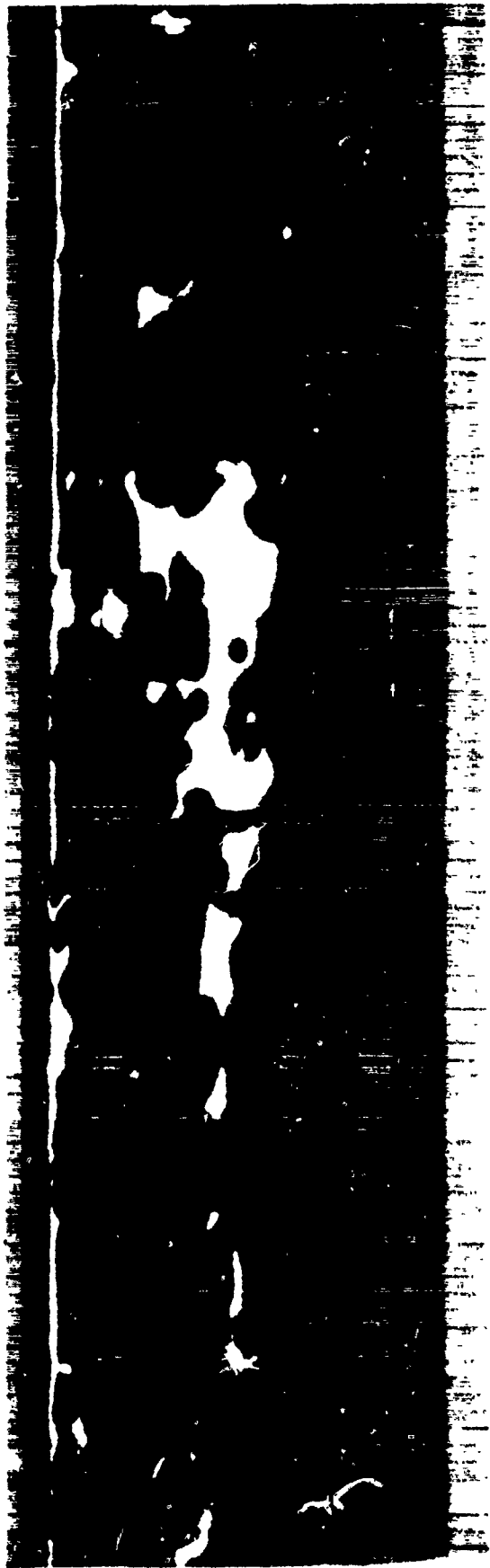


Figure D-3. Ultrasonic Through-Transmission Schematic

---

Tape on  
AL to keep  
Cylinder  
from slipping  
on fixture

360°



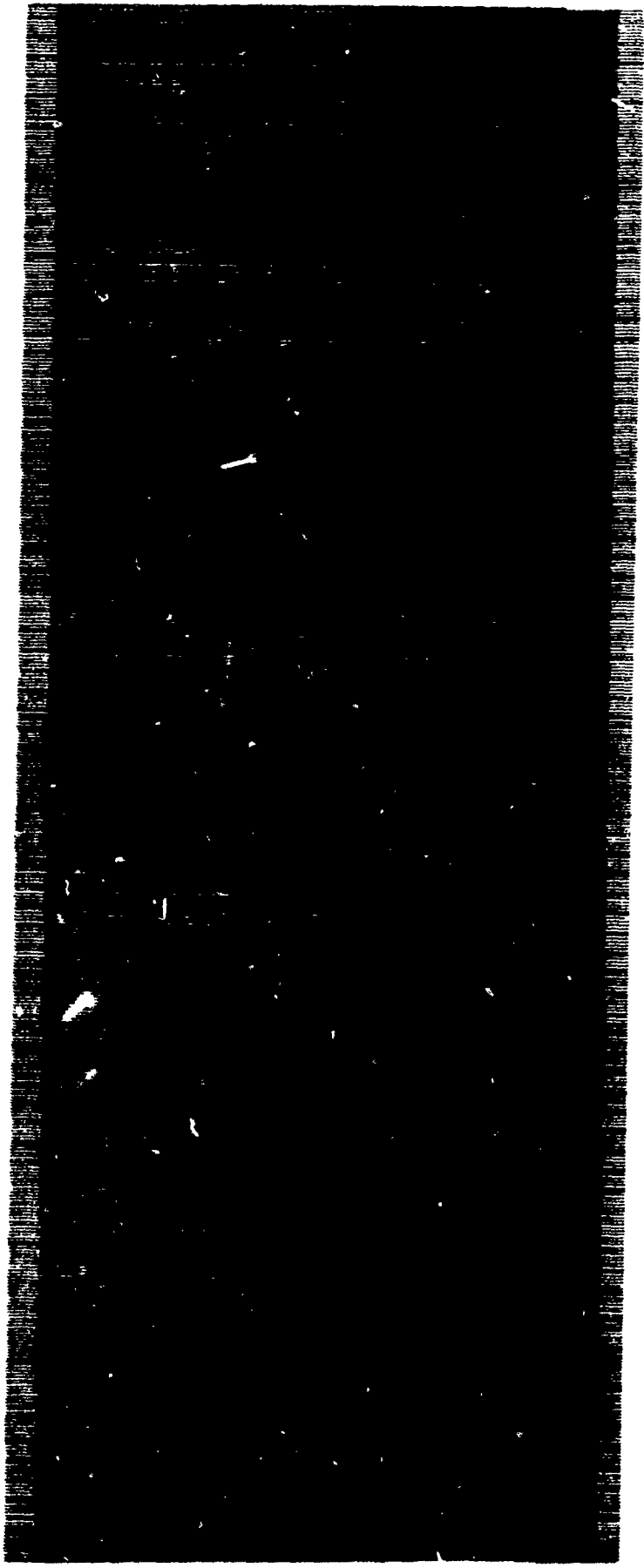
0°

Ultrasonic inspection (thru-transmission) UpSTAGE cylinder Refrasil on AL bonded with EC 2320 and AF 126-2  
Transmitter-Receiver I.OMC .500" dia. #SFZ 57A3131  
Recorded at I.OMC low freq. adapter Attenuator "A"  
Recorded at 24db

Figure D-4. AF 126-2 Adhesive Bonded Insulation

0°

360°



Ultrasonic Inspection (Thru-Transmission) UpSTAGE Cylinders Refrasil on Al, bonded with EC 1459 and AP 31  
Transmitter-Receiver-I.OMC .500" dia. #SFZ 57A3131  
Recorded at I.OMC Low Freq. Adapter Attenuator "A"  
Recorded at 30db

Figure D-5. AF-31 Bonded Insulation

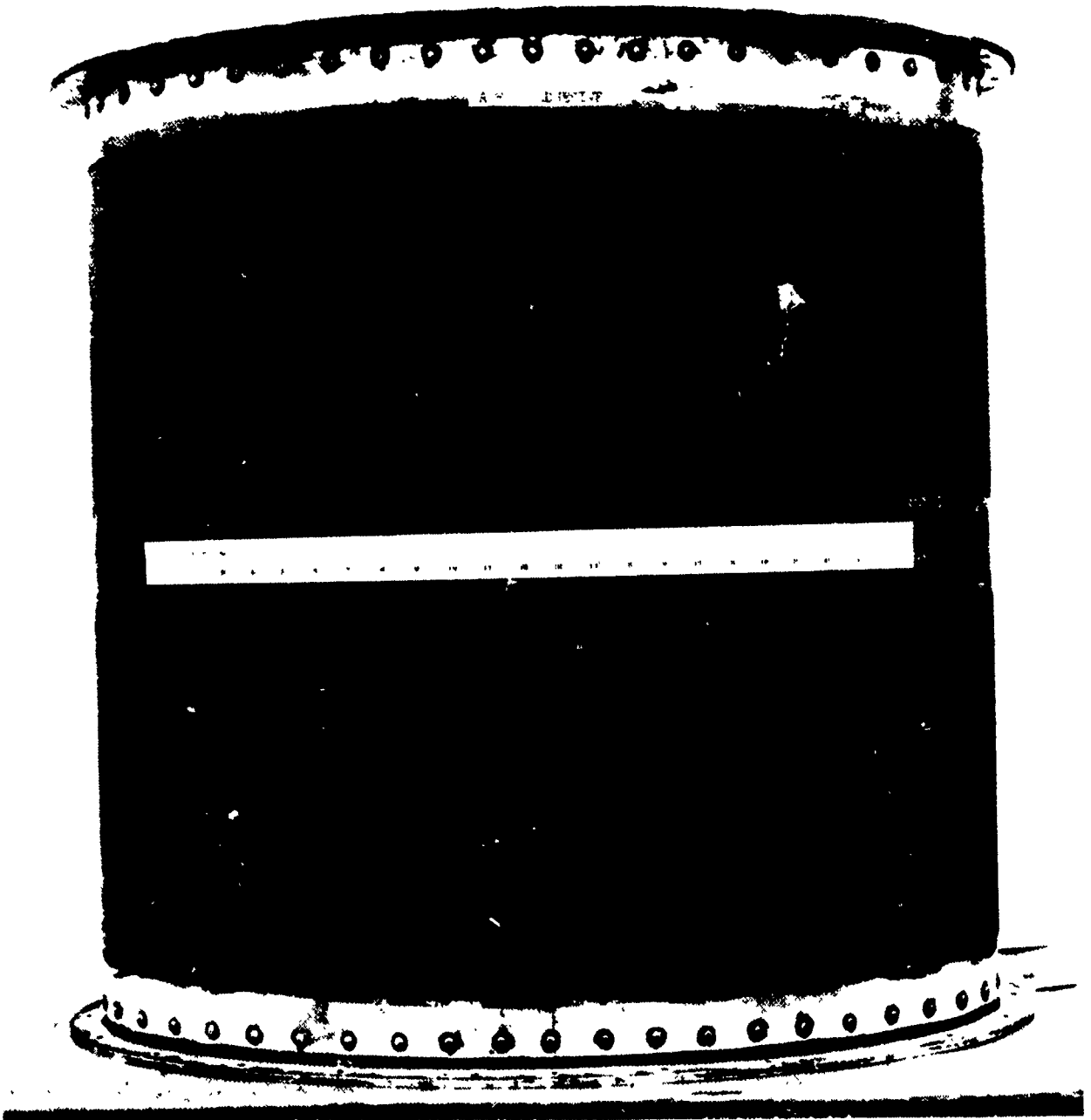


**Figure D-6. Elliptical Cylinder, Insulation Bonded with AF-31 Adhesive**

---



MISSILE & SPACE SYSTEMS DIVISION  
DOUGLAS AIRCRAFT COMPANY, INC.

FORM 37-00 (REV. 1-62)

MATERIAL & PROCESS ENGINEERING  
LABORATORY REPORT

CATALOG NO. PDL 104183

SERIAL NO. MP 51,736

DATE 3-11-70

ASSIGNED TO S. E. Gordon, A-255

TITLE THERMAL ANALYSIS OF REFRASIL  
PHENOLIC PREPREG AND AF31 NITRILE  
ADHESIVE FOR UpSTAGE

1. MATERIALS

- 1.1 C-100-96 Refrasil/DP-24-2 Phenolic Resin  
Prepreg, Lot No. 9806  
Vendor Material Designation, WB 2262/96  
Ferro-Cordo Corp., Culver City, Calif.
- 1.2 AF31 Film Adhesive, Batch No. 22H  
DPM 3915, STM 0030-03  
3-M Company, St. Paul, Minnesota

2. OBJECT

To perform Thermogravimetric Analysis (TGA) and Thermomechanical Analysis (TMA), to determine the effect of temperature on Refrasil Prepreg and AF31 Adhesive to be used for UpSTAGE heat shield insulation.

3. PROCEDURES

3.1 Prepreg Physical Property Tests

Incoming quality control tests to determine percent resin flow, volatiles and resin solids on the C-100-96 Refrasil/DP-24-2 were conducted per MRD 11247171-Cloth, Impregnated-High Silica Phenolic, Heavy-Weight.

For results see Table 1 (Prepreg Physical Properties).

3.2 Curing of Single Ply Prepreg and Single Layer Adhesive

One 6" x 6" ply of C-100-96 Refrasil/DP-24-2 phenolic resin prepreg and one 6" x 6" layer of AF31 film adhesive were individually placed on a .125" thick aluminum caul-plate using polytetrafluoroethylene as a release film. A 28-gauge iron-constantan thermocouple was inserted between the single ply of Refrasil and the release film, one-inch from one corner, to monitor part temperature. The specimen was vacuum-bagged and placed in an autoclave at ambient temperature. The autoclave was purged and then pressurized with nitrogen to 50 psig. The autoclave controllers were then set to give a 300°F part temperature. After three hours holding time at 300° ± 5°F, the temperature controllers were turned off and the part cooled to ambient while maintaining pressure.

### 3.3 Thermogravimetric Analysis

The TGA's of AF31 adhesive in argon and Refrasil phenolic prepreg in argon and air were performed on a DuPont Model 950 Thermogravimetric Analyzer. A Cahn Mark II Time Derivative Computer was used, along with a Mosley Model 7001A X-Y Recorder, to obtain the first derivative of the TGA Thermogram. This mixed system has the capability of producing both the normal TGA curve of % weight loss vs. temperature, and the first derivative of the weight loss (or rate of weight loss) vs. temperature, simultaneously. Thus, a peak on the derivative TGA corresponds to the point of maximum slope on the normal curve. The derivative of the TGA Thermogram magnifies changes in the weight loss curve which are easily overlooked in the conventional mode.

### 3.4 Thermomechanical Analysis (TMA)

The TMA's of AF31 adhesive and Refrasil prepreg were performed in argon using a DuPont Model 940 Thermomechanical Analyzer. The Cahn Mark II and Mosley 7001A were used to obtain first derivative of the dimensional change vs. temperature.

## 4. RESULTS

- 4.1 The TGA's 1088 and 1094 of AF31 show that two small weight losses occur in the temperature ranges of 75-175°C (167-347°F) and 200-290°C (392-554°F). A very rapid weight loss in argon begins at about 340°C (644°F).
- 4.2 The TMA's 736 of AF31 show continual shrinking with increasing temperature; however, the rate is not constant. Beginning at about 150°C (302°F) and continuing to 240°C (464°F) there is a noticeable increase in the rate of shrinkage. During decomposition the material undergoes considerable shrinkage.
- 4.3 The TGA's 1093 of DP-24-2 in argon show a large weight loss starting at 390°C (734°F). The TGA's 1090 of DP-24-2 in air show a large weight loss starting at 330°C (626°F).

In both air and argon the phenolic shows a weight loss between 200-300°C (392-572°F).

- 4.4 The TMA's 735A, 727 and 737 in argon of DP-24-2 show a softening between 150-250°C (302-482°F). Beginning at 390°C (734°F) rapid contractions and expansions take place, due to bubbling of the phenolic.

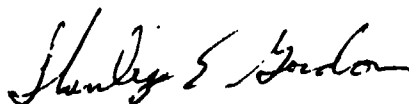
## 5. SIGNIFICANCE OF DATA

- 5.1 The AF31 in the temperature range of 75-240°C (167-464°F) shrinks while evolving water in the gas phase due to further curing. At 340°C (644°F) total decomposition of the material begins with rapid gas evolution, size decrease, and charring.

5.2 The DP-24-2, with a 60°C (140°F) lower oxidation temperature than inert gas decomposition temperature, burns before it can char. The material also undergoes further curing with gas-phase water evolution in the temperature range of 150-300°C (302-572°F).

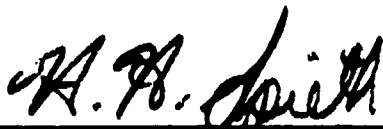
6. REFERENCES

S.O. 3859-6320  
EWO 11069  
S.A. 7014  
Case Sheet 90327  
TGA Run No. 1088, 1090, 1093, 1094  
TMA Run No. 727, 735A, 736, 737  
TR 9940, page 15; TR 9940, page 46 "Prepreg Physical Properties"  
TR 12071, pages 2-7, "Cure of Materials".



---

S. E. Gordon  
Analytical Chemistry Section



---

H. H. Spieth, Section Chief  
Analytical Chemistry  
Materials & Methods -  
Research & Engineering

TABLE 1  
PREPREG PHYSICAL PROPERTIES

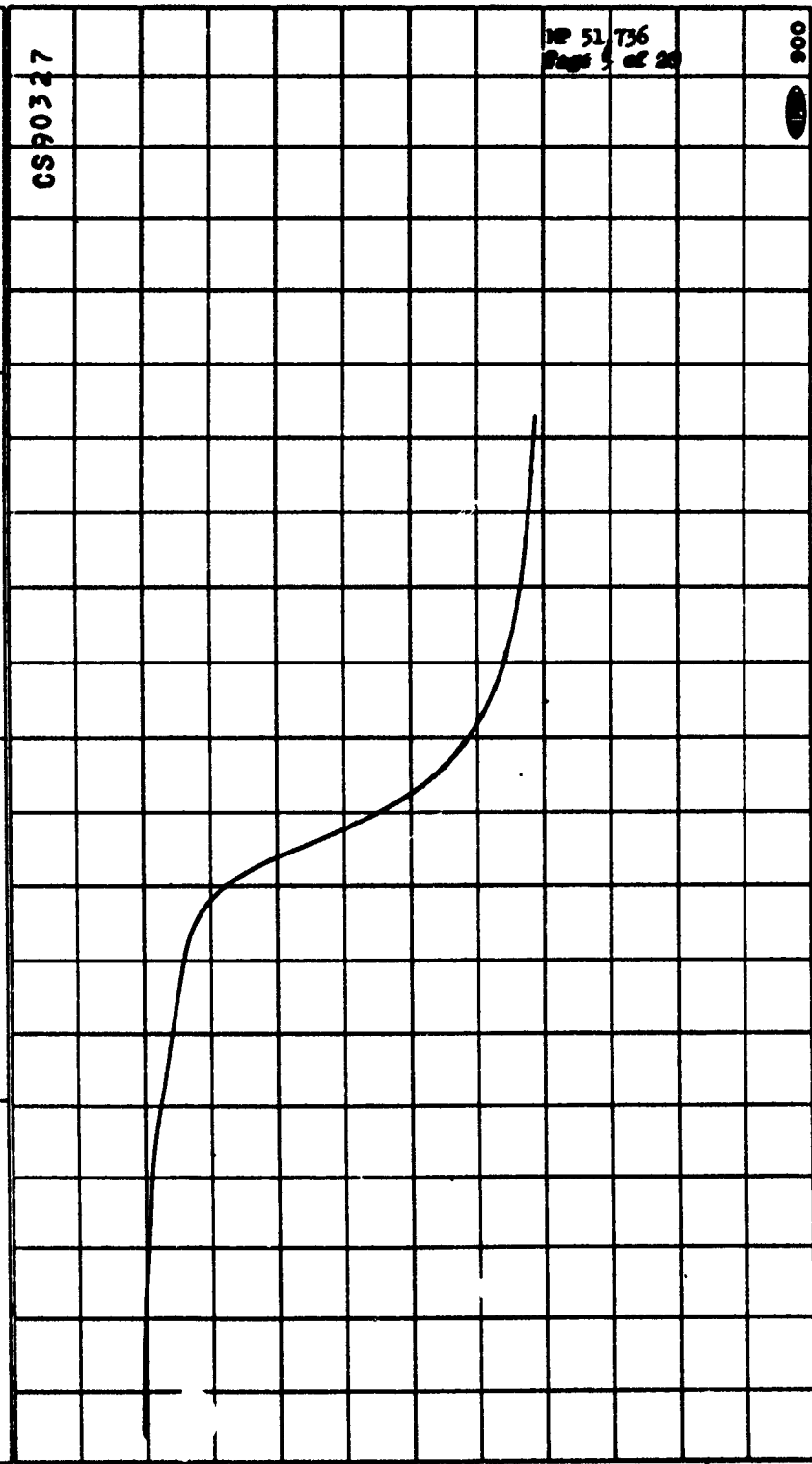
Material Description	Date of Tests	% Resin Flow	% Volatile Content	% Resin Shrink
C-100-96/DP-24-2 Lot No. 9806 WB 2262/96 Average	2-14-69	10.1	5.1	28.7
		9.9	5.1	28.7
		10.8	5.1	29.2
		<u>11.8</u>		
		10.7	5.1	28.9
Average	10-30-69	11.7	4.2	31.2
		11.2	4.5	30.4
		<u>11.6</u>	<u>4.3</u>	<u>29.9</u>
		11.5	4.3	30.5

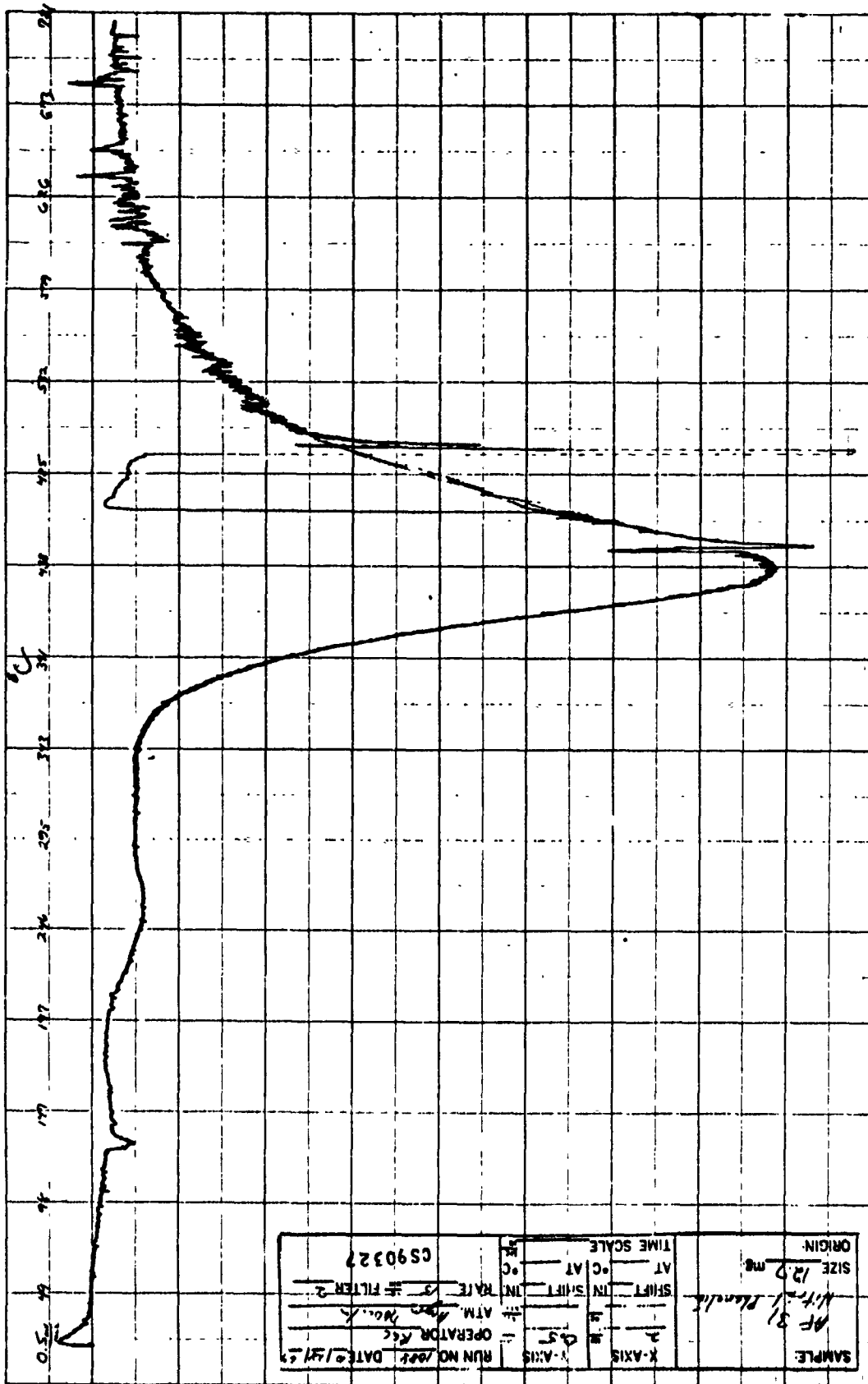
RUN NO. 031 DATE 11-18-59  
 OPERATOR RCC  
 HEATING RATE 15 °C/min.  
 ATM. Atmos. Pressure  
 TIME CONSTANT 1 sec.

Y-AXIS  
 SCALE 20.27  $\frac{mV}{inch}$   
 (SCALE SETTING X 2)  
 SUPPRESSION 50 mg.

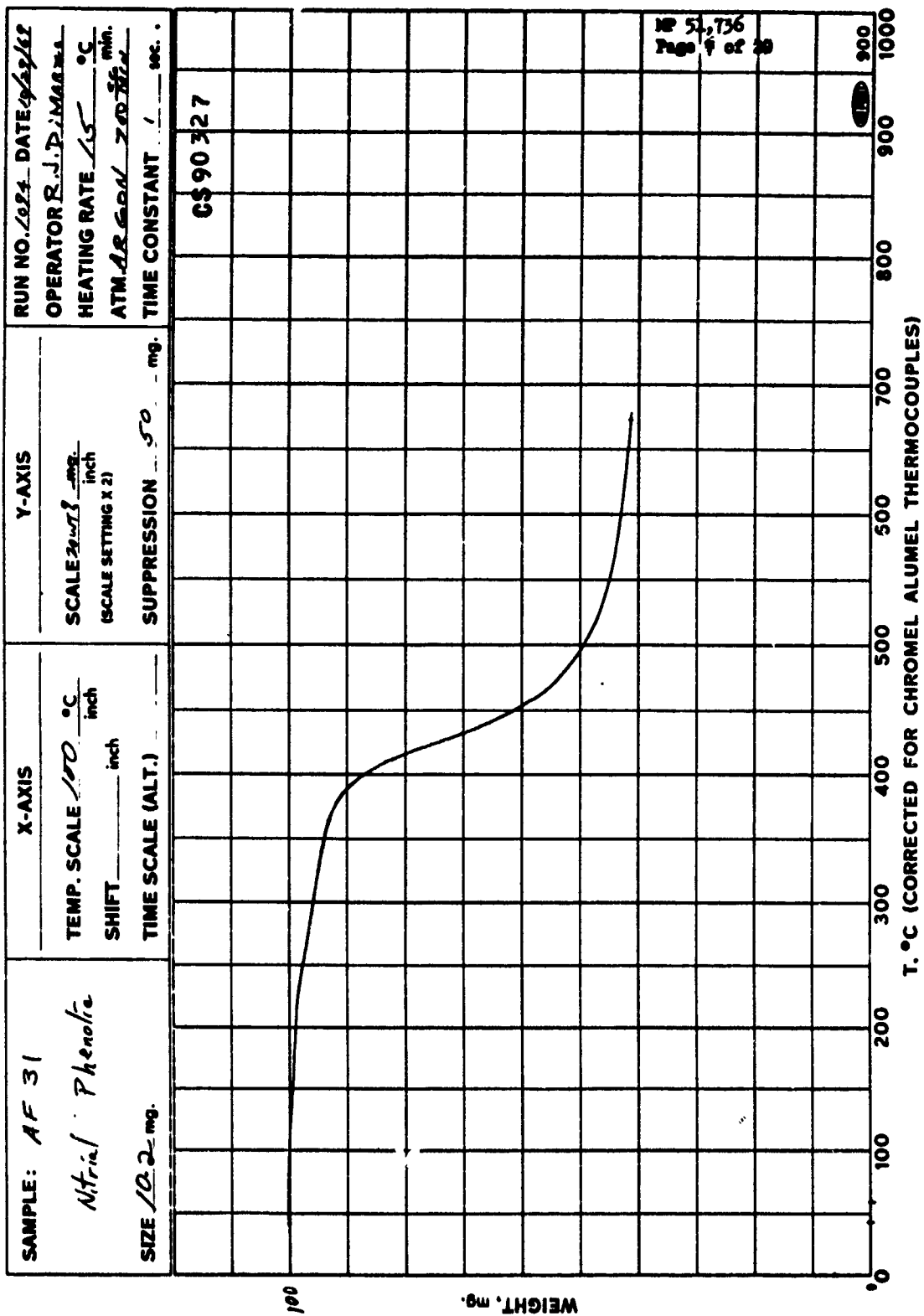
X-AXIS  
 TEMP. SCALE 100 °C/inch  
 SHIFT \_\_\_\_\_ inch  
 TIME SCALE (ALT.) \_\_\_\_\_

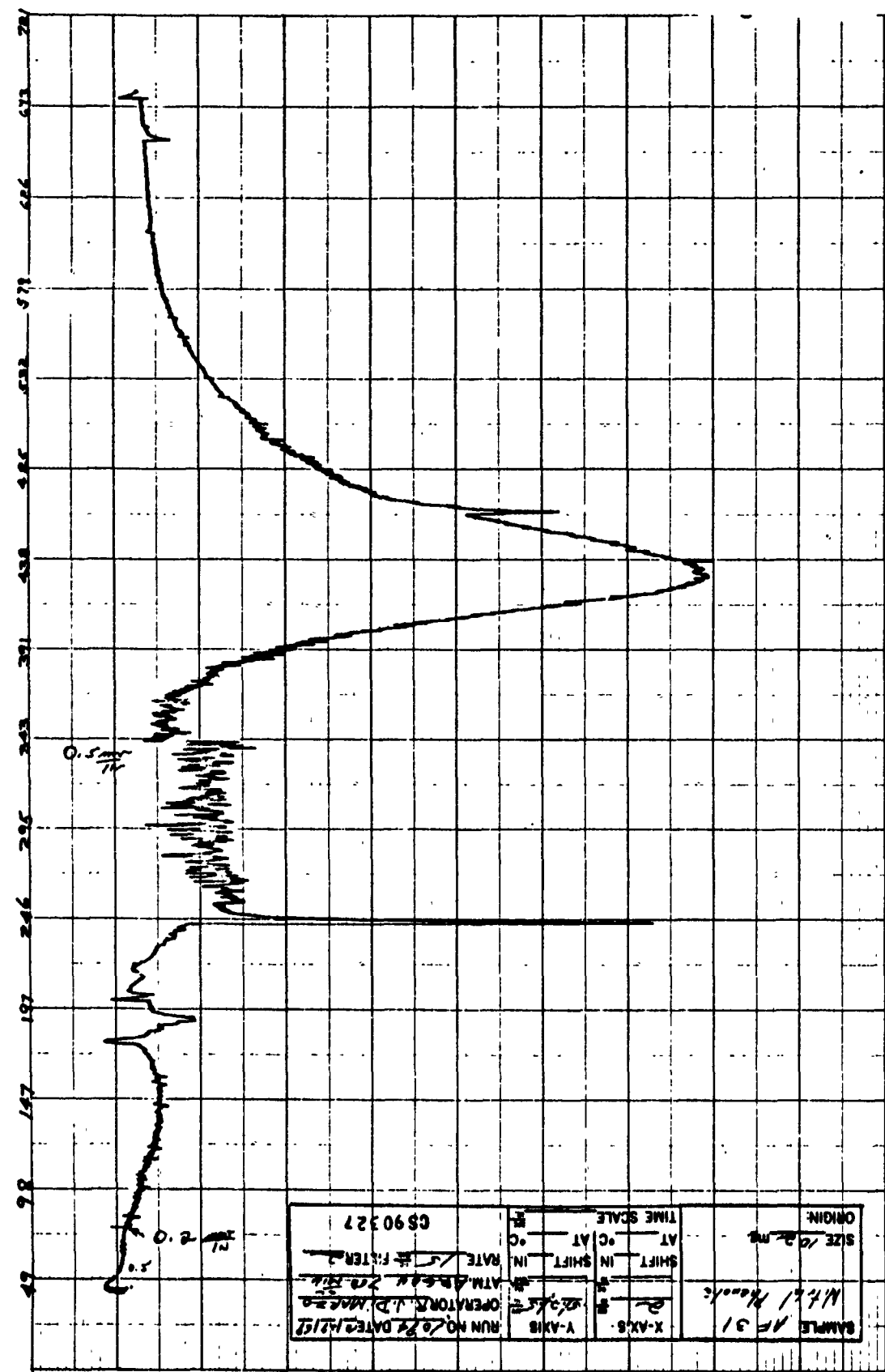
SAMPLE:  
AF 31  
Nitrid Phenolic  
 SIZE 2.7 mg.





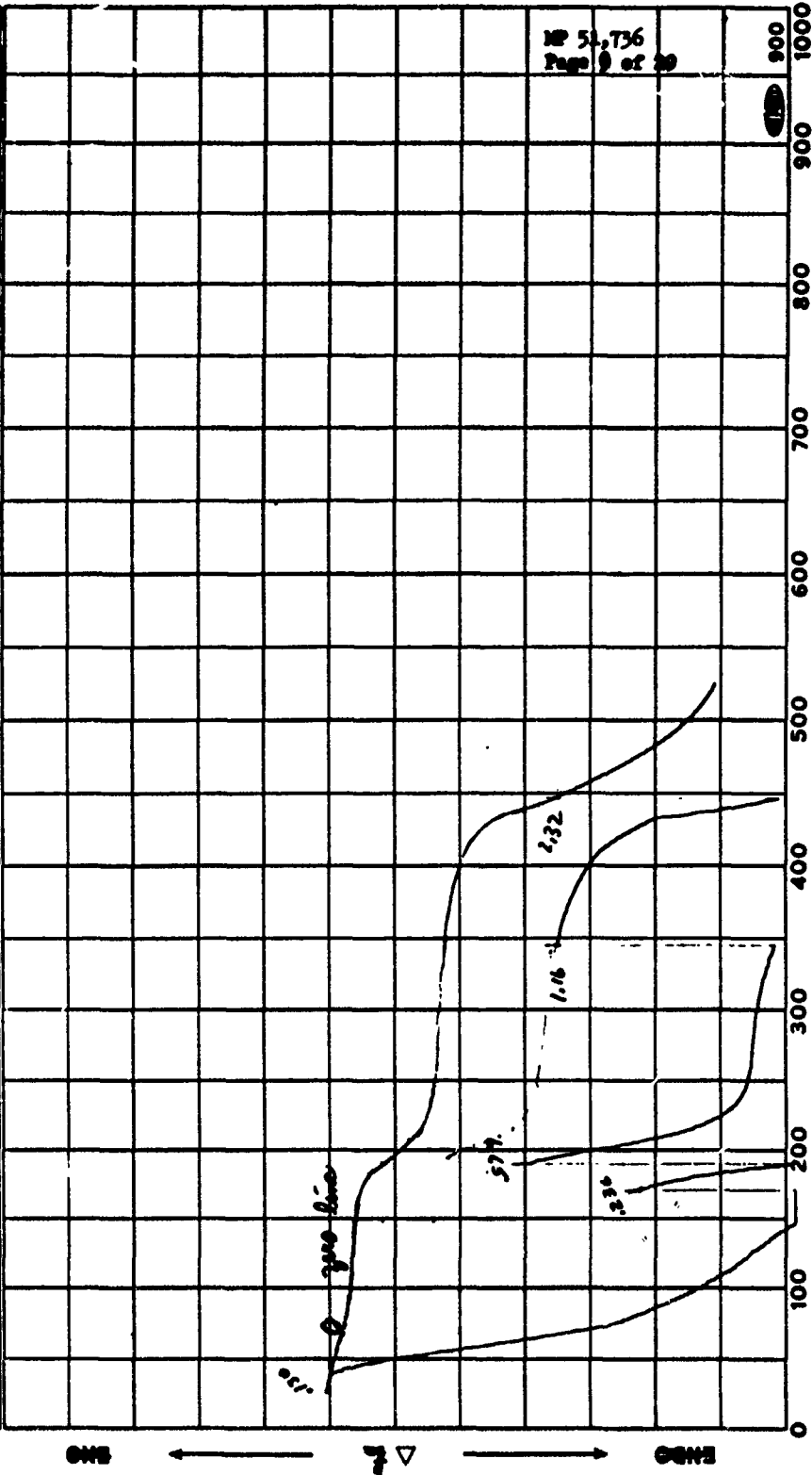
SAMPLE		AF 31		Mtr. 1		Mtr. 2		Mtr. 3		Mtr. 4	
SIZE		12.0 mg.									
ORIGIN											
X-AXIS	2	Y-AXIS	0.5	SHIFT	IN	IN	IN	IN	IN	IN	IN
TIME SCALE		AT	0	AT	0	AT	0	AT	0	AT	0
RUN NO.	1000	DATE	1/11/59	OPERATOR	RKC	ATM. No.	A	RATE	3	FILTER	2
CS90327											

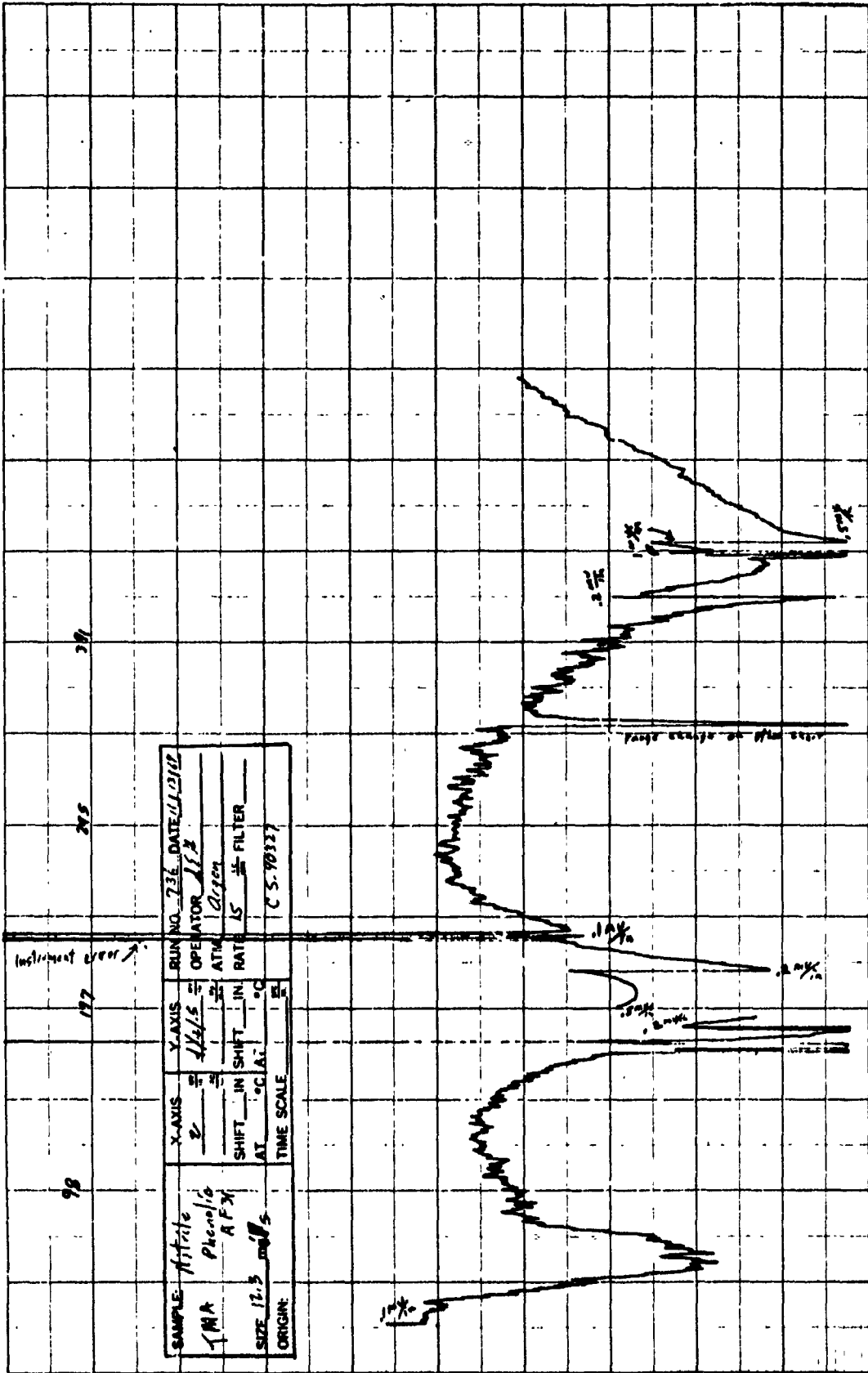


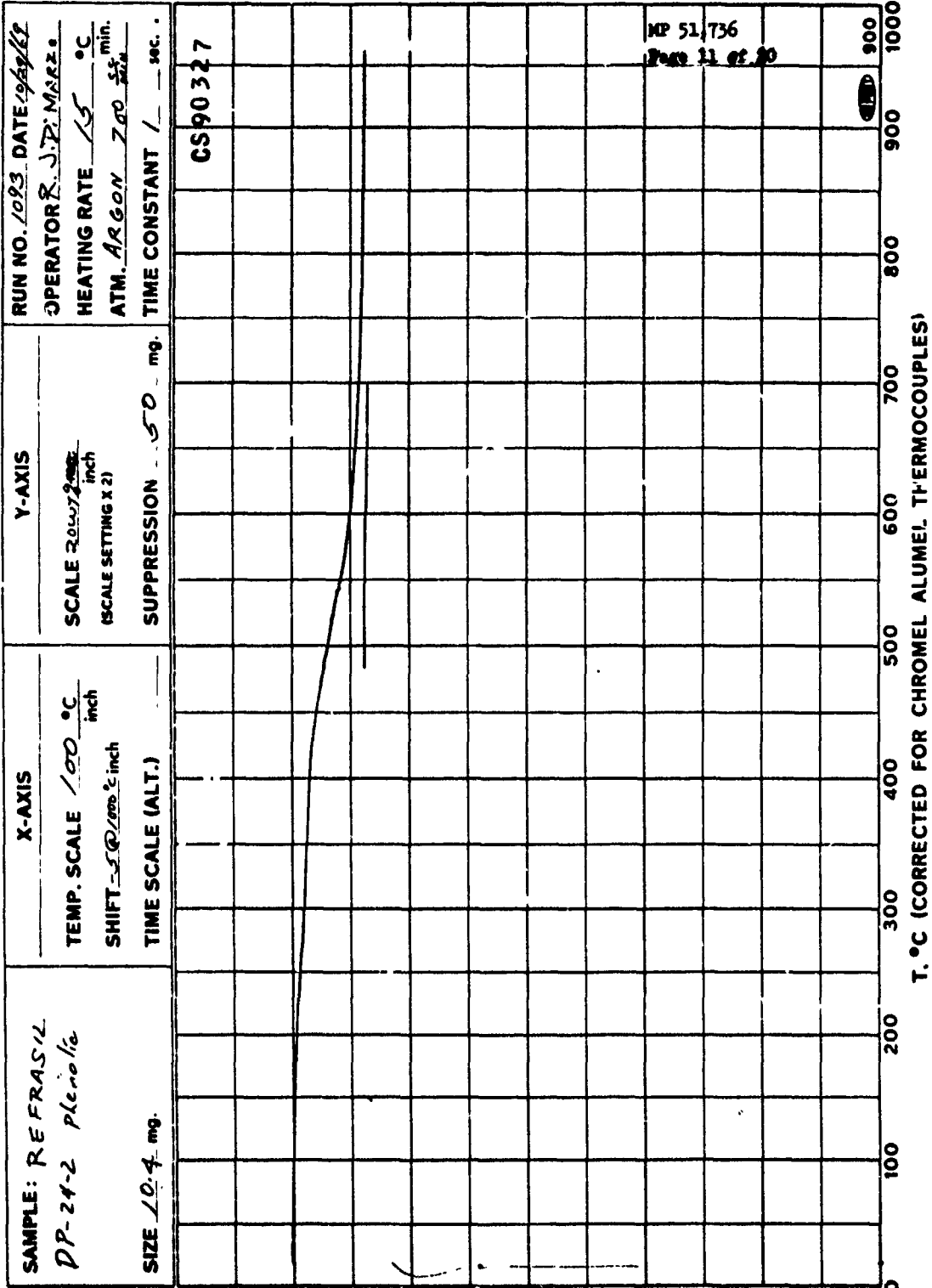


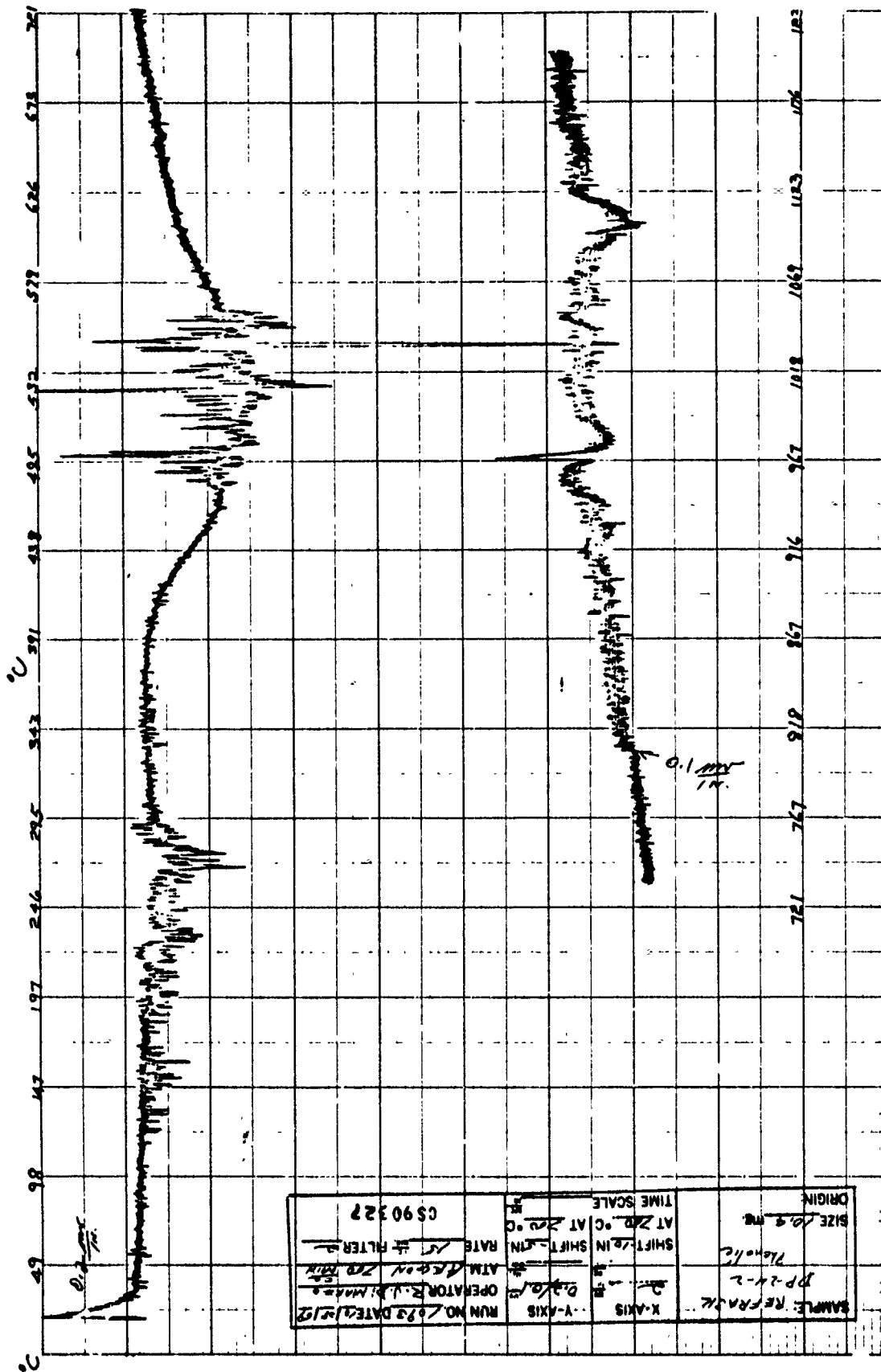
2

SAMPLE: Nitro Phenolic AF 31	SIZE 12.2 - 16	RUN NO. 726
	REF.	DATE 11/13/69
ORIGIN: Lead 22.5051	PROGRAM MODE Heat	OPERATOR JEA
	RATE 15 START °C	CS 90327
ATM. Argon		
	T	Δ T
	SCALE 100	1.00/2x
	SETTING .579/1.04/0.17	1/2







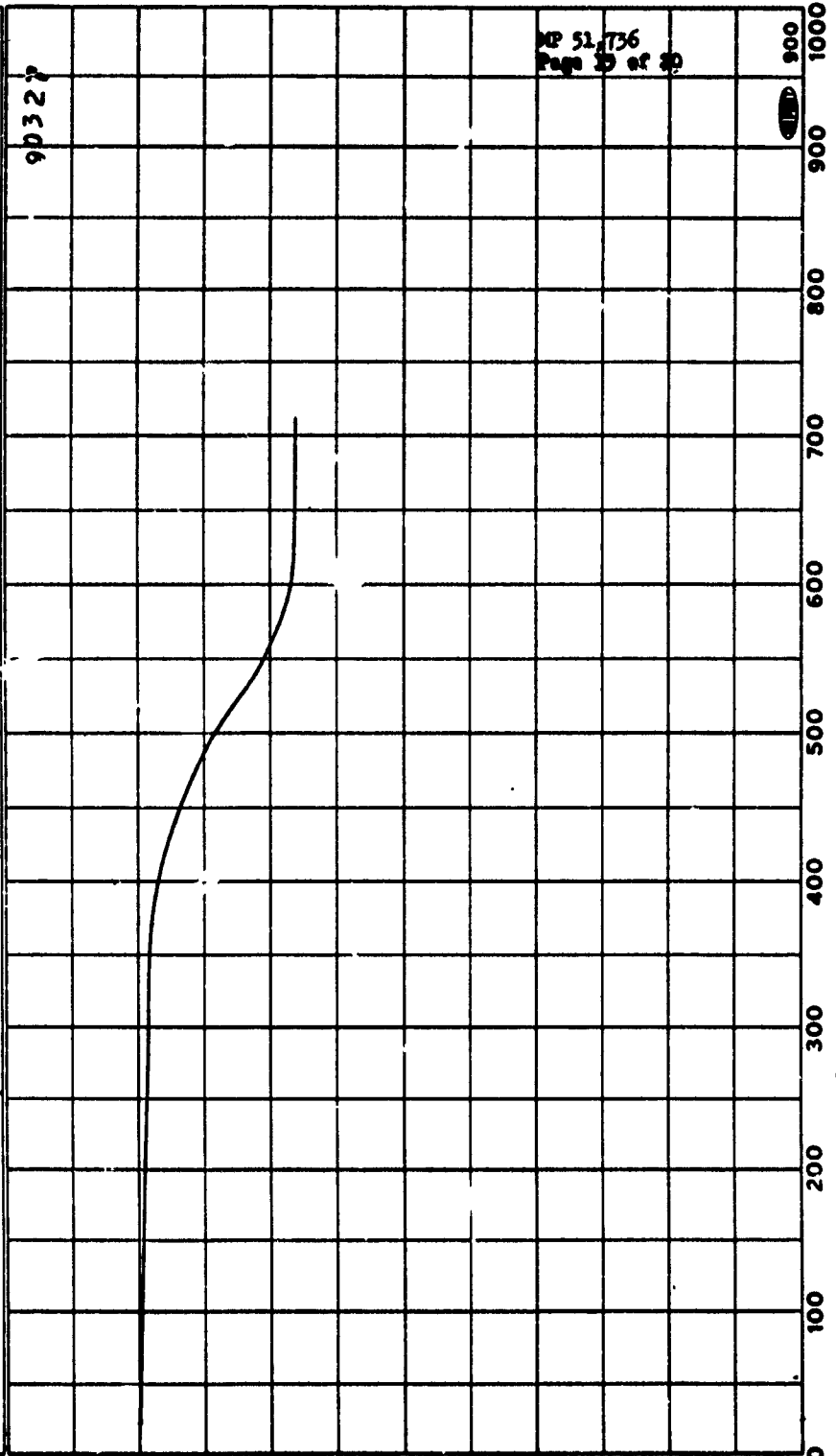


RUN NO. 1070 DATE 4-24-59  
 OPERATOR FCC  
 HEATING RATE 15 °C/min.  
 ATM. AL<sub>2</sub>O<sub>3</sub> 700  
 TIME CONSTANT 1 sec.

Y-AXIS  
 SCALE 20/10 inch  
 (SCALE SETTING X 2)  
 SUPPRESSION 50 mg.

X-AXIS  
 TEMP. SCALE 100 °C/inch  
 SHIFT \_\_\_\_\_ inch  
 TIME SCALE (ALT.) \_\_\_\_\_

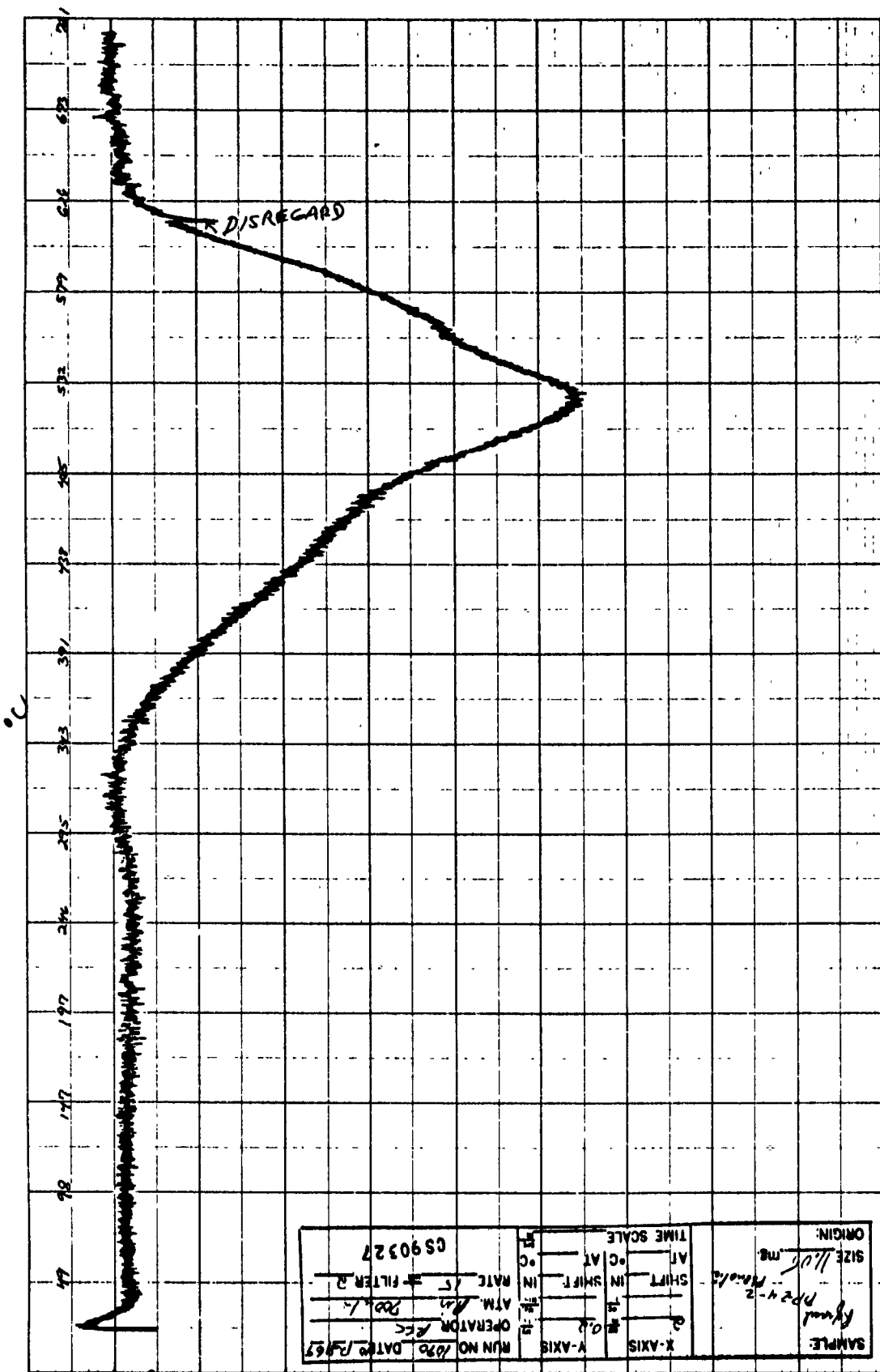
SAMPLE:  
REFRASIL  
DP-24-2 phenol<sub>2</sub>  
 SIZE 11.05 mg.



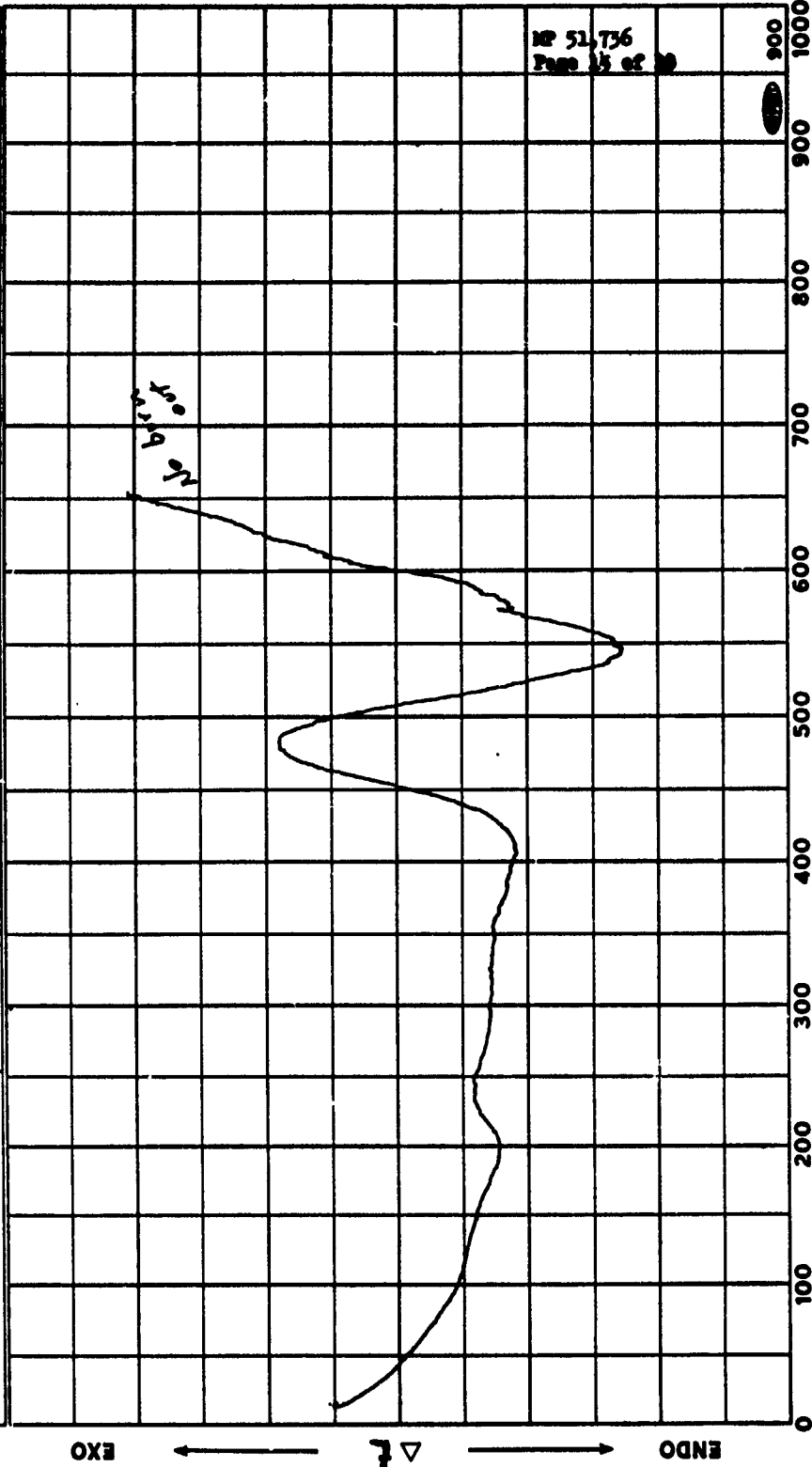
MP 51,736  
 Page 23 of 20

WEIGHT, mg.

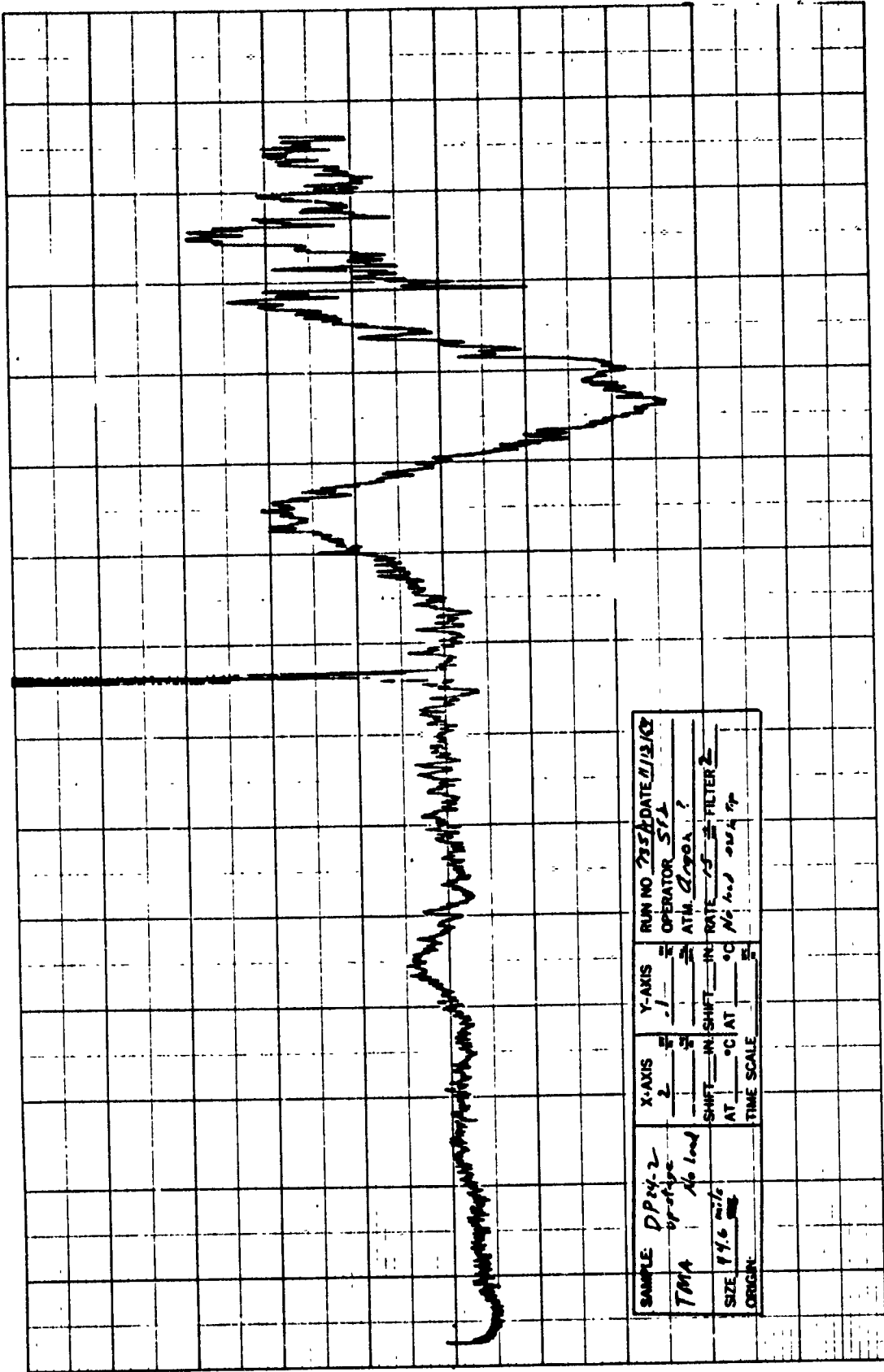
T. °C (CORRECTED FOR CHROMEL ALUMEL THERMOCOUPLES)



SAMPLE: TMA	DP 242 Retrasil No load	SIZE 44.6 mils	ATM. Argon	RUN NO. 726-721A
	ORIGIN:	REF.	T 100 SCALE SETTING	DATE 11/3/59
	PROGRAM MODE Heat	RATE 15	$\Delta T$ 130 mil	OPERATOR SG CS90327

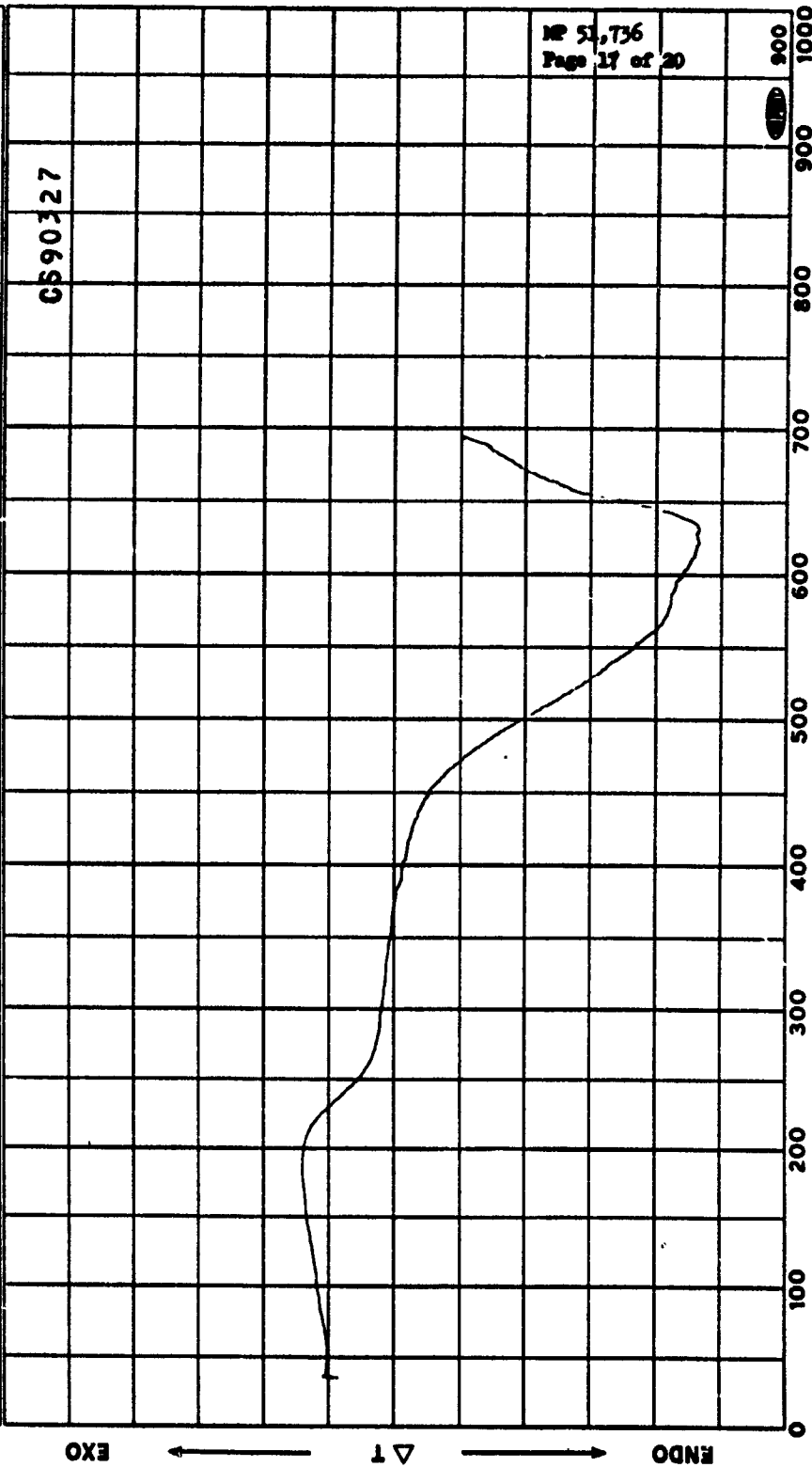


T, °C (CORRECTED FOR CHROMEL ALUMEL THERMOCOUPLES)

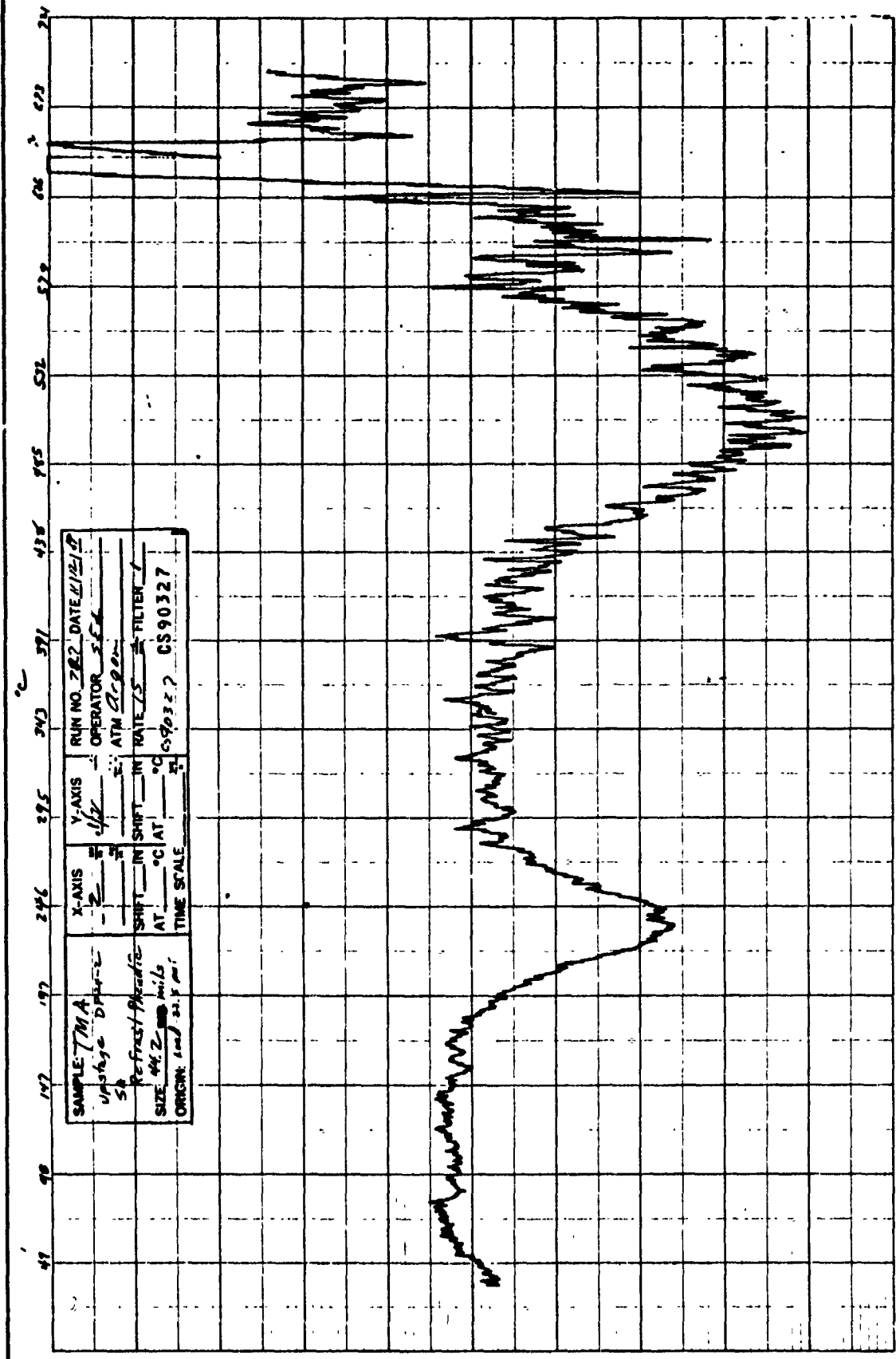


SAMPLE	DP 4.2	X-AXIS	2	Y-AXIS	1	RUN NO	733	DATE	11/2/62
TMA	up slope No low	SHIFT	IN	SHIFT	IN	OPERATOR	SFA		
SIZE	996 mils	AT	°C	AT	°C	ATM	CLYDA		
ORIGIN		TIME SCALE				RATE	5	FILTER	2
							16	had	only 7p

SAMPLE: DP-24-2  
 SIZE 44.2 mils  
 REF.  $\Delta T$   
 PROGRAM MODE Heat  
 RATE 15  $\frac{^\circ\text{C}}{\text{min}}$  START  $^\circ\text{C}$   
 ATM. Argon  
 SCALE SETTING 100  $\frac{\mu\text{V}}{^\circ\text{C}}$   
 RUN NO. 727  
 DATE 11/12/59  
 OPERATOR SFA  
 P.S. 90327



MP 51,736  
 Page 17 of 20



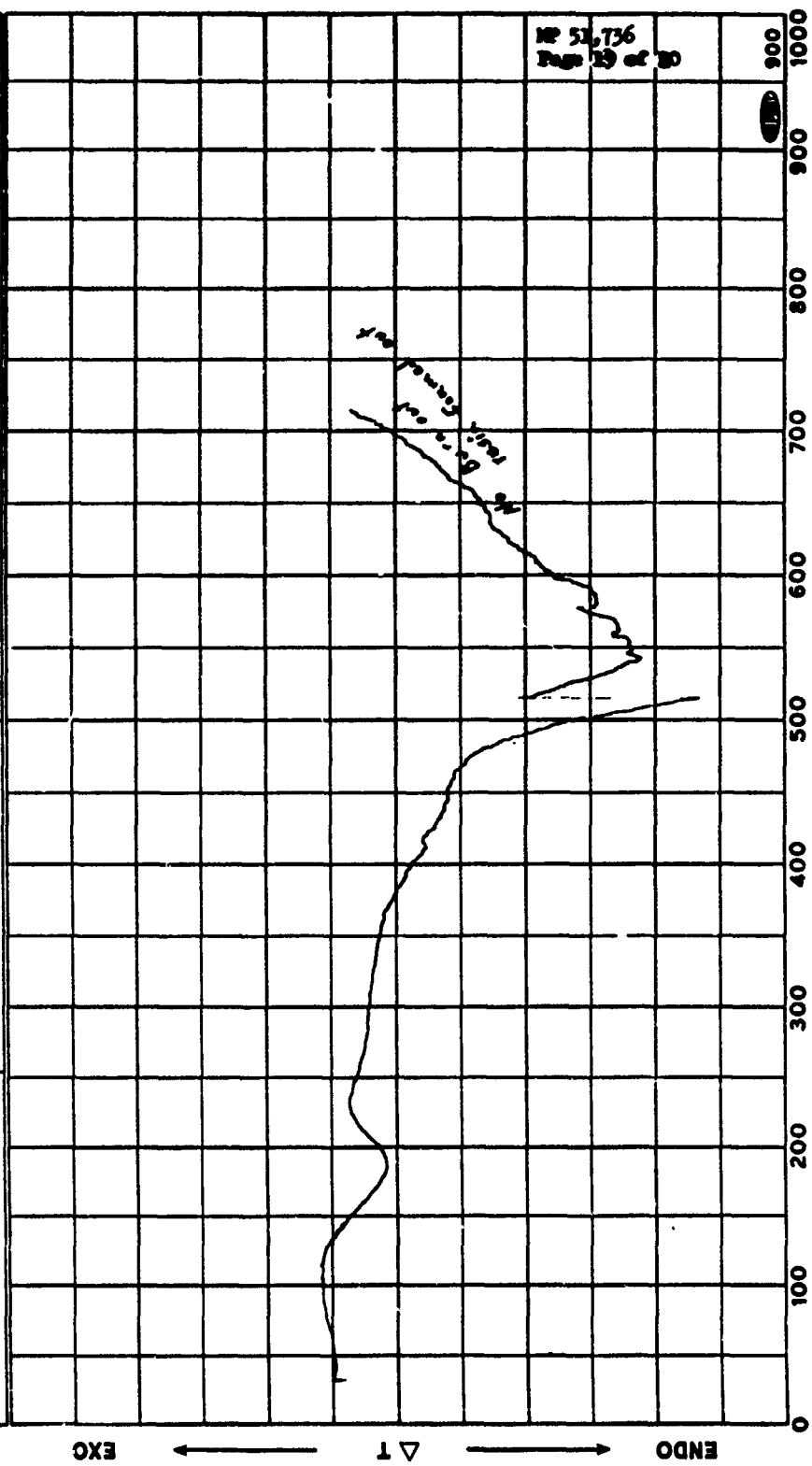
SAMPLE: TMA	X-AXIS	Y-AXIS	RUN NO. 282	DATE 11/21/82
upstage DPA-2	2	1/2	OPERATOR S.F.	
50			ATM 2000	
Refract/Refract	SHIFT	IN	RATE 25	FILTER 1
SIZE 4% 200 mesh	AT	°C	CS90327	CS90327
ORIGIN: 1000 20.5 ml	TIME SCALE			

SAMPLE: DP 24-2  
 TGA  
 ORIGIN:

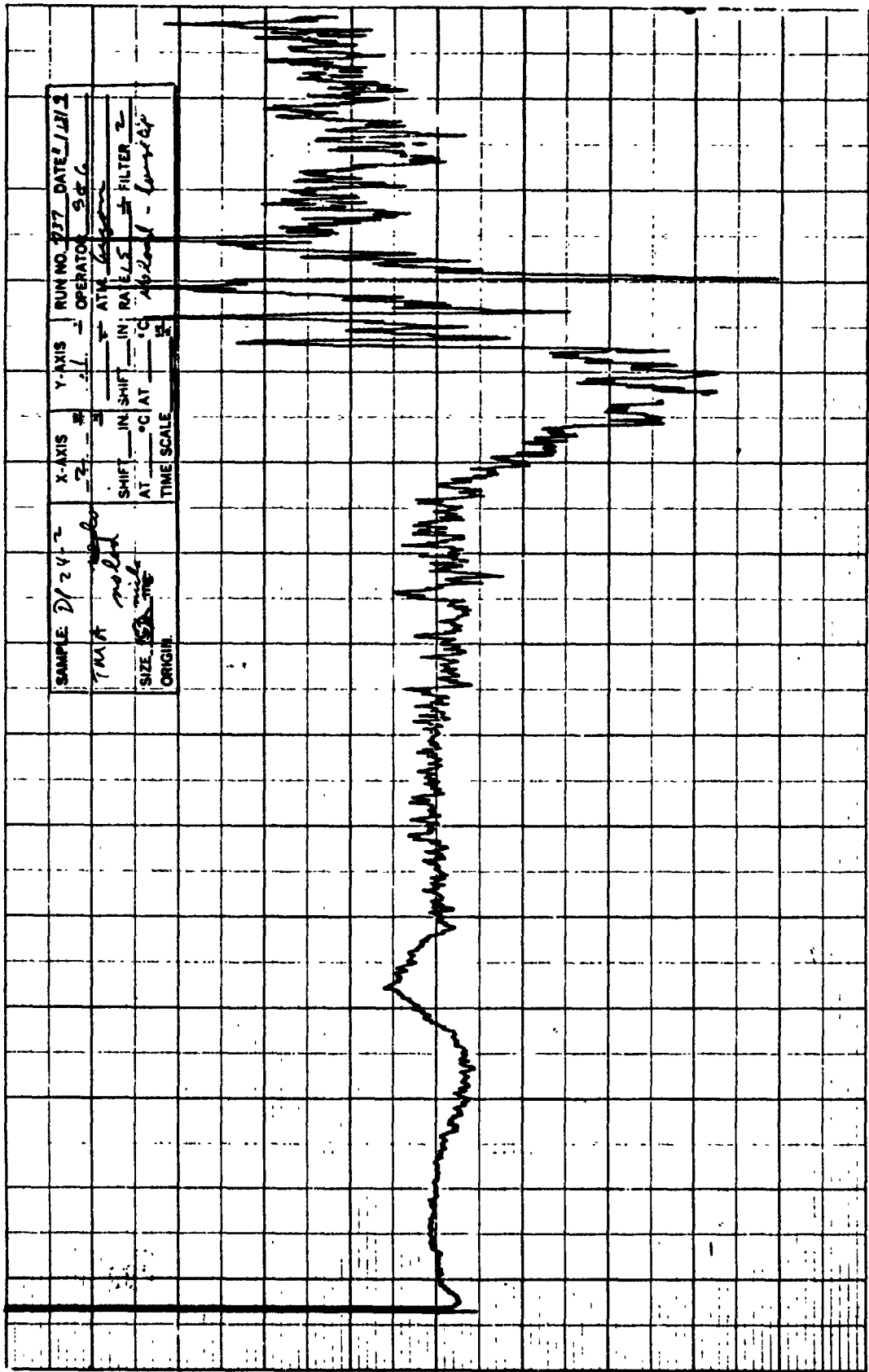
SIZE US-1 units  
 REF. \_\_\_\_\_  
 PROGRAM MODE rest  
 RATE 15 °C START °C

ATM. open  
 T Δ  
 SCALE 100 150  
 SETTING

RUN NO. 157  
 DATE 11/13/79  
 OPERATOR SEG  
C5903a7



T. °C (CORRECTED FOR CHROMEL ALUMEL THERMOCOUPLES)





MISSILE & SPACE SYSTEMS DIVISION  
DOUGLAS AIRCRAFT COMPANY, INC.

FORM 37-99 (REV. 1-62)

MATERIAL & PROCESS ENGINEERING  
LABORATORY REPORT

CATALOG NO. PDL 104345

SERIAL NO. MP 51,731

DATE 22 April 1970

TITLE 300°F CURE STUDIES OF C-100-96/DP24-2  
PREPREG AND AF31 FILM ADHESIVE FOR  
UpSTAGE

ASSIGNED TO R. W. Hunter, A-255

1. MATERIAL

- 1.1 C-100-96 Refrasil High Silica Fabric/DP24-2  
Phenolic Resin Prepreg  
Vendor Code: WB2262/96  
Western Backing  
Culver City, California
- 1.2 AF31 Film Adhesive - Nitrile phenolic adhesive  
Douglas Specifications DPM 3915 and STM 0030-04  
Vendor Lot: 22H  
3M Company  
St. Paul, Minnesota

2. OBJECT

- 2.1 To determine if a 3 hour cure cycle at 300°F is sufficient to cure the C-100-96/DP24-2 prepreg and AF31 adhesive.
- 2.2 To determine if a 3 hour cure cycle at 300°F will cause degradation in the mechanical properties of the C-100-96/DP24-2 prepreg or the AF31 adhesive.

3. PROCEDURE

3.1 Material Quality Control Tests

- 3.1.1 Prepreg incoming quality control tests were run in accordance with the requirements of the procedure in MRD 11247171, "Cloth, Impregnated-High Silica, Phenolic, Heavyweight."
- 3.1.2 Adhesive incoming quality control tests were run in accordance with the requirements of MMM-A-132, Type IV.

3.2 Cure Studies

3.2.1 Specimen Preparation -

Rectangular beams approximately 3/8 inch wide by 1-1/2 inches long were prepared from the prepreg and adhesive materials as follows:

### 3.2.1 (Cont'd)

One ply prepreg specimens were prepared. All specimens were cut with the same orientation.

AF31 adhesive is supplied as a thin calendered film. It was necessary to laminate plies of the film together to form a sheet of adequate thickness. The laminated sheets were given a short press pre-cure (10 minutes at 300°F and contact pressure) prior to preparation of the specimens. The pre-cure was found necessary to prevent foaming of the specimens at 300°F. The pre-cure time was included in the final cure time of the adhesive.

### 3.2.2 Cure Studies -

The vibrating reed apparatus (VRA) was used to monitor the 300°F cure cycles of the AF31 adhesive and C-100-96/DP24-2 prepreg. A specimen beam was clamped onto the vibrating reed driving rod in the VRA chamber and its room temperature resonance characteristics determined. The chamber was closed and heated to 300°F  $\pm$  5°F (approximately 6 minutes). The resonance characteristics of the specimen beam were periodically determined until the 3 hour cure cycle was completed. The test is nondestructive and a complete cure cycle can be monitored with a single specimen.

The resonance frequency characteristics measured during the test are a function of (1) the physical measurements and specific gravity of the specimen, and (2) the modulus and energy absorption characteristics of the material used to fabricate the specimen. Since the modulus and energy absorption characteristics are a function of cure, the resonance frequency will change as the cure progresses. Therefore, the VRA can be used to monitor cure cycles.

## 4. RESULTS

The results of the prepreg quality tests are contained in Table I. The adhesive quality control test data are contained in MP Report 51,732. The VRA cure data are contained in Figures 1 through 4.

## 5. SIGNIFICANCE OF DATA

### 5.1 AF31 Adhesive

The adhesive showed very little change in properties during the cure cycle, and in room temperature properties before and after cure.

The cure reaction that occurred took approximately 2 hours (110 minutes). No degradation was evident after 3 hours. The modulus increased as expected, as the temperature dropped, but the damping factors increased indicating that the glass transition of the adhesive is at or near room temperature.

5.2 C-100-96/DP24-2 Prepreg

The prepreg was 95% cured in approximately 1 hour as indicated by the change in modulus and damping factors, but the modulus had leveled off after 3 hours.

6. REFERENCES

MP Report 51,732  
TR 11392  
S.O. 3859-6320  
S.A. 7014  
EWO 11069  
TR 9940, Pg. 15  
TR 5988, Pg. 46

*RW Hunter*

---

R. W. Hunter  
Non-Metallics Materials Properties  
Materials & Methods -  
Research & Engineering

*F. P. Chiavetta*

---

F. P. Chiavetta, Section Chief  
Non-Metallics Materials Properties  
Materials & Methods -  
Research & Engineering

RWH:rtt  
2/11/70

TABLE I  
PREPREG PHYSICAL PROPERTIES

Material Description	Date of Test	% Resin Flow	% Volatile Content	% Resin Solids
C-100-96/DP24-2 Lot No. 9806 WB 2262/96	2-14-69	1 10.1	5.1	28.7
		9.9		
		2 10.8		
	3 11.8	5.1	29.2	
Average	10.7	5.1	28.9	
C-100-96/DP24-2 Lot No. 9806 WB 2262/96	10-30-69	1 11.7	4.2	31.2
		2 11.2		
		3 11.6		
	Average	11.5	4.3	29.9

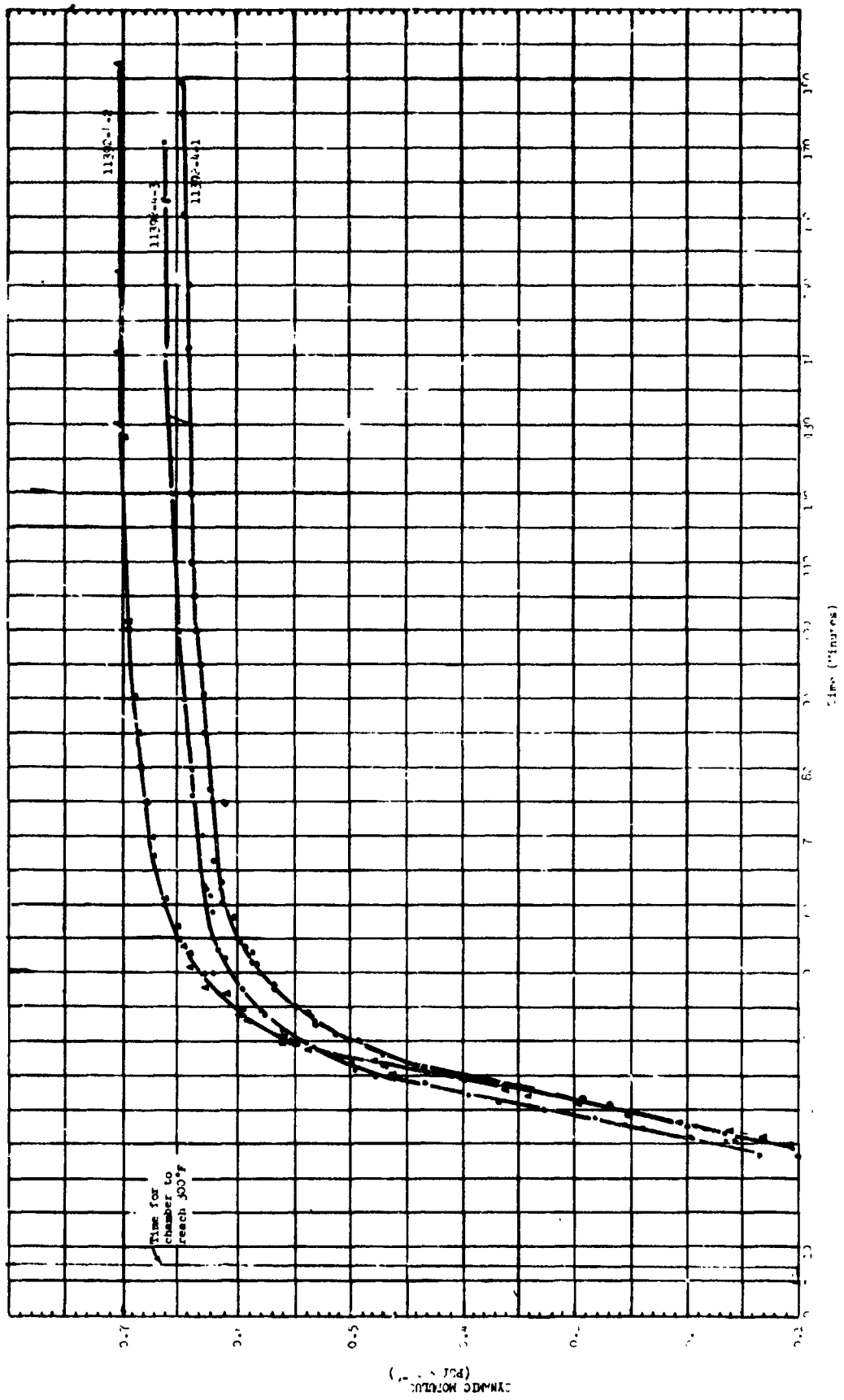


Figure 1. VRA Cure Data

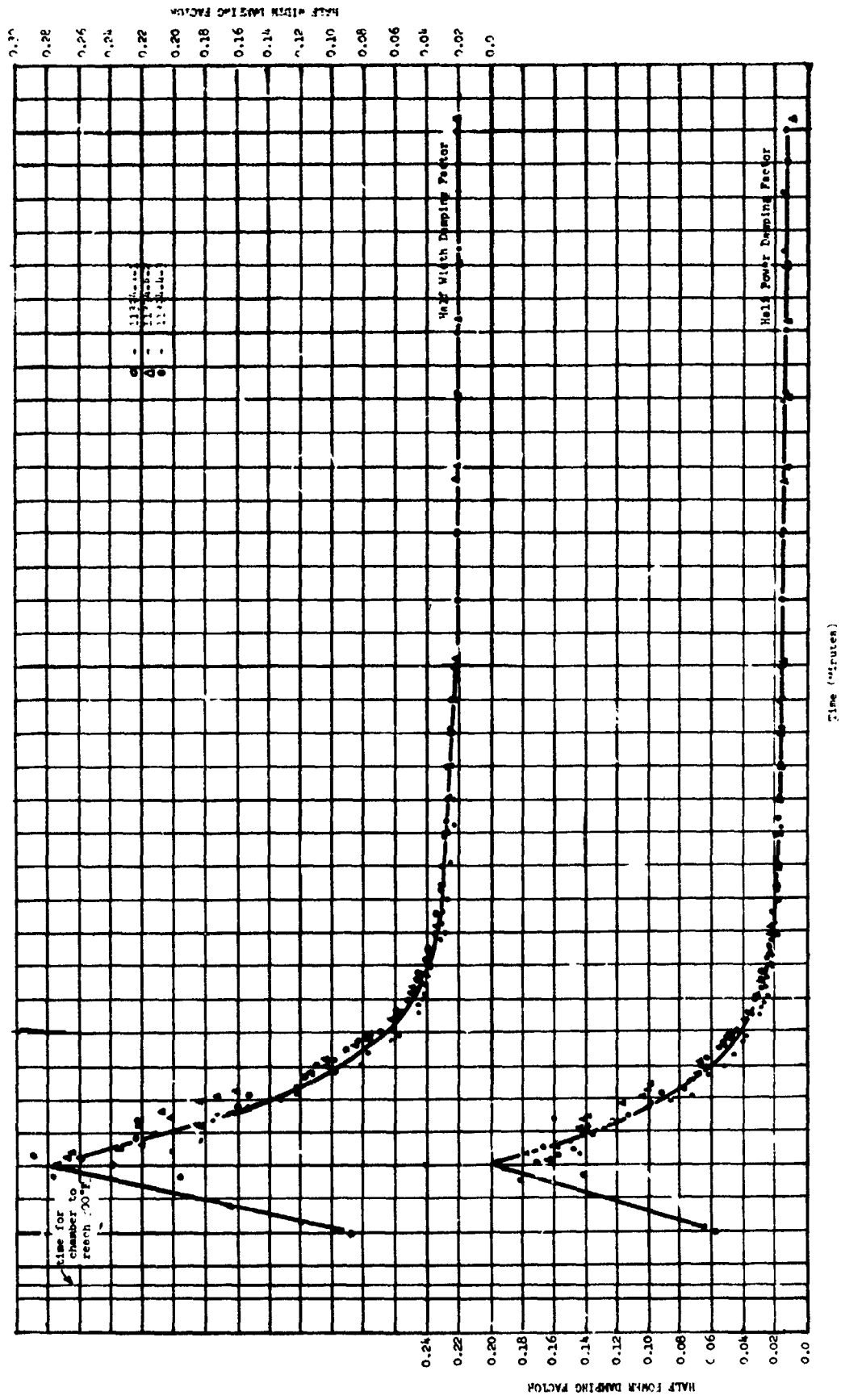


Figure 2. VRA Cure Data

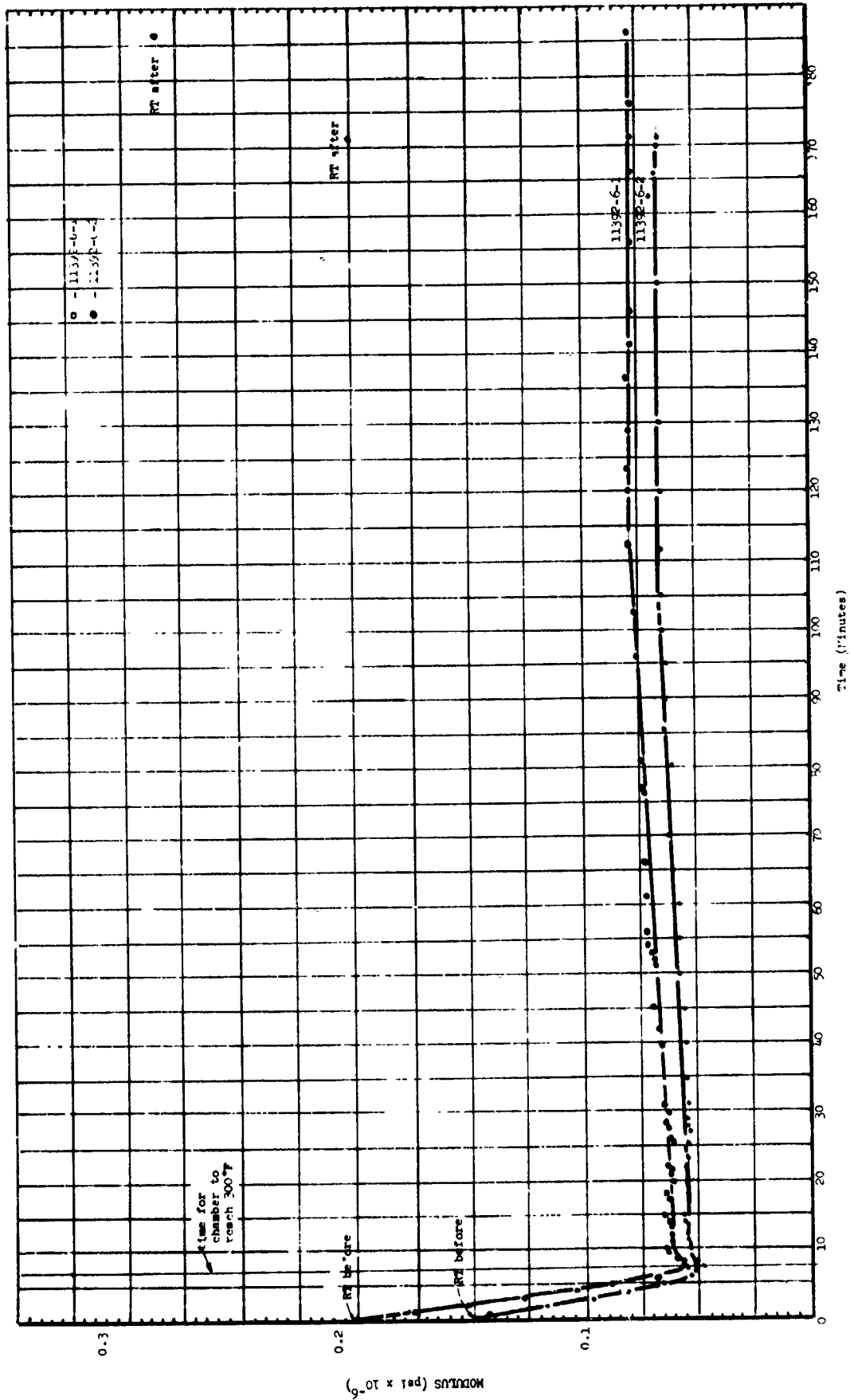


Figure 3. VRA Cure Data

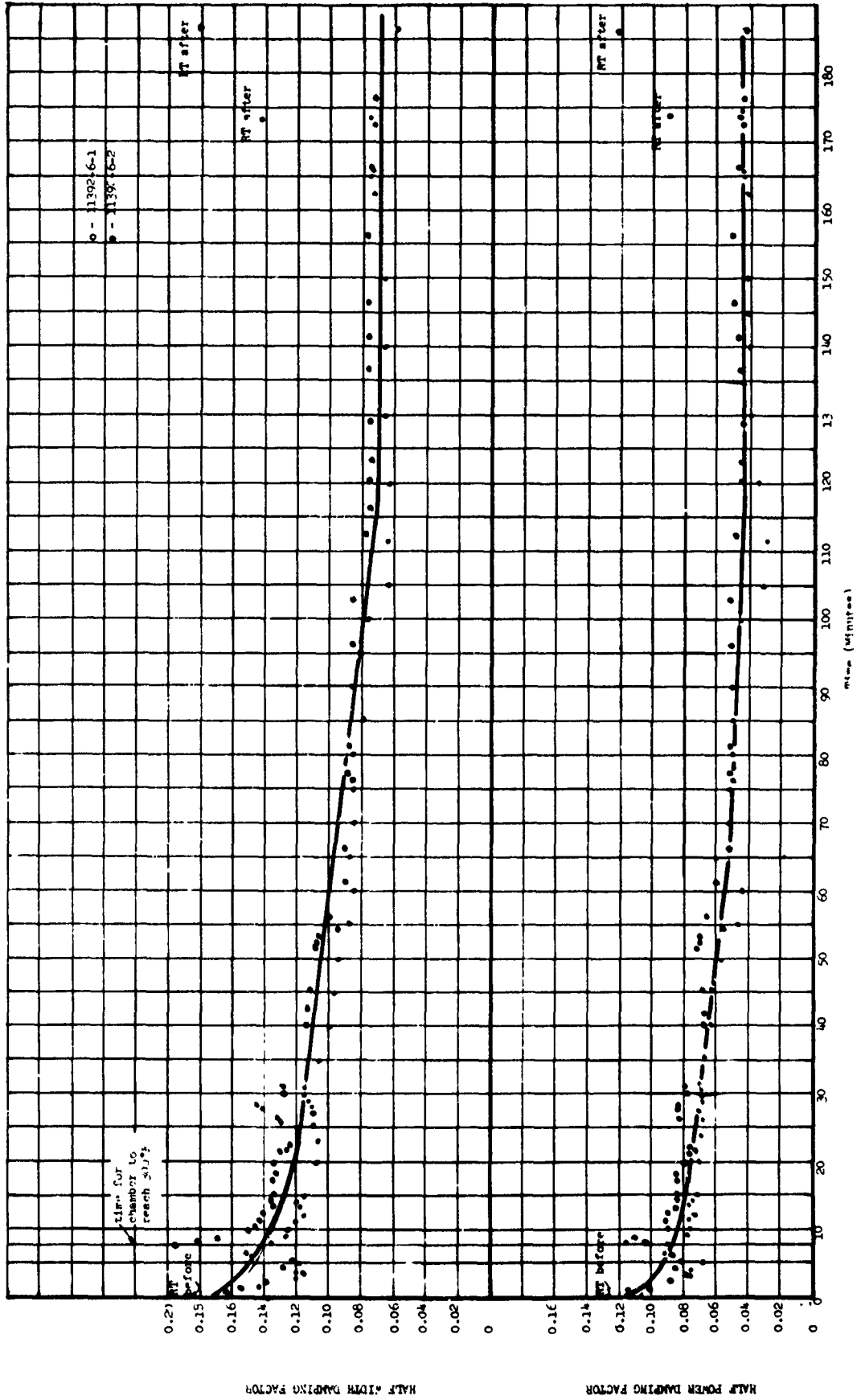


Figure 4. VRA Cure Data



MISSILE & SPACE SYSTEMS DIVISION  
DOUGLAS AIRCRAFT COMPANY, INC.

FORM 37-60 (REV. 1-62)

MATERIAL & PROCESS ENGINEERING  
LABORATORY REPORT

CATALOG NO. PDL 104348  
SERIAL NO. MP 51,732

DATE 23 April 1970

TITLE PLASMA JET SPECIMEN PREPARATION

ASSIGNED TO F. B. Jones, A-256

1. MATERIALS

- 1.1 AF31 Film Adhesive, Batch 22H  
DPM 3915, STM 0030-03  
3M Company  
St. Paul, Minnesota
- 1.2 EC 1459 Adhesive Primer, Batch 5B8P  
DPM 2131, 9020212  
3M Company  
St. Paul, Minnesota
- 1.3 C-100-96 Refrasil/DP24-2 Phenolic Resin Prepreg  
Lot No. 9806  
Vendor Designations: WB 2262/96  
Ferro-Cordo Corp., Culver City, Calif.
- 1.4 HT-424 .08 PSF Film Adhesive, Batch B-7377  
DPM No. 2857, 9709014, Type I  
American Cyanamid Company  
Havre de Grace, Maryland
- 1.5 HT-424B Adhesive Primer, Batch 105  
DPM 2978, 9709475  
American Cyanamid Company  
Havre de Grace, Maryland
- 1.6 Aluminum Alloy 2024-T3 clad .032 x 1 x 10 inches
- 1.7 Aluminum Alloy 2024-T3 clad .020 x 1 x 10 inches
- 1.8 Aluminum Alloy 2014-T6 bare .063 x 1 x 3 inches

2. OBJECTIVE

The proposed method of insulating the UpSTAGE airframe involves adhesive bonding of a single layer of phenolic Refrasil to the structure, using AF31 Film Adhesive and using a lay-up and curing process developed earlier in the Program. To confirm the thermal and mechanical design criteria using this material and process, plasma jet test specimens were prepared and mechanical strength data were developed for AF31 Film Adhesive.

2. OBJECTIVE (Cont'd)

Note: During the plasma jet tests, the AF31 bondline reached a higher temperature than that predicted and the adhesive failed. Afterwards, the plasma jet test was repeated (with a selected specimen configuration) substituting HT-424 Film Adhesive. The HT-424 material proved to be satisfactory. The results of the plasma jet tests are being reported by the cognizant design group.

3. PROCEDURES

3.1 Prepreg Physical Property Tests

Incoming quality control to determine per cent resin flow, volatiles and resin solids on the C-100-96 Refrasil DP24-2 phenolic resin prepreg was conducted per MRD 11247171 - Cloth, Impregnated-High Silica Phenolic, Heavyweight. For results, see Table VII (Prepreg Physical Properties).

3.2 Specimen Preparation - Quality Control AF-31 per MMM-A-132

The aluminum specimens were prepared for bonding per 1P00094, Type I (hot etch). The aluminum was primed with EC-1459 (9020212) and air dried 30 minutes at room temperature followed by 30 minutes at  $67 \pm 6^\circ\text{C}$  ( $170 \pm 10^\circ\text{F}$ ). The AF31 was applied and the lapshear specimens and T-peel specimens were cured one hour at  $177^\circ\text{C}$  ( $350^\circ\text{F}$ ) under vacuum and 50 psig autoclave pressure. Specimen configuration was per Federal Test Method Standard No. 175, Method 1033.1 for the lap shears and per ASTM 1876 for the T-peels.

3.3 Specimen Preparation - Quality Control HT-424

The quality control specimens were fabricated, cured and tested per above paragraph 3.2, except that the cure was for 3 hours at  $300^\circ\text{F}$ .

3.4 Specimen Preparation - Mechanical Properties AF31

The mechanical property specimens were prepared per the design constraints requiring the non-standard cure at  $149^\circ\text{C}$  ( $300^\circ\text{F}$ ) rather than  $177^\circ\text{C}$  ( $350^\circ\text{F}$ ) and grit blast surface preparation. The lower cure temperature was imposed to stay below the maximum allowable heat which could be tolerated by the 2024-T6 aluminum substructure material. Grit blasting was required instead of etching to eliminate acid residues which could contaminate the substructure. The aluminum was primed and dried per 3.2 above. The specimens were cured 3 hours at  $149^\circ\text{C}$  ( $300^\circ\text{F}$ ) under vacuum and at 50 psig autoclave pressure. The single lap shear specimen configuration was per Federal Test Method Standard No. 175 Method 1033.1. The double lap shear specimen configuration was per Figure 1. The bell-peel specimen configuration was per DLP 13.012.

Note: Mechanical property specimens were not required per SA 7014 (Phase I) for HT-424 adhesive, since this requirement was introduced after completion of Phase I.

### 3.5 Specimen Preparation - Plasma Jet (AF31 Bonded)

The aluminum substructure was prepared for bonding by hand sanding with #400 grit paper and followed by solvent wiping, per 1P00094 - Type IV. The aluminum was primed with EC 1459 (9020212) and air dried 30 minutes at room temperature followed by 30 minutes at 67°C (170° + 10° F). The AF31 film adhesive (MM-A-132) was applied to the specimens and lightly heat tacked into position prior to application of the Refrasil. The Refrasil was positioned with the fill in the longitudinal direction; the specimens were bagged (in groups of four) and the materials were cured 3 hours at 149°C (300°F) under vacuum (25" to 28" Hg) and 50 psig autoclave pressure. The plasma jet specimens were fabricated per 1T 36044B. See Figures 2, 3, 4, 5, and 6.

### 3.6 Specimen Preparation - Plasma Jet (HT-424 Bonded)

The surfaces were prepared for bonding per 1P00094-Type IV similar to those of paragraph 3.5 above. The aluminum was primed with HT-424B (9709475) and air dried 30 minutes at room temperature followed by 30 minutes at 67 + 6°C (170° + 10° F). The 0.08 pounds per square foot HT-424 adhesive film (9709014-Type I) was applied to the specimen, the Refrasil was positioned and the specimens were cured per paragraph 3.5 above. Three plasma jet specimens were fabricated per the -505 configuration (Figure 4).

## 4. TEST METHODS

The single shear specimens were tested at 600 to 700 pounds per minute. The T-peel and Bell-peel specimens were tested at 3 inches per minute. The elevated temperature specimens were soaked 10 minutes at test temperature in a convection oven and tested in situ.

## 5. RESULTS

- 5.1 The thickness of the cured and bonded Refrasil on each plasma jet specimens appears in Table I.
- 5.2 The density of the cured Refrasil was 1.32 grams per cubic centimeter.
- 5.3 The mechanical strength test data of AF31 adhesive are tabulated in Table II, III and IV. The quality control test data appear in Tables V and VI for the AF31 and HT-424 adhesives.

## 6. SIGNIFICANCE OF DATA

- 6.1 The overall thickness of the cured insulation on the plasma jet specimens was less than that of the total thickness of the uncured material (consisting of primer, adhesive and B-stage Refrasil). The B-stage Refrasil is porous and the curing process allows the adhesive and Refrasil resins to intermix and densify.

- 6.2 The mechanical strength data of AF31 adhesive is representative of the process originally proposed for the design and is identical to that employed in producing the plasma jet specimens. Data are tabulated on Tables II, III and IV. These data indicate that AF31 adhesive with EC-1459 primer is heat stable to at least 260°C (500°F), which is 111°C (200°F) above the predicted glue-line temperature originally expected during the plasma jet tests.
- 6.3 The HT424 quality control data recorded in Table VI exceeds the 2250 psi lapshear strength requirements of Specification 9709014 at room temperature. No specification requirement exists for aluminum lapshear specimens (grit blasted surface preparation) when tested at 260°C (500°F). Additional HT424 adhesive mechanical test data and thermal property test data were not run, because they had been generated for prior missile and space projects like Zeus, Spartan and Saturn.

*F. B. Jones*  
\_\_\_\_\_  
F. B. Jones  
Non-Metallics Materials Properties  
Materials & Methods -  
Research & Engineering

*F. P. Chiavetta*  
\_\_\_\_\_  
F. P. Chiavetta, Section Chief  
Non-Metallics Materials Properties  
Materials & Methods -  
Research & Engineering

FBJ:rtt  
2/12/70

TABLE I

Thickness of Cured Refrasil  
Plus Cured Adhesive

AF31/EC 1459

Specimen Number	Overall Average Thickness (Inches)
501-2	.048
505-1	.061
505-2	.061
507-1	.060
509-1	.055
509-2	.055

Thickness of Cured Refrasil  
Plus Cured Adhesive

HT424/HT424B

Specimen Number	Overall Average Thickness (Inches)
505-4	.053
505-5	.051
505-7	.050

TABLE II  
AF31/EC1459  
Mechanical Properties Data  
(Grit Blast Surface Preparation)

Lap Shear at Ambient Temperature

Specimen No.	Type Lap	Load Pounds	Lap Inches	Stress psi	Failure	
1	Single	1500	.48	3120	Primer/Metal	
2	Single	1502	.48	3125	Primer/Metal	
3	Single	1502	.48	3125	Primer/Metal	
4	Single	1450	.48	3020	Primer/Metal	
5	Single	1425	.48	2970	Primer/Metal	
6	Single	1585	.48	3300	Primer/Metal	
7	Single	1500	.48	3120	Primer/Metal	
8	Single	1470	.48	3060	Primer/Metal	
9	Single	1570	.48	3270	Primer/Metal	
10	Single	1525	.48	3180	Primer/Metal	
				Average	3129	
11	Double	3410	.48	3550	Primer/Metal	
12	Double	3530	.48	3680	Primer/Metal	
13	Double	3412	.48	3550	Primer/Metal	
14	Double	3490	.48	3640	Primer/Metal	
15	Double	3555	.48	3700	Primer/Metal	
16	Double	3490	.48	3640	Primer/Metal	
17	Double	3585	.48	3740	Primer/Metal	
18	Double	3600	.48	3755	Primer/Metal	
19	Double	3630	.48	3780	Primer/Metal	
20	Double	3320	.48	3460	Primer/Metal	
				Average	3650	

TABLE III  
AF31/EC1459  
Mechanical Properties Data  
(Grit Blast Surface Preparation)

Lap Shear at 260°C (500°F)

Specimen No.	Type Lap	Load Pounds	Lap Inches	Stress psi	Failure
21	Single	250	.48	520	Primer/Metal
22	Single	232	.48	483	Primer/Metal
23	Single	249	.48	519	Primer/Metal
24	Single	258	.48	537	Primer/Metal
25	Single	245	.48	510	Primer/Metal
26	Single	286	.48	596	Primer/Metal
27	Single	250	.48	520	Primer/Metal
28	Single	261	.48	543	Primer/Metal
29	Single	273	.48	568	Primer/Metal
30	Single	252	.48	525	Primer/Metal
				—	
				Average	532
31	Double	364	.48	**	Primer/Metal
32	Double	510	.48	532	Primer/Metal
33	Double	751	.48	784	Primer/Metal
34	Double	525	.48	546	Primer/Metal
35	Double	438	.48	456	Primer/Metal
36	Double	590	.48	615	Primer/Metal
37	Double	668	.48	696	Primer/Metal
38	Double	620	.48	646	Primer/Metal
39	Double	640	.48	629	Primer/Metal
40	Double	566	.48	590	Primer/Metal
				—	
				Average	610

\*\* Outlier at approximately 90% confidence level and not included in average

TABLE IV  
AF31/EC1459  
Mechanical Properties Data  
(Grit Blast Surface Preparation)  
Bell-Peel (.063 to .020 Metal)  
Ambient Temperature

Specimen No.	Load Pounds Per Inch	Failure
1	14	Primer to .020 Metal
2	16	Primer to .020 Metal
3	15	Primer to .020 Metal
4	16	Primer to .020 Metal
5	17	Primer to .020 Metal
6	14	Primer to .020 Metal
7	17	Primer to .020 Metal
8	16	Primer to .020 Metal
9	16	Primer to .020 Metal
10	16	Primer to .020 Metal
	—	
Average	16	

TABLE V

Quality Control Data  
(Hot Etch Surface Preparation)

AF 31 22H Adhesive  
EC 1459 5B8P Primer

Single Lap Shear

Test Temp.	Load Pounds	Overlap Inches	Stress psi	Failure
R.T.	1800	.48	---	*
	2260	.48	4708	Cohesive
	2200	.48	4583	Cohesive
	2340	.48	4875	Cohesive
	2015	.48	4198	Cohesive
	Average			4591
+260°C (500°F)	500	.48	1042	Primer to Metal
	580	.48	1208	Primer to Metal
	605	.48	1260	Primer to Metal
	595	.48	1240	Primer to Metal
	560	.48	1167	Primer to Metal
	Average			1183

T-Peel

Test Temp.	Load Pounds/Inch	Failure
R.T.	25	Cohesive
	25	Cohesive
	26	Cohesive
	21	Cohesive
	24	Cohesive
Average		24

\* Metal failure when pinhole failed in bearing  
D-48

TABLE VI

Quality Control Data  
(Grit Blast Surface Preparation)

HT-424 .08 PSF Batch B7377  
HT-424B Primer Batch 105

Single Lap Shear

Test Temp.	Load Pounds	Overlap Inches	Stress psi	Failure
R.T.	1415	0.50	2830	100% Cohesive
	1430	0.50	2860	100% Cohesive
	1460	0.50	2920	100% Cohesive
	1395	0.50	2790	100% Cohesive
	1405	0.50	2810	100% Cohesive
				Average
+260°C (500°F)	460	0.50	920	100% Cohesive
	490	0.50	980	100% Cohesive
	482	0.50	964	100% Cohesive
	500	0.50	1000	100% Cohesive
	407	0.50	814	100% Cohesive
				Average

TABLE VII

Prepreg Physical Properties

Material	Date of Test	% Resin Flow	% Volatile Content	% Resin Solids
C-100-96/DF24-2	10-30-69	11.7	4.2	31.2
Lot No. 9806		11.2	4.5	30.4
WB 2262/96		11.6	4.3	29.9
		—	—	—
	Average	11.5	4.3	30.5

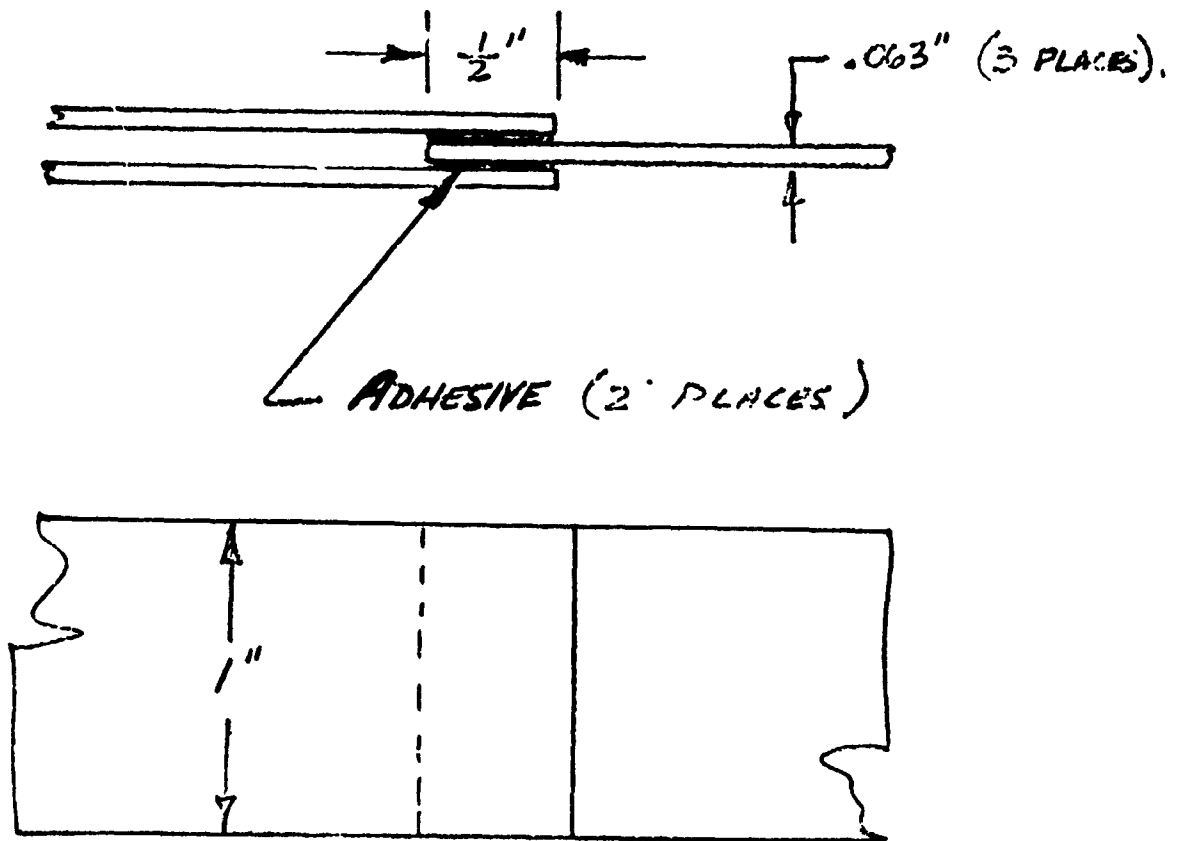
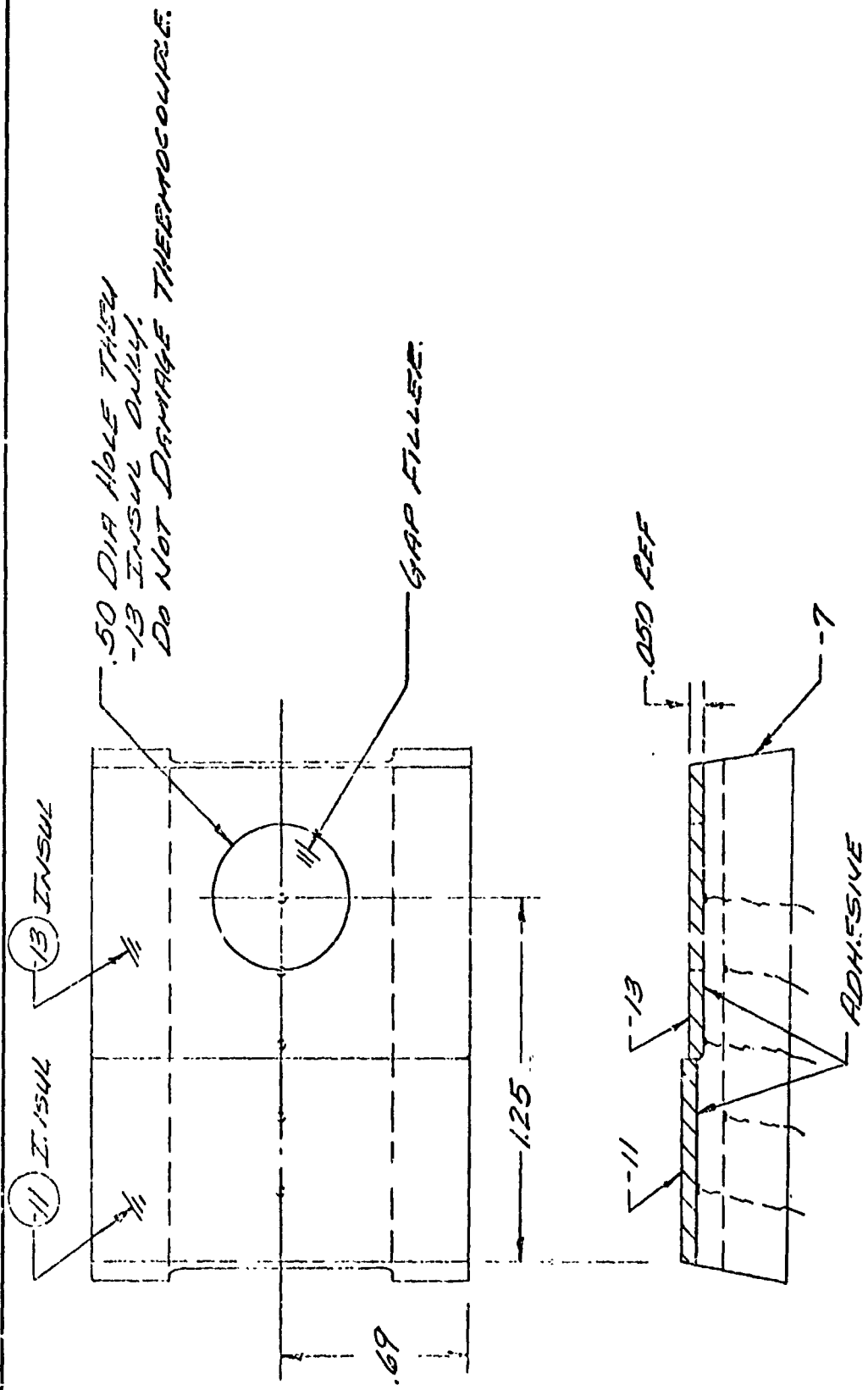


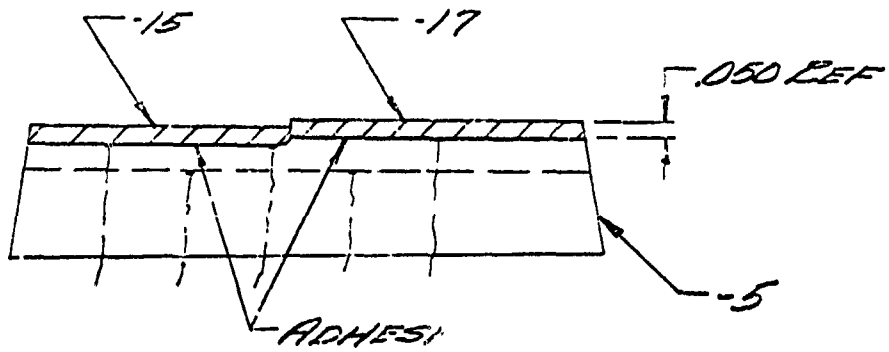
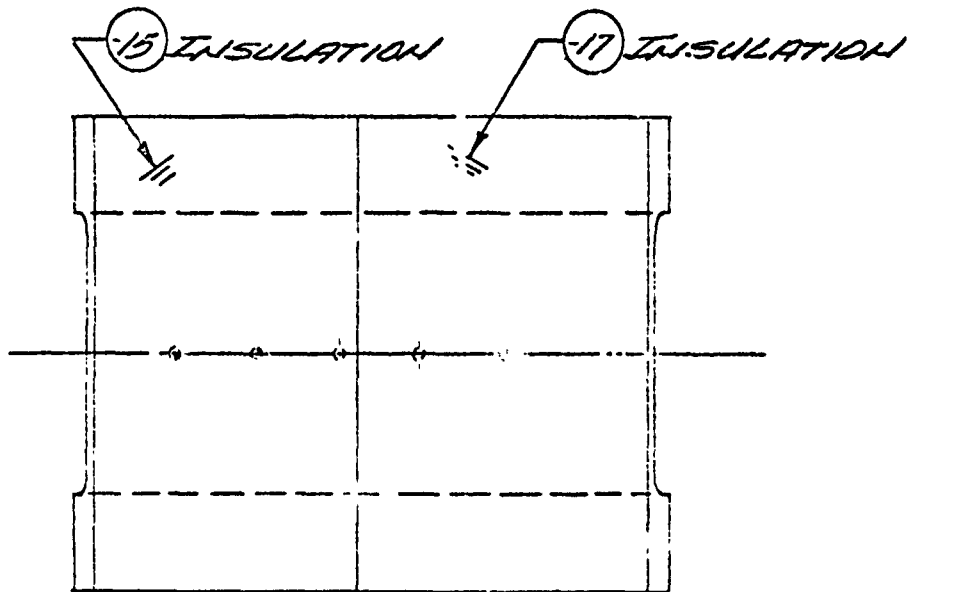
Figure 1. Double-Lap Shear Configuration



173604A-501

(2 REF)

Figure 2. Plasma Jet Specimen-501



LT36044-503  
(2 REF)

Figure 3. Plasma Jet Specimen-503

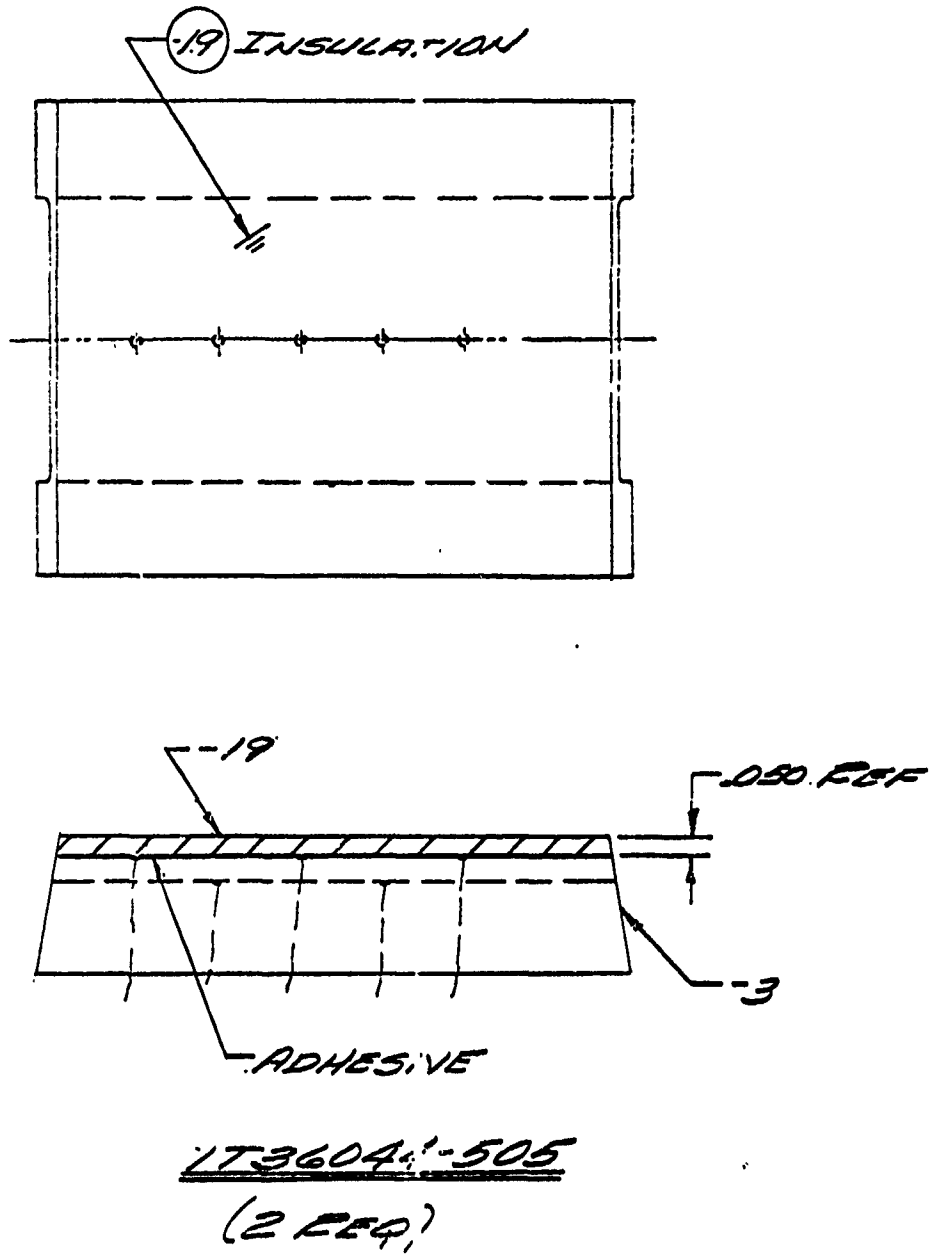
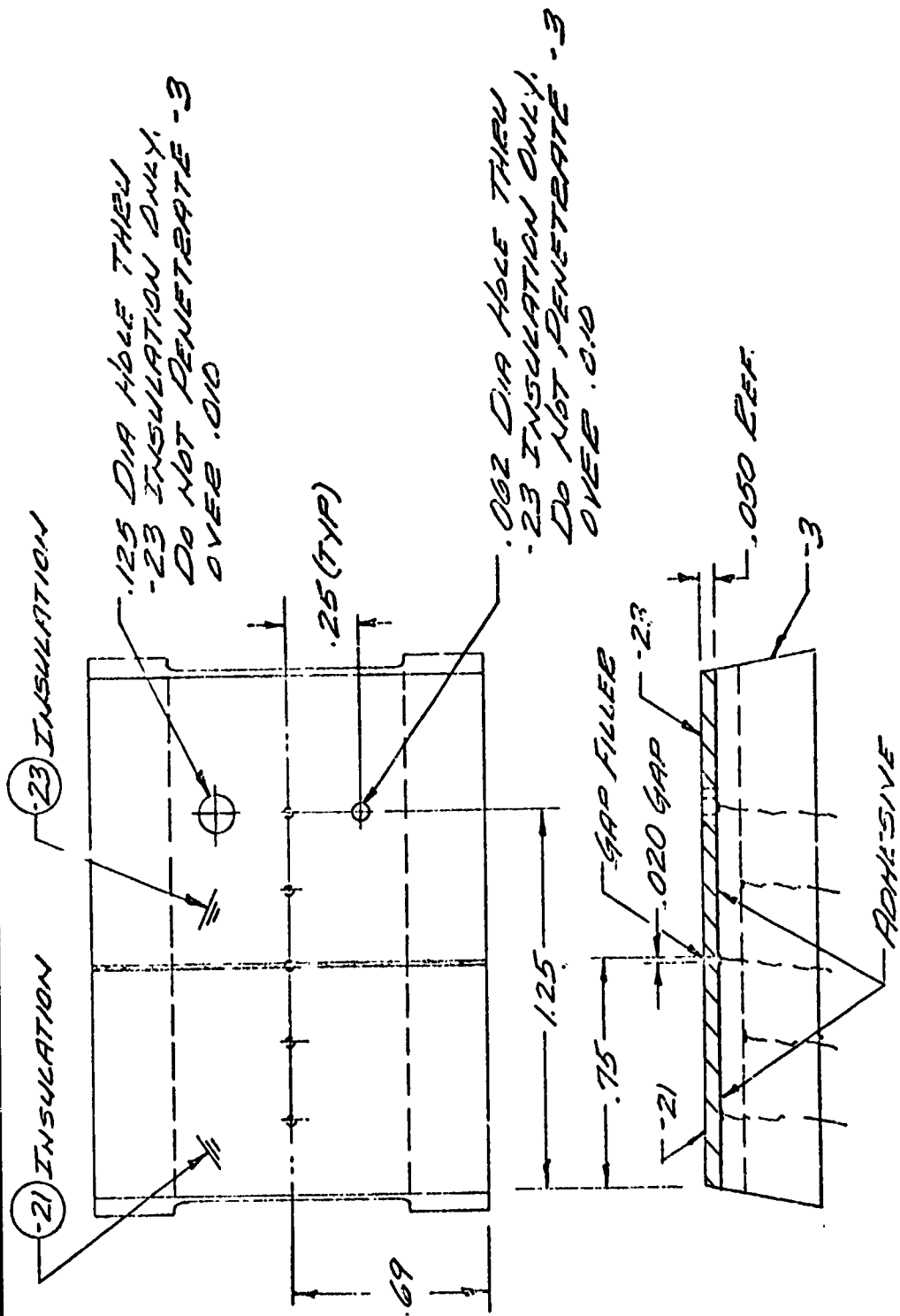
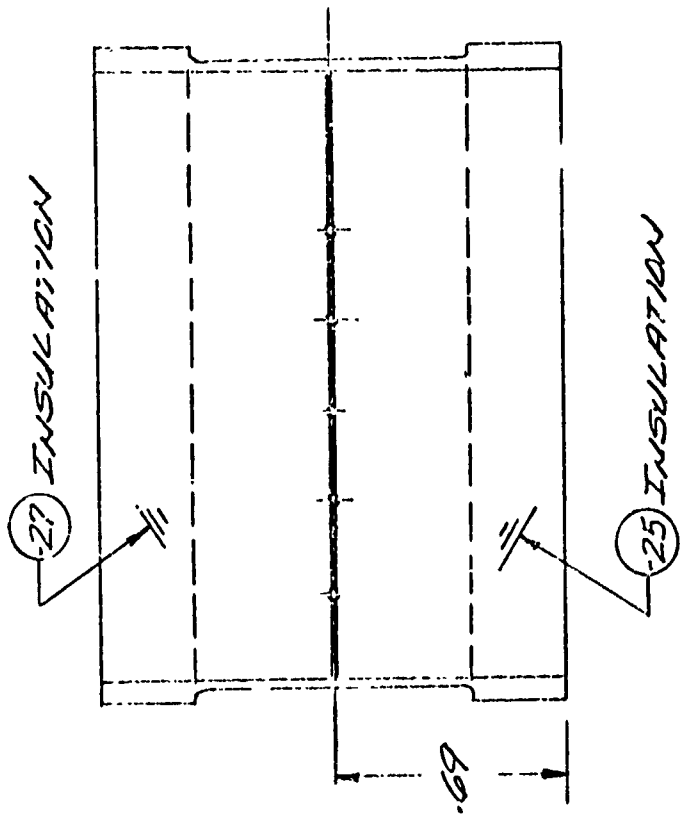


Figure 4. Plasma Jet Specimen-505



173604.1-507  
 (2 REF.)

Figure 5. Plasma Jet Specimen-507



17.36.044-509 (2 REF)  
17.36.044-511 (2 REF)

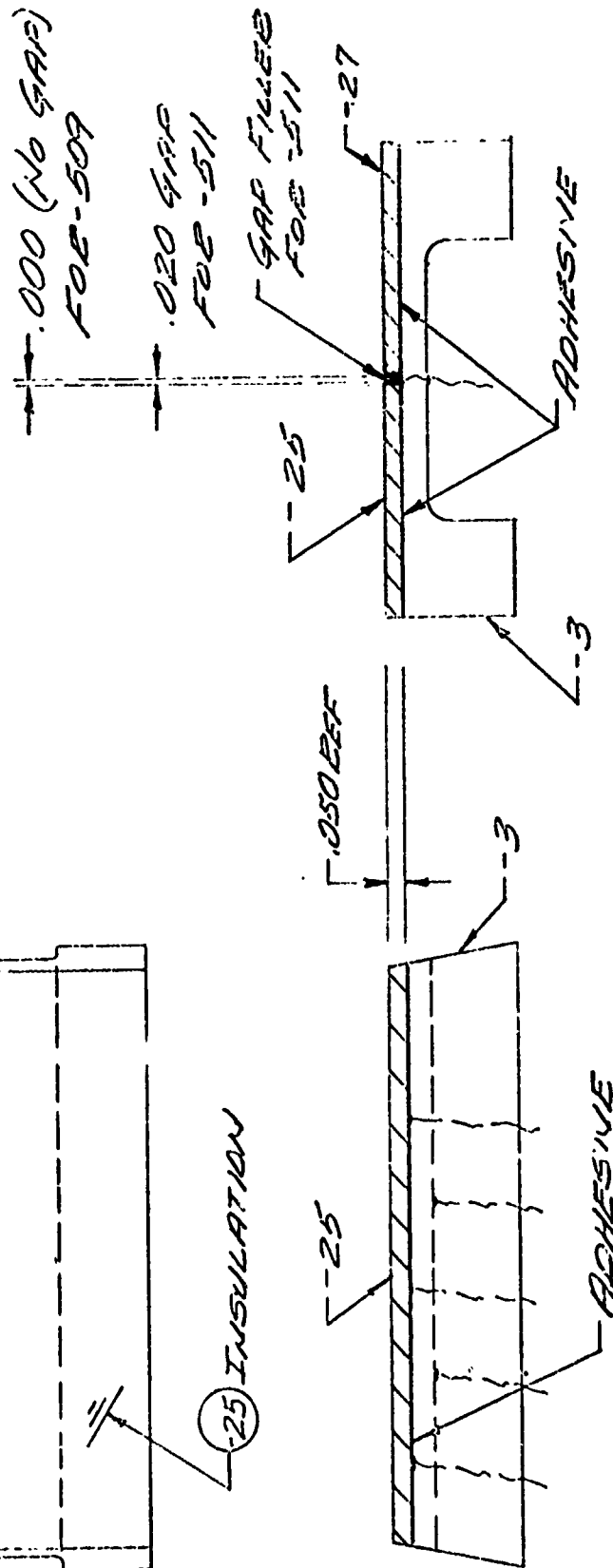


Figure 6. Plasma Jet Specimen-509 and -511

**MISSILE & SPACE SYSTEMS DIVISION  
DOUGLAS AIRCRAFT COMPANY, INC.**

MM 37-88 (REV. 1-62)

**MATERIAL & PROCESS ENGINEERING  
LABORATORY REPORT**

CATALOG NO. PDL 104336

SERIAL NO. MP 51,741DATE 21 April 1970ASSIGNED TO G. D. Shepherd, A-253

**TITLE** BONDING REFRASIL PREPREG TO  
ALUMINUM USING HT-424 ADHESIVE  
FOR UpSTAGE

**1. MATERIAL**

- 1.1 C-100-96 Refrasil/DP24-2 Phenolic Resin Prepreg  
Lot No. 9806  
Vendor Material Designation: WB2239/96  
Ferro Corp., Cordo Division  
Culver City, California
- 1.2 HT-424 Epoxy-Phenolic Film Adhesive, 0.08 lb/ft<sup>2</sup>  
Batch 7377, DPM 2857, STM 0019-01
- 1.3 HT-424B Epoxy-Phenolic Primer  
Batch 105, DPM 2978
- 1.4 Hi Shrink Tape, DPM 3141

**2. OBJECT**

To develop a method of bonding C-100-96 Refrasil prepreg to aluminum with HT-424 Film Adhesive for the UpSTAGE Program.

**3. INTRODUCTION**

The failure of the plasma jet specimens (a single layer of .050 inch thick Refrasil bonded to an aluminum substrate using AF31 adhesive) during the high temperature testing environment (4000°F) necessitated a change to HT-424 epoxy-phenolic adhesive. Standard methods of simultaneously curing the Refrasil prepreg and the HT-424 adhesive to a large area of aluminum substructure resulted in large unbonded areas and wrinkles in the Refrasil probably due to the outgassing characteristics of the adhesive during the cure. Modified bagging and curing techniques were required to overcome these problems.

**4. PROCEDURE****4.1 Surface Preparation (All Specimens)**

- 4.1.1 The aluminum surfaces were washed twice with methyl ethyl ketone and then air dried for 30 minutes.

- 4.1.2 The aluminum faying surfaces were grit blasted with #80 aluminum oxide grit.
- 4.1.3 The aluminum was primed with HT-424B primer. The primer was air-dried for 30 minutes at ambient temperature followed by a 1 hour exposure at 82°C (180°F) in an oven.

#### 4.2 Specimen Preparation

The adhesive, Refrasil, and bleeder were placed on 0.125" x 12" x 12" aluminum panels and 7 inch diameter x 9 inch long aluminum cylinders in the following sequence.

##### 4.2.1 Standard Lay-up Procedure -

- (a) One ply of 0.08 lb/ft<sup>2</sup> HT-424 adhesive film
- (b) One ply of C-100-96 Refrasil prepreg
- (c) Three plies of silicone treated fabric for release
- (d) Two plies of 1584 glass cloth for bleeder
- (e) Vacuum bag

##### 4.2.2 Modified Lay-up Procedure No. 1 -

- (a) One ply of 0.08 lb/ft<sup>2</sup> HT-424 adhesive film
- (b) One ply of C-100-96 Refrasil prepreg
- (c) One ply of perforated Armalon
- (d) Eight plies of 1584 glass cloth for bleeder
- (e) Vacuum bag

##### 4.2.3 Modified Lay-up Procedure No. 2 -

Same as No. 1 above except 1/2 inch thick silicone rubber foam was placed between the bleeder and the vacuum bag.

##### 4.2.4 Modified Lay-up Procedure No. 3 -

- (a) One ply of 0.08 lb/ft<sup>2</sup> HT-424 adhesive film
- (b) One ply of C-100-96 Refrasil prepreg
- (c) One ply of perforated Armalon
- (d) One complete wrap of perforated shrink tape (DPM 3141)

4.2.4 Modified Lay-Up Procedure No. 3 (Cont'd)

- (e) Eight plies of 1584 glass cloth for bleeder
- (f) One complete wrap of shrink tape
- (g) Vacuum bag

4.3 Specimen Cure

The specimens were then cured for three hours at 149°C (300°F) under vacuum and 50 psig in an autoclave. They were then cooled to 66°C (150°F) under vacuum and pressure.

5. RESULTS

Using the manual sonic technique large unbonded areas were found in the specimens fabricated using the standard method of bonding.

Using Procedure No. 1, with the increase in the number of bleeder plies, successfully removed the gases producing a complete bond. However, this method created wrinkles in the Refrasil surface.

Method No. 2, by the inclusion of silicone rubber foam during the lay-up, wrinkles were reduced in size and number but were still unacceptable.

Method No. 3, by using shrink tape, reduced the wrinkles to an acceptable level. No unbonds were detected.

6. SIGNIFICANCE OF DATA

Method No. 3 was the most successful and will be used for bonding Refrasil to the UpSTAGE structure.

7. REFERENCES

SO 3859-6320  
EWO 11069  
SA 7030

  
\_\_\_\_\_  
F. P. Chiavetta, Section Chief  
Non-Metallics Materials Properties  
Materials & Methods -  
Research & Engineering

  
\_\_\_\_\_  
G. D. Shepherd  
Non-Metallics Materials Properties  
Materials & Methods -  
Research & Engineering

Appendix E

- MDAC Report MP51, 603 (A. Koivu), Evaluation of Warm Gas Manifold Liner Materials, 20 August 1969.



FORM 10 (REV. 1-67)

MISSILE & SPACE SYSTEMS DIVISION  
DOUGLAS AIRCRAFT COMPANY, INC.

MATERIAL & PROCESS ENGINEERING  
LABORATORY REPORT

Catalog No. PDL 101848

SERIAL NO. 51,603

DATE 20 August 1969

ASSIGNED TO A. Kotvu, A-263

TITLE EVALUATION OF WARM GAS MANIFOLD LINER  
MATERIALS

1. MATERIALS

1.1 Milable Rubbers

- 1.1.1 K-1255 Silicone Rubber  
Union Carbide Silicones Division
- 1.1.2 K-1347 Silicone Rubber  
Union Carbide Silicones Division
- 1.1.3 Silastic 55 Silicone Rubber  
Dow Corning Corporation
- 1.1.4 Silastic 75 Silicone Rubber  
Dow Corning Corporation
- 1.1.5 SS-2365-2024N Silicone Rubber  
General Electric - Silicones Division

1.2 Castable Rubbers

- 1.2.1 RTV-630 Silicone Rubber  
General Electric - Silicones Division
- 1.2.2 TSS-758 Silicone Rubber  
General Electric - Silicones Division
- 1.2.3 DC-93-044 Silicone Rubber  
Dow Corning Corporation
- 1.2.4 DC-20-103-2 Silicone Rubber  
Dow Corning Corporation
- 1.2.5 RTV-60 Silicone Adhesive Sealant  
General Electric - Silicones Division
- 1.2.6 DC-731 Silicone Adhesive Sealant  
Dow Corning Corporation

1.3 Metal Adhesion Primer

- 1.3.1 SS-4155 Silicone Primer  
General Electric - Silicones Division

1.3.2 Thixon AM-2 Nitrile Rubber Primer  
Dayton Chemical Products Co.

1.3.3 Epon 934 Epoxy Primer/Adhesive  
Shell Chemical Co.

1.4 Control Materials

1.4.1 TFE Teflon  
E.I. duPont deNemours Co. - Plastics Division

1.4.2 V-44 Nitrile Rubber Ablative Insulation  
General Tire and Rubber Co.

1.5 Miscellaneous Materials

1.5.1 Aeroder Specimen Mounting Plates - 1025 Steel 6-1/2"x1"x.062"

1.5.2 Heat Transfer Gas - Dry Nitrogen

2. OBJECT

The object of these tests was to compare the physical properties and the thermal insulating characteristics of selected millable and castable silicone rubbers proposed for insulating the interior of the warm gas manifolds of the EB and JI propulsion systems.

3. PROCEDURE

3.1 Preparation of Test Insulating Materials

3.1.1 Millable Rubbers - The rubbers were catalyzed on the two roll rubber mill in accordance with the formulae shown in Table 1, and then cured in a 6"x6"x.050" mold to the schedule prescribed by the manufacturer. The press cure molded sheets were given an oven post cure as recommended by the manufacturer.

3.1.2 Castable Rubbers - The rubbers were hand mixed in a suitable container in accordance with the formulae shown in Table 2, degassed, and cast into sheets approximately .045" thick between glass plates using spacers. All materials were cured at room temperature with no oven post cure.

TABLE 1

FORMULAE FOR MILLABLE RUBBERS

	<u>K-1255</u>	<u>K-1347</u>	<u>Silastic 55</u>	<u>Silastic 75</u>	<u>SE-2369-2-200</u>
Polymer, pts/wt	100	100	100	100	
Luperco, CST pts/wt	0.7	1.5	1.3	-	(1)
Varox, pts/wt	-	-	-	1.2	-
(1) Compound supplied already catalyzed by supplier					

TABLE 2

FORMULAE FOR CASTABLE RUBBERS

	<u>RTV-630</u>	<u>TBS-758</u>	<u>DC-93-044</u>	<u>DC-20-103-2</u>
Polymer, pts/wt	100	100	100	100
Catalyst, pts/wt	10	10	10	10

3.2 Preparation of Aeroder Specimens

The 6-1/2"x1"x.062" steel mounting plates were vapor degreased and grit blasted before bonding the test insulation. Specimens bonded with RTV-60 were made with metal mounting plates primed with SS-4155 primer to assure good adhesion between the adhesive and the metal. No primer was used, or needed, to obtain adhesion to the metal mounting plate with the DC-731 adhesive. The adhesive was applied to both the rubber and metal surfaces and then the specimen was assembled and loaded with a light weight. Specimens bonded with DC-731 were exposed to the atmosphere for five minutes prior to assembly. This procedure was required to provide sufficient moisture from the air to activate the catalyst (acetic anhydride) in the adhesive. All bonding was performed at room temperature. Finally, an iron-constantan thermocouple was spot welded to the backside of the metal plate so that the backside temperature rise could be measured when the specimens were exposed during the Aeroder test. Control specimens were bonded to the mounting plates with adhesives suitable for each particular material. Thixon AM-2 was used to bond the V-44 specimen to the mounting plate at the same time the V-44 was cured. Bonding of the Teflon control to the mounting plate was accomplished by bonding the surface of the Teflon and cementing to the mounting plate with Epon 934.

3.3 Test Procedures

- 3.3.1 Stress/strain data were determined in accordance with ASTM D-412-66.
- 3.3.2 Hardness was determined in accordance with ASTM D-2240-64T.
- 3.3.3 Aeroder testing was performed in accordance with DLP 13,474.

4. RESULTS

Results are presented in Tables 3 and 4 and Figures 1 and 2.

5. SIGNIFICANCE OF DATA

5.1 Stress/Strain Properties

Analysis of the data in Table 3 indicates the millable rubbers have higher tensile strength and greater elongation than the castable rubbers. Of these rubbers, Silastic 55 and 75 have the highest

tensile and elongation. These properties are important considerations when inserting and bonding the insulation to the interior of the EB warm gas manifold.

RTV-630 and TBS-758 have the highest tensile values of the castable types with RTV-630 possessing the greatest percent elongation. RTV-630 has the lowest uncured viscosity and is best suited for injection casting of insulation for the interior of J1 warm gas manifold hardware.

## 5.2 Thermodynamic Properties

Aeroder test data are shown in Table 4. The data of test numbers 3428 through 3431 are not believed valid because of difficulties experienced with instrumentation but are included in this report to illustrate the importance and sensitivity of the instrumentation used to measure and control test parameters. Particular difficulty experienced in these four runs was because of a delay in the response of the Speedmax Recorder. Also, the top bed temperature did not appear stabilized. The following observations can be made:

- 5.2.1 With the exception of the GE-2365-2-2024N compound, all silicone materials exhibited lower backside temperature rise and ablation rate than the V-44 control material.
- 5.2.2 With the exception of the GE-2365-2-2024N compound, all silicone materials exhibited lower backside temperature rise than the Teflon control although the thickness of the Teflon was approximately 3-1/2 times greater. The duration of the test was increased in order to compensate for this thickness.
- 5.2.3 Generally, materials with the lowest ablation rate demonstrated the highest backside temperature rise. This is especially evident for the GE-2365-2-2024N system. However, the V-44 control exhibited both high ablation rate and backside temperature rise.
- 5.2.4 Weight loss is not an accurate means of determining the value of a material as a thermal insulation for this application. The specific gravity of the materials varies greatly so a high specific gravity material might show a high weight loss and a low specific gravity material shows a low weight loss. This is demonstrated when comparing the data of the DC-20-103-2 and K-1255 systems. The ablation rate for these two materials is identical although the backside temperature rise for the K-1255 is lower. For this application, the K-1255 is considered the preferred material.
- 5.2.5 The depth of ablation obtained with these materials indicates that the specimens might be reduced in thickness and still perform satisfactorily under the conditions of the test. In these tests, temperatures approached those expected in actual application.

However, the pressure of the gas, the particle content and the composition were quite different. It appears prudent to continue with the selected insulation thickness (0.40" for the EB and 0.90" for the JI concepts) until other data are obtained to indicate a reduction in insulation thickness may be feasible.

- 5.2.6 The backside temperature rise with all of these materials is considered relatively moderate. A far greater temperature rise can probably be tolerated before design limits of the manifold, metal are exceeded. With this possibility in mind, depth of erosion might be a more realistic criteria for selection of the insulation since a thinner section might be sufficient to meet design requirements. In this manner, a weight saving may be realized.
- 5.2.7 From a review of the backside temperature rise data, the Silastic 55 system appears to be the preferred material for the EB configuration. For the JI configuration, which requires a castable material suitable for injection molding, the RTV-630 system is preferred.
- 5.2.7 Based on backside temperature rise, the test results indicate the effectiveness of the materials, on a declining scale, to be as follows:

Solid millable rubbers

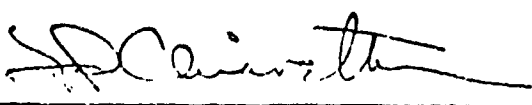
Silastic 55  
 Silastic 75  
 K-1347  
 K-1255  
 GE-2365-2-2024N

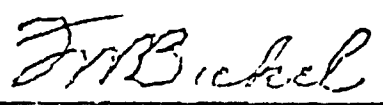
Castable liquid rubbers

RTV-630  
 DC-93-044  
 TBS-758  
 DC-20-103-2

6. REFERENCES

SO 3850-6320'  
 EWO 11069  
 SA 7013  
 TR 10862  
 TR 69076  
 ALB pgs. 6-9

  
 F. P. Chivetta, Section Chief  
 Non-Metall. Product Development  
 Materials & Methods -  
 Research & Engineering

  
 F. W. Bickel  
 Non-Metallics Products Development  
 Materials & Methods -  
 Research & Engineering

  
 A. Koivu  
 Non-Metallics Product Development  
 Materials & Methods -  
 Research & Engineering

TABLE 3

PHYSICAL PROPERTIES OF INSULATIONS

MATERIAL	TENSILE STRENGTH (PSI)	ELONGATION (PERCENT)	HARDNESS (SHORE A)
<u>Milable Rubbers</u>			
K-1347	1135	380	68
K-1255	1125	275	62 <sup>1)</sup>
Silastic 55	1385	480	56
Silastic 75	1190	375	70
GE-2365-2-2024N	855	215	65
<u>Castable Rubbers</u>			
HTV-630	680	250	52
DC-20-103-2	470	130	57
DC-93-044	265	60	62
TBS-758	900	100	79
<u>Controls</u>			
Teflon (Typical)	2100	300	55 (1)
V-44 Nitrile Insulation	1700	730	70

(1) Shore "D"

TABLE 4

AERODER TEST DATA: WAMM - GAS MANIFOLD LINER

TEST NUMBER	MATERIAL CODE	INITIAL AERODER TEST BED TEMPERATURE			TEST DURATION (SEC.)	SPEC. DENSITY (GM/CC)	SP.C. OVER-THICKNESS (IN.)	MAX. ABLATION DEPTH (IN.)	SPEC. WT. LOSS (G/G)	ABLA-TION RATE (IN/SEC)	CHAMBER PRESSURE (PSI)	MAX. BACK FACE TEMP (°F)*	AVG. TOP BED TEMP (°F)
		TOP (°F)	MIDDLE (°F)	BOTTOM (°F)									
3428 (4)	K-1255	3500	1560	1410	2.26	1.25	.103	.011	0.9	0.0049	100	85	2950
3429 (4)	K-1347	3500	1540	1260	2.28	1.17	.114	.012	0.8	0.0053	100	70	3000
3430 (4)	Silastic 55	3500	1530	1200	2.19	1.17	.114	.015	1.3	0.0068	100	70	3075
3431 (4)	RTV-630	3500	1520	1200	2.23	1.28	.109	.022	1.5	0.0099	100	68	3175
3432	Silastic 75	3500	1500	1180	2.23	1.20	.112	.017	1.0	0.0076	100	75	3165
3433	CE-2365-2-202M	3500	1500	1180	2.20	1.23	.107	.005	0.4	0.0023	105	113	3175
3434	TBS-758	3500	1500	1180	2.13	1.30	.118	**	0.25	**	104	95	3175
3435	DC-93-044	3500	1490	1170	2.43	0.67	.107	B.T.	2.2	B.T.	106	75	3185
3436	DC-20-103-2	3500	1480	1160	2.36	1.45	.110	.014	1.5	0.0059	108	103	3175
3437	V-44 (Control)	3500	1470	1160	2.26	1.37	.094	.030	2.7	0.0133	109	108	3140
3438	K-1255	3500	1470	1160	2.37	1.25	.102	.014	1.15	0.0059	115	96	3125
3439	K-1347	3500	1460	1160	2.33	1.17	.114	.022	2.33	0.0094	103	77	3175
3440	Silastic 55	3500	1450	1160	2.21	1.17	.106	.019	1.7	0.0086	108	72	3150
3441	RTV-630	3500	1450	1200	2.32	1.28	.112	.025	2.0	0.0108	106	70	3165
3442	Teflon (Control)	3500	1450	1170	9.76	2.16	.181	.047	6.7	0.0048	108	85	3160

\* Back face temperature monitored with Speedomax Recorder, Type G.

\*\* Surface charred considerably thus causing slight increase in thickness.

NOTES:

- (1) Angle of attack for all tests - 10 degrees.
- (2) Nitrogen-gas used to pressurize Aeroder chamber.
- (3) B.T. burn thru.
- (4) Test numbers 3428 thru 3431 were not used in the analysis due to instrumentation malfunction.

Appendix F  
HiBEX-U MOTOR DESCRIPTION  
(This Appendix is Unclassified)

Based on "UpSTAGE Program-HiBEX-U Rocket  
Motor, Final Technical Report, " Volumes 1, 2, and 3),  
Hercules, Inc., February 1972,

Contract No. DACA68-8012

Appendix F  
HERCULES HiBEX-U MOTOR

The HiBEX motor which was developed under the ARPA HiBEX program (Contract No. DA-01-021-AMC-10696Z) was used with some modifications on the UpSTAGE Experiment program. The modifications included design changes to the nozzle by removing the TVC hardware, thus lightening the weight by approximately 30 lb; incorporation of safety improvements in the igniter; and use of a liquid carrier heptane as a casting-power processing aid.

Hercules manufactured 15,500 lb of new FDN-80 casting powder which was blended with 6,500 lb powder from the ARPA HiBEX program. Hercules also manufactured additional motor cases, propellant grains, nozzles, igniters, and sundry components, as well as statically testing various components.

The rocket motor assembly (see Figure F-1) consists of three major components: the loaded case assembly, the nozzle and closure assembly, and the igniter loaded assembly.

The loaded case assembly is made up of a conical fiber glass case with fiber glass skirts extending fore and aft, terminating in aluminum skirt attachment rings. The case contains FDN-80 composite-modified double-base propellant in a single-perforated, 11-point star configuration. The propellant is bonded to the case with a bimodal powder embedment case bond system. The propellant-base burn rate is increased by the use of zirconium staples in the casting powder which are randomly dispersed throughout the propellant mass. The case is internally protected from the high-temperature combustion gases at the forward end (igniter end) and at the aft end.

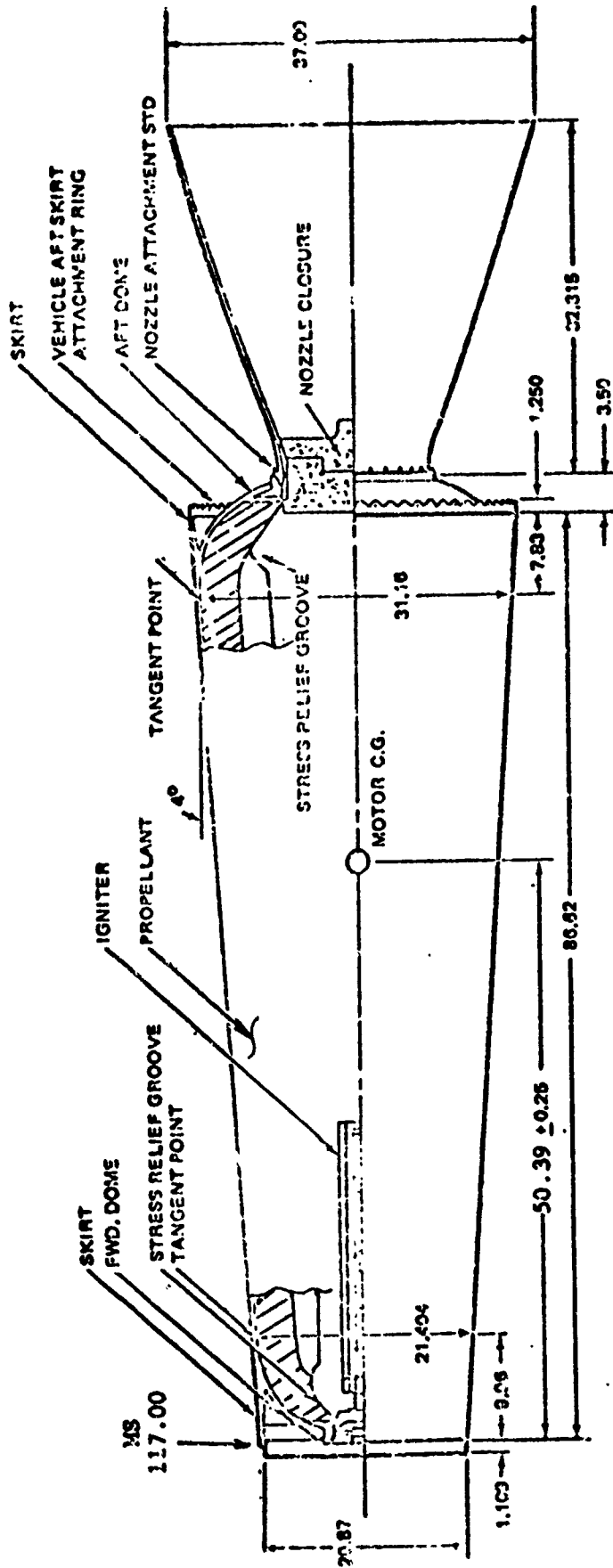


Figure F-1. HiBEX Rocket Motor Assembly

An aluminum forward pole piece, which is an integral part of the fiber glass case, houses a pyrotechnic igniter assembly containing a 6.5-lb boron/potassium nitrate pellet ignition charge. The igniter assembly consists of a concave aluminum pressure plate, which seals the forward port opening, and a stainless steel primary tube surrounded by a stainless steel wire-mesh secondary annular basket, both of which contain the pellet charge. The igniter has an electrical circuit, including two electric squibs and a safe-and-arm mechanism.

An aluminum aft pole piece, which is an integral part of the fiber glass case, provides for attachment of the nozzle and closure assembly. The nozzle and closure assembly consists of an aluminum structural conical shell, a compression-molded carbon-phenolic tape-wrapped exit cone liner, an asbestos-phenolic throat insert, and a two-piece cellular polystyrene nozzle closure.

#### F.1 LOADED CASE ASSEMBLY

The loaded case assembly consists of the case subassembly, the propellant grain, a hot gas seal, and miscellaneous components. The conical fiber glass case, with metal skirt attachment (splice) rings and adapters, contains FDN-80 propellant. The loaded case is manufactured and shipped separately from the igniter and nozzle since additional subassemblies of the UpSTAGE vehicle are integrated with these components during booster stage buildup.

##### F.1.1 Case

The case is a truncated cone 86.62 inches long, having a 32.984-inch diameter at the aft splice ring and a 20.87-inch diameter at the forward splice ring. The case is divided into two main structural sections, the skirts and the pressure vessel. The pressure vessel has port openings in the center of each dome. Aluminum adapters are located at each port. The forward adapter accommodates an igniter, and the aft adapter accommodates a nozzle in the loaded motor assembly. The forward and aft domes of the pressure vessel are internally insulated to protect the case from propellant combustion. The conical section is protected with propellant during motor operation and therefore requires no insulation. The inert slivers are placed longitudinally in the

conical section of the case to provide desired ballistic parameters. Splice rings have been riveted at the end of each skirt to provide attachments to adjacent missile sections.

#### F. 1. 1. 1 Adapters

At the two polar openings of the case, metal adapters (7075T652 aluminum forgings) are wound into each dome. The forward adapter accommodates the igniter, and the aft provides attachment for the nozzle. The adapters are also used during propellant manufacturing. The forward adapter provides access to the case interior for propellant casting and machining while the aft adapter is used to align and hold the core tooling.

#### F. 1. 1. 2 Insulators

The forward and aft domes and adapters are protected from propellant combustion gases by insulating material. The aft dome is covered by asbestos-filled styrene butadiene rubber (SBR) in conjunction with a ring of asbestos-phenolic adjacent to the nozzle entrance. The forward dome is protected from the combustion gases by silica-filled SBR. No rubber insulation was provided for the tapered conical chamber section since it is protected by the propellant grain during motor operation.

#### F. 1. 1. 3 Pressure Vessel and Skirts

The fiber glass portion of the case consists of two main sections, the pressure vessel and the skirts. The pressure vessel is an orthotropic structure fabricated from continuous glass filaments bonded with ERL-2256 resin and m-phenylene-diamine (CL) hardener. The vessel has a nominal burst pressure of 4,020 psig. The pressure-vessel center section has a conical shape with approximately a 4-deg taper. The domes are basically geodesic ovaloids with deviations from the theoretical to account for unequal polar openings and conical shape and to facilitate winding. The conical section is fabricated from helical and hoop windings. There are 17 helical layers; the number of hoop layers, varied along the case to maintain a relatively constant hoop filament stress, ranges from 20 at the aft major diameter to 14 at the forward tangent. The transitions between the conical section and the aft dome are reinforced with five layers of fiber glass mat. The mats are dispersed through the case

wall thickness and staggered radially and axially to prevent large discontinuities at the mat edges. The mat system is required to reinforce the area affected by bending discontinuities that are caused by the juncture of the dome to the conical section and the juncture of the skirts.

The skirts are also orthotropic structures fabricated from continuous glass filaments and glass cloth bonded with ERL-2256 resin and m-phenylenediamine (CL) hardener. The skirts are fabricated by alternating layers of glass cloth and hoop windings.

#### F. 1. 1. 4 Splice Rings

The splice (skirt attachment) rings are used to connect the rocket motor through the skirts with adjacent missile sections. These rings are fabricated from 2014-T652 aluminum rolled ring forgings and are potted in place with a high-modulus resin (Epon 901 B1). Final structural attachment to the stub is made with aluminum rivets.

#### F. 1. 1. 5 Inert Sliver

The inert sliver is a lightweight component bonded to the inside conical wall of the rocket motor case in line with each propellant star point. The purpose of the sliver is to replace heavier propellant that remains after the desired burn time and to produce more desirable pressure tailoff results. The inert sliver does not account for all of the propellant sliver. The previous HiBEX program picked up additional impulse by allowing some propellant sliver. Eleven slivers weighing 25.6 lb (total) replace 54.8 lb of unusable propellant. This weight savings was achieved by utilization of a sliver resin system filled with phenolic microballoons.

#### F. 1. 2 Hot Gas Seal

The hot gas seal is an asbestos-filled styrene butadiene rubber insert, bonded to the motor case aft adapter (metal polar opening). It serves as the nozzle approach interface and allows some relative motion between the motor case and the nozzle during pressurization. Its primary function is to prevent hot gases and molten metal particles (propellant combustion products) from impinging on the O-ring seals between the nozzle and the motor case. The

stepped outer diameter provides a retention system for bonding with the truncated cone, providing an interference fit with the nozzle approach section.

## F. 2 IGNITER LOADED ASSEMBLY

The HiBEX-U igniter is a forward-mounted, perforated basket containing a pyrotechnic pellet charge. Its function is to initiate burning of the rocket motor propellant in a timely, controlled, and stable manner. Initiation is accomplished by an electric squib housed in a remotely actuated safe-and-arm assembly. The igniter features the following:

- A. Remote electrical arming with automatic safing in event of power loss.
- B. Firing circuit electrically independent of arm and monitor circuits; all circuits are RF (radio frequency) shielded.
- C. Redundant 1 amp, 1 w, no-fire electric squibs.
- D. Open firing circuit with squib leads grounded and squib discharge blocked in the SAFE position.
- E. Mechanical locking in the SAFE position for handling and storage.

### F. 2. 1 Safe-and-Arm Assembly

The safe-and-arm assembly (S/A) combines the complete electrical circuit with the mechanical squib diversion of the igniter and simultaneously serves as the motor case forward closure. The dual squibs are the only pyrotechnics in the S/A device.

Application of the arming voltage causes the solenoid to rotate 90 deg. The solenoid shaft engages the driven shaft which transmits this rotary motion through the base plate and turns the blocking rotor. The blocking rotor also rotates 90 deg to align through-holes ahead of the squibs and simultaneously turns the rotary switch that closes the firing circuit in the last few degrees of travel.

Only the firing circuit passes through the base plate, as the arming circuit and monitoring circuit are external to the base plate. The monitoring circuit monitors the angular position of the solenoid shaft, thus providing a positive and electrically isolated indication of the directly connected firing switch and blocking rotor.

### F. 2. 2 Primary Igniter Assembly

The primary igniter assembly is a booster charge for the squibs. It mounts on the barrel section of the S/A and indexes to the squibs through engagement of the indexing tongue with the booster (primer) housing. The two primers receive the squib discharge when the S/A is in the armed position upon firing command. The primers in turn initiate each end of a pyrocore loop running the length of the primary charge basket. Within this basket are 320 grams of boron potassium nitrate pellets alternately positioned by styrofoam spacers down the length of the charge basket. A conductive plastic bag lines the steel tube and provides a moisture barrier for the pellets. With the pyrocore initiated, the pellets rapidly ignite and the resulting gases pass through the radial perforations of the basket to initiate the main secondary charge. The primers are bonded into the booster housing with conductive epoxy (ABLEBOND) which is also in contact with the lead sheath of the pyrocore, providing a static discharge path. The rubber grommet of the primer is also conductive.

### F. 3 NOZZLE AND CLOSURE ASSEMBLY

The HiBEX-H nozzle and closure assembly has been reconfigured for use in the UpSTAGE program from the original HiBEX nozzle design by the elimination of the HiBEX TVC system and mounting provisions. The nozzle assembly less the closure weights of 74.3 lb is composed of three basic components: (1) an ablative exit cone liner, (2) an ablative throat insert, and (3) an aluminum structural shell.

#### F. 3. 1 Exit Cone Liner

The HiBEX-U nozzle exit cone liner has an overall length of 32.415 inches and a maximum diameter of 26.604 inches. Radial thickness ranges from a maximum of 1.242 inches at the forward end to a minimum of 0.098 inch at the aft end.

The 25-lb liner is fabricated of Fiberite Corporation MX-4926 carbon phenolic tape cut on a 45-degree bias. Splice joints in the tape are lapsewn using cotton phenolic tape to minimize voids and pits and to withstand winding tension.

### F. 3.2 Exit Cone Shell

The loads exerted upon the HiBEX-U nozzles are transmitted through the full-length 7075-T652 aluminum exit cone shell. The exit cone shell has a minimum wall thickness of 0.100 inch and weighs 41.4 lb. The shell is machined from a die forging having the physical properties listed below. The exit cone shell OD is protected from corrosion by an Alodine 1200 chromate conversion coating.

HiBEX-U NOZZLE EXIT CONE SHELL MINIMUM  
MECHANICAL PROPERTIES

	Yield Strength (psi)	Tensile Strength (psi)	Elongation (%)
Longitudinal	65,000	75,000	7
Transverse	62,000	71,000	3

### F. 3.3 Throat Insert

The HiBEX-U nozzle throat insert is fabricated from molded 150-RPD asbestos phenolic and weighs 4 lb. This material has excellent ablative characteristics, good strength, and a long history of use in rocket nozzles.

The axial load exerted upon the throat insert by internal pressure is transmitted into a 0.145-inch wide step in the aluminum shell. Pressure force analysis indicates that this design bearing load amounts to 46,440 lb, which is equivalent to a design bearing stress of 7,200 psi. The resultant margin of safety is therefore greater than 5.

### F. 3.4 Nozzle Closure

The HiBEX-U nozzle closure is a two-piece assembly of low density (1.9 lb/ft<sup>3</sup>) expanded polystyrene (designated Styrofoam FR) produced by Dow Chemical Company. The closure assembly weighs 1.1 lb. Styrofoam FR is blue and is considered flame retardant. The aft face and outside taper of the aft closure are coated with a 0.015- to 0.035-inch thick layer of Westchester Chemical Company Lagz No. 1. This is a latex material having good resistance to moisture absorption.

The minor outside diameter of the forward closure is designed to have a nominal 0.010-inch interference fit with the nozzle throat. The aft closure is bonded to the forward closure. This design feature bypasses the need for bonding to the nozzle which could result in nozzle damage during closure blowout.

Appendix G  
HAZARDS EVALUATION OF HiBEX LIQUID CARRIER PROCESS

(This Appendix is Unclassified)

by

R. G. Hunt  
Allegany Ballistics Laboratory  
Hercules, Inc.

31 December 1969

## GLOSSARY

Impingement	Collision of casting powder with a portion of processing equipment or another powder granule.
Sparkle	Burning zirconium particle.
Threshold free fall velocity	The velocity at which sparking of casting powder does not occur when impinged.
TiL	Threshold initiation level - defined as the level above which initiation can occur as established by 20 consecutive failures obtained at that level.
ABL 2849 ABL 2888	Designation for casting powder compositions and manufacturing lots.
Transition Characteristics or critical height to explosion	Defined as the confined material height above which an explosion can occur when subjected to bottom flame initiation produced by a 12 gram bag igniter.
LEL	Lower Explosive Limit

Appendix G  
HAZARDS EVALUATION OF HiBEX LIQUID  
CARRIER PROCESS

OBJECTIVE

To determine the operational safety margins in the production of HiBEX motors by the liquid carrier process. The operations analyzed were (1) casting powder manufacture, (2) casting powder finishing, and (3) mold loading.

The HiBEX system utilizes a high rate propellant formulation. The casting powders made to this formulation differ from formulations normally processed by the cast double base manufacturing process. During impact, friction, and electrostatic testing a sparking reaction occurs at a low level energy input. The sparking reaction and low level electrostatic energies are capable of igniting dust clouds containing processing residues inherent in powder handling techniques. This sparking reaction was also found to occur at freefall height necessary to load the units with initiation by impingement. Powder critical heights were such that transition to explosion hazards were apparent in many of the process steps.

A method was devised utilizing a heptane liquid carrier system to limit powder particle velocities, reduce potential dust clouds and reduce the critical height problems. While correcting the major problem areas, the heptane carrier process introduced a new flammable material to the system and required additional processing steps. The system also had little effect on the powder frictional thresholds. The processing techniques did however limit the powder movements to levels below the frictional thresholds.

This report is a summary of the hazard analysis of the operations in the liquid carrier process and a compilation of the safety margin. These margins were derived from a comparison of the in-process potentials expressed in engineering terms and the response of process material to these stimuli expressed in like engineering terms.

## A. Casting Powder Manufacture

The casting powder for this program was manufactured at the Hercules Incorporated/Kenvil Plant. The manufacturing phase at Kenvil include mixing, extrusion, granulation and packaging the green powder under heptane. The additional steps required to package the powder in heptane is the only deviation from normal production of high energy powders and is the first use of the liquid carrier concept.

1. Mixing—Mixing is accomplished with a Day horizontal blade 400 lb mixer equipped with a remote ingredient feed system for the addition of the oxidizer and metal staples.

Preproduction safety checks of the system included (1) safety wiring and potting of overhead bolts to reduce the possibility of foreign material entering the mixer. (2) Measurement of blade clearances between the blades and the mixer and the mixer glands. This is to insure no metal to metal friction can occur during the mix cycles.

During mixing an acetone mist system applies acetone to the mixer glands to prevent dry propellant from building up in the glands. Such a buildup could present a potential source of initiation through friction. The glands are fabricated from non-metallic material to further reduce friction hazards.

Transition to explosion hazards during mixing were reduced by maintaining the total volatile level  $> 15\%$  during mixing. Transition characteristics were found to be independent of the alcohol/acetone ratio of the mix solvent within the range of 60-80% allowing the original 65/25 ratio to be modified to 75/25 to increase powder quality. The transition data was based on a previous study of an AP, aluminum staple CMDB propellant system, Figure XI. No data of this type is available on the actual HiBEX green mix.

The green mix is removed from the mixer by rotating the bowl  $90^\circ$  and using the blade action to move the mix into a powder bin where it is bagged and shipped to the extrusion area. Residual mix is removed from the mixer manually with a wooden powder hoe. The safety margin for an operator using the hoe during normal operation is 1, 200, presenting no hazard.

Mixer cleanup is accomplished by using a high pressure water stream and mechanical scrapping. The 600 psi pressure of the pump is insufficient to cause ignition. The use of the metal scrapper could cause initiation if the force is concentrated on the corner or by dropping the implement. It was recommended that the metal scrapper be replaced with a non-metallic scrapper.

2. Extrusion and Granulation—The green mix is extruded into strands for granulation using a 4" diameter press with approximately 8" of material height of a maximum pressure of 3,000 psi. Prior to use with explosive materials the hydraulic ram and basket assembly were disassembled and aligned to insure that no metal to metal contact would occur between the ram and the basket. During normal operation the press ram will build up a propellant flashing on the ram exerting frictional pressure equal to the press ram pressure on the wall of the basket with a friction initiation safety margin of  $> 2.4$ . A remote operated ratchet device has been installed on the press to remove the die for cleaning after the pressing operation is complete.

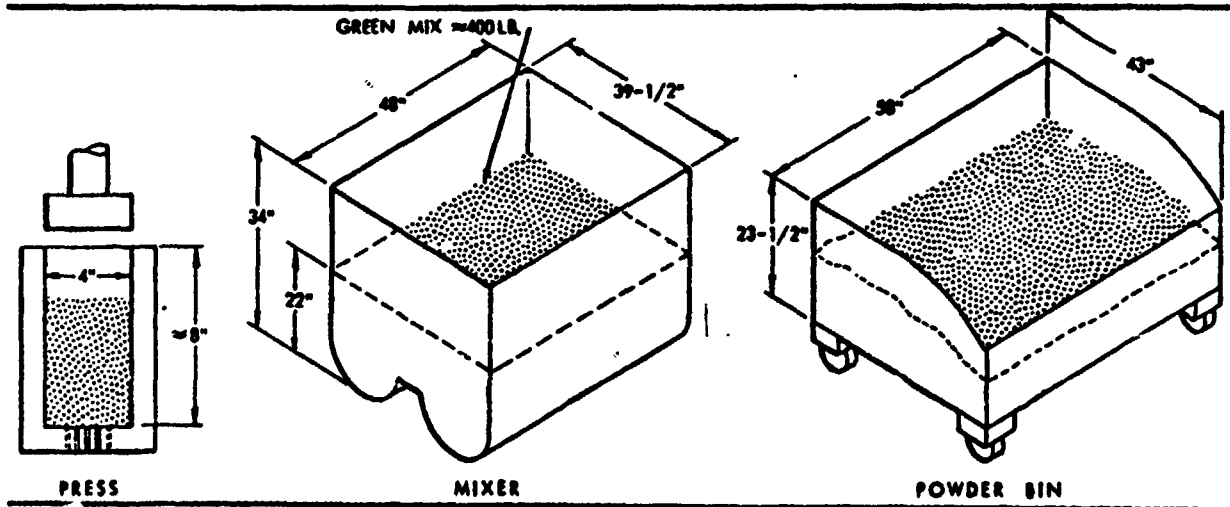
The powder is granulated on a cutting machine with a blade tip velocity of approximately 85 ft/sec across the cutting bar. At this velocity small frictional pressures could cause initiation during granulation. To reduce the friction hazard the standard metal cutting bar was replaced with a non-metallic bar with alcohol drip and mist systems providing lubricant and cooling to the cutting zone. The blade/bar gap setting cannot be set large enough to exclude all friction hazards since this adjustment is very important to the quality of the product. For this reason cutting operations are a potential source of fires. The product delivery tube between the cutting blade and the collection bag contains a volatile vapor atmosphere subject to ignition from granule sparkles or burning in the cutter. To minimize potential flame propagation to the powder bag, an exhaust system was added to the tube to keep the vapors below the lower explosive limit. A Primax deluge system with a light sensitive head is located in the powder delivery tube should ignition occur. No more than 20-25 lbs of cut powder are allowed to accumulate at one time at the cutting machine.

Figure 1 summarizes the process hazard survey of the mixing, extrusion and cutting operation indicating the engineering analysis and the safety margins.

3. Drum Loading and Rotating—The bags of cut powder are hand carried in buckets to the drum loading and rotating area. To minimize granular friction during powder handling and to reduce granule clustering the cut powder is submerged under heptane in the shipping drums within 15 minutes after cutting. Sufficient heptane is added to the drums to maintain a head of heptane over the powder during shipping to keep the powder in the green state.

The sealed drums are rotated at 20 rpm for 10 minutes to completely wet all surfaces with the liquid carrier heptane. The powder bag movement and granular friction stimuli during rotation has been analyzed with safety margins ranging from 2.6 to 3,216. Abnormal situations can produce hazards if drums fall off of the rotator causing excessive friction or heptane leaks during rotating producing explosive vapor concentrations in the area. The situation of dropping a drum would only result from careless operation and the potential hazard of heptane vapors is minimized by the lack of an ignition source. If ignition should occur in the heptane immersed powder, critical height to explosion data indicates the material should not transit to an explosion. The sealed drums are stored in a magazine maintained at  $> 55^{\circ}\text{F}$  to keep the  $< 1.0\%$  NG dissolved in the heptane from precipitating and introducing a liquid explosive into the process. This temperature specification is maintained through the process. Figure 2 shows the drum rotating arrangement and the appropriate engineering analysis safety margins.

4. Powder Shipment—The drums of casting powder immersed in heptane are shipped from Kenvil to ABL by commercial carrier. The drums are placed in the truck four abreast with two bars locked into the side of the truck to restrain the drums. Each layer of 4 drums is restrained in the same manner. Excessive granular motion during normal transportation is reduced since each drum contains 3-5 bags of powder, rather than loose bulk powder. The powder in the bags is covered with a head of heptane at all times, eliminating drying of the powder granules. Abnormal situations could arise from leaking containers during shipment presenting an explosive vapor hazard in



**TRANSITION AND PROPAGATION HAZARDS**

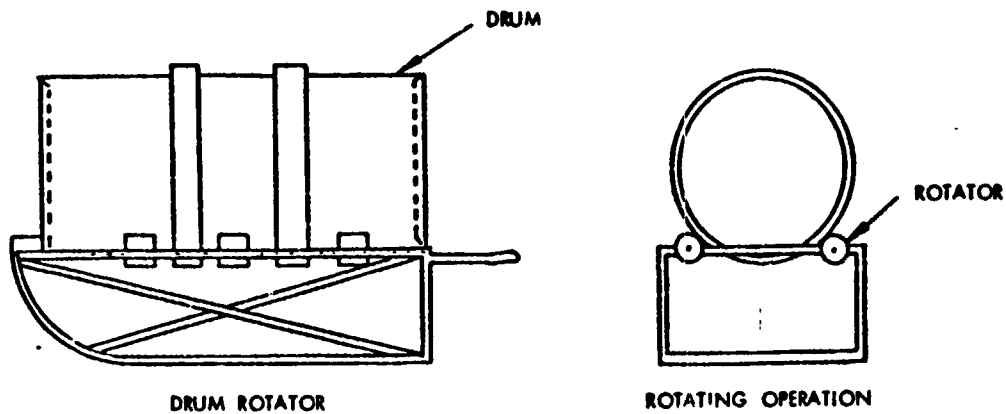
Processing Phase	In-Process Condition Height/Diameter	Test Data <sup>1,2/</sup> Height/Diameter	Hazard	Safety Margin
Propellant Mixing ≈ 15% Solvent Level	22"/40"	≈ 40"/40"	No	1.8
Propellant Pressing ≈ 17% Solvent Level	6"/4"	6"/4"	Yes	None
Propellant in Powder Bin ≈ 17% Solvent Level	22"/43"	≈ 40"/43"	No	≈ 1.8

(1) Sensitivity data is for a perchlorated, aluminum staple, GMD type propellant - ABL Type 2888.  
 (2) Critical height to emission values are obtained from an extrapolated values shown in Figure XI.

**PROCESS HAZARD SURVEY OF MIXING, EXTRUSION AND GRANULATION OPERATIONS**

Normal Operation	Observations		Engineering Analysis In-Process Potential	Test Analysis	Hazard	Safety Margin
	Combustible	Initiation Mode				
<b>Mixing</b>						
1. Rubbing of Mixer Blades on Mixer Bowl	Green Mix	Friction	No physical contact - Clearances verified prior to use of the mixer.	No Hazard	No	-
2. Rubbing of Blade Shaft on Mixer Glonds	Green Mix	Friction	No contact clearances verified prior to use of the mixer	No Hazard	No	-
3. Removing powder from the Mixer with a Wooden Powder Sco.	Green Mix	Friction	6 psi @ 1 ft/sec	7,234 psi @ 6 ft/sec	No	1,200
4. Cleaning Mixer with AMPCO K-30 BR-CU scraper (Sharp Edge)	Green Mix	Friction	Flat 12,500 psi @ 1 ft/sec	≈ 90,000 @ 1 ft/sec ≈ 234 psi @ 6 ft/sec	No	2.4
<b>Abnormal Operation</b>						
3. Cleaning mixer with scraper pressing on one corner	Green Mix	Friction	Corner 6 x 10 <sup>4</sup> psi @ 1 ft/sec	> 234 psi @ 6 ft/sec	Yes	None
6. Dropping Scraper on to Green Mix (1 ft/drop)	Green Mix	Impact	Corner 6.25 x 10 <sup>4</sup> ft-lb/in <sup>2</sup>	22 ft-lb/in <sup>2</sup>	Yes	None
<b>Pressing</b>						
1. Ram Pressing Powder (Powder on Metal)	Green Mix	Friction	Normal 3,000 psi @ 6 ft/sec	7,234 psi @ 6 ft/sec	No	2.41
3. Metal/Metal	Green Mix	Friction	Abnormal 6,700 psi at 6 ft/sec	7,234 psi @ 6 ft/sec	Yes	None

Figure 1. Transition and Propagation Hazards



### ROTATING OPERATION

**Conditions:** Rotation - 20 rpm  
 Surface Velocity - 1.65 ft/sec  
 Powder - 3-5 bags - 75-125 lbs  
 Drum Gross Wt. - ~ 300 lbs.

**Operation:** The loaded drums are placed onto the rotator by hooking onto the drum in the upright position and then lowering the rotator into the horizontal position. At this stage the drum rests on two sets of rollers ready for rotation.

### PROCESS SURVEY

Potential Initiation Source in the Operation	Observations		Engineering Analysis In-Process Potential	Sensitivity Test Analysis	Safety Margin
	Combustible	Initiation Mode			
<b>NORMAL OPERATION</b>					
1. Powder bag sliding on the inside of the drum during rotation.	Heptane wet C.P. residue	Friction	18.5 psi @ 1.65 ft/sec	16,000 psi @ 1.65 ft/sec	864
2. Sewed corner of a powder bag sliding on the inside of the drum during rotation.	Heptane wet C.P. Residue	Friction	410 psi @ 1.65 ft/sec	16,000 psi @ 1.65 ft/sec	39
3. Casting powder granule experiencing granular friction between powder bag and the drum during rotation.	Heptane wet green casting powder	Friction	18.5 psi @ 1.65 ft/sec	59,500 psi @ 1.65 ft/sec	3,216
4. Casting powder granule experiencing granular friction between powder bag sewed corner and the drum during rotation.	Heptane wet green casting powder	Friction	23,000 psi @ 1.65 ft/sec	59,500 psi @ 1.65 ft/sec	2.6
5. Granular friction inside of the powder bags during drum rotation.	Heptane wet green casting	Granular Friction	18.5 psi @ 3.3 ft/sec	> 2400 psi @ 4 ft/sec	129
<b>ABNORMAL OPERATIONS</b>					
1. Heptane leaks out of the drum causing an explosive atmosphere	Heptane	Electrostatic Human Spark	No voltage accumulation	2 milli-joules	Potential Hazard
2. Drum falls off of rotating stand	Green Casting Powder	Internal Impact and Friction	Undefined	-	Undefined
3. Falling drum impacts casting powder granules on the floor	Green Casting Powder	Impact	600 ft-lb/in <sup>2</sup>	22 ft-lb/in <sup>2</sup>	None
4. Transition of reaction to explosion if initiation should occur in the drum	Green Casting powder in heptane	Transition	Container 18" dia. powder @ ~ 20"	> 24" @ 4" dia.	> 1.2

Figure 2. Drum Rotating Operation (After Initial Loading of Drums)

the truck. Should this situation be found when the truck reaches its destination the vapor concentration should be lowered to a safe level prior to moving the containers. Accidents where the truck overturns could present hazardous situation from excessive movement of the powder. The shipping arrangement is shown in Figure 3 with the appropriate hazard analysis data.

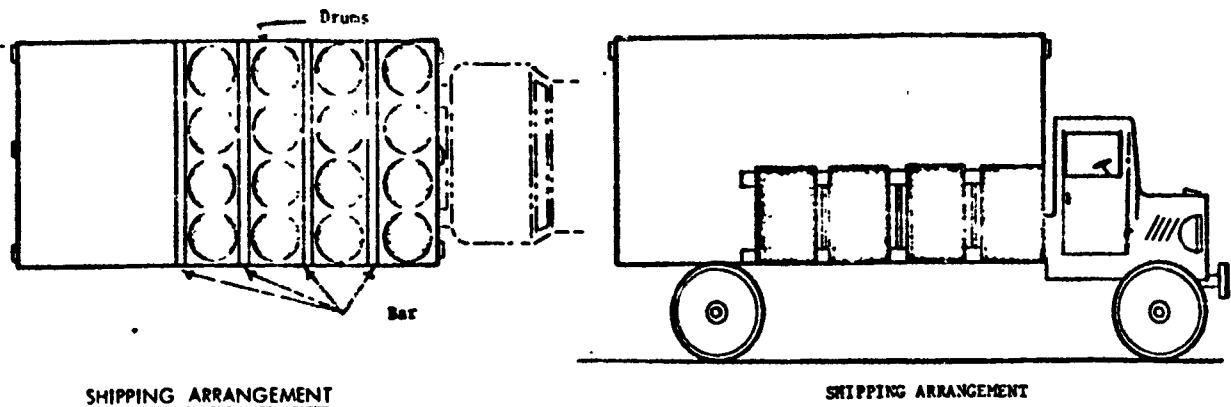
#### B. Casting Powder Finishing

Casting powder manufactured by the inert carrier process required certain portions of the manufacturing process to be completed at ABL. These steps include powder unloading, powder drying, powder rewetting and packaging into 14 gallon drums, powder shaping, powder screening and powder blending.

1. Powder Unloading and Drum Rotating—The casting powder drums received at ABL are removed from the shipping truck by utilizing a truck mounted hydraulic tailgate as an elevator, as shown in Figure 4. The individual drums are removed with a drum cart. One operator handles the cart and another stabilizes the drum. Movement is such that the bag and granule movement inside of the drum should not exceed 410 psi at 1 ft/sec. This relatively gentle motion affords a safety margin from 39 to 145. Under accidental conditions should a drum drop off of the truck, the granular friction would be in excess of the threshold sensitivity of the powder.

In order to breakup any powder clusters which may have formed during shipment, the drums are rotated when received. This operation can be accomplished with the same safety margins of 39 to 3,217 as found for drum rotation prior to shipping. Additional steps are required to lower the drum to a horizontal position and to lift the drums onto the rotator (Figure 5). Normal operation in these sequences does not introduce additional hazards. An abnormal situation where a strap breaks dropping the drum could present initiation hazards from granular friction. Figure 5 includes the additional hazard analysis data.

2. Drum Unloading and Drying—The powder as received at ABL is still green powder containing residual alcohol and acetone. To be utilized to manufacture propellant the powder must be dried. Removing the powder from the drums is accomplished by the setup as shown in Figure 5. An operator stands



SHIPPING CONDITIONS

Carrier: Truck

Securing Mechanism:

Powder drums are secured in the truck with bar attached to each side of the truck restraining each row of drums. Drums are located in an upright position.

PROCESS HAZARDS SURVEY

Operation	Observations		Engineering Analysis In-Process Potential	Sensitivity Test Analysis	Safety Margin
	Combustible	Initiation Mode			
<u>NORMAL OPERATIONS</u>					
1. Granular Friction in Shipping Containers	Green Casting & Heptane Powder	Friction	No friction expected during normal transportation due to settling effect of bagged powder in drums.		
2. Impact of Powder on Drum-sides	Green Casting Powder	Impact	No impact due to powder being restrained from moving.		
<u>ABNORMAL OPERATIONS</u>					
1. Vapor leaking into truck	Green Casting Powder and Heptane	Electrostatic	Potential hazard would depend on the accumulation of an explosive atmosphere during transit time and source of initiation		
2. Impact and friction inside of drums causing ignition of powder in the case of an accident where the vehicle overturns.	Green Casting Powder and Heptane	Impact and Friction	Undefined		
A. No container rupture	C.P. & Heptane	Transition	≈ 20" height @ 18" diameter	>24" @ 4" dia	> 1.3
B. Container ruptures	Heptane w/c C.P.	Transition	≈ 20" height @ 18" diameter	≈ 14" height @ 18" dia.	None

Figure 3. Drum Arrangement in Shipping Truck

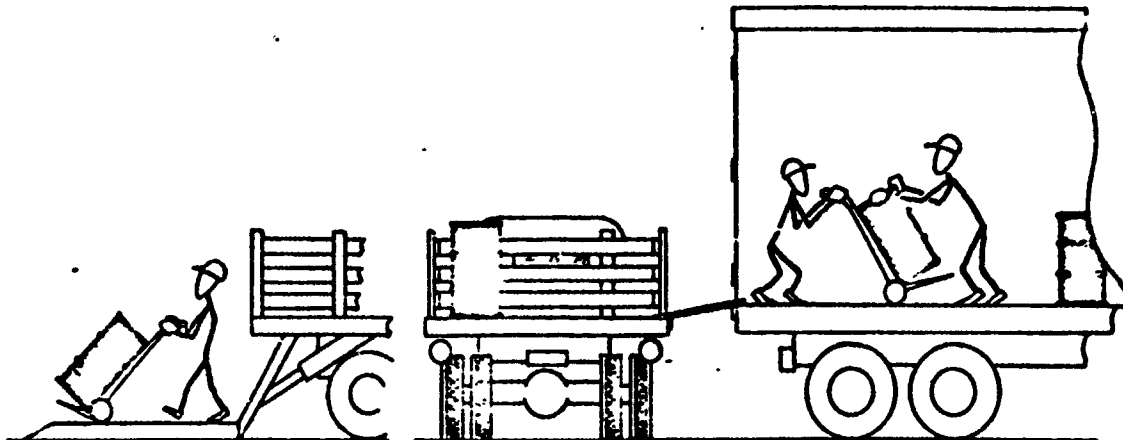


Figure 4. Unloading HIBEX Truck

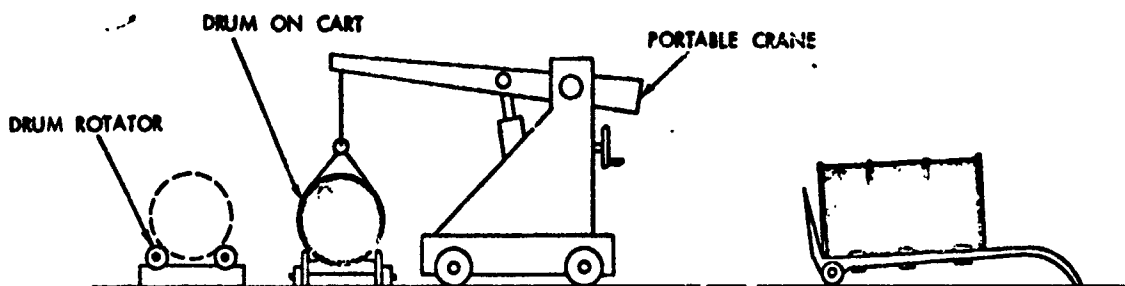


Figure 5. Drum Rotating—(Prior to Unloading Bags)

PROCESS SURVEY OF TRUCK LOADING

Operation	Observations		Engineering Analysis In-Process Potential	Sensitivity Test Analysis	Safety Margin
	Combustible	Initiation Mode			
<b>NORMAL OPERATIONS</b>					
1. Removing of the powder drums to hydraulic tail gate and moving of drums to a storage area with a hand truck.	Green Casting Powder and heptane	Granular Friction	410 psi @ 1 ft/sec	59,500 psi @ 1 ft/sec	145
		Friction from powder bags on casting powder residue	410 psi @ 1 ft/sec	16,000 psi @ 1 ft/sec	39

**ABNORMAL OPERATIONS**

1. Drum drops off of truck (4 ft)	Green Casting Powder and Heptane	Granular Friction	> 20 psi @ 16 ft/sec	< 700 psi @ 8 ft/sec	None
-----------------------------------	----------------------------------	-------------------	----------------------	----------------------	------

**LOADING ROTATOR**

**NORMAL OPERATIONS**

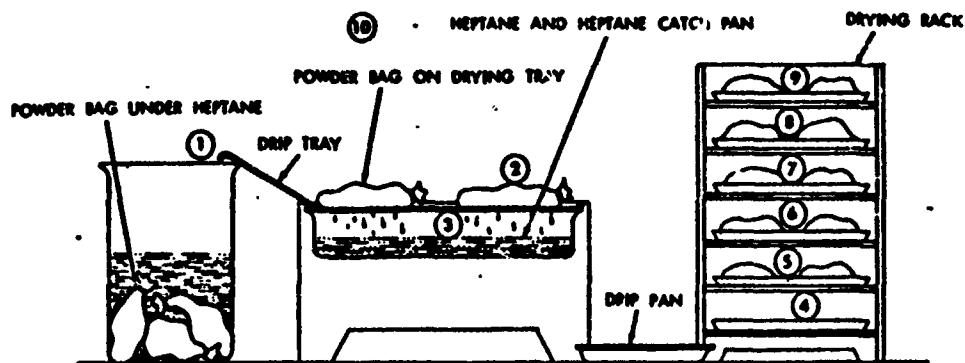
1. Lowering drum from upright to horizontal position	Green Casting Powder and Heptane	Granular Friction	27 psi @ 1 ft/sec	16,000 psi @ 1 ft/sec	392
2. Rotation of Powder in drum	Same analysis and conclusions as for the initial drum rotation.				

**ABNORMAL OPERATIONS**

1. Strap breaks dropping drum	Green Casting Powder in Heptane	Granular Friction	2,100 psi @ 11 ft/sec (2 ft drop)	< 700 psi @ 8 ft/sec	None
2. Transition to explosion if powder ignites	Green Casting Powder in Heptane	Transition	St. Dia. 30/16"	St./Dia. > 24"/4"	None

on each side of the drum, reaches into the drum, picks up a bag of powder and holds it at the top of the drum until most of the residual heptane drains back into the drum. The bag is then placed on a perforated tray over a grounded heptane collection bin. The bags continue to drip through the tray into the bin until another tray has filled. The tray is then placed in a drying rack and has essentially stopped dripping heptane. The bottom tray on the drying rack is solid to retain any residual heptane drippings. Heptane vapors are within the explosive range within 2-3" of the powder bags during unloading and in the drying racks (Figure 6). This potential hazard is minimized by the absence of excessive movement of the powder resulting in no detectable voltage accumulations. Heptane vapors are concentrated enough at the drum unloading area to require the operators to wear protective masks to prevent toxic effects. This concentration is limited to the immediate area of the drum as shown in Figure 6. The background vapor level in the room was approximately 5% of the LEL with no detected dead spots where vapors were excessive. The only explosive vapor concentrations in the drying bay during powder loading were within 2-3 inches of the powder bags. No personnel are allowed to enter the dry bay during the elevated temperature drying operation, preventing human spark ignition of heptane vapors. Previous checks on electrostatic buildup during drying indicated no voltage accumulates on the bags from drying during this phase. Electrostatic voltage checks after the cool down cycle indicated no voltage on the bags prior to removal from the bay.

3. Powder Rewetting and Packaging—The bags of powder removed from the drying bay must be rewetted with heptane to prevent movement of dry powder, opened and placed in containers as loose granules. The rewetting operation is accomplished by depositing the entire tray containing 2 powder bags into a heptane bath with no physical movement of the granules until they are heptane wet. When the bags are completely wet, the tie string is cut with an exacto knife with no contact between the blade and the casting powder. The powder, covered with heptane is poured into a grounded drum containing sufficient heptane to cover the powder. Free powder drop heights do not exceed 12" with a safety margin of 5. Explosive vapor concentrations are located in the receiving pot and the rewetting heptane tray. No electrostatic



DRUM UNLOADING SETU WITH HEPTANE VAPOR LEVELS - DURING DRUM UNLOADING

VAPORS	
1 -	23%
2 -	30%
3 -	>EXPLOSIVE RANGE
4 -	>EXPLOSIVE RANGE
5 -	>EXPLOSIVE RANGE
6 -	>80% OF LEL
7 -	30-40% OF LEL
8 -	10% OF LEL
9 -	6% OF LEL
10 -	ROOM ≈ 5% OF LEL

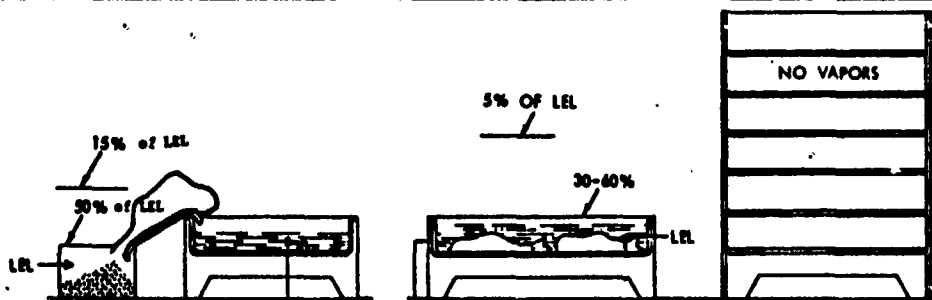
**OPERATING CONDITIONS**

**Drum Unloading Setup:**

1. Open Drum
2. Remove bag allowing majority of the solvent to drop back into the drum
3. Place bag on porous tray on drip rack
4. Place tray on drying rack
5. Recool empty drum

**Emptying Bags into 14 Gallon Drums:**

1. Remove tray from rack
2. Submerge tray under heptane
3. Cut Cord
4. Lift bag and pour contents into 14 gal container
5. After bags seal container



POWDER REWETTING AND TRANSFER TO 14 GALLON CONTAINERS

**PROCESS HAZARDS SURVEY**

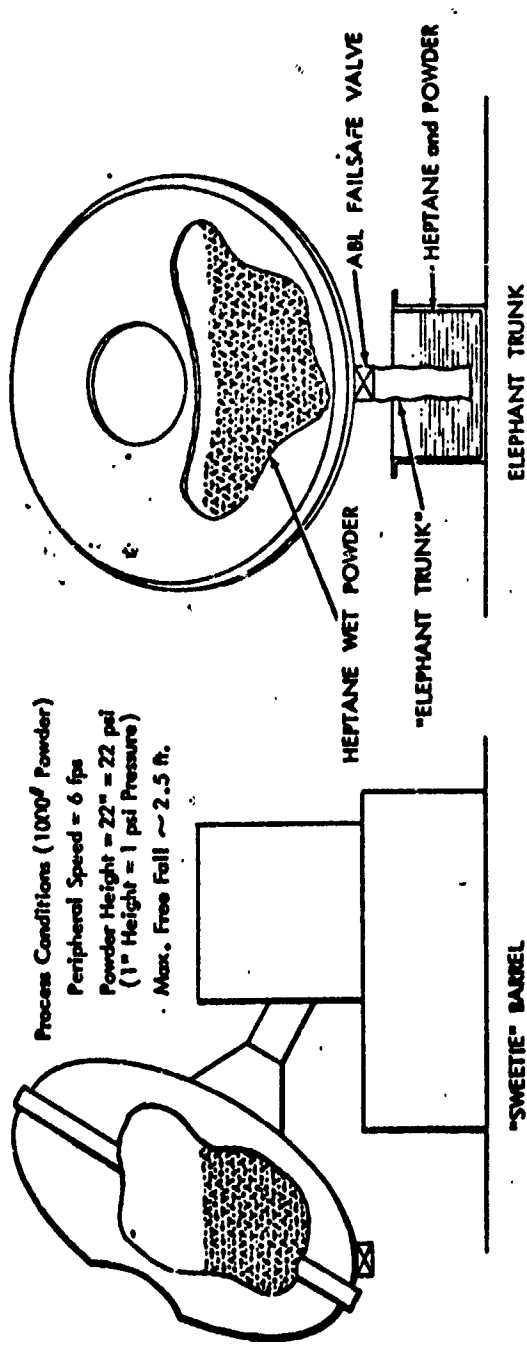
Operation	Observations		Engineering Analysis In-Process Potential	Sensitivity Test Analysis	Safety Margin
	Combustible	Initiation Mode			
<b>Normal</b> 1. Potentially Hazardous Vapor Accumulation	Heptane	Electrostatic Discharge	No Voltage Generation	> 6 Millijoules	Undefined
<b>Abnormal</b> 1. Dropping of Powder Bags	Green Coating Powder & Heptane	Granular Friction	~ 3-4 ft drop	No initiation after dropping powder bag 8 ft 20 times.	> 2
2. Electrostatic Generation	Heptane	Electrostatic Discharge	No Voltage	No electrostatic hazard is present in the operation since no voltage is accumulated.	
a. Bags in Dry House After Cool Down	"	"	" "		
b. Dumping Heptane into Dip Pan	"	"	" "		
c. Dumping powder	"	"	" "		
3. Freefall Dropping of Powder as the Granules Leave the Bag	"	Impingement	1 ft Drop	3 ft TIL	3

Figure 6. Hazard Analysis of Process to Remove Powder Bags from Drums, Rewet Powder after Drying and Loading Dry Powder into 14 Gallon Containers

voltage accumulations were present in the operation minimizing the potential vapor hazards. No physical movement of the powder was made until the powder was heptane wet. Figure 6 includes the in-process data on the rewetting operation.

4. Powder Shaping—Powder shaping and blending is accomplished in a "sweetie" barrel in approximately 1,000 lb lots. The barrel is precharged with sufficient heptane to maintain a heptane head on the powder bulk as the individual powder containers are dumped into the barrel. Powder shaping is accomplished by the intragranular action as the barrel turns. The finished product is removed from the barrel and repackaged in the handling containers by the use of an "elephant trunk" system. The "elephant trunk" is a flexible duct leading from an ABL designed fail safe pinch valve. The duct is placed in the receiving container with a set distance between the bottom of the container and the duct outlet. When the valve is opened 50 lbs of powder flows into the receiving pot, while the head of powder outside the trunk stops the flow. The valve is then closed and the receiving drum is removed, sealed and a clean drum put in its place. This is repeated until the powder is completely removed. The loading, operating, and unloading phases of the shaping and blending operation have sufficient safety margins ranging from 2 to 23 as shown in Figure 7.

5. Powder Screening—Powder screening is accomplished with a Sweco 30" screener with heptane circulating through the system to prevent powder dust buildup. The powder is introduced into the screener with a special arrangement consisting of a drum turning apparatus and dump valve. Using this arrangement the powder can be introduced remotely with heptane flowing through the screener. The screened powder automatically separates into a container ready to be resealed. Clusters and fine material are separated into containers, which are sent to the scrap disposal area heptane wet. Instrumented measurements of the acceleration during vibration and calculations of particle velocities have established adequate safety margins for this operation during normal operating conditions (2.0 to 83,000). Abnormal situations where a foreign object enters the screener could create a hazard from friction.



Process Conditions (1000<sup>g</sup> Powder)  
 Peripheral Speed = 6 fps  
 Powder Height = 22" = 22 psi  
 (1" Height = 1 psi Pressure)  
 Max. Free Fall ~ 2.5 ft.

PROCESS HAZARDS SURVEY

Operation	Observations		Engineering Analysis In-Process Potential	Sensitivity Test Analysis	Safety Margin
	Combustible	Initiation Mode			
1. Pumping Powder into Sweetie Barrel	Casting Powder & Heptane	Impingement	Max. Height 2.5 ft	5' drop ht. T11	No 2
2. Operating Barrel	Casting Powder & Heptane	Granular Friction Powder/Powder (G/Powder/Dust/Brass) Freefall	22 psi/6 fps 22 psi/6 fps ~ 2.5 ft	500 psi/6 fps > 10,000 psi @ 6 fps 5.0 ft	No 23 No > 470 No ~ 2
3. Unloading Barrel	Casting Powder & Heptane	Fail-safe Valve Freefall	Electrostatic Initiation Safe operation determined by previous analysis as reported in Ref. 1	(Equipment grounded)	No - 5' drop ht. T11

Figure 7. Hazards Analysis of Powder Shaping and Blending Operation

Screener cleanup requires flushing the inside surfaces of the screener with water to remove residual casting powder fines prior to removing the section restraining bands.

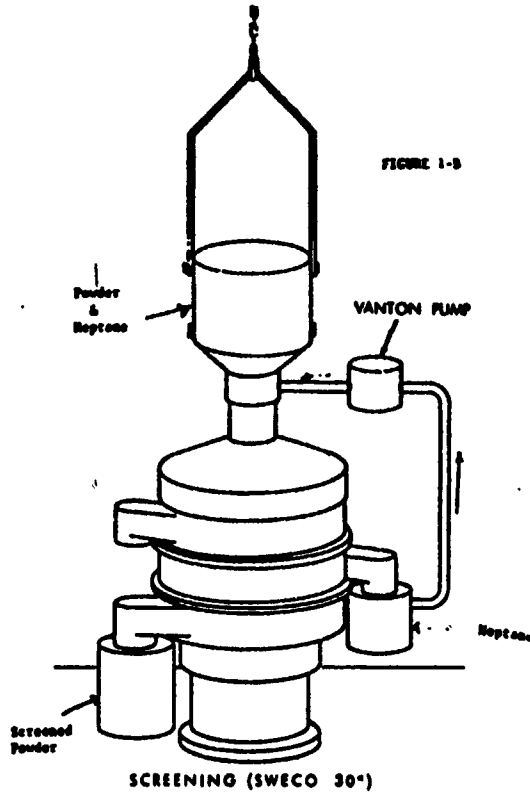
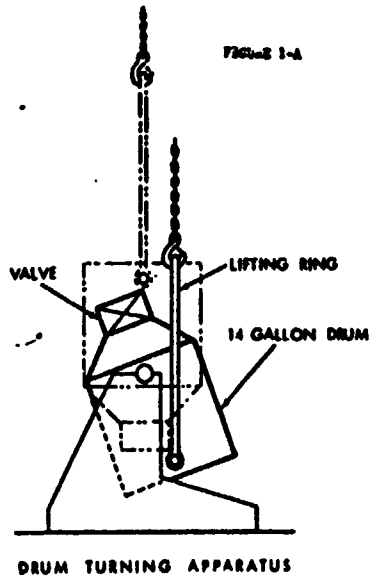
Figure 8 shows the screener operation and the safety margins during operation.

### C. Mold Loading

Mold loading, via the liquid carrier system, limits the powder particle velocities to a safe level. The process steps are, (1) filling the main hopper with powder from the smaller 14 gallon transporter cans, (2) mold loading, (3) mold transportation, and (4) mold unloading. These steps can be accomplished safely by this system with safety margins for normal operating conditions between 2 and 1,562.

1. Powder Dumping into Hoppers—Powder is received in the mold loading area in 14 gal drums containing 50 lb of powder and 3 gallons of Heptane. These drums are emptied into a single hopper for mold loading. The powder dumper arrangement used to empty the drums operates with sufficient margins of safety (of 2 to 1,562) and does not introduce any granular friction problems. Freefall drop height from the dumper to the bottom of the hopper does not exceed the 5' freefall limitation. This safety margin is increased by maintaining a head of Heptane over the powder in the hopper. Critical height to explosion data indicates that the powder in the 14 gallon drum or in the hopper should not transit to an explosive reaction if ignition should occur. Figure 9 shows hopper loading setup.

2. Powder Mold Filling—The height of the HiBEX unit is in excess of the freefall impingement threshold level. This was one of the reasons for introducing the liquid carrier system. Mold loading by the liquid carrier process reduces the powder particle velocities to 1.4 ft/sec, considerably below the 17.5 ft/sec threshold level. Hazardous dust clouds are also eliminated during the loading since casting powder residue will be suspended in the liquid media. Electrostatic voltages are not generated at the particle velocities of the loaded powder as indicated by in-process measurement of less



**SWECO 30" VIBRO-ENERGY SEPARATOR**

**Hazard Analysis for Screening Nitro Powder**

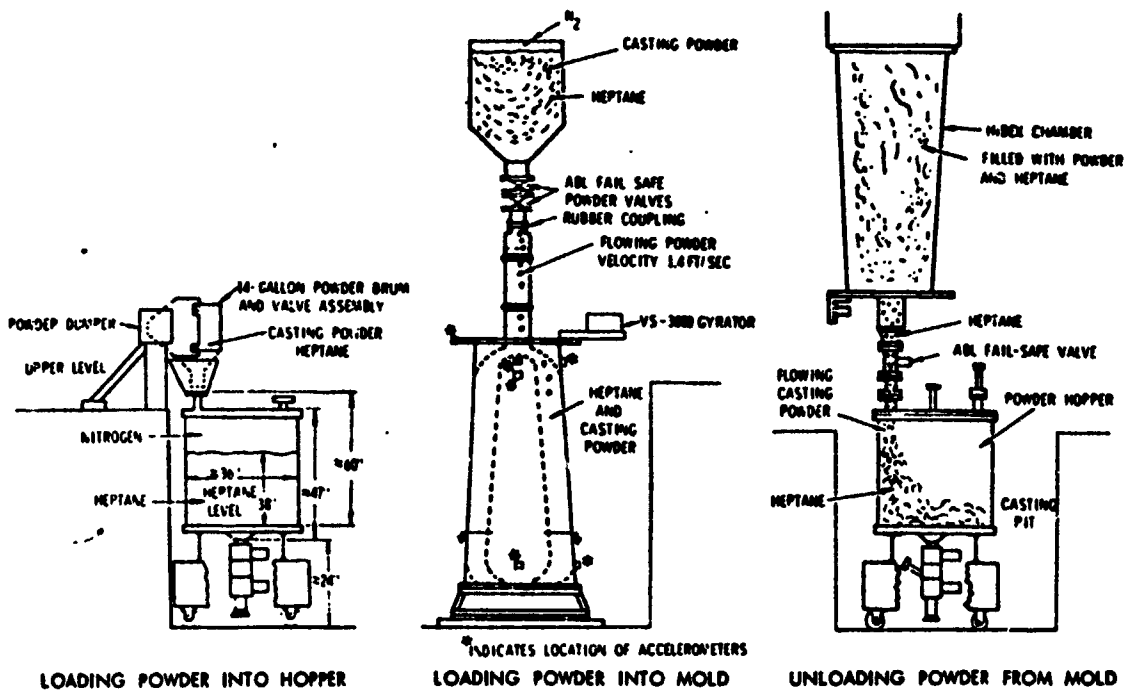
Condition Analyzed	Type of Material	In-Process Data	Quantity Data	Safety Factor
<b>Normal</b> Granular friction due to lateral motion of screener	(Heptane Wet) Granule/Granule			
	Single Granule	6 psi @ 4 ft/sec	2700 psi/4 ft/sec	450
	4 gm Cluster	15 psi @ 4 ft/sec	2700 psi/4 ft/sec	180
	(Heptane Wet) Granule/Metal			
	Single Granule	6 psi @ 4 ft/sec	25,000 psi @ 6 ft/sec	4,166
	4 gm Cluster	15 psi @ 4 ft/sec	25,000 psi @ 6 ft/sec	1,666
Granular friction on side of screener	(Heptane Wet) Granule/Granule			
	Single Granule	.30 psi @ 4 ft/sec	2,700 psi @ 4 ft/sec	9,000
	4 gm Cluster	1.9 psi @ 4 ft/sec	2,700 psi @ 4 ft/sec	1,421
	(Heptane Wet) Granule/Metal			
	Single Granule	.30 psi @ 4 ft/sec	25,000 psi @ 6 ft/sec	83,300
	4 gm Cluster	1.9 psi @ 4 ft/sec	25,000 psi @ 6 ft/sec	13,158
Granules impinging on the screener side	(Dry) Granule & Resid/Metal			
	Single Granule	.30 psi @ 4 ft/sec	3,640 psi @ 4 ft/sec	12,133
	4 gm Cluster	1.9 psi @ 4 ft/sec	3,640 psi @ 4 ft/sec	1,916
<b>Abnormal</b> Screen plates moving in recessed area of screener body	Impingement			
	1-3 Granule Cluster	4.0 ft/sec	17.3 ft/sec	4.37
Transition to Explosion	4 gm Cluster	4.0 ft/sec	4.0 ft/sec (cal.)	1.20
	Friction			
Transition to Explosion	C.F. Residue (Dry)	16,300 psi @ 4 ft/sec	8,000 psi @ 4 ft/sec	None
	C.F. Heptane (Dry)	16,300 psi @ 4 ft/sec	29,000 psi @ 4 ft/sec	1.76
Transition to Explosion	Critical	W/Dia	W/Dia	No
Transition to Explosion	W/Dia.	6"/30"	24"/4"	Hazard

Figure 8. Hazards Analysis of the Screening Operating

CONTAINER TURNING OPERATION

<u>Condition Analyzed</u>	<u>Type Hazard and Material</u>	<u>In-Process Data</u>	<u>Sensitivity Data</u>	<u>Safety Factor</u>
<u>Hazard Analysis for Screening Hibex Powder</u>				
<u>C7 Immersed</u>				
Granular Friction Powder/Powder	Friction	16 psi @ 1.6 ft/sec	> 2700 psi @ 1.6 sec	169
<u>C7 Immersed</u>				
Granular Friction Powder/Metal	Friction	16 psi @ 1.6 ft/sec	>25,000 psi @ 1.6 ft/sec	1,562
<u>Dry Material</u>				
Granular Friction Powder/Powder & Dust	Friction	16 psi @ 1.6 ft/sec	> 3,636 psi @ 1.6 ft/sec	227
<u>Dry Material</u>				
Freefall Velocity	Impingement	8.5 ft/sec	17.5 ft/sec	2
Transition from burning to explosion while immersed in C7	Transition	Max 16" Height in 21" diameter	>24" height in 4" dia pipe	No transition hazard
Transition from burning to explosion while dry	Transition	Max 16" Height in 21" diameter	2" Height at 2" dia 2" Height at 4" dia 6" Height at 8" dia (Extrapolated) > 24" at 21" dia.	

Figure 8. Hazards Analysis of the Screening Operating (Continued)



**PROCESS HAZARDS SURVEY**

Operation	Observations		Engineering Analysis		Safety Margin
	Combustible	Initiation Mode	In-Process Potential	Sensitivity Test Analysis	
	<u>(Powder Dumping into Hopper)</u>				
Powder Movement during turning operation		Some Analysis as found in Figure VII.			2-1,562
Freefall drop of Powder	Casting Powder & Heptane	Impingement	~ 2 ft drop into Heptane	5' TII	~ 2.5
			<u>(Mold Loading)</u>		
Powder falling in Heptane	Casting Powder & Heptane	Impingement	1.4 ft/sec	17.5 ft/sec	12.5
Electrostatics	Casting Powder & Heptane	Electrostatic Discharge	~ 300 volts		Undefined
Temperature Rise due to Vibration	Casting Powder & Heptane	Thermal Ignition	~ 10°F rise 80°F	Auto Ignition ~ 400°F	4.4
Friction due to vibration	Casting Powder & Heptane	Granular Friction	Hibex unit 84 psi @ 1.5 ft/sec	5,200 psi @ 1.5 ft/sec	62
			Powder Hopper 72 psi @ .5 ft/sec	62,000 psi @ .45 ft/sec	861
			14 gal Drum 22 psi @ 3.5 ft/sec	270 psi @ 3.5 ft/sec	122
			<u>(Mold Unloading)</u>		
Some Analysis as mold loading					4.4-62

**Figure 9. Hazard Analysis of Mold Loading and Unloading Operation**

than 300 volts accumulated during mold loading operations. The ABL designed fail safe pinch valves have been tested extensively to insure that the opening and closing of the valve does not present a hazard. Safety margins have been established for this operation ranging from 2 to 1,562. A potential hazard exists if the rubber boot in the valve should fail releasing the powder and heptane in the hopper. The new type neoprene NE-604 elastomer body was subjected to a contamination and endurance test to provide assurance that the valve would not fail.

Vibration is used on the 14 gallon handling drums, the casting powder hopper and the mold during mold loading operations. Potential granule motion levels are below that required to cause initiation. Safety factors for the vibrations exist from 62 to 122. Temperatures were monitored as suspected sources of friction heating during the mold vibration resulting in only 10° above ambient being detected. Figure 9 shows the powder loading setup.

3. Powder Unloading—A powder unloading technique was developed to remove the powder from the mold in the event that poor loading efficiency or other unacceptable condition occurred. The system in effect reverses the mold loading technique and allows for the powder to be cast back into the 1,500 lb hopper without free fall problems. Due to the inert carrier technique, a few granules adhered to the mold and fell after the unit was removed from the hopper during dummy powder tests. The drop height of these particles could exceed the 5 ft Til height, due to the length of the motor case. This problem is however minimized by the fact that only ≈ 2 lb of powder remain in the unit with water or heptane to remove these particles prior to disassembling the mold. Figure 9 shows the unloading setup. Included in Figure 9 is a process hazards survey of the mold loading and unloading phases.

#### Heptane Handling

Special procedures have been adopted for heptane loading and unloading of the units and hoppers used during the process. A 3,000 lb grounded desiccator is used as a supply source of heptane during loading of the units and during draining operations. A nitrogen atmosphere (< 8% O<sub>2</sub>) is maintained in the desiccator and the receiving containers during loading and unloading of the

units to reduce explosive atmospheres. A Coppus blower is used to remove the escaping vapors during heptane handling. Nitrogen is again introduced into the hoppers and the units when the heptane is removed after loading. Figure 10 shows the major heptane handling areas and indicates that at all times the heptane receiver and supply vessels are always blanketed with nitrogen, and that adequate ventilation exists in the various areas.

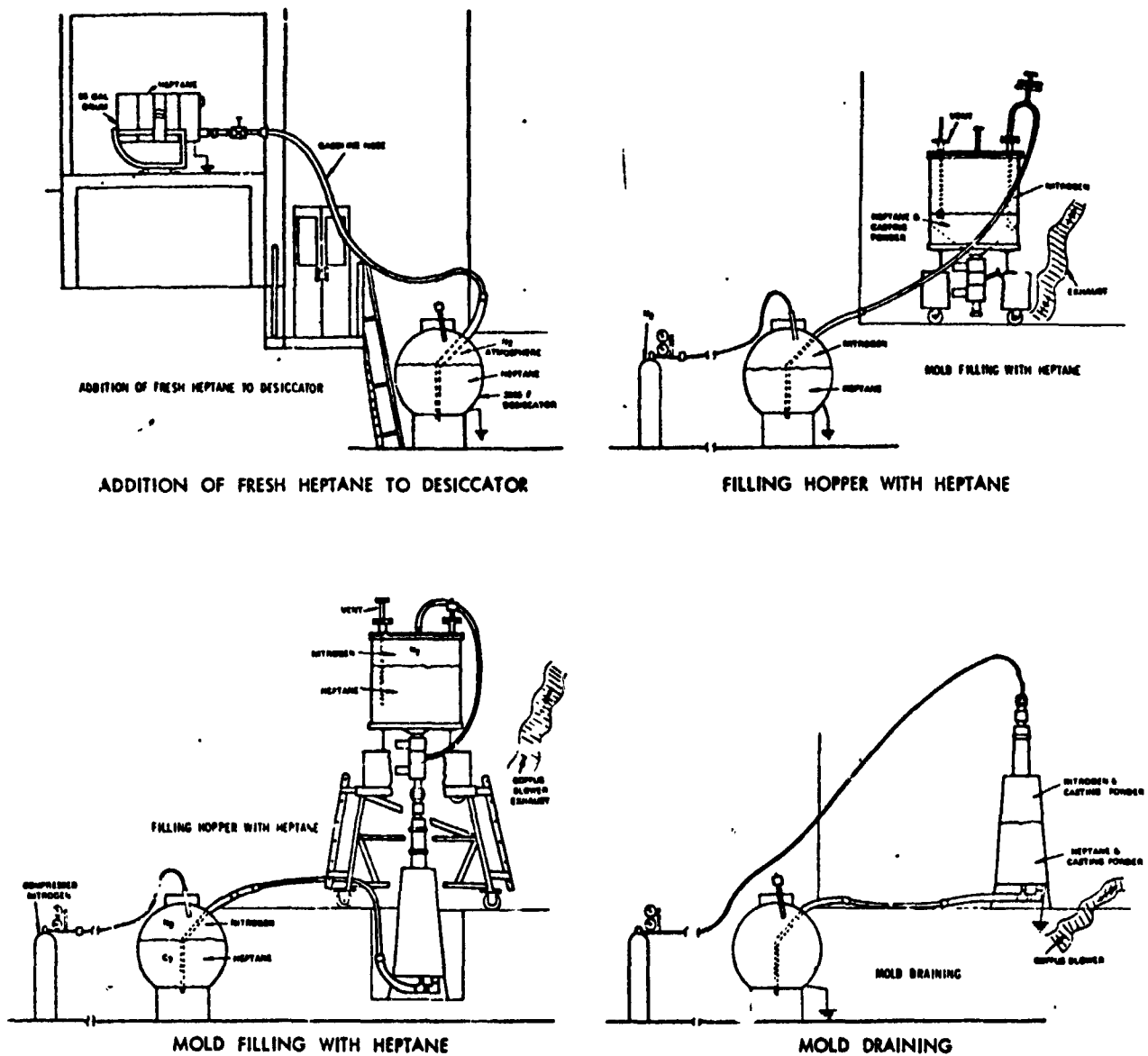
#### Material Sensitivity

The transition characteristics of the 2849 casting powder has been determined by defining the critical height to explosion with and without heptane and by extending the data to the diameters found in the process. Figure 11 shows these data for dry and heptane immersed conditions. The transition of the green mix was analyzed by a comparison with the data established for a perchlorated, aluminum staple, CMDB formulation, ABL 2888, Figure 12, as a function of volatile solvent level. No data was available similar to this for 2849 casting powder.

Impact, friction and electrostatic values of the materials are summarized in Table I in engineering terms. This information will be extended by obtaining data on the new powder being processed as samples become available.

### CONCLUSIONS AND RECOMMENDATIONS

Two potentially hazardous areas exist in the green powder processing operations which are not part of the liquid carrier systems but are part of the casting powder manufacturing process. They are (1) a transition to explosion hazard in the press during extrusion and (2) fire hazard due to friction in the cutting operation.



### HAZARD ANALYSIS OF HEPTANE HANDLING TECHNIQUES

1. Electrostatics - None--All systems grounded.
2. Explosive Vapors - None--Nitrogen purge use to displace the air from the systems prior to filling with Heptane and during draining.

Figure 10. Heptane Handling

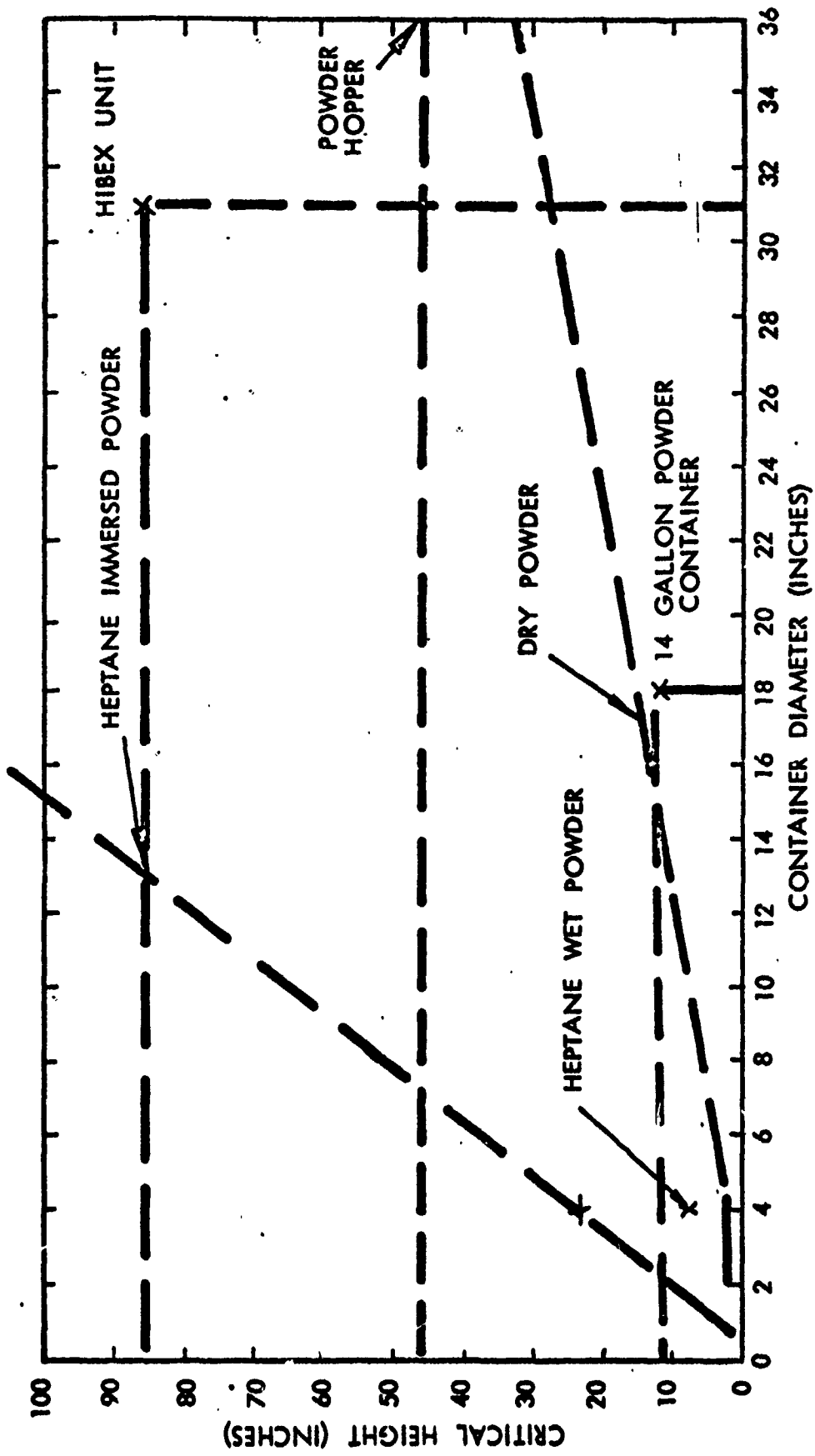


Figure 11. Transition Characteristics of 2847 Casting Powder

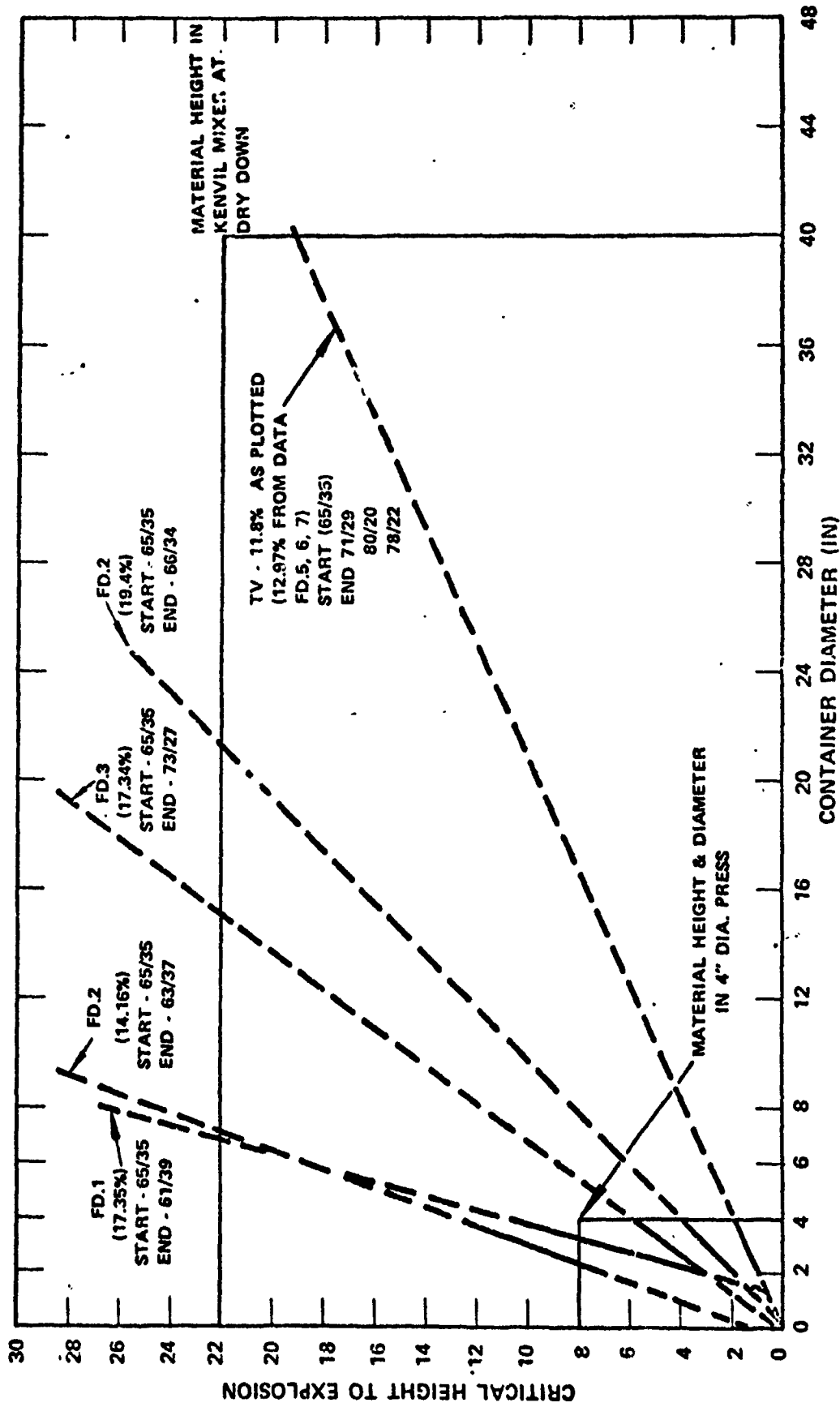


Figure 12. Effect of Volatile Solvent Concentration on Green Mix Transition Properties

Table I  
**SENSITIVITY THRESHOLD CHARACTERISTICS OF  
 FDN CASTING POWDER**

<u>Friction</u>	<u>Dry</u> <u>(psi/ft/sec)</u>	<u>Wet</u> <u>(psi/ft/sec)</u>
A. <u>2849 Green Mix</u>		
1. <u>Steel/Steel</u>	7, 000/8	---
B. <u>Green Casting Powder</u>		
1. <u>Steel/Steel</u>	---	51, 000/8 ft/sec 103, 000/6 ft/sec *Undefined
2. <u>Granule/Granule</u>	---	
C. <u>Dry Casting Powder</u>		
1. <u>Granule/Granule</u>	70/9 630/5 2, 700/4	< 700/8 < 700/6 2, 700/4
2. <u>Granule/Granule</u>	< 700/8 2, 700/6 6, 150/5	< 700/13 8, 400/8 25, 000/6
3. <u>Granule/Brass</u> <u>with Dust</u>	--- ---	>10, 000/8 >10, 000/6
4. <u>Steel/Steel (psi/fps)</u>	1, 500/8	10, 000/8
<u>Impact</u>	<u>(ft-lb/in<sup>2</sup>)</u>	<u>(ft-lb/sec-in<sup>2</sup>)</u>
A. <u>Green Mix</u>	19.5	56, 000
B. <u>Green Casting Powder - Wet</u>	19.5	56, 000
C. <u>Dry Casting Powder - Dry</u>	16	44, 720
<u>- Wet</u>	39	110, 000
<u>Electrostatic Discharge</u>	<u>Joules</u>	
A. <u>Green Mix</u>	< 0.001	
B. <u>Dry Casting Powder</u>	0.0016	
<u>Screener Residue</u> (Run Heptane Wet)	<u>Impact</u> <u>(ft-lb/in<sup>2</sup>)</u>	<u>Friction</u> <u>(psi/ft/sec)</u>
A. <u>2849 C. P. Fines</u>	1.0	< 2, 000/8 < 2, 000/6 2, 000/5 10, 000/4
B. <u>2849 C. P. Sludge</u>	46	2, 500/8
C. <u>2849 C. P. Wafers</u>	8.5	36, 500/8

These problems are inherent to the operation and are not related to the hazards of the liquid carrier system.

Granular movement and dust clouds have been reduced to a safe level by the liquid carrier principal and transition to explosion hazards have been reduced.

#### EXPERIMENTAL

Standard impact, friction, electrostatic discharge, freefall, impingement, and critical height to explosion tests were conducted to derive the required sensitivity data.